JCR-7

Monograph

North Sea Chalk

Editors

Svein M. Skjæveland
Professor of Reservoir Engineering at
University of Stavanger.
and

Ola Ketil Siqveland
Senior Engineer at
University of Stavanger.

Web version

JCR 7

November, 2019

We thank Morten Leth Hjuler for
the front page photo of this monograph.

ISBN 978-82-7644-733-0

Authors and Editors

Olav Inge Barkved is currently a geophysicist with Petoro AS. He has more than 20 Years of experience from chalk field geophysics, production and development. Olav received his master's degree in oil and gas exploration from the Norwegian Institute of Technology in 1983 and started his career as a research scientist with Geco. He worked in seismic reservoir characterization, interpretation technology, and processing, primarily based in Norway but including a short stay at Schlumberger Doll Research and at Schlumberger Cambridge Research. In 1992, Olav joined Amoco and remained there through the merger with BP in 1998 and until late 2013. In BP, he was area geophysicist, technology coordinator, and global advisor. Olav is an active member of SEG, EAGE, and NPF. He and his former colleagues at Amoco and BP received the EAGE award for best paper in 1997 and 2009, the Louis Canard Award in 2008, and the award for best paper in The Leading Edge in 2008. In 2006, he received the Norwegian Geophysical Award. Olav served as an EAGE Distinguished Lecturer in 2010. In 2012–2013, he presented EAGE's worldwide Education Tour VI on seismic surveillance.

Roman Berenblyum holds a PhD (2004) on reservoir streamline simulation accounting for capillary effects from Danish Technical University. Since 2006 he has worked in IRIS focusing on reservoir simulation activities related to IOR/EOR as well as carbon utilisation and storage. Roman has been involved in and coordinated multidisciplinary research and industry-oriented projects in Norway, Middle East, Latin America and Russia. He currently holds a position of Research Director, Multiscale Reservoir Studies.

Harald Berland is scientist in the enhanced oil recovery group at IRIS energy department. He holds a MS-degree in microbial ecology, from the University of Bergen. His research focuses are on EOR chemicals and microbial processes and ecology with the emphasis on mechanisms in fluid flooded rock matrix. His scientific interest include EOR polymers, biogenic energy production, degradation processes and technologies improving these processes. In collaboration he has been involved in more than 10 publications with a numerous of scientific reports at the IRIS energy and microbiology department.

Helle Foged Christensen is Chief Engineer at Geo (former Danish Geotechnical Institute). She holds a M.Sc. from the Technical University of Denmark in Geotechnics and structural engineering. More than 10 years of experience as Associate professor/referee, teaching and evaluation on Master and Phd level. Her main interest is the application of rock mechanics, especially in relation to laboratory testing and rate type modelling. Her favorite projects involve partners from both the universities and the industry, and provides practical solutions to engineering problems.

Finn Engstrøm is currently Senior Principal Petrophysicist at Maersk Oil. He has more than 30 years of experience with petrophysics of chalk and other small grained carbonates. Finn holds a M.Sc. in eletrotechnical engineering (1979) and a Ph.d. in petrophysics (1982) from the Technical University of Denmark. He started his professional life as wellsite engineer/petrophysicist for Shell in Oman (1982-1985). From 1985 he has worked for Maersk Oil as petrophysicist in various positions in Denmark and UK. During his 30+ years in petrophysics Finn has been working on the majority of the North Sea chalk fields doing log analysis, developing petrophysical rock models and saturation-height models for static/dynamic modelling, mud gas analysis, core analysis and compaction/subsidence analysis. He has more specifically been working on non-equilibrium condition chalk fields with dipping contacts and a General Petrophysical Chalk Model. He has a significant interest in petrophysical research and has acted as Msc./PhD project super visor and research project initiator/company representative on many occasions. Finn has participated in JCR since 1985 as project leader and steering committee representative and is chairman for JCR-7.

Geir Ersland is an Associate Professor in Reservoir Physics at the Dept. of Physics and Technology at the University of Bergen (UoB), Norway. His experimental work is focused on imaging and visualization of flow in porous media. His main scientific interests are CO_2 storage, fractured reservoirs, CO_2-EOR and sedimentary hosted gas hydrates.

Ida Lykke Fabricius is professor in applied geology and petrophysics at Department of Civil Engineering, Technical University of Denmark. She holds a dr.techn. degree in applied geology from Technical University of Denmark. Her main interest is integration and interpretation of petrophysical, rock physical, rock mechanical, sedimentological, geochemical and petrographic information

Charles Tibbals Feazel retired in 2010 from ConocoPhillips to form Feazel GeoConsulting LLC, where he assists oil and gas companies and their investors in determining reservoir quality and its impact on asset value and prediction of future production. At least half of his 35+ years with ConocoPhillips involved North Sea chalk reservoirs at scales from microscopic to seismic. He holds a BA from Ohio Wesleyan University and MA and PhD degrees from The Johns Hopkins University. A veteran of numerous research cruises from Arctic to Mid-Atlantic waters, he specializes in comparative sedimentology of carbonate rocks and their modern depositional analogs.

Ingebret Fjelde is Chief Scientist in Improved Oil Recovery at the International Research Institute of Stavanger (IRIS) and is also Adjunct Professor at the Institute of Petroleum Technology at the University of Stavanger. He holds a PhD (1995) in Chemistry from the University of Bergen. His main research interests are enhanced recovery methods in both sandstone and carbonate reservoirs (surfactant flooding, polymer flooding, low salinity water flooding, wettability alteration, carbon dioxide flooding, and foam) and evaluation of original wettability conditions. He has also studied oil field chemistry and formation damage.

Martin Anders Fernø is an Associate Professor in the Petroleum and Process Technology research group at the Department of Physics and Technology, University of Bergen. His research focuses on flow, oil recovery and CO_2 storage in heterogeneous, fractured reservoirs with emphasis on in situ imaging. His scientific interests include spontaneous imbibition, foam flow and combined CO_2 storage and enhanced oil recovery. He has published over 70 scientific publications and supervised more than 50 PhD and master students in Petroleum Technology at the Dept. of Physics and Technology.

Per Gunnar Folstad is Director, Geophysical Implementation within the Greater Ekofisk Area Development department at ConocoPhillips in Norway. He holds an MSc in Technical Physics from NTNU, Norway. He is interested in all aspects of geophysics with a special focus on 4D seismic for reservoir monitoring.

Arne Graue is Professor of Physics at the Department of Physics and Technology, University of Bergen, where he is Head of the Petroleum and Process Technology Research Group. His scientific interest is within Reservoir Physics emphasizing heterogeneous and fractured reservoirs, multiphase flow in porous media, in-situ fluid saturation imaging, laboratory investigation of Integrated EOR-techniques, CO_2 sequestration and gas hydrates. He has published more than 200 scientific publications and supervised 120 PhD and MS students. He has MS-degree in Exp. Nuclear Physics and PhD degree in Reservoir Physics; all from U. of Bergen. Graue is currently international coordinator for a collaboration of 11 universities in 5 countries on EOR in fractured reservoirs, coordinator for Carbon Capture Utilization and Storage (CCUS) research collaboration between Norway and the USA, Chairman of the Executive Board of the Petroleum Research School of Norway and Chairman of the Board of NorTex Petroleum Cluster.

Ying Guo is currently employed as Research Director for the EOR Group at International Research Institute of Stavanger, Norway (IRIS). She holds PhD degree in Reservoir Engineering (1989) from Norwegian Technology and Natural Science University (NTNU), and has worked on various subjects, in particular SCAL, chemical and CO2 EOR, numerical modelling, E&P data management and research coordination in Rogaland Research (now IRIS), IBM, Landmark Graphics and Total E&P Norway. For a period of about 10 years, she served as head of R&D Subsurface section at Total E&P Norway when she was involved in the IOR/EOR for chalk fields, and contributed in the Joint Chalk Research programs.

Marte Gutierrez is the James R. Paden Distinguished Professor at the Department of Civil and Environmental Engineering of Colorado School of Mines. Formerly, he was Post-Doctoral Fellow, Senior Engineer and Program Leader at the Norwegian Geotechnical Institute, and Associate Professor/Professor at Virginia Tech. He has held visiting professorship and researcher positions in China, Chile, France, Japan and South Korea and UAE. He has published more than 220 papers in book chapters, journals and conference proceedings, and has given keynote and invited lectures at a number of conferences. He is a member of the Editorial Board of four International Journals. He is the recipient of the 2011 Geotechnical Research Medal from UK's Institute of Civil Engineers, and the Peter A. Cundall Honorable Mention Award. Dr. Gutierrez's main research interests are in Geomechanics, and Energy and Environmental Sustainability.

Nina Elisabeth Bjørnevoll Hagen is Director of Reservoir Characterization within the Greater Ekofisk Area in ConocoPhillips Norway. She holds a Cand Scient degree in Structural Geology from University of Bergen. Her main interests cover all aspects related to fluid flow in reservoirs, Chalk reservoirs in particular. Previous experience includes operational geology, improved oil recovery, well planning, and reservoir modelling gained through working for Sperry Sun, IUGS, Norsk Hydro and the last 20 years for ConocoPhillips.

Harald Johansen held a position of Principal Research Scientist at the Institute of Energy Technology in Norway, until his retirement in 2015. He holds a Cand Scient in Mineralogy at the University of Oslo, Norway. His research has been directed towards water-rock interaction and the use of naturally occurring tracers in the study of geological processes.

Aksel Hjort is a Professor at the University of Stavanger within reservoir technology, and Chief Scientist at IRIS. He has a PhD within theoretical physics from University of Oslo. The last 10 years he has been working on understanding multiphase-flow in porous media by designing lab experiments, developing physical models and numerical simulation codes. In particular he has worked on improving flow models by taking into account chemical interactions with the fluid and the rock phase inside a porous medium. In 2013 he was part of the management team that was awarded the Norwegian national center within improved oil recovery by the Norwegian research council. Since then the main research interest has been to upscale laboratory results and pore scale mechanism to larger scale. Together with IFE he is currently working on a simulator (IORSim) that makes it possible to add rock fluid interactions to industry standard reservoir models (Eclipse) in order to predict the impact of chemical EOR in mature fi elds on the Norwegian Continental Shelf. The work has led to SR Bank's Innovation Award in 2010, the NPD's IOR prize in 2010 as part of the COREC team and Lyse's Research Award in 2013. Hiorth has more than 50 publications in per reviewed journals, and 40 international conference papers.

Hans Kleppe is an Associate Professor at the Department of Petroleum Engineering, University of Stavanger. He holds a MS-degree from the University of Oslo and a PhD degree from MIT, both in mathematics. His scientific interest is within Reservoir Simulation emphasizing solution of linear equations, upscaling and modeling of wettability alteration. From 1981 to 1986 he was with Rogaland Research (now IRIS) and from 1986 to date with the University of Stavanger. He spent one year from 1994 to 1995 as a Visiting Professor at Stanford University.

Dimitrios Georgios Hatzignatiou is a Tenured Professor of Petroleum Engineering at University of Houston's (UH) Cullen School of Engineering, and an ORISE Faculty Research Associate. For the last 11 years he was also the Center of Oil Recovery (COREC) Professor II of EOR at University of Stavanger (UiS). Hatzignatiou previously held several senior-level technical and management positions with RF/IRIS and Schlumberger, and served as reservoir engineering principal consulting advisor and tenured associate professor of petroleum engineering at University of Alaska Fairbanks. Hatzignatiou holds a PhD degree in petroleum engineering from the University of Tulsa, and his areas of specialization include, among others, EOR/IOR, reservoir engineering, reservoir characterization, production optimization, reservoir simulation, water management, and CO2 sequestration. He is a chartered engineer and registered professional engineer in Europe, and serves as an associate editor of the SPE Reservoir Evaluation and Engineering journal and technical editor in several scientific journals.

Ole Jørgensen is a principal reservoir engineer with Maersk Oil. He holds a PhD in solid mechanics from the technical university of Denmark. His main interest is in field development planning, water flooding and reservoir monitoring and diagnostics. He took part in the early developments of the Halfdan field, where the concept of FAST (Fracture Aligned Sweep Technology) was created. FAST takes the effect of pressure gradients and their effect on magnitude and direction of horizontal stresses into account. FAST makes it possible to propagate injection fractures at reduced risk of creating short-circuits.

Tron Golder Kristiansen is applying geomechanics to solve various challenges in the oil and gas industry. This includes areas such as: solids production, hydraulic fracturing, well design in hostile environments, wellbore stability, drill cuttings re-injection and waste disposal, P&A, compaction and subsidence prediction, reservoir engineering, petrophysics, rock physics and geophysics. He started his work with Amoco including work at their research center in Tulsa, Oklahoma. He was a Global Geomechanics Advisor for BP from 2003 to 2016 in the central geomechanics team in the Global Wells Organization located in London and Houston. He was involved in both BP and partner operated projects, and R&D, around the world. He is currently Operations Geology and Rock Mechanics Manager in Aker BP in Stavanger and Trondheim. He has an MSc in Petroleum Engineering from Stavanger in 1992.

Martin Landrø received an M.S. (1983) and Ph.D. (1986) in physics from the Norwegian University of Science and Technology. From 1986 to 1989, he worked at SERES A/S. From 1989 to 1996, he was employed at IKU Petroleum Research as a research geophysicist and manager. From 1996 to 1998, he worked as a specialist at Statoil's research center in Trondheim. Since 1998, Landrø has been a professor at the Norwegian University of Science and Technology, Department of Petroleum Engineering and Applied Geophysics. He received the Norman Falcon award from EAGE in 2000 and the award for best paper in GEOPHYSICS in 2001. In 2004 he received the Norwegian Geophysical award, and in 2007 Statoil's researcher prize. He received the SINTEF award for outstanding pedagogical activity in 2009. In 2010 he received the Louis Cagniard award from EAGE and in 2011 the Eni award (New Frontiers in Hydrocarbons). In 2012 he received the Conrad Schlumberger award from EAGE. Landrø's research interests include seismic inversion, marine seismic acquisition, and 4D and 4C seismic. This includes geophysical monitoring of CO_2 storage. In 2014 he received the IOR award from the Norwegian Petroleum Directorate. He is a member of EAGE, SEG, The Norwegian Academy of Technological Sciences and The Royal Norwegian Society of Sciences and Letters.

Merete Vadla Madland is professor at University of Stavanger within reservoir engineering, and in autumn 2013 she became director of the new national research centre for improved recovery of petroleum resources on the Norwegian Continental Shelf. She has a Dr.ing within geomechanics from the University of Stavanger. The last 20 years she has worked on how to most effectively extract oil from reservoir rocks. She has been heading several RCN funded projects and numerous industry funded projects.The research has focused on understanding the physical and chemical interactions between rocks and fluids on the pore (micro) scale and how these can be transferred to the field (macro) scale. The work has led to SR Bank's Innovation Award in 2010, the NPD's IOR prize in 2010 as part of the COREC team and Lyse's Research Award in 2013. Madland has more than 50 publications in per reviewed journals, and 70 international conference papers. She has been invited speaker and held several keynote presentations at national and international conferences/symposiums.

Anna Matthews is currently Lead carbonate geologist for the Middle East Region at BP. Interest in the North Sea Chalk began when researching the reservoir heterogeneity of the Valhall and Hod Field chalks for her PhD, awarded in 1998 by Reading University, UK. During 14 years as a consultant Reservoir Geologist with Robertson's, North Wales, she led numerous North Sea chalk sedimentology, diagenesis and modelling projects in the Norwegian, Danish and UK sectors. She also worked extensively on the sedimentology and diagenesis of Middle Eastern, Mexican and Far Eastern carbonates and clastics during this time. Since 2012 Anna has been a carbonate sedimentologist at BP, working once again on the reservoir characterisation of the Valhall Field, amongst other global projects.

Mona Wetrhus Minde holds a PhD in Petroleum Technology, carried out with the National IOR Centre of Norway, University of Stavanger. At the Centre, she contributes to leading one of the tasks focusing on "Mineral fluid reactions at nano/submicron scale´´. She is employed at UiS at the Department of Mechanical and Structural Engineering and Materials Science. The focus of Dr. Mindes work is micro- and nano-analytical tools to study materials and their microstructure, with particular interest in fine-grained sedimentary rocks (chalk) in an EOR perspective. In practical terms, this work involves studying rock samples at nano-scale to investigate the mineralogical changes induced by injection of non-equilibrium brines, and link these alterations to the geo-mechanical properties of the rock, reservoir properties and EOR simulation. Her main methods of expertise are within electron microscopy, analysing most materials ranging from rocks, metal, concrete and ceramics, all the way to biological material such as fish-proteins.

Hardy Hartmann Nielsen received a Cand. Scient. degree in geophysics from the University in Aarhus in 1981. He worked for 34 years in the oil service and oil industry. From 1982-1987 he worked with seismic processing and interpretation of data from NCS, Danish North Sea and the Arabian Gulf in GECO AS. He joined Mobil exploration Norway in 1988 and worked on exploration projects in the Barents Sea and Mid Norway until 1994, where he joined ConocoPhillips. In ConocoPhillips he has had positions as well planner for the Ekofisk II project, director for Ekofisk area reservoir characterization, 5 years as chief geophysicist, director for Ekofisk area overburden characterization and finally until he retired as director for Ekofisk area geoscience well planning. The positions have provided deep insights into NCS exploration and the chalk reservoir exploitation, reservoir and overburden seismic 4D monitoring of production and water/waste injection, well planning, geo-steering, reservoir and overburden geomechanics and mentoring. He retired spring 2016.

Erling Stenby is professor of applied thermodynamics at DTU since 1996. He is currently the Scientific Director for EOR at Centre for Oil and Gas, DTU and the Head of Department of Chemistry, DTU. He acted as the director of the Center for Energy Resources Engineering (DTU), the chairman of the Danish Council for Independent Research (Technology and Production Sciences), and the Chairman of the Executive Committee of the IEA Collaborative Project on EOR. He has co-authored more than 190 scientific journal papers and supervised or co-supervised more than 50 PhD students. He has participated in several EU funded projects and has a strong international network of academic and industrial collaborators. Besides the academic activities Erling H. Stenby has been a board member and advisor for various types of technology companies. He has on a number of occasions acted as a consultant for major international companies. He is the co-founder of the spin-off company Tie-Line Technology.

Henrik Olsen received an M.S. (1980) from the Technical University of Denmark. He has more than 30 years of experience in reservoir engineering and reservoir simulation, mentoring younger engineers and defining workflows and processes within the reservoir engineering community. His key experience is within field development planning, with some exposure to data room evaluations. Reservoir engineering skills comprise reservoir engineering evaluations at many levels, particularly construction and history matching of simulation models for a variety of reservoir types, thereby enabling characterisation of fluid and reservoir properties to identify and optimize efficient development options. Recently also developed procedures to integrate subsurface uncertainties into probabilisticly derived recovery ranges. He has acquired an excellent knowledge of computer applications and plays a key role in selection of software for reservoir studies. Mr. Olsen has previously worked as a consultant to Oil companies and Government Authorities in Denmark and abroad within a wide range of reservoir engineering disciplines.

Svein Magne Skjæveland is a reservoir engineering professor at the University of Stavanger (UiS) with a PhD from the Norwegian University of Science and Technology (NTNU) in engineering physics and a PhD in petroleum engineering from Texas A&M University. At UiS he worked to establish the master and PhD programs in petroleum engineering and geoscience and to develop the research organization IRIS (Rogaland Research). He is an appointed "Oil Man of the Year", and has won many prizes. During 1992–94 he was an elected rector and has held many administrative positions in academia. He enjoys teaching and has published many papers in the fields of physics, reservoir engineering, and multiphase flow in porous media.

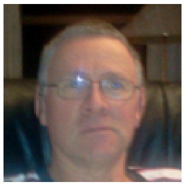

Ola Ketil Siqveland is a Senior engineer at University of Stavanger. He holds a Master of Science, Petroleum Technology (University of Stavanger, Norway), 1985. He has more than 30 years of experience at laboratory work and student guidance at the University. He also has participated in many research projects at the University of Stavanger.

Sigmund Stokka holds a PhD in Applied Physics (1981) from the Norwegian University of Science and Technology (NTNU). Since 1981 he has worked with research and development, research coordination and team management within drilling and well technology and improved oil recovery, 28 years with Rogaland Research/IRIS and 6 years in the oil and gas industry. He has filed patents concerning the innovative drilling concepts Badger Explorer and Hole in One Producer. He is currently a Research Director at IRIS and manager of the DrillWell Centre.

Leonid Surguchev is a Managing Director of LUKOIL Overseas North Shelf AS in Norway, previously Senior Vice President of IRIS AS (International Research Institute of Stavanger), Senior scientist with Russian Academy Institute of Oil and Gas Research, various positions with Russian oil company SIBNEFT, Algerian oil company SONATRACH and Norwegian Smedvig Technologies. His scientific interests are within hydrogen technologies, reservoir modelling, field development and Improved Oil Recovery (IOR) methods. Surguchev graduated as a petroleum engineer from Moscow Gubkin Oil and Gas Academy and holds PhD in reservoir engineering from the same university. He received Doctor of Technical Sciences (Oil and Gas Field Development) degree from VNIIneft Institute Scientific Board approved by VAK of Russian Federation. In 1995 Surguchev was awarded the best scientist of the year research prize of Rogaland Research in Norway. Authorship in more than 100 scientific papers and 15 monographs.

Michel-Bøgh Thomas has a PhD in Applied Geology (1977) from the University of Besancon (France), where he first studied the carbonates in the Jura mountains. He has been a geologist at Elf and Total for more than 35 years working in very different geological domains: diagenesis and sedimentology, basin modelling, reservoir geology, exploration, field follow-up… and in different countries: France, Norway, United Kingdom and United Arab Emirates. He got a good knowledge / experience of low permeability carbonates both in the UAE and in Norway where he has been working in Licence Projects with / at both ConocoPhillips Norge (Ekofisk, Eldfisk, Tor) and BP Norge (Valhall). During almost 10 years, he followed and worked on different Norwegian chalk projects, initiating and monitoring a few PhD and MSc projects on the chalk both at regional and field scales, and also following / leading JCR projects.

Ole Torsæter is Professor in Reservoir Engineering at the Department of Petroleum Engineering and Applied Geophysics, Norwegian University of Science and Technology (NTNU), where he is Head of the Reservoir Engineering and Petrophysics Group. He is Siv.ing. (1975) and Dr.Ing. (1983) in petroleum engineering from Norwegian Institute of Technology (NTH). Torsæter had research positions with SINTEF, Phillips Petroleum Co., USA and ResLab AS before he became professor. He was Department head in 1993-1996 and he has been visiting professor at New Mexico Tech, Texas A & M, University of Bordeaux and he is visiting investigator at A*STAR in Singapore (2014–2017). Torsæter has been the main supervisor for 160 Master thesis and 21 PhD thesis, and he is author/coauthor of 150 research publications. Torsæter received the Darcy Award in 2014 from the Society of Core Analysts and he is awarded membership in The Norwegian Academy of Technological Sciences (2015). The subject areas for his teaching and research are experimental reservoir engineering, flow in porous media, fractured reservoirs and enhanced oil recovery methods. Presently Torsæter's research activity is focused on methods for mobilizing residual oil by using either bacteria, surfactants or nanofluids.

Anette Uldall is Senior Lead Geophysicist in Mærsk Oil, Copenhagen Denmark. She holds a MS in Geology specializing in Geophysics from Århus University in Denmark. Her main work interest is interpretation in the cross field between rock physics, seismic inversion, seismic interpretation and seismic processing in integration with other geo disciplines. She finds the North Sea Chalk to be an intriguing layer package for testing and applying integrated interpretation methods.

Ole Vejbæk is a Senior Geophysical Advisor at Hess and has more than 30 years experience working as geologist/geophysicist mainly with North Sea exploration and production related issues. He has been with Hess for over 8 years and was employed at the Geological survey of Denmark prior to that. Mr. Ole Vejbæk holds a PhD degree in Geology from the University of Copenhagen

Wei Yan Yan is an Associate Professor in high pressure phase behavior at the Technical University of Denmark. His research interests are experimental and modeling studies related to high pressure phase behavior and efficient phase equilibrium calculation algorithms. He has been involved in projects on HPHT fluids, CO2 enhanced oil recovery, and compositional reservoir simulation. He has over 40 technical papers including around 30 peer-reviewed scientific journal papers. He acts as associate editor of Journal of Petroleum Science and Engineering.

Adrian Zett is the Production Petrophysics Advisor in BP. He holds a MSC in Geophysics and a PhD in Formation Evaluation from the University of Bucharest.His current role within Reservoir Development is to lead and develop Production Petrophysics globally in BP. His Oil and Gas activity spans over 28 years in various Petrophysical roles. He has spent most of his career working mature fields in a combination of well service, petrophysical and technology developments roles. He has a specific interest in surveillance applications in wells and reservoir management. Adrian has published over 30 papers on petrophysical surveillance, new technologies and integrated petrophysical solutions. He is a member of SPE and SPWLA and participates in numerous SPE and SPWLA Workshops and Chapter Events. He is a technical reviewer for SPE Formation Evaluation and PetroWiki moderator. Adrian is an executive member of Nuclear SIG at SPWLA and serves in the SPWLA Technology Committee. He is the Well and Reservoir Surveillance associate editor for Petrophysical Journal.

Arvid Østhus received an Master of Science, Petroleum Technology (University of Stavanger, Norway), 1989. He has about 25 years of experience in the oil industry in Norway and US, including 1 year in a servive company (Geoservices) and 23 years with a major oil company (Phillips Petroleum / ConocoPhillips). Both technical and leadership roles. Experience with development projects and improved oil recovery projects. Joined Norwegian Petroleum Directorate (NPD) in 2014. Work as a Senior Advisor in Reservoir Technology in NPD for the Norwegian sector. Also involved in international activities, including project leader for NPD's activities in Sudan.

Contents

Preface

Finn Engstrøm and Tron Golder Kristiansen

The chalk formations in the southern part of the Norwegian North Sea and in the Danish part of the North Sea were among the first fields to be discovered and developed offshore Norway and Denmark. The uniqueness of these reservoirs has challenged both the involved oil companies and authorities throughout the years. These days we would have called these reservoirs unconventional resources. The Danish Energy Agency (DEA) and the Norwegian Petroleum Directorate (NPD) recognized early the need for mutual research and understanding to help solve the common problems of these low permeable, low recovery reservoirs with challenges such as chalk stability and later seafloor subsidence. The initiative to create a common research forum was taken in 1980 when oil companies were invited to Copenhagen for a three day seminar on chalk reservoirs. This seminar led to the establishment of the Joint Chalk Research Program (JCR) which has since 1981 become an ongoing forum for common research concerning the chalk fields. The JCR is unique in that many different disciplines have been gathered (geologists, reservoir engineers, rock mechanics experts, fundamental researchers etc.) in a continuous, common research program. The multi-disciplinary approach has most certainly benefited the involved parties in understanding the diversity of the chalk.

In the fourth phase of JCR Mark Andersen summarized the understanding of chalk reservoirs up until around 1995 in a chalk monograph sponsored by JCR. Mark Andersen was seconded from his position at Amoco Tulsa Research Center to Amoco Norway and Rogaland Research to write the monograph during a two year period. The monograph has been a useful reference book for engineers and geoscientists working on extracting hydrocarbons from the chalk fields in the North Sea.

As said above, the chalk fields would most likely have been characterized as non-conventional reservoirs today. It is therefore also interesting to see that a technology like horizontal wells with multi-zone stimulations, as implemented in the North Sea chalks in the nineties, was also the key technology that unlocked another low permeable unconventional resource many decades later, the shale gas and oil onshore in the United States of America.

In the seventh phase of JCR it was decided to initiate several knowledge management projects within the JCR community. A JCR Library was made available on the web. It was also decided to make a more updated monograph available, also including the last 2 decades of research and experiences from the chalk fields. The monograph was designed to be a textbook on chalk that could be used in a MSc. program at University. It was also decided to make the book available on the web as a chalk-i-pedia, meaning that it can be kept alive and updated as our understanding of chalk reservoirs is progressing with time, long after the seventh phase of JCR is ended. A large number of chalk experts have contributed to this textbook. The Chief Editor has been Svein Skjæveland and Ola Ketil Siqveland, both at University of Stavanger/IRIS. Assisting editors from the sponsoring companies have been Nina Hagen (CoP), Helge Rutledal (Statoil), Michel-Bøgh Thomas (Total), Ying Guo (Total/IRIS), Finn Engstrøm (Mærsk) and Tron Kristiansen (BP/Aker BP).

We wish to thank all the authors that have contributed to this book, the editors for their work and the sponsoring oil companies that made this happen. We hope you find this chalk textbook interesting and useful in your work to increase recovery from the chalk fields in the North Sea. We also hope you contribute with your discoveries to make sure the chalk textbook for always stays alive and always is updated on the latest and greatest related to the chalk fields via the chalk-i-pedia version on the web.

Finn Engstrøm
JCR 7 Steering Committee Chairman
Mærsk Oil & Gas

Tron Golder Kristiansen
JCR 7 Textbook Project Leader
Aker BP

Part I

Fundamentals

Chapter 1

Geology

Charles Tibbals Feazel and Anna Matthews

1.1 Distribution of chalk

The distribution of chalk, a pelagic sediment predominantly composed of disseminated coccoliths and tests of planktonic foraminifera, is influenced by biological, chemical and physical factors which control its stratigraphic and geographic extent. Chalk was deposited and preserved from early Cretaceous times onwards, but the late Cretaceous global paleogeography was ideally configured for the accumulation of thick chalk deposits, with the development of warm, expansive, epeiric seas, **Fig 1.1**. An extensive review of the oceanographic controls on late Cretaceous chalk deposition is given by Hay (2008), discussing a number of the complexities of chalk, including epeiric deposition, water depths and the existence (or absence) of significant shelf-slope breaks during the late Cretaceous.

1.1.1 Unique aspects of Cretaceous seas

Modern, deep sea globigerina/nanoplankton oozes are most analogous to the chalk, but the Cretaceous seas represented a unique environment due to high sea levels, expansive epeiric seas, greenhouse conditions and the arrangement of the continents. Land masses were covered by shallow continental oceans and inland seas and the paleogeography was dominated by the widening of the Atlantic rift, Fig 1.1. Unusually high rates of oceanic spreading during Aptian-Albian times contributed significantly to the evolution of ocean chemistry at this time, probably resulting in increased methane and carbon dioxide levels. Oceanic temperatures also became very high, reaching over 30°C in equatorial regions during the Albian-Campanian times (Jenkyns and Wilson 1999; Hay 2008). High, relatively uniform oceanic temperatures, with warm polar regions, are thought to have persisted throughout most of the Cretaceous and indicate good horizontal oceanic mixing. However, poorer vertical mixing is suggested by the development of anoxic shales in deeper, restricted parts of the basin (Kazlev 2003). Oxygen isotopic data suggest that during the latest Cretaceous and early Tertiary, low latitude surface oceanic temperatures fell below 30°C and possibly below 25°C (Jenkyns and Wilson 1999).

It is likely that the extreme oceanic conditions of the mid to late Cretaceous at least partly influenced the explosion of micro-organisms with mineralized skeletons, with many new forms of foraminifera, coccolithophores, armoured algae and diatoms evolving at this time. Planktonic foraminifera and calcareous nannoplankton have their evolutionary origins in the Jurassic (BouDagher-Fadel, Banner et al. 1997) and Triassic (Bown, Lees et al. 2004), respectively, where they were restricted to epeiric seas. However, during Early Cretaceous times they expanded their habitat into the open ocean, resulting in the formation of deep sea oozes (Roth 1986). This habitat expansion may have been related to a lowering of oceanic salinity after the deposition of the south Atlantic salt in Aptian times (Hay, Wold et al. 2001; Hay, Migdisov et al. 2006). It is also considered likely that a fall in the ocean Mg/Ca ratio, to below 2 (Stanley and Hardie 1999; Berner 2004), might have increased coccolith production, as low Mg/Ca ratio conditions appear to enhance modern coccolith production. Since the early Tertiary a diverse assemblage of calcareous nanoplankton has been present in shallow, epicontinental seas (Hay 2008), but they have only been rock forming in deeper, oceanic settings, forming a carbonate sink that controls the saturation state of $CaCO_3$ in the oceans (Ridgwell 2005). Closer to the continents, carbonate sediments are commonly diluted by influx of clastics.

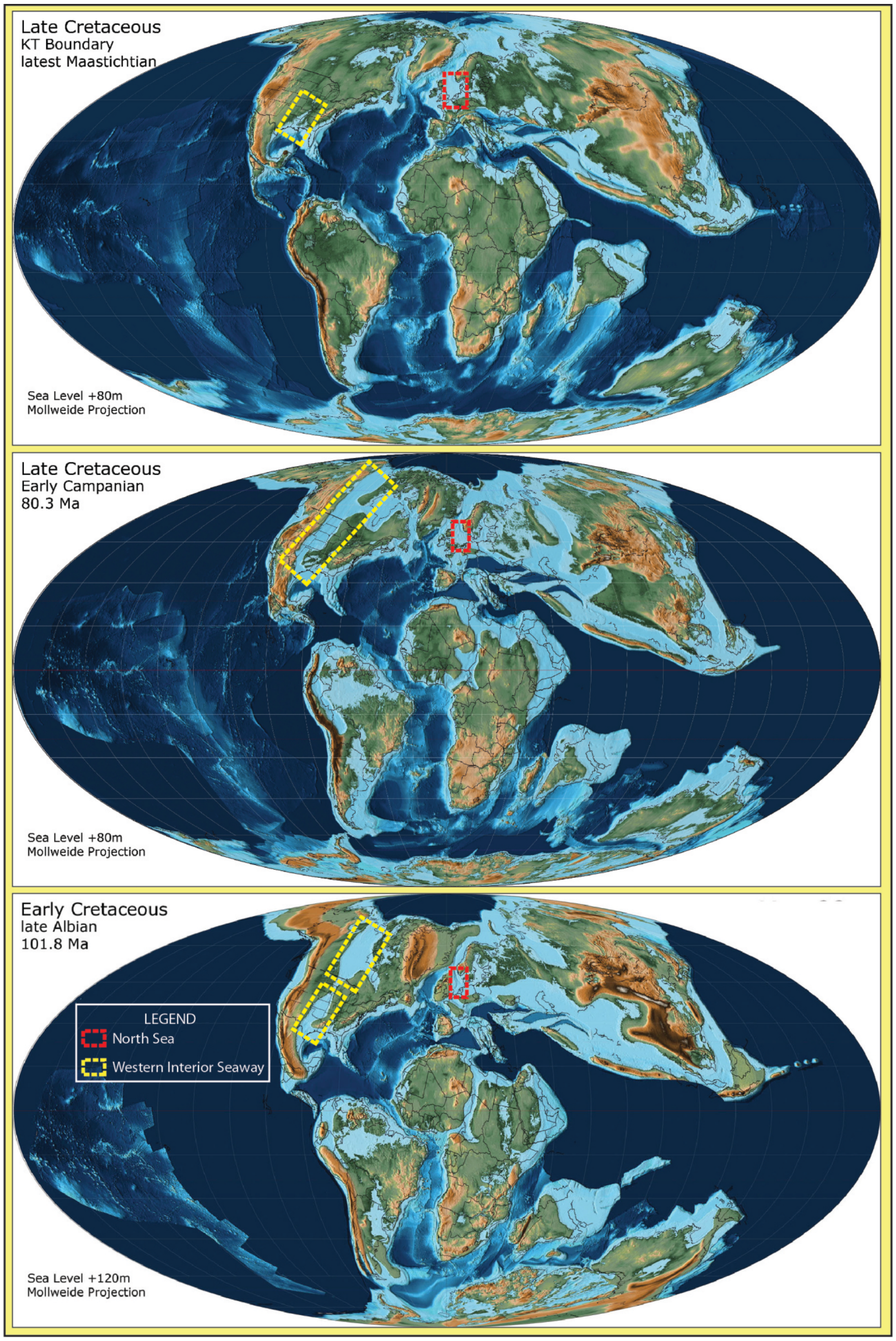

Figure 1.1: Late Cretaceous global palaeogeography, KT (Cretaceous Tertiary), Ma (megaannus, one million year), palaeoreconstructions from Scotese (2014b,a)

1.1.2 Global distribution of chalk and analogous sediments

Extensive pelagic, epeiric limestone sediments are rare in the rock record, comprising: the Cretaceous-Tertiary chalks of northwestern Europe and the Western Interior Seaway (USA) (Tucker and Wright 1999); Tethyan pelagic limestones of the Mediterranean area, Devonian Cephalopodenkalk and Griotte of western Europe and Ordovician *Orthoceras* limestones of Scandinavia.

The Western Interior Seaway (USA) was an epeiric sea filling a Late Jurassic and Cretaceous Andean-style foreland basin. During the middle Cenomanian to middle Turonian highstand the seaway reached as far north as the arctic Ocean and as far west as central Montana, connecting to the Tethys Sea (Gulf of Mexico) (Sageman and Arthur 1994), but retreated southwards and eastwards during the latest Cretaceous, Fig 1.1. Two economic Chalk reservoirs were deposited in the Western Interior Seaway, the Niobrara Formation and the Austin Chalk. In addition, the Eagle Ford "shale" of Texas and the Second White Specks "shale" of Canada, both significant resource plays, are roughly stratigraphically equivalent to Niobrara. The Turonian-Campanian Niobrara chalk forms thick deposits through Nebraska, Colorado, Wyoming, Kansas into Oklahoma, and is directly analogous, in both time and facies, to the Hod and lowermost Tor Formations of the North Sea, **Fig 1.2.** The Niobrara chalk forms a high porosity (25–46%), low permeability (0.1–3md), shallow (<1000m) gas play. In comparison, the Austin chalk of Texas, Louisiana and Mississippi is more restricted in age, Lower Coniacian to Upper Santonian, equivalent to the middle and upper Hod Formation in the North Sea. The Austin Chalk has much lower matrix porosity (3–10%) and permeability (avg 0.5md) than the Niobrara, with the main reservoirs being at 3000–4000m depth. The Austin Chalk produces oil and gas from major fractures parallel to the underlying lower Cretaceous shelf margin, which locally increase permeability to over 2 darcies (Pearson 2012).

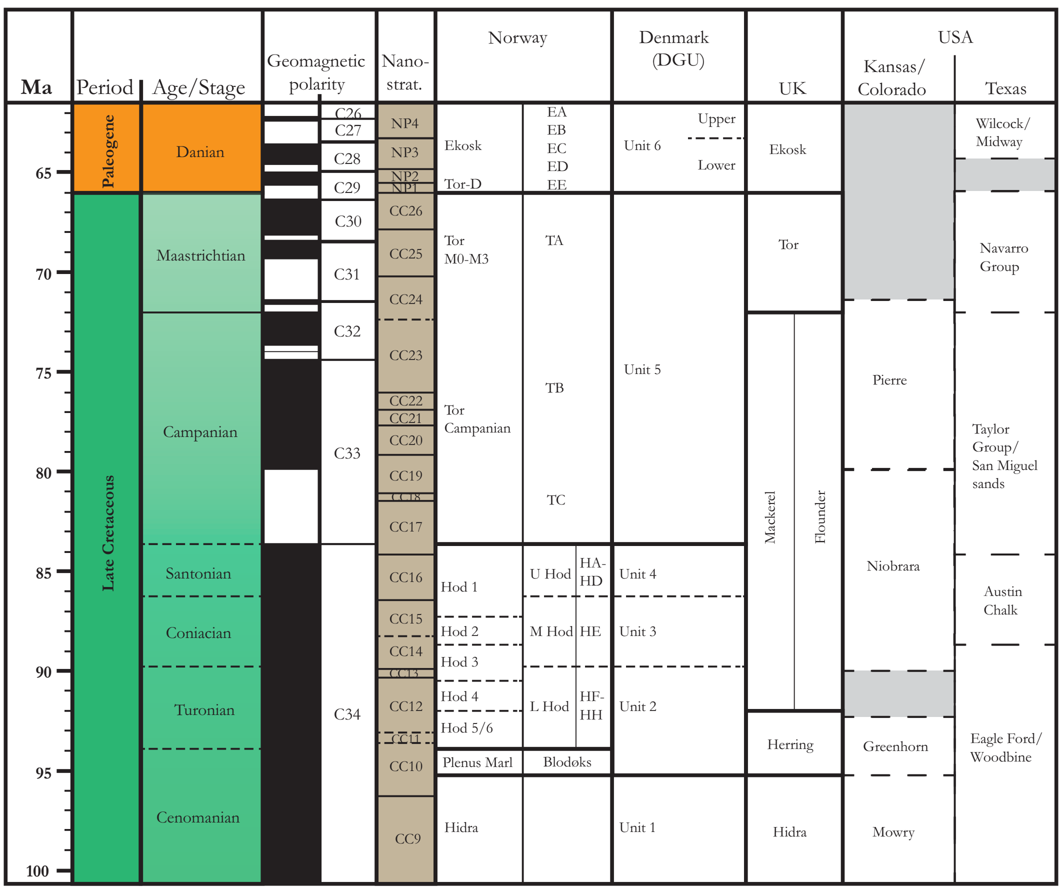

Figure 1.2: Late Cretaceous comparative stratigraphy for chalk sediments in northwest Europe and the Western Interior Seaway (USA). Modified from Surlyk, Dons et al. (2003); Andersen (1995).

The Tethyan Triassic-Jurassic pelagic limestones of the Mediterranean provide a depositional analogue for the pelagic chalk, comprising stratigraphically condensed limestones on palaeohighs and thick, nodular limestones and marls in deeper basins, with local slump and calciturbidite reworking also present. The Devonian Griotte was deposited in a series of basins and comprises micritic limestones containing pelagic cephalopods, bivalves, conodonts and ostracods. The limestones pass laterally into nodular and marly limestones, indicating an adjacent deeper basinal setting, with well developed debris flows, slumps and calciturbidites on the paleoslope providing an analogue for the redeposited chalk. The *Orthoceras* limestones of the Baltic Shield comprise a thin, condensed interval of micritic thin-bedded to nodular, shaley limestones and as such can be considered an analogue for some of the condensed 'Dense Zones' within the chalk.

1.1.3 Northern Europe

Chalk is widespread across Europe, with thick accumulations from the Mediterranean, across central Europe to the northern North Sea. The chalk forms a thick blanket from around 200m at outcrop in the UK and mainland Europe to over 1200m in parts of the Central Graben, **Fig 1.3.** In northwest Europe the chalk forms an important economic resource, being both a major aquifer in onshore areas and a major hydrocarbon reservoir in the North Sea Basin. The chalk forming the hydrocarbon reservoirs of the North Sea was deposited at a latitude similar to the present day Mediterranean Sea, in warm platform seas. The distribution of the chalk is controlled by the location and timing of activity on a number of faults in the basin, forming depositional basins and structural highs and influencing later redeposition of the sediments. The best chalk hydrocarbon reservoirs are located in the Central Graben, comprising the Greater Ekofisk area fields, where chalk was subject to early redeposition resulting in the present day high porosities. However, good hydrocarbon reservoirs are also found in variably pelagic and resedimented chalks of the southern North Sea (Danish and Dutch Sectors) and Eastern Central Graben (UK sector) where they are commonly underlain by salt diapirs and at a shallower depth.

The chalk oilfields of the North Sea were first discovered in the Danish Sector at well A–1X (Kraka Field) in 1966, with the first Norwegian chalk field, Valhall, discovered in 1969, followed by Ekofisk field later the same year. The producing fields comprise both structural and stratigraphic traps, with additional complexities such as tilted free-water levels, gas clouds, variable compaction and fracture distribution adding to uncertainty during exploration, development and production. Despite the North Sea chalk being a mature exploration target, fields such as Halfdan and South Arne show that there may be considerable reserves present in downflank areas of existing chalk fields, particularly where stratigraphic and tilted free-water level trapping mechanisms are at play (Megson and Tygesen 2005). A more detailed discussion of a number of fields is given in Chapter 25: Field Histories, with field data provided in Chapter 25.

1.2 Age of chalk deposition

1.2.1 Stratigraphic zonation of the North Sea chalk reservoirs

Chalk sedimentation and preservation began in the early Cretaceous, but the majority of preserved chalk was primarily deposited from Cenomanian to Danian times, forming the Shetland Group. A number of different nomenclatures are used to describe the chalk stratigraphy across the North Sea, Fig 1.2, but the use of absolute ages determined from detailed biostratigraphy means that these different stratigraphic naming systems can be directly compared. The stratigraphy of the chalk continues to evolve as both the biostratigraphy and reservoir stratigraphy are refined, but it should be noted that finer scale sub-divisions of the gross stratigraphy commonly vary between operating companies and may contain a degree of pragmatism related to reservoir zonation and production issues rather than true stratigraphic principles.

The Cenomanian aged Hidra Formation generally comprises non-reservoir pelagic, argillaceous chalk interbedded with shales. The Blodøks Formation is a carbonaceous shale representing the regionally and globally distinct, Cenomanian-Turonian OAE2 marker horizon in the North Sea (Jarvis, Gale et al. 2006; Jenkyns 2010).

Within the North Sea Basin the Turonian to Campanian Hod Formation comprises a mixture of pelagic and redeposited, variably argillaceous and siliceous chalks, commonly with 20% to >30% non-carbonate fraction. Cleaner intervals may attain very high porosities and locally form good quality secondary, and even primary reservoirs. Subdivision and stratigraphic nomenclature of the Hod Formation varies across the North Sea area from a simplistic Lower, Middle, Upper scheme in parts of the UK to full micro/nanofossil biostratigraphic zonations in some fields e.g. Valhall, Ekofisk, Dan Fields. The stratigraphic sub-division of the Hod Formation is dependent on the country and level of development of the formation.

The Tor Formation is predominantly Maastrichtian in age, although the lowermost interval is Campanian and the uppermost interval was locally reworked in Danian times, but is commonly considered a part of the Tor Formation for production purposes as it has similar reservoir properties to the Maastrichtian Chalk. Subdivision of the Tor Formation again varies across the North Sea Basin and from field to field, usually on the basis of identified micro/nanofossil or reservoir zones and dense interbeds. The Tor Formation is typically much cleaner (>95% carbonate) than the Hod Formation, with little siliceous material and very high porosity (locally up to, and over, 45%). The best reservoir intervals are generally reworked, although this is not always the case,

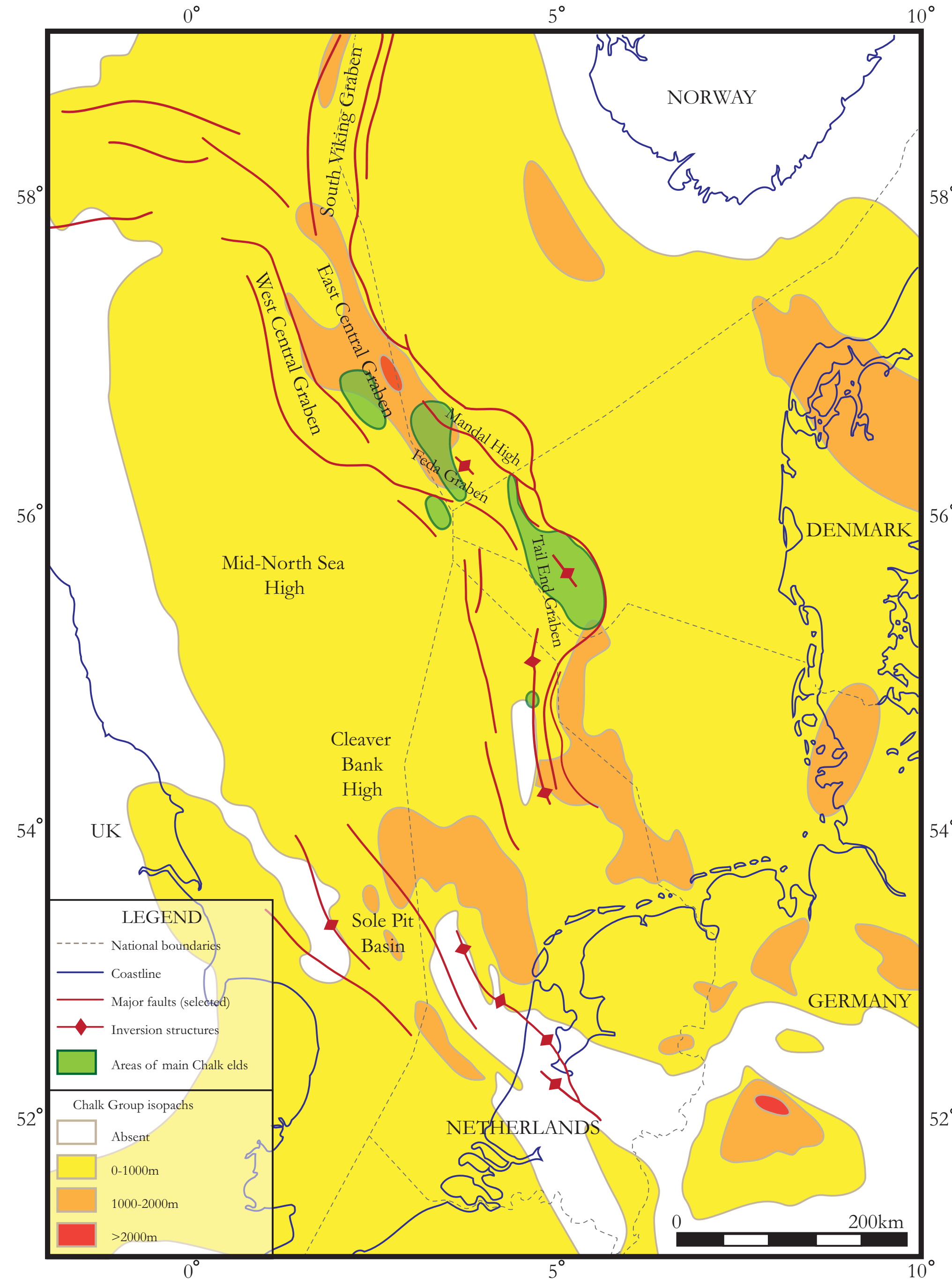

Figure 1.3: Chalk distribution across the North Sea area, modied from Gennaro (2011)

as is seen in many of the Danish chalk fields where productive reservoirs are found in pelagic Tor Formation sediments.

The Ekofisk Formation is Danian in age and is commonly dominated by pelagic cycles of more and less argillaceous chalk. The Ekofisk Formation is typically thinner than the Hod and Tor Formations, varying in thickness from being absent over palaeotopographic highs (e.g. parts of the Lindesnes Ridge) to >150m thick in Central Graben depocentres. Locally, the Ekofisk Formation forms a primary or secondary reservoir, often in the more shallowly buried fields in the southern North Sea (Danish Sector). A similar porosity range is present in the Ekofisk and Tor Formations, although the finer grain size of the coccoliths in the Danian results in a slightly lower permeability (up to an order of magnitude) for any given porosity in the Ekofisk Formation than the Tor Formation (Jakobsen, Ineson et al. 2004).

The stratigraphic nomenclature of the onshore and non-reservoir chalk successions across Europe is typically based on local or regional markers and legacy names, and is therefore not easily comparable, although a number of authors have tried to standardize the nomenclature and correlation on regional scales, e.g. Hopson (2005) for the UK onshore chalk, Jarvis, Gale et al. (2006) and Thibault, Harlou et al. (2012) for wider European correlation using carbon isotopes and nanofossil assemblages.

1.2.2 Biota

The majority of chalk sediment is composed of disaggregated armored nanoplankton (coccolithophores and rhabdoliths), which lived near the top of the oceanic water column. Armored nanoplankton are known from the late Triassic/early Jurassic and their abundance appears to be somewhat related to sea level, with maximum productivity in the late Cretaceous. The coccoliths and rhabdoliths in chalk are typically disaggregated, having been predated in the water column and transported, as fecal pellets, to the sea floor where they commonly form 60–95% of the chalk rock volume. In very deep basins the nannoplankton may never reach the sea floor due to dissolution of the grains below the calcite compensation depth (CCD) – the depth at which dissolution equals the rate of calcitic skeletal supply from above (Tucker and Wright 1999).

A wide variety of additional biota are found in chalk sediments, dependent upon factors such as depositional depth, energy, climate, age and distance from the palaeo-coastline. Planktonic foraminifera are typically the most abundant secondary fauna in the chalk, locally comprising a significant volume of the sediment. Semi-quantitative and quantitative analysis of planktonic foraminiferal assemblages, coupled with nanofossil analysis, can provide reliable age analysis in the Cretaceous and Tertiary section, along with qualitative information regarding the depositional setting. However, more simplistic relationships can also be used: such as a relative abundance of keeled planktonic foraminifera indicating deposition in a deep marine setting (Boersma and Silva 1983), or a dominance of unkeeled examples generally indicating an intermediate marine setting. The planktonic/benthonic foraminiferal ratio can be used as a simple proxy for depositional setting with low P/B ratios in shallow settings increasing with depth.

Calcispheres are commonly volumetrically important secondary fauna and are assumed to be planktonic in origin, although their affiliation remains uncertain with foraminiferal, dinoflagellate and green algae origins postulated. Thin walled bivalves and larger, *Inoceramus* bivalves, which became extinct at the end of the Cretaceous, are common in chalk and can provide a useful stratigraphic marker, although care must be taken where there is reworking. Green algae, echinoderm ossicles, bryozoan fragments, belemnites, sponge spicules, brachiopods and coral debris are also locally seen in chalk, although they are more common in proximal areas or those areas where chalk has been resedimented from shelf and slope locations. In areas affected by resedimentation there may also be common intraclasts from either local reworking of partly lithified chalk or distal reworking from shallower settings.

Trace fossils are common within the chalk, dominated by *Thalassinoides* (crustacean dwelling burrow) in shelf seas and by *Chondrites*, *Zoophycos* and *Planolites* (deposit feeding worm like organisms) in both shelf seas and deep sea chalks (Ekdale and Bromley 1984). Tiered, overlapping assemblages are often diagnostic of pelagic chalk, with strongly bioturbated chalk commonly forming low reservoir quality facies in the Central Graben chalk fields.

1.3 Chalk depositional processes

Pelagic coccolith-foraminiferal ooze, the precursor of chalk, is widely distributed in today's oceans wherever sands and muds derived from continental sources are not present to dilute it. Pelagic ooze is considered "background sediment" that would be deposited almost everywhere in the ocean without detrital influx. Closer to continental sources, distal fine-grained sediment, termed hemipelagic, contains abundant coccoliths, foraminiferal tests, and other components of chalk, in a mud matrix consisting of clays, silts, and organic fragments. Most chalks, and especially those of northern Europe and northeastern North America, are characterized by layers of homogenous chalk, interspersed with argillaceous layers of hemipelagic deposits, representing times of greater clastic influx. Argillaceous chalk is commonly termed marl, and commonly contains sufficient organic matter to represent a resource target where thermally mature (e.g., Niobrara chalk, Eagle Ford "shale," in the U.S. and their depositional equivalents in Canada).

Global greenhouse conditions during Cretaceous chalk deposition limited sea level fluctuations to a few tens of meters at the most (Wilgus, Hastings et al. 1988) Resulting shallow-shelf chalks display repetitive layers in outcrop described as rhythmites, made especially visible by their dark chert layers, **Fig. 1.4**. In the deeper-deposited North Sea basin, the chalks serving as petroleum reservoirs, such rhythmites are absent, and the biotic content is more restricted, raising numerous questions about the use of the outcropping chalks as analogs to the reservoir chalks.

Figure 1.4: Outcrop of North Sea chalk on the Normandy coast. Upper portion shows 2–5 meter cycles capped by burrowed hardgrounds made visible due to abundant dark brown to black chert, with lighter chalk beneath. Lower portion shows pinch-and-swell stratal geometry.

1.3.1 Water column

Chalk deposition begins with primary productivity (photosynthesis) in the photic zone: the uppermost 50-200 meters of the ocean where sunlight penetrates. The depth of the photic zone varies with water clarity (deeper) or turbidity (shallower). Algae, especially Coccolithophoridae, flourish within the photic zone in every ocean today. They appear to have been especially productive in the chemistry of Cretaceous seawater (Stanley, Ries et al. 2005). Chalk accumulates as fine-grained skeletal ooze, **Fig. 1.5**, containing up to 70 % water-filled porosity in shelf, slope and deep-water settings typically well below the photic zone. Coccoliths typically comprise 80–90 % of the skeletal grains in pelagic ooze, with the additional fauna varying according to depositional setting.

1.3.2 Sea floor

Once the skeletal fragments reach the sea floor, they may encounter oxygenated bottom water, or varying levels of dysoxia or anoxia. Together with the firmness or fluidity of the substrate, dissolved oxygen determines what epifauna and infauna will leave feeding traces, escape structures, and habitation burrows in the sediment. The abundance and diversity of such ichnofossils has been described extensively from outcrops and cores (Ekdale and Bromley 1984; Bromley and Ekdale 1984, 1986) in efforts to understand chalk depositional processes and

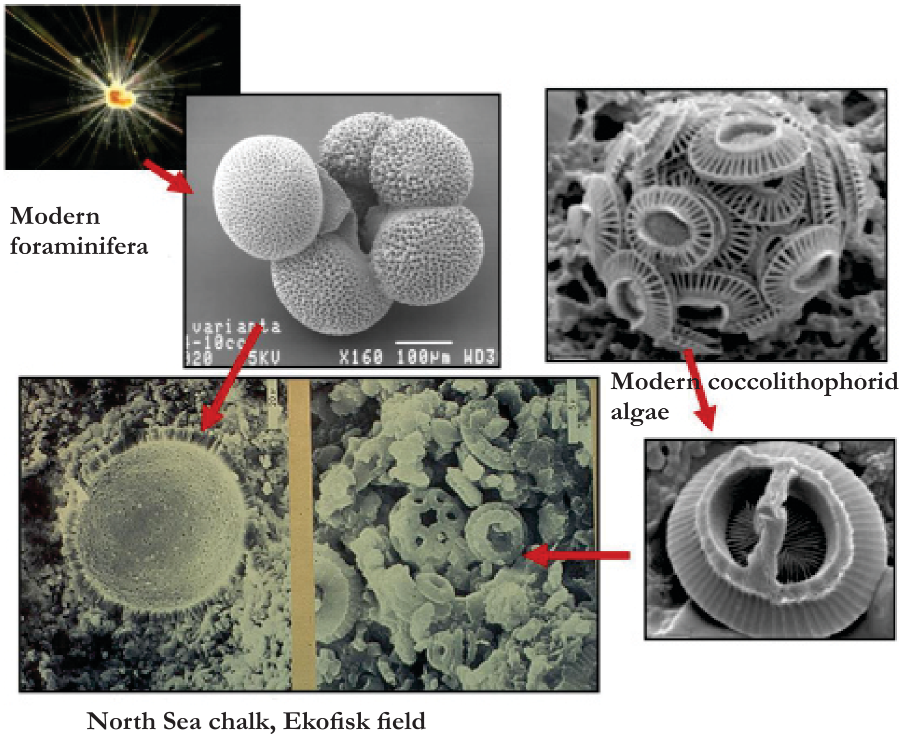

Figure 1.5: Chalk is deposited as an ooze containing predominantly coccoliths and foraminiferal tests.

paleo-oceanographic conditions.

Where burrows facilitate water escape and sediment compaction, a grain-supported matrix forms relatively quickly, and minor cement may precipitate, resulting in firmgrounds and hardgrounds that affect subsequent faunal content.

1.3.3 Resedimentation

On the sea floor, foraminiferal-coccolith ooze may be modified by various sediment-redistribution processes, from downslope creep to mass transport to traction currents and turbidity currents, **Fig. 1.6**. Resulting sedimentary features are visible in core and outcrop at scales ranging from microscopic to seismic. Re-suspension of the ooze seems to winnow clay particles, as the thickest redeposited chalks are also the cleanest, containing very little clay. They also lack significant bioturbation, suggesting rapid deposition of a blanket of ooze so thick that the organisms typically occupying the uppermost meter of sea-floor sediment couldn't burrow deeper.

Modern analogs include the southeastern coast of Australia, where slump blocks and their debris trains dominate portions of the continental shelf, **Fig. 1.7**. The sediments within and surrounding the transported blocks are foraminiferal-coccolith ooze very like many Cretaceous chalks.

1.3.4 Resulting depositional facies

A core-based facies scheme generated during Joint Chalk Research Phase IV and published by the Norwegian Petroleum Directorate (Fritsen 1996) listed the following chalk lithofacies in the Central Graben:

- Massive chalk mudstone
- Massive chalk wackestone
- Massive chalk packstone
- Laminated chalk mudstone
- Laminated chalk packstone
- Laminated chalk grainstone
- Massive pebbly chalk mudstone

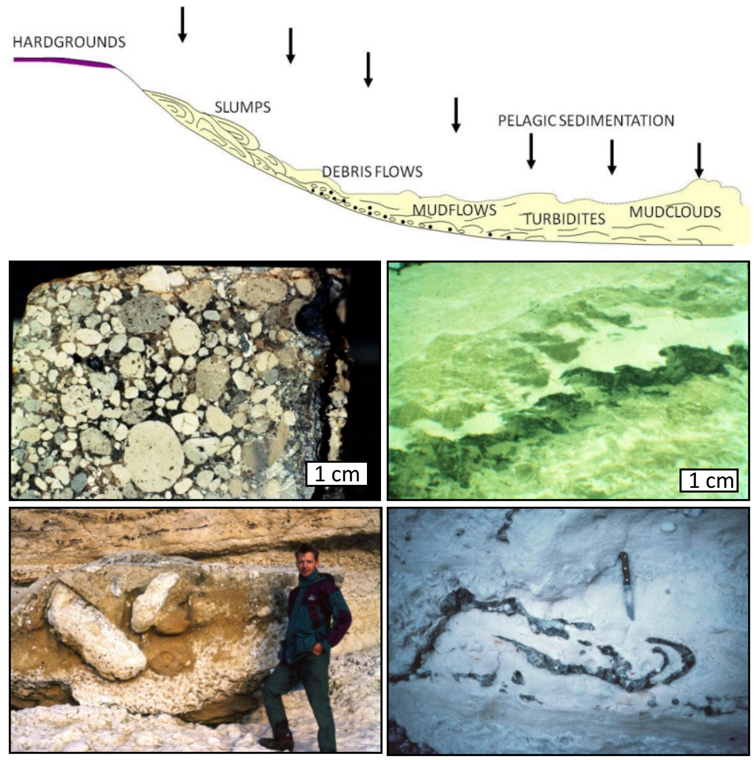

Figure 1.6: The depositional mode preserved in basinal North Sea chalks was not the quiet settling termed "marine snow',' but rather resedimentation by gravity flow, shear, and creep. Transported pebbles and boulders (left) characterize chalk debrites. Shear deformation of underlying layers - initially horizontal light and dark laminae (right) reflects downslope creep and slumping. Top photos are from cores, bottom from outcrops. Lower right shows shear folding in a chert band, suggesting early silicification, or later chert replacement of a deformed precursor (knife for scale).

- Laminated argillaceous chalk mudstone
- Massive argillaceous chalk wackestone
- Burrowed massive chalk mudstone
- Burrowed laminated argillaceous chalk mudstone
- Deformed chalk mudstone
- Deformed pebbly chalk mudstone
- Deformed laminated pebbly chalk mudstone
- Deformed chalk wackestone
- Deformed burrowed chalk mudstone
- Graded laminated chalk

These lithofacies have been adopted by most chalk researchers throughout the North Sea, region, though a lithogenetic scheme based on depositional processes has been adopted for better integration with wireline log data as input to maps and models.

1.4 Chalk diagenesis

1.4.1 Early diagenesis

Diagenetic modification of coccoliths, foraminiferal tests, and other carbonate skeletal components of chalk begins in the water column, which is increasingly hostile to calcium carbonate with depth due to the increased

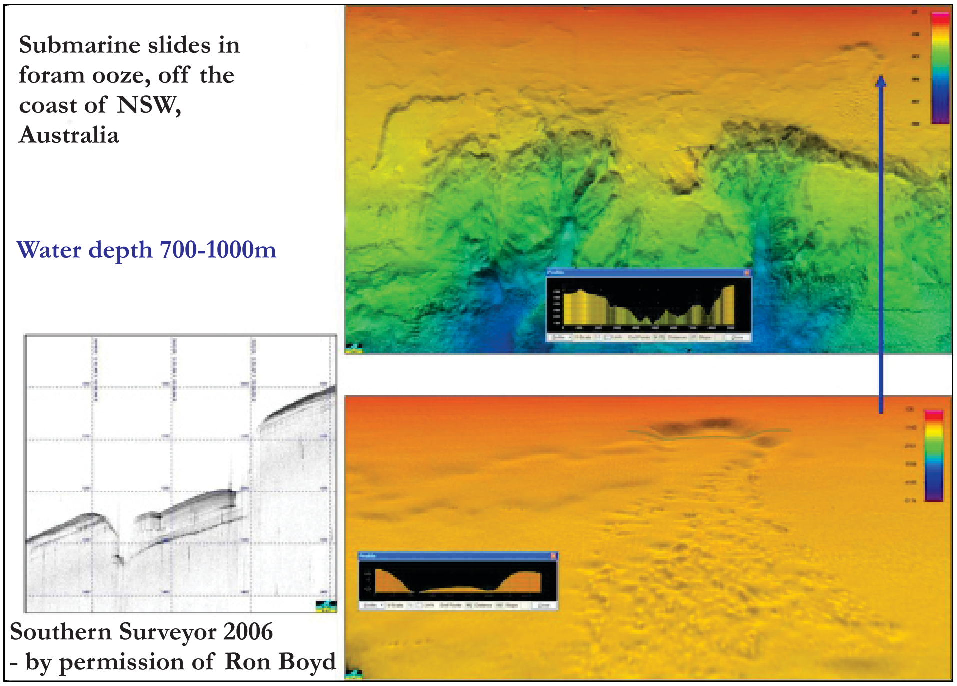

Figure 1.7: Mass transport via slumping and sliding of large blocks and slabs of Tertiary coccolith-foraminiferal ooze from outer shelf locations to deep water, New South Wales, Australia. Ron Boyd, pers. comm.

partial pressure of dissolved CO_2. A significant level in the ocean known as the lysocline is marked by the onset of corrosion of carbonate skeletons. Below the lysocline the biotic assemblage is altered, and only robust forms may be preserved. Presently the lysocline occurs at approximately 5000 meters in the Atlantic Ocean, and 4000 meters in the Pacific. The compensation depth, where the rate of supply from the surface equals the rate of dissolution, lies deeper (6000m Atlantic; 4500m Pacific). Both the lysocline and compensation depth vary by mineralogy (aragonite being more soluble than calcite) and by latitude (cold polar waters contain more CO_2 than tropical and equatorial waters). In the geological past, compensation depths varied significantly. During chalk deposition (Cretaceous - Eocene) the calcite compensation depth was much shallower globally than at present due to intense volcanic activity and resulting higher atmospheric CO_2 concentrations (Arthur and Dean 1986).

Once the sediments reach the sea floor, burrowing organisms modify the chemistry of interstitial waters. Two processes may have been synsedimentary, or began soon after deposition. These involve dissolution and reprecipitation of silica, and precipitation of calcite cement on and between skeletal grains. Organisms with siliceous skeletons (radiolarian, diatoms, sponge spicules, and others) were especially abundant in the shallow shelf waters that gave rise to the chalks outcropping on both sides of the English Channel. Remobilization of silica from their skeletal remains appears to pre-date lithification of the chalk due to its complex deformation by soft-sediment processes (though an argument can be made that the silica infiltrated later and was emplaced in, or replaced, host layers, burrows, or fracture fills of carbonate minerals). Fig. 1.6 Outcropping chalks are much richer in chert (flint) nodules, bands, and burrow-replacements than reservoir chalks in the Central Graben, but within the producing fields, silica-rich layers may cause drilling difficulties and act as flow baffles. Early carbonate cements are evident in layers showing brittle deformation beneath slump folds and glide planes, **Fig. 1.8**. Even allowing for compaction, these features must have developed at burial depths of only a few meters. The onset of brittle mechanical behavior is an important time in reservoir history, as microfractures offer pathways for hydrocarbon entry and water escape.

1.4.2 Late diagenesis

Burial diagenesis, commonly defined by the initiation of stylolites, has greatly affected the chalks of the Central Graben of the North Sea, especially those above salt-cored structures. Fluids rising from the Jurassic (Zechstein) salt have precipitated exotic minerals within the chalk in addition to the more common suite of calcite, clays and pyrite typical of most chalks, **Figs. 1.9 and 1.10**, and several of the chalk fields have complex diagenetic histories. Barite ($BaSO_4$) and celestite ($SrSO_4$) are especially notable. Diagenetic dolomite has precipitated in

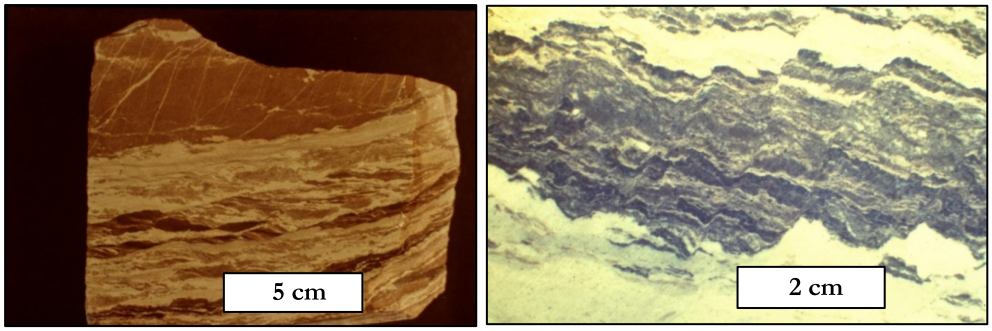

Figure 1.8: Incipient brittle deformation: small fault offset 35–40 cm below allochthon glide planes in Central Graben chalk, suggesting some degree of early cementation at very shallow burial.

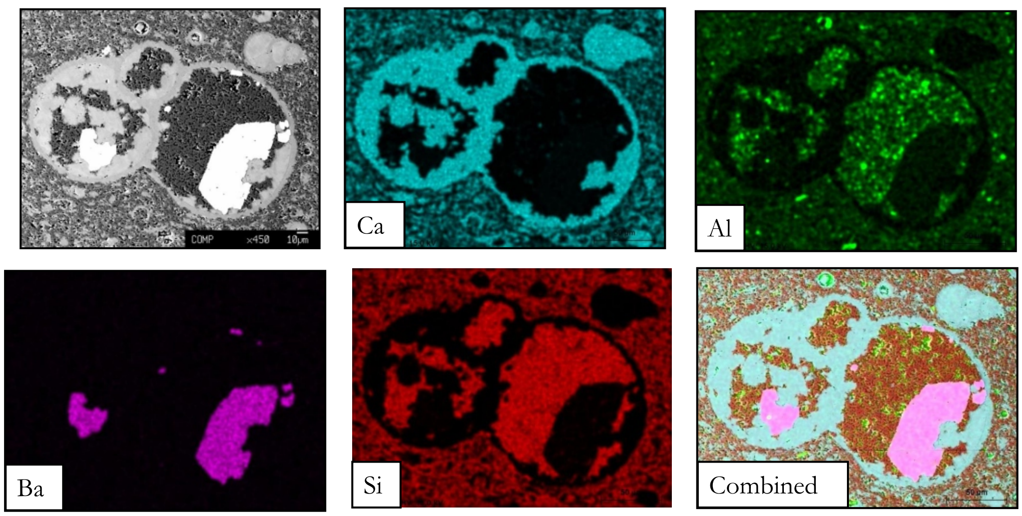

Figure 1.9: Microprobe element maps of barite and clays occluding intraskeletal porosity in frominiferal chambers. 10,065 ft 2/4-8AX.

the chalk matrix and in some samples, also dissolved by interaction with later-introduced fluids, **Fig. 1.11**.

Fluid inclusions, especially those containing hydrocarbon phases, document the thermal environment of many of these diagenetic alterations. Similarly, co-precipitation of minerals, **Fig. 1.12**, constrain the temperature regime at the time they grew in the chalk. Most diagenetic events at Ekofisk field occurred at temperatures lower than reservoir temperatures at the time of discovery (e.g., dolomite, **Fig. 1.13**). The hydrocarbon inclusions (particularly those in barite, **Fig. 1.14** and dolomite **Fig. 1.15**, document petroleum migration during growth of the hosting crystals.

Stylolites are a common feature in the Central Graben of the North Sea . They appear in many forms, from incipient solution seams “horsetails”, **Fig. 1.16** in argillaceous chalk to high-amplitude stylolites containing insoluble minerals (notably detrital and authigenic clays, pyrite, quartz) and organic matter. High-amplitude stylolites are most prevalent in “cleaner” chalks with little clay content, and occur in many orientations, especially in structures that have experienced compressive tectonic forces or halokinesis. Stylolites are typically surrounded by thin zones of enhanced porosity and permeability, but in general, they are the sources of calcite cement, remobilized and reprecipitated as overgrowths on and in skeletal grains.

Fracturing accompanied lithification: brittle behavior is documented in chalks at relatively shallow burial depths, Fig. 1.8. As matrix permeabilities are very low in chalks, an extensive fracture network is essential to production of oil and gas. Stylolite-associated fractures may contribute to horizontal permeability, but tectonic fractures (halokinesis plus regional deformation) are likely the main pathways for wellbore deliverability, **Fig. 1.17**.

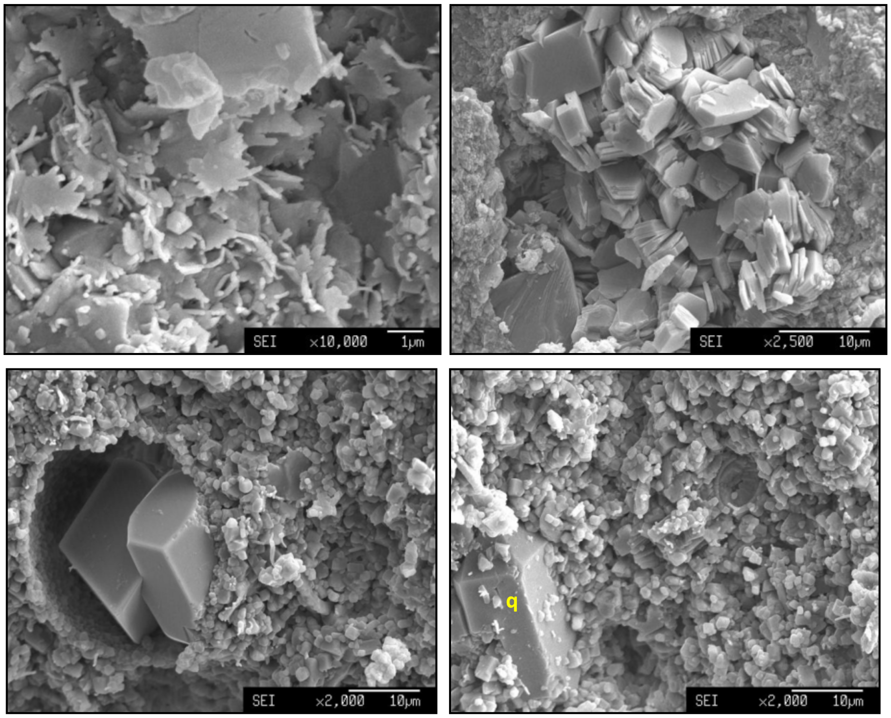

Figure 1.10: Authigenic minerals in North Sea chalk. Top left: fibrous and platy illite. 10,484ft. Top right: kaolinite, 10,163ft. Bottom left: calcite, 10,499ft. Bottom right: quartz, 10,499ft. All from 2/4-8AX.

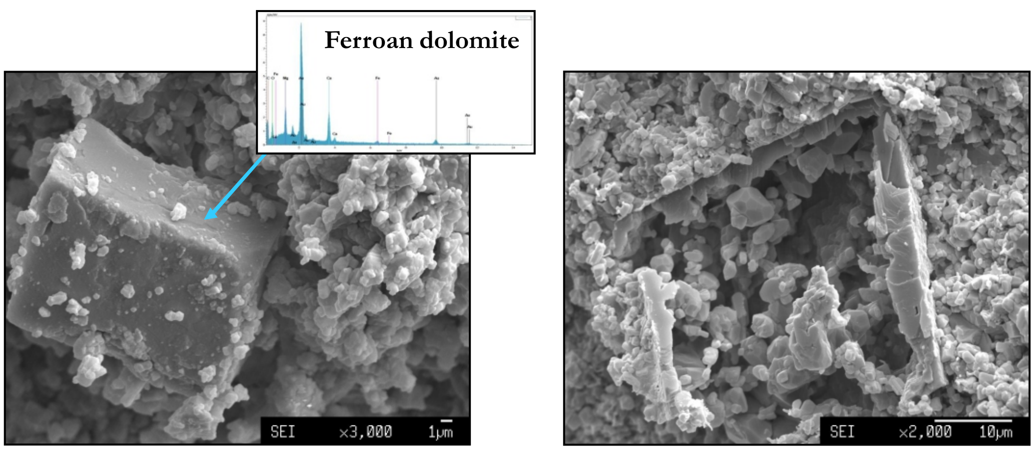

Figure 1.11: Authigenic Fe-dolomite (left) 10,439ft. Skeletal dolomite crystal (right), suggests partial dissolution. 10,409ft, both from 2/4-8AX.

1.5 Consequences of depositional and diagenetic processes to reservoir properties

Brasher and Vagle (1996) considered resedimentation and early oil entry to be the significant processes determining chalk reservoir flow units, **Fig. 1.18.** They listed five factors having the greatest influence on chalk's diagenetic pathway: burial depth, chalk type, overpressure, hydrocarbon presence, and original grain size. Resedimentation offers the opportunity for winnowing of clays, leaving the redeposited chalk more porous and homogenous and less argillaceous. Resedimented units can be several meters thick with uniform properties —both sedimentological and geomechanical —making them productive reservoir flow units, typically

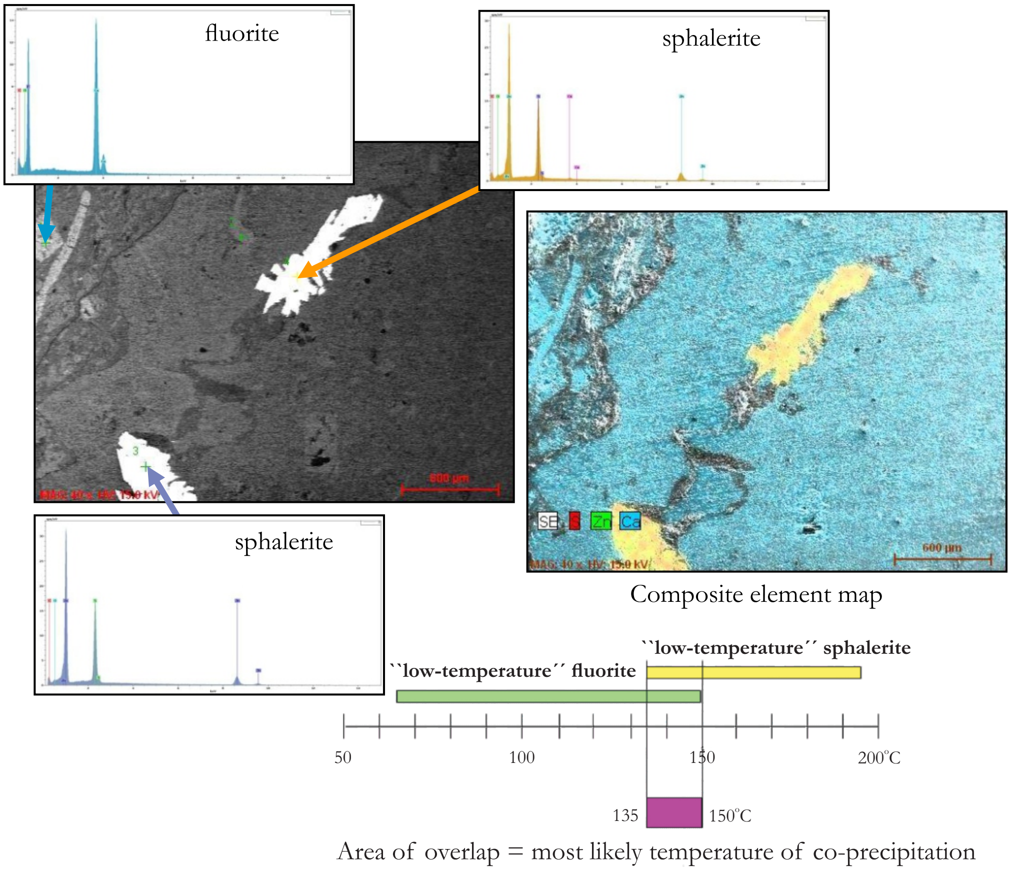

Figure 1.12: Coprecipitation of sphalerite and fluorite suggests a temperature window between 135 and 150°C, 11,611ft, 2/7A-13Bt2.

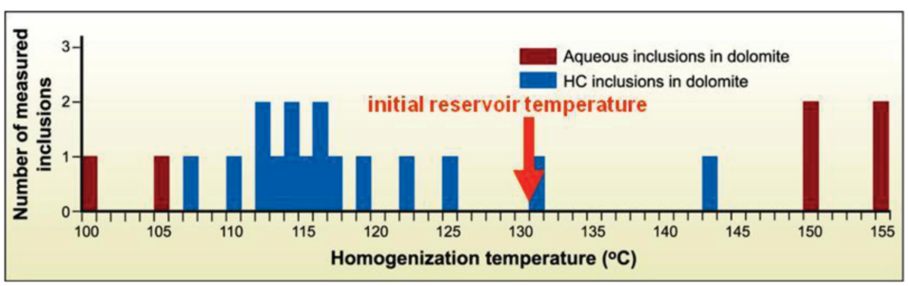

Figure 1.13: Homogenization temperatures (107–143°C) of hydrocarbon fluid inclusions suggest dolomite precipitation under reservoir conditions during or after charge. Aqueous inclusions are very small (<10μm), lending ambiguity to their homogenization temperatures (100–155°C), Samples from 2/4X-32. Paleothermometry by Anita Csoma.

with homogenous matrix properties and abundant fractures. Argillaceous chalk, with enhanced ductility due to clay content, does not fracture as readily, and likely does not contribute to reservoir deliverability.

The dominant process determining porosity evolution is precipitation of calcite overgrowth cements on skeletal elements. High-porosity intervals exhibit little cement, whereas low-porosity chalks show a preponderance of cement over skeletal fragments, **Fig. 1.19.** Most of the cement may be derived via chemical compaction (stylolitization), but at least some have precipitated from seawater or shallow-burial pore waters, perhaps facilitated by burrowing organisms. Hardgrounds and other low-porosity intervals were likely formed syndepositionally, and were buried with the lower-quality reservoir properties that they retain today.

Anderskouv and Surlyk (2012) confirmed that resedimented mass-transport deposits in Danish chalks are on average more porous than pelagic chalks, though chalk turbidites are less porous, given similar composition, burial and hydrocarbon migration histories. They concluded that grain packing of consolidated sediment was responsible for facies-dependent porosity variation, and that bioturbation caused relatively tight grain

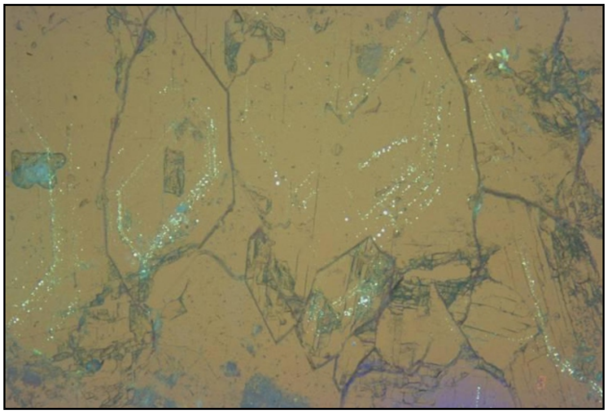

Figure 1.14: UV epifluorescence image of hydrocarbon fluid inclusions in a vein cemented by barite. Lower Ekofisk Fm., 2/7-13X. Clearly hydrocarbons were migrating during cementation of the tension fracture. Photomicrograph courtesy of Matt Reppert/IFE.

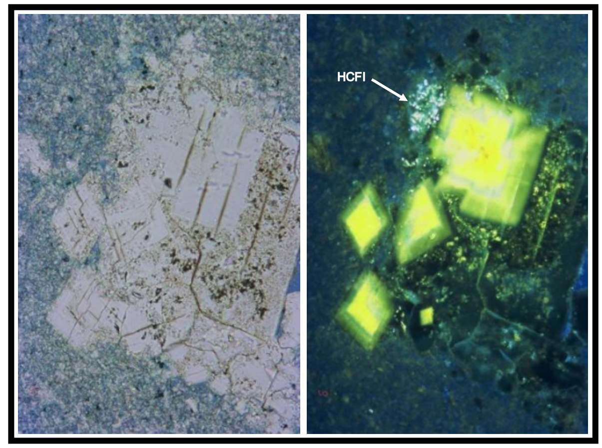

Figure 1.15: Phomicrograph showing calcite and zoned dolomite crystals in transmitted light (left) and UV epifluorescence (right). Greenish white fluorescing hydrocarbon fluid inclusions (HCFI) occur in the dolomite-calcite crystal aggregates in the martrix. 3210.6m, Tor Fm., 2/4-6X. Courtesy Matt Reppert/IFE.

Figure 1.16: Compaction in burrowed argillaceous chalk typically produces "horsetails," or solution seams. 10,657ft., 2/4X-32.

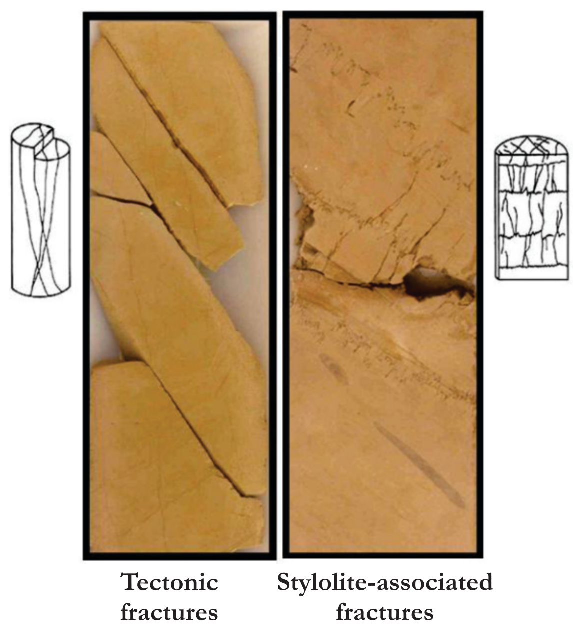

Figure 1.17: Most fractures in Central Graben chalks are of tectonic or stylolitic origin. Without such fractures, the low-permeability chalk would make a poor reservoir. Courtesy, Helen Farrell.

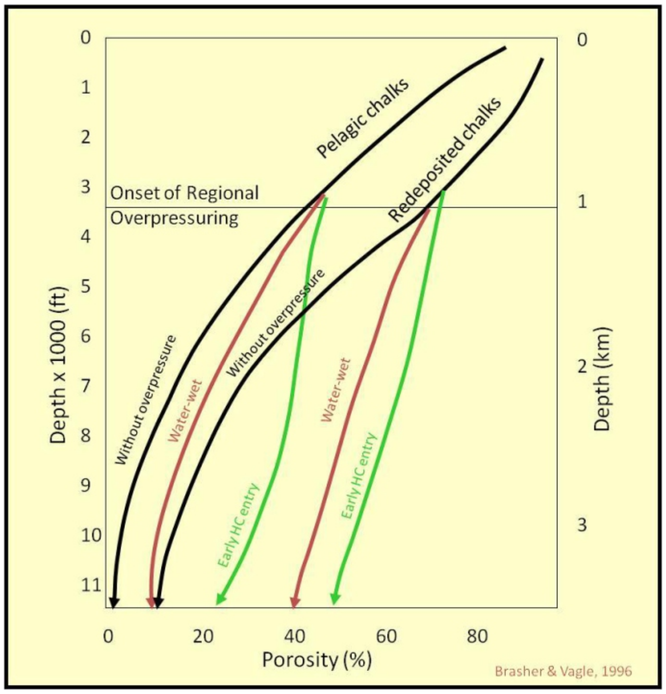

Figure 1.18: Porosity preservation in North Sea chalk depends on (a) redeposition, (b) overpressure, and (c) early oil entry. Modified after Brasher and Vagle (1996). AAPG©[1996] reprinted by permission of the AAPG whose permission is required for further use.

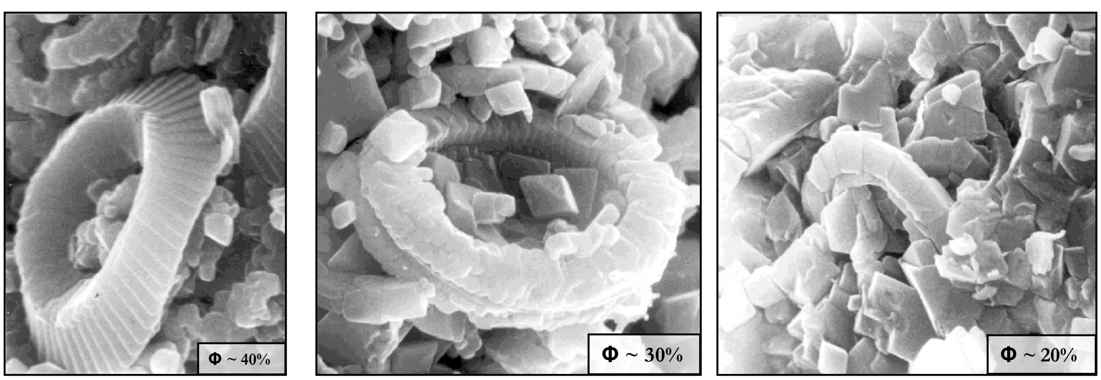

High-porosity intervals contain coccoliths with very little cement.

Medium-porosity intervals contain coccoliths with overgrowths of secondary calcite.

Low-porosity intervals contain abundant secondary calcite.

Figure 1.19: Typical SEM appearance of North Sea chalk.

packing compared to deposits that escaped bioturbation. Early plastic shear deformation of tightly packed bioturbated units resulted in dilative behavior, increasing porosity, whereas more loosely packed units responded contractively, decreasing porosity.

Clearly the role of fractures in production is dominant over matrix properties. Combined with the ability of chalk to imbibe seawater and displace oil and gas, these rock characteristics allow initial production to be supplemented by waterflooding, and offer hope for various proposed methods of tertiary recovery as well.

References

Andersen, M.A., 1995. *Petroleum Research in North Sea Chalk.* RF-Rogaland Research. Joint Chalk Research Program Phase IV.

Anderskouv, K. and Surlyk, F., 2012. The influence of depositional processes on the porosity of chalk. *Journal of the Geological Society*, **169**: 311–325. May. URL `http://dx.doi.org/10.1144/0016-76492011-079`.

Arthur, M.A. and Dean, W.E., 1986. Decade of North American Geology, Western North Atlantic Basin Synthesis, In *Decade of North American Geology, Western North Atlantic Basin Synthesis Volume*, eds., B.E. Tucholke and P.R. Vogt, , Chap. Cretaceous paleoceanography, 617–630. Geological Society of America Special.

Berner, R.A., 2004. A model for calcium, magnesium and sulfate in seawater over Phanerozoic time. *American Journal of Science*, **304** (5): 438–453. URL `http://dx.doi.org/10.2475/ajs.304.5.438`.

Boersma, A. and Silva, I.P., 1983. Paleocene Planktonic Foraminiferal Biogeography and the Paleooceanography of the Atlantic Ocean. *Micropaleontology*, **29** (4): 355–381. URL `http://www.jstor.org/stable/1485514`.

BouDagher-Fadel, M.K., Banner, F.T., and Whittaker, J.E., 1997. *The early evolutionary history of planktonic foraminifera*. Chapman & Hall. URL `http://dx.doi.org/10.1007/978-94-011-5836-7`.

Bown, P.R., Lees, J.A., and Young, J.R., 2004. Calcareous nanoplankton evolution and diversity through time. In H. Thierstein and J. Young, eds., *Coccolithophores*, 481–508. Springer Berlin Heidelberg. ISBN 978-3-642-06016-8. URL `http://dx.doi.org/10.1007/978-3-662-06278-4_18`.

Brasher, J.M. and Vagle, K.R., 1996. Influence of lithofacies and diagenesis on Norwegian North Sea chalk reservoirs. *AAPG Bulletin*, **80** (5): 746–769. URL `http://archives.datapages.com/data/bulletns/1994-96/data/pg/0080/0005/0700/0746.htm`.

Bromley, R.G. and Ekdale, A.A., 1984. Trace fossil preservation in flint in the European chalk. *Journal of Paleontology*, **58** (2): 298–311. URL `http://www.jstor.org/stable/1304785`.

Bromley, R.G. and Ekdale, A.A., 1986. Composite ichnofabrics and tiering of burrows. *Geological Magazine*, **123**: 59–65. Jan. URL `http://dx.doi.org/10.1017/S0016756800026534`.

Ekdale, A.A. and Bromley, R.G., 1984. Comparative ichnology of shelf-sea and deep-sea Chalk. *Journal of Paleontology*, **58** (2): 322–332. URL `http://www.jstor.org/stable/1304787`.

Fritsen, A., ed., 1996. *Description and Classification of Chalks North Sea Central Graben*. Joint Chalk Research Phase IV. Norwegian Petroleum Directorate, Stavanger.

Gennaro, M., 2011. *3D seismic stratigraphy and reservoir characterization of the Chalk Group in the Norwegian Central Graben, North Sea*. Ph.D. thesis, University of Bergen. URL `https://bora.uib.no/handle/1956/5396`.

Hay, W.W., 2008. Evolving ideas about the Cretaceous climate and ocean circulation. *Cretaceous Research*, **29**: 725–753. URL `http://dx.doi.org/http://dx.doi.org/10.1016/j.cretres.2008.05.025`.

Hay, W.W., Migdisov, A. et al., 2006. Evaporites and the salinity of the ocean during the Phanerozoic: Implications for climate, ocean circulation and life. *Palaeogeography, Palaeoclimatology, Palaeoecology*, **240** (1–2): 3–46. Evolution of the System Earth in the Late Palaeozoic: Clues from Sedimentary Geochemistry. URL `http://dx.doi.org/http://dx.doi.org/10.1016/j.palaeo.2006.03.044`.

Hay, W.W., Wold, C.N. et al., 2001. Evolution of sediment fluxes and ocean salinity. In D. Merriam and J. Davis, eds., *Geologic Modeling and Simulation: Sedimentary Systems. Kluwer*, 153–167. Academic/Plenum Publishers, Dordrecht, The Netherlands. URL `http://dx.doi.org/10.1007/978-1-4615-1359-9_9`.

Hopson, P., 2005. *A stratigraphical framework for the Upper Cretaceous Chalk of England and Scotland with statements on the Chalk of Northern Ireland and the UK Offshore Sector*. British Geological Survey. ISBN 0 85272 517 5. URL `http://nora.nerc.ac.uk/3230/1/RR05001.pdf`.

Jakobsen, F., Ineson, J.R. et al., 2004. Characterisation and zonation of a marly chalk reservoir: the Lower Cretaceous Valdemar Field of the Danish Central Graben. *Petroleum Geoscience*, **10**: 21–33. January. URL `http://dx.doi.org/10.1144/1354-079303-584`.

Jarvis, I., Gale, A.S. et al., 2006. Secular variation in Late Cretaceous carbon isotopes: a new δ^{13}C carbonate reference curve for the Cenomanian-Campanian (99.6–70.6 Ma). *Geological Magazine*, **143**: 561–608. September. URL `http://dx.doi.org/10.1017/S0016756806002421`.

Jenkyns, H.C., 2010. Geochemistry of oceanic anoxic events. *Geochemistry, Geophysics, Geosystems*, **11** (3): 1–30. URL `http://dx.doi.org/10.1029/2009GC002788`.

Jenkyns, H.C. and Wilson, P.A., 1999. Stratigraphy, paleoceanography, and evolution of Cretaceous Pacific guyots; relics from a greenhouse Earth. *American Journal of Science*, **299**: 341–392. 1 May. URL `http://dx.doi.org/10.2475/ajs.299.5.341`.

Kazlev, M.A., 2003. The Mesozoic Era. URL `http://palaeos.com/mesozoic/index.html`.

Megson, J. and Tygesen, T., 2005. The North Sea Chalk: an underexplored and underdeveloped play. *Geological Society, London, Petroleum Geology Conference series*, **6**: 159–168. URL `http://dx.doi.org/10.1144/0060159`.

Pearson, K., 2012. Geologic models and evaluation of undiscovered conventional and continuous oil and gas resources: Upper Cretaceous Austin Chalk. Tech. rep., US Geological Survey. URL `http://pubs.er.usgs.gov/publication/sir20125159`.

Ridgwell, A., 2005. A Mid Mesozoic Revolution in the regulation of ocean chemistry. *Marine Geology*, **217** (3): 339–357. URL `http://dx.doi.org/10.1016/j.margeo.2004.10.036`.

Roth, P.H., 1986. Mesozoic palaeoceanography of the North Atlantic and Tethys oceans. *Geological Society, London, Special Publications*, **21** (1): 299–320. URL `http://dx.doi.org/10.1144/GSL.SP.1986.021.01.22`.

Sageman, B.B. and Arthur, M.A., 1994. Early Turonian palaeogeographic/paleobathymetric map, Western Interior, U.S. In M. Caputo, J. Peterson, and K. Franczyk, eds., *Rocky Mountain Section (SEPM)*. Rocky Mountain Section (SEPM), Mesozoic Systems of the Rocky Mountain Region, USA. URL `http://archives.datapages.com/data/rocky_sepm/data/032/032001/457_rocky_mount320457.htm`.

Scotese, C.R., 2014a. Atlas of Early Cretaceous Paleogeographic Maps, PALEOMAP Atlas for ArcGIS. *The Cretaceous, Maps 23-31, Mollweide Projection, PALEOMAP Project, Evanston, IL.*, **2**. The Cretaceous, Maps 23–31, Mollweide Projection, PALEOMAP Project, Evanston, IL. a. URL `https://uta.academia.edu/ChristopherScotese`.

Scotese, C.R., 2014b. Atlas of Late Cretaceous Paleogeographic Maps, PALEOMAP Atlas for ArcGIS. *The Cretaceous, Maps 16–22, Mollweide Projection, PALEOMAP Project, Evanston, IL.*, **2**. b. URL `https://uta.academia.edu/ChristopherScotese`.

Stanley, S.M. and Hardie, L.A., 1999. Hypercalcification: Paleontology Links Plate Tectonics and Geochemistry to Sedimentology. *GSA Today*, **9** (2): 1–7. URL `ftp://rock.geosociety.org/pub/GSAToday/gt9902.pdf`.

Stanley, S.M., Ries, J.B. et al., 2005. Seawater chemistry, coccolithophore population growth, and the origin of Cretaceous chalk. *Geology*, **33** (7): 593–596. URL `http://dx.doi.org/10.1130/G21405.1`.

Surlyk, F., Dons, T. et al., 2003. Upper Cretaceous. In *The Millennium Atlas: petroleum geology of the central and northern North Sea*, 213–233. Geol. Soc. Of London. URL `https://www.researchgate.net/profile/Finn_Surlyk/publication/285129506_Upper_Cretaceous_In_The_Millennium_Atlas_Petroleum_Geology_of_the_Central_and_Northern_North_Sea/links/5ab2403faca272171000a2a7/Upper-Cretaceous-In-The-Millennium-Atlas-Petroleum-Geology-of-the-Central-and-Northern-North-Sea.pdf`.

Thibault, N., Harlou, R. et al., 2012. Upper Campanian–Maastrichtian nannofossil biostratigraphy and high-resolution carbon-isotope stratigraphy of the Danish Basin: towards a standard δ 13 C curve for the Boreal Realm. *Cretaceous Research*, **33** (1): 72–90. February. URL `http://dx.doi.org/10.1016/j.cretres.2011.09.001`.

Tucker, M.E. and Wright, V.P., 1999. *Carbonate Sedimentology*. John Wiley & Sons.

Wilgus, C.K., Hastings, B.S. et al., 1988. Sea-level changes: an integrated approach. *SEPM Special Publication*, **42**. URL `http://listbestselling.info/sea-level-changes-an-integrated-approach-etexts-library-cheryl-k-wilgus.pdf`.

Chapter 2

Geophysics

Martin Landrø and Olav Inge Barkved

2.1 Introduction

Exploration and production geophysics span over a wide range of methods such as gravimetric, magnetometric, seismic, altimetric methods such as Interferometric Synthetic Aperture Radar (InSAR), electrical and electromagnetic methods. We will put most emphasis on the marine seismic method, since this is by far the most used method in both exploration and production of hydrocarbons in the chalk fields of the North Sea. In the late 1950s, some geologists concluded that there were low possibilities for hydrocarbon discoveries offshore Norway. Some years later and after the discovery of the Groningen field, in 1964, professor Harald Bjørlykke wrote a short note for the Norwegian Shelf Committee entitled "Possibilities for presence of oil at the Norwegian Continental Shelf". The note clearly states, "it is probable that some of the Mesozoic layers might contain oil". He further stated that it is necessary to acquire seismic data to qualify the assumption further. Today we know that professor Bjørlykke was correct in his assumptions and it is also correct that seismic data have played a crucial role in exploration and production offshore Norway.

Norway as a shipping nation, with a lot of experience in both building and maintenance of ships, was able to rapidly build up a milieu for marine seismic investigation. Anders Farestveit founded Geco in 1972, a company that rapidly picked up and developed new technology that was effective for marine seismic acquisition. At first sight, there are no major differences between using geophysical methods for chalk and other lithologies such as for instance sand. However, there are differences in rock physics and reservoir properties that make some geophysical methods more challenging for chalk. In addition, chalk exhibits other properties that enable methods that are not commonly used for other types of reservoir rocks. In this section we will discuss marine seismic investigations in general, with a special focus on chalk.

2.2 Seismic exploration and discoveries of the North Sea chalk fields — the early days

The chalk fields are amongst the earliest oil discoveries in the North Sea. In 1966 the first oil discovery in the Danish sector was made. When the A–1X well found oil in the Kraka field (Jorgensen and Andersen 1991) The Harlingen, a Dutch chalk gas field had been discovered onshore the year before, and the Hanze field, Netherlands only producing offshore oil field, was found in 1996. According to Megson and Tygesen (2005) the chalk discoveries in the UK sector contains an estimated 1171 MMBOE in place. The first hydrocarbon discovery in UK was the Machar field in 1976.

Esso drilled the first exploration well on the Norwegian Continental Shelf in 1966. **Fig. 2.1** shows a 2D seismic line that was used for placing the well. This well was dry, and more than 30 dry wells were drilled prior to the 2/4–1AX or (2/4–2) **(Fig. 2.2)** well that discovered an oil bearing layer on 25 October 1969. A giant chalk field had be found, the Ekofisk field. The quality of the seismic data was limited, and misinterpretations and educated guessing were unavoidable. Three appraisal wells were drilled, and based on the seismic interpretation it was assumed that the center of the structure was a depression, and therefore this area was avoided for appraisal drilling. First when well 2/4 C–8 was drilled in 1974 it was realized that a gas cloud above the center of the field affected the seismic, and that the field actually was a doubly plunging anticline.

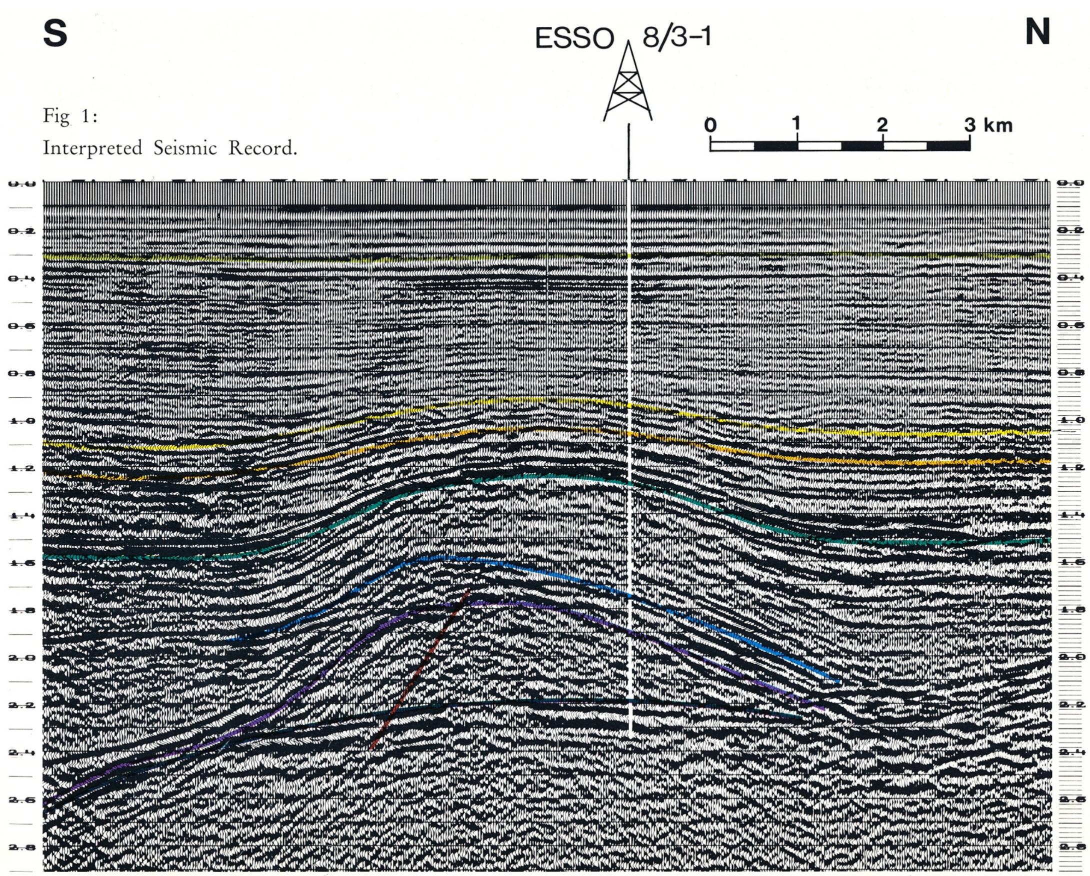

Figure 2.1: Seismic 2D line (top) used to drill the first exploration well 19 July 1966 by Esso. The well was dry and drilled into the basement. The purple bump above the basement is interpreted as salt. Top chalk is a the orange horizon, around 1050 msec in the well, a base is just above the green horizon (Myhre 1975).

Another example of seismic data from the 1960s is shown in **Fig. 2.3**, from the Valhall area. This is a South-North line including two wells, 2/11–1 and 2/8–1, and is quite representative for the seismic quality at this point in time. The 2/8–1-well, spudded in November 1967, was the eight and the most southern well to be drilled in Norwegian waters. This was the first well to be drilled from a drilling ship in Norway. Bad weathers and technical problems made the operation challenging. In January 1968 a storm, only to be expected every 75–100 years, occurred with sea waves up to 15–17 m. After the storm the drill-ship had to be repaired and the drilling was stopped after reaching a depth of 2595 m, above the chalk formation.

The chalk fields of the North Sea Central Graben have a geologic history that in many ways makes them unique in the world. The sequence of geological events combined with the conditions led to the prolific producers of hydrocarbons we find today. "The happy co-joining of high porosity, overpressure, extremely high saturation of a live oil and fracture permeability makes the fields economic to produce" (Andersen 1995).

The chalk fields of the North Sea are mainly located in the Norwegian and Danish Sectors in the Central Graben area, with a few fields also located on the UK continental shelf. The fields have generally been characterized as fractured, over-pressured, high porosity chalk. However, subtle changes in deposition processes and rates and burial history can, in some cases, result in a reservoir, but in others, a perfect seal. The awareness that producible hydrocarbon can also be available in lower porosity chalk has grown, as operators have been testing more and more of the deeper part of their fields. The use of horizontal wells, which dominates as the preferred depletion strategy, has allowed using an extended toe section to appraise the upside of the lower flanks of existing fields and push the presence of the reservoir deeper. Chalk is a carbonate and shares most carbonate characteristics, including that carbonates can function both as reservoirs and seals, introducing a range of exploration opportunities.

Chalk reservoirs appears to be controlled by four factors; the purity in terms of the calcium carbonate of the sediments, the rate of deposition, the tectonic settings during deposition and the size distribution of the coccoliths being deposited (Hardman 1982). In addition the timing and the structural setting at the time when oil migration started appears to be important, as the presence of oil halts the chemical diagenesis.

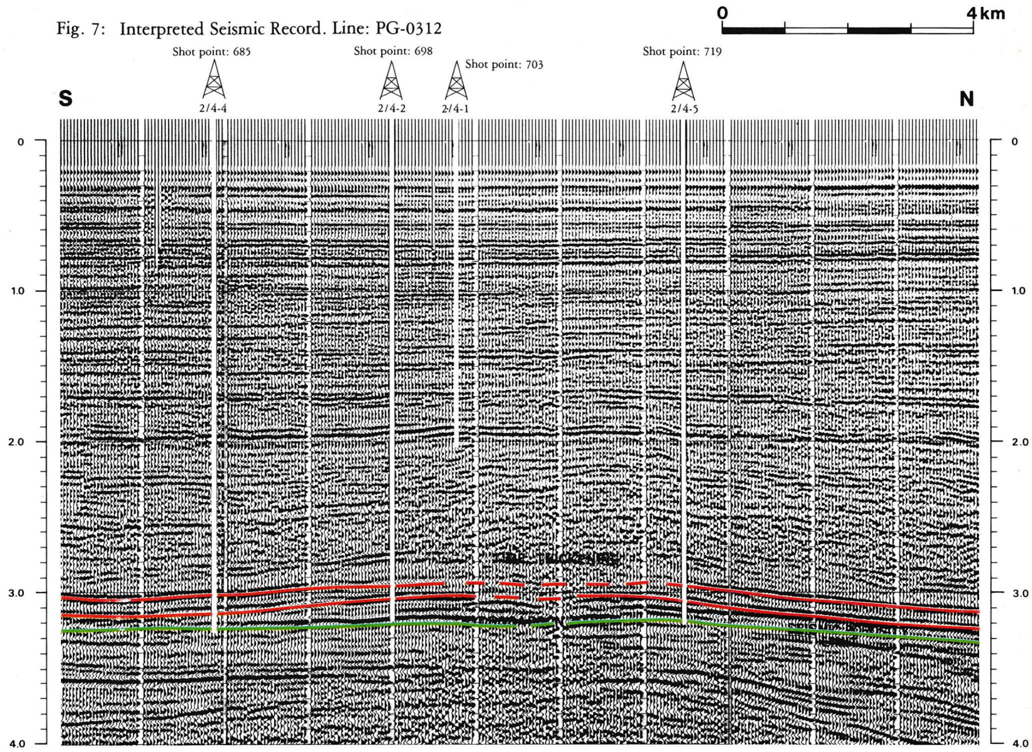

(a)

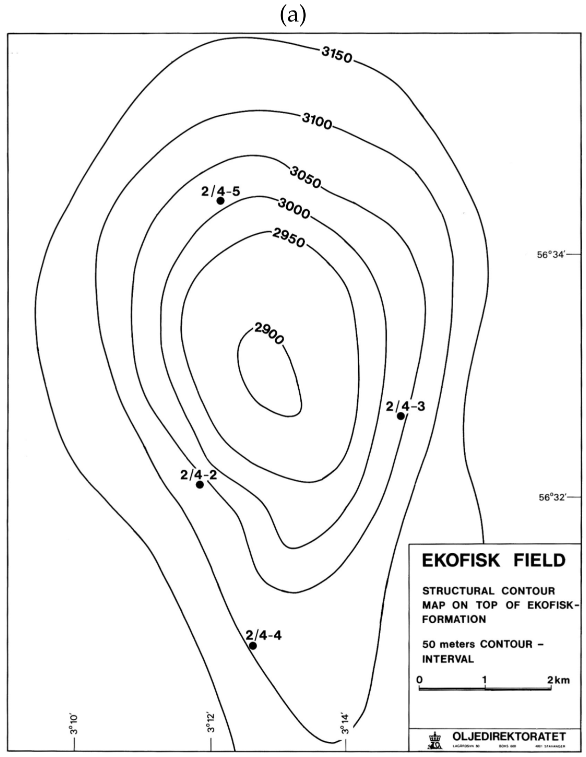

(b)

Figure 2.2: (a) Seismic 2D line from Ekofisk, (b) and structural contour map of the Ekofisk formation (Strass 1980).

Structural closure is the most dominant trapping mechanism for the chalk reservoirs. Both inversions-generated closure (i.e., Valhall, Roar, Tyra, Hod and South Arne), salt domes influenced with minor inversion element (i.e., Ekofisk and Dan), to salt diapers driven structures (Machar and Skold), may be found.

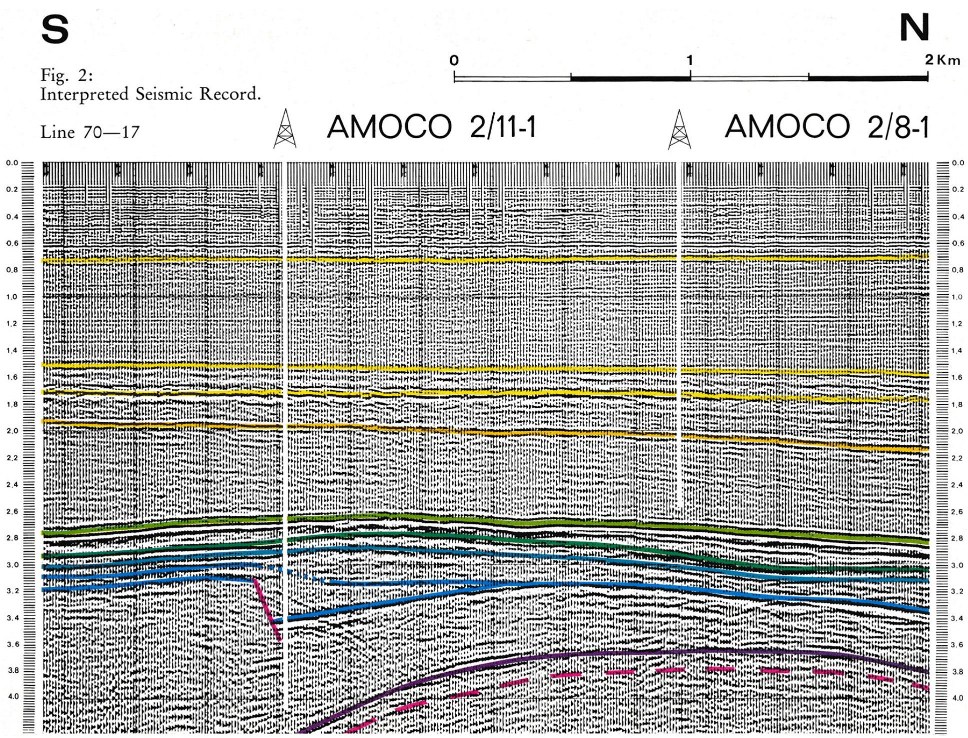

(a)

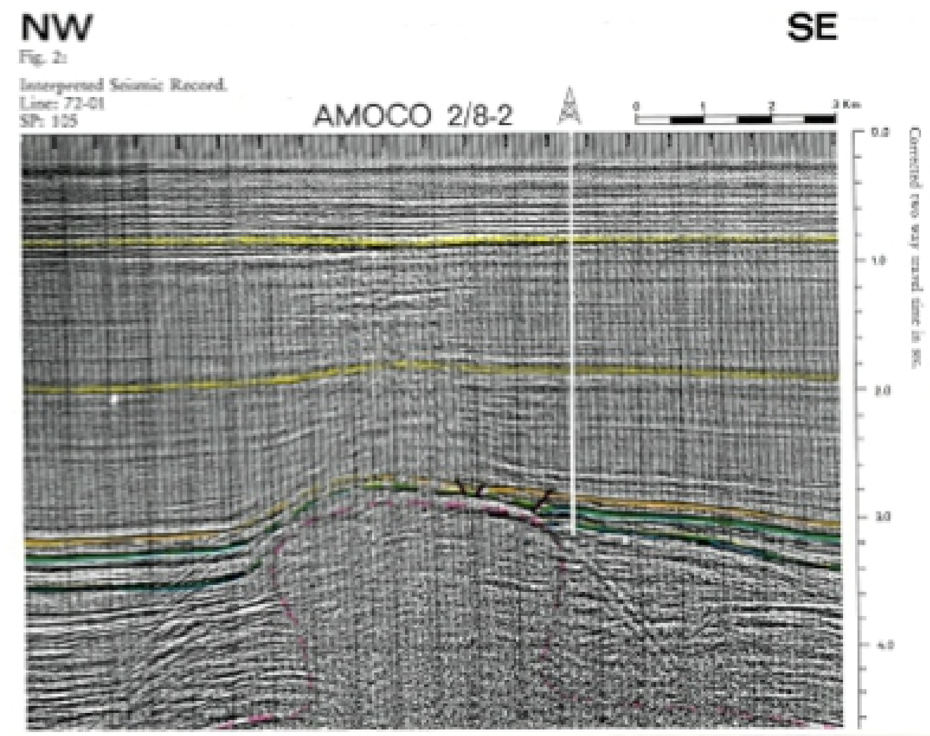

(b)

Figure 2.3: (a) seismic 2D line from Valhall, 1960s. Well 2/8-1 is located east of the Valhall field. Well 2/11-1 was drilled July 1969 and classified as a minor discovery, situated at the rim of the Valhall field (Myhre 1977). (b) 2D line north of the Valhall field. Well 2/8-2 was drilled in 1970. Shows of oil were encountered. The chalk layers are defined by a green curve above and below (Riise 1977).

Stratigraphic trapping mechanisms are believed to occur commonly. One example is the Halfdan field. The Hod Pod discovery is also believed to be a true stratigraphic trap. These traps are formed by a combination of initial chalk properties linked to the actual marine environment, depositional processes, over-pressuring due and early hydrocarbon invasion which preserved the quality of the reservoir rock during burial (D'Angelo, Brandal et al. 1997; Anderson 1999).

2.3 Rock physics and relation to key seismic parameters.

There are two major types of body waves that propagate in solid rocks: Pressure waves (P-waves) and shear waves (S-waves). A pressure wave is characterized by that the wave propagation direction and the particle motion is parallel. For a shear wave the particle motion is normal (perpendicular) to the propagation direction. In addition to these two wave types, there are surface waves, where the Rayleigh wave (always detected for earth quakes) is well known. The P- and S-waves are related to the bulk (K) and shear modulus (G) in the following way

$$v_P = \sqrt{\frac{K + \frac{4}{3}G}{\rho}}, \tag{2.1}$$

$$v_S = \sqrt{\frac{G}{\rho}}, \tag{2.2}$$

where ρ is the rock density.

We notice that the P-wave velocity is always larger than the S-wave velocity. Hence, the shear wave event will appear later than the compressional or pressure event on seismic records. Here P is used as a shortcut both for pressure and primary and S for shear and secondary.

We see from these equations that both the bulk and shear modulus are key factors determining the velocities of the rock. We might say that the two moduli and the density of the rock is closer to geology than the velocities, and we often state that rock physics is the glue or link between geology and seismic parameters. Eqs. 2.1 and 2.2 demonstrate another challenge related to seismic exploration: there are three unknowns (two moduli and the density) on the rock physic side, and only two velocities. To be able to determine more rock parameters it is therefore common to also measure seismic amplitudes in addition to travel-times. This offers extra equations to determine as many parameters as possible from a seismic survey. However, in most cases, the number of parameters we want to determine is much larger than what can reliably be determined from the seismic experiment. It is therefore necessary to do rock physics laboratory measurements of rock samples. Such experiments are used to obtain empirical relations for seismic analysis.

One example of how such a rock physics relationship might be obtained is to plot seismic parameters measured in a well versus for instance porosity, and then use statistical regression analysis to obtain a mathematical equation relating the parameters. **Fig. 2.4** shows an example from the Valhall field.

The porosities are known to have a first order impact on the elastic properties of a rock (Mavko, Mukerji et al. 2009). The strong correlation shown in Fig. 2.4, which is representative for chalk in general, may explain why prediction of porosity so often are successfully made from seismic amplitude data. Although there are several papers promoting prediction of the fluid in porous chalk, this capability has often been debated. Uldall and Ødum (1994) discuss the fact that the phase of the seismic response changed between what in their case was a gas-bearing crest to water filled flank. They also showed that this effect could be better modeled using a Toksøs based inclusion model instead of the more commonly used Gassmann model.

The phase reversal effect at top chalk was not new to geophysicists working within chalk exploration. This insight has been used with successes and failures a number of times, primarily with the intention of defining porous chalk (Campbell and Gravdal 1995; Barkved 1996). The regional strong and distinct reflector at top chalk level reflected, "Top hard chalk" and not necessary the top chalk. By making an isopach map between the Balder Formation (= Top Rogaland Group) and the strong reflector at top chalk level, the increase in thickness may reflect presence of porous Tor Formation and not necessarily increase in shale thickness.

These techniques require high fidelity processing and skills by the interpreter and failure in any of these have resulted in wrongly placed exploration wells, i.e. on a local high that represents chalk, but no reservoir. During the eighties the simple reversal sign processing had become quite robust, but as late as in 1994 a prospect was drilled on a "false" phase anomaly. Unfortunately, no paper documents these cases.

Logs and laboratory tests show that the fluid variations are reflected in the elastic measurements but it is debated to what extent there exist a distinct trend and if so to what extend this is universal. See for example (Landrø, Buland et al. 1995; Walls, Dvorkin et al. 1998; Anderson 1999; Askim 2003; Gommesen, Hansen et al.

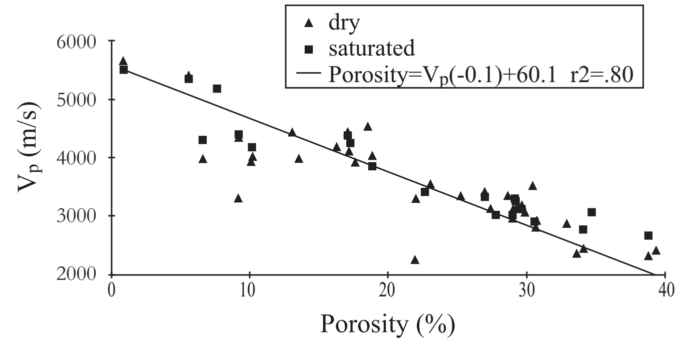

(a)

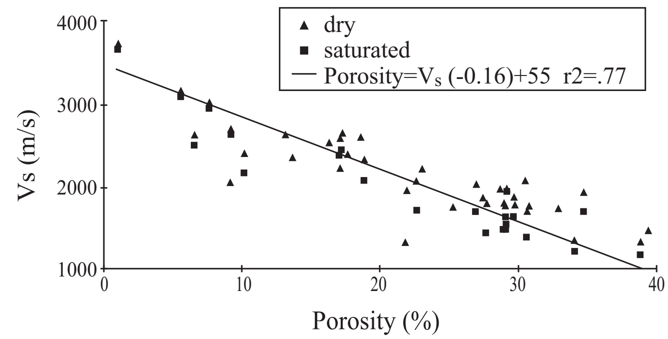

(b)

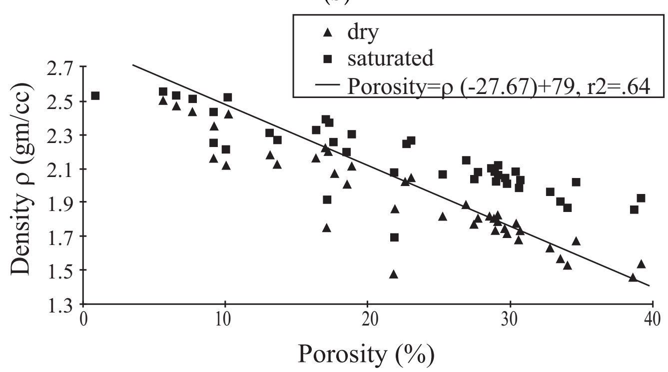

(c)

Figure 2.4: Scatter plot of (a) P- and (b) S-wave velocities and (c) densities versus porosity for 41 chalk core samples.

2004; Lindgård, Lehocki et al. 2011; Herbert, Escobar et al. 2013). It appears that estimating fluid distribution in chalk remains a difficult task. Factors like cement, mineralogy and the shape and nature of the pore volumes may be the reasons for these challenges, and different authors might be biased by their relative focus and data sets. The general opinion though seems to be that the Gassmann model is adequate, but have to be used with great care.

2.4 Seismicity & chalk; opportunities and challenges

Seismic data is obviously the key to structural definition of the reservoir. In addition, the petrophysical properties of chalk may vary dramatically and there are especially good correlations between porosity and acoustic impedance. The latter implies that the presence of porous chalk in some cases may be "read" directly from the seismic amplitude data. Secondly it means that more advanced techniques like acoustic impedance inversion may be especially useful for mapping the extent of the reservoir.

The chalk may serve both as a cap rock as well as a reservoir. The best quality reservoir is found in the late Campanian to Danian (Magne and Tor Formation) and in the Upper Turonian to Lowe Santonian Lower Hod Formation (Hardman 1982). These formations are the ones least polluted by terrigenous material, which appears to be linked to sea levels. During the Upper Turonian to Lower Santonian times the sea level was apparently lower, and the distance to sources of the unfavorable clay minerals shorter.

Due to the strong acoustic contrast often observed within and between the chalk sediment and the shales above and below, the chalk layer complicates the imaging below and intra-bed multiples including the ones set up between the Balder Formation and the top hard chalk sediments introduce multiple reflections which are difficult to remove and therefore challenge the inversion technique.

The biggest challenges associated with seismic imaging of chalk reservoirs are undoubtedly linked to the presence of gas in the sediments above. The difficulties in imaging significant part of the largest chalk reservoirs, like Ekofisk, Valhall and Eldfisk, is probably why the 3D seismic technology was introduced late compared to other fields of similar value. Seismic 2D data, sometimes in combination with VSP (Vertical Seismic Profiling) was for long the dominant seismic data used in the development phase of these giants. The first chalk discovery to have a 3D data-set to be acquired across it is probably the Dan field in 1988. The Ekofisk field was covered by 3D seismic in 1989, the Hod field in 1990 and by then the development of horizontal drilling and the demonstration of the superiority of the 3D technology over 2D made 3D coverage part of best practice.

The seismic imaging problem associated with several of the latest chalk fields was addressed through dedicated seismic processing scheme and acquisition techniques. These include the use of VSP Ocean bottom seismic systems for undershooting of the gas and use of shear waves.

It took another 10 years after accepting 3D seismic as a state of the art technology before the 4D seismic technology was introduced when turning the millennium. Contrary to many concerns, this technique turned out to be very well suited to address several of the challenges that are common for chalk reservoirs. Ten years later, two of the largest chalk reservoirs in the North Sea, the Valhall and the Ekofisk system has dedicated permanent seismic systems in place to help optimizing the recovery from the reservoir as well as managing the overburden.

Advanced processing of conventional 2D seismic combined with extensive use of normal-incidence VSP data was used to undershoot the overburden gas accumulations. Many of the wells were drilled as high angle deviated wells. A seismic geophone was lowered into the well and moved in steps of for instance 20 m, and a seismic source was fired at the surface vertically above the geophone for every geophone position. Reasonable image quality of the geology below the wells was achieved, as long as the seismic wave only traveled once through the overburden gas layers. In more complex chalk fields, where thicknesses could vary abruptly, these VSP's were used to identify new locations for side-track drilling due to lack of reservoir or in case of permanent well-failures, see Leonard and Munns (1987). The chalk fields became an important market for advanced VSP technology in this way. The world's first walk-away VSP was probably acquired in the A–5 well at Valhall in 1984, D. Miller (pers. Comm.). In this configuration the VSP geophones are placed in the well at a certain depth below the most significant gas layers. A seismic source towed by a supply vessel was fired at regular intervals along a line across the position of the geophones in the well. In this manner it was possible to image also along 2D sections orthogonal to the well. The first Valhall walkaway VSP was not a success. The images created were great, but the location of the resulting seismic section was highly uncertain due to lack of navigation data.

The first successful walkaway VSP was acquired at Ekofisk in 1985. This was apparently so successful that a few years later a full 3D VSP survey with 58 shot lines was performed over the same field to improve the resolution of the seismic response at the reservoir (Farmer and Barkved 1999). The final result was regarded as "the best image obtained of the Ekofisk reservoir", and is shown in **Fig. 2.5** (Dangerfield 2004).

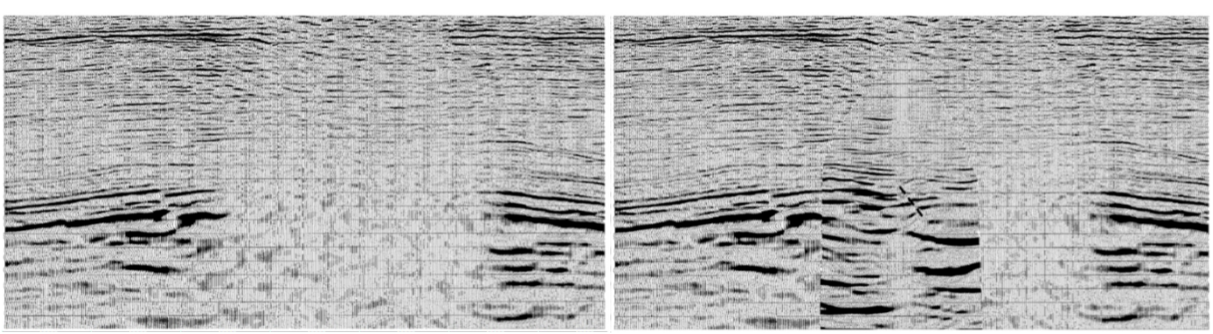

Figure 2.5: Left: Gas-affected seismic line in the borehole profile area. Right : Seismic line with the corresponding borehole profile line inserted. Nielsen, Dangerfield et al. (1999)

Since then 3D VSP's were acquired in several other wells. Quite a bit of efforts went into merging this image to fill in the "hole" caused by the gas above the reservoir (Smith, Ventzel et al. 2000). The 3D VSP image data was not directly comparable to surface seismic data. This is mainly caused by the limited fold in such data, which leads to a lower signal/noise level. Another difference between VSP and conventional imaging is that reflectors tilting towards the wellbore will be enhanced on the VSP image, and those tilting away from the wellbore will be attenuated. Finally, establishing a 3D velocity model that honors all the data sets that enables a unique image is difficult.

The efforts in the late 80's/early 90's were limited by the fact that only a certain number of geophone stations could be used simultaneously, typically 6 levels. This limits the vertical aperture or may result in aliased recordings if the spacing between adjacent receiver stations is too large. Today there are system in place that can deal with hundreds levels active at the same time. Such acquisition will make a significant better starting point for high quality unique imaging.

The Valhall license selected another approach and looked into the possibilities in using, at that time, the emerging 4–component ocean bottom seismic (4C OBS) technology, which also allowed for imaging using shear waves, which are "not" impacted by the fluid in the rocks. This technology was first used at the Tommeliten field for imaging below gas (Berg, Svenning et al. 1995).

The Valhall field became one of the key assets for demonstrating the viability of imaging below gas using converted shear waves recorded by 4C sensors on the seafloor (Thomsen, Barkved et al. 1997). Converted (shear) waves are reflected shear energy from down-going compressional (P-wave) seismic energy, at the acoustic interfaces in the subsurface. One of the world's first 3D, 4C seismic datasets was acquired at Valhall in 1997 (Rosland, Tree et al. 1999; Barkved, Mueller et al. 1999). Images constructed from this dataset were critical for planning and drilling several of the subsequent wells drilled in the field, **Fig. 2.6**.

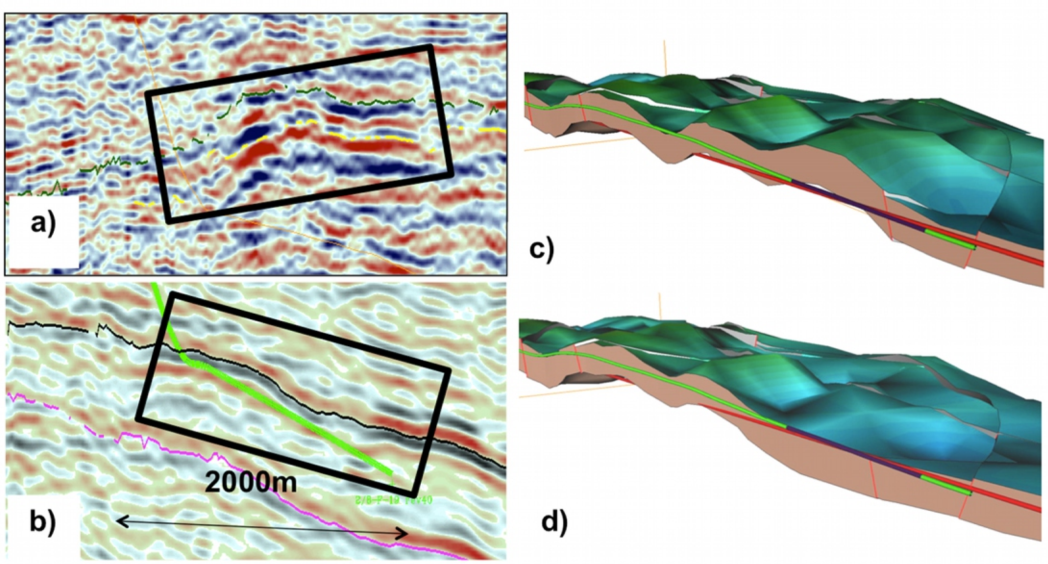

Figure 2.6: Converted wave images were critical in drilling several wells. a) P-wave section in P-wave time, the data was of little help in defining the entry and the first 500 m of the well (black box). b) C-wave in C-wave time provided enough confidence to drill the well. As we see, the prognosis from the C-wave in c), matched the final trajectory in d) fairly well (Barkved 2004).

Depth Migration (DM) is required to obtain optimal quality seismic images in a structurally complex subsurface. Gas charging in the overburden, of the types we see across several fields of the North Sea Central Graben, typically results in strong lateral variations, which are addressed more correctly with seismic depth processing. The same is also true for some of the highly dipping and structurally complex reservoir's Pre-stack depth migration (PSDM) was first applied to 2D seismic lines across some of the chalk fields in the early nineties (Whitmore Jr., Felinski et al. 1993) and the first 3D applications a few year later (Campbell, Gunn et al. 2003).

The presence of gas in the overburden distorts the seismic images by complicating the travel paths and attenuating the energy of the seismic wave fields. Advanced finite difference modeling and migration might give a significant uplift in seismic image quality if a detailed and accurate velocity distribution is known, see **Fig. 2.7**. More details may be found in O'Brien, Brandsberg-Dahl et al. (1999). This study was limited to elastic simulation and unelastic attenuation is not addressed.

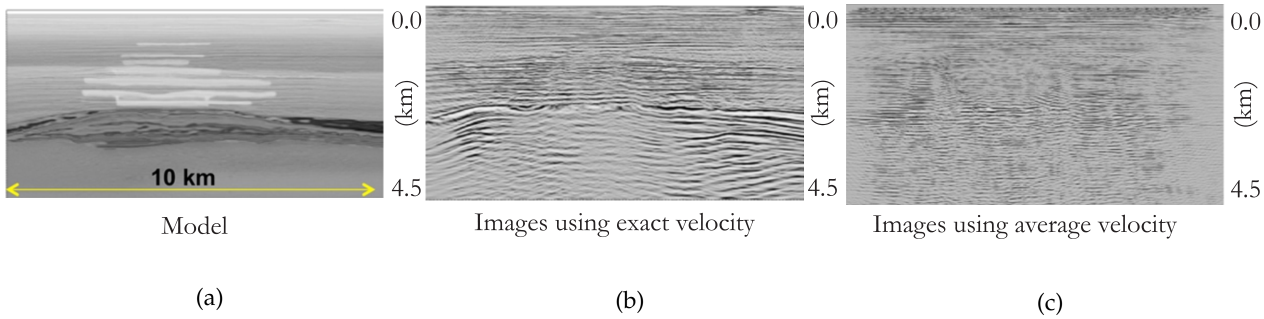

Figure 2.7: a) model used for full elastic modeling of a line across the Valhall field, b) the images from migrating with the exact velocities field. c) migrated with a smoothed velocity field (O'Brien, Brandsberg-Dahl et al. 1999).

The key observation is that the poor imaging in the presence of gas over the reservoir may be due to inaccurate or "too smooth" velocity fields and not necessarily attenuation. This is consistent with observation in wells, where down-going seismic energy in the most severe data degradation areas has been recorded. Following the insights from these numerical studies resulted in a strong focus on defining the best possible velocity definition across the field. A real breakthrough came with the use of Full Waveform Inversion (FWI) (Sirgue, Barkved et al. 2009). **Fig. 2.8** shows a cross-section through the Valhall field of the best tomographic velocities and the resulting seismic images when migrated with the best possible velocity field from tomography, compared to what was achieved using the Full Waveform Inversion (FWI) velocity. The inherent properties of the data acquired across the permanent seismic array at Valhall, low frequency and large offsets, made these results possible. These results (Fig. 2.8), demonstrate that considerable P-wave energy does make it through the "cloud". Full waveform inversion was able to find a velocity model that could produce a significantly better image compared to the image that was obtained from conventional tomography analysis.

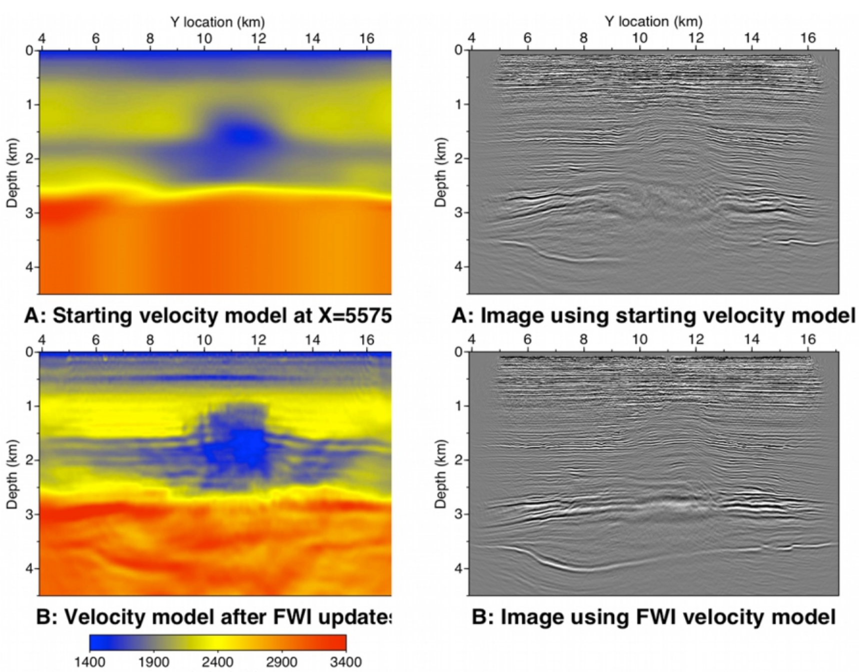

Figure 2.8: Left: Section through the starting 2007 velocity model from conventional tomography and (B), the corresponding section through the final 2009 velocity model from full-waveform inversion. Right: the pre-stack depth-migrated images corresponding to the velocity models A and B (Sirgue, Barkved et al. 2009).

A similar approach was later applied to the LoFS (Life of Field Seismic) recordings from the Ekofisk field. This array was installed in 2010, and is discussed in more details in Chapter 15. The resulting image, shown to the right in **Fig. 2.9**, is constructed by PSDM (Pre-Stack Depth Migration) utilizing a velocity model based on a combined FWI and tomography work flow (Bertrand, Folstad et al. 2013).

Although converted wave imaging produced images in areas that were poorly imaged on conventional P-

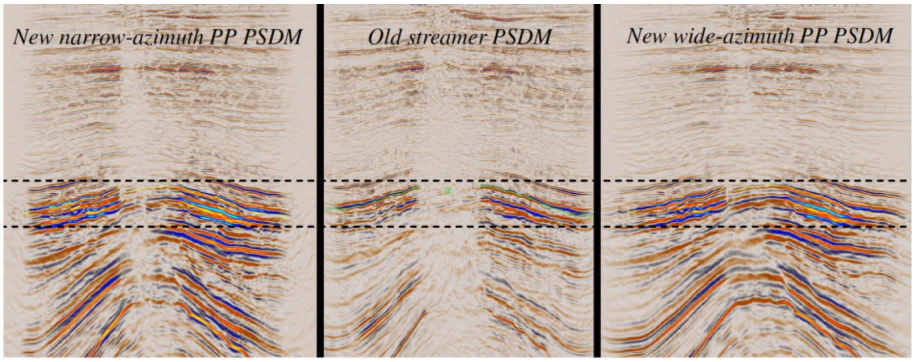

Figure 2.9: (left) narrow azimuth PP-stack from new PSDM; (middle) previous PSDM stack; (right) wide-azimuth PP-stack from new PSDM. The reservoir interval is located between the dotted lines (Bertrand, Folstad et al. 2013).

wave data due to the presence of gas in overburden (Barkved, Heavey et al. 2010) there were several remaining challenges. As a converted wave per definition consists of a down going P-wave leg, and an up going or reflected shear wave leg, we will still need the P-wave velocity in order to make a good image. Conversely we can establish a P-wave velocity by using the converted wave as input to a tomography process and jointly invert for P- and S-wave velocities. The best source for estimating the P-wave velocity will always be a pure P-wave dataset. The most severe imaging problems at Valhall and Ekofisk fields start below 1000–1500 m. Above this interval it appears that the improved resolution velocities from FWI provide a significant better starting point. **Fig. 2.10** shows the improvement in PS and PP imaging after using a combined FWI and tomography workflow (Barkved, Heavey et al. 2010).

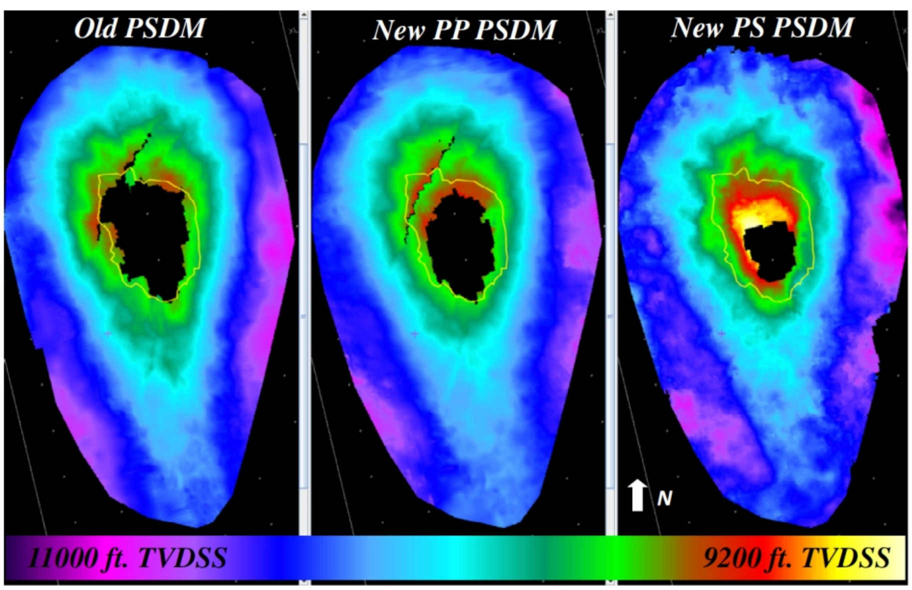

Figure 2.10: Auto-tracked top reservoir horizon at Valhall for the previous PSDM streamer data (left), new PSDM PP- data (middle) and new PSDM PS-data (right). The black area in the middle corresponds to the SOA (Seismic Obscured Area). The yellow polygon corresponds to the SOA on PSTM data. The SOA is reduced by 25% for the PP, and by 68% for the PS data compared to the previous PSDM (Barkved, Heavey et al. 2010).

As we see from Fig. 2.10 an area still remains black (no image obtained) under the most central part of the gas affected area. However, the Valhall 4D team realized that it was possible to fill this hole by carefully differencing of subsequent 3D data sets, **Fig. 2.11**. As the gas appears in thin and distinct silt layers in what generally is a fairly weak sequence, there is a high risk that strong intra-bed multiples may be generated. Even though there might be some stress induced time-lapse effects in the overburden, the 4D differencing appears to cancel the multiples so that a clear 4D image is obtained also in the most obscured areas below the gas cloud. It is believed that a more rigorous scheme including attenuation correction will most likely improve the 3D images further.

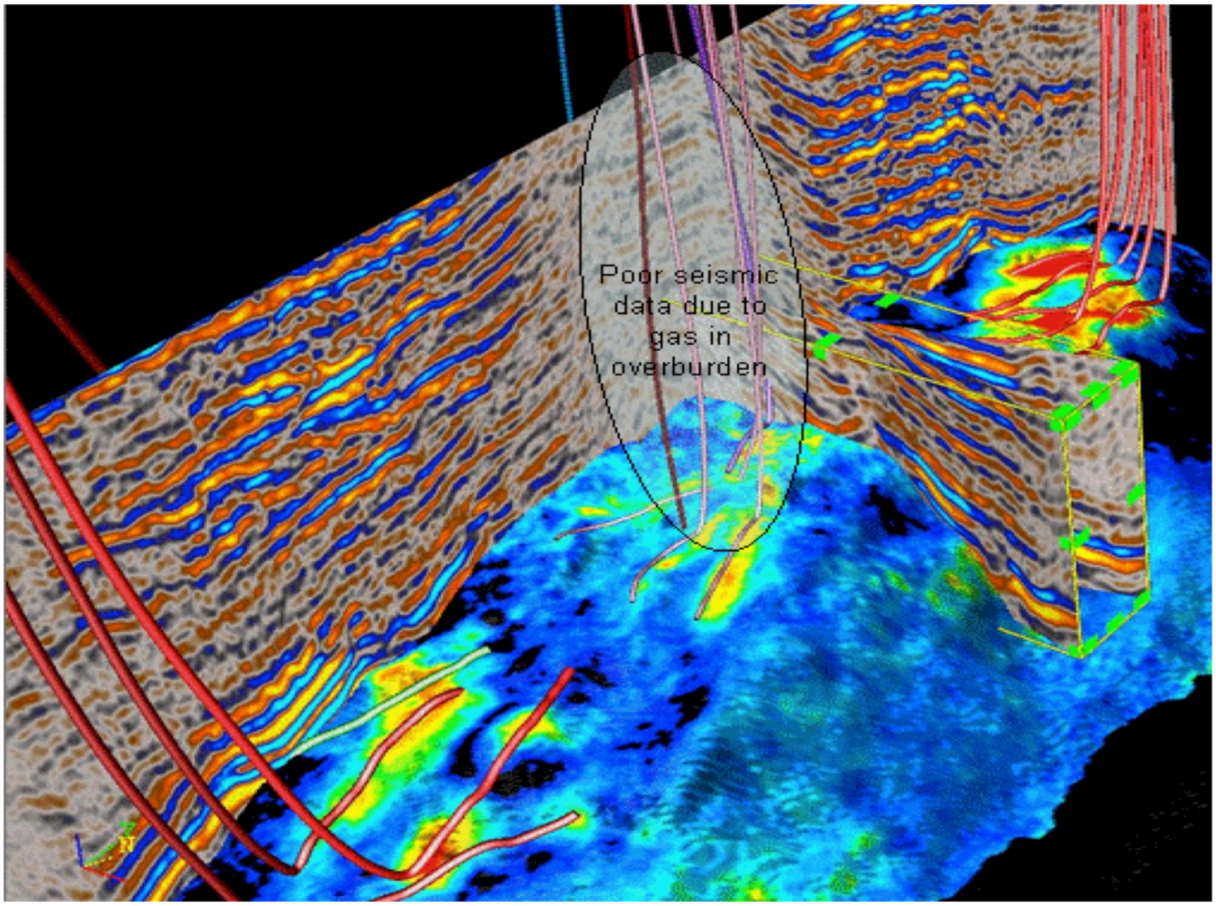

Figure 2.11: Migrated 3D volume of data (vertical sections) and a 4D difference map at reservoir level. An updated velocity model using FWI has been applied. The 4D difference shows changes that correspond to well production, while the 3D volume still struggle to show a the continuous reflector across the reservoir in the gas effected zones.

2.5 Inversion methods

Seismic inversion is one of the tools that present data in a format that is more readily available to geologists and reservoir engineers. Inversions transform seismic amplitude data into a layered model of density, P- and S-wave velocities. Alternatively we can invert for other properties like porosity or saturation, if the relation to the seismic response is known. The technique is referred to as inversion since it is the inverse of seismic modeling. Seismic modeling is used to construct the seismic response of a reservoir or subsurface model by combining its corresponding elastic properties with a seismic pulse or wavelet. The simplest form of seismic inversion converts a vertical incidence seismic trace into a layered model of the acoustic impedance. Known relations or a rock physics model can be used to make an estimate of the corresponding seismic velocities, and produce a synthetic sonic log.

One of the earliest commercial seismic inversion products used for chalk reservoirs was *Seislog*. This was based on the assumption that a trace in a stacked seismic section "has been processed to approximate the reflection coefficient series of a sedimentary section" (Lindseth 1979). Inversion of the seismic trace will then produce a relative impedance log, showing the changes between the layered sediments. By including velocity-density relations and adding the low frequency or background model from logs, a synthetic sonic log could be produced.

Seislog was used extensively by companies like Amoco to support development well planning in the Valhall Field, and several successful wells were drilled using this as input. One of the few easily available abstracts describing successful application to a chalk reservoir is from the Dan Field (Mummery 1985). The method eventually lost some of its credibility as the results were presented without an objective reference to the data quality. At Valhall, nice colorful "sonic log" sections were produced also in areas were the seismic imaging was severely challenged, like in gas affected areas. According to the anecdotes the validation of the result were made on the similarity to geology, e.g., how well it reflected channel features rather than on the physical basis of the methods.

Fortunately, the knowledge that porous chalk has a detectable seismic response did not get lost, but the focus turned into detailed analysis of amplitude at top chalk level for a while. Neff and West (1993) introduced a method named incremental pay thicknesses (IPT). They created several hundreds of perturbations changing thicknesses, saturation and porosity. IPT were tested on Zechstein carbonates as well as high probity cretaceous chalk. The results were used to support a statistical evaluation of new well targets (Hermansen, Neff et al. 1994).

In the 1990s several seismic inversion software packages became available. Hamson Russels Strata and Beicip Franlab's Interwell and Jason's Integrate were amongst these (Campbell and Gravdal 1995). In addition dedicated products were offered by various service providers. A product from Entec Energy Consultants based on a target oriented wavelet-processing and subsequent least square inversion appears to handle the noise in the gas affected area better than others. Apparently, the objective functions were designed in such a manner that the high frequency noise made the inversion to stop. While the main gas affected area still remains a challenge, several success stories made seismic inversion return as a "bread and butter" tool for chalk development, (Barkved 1996; Barkved, Kunz et al. 1998) tested a method with automated geo-body extraction. Top and base Tor reservoir of the Valhall field were defined based on acoustic impedance, within a maximum thickness from pre-inversion amplitude analysis and combined with fault planes extracted from coherency cubes from the same data set. The method works well for high porous reservoirs, but in the transition zones it was impossible to separate the reservoir of around 30% porosity from the Lista shale above.

AVO inversion techniques are used to extract elastic layer parameters, which may be used to separate lithologies. Pickett (1963) showed that in limestone $v_p/v_s = 1.9$ while in dolomite $v_p/v_s = 1.8$. The published numbers appear to have some spread but it is not common to see numbers above 2.0. There still remains some none-uniqueness in measured shear velocities for highly porous chalk based on cores, especially for porosities above 45%. The v_p/v_s ratio in the shale above the chalk section is typically around 2.5–3.5 (Mueller, Barkved et al. 1997) The development of dipole sonic tools in the nineties opened for measurements of slow shear velocity, which added confidence to another "chalk exploration secret". In areas where the Tor Formation represented the uppermost chalk section and was considered as an exploration target, the acoustic properties could be such that there were none or small contrast between porous reservoir chalk and the shale above, which could make it difficult to map the top reservoir. However, the strong contrast in the shear velocities between the shale cap rock and the chalk reservoir may be such that the shear wave response could detect this. Hansen, Escobar et al. (2011) has a very nice example of how this technique may work, as shown in **Fig. 2.12**.

One of the very early applications of AVO inversion applied in chalk is described in Landrø, Buland et al. (1995). They used a combination of travel time information and reflection amplitudes to extract P– and S–wave velocities and densities from data from the Valhall and Hod fields. Since P–wave velocity affected both travel time and reflection strength, it is the best resolved parameter. S-wave velocities are mainly determined from variation of reflection amplitude with angle of incidence. The results from this analysis combined with a seismic stratigraphic analysis of the conventional stacked amplitude data formed the basis for drilling and confirming the Hod pod prospect in 1994, as described by D'Angelo, Brandal et al. (1997).

Turning the millennium the use of seismic inversion for chalk prospects was reasonable well understood, and most chalk reservoirs was modeled based on acoustic impedance volumes as part of the workflow. Prediction of porosity was commonly accepted as robust products, given that the reservoir thickness was sufficient (Anderson 1999; Øxnevad and Taylor 1999). However, the opinions on predicting saturation remained mixed, and more work was necessary to clarify the situation. Ocean bottom and 4D Seismic data have been introduced and approaches aiming at simultaneously inverting all these data, also utilizing the offset dependencies, were introduced, e.g., (K. B. Rasmussen and and Pedersen 2004). Unfortunately, some practical challenges made it difficult to establish this as a routine process. The shear wave data remained at lower frequency than P-wave data, and 4D data may be influenced by stress changes, resulting in non-unique AVO responses (see next section).

The rock physics work done after the millennium helped t consolidate the understanding, see for example (Gommesen, Hansen et al. 2004; Japsen, Bruun et al. 2004; Britze, Nielsen et al. 2000) that the presence of clay in the chalk could complicate a unique estimation from seismic recordings only, and suggest a method that allows qualitative discrimination between clean, porous and tight chalk based on the continuity of the reflection pattern. Herbert, Escobar et al. (2013) combine elastic inversion, rock physics insights and a Bayesian classification system with geo-modelling to estimate porosity and saturation.

The lack of low frequencies has always represented a large uncertainty limiting independent use of seismic

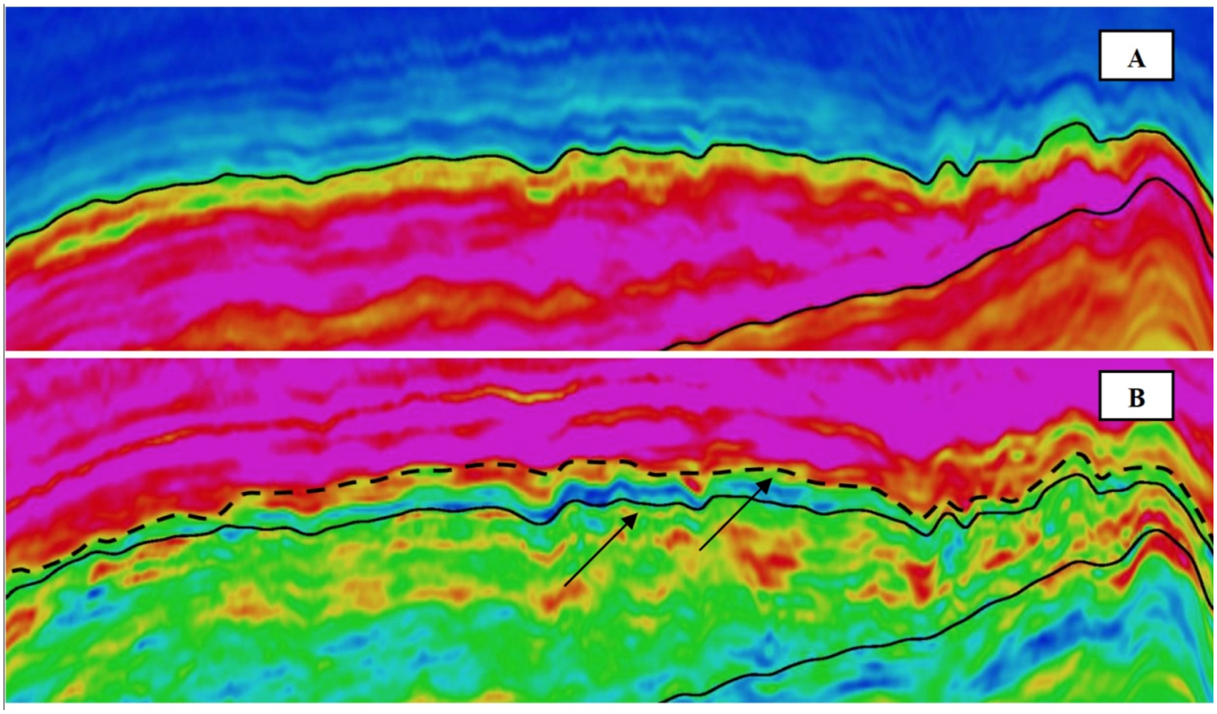

Figure 2.12: A: Inverted AI using the stratigraphic grid from the original horizons interpreted on the Seismic (solid black lines). B: Inverted V_p/V_s reveals the actual location of the top-reservoir being the lithological interface between overburden shale material and the reservoir chalk (dashed black line). The stratigraphic grid is updated using this new horizon and the inversion is repeated. After this the reworked marls are easily mapped (arrowed).

inversion. The low frequency model typically came from filtering well logs or from seismic derived velocities. Combining the low frequency model with the higher frequency inversion results is not trivial, and may require subjective input linked to structure or assessment when weighting the two models. Full waveform inversion (FWI) was introduced in the oil & gas industry around 1984 (Tarantola 1984). But it was not until 2007 we started to see the first industry applications of the technique, which until then has suffered from the absence of low frequencies in the data and also lack of sufficient computer resources.

One of the first successful industry applications of FWI was from the Valhall permanent seismic array (ref Chapter 15). The generally lower frequencies and very large offsets gave the necessary low wave numbers required to get successful results (Sirgue, Barkved et al. 2009). The FWI algorithm fully utilized the refracted and diving waves present in the data, which provided a significant improvement in lateral resolution, as shown in **Fig. 2.13**. The resulting velocity field obtained from full waveform inversion is a very useful seismic attribute, but is still limited in vertical resolution, and is therefore generally used in combination with conventional migration that includes the higher frequency in conventional amplitude display (Barkved, Heavey et al. 2010). Interestingly there has been none published result from combining a classical seismic amplitude inversion scheme with the lower frequency velocity model arising from FWI. Full waveform inversion are typically run down to about 3 to 4 Hz on OBC data set, and the results appears to be generally better above the shale, possible because the diving waves are limited to at best include the top chalk. However, by pushing the frequency lower, there might be better possibilities for inverting the velocities of the chalk layers, provided that the offsets are sufficiently large.

A lot of focus has been on using the velocities from full waveform inversion to improve the quality of the seismic imaging, see section above. FWI are typically utilized in combination with tomography for better conditioning of the deeper layers (Bertrand, Folstad et al. 2013).

2.6 Future aspects

Seismic data has played a key role in finding and deliberating chalk reservoirs. Although key challenges like gas saturated layers above the reservoir has remained, innovative use of seismic technology has demonstrated that this problem can be reduced significantly.

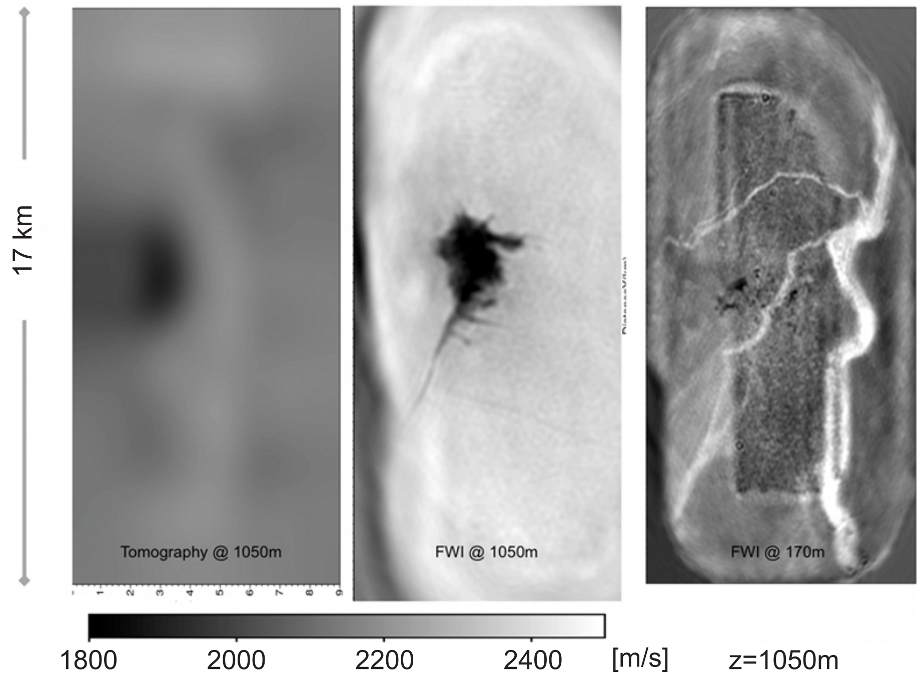

Figure 2.13: Right and center: details from the FWI data (Valhall) at 1050 m and 170 m below seabed. Left-hand image shows the resolution commonly seen in the tomographic-based velocities at 1050 m. Data from the LoFS array (Sirgue, Barkved et al. 2009).

1. At the turn of the century, the chalk reservoirs were not considered optimal candidates for seismic monitoring. From this background it is interesting that some of the 4D responses observed for producing chalk reservoirs are amongst the most impressive seen across the industry. The Valhall and Ekofisk fields are among the few fields in the world that are equipped with full field coverage of permanent seismic recording systems.

2. Seismic data will play an even more important role in the 50 years of production remaining from the North Sea giant chalk reservoirs. The remaining resources are significant and therefore it is very likely that improved seismic imaging and monitoring methods will contribute significantly to the remaining production.

3. The seismic technology will remain the key remote technique that will be able to delineate the stress state and the remaining resources in the reservoirs from surface for the foreseeable future.

4. The computer technology will allow us to utilize the right type of imaging algorithms, that support teethe complexities of the overburden often seen across the chalk reservoirs. We expect that the FWI technology will continue to be developed and that solutions which include inverting for anisotropy may be industry standards in the next 5 years. Continued work will also make it possible for S-wave velocities to be part of the solution within the next 10 years.

5. Shale gas & oil is likely to support renewed interest in methodology that the low permeable chalk reservoirs might benefit from, including S-waves and AVOA.

6. While it is beyond doubt that seismic will continue to add value to the production from our chalk fields, the difference between value adding and substantial commercial impact sits primarily within the geophysical community. Focus needs to be on cost effective ”answer” products utilizing other disciplines insights rather than re-inventing them with a geophysical mindset. Looking back on the last 20 years of chalk seismology, we may conclude that the seismic theory turned out to be correct, although we will always struggle to find efficient and robust ways to exploit the theory in practice.

Nomenclature

G = shear modulus, m/Lt^2
K = bulk modulus, m/Lt^2
v_P = velocity P-wave, L/t, m/s
v_S = velocity S-wave, L/t, m/s
ρ = rock density, m/L^3, gm/cc

Subscripts

P = P-wave
S = S-wave

Abbreviations

AI = acoustic impedance
AVO = amplitude versus offset
AVOA = azimuthal AVO
DM = depth migration
FWI = full waveform inversion
IPT = incremental pay thicknesses
LoFS = life of field seismic
MMBOE = millin of barrels oil equivalent
OBC = ocean bottom cables
P-wave = pressure (or primary) wave
PP = PP-event (used to point out that an observed reflected events are caused by an incident p-wave and reflected as p-wave)
PS = PS-event (used to point out that an observed reflected event are caused by an incident p-wave and reflected as s-wave)
PSDM = pre-stack depth migration
PSTM = pre-stack time migration
S-wave = shear (or secondary) wave
SOA = seismic obscured area
VSP = vertical seismic profiling

References

Andersen, M.A., 1995. *Petroleum Research in North Sea Chalk.* RF-Rogaland Research. Joint Chalk Research Program Phase IV.

Anderson, J.K., 1999. The capabilities and challenges of the seismic method in chalk exploration. *Geological Society, London, Petroleum Geology Conference series*, **5**: 939–947. URL http://dx.doi.org/10.1144/0050939.

Askim, O.J., 2003. Seismic Forward Modeling in a Chalk Reservoir with Permanent Monitoring. Paper presented at 65th EAGE Conference & Exhibition. 02 June. URL http://www.earthdoc.org/publication/publicationdetails/?publication=3112.

Barkved, O., 1996. Succesfull use of seismic attribute maps and poststack inversion in horizontal well planning. Paper presented at 58th EAGE Conference and Exhibition. 06 June. URL http://dx.doi.org/10.3997/2214-4609.201409039.

Barkved, O., Heavey, P. et al., 2010. Business Impact of Full Waveform Inversion at Valhall. In *SEG Technical Program Expanded Abstracts 2010*, 925–929. Society of Exploration Geophysicists. January. URL http://dx.doi.org/10.1190/1.3513929.

Barkved, O.I., 2004. Continuous seismic monitoring. In *SEG Technical Program Expanded Abstracts 2004*, 2537–2540. Society of Exploration Geophysicists. January. URL http://dx.doi.org/10.1190/1.1851258.

Barkved, O.I., Kunz, T., and Whitman, D., 1998. Automated Extraction of Faults And Porous Reservoir Bodies -Examples From The Valhall Field. NPF conference.

Barkved, O.I., Mueller, M.C., and Thomsen, L., 1999. Vector Interpretation of the Valhall 3D/4C OBS dataset. 61st EAGE Conference and Exhibition. 07 June. URL http://dx.doi.org/10.3997/2214-4609.201407831.

Berg, E., Svenning, B., and Martin, J., 1995. SUMIC, a new strategic tool for exploration and reservoir mapping. *Journal of Applied Geophysics*, **2** (34): 139–140. URL http://dx.doi.org/10.1016/0926-9851(96)80868-8.

Bertrand, A., Folstad, P.G. et al., 2013. The Ekofisk Life of Field Seismic (LoFS) System - Experiences and Results after Two Years in Operation. Paper presented at 75th EAGE Conference & Exhibition incorporating SPE EUROPEC 2013. 10 June. URL http://dx.doi.org/10.3997/2214-4609.20130424.

Britze, P., Nielsen, E.B. et al., 2000. North Sea chalk porosity resolved by integration of seismic reflectivity and well data. Paper presented at EAGE Conference on Exploring the Synergies between Surface and Borehole Geoscience - Petrophysics meets Geophysics. 06 August. URL http://www.earthdoc.org/publication/publicationdetails/?publication=5197.

Campbell, A., Gunn, C. et al., 2003. Anisotropic Depth Migration - A New Attempt to Image the Banff Chalk Reservoir. Paper presented at 65th EAGE Conference & Exhibition. 02 June.

Campbell, S.J.D. and Gravdal, N., 1995. The prediction of high porosity chalks in the East Hod Field. *Petroleum Geoscience*, **1** (1): 57–69. February. URL http://pg.eage.org/publication/publicationdetails/?publication=36436.

D'Angelo, R.M., Brandal, M.K., and Rørvik, K.O., 1997. 13. Porosity Detection and Mapping in a Basinal Carbonate Setting, Offshore Norway. In I. Palaz and K.J. Mafurt, eds., *Carbonate Seismology*, Chap. 13, 321–336. Society of Exploration Geophysicists. URL http://dx.doi.org/10.1190/1.9781560802099.ch13.

Dangerfield, J.A., 2004. *AAPG Special Volumes*, , In ed., , Chap. Case History 9: Shallow 3-D Seismic and a 3-D Borehole Profile at Ekofisk Field, 383–391. The American Association of Petroleum Geologists and the Society of Exploration Geophysicists. URL http://archives.datapages.com/data/specpubs/memoir42/ch09_09/ch09no09.htm?q=%2BauthorStrip%3Adangerfield#purchaseoptions.

Farmer, C.L. and Barkved, O.I., 1999. Influence of syn-depositional faulting on thickness variations in chalk reservoirs– Valhall and Hod fields. *Geological Society, London, Petroleum Geology Conference series*, **5**: 949–957. URL http://dx.doi.org/10.1144/0050949.

Gommesen, L., Hansen, H.P. et al., 2004. Rock Physics Templates and Seismic Modelling of Chalk Reservoirs in the South Arne Field of the Danish North Sea. Paper presented at 66th EAGE Conference & Exhibition. 07 June.

Hansen, H.P., Escobar, I., and Cherrett, A.J., 2011. Fast Deterministic Geostatistical Inversion - A Case Study. Paper presentet at 73rd EAGE Conference and Exhibition incorporating SPE EUROPEC 2011. 23 May. URL http://dx.doi.org/10.3997/2214-4609.20149298.

Hardman, R.F.P., 1982. Chalk Reservoirs of the North Sea. *Bulletin of the Geological Society of Denmark*, **30** (3–4): 119–137. URL http://2dgf.dk/xpdf/bull30-03-04-119-137.pdf.

Herbert, I., Escobar, I., and Arnhild, M., 2013. Modelling Fluid Distribution in a Chalk Field Using Elastic Inversion. In *75th EAGE Conference & Exhibition incorporating SPE EUROPEC 2013*. EAGE Publications BV. URL http://dx.doi.org/10.3997/2214-4609.20130878.

Hermansen, H., Neff, D.B. et al., 1994. Reservoir characterization and management studies of the Tor Field, Norway. Paper presented at EAPG/AAPG Special Conference on Chalk. 09 September. URL http://dx.doi.org/10.3997/2214-4609.201407543.

Japsen, P., Bruun, A. et al., 2004. Influence of porosity and pore fluid on acoustic properties of chalk: AVO response from oil, South Arne Field, North Sea. *Petroleum Geocience*, **10** (4): 319–330. October. URL http://dx.doi.org/10.1144/1354-079303-586.

Jorgensen, L.N. and Andersen, P.M., 1991. Integrated Study of the Kraka Field. Paper SPE 23082, presented at the Offshore Europe Conference, Aberdeen. 3–6 September. URL http://dx.doi.org/10.2118/23082-MS.

K. B. Rasmussen and, A.B. and Pedersen, J.M., 2004. Simultaneous Seismic Inversion. Paper presented at 66th EAGE Conference & Exhibition. 07 June. URL http://www.earthdoc.org/publication/publicationdetails/?publication=2382.

Landrø, M., Buland, A., and D'Angelo, R., 1995. Target-oriented AVO inversion of data from Valhall and Hod fields. *The Leading Edge*, **14** (8): 855–861. August. URL `http://dx.doi.org/10.1190/1.1437171`.

Leonard, R.C. and Munns, J.W., 1987. Valhall Field. In A. Spencer, ed., *Geology of the Norwegian Oil and Gas Fields: An Atlas of Hydrocarbon Discoveries, Containing Full Descriptions of 37 of Norway's Major Oil and Gas Fields and Finds*, 153–163. Graham & Trotman, Limited. ISBN 9780860109082. URL `http://books.google.no/books?id=CVQZAQAAIAAJ`.

Lindgård, J.E., Lehocki, I. et al., 2011. Seismic Porosity Prediction in Chalks - Pitfalls and Potential. Paper presented at 73rd EAGE Conference and Exhibition incorporating SPE EUROPEC 2011. 23 May. URL `http://www.earthdoc.org/publication/publicationdetails/?publication=50823`.

Lindseth, R.O., 1979. Synthetic sonic logs - a process for stratigraphic interpretation. *GEOPHYSICS*, **44** (1): 3–26. January. URL `http://dx.doi.org/10.1190/1.1440922`.

Mavko, G., Mukerji, T., and Dvorkin, J., 2009. *The Rock Physics Handbook*. 2nd ed., Cambridge University Press. Isbn: 9780521861366. URL `http://dx.doi.org/10.1017/cbo9780511626753`.

Megson, J. and Tygesen, T., 2005. The North Sea Chalk: an underexplored and underdeveloped play. *Geological Society, London, Petroleum Geology Conference series*, **6**: 159–168. URL `http://dx.doi.org/10.1144/0060159`.

Mueller, M.C., Barkved, O.I., and Thomsen, L.A., 1997. Dipole sonic results (Valhall area)-implications for AVO and OBS interpretation. In *59th EAGE Conference & Exhibition*. URL `http://www.earthdoc.org/publication/publicationdetails/?publication=24678`.

Mummery, R.C., 1985. Use of {SEISLOG} for basin evaluation and field development. *Energy*, **10** (3–4): 383–401. Proceedings of the Second EAPI/CCOP Workshop. URL `http://dx.doi.org/http://dx.doi.org/10.1016/0360-5442(85)90055-6`.

Myhre, L., ed., 1975. *Lithology. Well no 8/3-1*. Oljedeirektoratet (Norwegian Petroleum Directorate), Stavanger. NPD Paper No. 1.

Myhre, L., ed., 1977. *Lithology. Wells 2/8-1 and 2/11-1*. Oljedeirektoratet (Norwegian Petroleum Directorate), Stavanger. NPD Paper No. 7. URL `http://www.npd.no/engelsk/cwi/pbl/NPD_papers/168_01_NPD_Paper_No.7_Lithology__Well_2_11_1.pdf`.

Neff, D.B. and West, K.L., 1993. Integrated Interpreation of North Sea Carbonates using Automated seismic modelling. Paper presented at 55th EAEG Meeting. 9 June. URL `http://dx.doi.org/10.3997/2214-4609.201411420`.

Nielsen, H.H., Dangerfield, J. et al., 1999. Three-component 3D borehole profile imaging program on Ekofisk Field. *Geological Society, London, Petroleum Geology Conference series*, **5** (1): 1255–1264. URL `http://dx.doi.org/10.1144/0051255`.

O'Brien, M. J.and Whitmore, N.D., Brandsberg-Dahl, S., and Murphy, G.E., 1999. Multicomponent modeling of the Valhall field. EAGE expanded abstract, 4-27.

Øxnevad, I.E.I. and Taylor, M.S.G., 1999. An integrated approach to hydrocarbon emplacement in chalk, Norwegian North Sea Central Graben. *Geological Society, London, Petroleum Geology Conference series*, **5**: 1221–1230. URL `http://dx.doi.org/10.1144/0051221`.

Pickett, G.R., 1963. Acoustic character logs and their applications in formation evaluation. *Journal of Petroleum Technology*, **15**: 659–667. June. URL `http://dx.doi.org/10.2118/452-PA`.

Riise, R., ed., 1977. *Lithology. Wells 2/8-2*. Oljedeirektoratet (Norwegian Petroleum Directorate), Stavanger. NPD Paper No. 13. URL `http://www.npd.no/engelsk/cwi/pbl/NPD_papers/155_01_NPD_Paper_No.13_Lithology__Well_2_8_2.pdf`.

Rosland, B., Tree, E.L., and Kristiansen, P., 1999. Acquisition of 3D/4C OBS data at Valhall. Presented at the 61st EAGE Conference and Exhibition. URL `http://earthdoc.eage.org/publication/publicationdetails/?publication=31785`.

Sirgue, L., Barkved, O.I. et al., 2009. 3D Waveform Inversion on Valhall Wide-azimuth OBC. Paper presented at 71st EAGE Conference and Exhibition incorporating SPE EUROPEC 2009. 08 June. URL `http://dx.doi.org/10.3997/2214-4609.201400395`.

Smith, A.B., Ventzel, N. et al., 2000. 3D VSP Imaging-Filling in the Ekofisk Gas Hole. In *62nd EAGE Conference & Exhibition*. 29 May. URL http://www.earthdoc.org/publication/publicationdetails/?publication=7387.

Strass, I.F., ed., 1980. *Litology. Wells 2/4-1, 2/4-2, 2/4-3, 2/4-4 and 2/4-5*. Oljedeirektoratet (Norwegian Petroleum Directorate), Stavanger. NPD Paper No. 25. URL http://www.npd.no/engelsk/cwi/pbl/NPD_papers/174_01_NPD_Paper_No.25_Lithology__Well_2_4_4.pdf.

Tarantola, A., 1984. Inversion of seismic reflection data in the acoustic approximation. *GEOPHYSICS*, **49** (8): 1259–1266. URL http://dx.doi.org/10.1190/1.1441754.

Thomsen, L.A., Barkved, O.I. et al., 1997. Converted-wave Imaging of Valhall Reservoir. Presented at the 59 EAGE Conference & Tech. Exhibition.

Uldall, A. and Ødum, M.R., 1994. Modelling the seismic response of highly porous chalk. Paper presented at 1994 EAPG/AAPG Special Conference on Chalk. 08 September. URL http://dx.doi.org/10.3997/2214-4609.201407541.

Walls, J., Dvorkin, J., and Smith, B., 1998. Modeling seismic velocity in Ekofisk chalk. In *SEG Technical Program Expanded Abstracts 1998*, 1016–1019. Society of Exploration Geophysicists. SEG Annual Meeting, New Orleans. January. URL http://dx.doi.org/10.1190/1.1820055.

Whitmore Jr., N.D., Felinski, W.F. et al., 1993. The application of common offset and common angle pre-stack depth migration in the North Sea. Paper presented at 55th EAEG Meeting. URL http://dx.doi.org/10.3997/2214-4609.201411444.

Chapter 3

Rock Physics

Ida Lykke Fabricius

Rock physics is the discipline linking petrophysical properties as derived from borehole data to surface based geophysical exploration data. It can involve interpretation of both elastic wave propagation and electrical conductivity, but in this chapter focus is on elasticity. Rock physics is based on continuum mechanics, and the theory of elasticity developed for statics becomes the key to petrophysical interpretation of velocity of elastic waves. In practice, rock physics involves interpretation of well logs including vertical seismic profiling (VSP) and analysis of core samples. The results of these procedures are then integrated with reflection seismic data (Japsen, Bruun et al. 2004; Al-Shuhail 2007).

3.1 Elastic moduli and elastic waves

The elasticity of an isotropic medium can be fully described provided two elastic moduli are known. In rock physics of isotropic rocks the preferred moduli are the bulk modulus, K, which describes stress per unit volumetric deformation with no change of shape (no shear) and the shear modulus, G, which describes shear stress required for half-unity average shear strain with no change of volume. Elastic shear waves involve translations in the direction perpendicular to wave propagation, which takes place with a velocity, v_S controlled by shear modulus, G and density, ρ, of the material:

$$v_s = \sqrt{G/\rho}. \tag{3.1}$$

Compressional P-waves involve one-dimensional (uniaxial) deformation in the direction of wave propagation and include change of volume as well as change of shape due to the one-directional change in volume. P—wave velocity, v_P depends on density and the compressional (or P-wave) modulus, $M = K + 4G/3$:

$$v_p = \sqrt{M/\rho}. \tag{3.2}$$

From logging data, v_S and v_P are found as the inverse interval travel times (or equivalently inverse slowness). For many wells, interval travel time is only available for P-waves, and v_S must then be estimated either by empirical relations to v_P or by rock physical modelling.

3.2 Elastic moduli and elastic waves in chalk

For porous rocks, G depends only on deformation of the solid frame and is independent of pore fluid, because the fluid is translated passively during the shear of the frame. The pore-fluid contributes to the bulk density, ρ, so the shear wave velocity decreases as fluid density increases. By contrast, pore-fluid contributes to M, because the volumetric part of the elastic deformation also includes the pore fluid, so because fluid density contributes positively to both ρ and M, v_P of chalk is typically less influenced by pore fluid than v_S.

Biot (1956) predicted that the velocity of elastic waves in a fluid-saturated rock will depend on specific surface of pore space, S_P, on fluid density, ρ_{fl}, and fluid viscosity, η as well as on frequency of the elastic wave. When specific surface and fluid viscosity is high while density of fluid and frequency is low, the wave will propagate in phase through the solid and fluid. Above a critical frequency, f_c, depending on specific surface of pore space, viscosity, and fluid density, the wave will propagate in the fluid out of phase with the propagation in the rock frame and the rock will stiffen and elastic wave velocity go up:

$$f_c = \frac{\eta S_p^2}{2c\pi\rho_{fl}}, \tag{3.3}$$

where c is Kozeny's factor (see Chapter 12)

For water saturated chalk, critical frequencies in the range 10–10^5 MHz was found (Fabricius, Bächle et al. 2010), whereas for air saturated (dry) chalk, critical frequency is ca. 15 times higher. These results would indicate that elastic wave velocities of chalk are independent of frequency in the entire range from 10 MHz (ultrasonic) to seismic velocity. Biot's theory only holds if the specific surface of pore space refers to a uniform pore size distribution, and if the solid frame has a homogeneous stiffness. Provided the chalk is not fractured, these conditions actually holds for chalk **(Fig. 3.1)**.

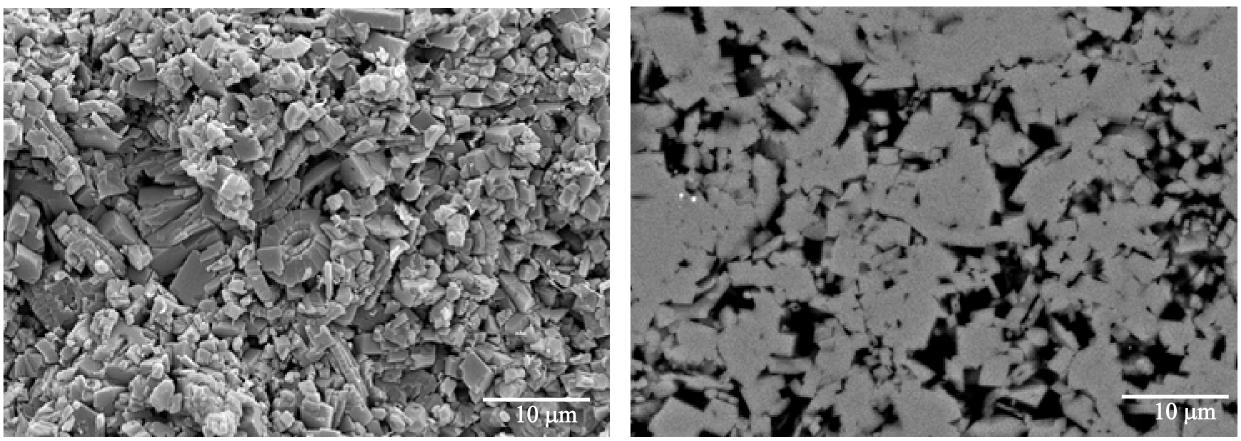

(a) (b)

Figure 3.1: Electron micrographs of sample of North Sea chalk close to an oil-water contact. It is massive, has microfossil bearing mudstone texture and 20% porosity. (a) is recorded on the broken surface by collecting secondary electrons, whereas (b) is recorded on the epoxy-impregnated, cut and polished sample by collecting backscattered electrons. The particle-aggregate nature of this low-porosity chalk is easy to see from (a), whereas the cemented nature of grain contacts is easy to see from (b).

Several authors have compared elastic modulus of water saturated chalk as derived from geomechanical testing to elastic modulus of water saturated chalk as calculated from density and ultrasonic velocities e.g. (Henriksen, Fabricius et al. 1999; Gommesen and Fabricius 2001; Alam, Borre et al. 2010) . The elastic modulus derived from ultrasonic data is found to be significantly higher than the modulus derived from geomechanical testing. A primary reason for this discrepancy is that ultrasonic data refer to an undrained state, where pressure builds up in the pore fluid during deformation, whereas geomechanical testing refers to a drained state where pore pressure is constant. It would seem obvious to compare moduli from undrained geomechanical testing to moduli from ultrasonic velocity, but this kind of experiments are difficult to perform. A second reason for the discrepancy is the scale of deformation in that geomechanical deformation is relatively high and can include elastic and plastic deformation, whereas ultrasonic deformation is in the nm scale and is purely elastic. It remains an open question whether there is an intrinsic difference between moduli measured in the two ways.

3.3 Biot's coefficient and pore stiffness

The stiffness of a chalk expressed as bulk modulus depends on the stiffness of the chalk frame, the stiffness of the pore fluid, and can be influenced by electrostatic effects controlled by the pore fluid (Nermoen, Korsnes et al. 2015). The stiffness of the rock frame, K_{fr}, is found by deformation at constant pore pressure with an inert pore fluid. For elasticity measured from ultrasonic velocities, this condition is approximately met for dry chalk.

Under assumption of an isotropic frame, the stiffness of the frame can be modelled either from Biot's coefficient **(Fig. 3.2a)** or by effective medium theory. Biot (1941) introduced Biot's coefficient, α, expressing how much a constant pore pressure counteracts elastic deformation of a rock frame. As expressed by Biot and Willis (1957):

$$\alpha = 1 - \frac{K_{fr}}{K_{\min}}, \tag{3.4}$$

where $K_{\min}$ is the elastic bulk modulus of the mineral. For chalk it is in most cases reasonable to assume $K_{\min}$ is the bulk modulus of calcite (c. 70 GPa). By rock mechanical testing of dry chalk a similar value for K_{fr} is found as when modelled from ultrasonic data (Olsen, Hedegaard et al. 2008). The coefficient, α, can be used to estimate pore stiffness, K_ϕ:

$$K_\phi = K_{fr}\frac{\phi}{\alpha}. \tag{3.5}$$

$1/K_\phi$ is an expression of pore compressibility. As illustrated in Fig. 3.2a, α decreases with increasing contact cementation or pore filling cementation of chalk. For this reason α is typically declining with decreasing porosity, ϕ, (Engstrøm 1992), but it should be noted that α in principle is independent of porosity although ϕ is the theoretical lower bound for α. The upper bound for α is 1. This value can be approached but never met for an elastic material.

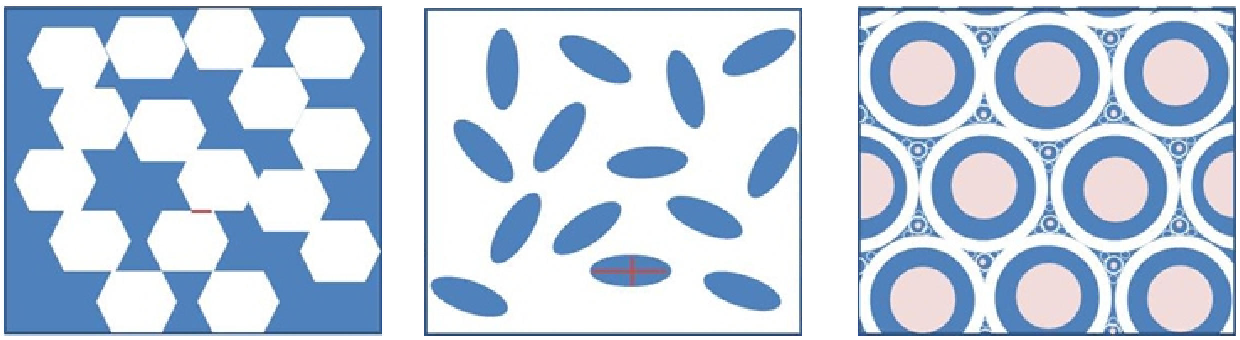

(a) (b) (c)

Figure 3.2: Concepts of chalk texture for modelling elastic properties. In all figures the blue areas indicate the pore fluid. In (a) (white) calcite crystals support each other via contact cement (red bar) but they are basically particles and the pore space is continuous. The area of particle contact illustrates one minus Biot's coefficient and determines elasticity for a given mineralogy, porosity and pore fluid. In (b) the calcitic (white) phase is continuous and encloses isolated pores. The aspect ratio of pores (red bars) determines elasticity for a given mineralogy, pore fluid and porosity. In (c) the iso-frame model is illustrated. The white spherical (calcite) shells represent the supporting frame. By filling smaller spherical shells in between the bigger ones, the white shells fill the space according to an upper Hashin Shtrikman bound. The pink spheres represent calcite which is not part of the frame. The fluid and the pink spheres fill the non-frame space according to a lower Hashin-Shtrikman bound. The fraction of the solid in the supporting frame defines the iso-frame value. Elasticity is then controlled by the iso-frame value for a given porosity, pore fluid and mineralogy.

3.4 Fluid substitution

If the pore-fluid has no chemical interaction with the rock frame and if the pore-space is homogeneous and well connected, it is possible to predict the undrained elastic moduli of the fluid-saturated rock from the elastic moduli of the dry (drained) rock (and vice versa). Necessary input data include porosity, ϕ, mineral bulk modulus, $K_{\min}$, and bulk modulus, K_{fl}, of the fluid. Elastic moduli will typically be calculated from elastic wave velocity and density. Simple expressions quantifying the effect on elasticity of fluid substitution were introduced by Gassmann (1951), where the suffix "sat" refers to the fluid saturated state:

$$G_{\text{sat}} = G_{\text{dry}}, \tag{3.6}$$

$$\frac{K_{\text{sat}}}{K_{\min} - K_{\text{sat}}} = \frac{K_{\text{dry}}}{K_{\min} - K_{\text{dry}}} + \frac{K_{fl}}{\phi(K_{\min} - K_{fl})}. \tag{3.7}$$

If the chalk only contains one pore fluid, Gassmanns equations are robust. If two fluids are present in the pore space, the effective bulk modulus of the fluid can with good approximation be predicted from wettability and fluid saturation. In an oil-bearing chalk in water-wet condition, and high water saturation S_w, the effective bulk modulus of the fluid becomes:

$$K_{fl} = S_w K_{\text{water}} + (1 - S_w) K_{\text{oil}}. \tag{3.8}$$

At low water saturation or in a mixed-wet condition K_{fl} can be estimated from (Hill 1952):

$$K_{fl} = (S_w K_{\text{water}} + (1 - S_w) K_{\text{oil}} + (S_w / K_{\text{water}} + (1 - S_w)/K_{\text{oil}})^{-1})/2. \tag{3.9}$$

In case of doubt, the average of the two expressions can be attempted.

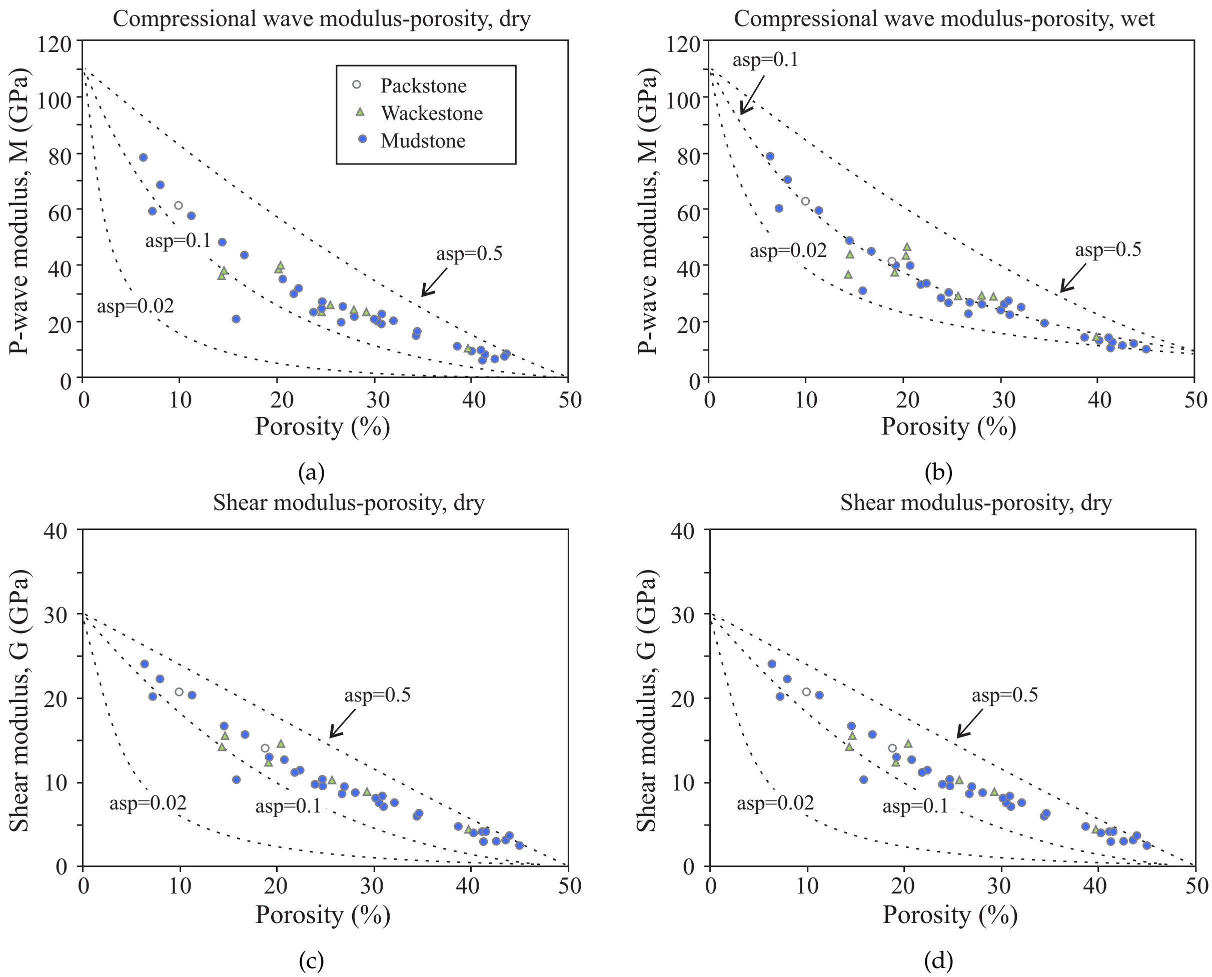

Figure 3.3: Elastic P-wave modulus and shear modulus for dry and for water saturated chalk samples (Fabricius, Bächle et al. 2010). The data are plotted on templates constructed according to a self consistent approximation (Berryman 1980). By this method elastic moduli are characterized by the aspect ratio of randomly oriented ellipsoidal pores. P-wave and shear modulus are consistent because they are modelled together for a given pore fluid, but the model is not consistent between different pore fluids.

3.5 Fluid effects on chalk stiffness

By rock mechanical testing Risnes (2001) found that the strength of chalk is highly influenced by the nature of the pore fluid, and Japsen, Høier et al. (2002) found that also frame elasticity as derived from ultrasonic velocity and density is influenced by pore fluid. When doing Gassmann substitution of water saturated to dry chalk, both bulk- and shear moduli were found to be lower than moduli measured on dry chalk (Fabricius, Bächle et al. 2010).

The softening is found to be reversible, so it is probably not caused by irreversible chemical action (precipitation or dissolution). The degree of softening depends on pore fluid composition; and Katika, Addassi et al. (2015) stated that a possible cause for the observed weakening is electrostatic repulsion between chalk particles

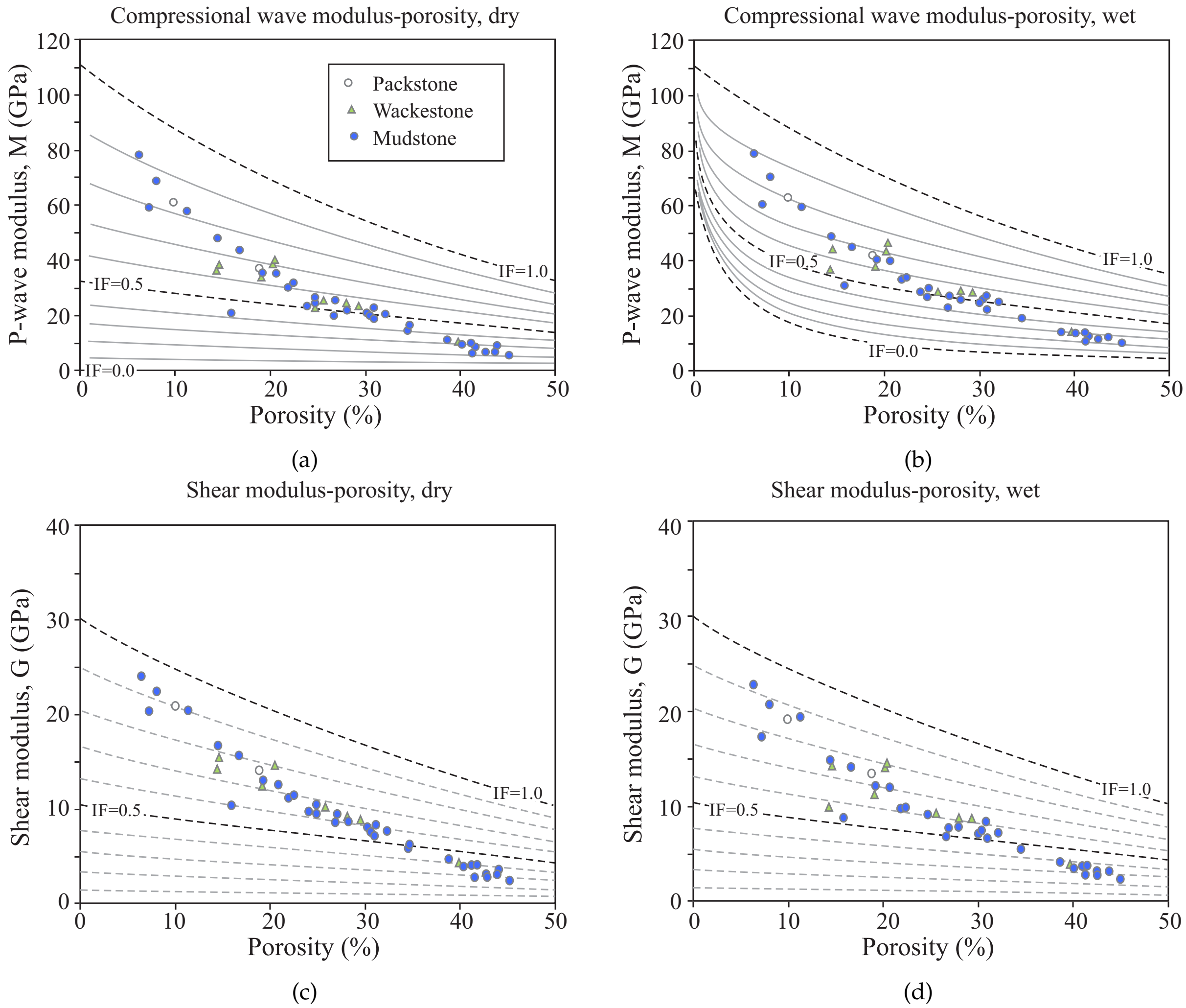

Figure 3.4: Elastic P-wave modulus and shear modulus for dry and for water saturated chalk samples (Fabricius, Bächle et al. 2010). The data are plotted on templates constructed according to the iso-frame model. Each modulus is modelled independently, and the iso-frame value is consistent among the two P-moduli and can be used for fluid substitution in the absence of shear modulus data (Røgen, Gommesen et al. 2004). Shear wave moduli of dry chalk tend to have higher iso-frame value than for water saturated chalk. The iso-frame value increases with increasing cementation and can be used to estimate Biot's coefficient from each data set independently.

in the water saturated state. It should be noted though, that the fluid influence on frame stiffness is a second order effect, and that Gassmann substitution gives a good approximation of the required data.

3.6 Rock physical modeling

Chalk can be modelled as an effective medium composed of calcite, water and hydrocarbons, and several authors have attempted to gain information on pore shape and texture from the relation between porosity and elastic moduli (Fabricius, Baechle et al. 2007; Gommesen, Fabricius et al. 2007; Olsen, Christensen et al. 2008; Saberi, Johansen et al. 2009). A typical procedure is to visualize the chalk as a medium composed of calcite serving as the host of ellipsoidal pores with a distribution of aspect ratios (Fig. 3.2 2, citations in Mavko, Mukerji et al. (2009)). Unfortunately no workers have so far demonstrated that an inclusion based model can result in the same pore shape information when data with different pore fluids are compared **(Fig. 3.3)**. A reason why this kind of models work so badly for chalk may be that "pores" in chalk rather than being concave tend to be convex (and thus very hard to model).

Aspect ratio models, though, have the benefit that they are flexible and relatively easily provide a function fitting a given data set (Fig. 3.3). This makes them useful for applications linking logging information and seismic information. A recommended procedure is to begin with a given petrophyscial data set, and (1) do Gassmann fluid substitution to model the dry state, (2) do aspect ratio modelling in the dry state, and (3) fluid substitute back to natural state by Gassmanns equations. It should always be borne in mind that the modelled aspect ratios have little chance of conveying information on the pore texture. By contrast, grain-contact models give a relatively consistent picture of the relation between porosity, bulk modulus and degree of contact cement as expressed by Biot's coefficient.

The fact that chalk is not well depicted as solid calcite frame with ellipsoidal holes in it, can to some extent be remedied by assuming that only a fraction of the calcite constitutes the frame according to an upper Hashin Shtrikman bound (Hashin and Shtrikman 1963), whereas the remaining solid is in suspension and mixed with pore fluid according to a lower Hashin Shtrikman bound (Fig. 3.2). The degree to which the solid is part of the frame is named the iso-frame value, and when a rock is practically monomineralic as is the case for chalk, the isoframe value can be modelled from porosity and a single elastic velocity (typically v_P, (Fabricius 2003; Fabricius, Bächle et al. 2010). The iso-frame value thus gives a measure of cementation, and from the relation between porosity and iso-frame value it can be evaluated if the cementation is pore filling or is mainly contact cement. To use the iso-frame value to fit a data series with a single iso-frame value, it is necessary to introduce an upper critical porosity (Fabricius 2003), but the physical meaning is then largely lost.

Nomenclature

c = Kozenys factor
f_c = critical frequency, 1/t, MHz
G = shear modulus, m/Lt^2, GPa
G_{dry} = shear modulus drained, m/Lt^2, GPa
G_{sat} = shear modulus saturated, m/Lt^2, GPa
K = bulk modulus, m/Lt^2, GPa
K_{fr} = stiffness of the rock
K_{dry} = bulk modulus drained, m/Lt^2, GPa
K_{min} = elastic bulk modulus of the mineral, m/Lt^2, GPa
K_{oil} = bulk modulus of oil, m/Lt^2, GPa
K_{sat} = bulk modulus saturated, m/Lt^2, GPa
K_{water} = bulk modulus of water, m/Lt^2, GPa
K_ϕ = pore stiffness
M = compressional modulus, m/Lt^2, GPa
S_P = specific surface of pore space
S_w = water saturation
v_P = P-wave velocity, L/t
v_S = velocity, L/t
α = Biot's coefficient
η = fluid viscosity, M/Lt
ρ = density, m/L^3
ρ_{fl} = fluid density
ϕ = porosity

Subscripts

c = critical
dry = drained
fl = fluid
fr = rock frame
min = mineral
oil = oil
P = P-wave
S = shear
w = water
sat = fluid saturated state
ϕ = pore

Abbreviations

asp = aspect ratio of ellipsoidal pores
VSP = vertical seismic profiling

References

Al-Shuhail, A.A., 2007. Fracture-porosity inversion from P-wave AVOA data along 2D seismic lines: An example from the Austin Chalk of southeast Texas. *GEOPHYSICS*, **72** (1): B1–B7. January. URL http://dx.doi.org/10.1190/1.2399444.

Alam, M.M., Borre, M.K. et al., 2010. Biot's coefficient as an indicator of strength and porosity reduction: Calcareous sediments from Kerguelen Plateau. *Journal of Petroleum Science and Engineering*, **70** (3-4): 282–297. February. URL http://dx.doi.org/10.1016/j.petrol.2009.11.021.

Berryman, J.G., 1980. Long-wavelength propagation in composite elastic media II. Ellipsoidal inclusions. *The Journal of the Acoustical Society of America*, **68** (6): 1820. June. URL http://dx.doi.org/10.1121/1.385172.

Biot, M. and Willis, D., 1957. The elastic coefficients of theory of consolidation. *J. Appl Elastic Coefficients of the Mech*, **24**: 594–601. URL http://www.math.purdue.edu/~santos/research/Lucas_2014/biot_willis_J_Ap_Mech_57.pdf.

Biot, M.A., 1941. General Theory of Three-Dimensional Consolidation. *Journal of Applied Physics*, **12** (2): 155–164. URL http://dx.doi.org/http://dx.doi.org/10.1063/1.1712886.

Biot, M.A., 1956. General solutions of the equations of elasticity and consolidation for a porous material. *J. appl. Mech*, **23** (1): 91–96.

Engstrøm, F., 1992. Rock mechanical properties of Danish North Sea chalk. In *Proceedings of 4th North Sea chalk symposium, Deauville*.

Fabricius, I.L., 2003. How burial diagenesis of chalk sediments controls sonic velocity and porosity. *AAPG bulletin*, **87** (11): 1755–1778. URL http://archives.datapages.com/data/bulletns/2003/11nov/1755/1755.htm?doi=10.1306%2F06230301113.

Fabricius, I.L., Bächle, G.T., and Eberli, G.P., 2010. Elastic moduli of dry and water-saturated carbonates — Effect of depositional texture, porosity, and permeability. *GEOPHYSICS*, **75** (3): N65–N78. May. URL http://dx.doi.org/10.1190/1.3374690.

Fabricius, I.L., Baechle, G. et al., 2007. Estimating permeability of carbonate rocks from porosity and $v_p?v_s$. *GEOPHYSICS*, **72** (5): E185–E191. September. URL http://dx.doi.org/10.1190/1.2756081.

Gassmann, F., 1951. Über die elastizität poröser medien: Vier. der Natur. *Gesellschaft Zürich*, **96**: 1–23. URL http://sepwww.stanford.edu/sep/berryman/PS/gassmann.pdf.

Gommesen, L. and Fabricius, I.L., 2001. Dynamic and static elastic moduli of north sea and deep sea chalk. *Physics and Chemistry of the Earth, Part A: Solid Earth and Geodesy*, **26** (1-2): 63–68. January. URL http://dx.doi.org/10.1016/S1464-1895(01)00024-2.

Gommesen, L., Fabricius, I.L. et al., 2007. Elastic behaviour of North Sea chalk: A well-log study. *Geophysical Prospecting*, **55** (3): 307–322. May. URL http://dx.doi.org/10.1111/j.1365-2478.2007.00622.x.

Hashin, Z. and Shtrikman, S., 1963. A variational approach to the theory of the elastic behaviour of multiphase materials. *Journal of the Mechanics and Physics of Solids*, **11** (2): 127–140. March. URL http://dx.doi.org/10.1016/0022-5096(63)90060-7.

Henriksen, A., Fabricius, I. et al., 1999. Core Density Scanning and Mechanical Properties of limestone in the Copenhagen Area. *Quarternary Journal of Engineering Geology*, **32**: 107–117. URL http://www.forskningsdatabasen.dk/catalog/108097203.

Hill, R., 1952. The elastic behaviour of a crystalline aggregate. *Proceedings of the Physical Society. Section A*, **65** (5): 349. May. URL http://dx.doi.org/10.1088/0370-1298/65/5/307.

Japsen, P., Bruun, A. et al., 2004. Influence of porosity and pore fluid on acoustic properties of chalk: AVO response from oil, South Arne Field, North Sea. *Petroleum Geocience*, **10** (4): 319–330. October. URL `http://dx.doi.org/10.1144/1354-079303-586`.

Japsen, P., Høier, C. et al., 2002. Effect of fluid substitution on ultrasonic velocities in chalk plugs, South Arne field, North Sea. In *SEG Technical Program Expanded Abstracts 2002*, 1881–1884. Society of Exploration Geophysicists. January. URL `http://dx.doi.org/10.1190/1.1817056`.

Katika, K., Addassi, M. et al., 2015. The effect of divalent ions on the elasticity and pore collapse of chalk evaluated from compressional wave velocity and low-field Nuclear Magnetic Resonance (NMR). *Journal of Petroleum Science and Engineering*, **136**: 88–99. December. URL `http://dx.doi.org/10.1016/j.petrol.2015.10.036`.

Mavko, G., Mukerji, T., and Dvorkin, J., 2009. *The Rock Physics Handbook*. 2nd ed., Cambridge University Press. Isbn: 9780521861366. URL `http://dx.doi.org/10.1017/cbo9780511626753`.

Nermoen, A., Korsnes, R.I. et al., 2015. Extending the effective stress relation to incorporate electrostatic effects. In *2015 SEG Annual Meeting*, 3239–3243. Society of Exploration Geophysicists, Society of Exploration Geophysicists. August. URL `http://dx.doi.org/10.1190/segam2015-5891149.1`.

Olsen, C., Christensen, H.F., and Fabricius, I.L., 2008. Static and dynamic Young's moduli of chalk from the North Sea. *GEOPHYSICS*, **73** (2): E41–E50. March. URL `http://dx.doi.org/10.1190/1.2821819`.

Olsen, C., Hedegaard, K. et al., 2008. Prediction of Biot's coefficient from rock-physical modeling of North Sea chalk. *GEOPHYSICS*, **73** (2): E89–E96. March. URL `http://dx.doi.org/10.1190/1.2838158`.

Risnes, R., 2001. Deformation and yield in high porosity outcrop chalk. *Physics and Chemistry of the Earth, Part A: Solid Earth and Geodesy*, **26** (1-2): 53–57. January. URL `http://dx.doi.org/10.1016/S1464-1895(01)00022-9`.

Røgen, B., Gommesen, L., and Fabricius, I.L., 2004. Methods of velocity prediction tested for North Sea chalk: a review of fluid substitution and v_S estimates. *Journal of Petroleum Science and Engineering*, **45** (1-2): 129–139. November. URL `http://dx.doi.org/10.1016/j.petrol.2004.04.003`.

Saberi, M.R., Johansen, T.A., and Talbot, M.R., 2009. Textural and burial effects on rock physics characterization of chalks. *Petroleum Geoscience*, **15** (4): 355–365. October. URL `http://dx.doi.org/10.1144/1354-079309-836`.

Chapter 4

Geochemistry

Harald Johansen

4.1 Introduction

4.1.1 Data sources and methods

The geochemistry of chalk has two major aspects: the solids (mineralogy) and their contained fluids (phases and composition). Several petrophysical properties (e.g. porosity, permeability, grain size, texture) are in addition of major importance for the geochemical behavior of the solids. When it comes to the fluids, the various phases (gas, water, oil) may show highly variable compositions (hydrocarbon molecules and cations, anions and neutral species that are dissolved in the formation water). The total geochemical characteristics of the chalk system is finally the geohistorical sum of all fluid-rock interactions, and the fluid flow in and out of the chalk system. Geochemical information is mainly collected from the following sources:

- Core and drill chip material
- Fluids extracted from core material
- Fluid and solid data from experiments conducted on core and analogue rock
- Fluid samples obtained during drilling
- Test fluids
- Produced fluids

Wireline log data will in addition give complementary information about fluid composition and properties. This class of data is however of a much more indirect nature, but it provides an important opportunity to view direct geochemical data in a geometrical context, and also to generalize and upscale geochemical information.

A very great part of the knowledge and data comes from the North Sea chalk fields, where a great number of cores and fluid samples have been obtained over the years. There is clearly a bias in this knowledge, in the sense that non-productive chalk elsewhere in the world is strongly under represented, when it comes to chalk evolution during burial. The study of outcrop chalk is the alternative, but this source of information is also biased, because uplift and secondary processes in this connection has resulted in alteration of the chalk mineralogy, petrophysics and fluid content.

4.2 Chalk evolution during burial

4.2.1 Burial and diaprism

Bjørlykke and Høeg (1997) presented a thorough discussion of the effects of burial diagenesis on stresses, compaction and fluid flow in sediments in general, and also included a discussion on chalk behavior. One feature that makes the burial of North Sea chalks somewhat special is the simultaneous operation of salt diapirism (Jensenius and Munksgaard 1989). These authors discussed the importance of large scale hot water migration around salt diapirs and their impact on diagenesis and compaction of chalk reservoirs. A similar discussion is also given by Davison, Alsop et al. (2000) and in Carruthers, Cartwright et al. (2013). Mallon and Swarbrick (2008) studied the diagenetic characteristics of low permeability, non-reservoir chalks from the Central North Sea, and pointed out the much better porosity preservation of oil-bearing chalk. Andresen (2012) discussed how we can get feedback from the study of fluid flow features in hydrocarbon plumbing systems, and what we can learn about basin evolution.

The most important driving force for the geochemical evolution of the chalk system is compaction and subsidence of the sedimentary layers. Increased temperature, pressure and stress, and the contact with fluids that originated elsewhere in the sedimentary basin will continuously offset the chemical and mechanical equilibria that would otherwise be established. This promotes various types of fluid-rock interaction. The texture, as well as its chemo-mechanical properties, makes chalk respond in a rather characteristic way to burial. Tectonic and structural geologic events in the basin (halokinesis, faulting, fracturing) will also have a superimposed effect on the geochemical evolution.

4.2.2 Chalk compaction - chemomechanical processes

Several investigations have been dedicated to the combined chemical and mechanical compaction of chalk sediments, and the relation to pressure evolution (Bjørlykke and Høeg 1997; Bolås, Hermanrud et al. 2008; Mallon and Swarbrick 2008, 2002; Croizet, Renard et al. 2013). Also, Liteanu, Spiers et al. (2013) discussed the influence of water and supercritical CO_2 on the failure behavior of chalk.

Chalk is a fairly soft material close to the seabed and shortly after deposition. In contrast to shaly materials, the mechanical strength may change markedly close to the sea bottom due to diagenetic processes (recrystallization; hardground formation). During further burial the control on chalk petrophysics will be more and more controlled by diagenetic effects, which become important already before the first kilometer of burial. This is in strong contast to siliciclastic sediments, which retain a dominantly mechanical porosity control during the first 2 km of burial. Pressure solution in chalk would, if it was allowed to operate unaffected by other important depositional or basinal processes, in most cases eliminate economically important porosity before 2 km burial depth. Sedimentary slumping, and the early introduction of hydrocarbon fluids, are two such processes that has strongly offset the "normal" compaction behavior of chalk. Overpressure is another mechanism that inhibit chalk compaction. The enhanced textural rigidity, and the reduced water content from hydrocarbon filling, cause a major retardation of diagenetic processes. This has strongly helped the preservation of porosity and permeability in chalk.

4.2.3 Chalk compaction - thermal control

Another difference between carbonate rocks like chalk on one hand, and siliciclastic sediments on the other, is the response to burial and temperature increase. Siliciclastics do mainly show prograde mineral solubility (increased solubility at higher temperatures), while carbonates behave in a retrograde fashion to increased temperature. This has an important effect of counteracting pressure solution, which would otherwise be even stronger than what is observed. The grain size effect of chalk (extremely small coccolith sub-plates) is the most important driving force for chalk recrystallization (pressure enhanced dissolution), due to the very high surface energy of micron- to submicron particles. The elimination of the smallest crystals by dissolution, and the coupled precipitation of larger crystals (crystal ripening) is a way to reduce the energy of the chalk system. The strong thermal influence on porosity reduction assumed for siliciclastics, is therefore not necessarily of the same importance for chalk sediments. Temparture is on the other hand of importance for the rate of diagenetic processes, so even if its ability to offset equilibria in chalk is less important than in siliciclastics, increased temperature will have the overall effect of accelerating the approach towards equilibrium.

4.3 Chemical compaction

4.3.1 Reservoir chalk

Mallon and Swarbrick (2008); Bolås, Hermanrud et al. (2008) addressed the relation between diagenetic processes and chalk reservoir quality, and made comparisons with the diagenetic behavior of low permeability, non-reservoir chalks from the Central North Sea.

The chemical (diagenetic) compaction of the carbonate grains in chalks is mainly influenced by these factors:

- Depositional mineralogy
- Grain/crystallite size

- Effective stress
- Salinity
- Pore water origin and composition
- CO_2 partial pressure

The effective stress is important in the sense that it controls the extent of microscale strain of particles, and their associated enhanced tendency for dissolution and recrystallization (compaction creep). The salinity of the formation water plays an important role because it increases the solubility of the carbonate minerals. Formation water salts that are introduced to the chalk system by fluid flow from external sediments, may on the other hand introduce both super- or undersaturation of the water with respect to carbonate minerals, depending on the concentration of Ca, Mg, Fe and carbonate species of the external formation water.

Stylolites are frequently observed in high numbers in chalks and other limestones. They represent a special kind of fracture, which is normally (but not always) subparallell to the bedding. Dissolution at stylolites is particularly effective if the stylolites are communicating with a larger scale, more vertically oriented fracture system, that can aid in the transport of reacted fluids away from the stylolite surface, and thus maintain the dissolution rate at the stylolite. The importance of fractures will be discussed in more detail in section 4.6

4.3.2 Non-reservoir chalk

Studies of pelagic chalks that have not been exposed to early infilling of hydrocarbons have revealed that the most frequent mode of these chalk type is a completely tight lithology, that can serve as vertical seals over large distances on the scale of basins. It is thus clear, that chalks that have not been exposed to early infilling of hydrocarbons have revealed that the most frequent mode of these chalk type is a completely tight lithology, that can serve as vertical seals over large distances on the scale of basins. It is thus clear, that chalks may not always be hydrocarbon reservoir rocks. This may be due to the original depositional process (slumped versus pelagic chalk), it may be due to the absence of fractures to aid the migration of hydrocarbon fluids into the chalk system, or it may be due to tectonic structuration of the basin that has not provided pathways from source rocks to potential chalk reservoirs. It may also be that the timing of maturation and migration has been too late, relative to porosity reducing reactions in the potential reservoir section. Early arrival of hydrocarbons into the structure would have the opposite effect, by reduction of the rate of diagenetic reactions, and consequently on porosity reduction.

4.4 Diagenesis and reservoir quality

4.4.1 Matrix porosity

The matrix porosity of chalk consists mainly of the interstices between tiny (submicron) coccolith platelets, that has been subjected to various degrees of mechanical and diagenetic compaction. A typical chalk reservoir rock at a burial depth between 2 and 4 km, would possess a grain matrix with very narrow pore apertures, even in the cases where a fair amount of total porosity has been preserved. These tiny pore throats have a tremendous effect on the matrix permeability of such chalks, which only rarely exceed a few milidarcies. The effective flow rate of hydrocarbons out of the matrix porosity, and the desired introduction of injection fluids and chemicals into the same pore system, to produce an effective sweep of hydrocarbons, is a major limitation to the global oil production rate from chalks, even when it is fractured.

4.4.2 Fracture porosity and porous networks

The importance of fractures as agents of enhanced large scale permeability is very large. Odling, West et al. (2013) discussed the fractional flow in fractured chalk based on experiences from flow and tracer tests.

Potential chalk reservoir sediments may be fractured for various reasons: overpressure release by hydraulic fracturing; fracturing driven by tectonic forces; or due to the uprising flow of salt. All three mechanisms are probably relevant for North sea chalk reservoirs. Fracture networks serve a wide range of functions, both during natural geologic processes, and also during injection of fluids and production of hydrocarbons or other fluids:

- Fractures aid hydrocarbon migration into reservoirs

- Fractures cause leakage out of reservoirs
- Fractures stimulate stylolite processes and other porosity reducing mechanisms
- Fractures increase the hydrocarbon storage capacity for hydrocarbons or other fluids
- Fractures provide large scale communication between injectors, interior reservoir and producers

The fracture porosity in itself may be small, compared with the matrix porosity, but when it comes to the effective large scale porosity, as observed by the quantities of produced fluids, the fracture porosity may play a much more important role than indicated by its actual volume. Dual porosity regimes is commonly considered and/or applied during reservoir modeling for chalk lithologies.

The ability of fractures to influence geochemistry on a large scale, as well as the productivity of fluids, depends on the relation between the stress regime, which controls fracture aperture, orientation, length, and the connectivity between individual fractures. En echelon shear fractures (secondary tension gashes) may for instance contribute very little to overall geochemical homogenization.

The total pore networks that need to be considered for geochemical evolution is strongly scale dependent. On the nano-micro scale (matrix porosity) we must consider the coccolith platelet grains, as well as silca and clay minerals in the same size class. Pore throats on this scale is typically on the order of tens to hundreds of nanometers, rendering pore fluids to be almost stagnant, at least on the timescale of human operations. The next scale of interest is the very largest pores (vugs, tension gashes and other small fractures). These contribute little to overall porosity, and may also be of limited geochemical importance, because they may be dependent on the matix porosity for larger scale communication. Fracture networks that contain individual fractures in the decimeter, meter, to tens of meter scale is the next element in the porous network hierarchy. At least on the geological time scale, these elements are the reasons way geochemical fluid compositions commonly show homogeneity, even on the larger scale.

4.4.3 Environments for carbonate diagenesis

Chalk (and other carbonate sediments) undergoes various degrees of diagenetic modification, which is largely dependent on their coexisting formation fluids, and the characteristic sedimentary environment that controls bot fluid composition and dynamics (local pore water regime). Potential water types include:

- normal Createaceous seawater
- meteoric water
- residual brines (evaporated seawater)
- evaporate brines (diapirs)
- external formation water (from other lithologies)

Various hydrocarbon fluids and non-hydrocarbon natural gases may also be present. The geological environments that are typically associated with the various water types includes (but are not limited to):

- seabed hardgrounds
- meteoric invasion zones
- sabkha reflux brines
- diapiric environments
- basin compactional regime

The coccolith particles are typically low Mg calcite, which are the least reactive carbonate minerals in the seawater environment. In the meteoric regime, all kinds of minerals will be variously influenced by dissolution, while the other formation water types may show so large chemical variation, that it is impossible to generalize about chemical stability or unstability. The typical thermal influence on carbonate stability, is that when all other factors are kept constant, the mineral become more stable with increasing temperature

4.4.4 Open or closed system diagenesis

Relatively thick chalk sequences are normally considered to be closed systems relative to the introduction of external fluids (maybe except gas), because of the extremely low matrix permeability. The exception is fractured chalk, which in many cases are effective conduits for non-chalk fluids. With reference to the discussion above on the dual porosity properties of fractured chalk, it is nevertheless questionable how large proportion of a fractured chalk that will become geochemically influenced by external fluids. Open system diagenesis usually results in much more recrystallization and porosity reduction than closed systems. One important feature is that pervasive stylolitization due to communication with extensive fracture networks, may cause a substantial amount of local reservoir compartmentalization. Early filling of hydrocarbons is open system behavior with respect to this fluid, but causes the opposite effect relative to aqueous fluids, by reducing the water phase communication and the diagenetic reactivity.

4.4.5 Silica diagenesis

Silica in chalk is a very frequent occurrence, and it may be manifest in many different ways: as discrete beds; as nodules (flint) or as more scattered quartz crystals. The silica is in most cases the polymorph α-quartz. The origin of the silica is however debated. Two of the most contrasting opinions are, on one hand an origin by subsurface recrystallization of biogenic silica (mainly sponge spicules), while on the other hand an origin by α-quartz deposition, which is a completely different mechanism. While the silica in itself is rarely a type of feature that affects the petrophysical properties of the chalk very strongly, its origin is of potential great interest as a stratigraphical marker, if it can be demonstrated that the silica is deposited as its present α-quartz polymorph.

4.5 Fluid evolution during burial

Published fluid data from chalk is not very common. Egeberg and Aagaard (1989) made a compilation of North Sea formation waters, including some samples from chalk fields, and Bjørlykke and Gran (1994) made a similar compilation of salinity data from North Sea wells, based both on direct water samples, and also from wireline log data. Apart from that, Egeberg and Saigal (1991): (cementation of fractures); Smalley, Lønøy et al. (1992): (Spatial $^{87}Sr/^{86}Sr$ variations in formation water and calcite) and Barnes and Worden (1998): (groundwater sources and movement using water chemistry and tracers), discussed the relation between fluid and mineral data in relation to studies of chalk diagenesis.

4.5.1 Pore water evolution

The water present during chalk deposition is Cretaceous to Early Tertiary seawater. The composition of this seawater is essentially not known, but it is assumed that its major element chemistry was not radically different from that of present day seawater. The evolution of marine waters during the first 1–2 km of burial is poorly documented due to the paucity of water samples from economic drilling in this depth range. Egeberg and Aagaard (1989) and Warren and Smalley (1994) has reported a large amount of formation water data from reservoirs in the North Sea area (both Norway and UK), and a subset of these water samples are collected from chalk reservoirs. These data show some very significant enrichment and depletions in comparison with present day seawater. These differences could in principle be partly explained by the differences between present an past seawaters, but an explantion involving burial diagenesis seems to be much more important. Mg, K and especially SO_4 is depleted, while elements like Na, Sr, Ba, Cl and Br are enriched. Alkalinity is also moderately enriched. $\delta^{18}O$ values are also strongly enriched, while δD values are depleted. Sr isotope values are normally just a little bit above the values expected from Cretaceous seawater, but in some deeper parts of the chalk in the Ekofisk area of the North Sea, significantly higher values are found in more marly chalks.

The knowledge about chalk pore water evolution thus has a wide gap concerning processes at intermediate (0–2 km) burial depths. Knowledge about the depositional environment, and the final water compositions at large depths, provide an opportunity for some deductions concerning the complete burial evolution. Sulphate is probably depleted very early in the burial history, close to the sea bottom, due to bacterial sulphate reduction. Mg is most likely depleted due to a limited amount of dolomitization of the chalk matrix. K is most likely spent by fixation and illitization of kaolinite and smectites, which occur in minor amounts in the more marly chalk horizons. The enrichments in Na, Cl and Br is most likely caused by fracture conducted flow of water from salt diapirs beneath the chalk and into the chalk intervals. The enrichments of Sr and Sr isotopes could also partly be explained by these mechanisms, but internal chalk processes involving calcite and clay diagenesis could also give the relevant contributions for these two indicators.

4.5.2 Content of natural gas and liquid hydrocarbons in chalk

The natural gases from reservoirs in the chalk reservoirs in the North Sea area are not significantly different from those in siliciclastic reservoirs. Neither the hydrocarbon gas, nor the CO_2 or H_2S content are very much different from those from non-chalk reservoirs. The low H_2S content is perhaps somewhat surprising, given the very low content of Fe in the chalks. High temperature hydrocarbon bearing limestones with a low amount of Fe-bearing minerals are commonly fairly H_2S rich, presumably due to thermochemical sulphate reduction (TSR). The low H_2S content of gas from the chalk fields in the Southern North Sea suggests that TSR is not a very important process, even though the contact with evaporate waters are very well documented. The hydrocarbon organic geochemistry of the chalk reservoirs do not show any significant differences when compared with hydrocarbons found in siliciclastic reservoirs.

4.6 Fluids in fractures

Very little is known about fluids in fractured chalk based on direct sampling or observations. Most knowledge is obtained from natural solid samples Egeberg and Saigal (1991), from observations on outcrop samples Richard and Sizun (2011), from fluid inclusion studies of fracture minerals Jensenius and Munksgaard (1989), from experimental studies Liteanu, Spiers et al. (2013); Monzurul Alam, Leth Hjuler et al. (2014); Puntervold and Austad (2008), or from tracer tests Hartmann, Odling et al. (2007).

4.6.1 Fractured chalk and the healing of fractures

The fractures in chalk reservoirs are in some cases partly or completely sealed by mineral precipitation. Studies on the geochemistry of vein minerals and fluid inclusions have shed light both on the timing of deformation, and on the nature of fluids that have been flowing through these fractures (Egeberg and Saigal 1991; Jensenius and Munksgaard 1989). The timing is commonly rather late in the burial history, and the mineralogy and fluids witness transport of non-chalk components into the reservoir (celestite, anhydrite, sulphides, oil, salts). It has been suggested Jensenius and Munksgaard (1989) from fluid inclusion homogenization temperatures and from stable isotope data that very hot (up to 130°C) fluids have been circulating in chalk reservoirs that are presently no warmer than 95°C. Egeberg and Saigal (1991) argued against this view on the basis of petrography, stable isotopes and heat modeling. Open system behavior has however been documented for both salts and $\delta^{13}C$ values of vein minerals. The cements in fractures are thus very valuable recorders of the composition and source of ancient fluids that have migrated in the fractures.

The mechanism of fracture cementation is of particular interest. Cooling of fluids that has migrated up fractures is not a viable cause of precipitation, as the retrograde behavior of calcite would tend to keep Ca and CO_2/HCO_{3-} in solution. A more likely mechanism would be the "champagne effect", whereby CO_2 degassing upon pressure drop due to fracturing would cause an increase in pH, and subsequent calcite precipitation. There are also other viable mechanisms for fracture cementation: one is the migration of water along stylolite planes down pressure gradients to the junctions with vertical fractures, where precipitation could occur due to degassing. Another possibility is the dilution of highly saline water from diapirs with less saline chalk pore water, which would also reduce the solubility of calcite.

4.7 Fluid behavior during production

The main sources for the understanding of fluid evolution and behavior during production are found in:

- Egeberg and Aagaard (1989); Warren and Smalley (1994): on analysis of co-produced formation water
- Hamouda, Karoussi et al. (2008); Taibi, Duperret et al. (2009); Zahid, Sandersen et al. (2011): on interpretation of water flooding behavior
- Andersen, Evje et al. (2012); Høgnesen, Standnes et al. (2006): on experiments combined with simulation

4.7.1 Reservoir connectivity and compartmentalization

Smalley, Lønøy et al. (1992) demonstrated that fluid flow and diagenetic reactions in the Ekofisk area chalks are influenced by underlying high salinity water, probably originating by dissolution of Zechstein diapiric salts. Downward gradients towards higher salt content and $^{87}Sr/^{86}Sr$ values of formation water were identified, and it was also recognized that the youngest chalk interval (Ekofisk Fm) was much less influenced by this external source, due to a field-wide barrier (The Ekofisk Tight Zone), where salinities and Sr isotope values are much more in line with assumed Cretaceous seawater values.

4.7.2 Fluid-rock interaction during production with seawater injection

The overall effects of seawater injection on oil productivity from chalk is considered to be positive, but there are also potentially negative side effects, such as enhanced compaction and scale precipitation. Compaction is a positive effect in the sense that it facilitates pressure maintenance, but is a negative effect in the sense that wells and infrastructure may be damaged. The ideal composition of injection water is still debated.

The content of Mg and SO_4 in seawater has been demonstrated to increase the degree of water wetting of the chalk matrix, which results in an improved microscopic sweep effect. The same seawater ions have for a long time been known to inhibit the growth of dolomite and low-Mg calcite. Distilled water has been shown to enhance the chalk strength, most likely because the absence of Mg and SO_4 allows Mg containing carbonates to precipitate, especially at high temperatures as a consequence of the retrograde solubility of carbonates. Quite a few important questions relevant to the short term flow characteristics and stability of chalk are thus not satisfactorily answered:

- What is the exact relation between wettability and water chemistry at various temperatures?
- Is chalk dissolution or recrystallization favorable for flow and sweep in chalks?
- Will there be more or less matrix compaction if produced water is reinjected?
- Will there be more or less scale precipitation if produced water is reinjected?
- What will be the impact from fluid rock interactions on the monitorability of chalks during production, if produced water is reinjected, or if injection water is modified in other ways?

4.7.3 Fluid tracing during production

A practical application of the research on Sr isotope behavior in chalk and its formation water is that reservoir zonation can be mapped prior to production from analyses of core material, residual salt Sr isotope analysis (SrRSA) (Smalley, Lønøy et al. 1992), and that the Sr isotopes of later produced water can also be used to monitor cross formational flow and injection water breakthrough. A particular useful combination for monitoring is the use of SrRSA in conjunction with injected water tracers. Such an application has been demonstrated for a non-chalk North Sea reservoir (Munz, Johansen et al. 2010). The value of this application can be further enhanced by the use of other water chemistry data from produced water, which can allow the deduction of mixing proportions, degree of reservoir interaction, sweep, and scale prediction. It has been shown (Munz, Johansen et al. 2010) that Sr isotope data can be used to identify the effect of operational changes (shut-in or opening of wells), and also that it is possible to establish new time-dependant baselines for water monitoring if a third water component (reinjected production water) is mixed with the original injection water.

4.8 CO_2 storage and EOR in chalks

The idea of a combined effect of partial CO_2 storage and oil mobility enhancement in chalk by CO_2 injection has attracted a lot of interest (Holt, Lindeberg et al. 2009; Vega and Kovscek 2010; Alvarado and Manrique 2010; Gallo, Fillacier et al. 2011; Mendelevitch 2014).

4.8.1 Chalk reservoirs for CO_2 EOR and storage

CO_2 has been suggested as a potentially powerful injection fluid component for enhanced oil production, and it has also been suggested that depleted chalk fields could be high capacity sites for CO_2 storage. Many of the same questions that were phrased and discussed in Sec. 4.7.2 are of relevance also for the consideration of CO_2 use or storage in chalks.

4.8.2 CO_2 mobility and EOR effect

CO_2 injection for EOR is commonly assumed to be used in a WAG mode. A very special issue is the low viscosity and high mobility of supercritical CO_2, compared with water. It it thus probable that a significant part of the CO_2 would bypass the chalk matrix, and only circulate in the porous network of fractures. If this happens, a very large amount of CO_2 will be produced during each cycle, and will have to be separated and reinjected a very high number of times.

4.8.3 CO_2 driven fluid-rock interaction

If CO_2 EOR injection should have a significant impact on oil recovery, the ability of this fluid to contact the chalk matrix must be improved. The use of surfactants (foams) has been suggested as a means of facilitating this. A potential negative effect of better matrix consistence with CO_2 (and water from WAG) is that enhanced dissolution of chalk matrix grains may occur, causing the same positive and/or negative effects as discussed in Sec. 4.7.2. CO_2 in contact with water dissolves and dissociates to H+ ions, which will very strongly affect the saturation index of calcite, promoting chalk dissolution.

4.8.4 Storage capacity of CO_2 in chalks

The potential success of obtaining a high storage capacity for CO_2 will to a large extent depend on the likelihood that a large proportion of the CO_2 will enter the matrix porosity, and not only the fracture porosity. The viscosity contrast may also represent a risk factor when it comes to CO_2 injectivity. Because the fracture network only constitutes a small fraction of the total porosity, pressure buildup may be very rapid and thus counteract injection, unless CO_2 injection is operated in such a mode that the utilization of the large matrix porosity is effectuated.

4.9 Summary and concluding remarks

This overview of selected geochemical topics is in particular addressing the behavior of chalk sediments that have a sufficiently high porosity and permeability to be of economic interest. Tight chalks are probably much more frequent than porous chalks, so this discussion has a fairly strong bias towards the less frequent chalk properties that allows some chalk locations to be very valuable hydrocarbon reservoirs. The tight chalks that owe their properties to less favorable geological processes, serves the purpose as a reference for comparison with porous chalks. The focus of this chapter is also biased towards the deeper part of the subsurface, again motivated by purely economic considerations. Finally the amount of knowledge on chalk behavior is also strongly biased in itself by the large amount of economic boreholes.

The geochemistry of chalk is fairly special compared with other sediment types, for several reasons:

- The almost monomineralic composition
- The very special grain morphologies and grain size distributions
- The very delicate textural patterns that are established in various depositional environments
- The rather fragile porous network system of chalks shortly after deposition
- The very high reactivity, related to fast kinetics of many important chemical reactions that affect carbonates in general, and chalk in particular
- The strongly contrasting petrophysical properties of tight chalks at deep burial, compared with chalks at similar depths, that for several important geochemical and geomechanical reasons have escaped the strong porosity reduction during deep burial.

Nomenclature

δD = isotope fraction deuterium
$\delta^{18}O$ = isotope fraction oxygen
$\delta^{13}C$ = isotope fraction carbon

Abbreviations

SrRSA = strontium isotope residual salt analysis
TSR = thermochemical sulphate reduction
WAG = water alternating gas

References

Alvarado, V. and Manrique, E., 2010. Chapter 8 - EOR's Current Status. In V.A. Manrique, ed., *Enhanced Oil Recovery*, 133–156. Gulf Professional Publishing, Boston. ISBN 978-1-85617-855-6. URL `http://dx.doi.org/http://dx.doi.org/10.1016/B978-1-85617-855-6.00014-0`.

Andersen, P., Evje, S. et al., 2012. A geochemical model for interpretation of chalk core flooding experiments. *Chemical Engineering Science*, **84** (0): 218–241. URL `http://dx.doi.org/http://dx.doi.org/10.1016/j.ces.2012.08.038`.

Andresen, K.J., 2012. Fluid flow features in hydrocarbon plumbing systems: What do they tell us about the basin evolution? *Marine Geology*, **332–334** (0): 89–108. Hydrocarbon leakage through focused fluid flow systems in continental margins. URL `http://dx.doi.org/http://dx.doi.org/10.1016/j.margeo.2012.07.006`.

Barnes, S. and Worden, R.H., 1998. Understanding groundwater sources and movement using water chemistry and tracers in a low matrix permeability terrain: the Cretaceous (Chalk) Ulster White Limestone Formation, Northern Ireland. *Applied Geochemistry*, **13** (2): 143–153. URL `http://dx.doi.org/http://dx.doi.org/10.1016/S0883-2927(97)00072-3`.

Bjørlykke, K. and Gran, K., 1994. Salinity variations in North Sea formation waters: implications for large-scale fluid movements. *Marine and Petroleum Geology*, **11** (1): 5–9. URL `http://dx.doi.org/http://dx.doi.org/10.1016/0264-8172(94)90003-5`.

Bjørlykke, K. and Høeg, K., 1997. Effects of burial diagenesis on stresses, compaction and fluid flow in sedimentary basins. *Marine and Petroleum Geology*, **14** (3): 267–276. URL `http://dx.doi.org/http://dx.doi.org/10.1016/S0264-8172(96)00051-7`.

Bolås, H.M.N., Hermanrud, C. et al., 2008. Is stress-insensitive chemical compaction responsible for high overpressures in deeply buried North Sea chalks? *Marine and Petroleum Geology*, **25** (7): 565–587. URL `http://dx.doi.org/http://dx.doi.org/10.1016/j.marpetgeo.2008.01.001`.

Carruthers, D., Cartwright, J. et al., 2013. Origin and timing of layer-bound radial faulting around North Sea salt stocks: New insights into the evolving stress state around rising diapirs. *Marine and Petroleum Geology*, **48** (0): 130–148. URL `http://dx.doi.org/http://dx.doi.org/10.1016/j.marpetgeo.2013.08.001`.

Croizet, D., Renard, F., and Gratier, J.P., 2013. Compaction and porosity reduction in carbonates: A review of observations, theory, and experiments. *Advances in Geophysics*, **54**: 181–238. URL `http://dx.doi.org/10.1016/B978-0-12-380940-7.00003-2`.

Davison, I., Alsop, I. et al., 2000. Geometry and late-stage structural evolution of Central Graben salt diapirs, North Sea. *Marine and Petroleum Geology*, **17** (4): 499–522. URL `http://dx.doi.org/http://dx.doi.org/10.1016/S0264-8172(99)00068-9`.

Egeberg, P.K. and Aagaard, P., 1989. Origin and evolution of formation waters from oil fields on the Norwegian shelf. *Applied Geochemistry*, **4** (2): 131–142. URL `http://dx.doi.org/http://dx.doi.org/10.1016/0883-2927(89)90044-9`.

Egeberg, P.K. and Saigal, G.C., 1991. North Sea chalk diagenesis: cementation of chalks and healing of fractures. *Chemical Geology*, **92** (4): 339–354. URL `http://dx.doi.org/http://dx.doi.org/10.1016/0009-2541(91)90078-6`.

Gallo, Y.L., Fillacier, S. et al., 2011. Technical challenges in characterization of future {CO2} storage site in a deep saline aquifer in the Paris basin. Lessons learned from practical application of site selection methodology. *Energy Procedia*, **4** (0): 4599–4606. 10th International Conference on Greenhouse Gas Control Technologies. URL `http://dx.doi.org/http://dx.doi.org/10.1016/j.egypro.2011.02.419`.

Hamouda, A.A., Karoussi, O., and Chukwudeme, E.A., 2008. Relative permeability as a function of temperature, initial water saturation and flooding fluid compositions for modified oil-wet chalk. *Journal of Petroleum Science and Engineering*, **63** (1–4): 61–72. URL `http://dx.doi.org/http://dx.doi.org/10.1016/j.petrol.2008.10.002`.

Hartmann, S., Odling, N.E., and West, L.J., 2007. A multi-directional tracer test in the fractured Chalk aquifer of E. Yorkshire, {UK}. *Journal of Contaminant Hydrology*, **94** (3–4): 315–331. URL `http://dx.doi.org/http://dx.doi.org/10.1016/j.jconhyd.2007.07.009`.

Høgnesen, E.J., Standnes, D.C., and Austad, T., 2006. Experimental and numerical investigation of high temperature imbibition into preferential oil-wet chalk. *Journal of Petroleum Science and Engineering*, **53** (1–2): 100–112. URL `http://dx.doi.org/http://dx.doi.org/10.1016/j.petrol.2006.04.002`.

Holt, T., Lindeberg, E., and Wessel-Berg, D., 2009. EOR and CO2 disposal - Economic and capacity potential in the North Sea. *Energy Procedia*, **1** (1): 4159–4166. Greenhouse Gas Control Technologies 9 Proceedings of the 9th International Conference on Greenhouse Gas Control Technologies (GHGT-9), 16–20 November 2008, Washington DC, USA. URL `http://dx.doi.org/http://dx.doi.org/10.1016/j.egypro.2009.02.225`.

Jensenius, J. and Munksgaard, N.C., 1989. Large scale hot water migration systems around salt diapirs in the Danish Central Trough and their impact on diagenesis of chalk reservoirs. *Geochimica et Cosmochimica Acta*, **53** (1): 79–87. URL `http://dx.doi.org/http://dx.doi.org/10.1016/0016-7037(89)90274-3`.

Liteanu, E., Spiers, C.J., and de Bresser, J.H.P., 2013. The influence of water and supercritical {CO2} on the failure behavior of chalk. *Tectonophysics*, **599** (0): 157–169. URL `http://dx.doi.org/http://dx.doi.org/10.1016/j.tecto.2013.04.013`.

Mallon, A.J. and Swarbrick, R.E., 2002. A compaction trend for non-reservoir North Sea Chalk. *Marine and Petroleum Geology*, **19** (5): 527–539. URL `http://dx.doi.org/http://dx.doi.org/10.1016/S0264-8172(02)00027-2`.

Mallon, A.J. and Swarbrick, R.E., 2008. Diagenetic characteristics of low permeability, non-reservoir chalks from the Central North Sea. *Marine and Petroleum Geology*, **25** (10): 1097–1108. URL `http://dx.doi.org/http://dx.doi.org/10.1016/j.marpetgeo.2007.12.001`.

Mendelevitch, R., 2014. The role of CO2-EOR for the development of a {CCTS} infrastructure in the North Sea Region: A techno-economic model and applications. *International Journal of Greenhouse Gas Control*, **20** (0): 132–159. URL `http://dx.doi.org/http://dx.doi.org/10.1016/j.ijggc.2013.11.007`.

Monzurul Alam, M., Leth Hjuler, M. et al., 2014. Petrophysical and rock-mechanics effects of {CO2} injection for enhanced oil recovery: Experimental study on chalk from South Arne field, North Sea. *Journal of Petroleum Science and Engineering*, **122** (0): 468–487. URL `http://dx.doi.org/http://dx.doi.org/10.1016/j.petrol.2014.08.008`.

Munz, I.A., Johansen, H. et al., 2010. Water flooding of the Oseberg Øst oil field, Norwegian North Sea: Application of formation water chemistry and isotopic composition for production monitoring. *Marine and Petroleum Geology*, **27** (4): 838–852. URL `http://dx.doi.org/http://dx.doi.org/10.1016/j.marpetgeo.2009.12.003`.

Odling, N.E., West, L.J. et al., 2013. Fractional flow in fractured chalk; a flow and tracer test revisited. *Journal of Contaminant Hydrology*, **147** (0): 96–111. URL `http://dx.doi.org/http://dx.doi.org/10.1016/j.jconhyd.2013.02.003`.

Puntervold, T. and Austad, T., 2008. Injection of seawater and mixtures with produced water into North Sea chalk formation: Impact of fluid-rock interactions on wettability and scale formation. *Journal of Petroleum Science and Engineering*, **63** (1–4): 23–33. URL `http://dx.doi.org/http://dx.doi.org/10.1016/j.petrol.2008.07.010`.

Richard, J. and Sizun, J.P., 2011. Pressure solution-fracturing interactions in weakly cohesive carbonate sediments and rocks: Example of the synsedimentary deformation of the Campanian chalk from the Mons Basin (Belgium). *Journal of Structural Geology*, **33** (2): 154–168. URL `http://dx.doi.org/http://dx.doi.org/10.1016/j.jsg.2010.11.006`.

Smalley, P.C., Lønøy, A., and Råheim, A., 1992. Spatial $^{87}Sr/^{86}Sr$ variations in formation water and calcite from the Ekofisk chalk oil field: implications for reservoir connectivity and fluid composition. *Applied Geochemistry*, **7** (4): 341–350. URL `http://dx.doi.org/http://dx.doi.org/10.1016/0883-2927(92)90024-W`.

Taibi, S., Duperret, A., and Fleureau, J.M., 2009. The effect of suction on the hydro-mechanical behaviour of chalk rocks. *Engineering Geology*, **106** (1–2): 40–50. URL `http://dx.doi.org/http://dx.doi.org/10.1016/j.enggeo.2009.02.012`.

Vega, B. and Kovscek, A.R., 2010. 4 - Carbon dioxide (CO_2) sequestration in oil and gas reservoirs and use for enhanced oil recovery (EOR). In M.M. Maroto-Valer, ed., *Developments and Innovation in Carbon Dioxide (CO_2) Capture and Storage Technology*, vol. 2 of *Woodhead Publishing Series in Energy*, 104–126. Woodhead Publishing. ISBN 978-1-84569-797-6. URL `http://dx.doi.org/http://dx.doi.org/10.1533/9781845699581.1.104`.

Warren, E.A. and Smalley, P.C., eds., 1994. *North Sea Formation Waters Atlas*. 15. Geological society memoir (london) ed., Geological Society.

Zahid, A., Sandersen, S.B. et al., 2011. Advanced waterflooding in chalk reservoirs: Understanding of underlying mechanisms. *Colloids and Surfaces A: Physicochemical and Engineering Aspects*, **389** (1–3): 281–290. URL `http://dx.doi.org/http://dx.doi.org/10.1016/j.colsurfa.2011.08.009`.

Chapter 5

Fluids

Roman Berenblyum

5.1 Introduction

This chapter provides an overview of fluids found in petroleum reservoirs and, specifically, chalks. Here the main goal is to familiarize the reader with types of fluids saturating a reservoir and an interaction between the fluids and the rock. The chapter focuses on the fluids as such leaving the aspects of the fluid flow to the other parts of the manuscript.

It is important to state that the term "fluid" represents anything saturating the reservoir pore space. Similar to other reservoirs, fluids saturating chalks could be divided into two large groups based on their origin: hydrocarbon fluids and brines. Hydrocarbon fluids in the reservoir could be in gaseous (commonly referred as "gas") or liquid ("oil") phase. The majority of hydrocarbons in the reservoir is, due to the non-polar nature, has very low solubility in aqueous phase. Brines are solutions of various salts in water. Brines are commonly referred to as an aqueous or water phase which is almost immiscible with oil. Interfacial tension between the water and hydrocarbon phases usually varies from approximately 72 dyne/cm for water/gas systems to 20 to 40 dyne/cm for water/oil systems.

In the early days of oil and gas development in a vast majority of cases, it was assumed that fluids neither interacted with themselves nor with reservoir rock. Porous media was considered unchanged through the reservoir lifetime. Hence the definition of "static" modelling in relation to geological modelling. The importance of chemical compositions of fluids and rock and their interaction came to attention relatively recently. It is important to stress that each reservoir is a complex chemical system in equilibrium (potentially local or partial) comprised of rock minerals, hydrocarbons, water with dissolved salts and microbiological cultures. Changing condition during production phase and especially introducing new fluids with different composition (CO_2 or other gasses or solvents, brines of different salt compositions, salinity, and microorganisms, chemicals for water comformance, etc.) would disturb the balance of this system. Such changes could result in, for example, scale formation due to water incompatibility and mixing (Lindlof and Stoffer 1983; Jordan 2009), chalk weakening (Sylte, Thomas et al. 1999; Austad, Strand et al. 2008), wettability alteration (Austad, Strand et al. 2008), souring (Burger, Jenneman et al. 2006). This chapter would scratch the surface of these processes leaving details to corresponding chapters in this manuscript.

5.2 Hydrocarbon fluids in place

This section assumes that a reader is familiar with basic concepts of phase state and phase diagrams. Details on which may be found in Hillert (2007) and Pedersen, Christensen et al. (2006).

Hydrocarbon fluids are complex mixtures of various hydrocarbons, that in a single or in a two phase state. In either case the reservoir could initially be classified as oil (liquid) with or without gas cap or gas with or without oil rim. For initially single phase reservoirs the classification as black or volatile oil and gas or gas condensate reservoir is obviously based on the phase state (liquid or gaseous) of an original fluid. For two-phase fluids it is the initial volume of each of the phases that will define the reservoir as a gas with an oil rim or an oil with a gas cap. The initial state of the reservoir and fluid composition plays vital role in defining the development strategy. Phase diagram in P, T coordinates with phase envelopes for typical reservoir types and a compositional path to normal conditions are shown in **Fig. 5.1**. Fluids with critical points (a point on a corresponding phase envelope) to the left of initial conditions IC are initially single phase liquids (oil reservoirs), the ones with critical point to the right are initially single phases gases. If, for example, the fluid described by a blue phase envelope and classified as a single phase oil reservoir at initial conditions IC would have been found at lower initial pressure $IC1$ it would form a single gas phase reservoir.

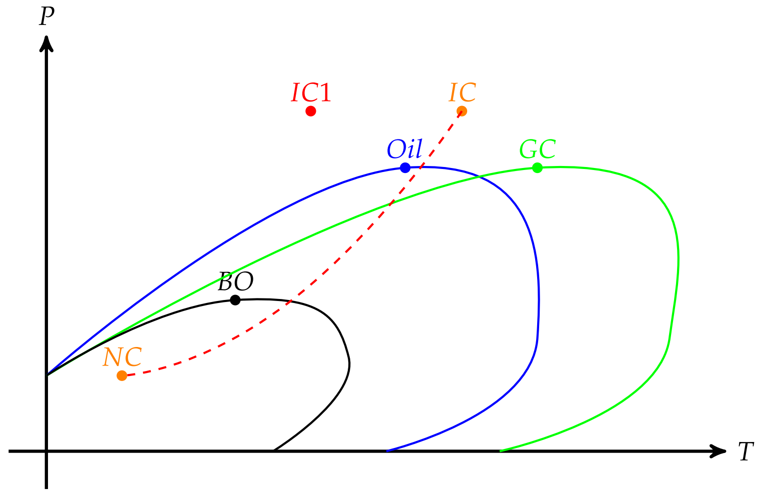

Figure 5.1: A sketch showing phase diagrams in P-T coordinates for Blackoil (BO) in black, Volatile oil (VO) in blue and gas condensate (GC) in green together with compositional production path from initial reservoir conditions (IC) to normal conditions (NC). Dots on phase diagrams correspond to location of critical point.

Fig. 5.2 shows a phase diagram for an initially two-phase reservoir. The phase envelope for initial compositions of oil (blue) and gas (green) phases intersect at initial conditions IC illustrating two fluids at equilibrium.

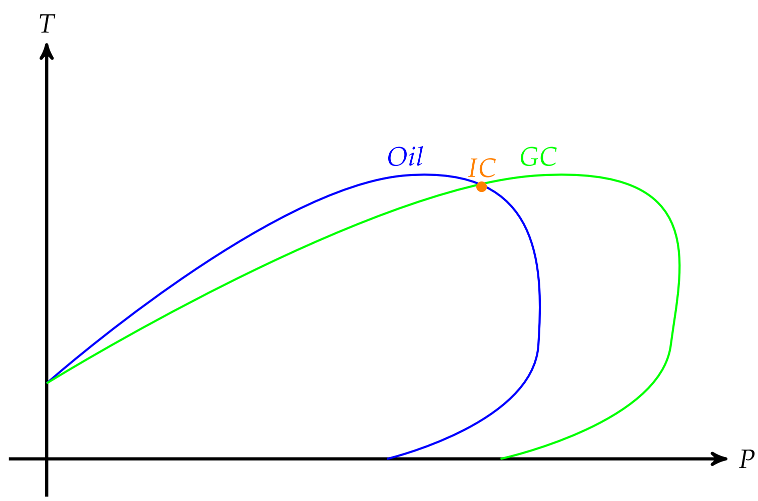

Figure 5.2: A sketch showing phase diagram in P-T coordinates for an initial two-phase reservoir. Blue phase envelope for oil phase and green for gas phase intersect at initial conditions IC as both fluids are originally at equilibrium.

The diagrams in Figs. 5.1 and 5.2 show phase envelopes for a number of hydrocarbon mixtures each of those with a defined and affixed composition. In reality, however, pressure and temperature gradients as well as gravity would cause hydrocarbon components to segregate as a function of depth (Muskat 1930; Whitson and Brulé 2000). Compartmentalisation (especially one occurred during migration process), vertically isolated (or partially isolated) reservoirs could also be a cause for a significant compositional variations in the reservoir prior to production start (Høier and Whitson 2001).

As the reservoir undergoes development processes and pressure declines, not necessarily on average in the whole reservoir, but most importantly in the vicinity of the production wells, the second phase may appear, increase or decrease in volume or totally disappear again. While appearance or increase of the second phase with pressure decline is rather obvious behavior, its decrease or disappearance often causes confusion.

Such *retrograde* effects need to be discussed in more detail and are illustrated in **Fig. 5.3**. The PVT diagram is representative of initially single phase gas condensate reservoir. The solid black line in Fig. 5.3 shows the two phase envelope, while dashed lines are, essentially, representing "topography" of fluid precipitated in two phase zone. The orange line shows the change in fluid composition from initial conditions point IC to final conditions FC. For ease of understanding the retrograde effects the path is simplified assuming constant temperature (isothermal) conditions in the reservoir followed by further depressurisation and cooling in the infrastructure system. During depressurisation from IC to point A the original fluid remains single phase gas. As pressure continues to decline from A to B the fluid is exhibiting expected growth in an amount of liquid phase precipitated. Further on from B to C the retrograde effects could be observed. As pressure declines our compositional path crosses the "topography" lines with decreasing liquid content illustrating condensate dissolution back into the gaseous phase. In extreme cases (illustrated here on the figure) all fluid could dissolve back to form single phase gas at low pressures.Whitson and Brulé (2000) is recommended for more information on retrograde effects.

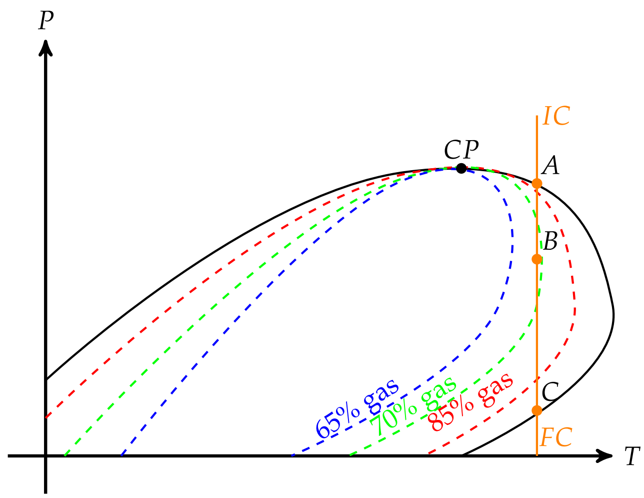

Figure 5.3: A sketch showing phase diagram of a reservoir fluid in P-T coordinates, it's critical point (black dot) and lines of constant liquid precipitation (dotted ones). Blue line indicates compositional path of the fluid exhibiting retrograde effects from initial conditions to normal conditions

Understanding initial fluid state and possible phase changes is very important in order to properly develop the asset and avoid loosing otherwise recoverable reserves. For gas condensate reservoirs, for example, formation of condensate bank around production wells as pressure declines could cause both significant decline of wells productivity (due to decrease of gas saturation and, therefore, mobility) and loss of valuable condensate as an immobile fluid in the low pressure areas. For oil reservoirs formation of gas in lower pressure zones may result in high gas-oil ratio and decrease in oil recovery rate.

The PVT experiments could be separated into four main groups:

- Conventional PVT measurements aimed at determining original composition: Separator test, Constant Composition (or Mass) Expansion - CCE or CME, Differential Liberation - DL and Constant Volume Depletion - CVD;
- Extended study necessary for evaluation of gas injection process: Swelling test, Slimtube experiment, Forward and Backward injection tests;
- Asphaltene and wax precipitation study;
- Hydrate formation study.

Conventional PVT measurements are necessary for any type of reservoir fluids regardless of expected production scenario as they provide basic insight into the volumetric behavior of the system. Extended study is carried out when gas injection is planned, such that the behavior of the various mixtures of the reservoir fluid with the injected gas may also be studied. If the hydrates or hydrocarbon solids were detected in the production wells or initial reservoir state, low temperature, high asphaltene and/or wax content of original reservoir fluid, indicate such risk an additional studies need to be carried out. Here conventional and extended experiments are briefly introduced and the main experimental results are presented. The experiments schematics and layout are presented based on the assumption that an oil sample is studied. For each individual project a detailed laboratory plan must be developed.

5.2.1 Conventional PVT measurements

Differential Liberation

This isothermal experiment starts at reservoir temperature and bubble point pressure. During the differential liberation experiment the pressure is declined in stages below the saturation pressure, see **Fig. 5.4**, modified from Whitson and Brulé (2000). After each stage of pressure reduction all gas is removed from the cell and the next stage of the pressure reduction is conducted. Oil shrinkage and gas volumes liberated are reported. Gas composition and properties (density, viscosity) at each stage and oil composition at the final stage are reported. The experiment mimics the depletion process in the oil reservoir.

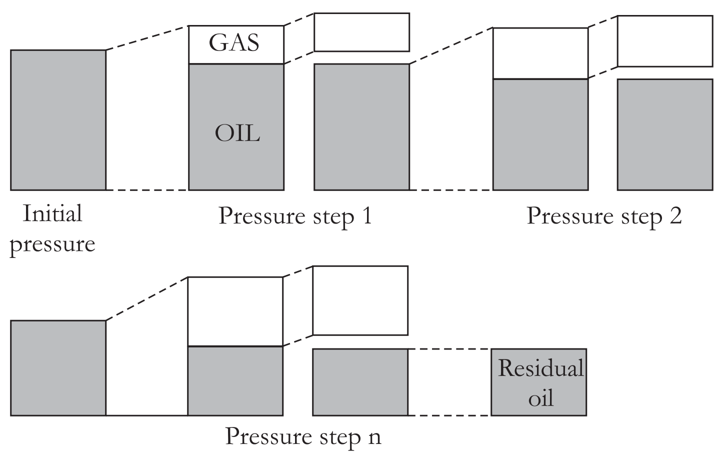

Figure 5.4: Differential liberation schematics

Constant Mass Expansion / Constant Composition Expansion

The experiment starts at reservoir conditions. While temperature is kept constant pressure is reduced in steps. The mass and the composition in the PVT cell remains constant, as the PVT cell remain closed through out the experiment. The volumes are reported relative to the volume at saturation pressure. The experiment is designed to reproduce fluid system behavior during flow through the well neglecting the effects of the heat losses. Gas and oil compositions are reported at the end of experiment. The schematic of the process is shown in **Fig. 5.5**, modified from Whitson and Brulé (2000).

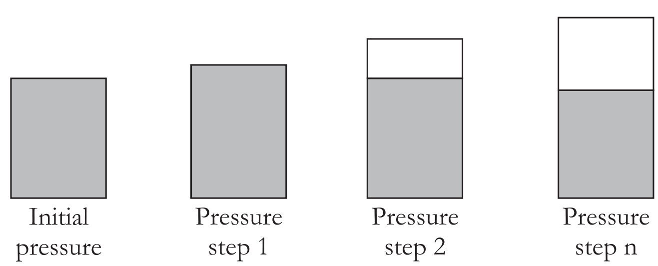

Figure 5.5: CME/CCE schematics

Separator test

Reservoir fluid is brought from reservoir to the surface conditions in a number of designed separator stages at specified T and P. Schematics of the process is shown in **Fig. 5.6**, modified from Whitson and Brulé (2000). During the separator test T, P and composition changes at each experiment step. The test is important for optimising the performance of the separators. Fluids properties and compositions are reported at each step.

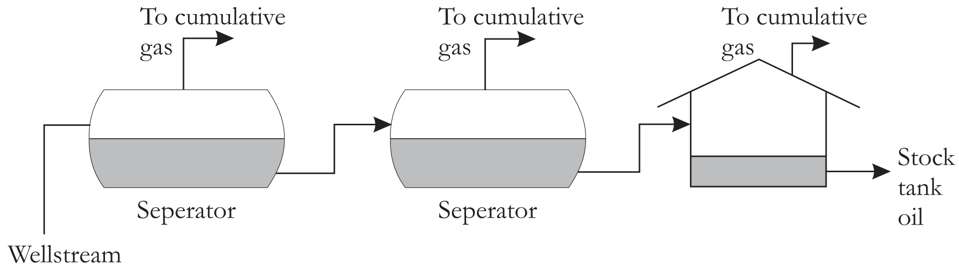

Figure 5.6: Separator test schematics

5.2.2 Solid phase

Appearance of the solid hydrocarbon phase is either due to formation of waxes or asphaltenes (Pedersen, Christensen et al. 2006) or as a result of hydrate formation (Whitson and Brulé 2000). Precipitation of heavy hydrocarbons would occur mostly due to the depressurisation process and may be induced by gas injection. The problem of hydrocarbon solid phase precipitation is not limited to heavy oil as one may naturally assume, but may also be very pronounced for light oils. Heavier oils would typically contain larger amounts of potential solids compared to the lighter ones, however solubility of solids in them is significantly higher as increase of light component concentration decreases miscibility of heavier ones. Light oils may have relatively low content of potentially precipitating hydrocarbons with virtually equal initial and precipitation pressures. Decline in reservoir pressure may cause precipitation of those solids causing permeability damage close to the producers. As pressure continue to decline and gas liberates from oil decrease in light components in liquid hydrocarbon phase would stabilise or cause some of the solid phase to dissolve back. To screen and evaluate potential and scale of solid hydrocarbon phase precipitation a set of experimental studies to determine wax appearance temperature at different pressures and asphaltene precipitation should be conducted (Pedersen, Christensen et al. 2006).

Hydrate formation would mostly affect gas transport systems, where low temperatures and small moisture contents causing formation of "snowlike" or "slush" reducing or completely plugging the pipelines. Interested reader should look into Pedersen, Christensen et al. (2006); Whitson and Brulé (2000) for details on types of hydrates, laboratory study and modelling approaches.

5.3 Brines

Water is always presented in the reservoir as a free phase (trapped water as a result of primary migration) and as an equilibrium moisture in hydrocarbon gas mixtures. In free form, as a result of establishing geochemical equilibrium with rock, the aqueous phase is represented by mixtures of large number of salts dissolved in water i.e. brines. Overall salinity, pH, and ion composition of both reservoir brines and water available for injection can range significantly from fresh, see (Advameg 2015) for example of compositions, to seawaters (Dittmar 1884). The formation and seawater compositions as wells as their various mixtures could, for example, be found in Puntervold and Austad (2008). The chemical interactions caused by mixing of waters with different compositions may lead to a number of effects in the reservoir or production tubing. While some of those effects (scale formation, for example) are fairly well understood, others, like "smart water" lacks a definition.

5.4 Fluids of IOR processes

Most common increased oil recovery fluid is water, followed by hydrocarbon gas and various chemical solutions. Both water and gas are initially present in the reservoir. However, injected fluids would typically differ in composition, creating a range of challenging engineering tasks discussed in this section.

5.4.1 Water injection

Water is the most common substance on Earth. Its composition however, types and concentration of salts (inorganic, or non-hydrocarbon components) dissolved in the water may significantly vary from fresh water of rivers in lakes to brines or salt water of underground aquifers or oceans.

Mechanical preparation on water has long become a standard procedure in thne oil and gas industry. The water is routinely cleaned and treated prior to injection or dumping from the production site (Bradley 1987). Mechanical preparation should, however be a first step in the process of tuning water properties to a particular reservoir. Chemical and microbiological composition of the water should also be treated with care.

Chemical composition of the water may significantly vary depending on the source of fluid. Formation water is in equilibrium with other fluids and reservoir rock as it has been in contact with them over geological time. Introducing water with other chemical composition will cause the equilibrium to cease and may result in a number of various processes, especially in rather chemically reactive carbonates. Water weakening, as a consequence of fluid-reservoir rock interaction in the pore, has been shown to dependen on water composition. Research carried out at UiS (Heggheim, Madland et al. 2004; Austad, Strand et al. 2008) showed seawater to cause at least twice as much weakening as distilled water. Precipitation of inorganic solids due to interaction of seawater containing sulphate (SO_4^{2-}) and carbonate (CO_3^{2-}) with formation water containing barium, calcium or magnesium, or even dissolution of reservoir rock calcium, would cause blockage of both pore space or tubing and installation and pipelines depending on where the two waters mix. An example of compositional differences between the formation and seawater are given in (Puntervold and Austad 2008). The scale could be prevented by squeeze treatments (Mackay and Sorbie 1999), permanent line injecting (Schlumberger 2015), adding inhibitor to injection fluid (Mackay 2005) or mechanically removed by cleaning, brushing and milling the wellbore. Millions of US dollars could be spent per well (Frampton, Craddock et al. 2002) as a direct consequence of such precipitation. The effect from injecting water with different chemical compositions may not, however, only be negative. "Smart water" or water with controlled physical-chemical properties can significantly increase oil recovery. While the mechanism for smart water applications still is debatable, the effect for carbonates seems to be associated with temperature and mineralogy (RezaeiDoust, Puntervold et al. 2009). Alteration of chemical composition by introduction of various silicates to water could also aid in water conformance control (Skrettingland, Giske et al. 2012; Stavland, Jonsbråten et al. 2011).

Microbiology is a subject that is not addressed above and seldom is investigated in the industry in general is changes to the reservoir microbial communities. Although some studies in the last few years have focused on microbial communities, there have been few in-depth investigations of the role of the microorganisms and of the changes which occur following reservoir flooding with seawater or other fluids. Some of the indigenous reservoir microorganisms have persisted in these environments over a geological timescale, others have evolved in more recent years in response to changes in the in-situ conditions following human activity. The introduction of fluids which may have altered in-situ acidity (pH), temperatures, ions, and oxygen content, as well as possible injection of minerals and nutrients, have all contributed to generating changes in reservoir conditions, in turn triggering changes in the microbial community structure and abundance. In addition, organisms originating for seawater, from animal or human sources may have been introduced in the reservoir, resulting in new populations adapting and competing inside the reservoir.

It has been well documented (Lazar, Petrisor et al. 2007; Brown 2010; Kaster, Hiorth et al. 2012; Youssef, Simpson et al. 2013) that many microorganisms could have a positive effect on oil recovery through the production of chemicals such as polymers, surfactants, solvents, or through the microbial biomass itself. Stimulating microbial activity or introducing key organisms to the reservoir could be used to increase oil recovery. It is also natural to suspect that some of microbial communities may have negative effect on oil recovery.

Many organisms, known as Sulfate Reducing Bacteria (SRB) have also been shown (Tabari, Tabari et al. 2011)to be a source of serious reservoir souring problems, due to their over-stimulation in the reservoir, often following injection of fluids. Therefore understanding reservoir microorganisms, their activity in the reservoir, and how the communities change during the oil recovery process, are important to both prevent souring and corrosion in the reservoir and boost oil recovery. With recent developments in molecular biology and metagenomics over the last decade, important questions related to the microorganisms and their functions should be addressed.

5.4.2 Gas injection

Natural gas liberated from recovered oil or produced as a free phase could be re-injected. Re-injection of produced gas, which is a fraction of produced fluid, can not compensate for the overall pressure loss, therefore the WAG (Water-Alternate-Gas) process or topping up gas with one available from other sources is required. Hydrocarbon gases from other near-by fields, nitrogen, CO_2, and even air, for oxidation process, could also be injected. Determining composition of initial and injected fluids and their interaction is of crucial importance the for gas injection process, and should be tested in a set of laboratory experiments.

Extended experiments need to be carried out to understand interaction of injected gas and reservoir fluid. One of the key parameters is the *Minimum Miscibility Pressure* (MMP). For the three-component systems, MMP could be found from the positions of oil and gas composition relative to the critical tie-line (Whitson and Brulé 2000; Pedersen, Christensen et al. 2006). For multicomponent systems, however, the solution is either to simplify the system to three component case. Or, alternatively to use a definition based on experimental observation of a breakpoint on recovery vs. pressure diagram for a set of slimtube experiment. Or, in cases where a breakpoing could not be clearly determined, selevt the pressure at which 95% recovery is reached.

The slimtube experiment is conducted in a packed thin and long tube (Whitson and Brulé 2000) essentially representing 1D flow and minimising viscous and gravity fingering. The slimtube is saturated with original reservoir fluid and is displaced by large volumes of gas in question until no oil is produced, at several different pressures. Recovery vs. pressure is then plotted on a diagram similar to the one sketched in **Fig. 5.7** and the MMP is determined.

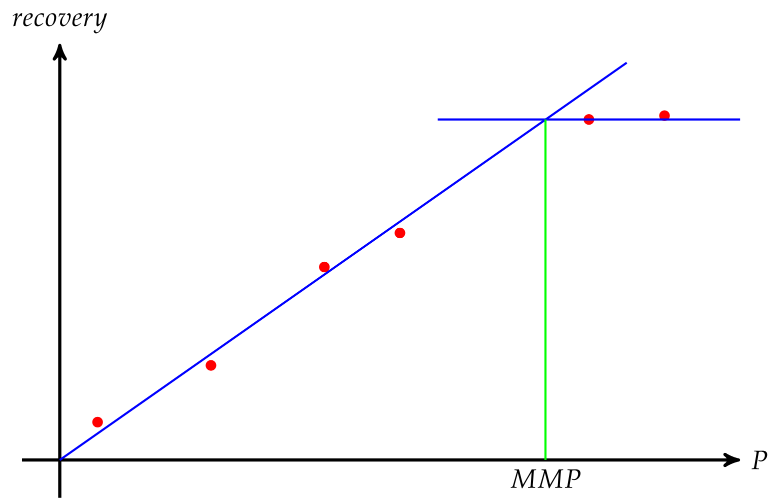

Figure 5.7: A sketch showing experimental points (red dots) on recovery vs. pressure diagram and straight lines drawn to determine MMP.

Swelling tests provide a way to measure PVT behavior of the various mixtures of original reservoir fluid with injected gas. Typical procedure includes mixing injection gas with reservoir oil in different proportions, bringing the mixture to single phase state by pressurising it and conducting CME experiment on it. The mixture vary from 10-20 mol% of gas, single phase mixture is typically liquid phase when pressurised, to high gas content up to and above 200%, being single phase gas when pressurised. It is important to have the mixture switch from liquid to gas in pressurised single phase if conditions allow for it. Behavior of resulting hydrocarbon mixture at each pressure is studied in a set of standard PVT experiments.

Forward and backward contact tests are not always conducted during an extended study. During the forward test equilibrium gas after each step is removed and mixed with new portion of reservoir oil. Forward test studies the vaporising-gas, miscible displacement. Flowing gas phase extracts hydrocarbon components from the reservoir oil while travelling through the reservoir. The enriched gas might reach full miscibility with reservoir oil. This experiment also shows to which extent gas should be enriched to be miscible with oil.

The backward test monitors the condensing drive mechanism, when reservoir oil composition is enriched with gas components. After each experimental step equilibrium liquid is removed and contacted by fresh injected gas. During the backward test the miscibility may also develop between altered reservoir oil and injected gas.

Schematics of both processes is shown in **Fig. 5.8**. Forward and backward contact test are seldom performed as a part of the extended study. However, these experiments may provide additional insight into PVT behavior of the system and the condensing a vaporising gas drive mechanisms.
If the miscibility conditions are established a gas injection strategy needs to be chosen: up- or down-dip, flank, WAG, SWAG (Simultaneous Water-Alternate-GAS) or FAWAG (Foam Assisted WAG) .

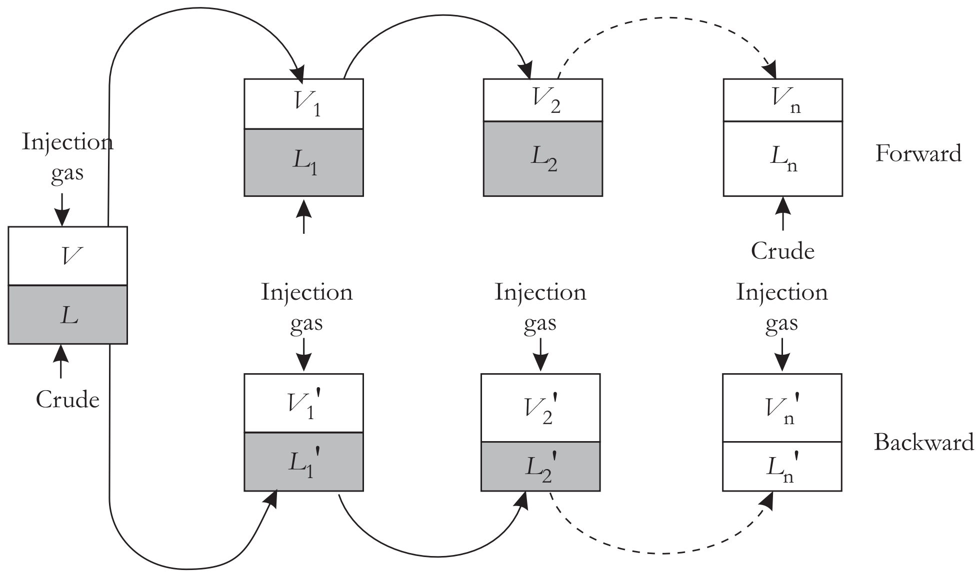

Figure 5.8: Schematics of forward and backward tests.

CO_2

While CO_2 often exhibits the lowest miscibility pressure with liquid hydrocarbons compared to hydrocarbon gases after separation, or to nitrogen, its application to EOR has several additional aspects:

- CO_2 at reservoir conditions is often in a supercritical state exhibiting fluid-like densities with gas-like viscosities.
- CO_2 is miscible in aqueous phase with concentration as high as 4–5%. As dissolved carbon dioxide concentration increase, the water gets heavier and sinks to the bottom of the formation, creating additional mixing and increasing the amount of CO_2 to be dissolved in aqueous phase.
- While hydrocarbon gas during vaporising gas drive evaporates light to medium hydrocarbons from the liquid phase, CO_2 evaporates components up to C_{30} (Whitson and Brulé 2000).
- Aqueous solution of CO_2 acts as a weak acid:

$$\mathrm{CO}_{2,aq} + \mathrm{H}_2 0 \rightarrow 2\mathrm{H}^+ \mathrm{CO}_3^{2-}$$

  Lowering acidity or pH will cause mineral dissolution. High concentration of CO_2, especially close to the injection point could cause significant damage to the rock structure and possible, the well collapse.

5.5 Reservoir information from fluids

Reservoir fluids may give more knowledge about the reservoir itself. Tracers are used to investigate flow paths, well connectivity and sweep (Bradley 1987). Tracers are also used to evaluate efficiency of IOR/EOR techniques (Dugstad, Viig et al. 2013) and well flow profile (Sira and Bjørnstad 2013). Composition and temperature of produced water may serve as a tracer and help better understand distribution of the fluid flow to and from the wells. Analysis of a well history including pressure transients can provide description of dynamics of well-reservoir parameters and their interaction during flowing and shut-in periods (Shchipanov, Kollbotn et al. 2011). In some cases this analysis gives unique opportunity to highlight impact of geological features like natural fracture networks and faults on reservoir fluid flow that may otherwise be undetectable. The value of such analysis is continuously increasing due to installation of Permanent Downhole Gauges (PDGs) in wells and progress in PDG interpretation approaches (Shchipanov, Berenblyum et al. 2014).

5.6 Summary

Hydrocarbon fluids may be present in the reservoir as liquid or gaseous phases with potential for solid precipitation. Phase effects and phase transformation could cause either loss of productivity and resources, precipitating solids, condensate banking, high gas-oil ratio, or could be used to enhance oil recovery, gas, including CO_2 injection.

The aqueous phase cannot be considered a single phase with constant composition. Chemical interaction between injected and reservoir fluids as well as with reservoir rocks could cause significant complications and financial losses, for example, scale precipitation, chalk water weakening, corrosion, souring, or could be used to boost and increase recovery, for example water conformance control; "smart water" and MEOR processes.

An in-depth laboratory study of reservoir and injection fluids, their interaction with each other and the reservoir rock may be needed.

Nomenclature

L = liquid
P = pressure, m/Lt^2
T = temperature, T
V = vapor

Abbreviations

CCE = constant composition expansion
CME = constant mass expansion
CVD = constant volume depletion
DL = differential liberation
FAWAG = foam assisted water-alternate-gas
MMP = minimum miscibility pressure
PDG = permanent downhole gauges
PVT = pressure volume temperature
SRB = sulfate reducing bacteria
SWAG = simultaneous water-alternate-gas
WAG = water-alternate-gas

References

Advameg, I., 2015. Water Encyclopedia. URL `http://www.waterencyclopedia.com/En-Ge/Fresh-Water-Natural-Composition-of.html`.

Austad, T., Strand, S. et al., 2008. Seawater in Chalk: An EOR and Compaction Fluid. *SPE Reservoir Evaluation & Engineering*, **11** (04): 648–654. Society of Petroleum Engineers. doi:10.2118/118431-PA. August. URL `http://dx.doi.org/10.2118/118431-PA`.

Bradley, H.B., ed., 1987. *Petroleum Engineering Handbook*. Society of Petroleum Engineers. ISBN 1-55563-010-3. URL `https://www.osti.gov/biblio/5770327`.

Brown, L.R., 2010. Microbial enhanced oil recovery (MEOR). *Current Opinion in Microbiology*, **13** (3): 316–320. Ecology and industrial microbiology * Special section: Systems biology. URL `http://dx.doi.org/10.1016/j.mib.2010.01.011`.

Burger, E.D., Jenneman, G.E. et al., 2006. Forecasting the Effect of Produced Water Reinjection on Reservoir Souring in the Ekofisk Field. Paper NACE-06661 presented at CORROSION 2006. 12–16 March. URL `https://www.onepetro.org/conference-paper/NACE-06661`.

Dittmar, W., 1884. Report on researches into tne composition or ocean water collected oy H. Mv. o. Chullenger 1873–76. Sci. Res. Voyage "Challenger", 1873–76. *Chem Phys*, **1**: 1–211.

Dugstad, Ø., Viig, S. et al., 2013. Tracer monitoring of enhanced oil recovery projects. *EPJ Web of Conferences*, **50**. 28 May. URL `http://dx.doi.org/10.1051/epjconf/20135002002`.

Frampton, H., Craddock, H.A. et al., eds., 2002. *Chemistry in the Oil Industry VII*. Royal Society of Chemistry. URL `http://dx.doi.org/10.1039/9781847550460`.

Heggheim, T., Madland, M.V. et al., 2004. A chemical induced enhanced weakening of chalk by seawater. *Journal of Petroleum Science and Engineering*, 171–184.

Hillert, M., 2007. *Phase Equilibria, Phase Diagrams and Phase Transformations*. 2nd ed., Cambridge University Press. ISBN 9780511812781. Cambridge Books Online. URL http://dx.doi.org/10.1017/CBO9780511812781.

Høier, L. and Whitson, C.H., 2001. Compositional Grading –Theory and Practice. *SPE Reservoir Evaluation & Engineering*, **4** (06): 525–535. SPE-74714-PA. December. URL http://dx.doi.org/10.2118/74714-PA.

Jordan, M.M., 2009. The Modelling, Application, and Monitoring of Scale Squeeze Treatments in Heterogeneous Reservoirs, North Sea. In *SPE International Symposium on Oilfield Chemistry*. Society of Petroleum Engineers. SPE-121142-MS. URL http://dx.doi.org/10.2118/121142-MS.

Kaster, K.M., Hiorth, A. et al., 2012. Mechanisms Involved in Microbially Enhanced Oil Recovery. *Transport in Porous Media*, **91** (1): 59–79. URL http://dx.doi.org/10.1007/s11242-011-9833-7.

Lazar, I., Petrisor, I.G., and Yen, T.E., 2007. Microbial enhanced oil recovery (MEOR). *Petroleum Science and Technology*, **25** (11): 1353–1366. 27 November. URL http://dx.doi.org/10.1080/10916460701287714.

Lindlof, J.C. and Stoffer, K.G., 1983. A case study of seawater injection incompatibility. *Journal of Petroleum Technology*, **35** (07): 1–256. SPE-9626-PA. URL http://dx.doi.org/10.2118/9626-PA.

Mackay, E.J., 2005. Scale Inhibitor Application in Injection Wells to Protect Against Damage to Production Wells. When does it Work. In *SPE European Formation Damage Conference*. Society of Petroleum Engineers. URL http://dx.doi.org/10.2118/95022-ms.

Mackay, E.J. and Sorbie, K.S., 1999. An evaluation of simulation techniques for modelling squeeze treatments. In *SPE Annual Technical Conference and Exhibition*. Society of Petroleum Engineers, Society of Petroleum Engineers (SPE), Houston, Texas. SPE-56775-MS. 3–6 October. URL http://dx.doi.org/10.2118/56775-MS.

Muskat, M., 1930. Distribution of non-reacting fluids in the gravitational field. *Physical Review*, **35** (11): 1384. 1 June. URL http://dx.doi.org/10.1103/PhysRev.35.1384.

Pedersen, K.S., Christensen, P.L., and Shaikh, J.A., 2006. *Phase Behavior of Petroleum Reservoir Fluids*. 2nd ed., CRC Press Taylor & Francis Group. 465 pages. 18 December. URL https://www.google.com/books?hl=no&lr=&id=O-vKBQAAQBAJ&oi=fnd&pg=PP1&ots=sKpcMWB8WY&sig=iKNDBFK0VoYnX8OTHphQyGGaiNE.

Puntervold, T. and Austad, T., 2008. Injection of seawater and mixtures with produced water into North Sea chalk formation: Impact of fluid-rock interactions on wettability and scale formation. *Journal of Petroleum Science and Engineering*, **63** (1–4): 23–33. URL http://dx.doi.org/http://dx.doi.org/10.1016/j.petrol.2008.07.010.

RezaeiDoust, A., Puntervold, T. et al., 2009. Smart Water as Wettability Modifier in Carbonate and Sandstone: A Discussion of Similarities/Differences in the Chemical Mechanisms. *Energy and Fuels*, **23** (9): 4479–4485. 12 August. URL http://dx.doi.org/10.1021/ef900185q.

Schlumberger, 2015. URL http://www.glossary.oilfield.slb.com/en/Terms/s/scale$_$inhibitor.aspx.

Shchipanov, A., Berenblyum, R., and Kollbotn, L., 2014. Pressure Transient Analysis as an Element of Permanent Reservoir Monitoring. In *SPE Annual Technical Conference and Exhibition*. Society of Petroleum Engineers. SPE-170740-MS. URL http://dx.doi.org/10.2118/170740-MS.

Shchipanov, A.A., Kollbotn, L. et al., 2011. How to Account for Dynamic Fracture Behaviour in Reservoir Simulation. In *EAGE Workshop-Naturally & Hydraulically Induced Fractured Reservoirs–From NanoDarcies to Darcies*. 10 April. URL http://dx.doi.org/10.3997/2214-4609.20146791.

Sira, T. and Bjørnstad, T., 2013. Tracer based flow measurement. World International Property Organization (WIPO). Pub. No.: WO/2013/135861 Publication Date: 19.09.2013.

Skrettingland, K., Giske, N.H. et al., 2012. Snorre In-depth Water Diversion Using Sodium Silicate - Single Well Injection Pilot. Paper SPE 154004 presented at SPE Improved Oil Recovery Symposium, Tulsa, Oklahoma, USA. 14–18 April. URL http://dx.doi.org/10.2118/154004-MS.

Stavland, A., Jonsbråten, H.C. et al., 2011. In-Depth Water Diversion Using Sodium Silicate - Preparation for Single Well Field Pilot on Snorre. Paper presented at the 16th European Symposium on Improved Oil Recovery, Cambridge, UK. 12–14 April. URL `http://dx.doi.org/10.3997/2214-4609.201404788`.

Sylte, J.E., Thomas, L.K. et al., 1999. Water induced compaction in the Ekofisk Field. In *SPE Annual Technical Conference and Exhibition*. Society of Petroleum Engineers, Houston, Texas. SPE-56426-MS. 3-6 October. URL `http://dx.doi.org/10.2118/56426-MS`.

Tabari, K., Tabari, M., and Tabari, O., 2011. Investigation of Reservoirs Souring Reasons after Water Flooding. *Australian journal of basic and Applied Sciences*, **5**: 952–954.

Whitson, C.H. and Brulé, M.R., 2000. *Phase behavior*. SPE Monograph Series Vol. 20, Richardson, Texas.

Youssef, N., Simpson, D.R. et al., 2013. In-situ lipopeptide biosurfactant production by Bacillus strains correlates with improved oil recovery in two oil wells approaching their economic limit of production. *International Biodeterioration & Biodegradation*, **81**: 127–132. July. URL `http://dx.doi.org/10.1016/j.ibiod.2012.05.010`.

Chapter 6

Rock Mechanics

Tron Golder Kristiansen, Helle Foged Christensen, and Merete Vadla Madland

6.1 Introduction

Rock mechanics is presenting a framework for characterizing rock types to predict how the rock will deform and potential fail under various load conditions in the subsurface rock mass, or close to a wellbore. To characterize the rock it has to be brought to the rock mechanics laboratory and exposed to the load (stress) and the temperature the rock will experience in situ.

The load, or stress, is defined as the force acting on an area of the rock. In the laboratory the force is most often acting on the circumference or the ends of a cylindrical specimen. Cubic specimens are also used in some cases. To characterise a rock type from a rock mechanics point of view, one has to expose it to various combinations of stresses and measure the resulting deformations. In the laboratory this is typically done on a cylindrical specimen that is wrapped in a thin sleeve so that the confining pressure, usually provided from pressurizing a fluid surrounding the cylindrical circumference of the specimen, while the axial load is supplied by a piston driven by a hydraulic ram. See various examples of test setups on chalk in **Figs. 6.1 and 6.2**.

(a) (b) (c)

Figure 6.1: (a) Instrumentation of a chalk sample with strain gauges before a triaxial test, (b) Instrumentation of a cubic chalk specimen with strain gauges prior to a true 3D triaxial test, (c) Tensile test on chalk applying the Brazilian test (courtesy GEO).

In rock mechanics the stresses that dictate the magnitude of deformation or the failure of the rock is termed the effective stress. In its simplest form the effective stress is the total stress (force divided on the area of the rock) minus the pressure in the pores of the rock, the pore pressure. Depending on the microstructure of the rock, the effectiveness of the pore pressure to unload the grains in the matrix has to be corrected for. This is typically done by the use of an effective stress coefficient that theoretically has the magnitude in the range between the porosity of the rock and 1. In many rock mechanics calculations for weak rocks a good starting point is to assume an effective stress coefficient of 1. The effective stress coefficient is often referred to as the Biot coefficient (Biot 1941, 1955, 1956) to account for the deformability of the rock grains and for three-dimensional deformation:

$$\sigma' = S - \alpha P_p, \tag{6.1}$$

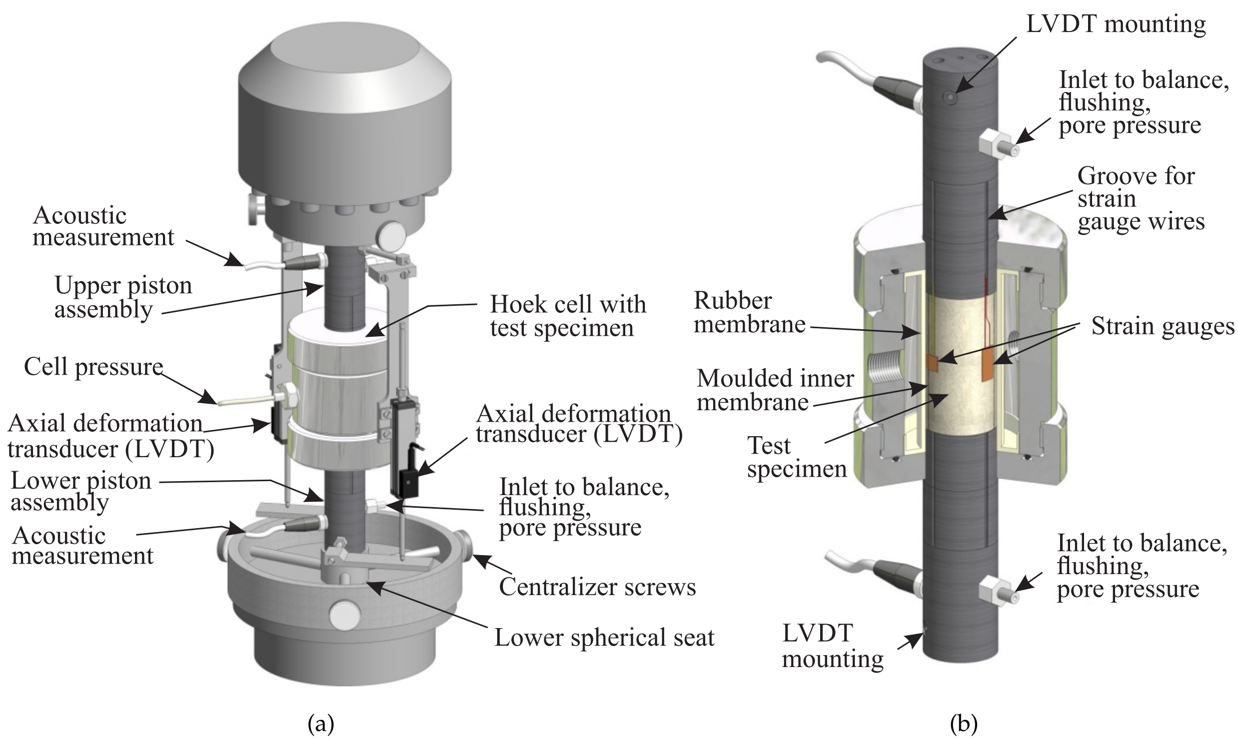

Figure 6.2: (a) Overview of a typical triaxial Hoek cell with instrumentation (courtesy GEO), (b) Typical cross sectional view through a typical triaxial Hoek cell with instrumentation (courtesy GEO).

where σ' is the effective stress, S the total stress, P_p the pore pressure, and α is the Biot coefficient, often referred to as the Biot-Willis poroelastic coefficient.

6.1.1 Stress

Inside the subsurface rock mass there exist 3 principal orthogonal stresses. It is always possible to orient a cube in the rock mass so that all the shear stress components τ_{ij} are zero, see **Fig. 6.3**.Then the cube faces represent the principal stress planes. The normal stresses on these planes are the principal stresses (Fjær, Holt et al. 2008).

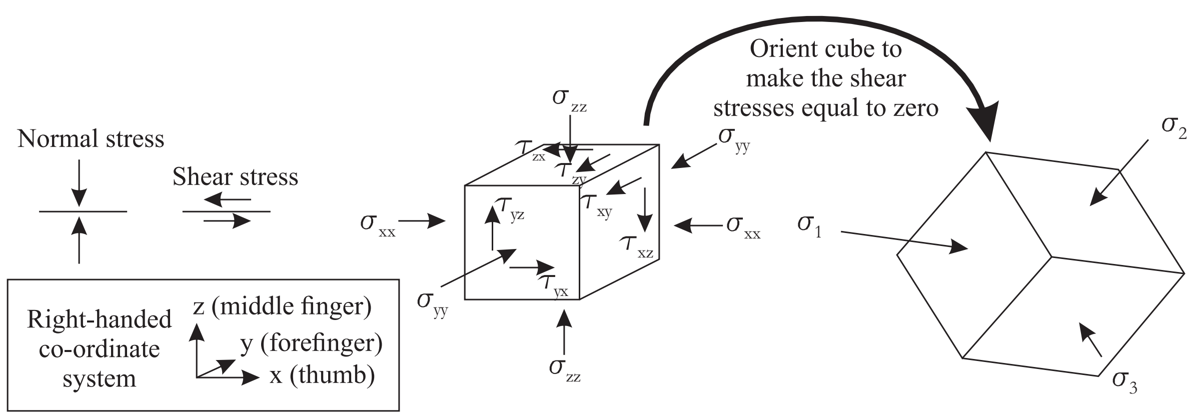

Figure 6.3: Illustration of the definition of principal stresses. The cube to the right has been rotated so that no shear stresses exist on the planes the principal stresses are working on.

The principal stresses rotate to be perpendicular and parallel to any free surfaces in the subsurface like wellbore walls, fault planes and salt walls, see **Fig. 6.4**. Close to the surface, seafloor, and in most locations in the subsurface one is vertical and the other two horizontal. The magnitude of the principal stresses vary with the geographic location and position in the subsurface. The vertical stress can be the largest one (normal faulting stress regime), the intermediate one (strikeslip stress regime) or the smallest one (reverse or thrust

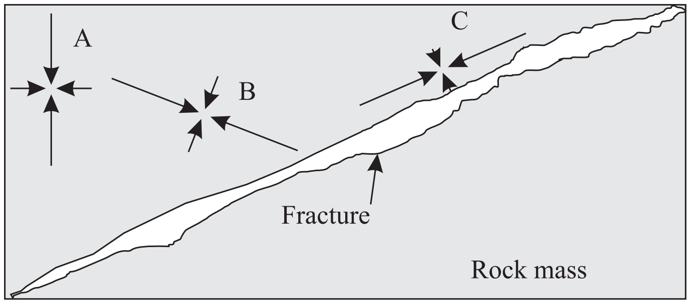

Figure 6.4: Illustration of how the principal stresses in a rock mass is reorienting themselves to be perpendicular to a free surface as wellbore wall, salt walls and in this case a fracture/fault.

stress regime) (Fjær, Holt et al. 2008). Most chalk reservoirs in the North Sea are found in a current day normal faulting stress regime. The faults interpreted from seismic data may have been formed in a different stress regime that existed at that location when the fault was formed. It is important to not mix the historic stress state with the current stress regime.

6.1.2 Deformation (strain)

In addition to load and stress, we need to measure the deformation of the rock as it is loaded. To do this the sample is instrumented with electrical deformation measurement devices as strain gauges, strain chains, and linear variable displacement transducers (LVDT). The definition of strain is the change in the length between two points in a sample divided by the initial length as illustrated in **Fig. 6.5**.

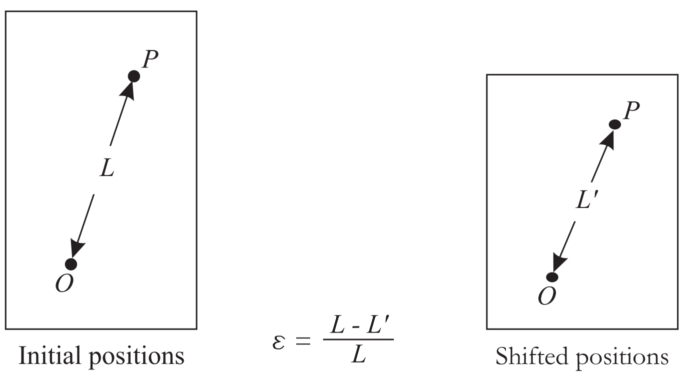

Figure 6.5: Definition of strain, ε.

6.1.3 Elastic moduli

Based on measurement of stress and deformations of the rock sample one can calculate several deformation properties, often referred to as elastic moduli. The most common ones measured in the laboratory are Young's Modulus (E), Poisson's Ratio (ν), Compaction Modulus (Oedometer Modulus) (M) and Bulk Modulus (K). The definitions of these are listed in **Table 6.1**.

Other parameters are more complicated to measure in the laboratory such as Lamé's first parameter (λ) and shear modulus or shear rigidity (G).

For perfect homogenous, isotropic, linear elastic materials, one can calculate the other elastic moduli from any two moduli. As an example if, Young's Modulus and Poisson's Ratio are measured, we have for the Bulk modulus:

$$K = \frac{E}{3(1-2\nu)}, \tag{6.2}$$

and for Lamé's first parameter:

$$\lambda = \frac{E\nu}{(1+\nu)(1-2\nu)}, \tag{6.3}$$

Elastic Parameter	Definition	Stress Path	Boundary Condition
Young's Modulus (E)	axial stress/axial strain	Triaxial	σ_3 =constant
Poisson's Ratio (ν)	-radial strain/axial strain	Triaxial	σ_3 =constant
Compaction Modulus (M)	axial strain/axial strain	Unixaial strain	$\sigma_2 = \sigma_3 = 0$
Bulk Modulus (K)	confining pressure/volumetric strain	Hydrostatic	$\sigma_1 = \sigma_2 = \sigma_3$

Table 6.1: Definitions of Young's Modulus, Poisson's Ratio, Compaction Modulus (Oedometer Modulus) and Bulk Modulus.

and the Shear modulus:

$$G = \frac{E}{2(1+\nu)}, \tag{6.4}$$

and the Compaction modulus:

$$M = \frac{E(1-\nu}{(1+\nu)(1-2\nu)}. \tag{6.5}$$

A complete set of relationships may be found in (Fjær, Holt et al. 2008).

If the elastic moduli from measurements of two others are calculated, the result is not very accurate. Rocks exposed to slow and relative large deformations in the laboratory are not often found to be perfectly homogenous or isotropic and may experience grain sliding and rotation. The relationships seem to work well for elastic properties determined from acoustic velocities and bulk density. These are often referred to as dynamic elastic moduli, while the ones calculated from measured stress and strain on a core are referred to as static elastic moduli. The dynamic and static elastic properties measured on the same core are not the same. The static ones are used to calculate subsurface deformations. The dynamic ones are typically much larger, but can be used to correlate borehole logs to core (applying a log to core shift).

6.1.4 Rock strength

Rock strength is typically used for a stress condition where the rock loses its load bearing capacity it has in the elastic regime. The rock loses its load bearing capacity when it starts to yield outside the elastic regime. When rocks are loaded past their elastic limit (i.e., permanently irreversible deformation), cracks start to grow in the cement between the grains which also start to crack. The cracks are initially distributed across the whole rock volume. However, as the cracking progresses, a localization of cracks takes place forming larger global fractures that can be observed by the naked eye. The way the global cracks develop depends on the external load and the rock properties.

The rock can start to fail in different modes. The three main modes are tension, shear, and pore collapse. In tensional yield a tensional fracture will form perpendicular to the local minimum principal stress. The microcracks have been concentrated in a plane with maximum tensile stress. This failure is brittle meaning that the load bearing capacity of the rock in tension then is zero. It is often assumed to be zero in many applications if natural fractures exist.

In shear failure mode a shear fracture (shear band) is formed at a certain angle relative to the maximum principal stress. As the load is increasing in one direction while it is kept constant or reduced in another, the microcracks will tend to coalesce to form global shear bands. The angle of the shear band, relative to the maximum principal stress, will be determined by a strength measure called internal friction angle. The load-bearing capacity is reduced to a residual value governed by the friction of the fracture surfaces and the stress state of the rock. This failure mode is called shear failure and is generally brittle.

During pore collapse there is a gradual yielding of the rock where the load bearing capacity drops, typically by a factor of 5–10. The loading condition with equal stresses around the specimen is referred to as hydrostatic. The rock is generally 'strong' under this loading condition. The microcracks will be distributed across the sample with no visible cracks in most cases. In other cases one can observe compaction bands. As the crack distribution reaches a certain density, the grains and fragments can find a new packing arrangement by reducing the porosity (pore collapse). The rock loses some of its load bearing capacity at pore collapse. It gets less stiff (softer) and the failure is ductile. With continued plastic deformation the rock may harden as it compacts and the grain packing is becoming denser and the load bearing capacity may increase again.

6.1.5 Laboratory tests

To characterize a rock type several tests are performed. A well characterized rock type will require 4 main types of tests as illustrated in **Fig. 6.6**. The main properties we can derive from these tests are summarized in **Table 6.2**. In addition, there also exist a number of special purpose tests like true 3D triaxial tests, hollow cylinder tests, thick wall cylinder tests, indentation tests, point load tests, scratch tests, strain rate tests, creep tests, flooding tests and more.

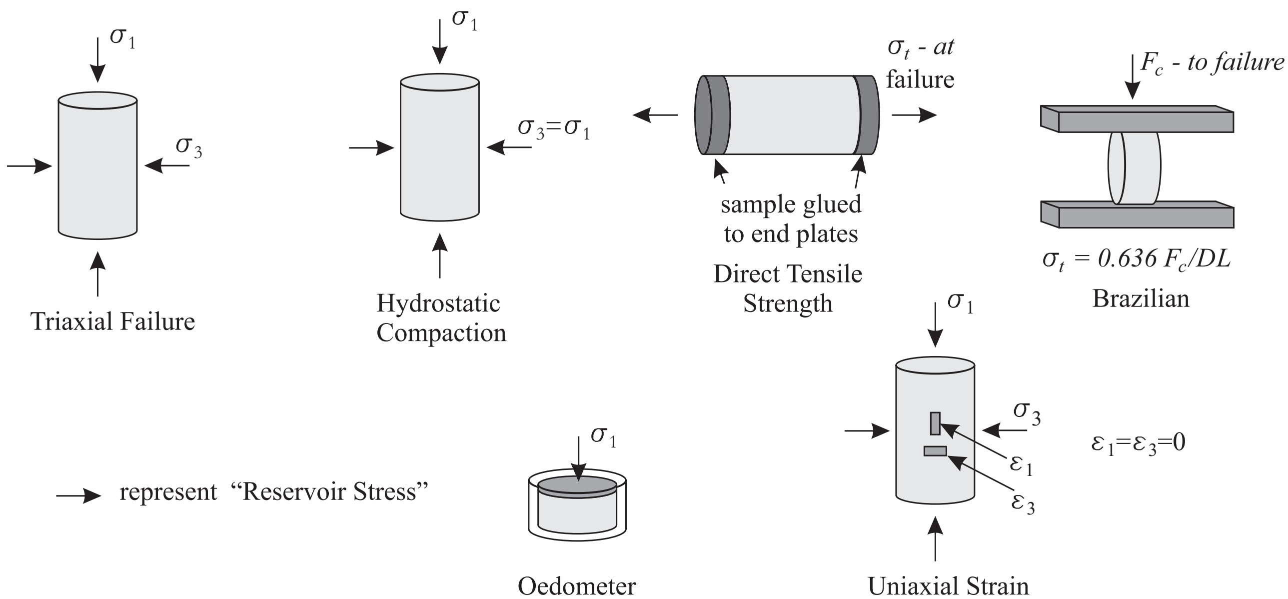

Figure 6.6: Overview of the 4 main types of rock mechanics tests used to characterize a rock type, triaxial, hydrostatic, tensile strength tests and uniaxial/oedometer tests (Fjær, Holt et al. 2008).

6.1.6 Failure diagrams

To summarize the characterization and derive additional parameters, some standard plots or failure diagrams are used. There is a number of them, but the most commonly used plots in the chalk community is the Mohr-Coulomb and the p'-q diagram. These plots are typically expressed in stress invariants, i.e., expressions which are independent of the orientation of the stress relative to the sample. In principle these plots differentiate between stress states or combination of principal stresses where the material behave elastic, i.e., returns to its initial shape after the load increase is removed and the stress states where irreversible or plastic deformations takes place, i.e., where the material does not return to its original shape after the load increase is removed. The reason for the irreversible deformations is the formation of microcracks and grain sliding and rotation in the microstructure of the rock. On a macroscale, the irreversible deformations are split in 3 main failure modes: tensile failure, shear failure and pore collapse. The principle of a failure diagram is shown in **Fig. 6.7**.

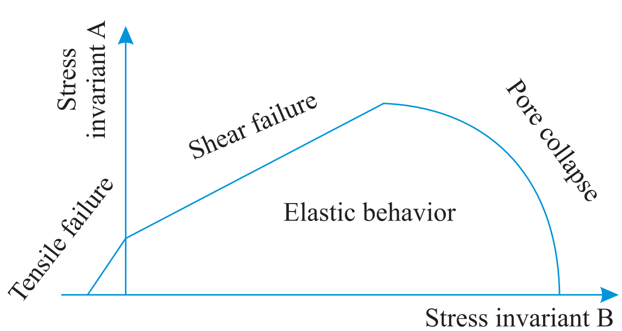

Figure 6.7: Principle of a failure diagram.

The Mohr-Coloumb diagram is mainly used to determine the shear strength of the material and properties like cohesion and internal friction angle. The axis are τ (shear stress) and σ' (normal stress). The diagram

<table>
<tr><th>Test</th><th>Main Properties</th></tr>
<tr><td>Triaxial compression</td><td>Most usual properties determined from test:
Young’s modulus (slope of axial stress/axial strain)
Poisson’s Ratio (negative ratio of lateral strain/axial strain)
Peak strength
UCS (confining pressure = 0)
Cohesion and internal friction angle (companion plugs at different confining pressures)
Pore volume compressibillity along triaxial stress paths
Failure envelope</td></tr>
<tr><td>Hydrostatic compaction</td><td>Most usual properties determined from test:
Bulk compressibility
Pore volume compressibillity
Bulk modulus
Hydrostatic yield (intercept of endcap with p′-axis)
Standard petrophysics tests are performed like this if stress is applied.
Stress path very seldom or never encountered in situ (no shear stresses), except inside a salt dome.</td></tr>
<tr><td>Tensile strength</td><td>Tensile strength, often used for wellbore stability hydraulic fracturing and solids production.</td></tr>
<tr><td>Unixial strain</td><td>Most usual properties determined from the test:
Oedometric or compaction modulus
Yield stress in uniaxial strain
K_0 (coefficient for earth at rest)
Pore volume compressibility
Strain rate data
Creep data
Time-dependent parameters (for rate type modelling)
Often including creep periods (days or weeks)
Industry standard for compaction tests</td></tr>
</table>

Table 6.2: Summary of main properties derived from the 4 main rock mechanics characterization tests.

is constructed by drawing circles (Mohr circles) on the σ' axes where the largest value on the σ' axis is the maximum effective stress in the triaxial test at peak stress and the smallest is the effective confining pressure.

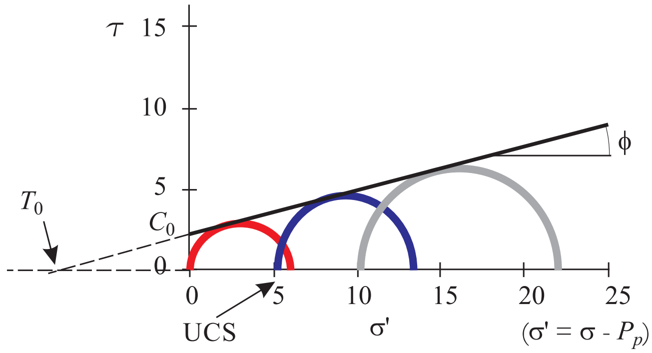

Figure 6.8: Mohr-Coulomb diagram.

From the Mohr-Coulomb diagram we can then draw the shear failure line with a slope equal to the internal friction angle ϕ. The intercept with the τ axis equals the cohesion (C_0) and tensile strength can be estimated by extending the shear failure line to the σ'-axis, although this often overestimate the tensile strength since the slope of the line on the other side of the τ-axis tends to be steeper. Typically the tensile strength is 1/8 to 1/12 of the UCS. Also note that a Mohr circle with the smallest σ' value at origo (zero), the maximum effective stress value will be equal to the unconfined compressive strength (UCS). So if you do not have a triaxial test with zero confining pressure you can estimate the UCS from drawing a circle with the smallest value equal to zero. There are also simple geometrical equations that link UCS, cohesion and internal friction angle to each other, (Fjær, Holt et al. 2008).

The p'-q diagram is used a lot in chalk rock mechanics since it can easily be used to show stress paths and is convenient to illustrate the onset of pore collapse. The axis are p' and q. The definitions of p' and q are:

$$p' = (\sigma_1' + \sigma_2' + \sigma_3')/3, \tag{6.6}$$

$$q = \frac{1}{\sqrt{2}} \sqrt{(\sigma_1' - \sigma_2')^2 + (\sigma_2' - \sigma_3')^2 + (\sigma_3' - \sigma_1')^2}, \tag{6.7}$$

where σ_i' are effective principal stresses. Note that for cylindrical laboratory samples ($\sigma_2' = \sigma_3'$) q simplifies to ($\sigma_1' - \sigma_3'$).

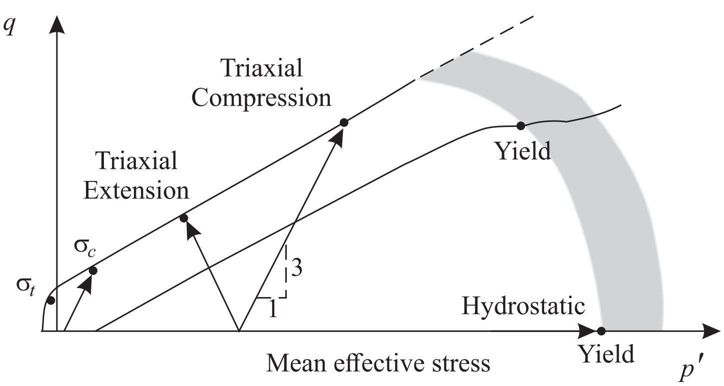

Figure 6.9: p'-q diagram.

6.1.7 Rock mechanical properties of chalk

The rest of this chapter focuses on the rock mechanical properties of reservoir chalk from the North Sea area, on the basis of studies from the Joint Chalk Research (JCR) program, literature, or information made available to the JCR partners during the various phases. Both high and low porosity chalk is discussed. In case no relevant information is available on reservoir chalk, reference will be made to studies on outcrop chalk. Further, details in relation to work carried out before 1994, reference is made to Andersen (1995). The plots and trend lines showing simple engineering correlations presented are generated from the JCR 6 database. Further details regarding the layout of the JCR database can be found in (Havmøller and Foged 1996; Chrisensen, Ditlevsen et al. 2007) .

6.2 Conceptual chalk model

The JCR database and much of the work done in the JCR since 1994 is related to the conceptual chalk model illustrated in **Fig. 6.10**. Geomechanic models are described in further details in a following section. The conceptual model is based on the assumption that chalk is behaving similarly to other soft rocks with a tension cut off line, a shear failure line (as in a Mohr-Coulomb criterion) and a compaction region illustrated with an endcap or also called yield cap. The tension cut off reflects that the tensile strength for chalk is significantly lower than the compressive strength. Thus the Mohr-Coulomb line cannot just be extended to the left in the (p,q)-diagram, so the strength in this area is reduced by a tension cut off line defined by the tensile strength (cf. Section 6.5.3). For high values of p' (mean) effective stress, the chalk gradually becomes less elastic, the stiffness decreases and the chalk starts to experience pore collapse and non-reversible deformations. At this stage, the chalk is said to have reached the yield cap. The yield surface and pore collapse is further described in Section 6.5.1.

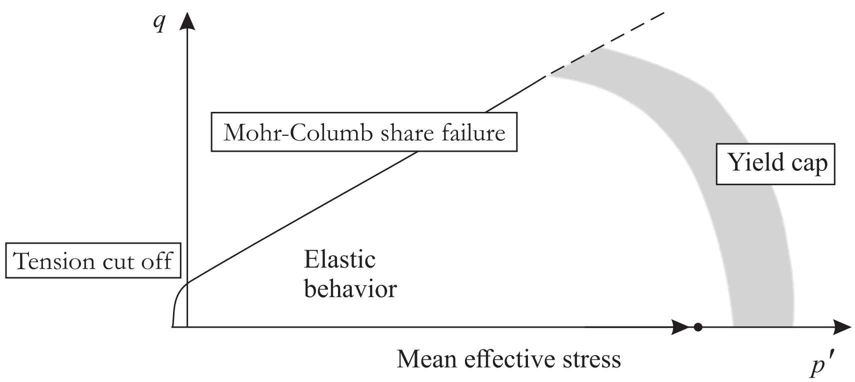

Figure 6.10: Conceptual chalk model

Inside the envelope defined by the tension cut off, the shear failure line and the end cap, the chalk is believed to behave close to linear elastic, although Risnes and Nygaard (1999) show that this is not strictly true for high porosity chalk. When a chalk specimen is loaded to a stress level on the shear failure line, a fracture is created and the specimen fails either in compression or in extension, depending on changes in the principal stresses. At the yield cap, the chalk compacts and the yield cap is updated (moves towards the right) as the porosity is reduced. If the specimen is unloaded to a lower stress level and then reloaded, the updated yield cap is encountered at a higher stress level.

Chalk is a rate type material, as described by de Waal (1986) and further developed for chalk byAndersen, Foged et al. (1992a). The rate type behavior implies that chalk experiences viscoelastic (time dependent) deformations. This in turn implies that laboratory test results are rate dependent and can not directly be applied to field conditions without a correction taking into account the stress or strain rate. The rate type model is further described in Section 6.4.4.

6.3 Core preparation

Comparing the rock mechanics data from various tests and laboratories, it was realized that the initial core preparation plays an important role in obtaining quality data from the tests. The preparation methods were discussed in e.g. JCR 3 by Springer (1992), introducing GCP (Good Core Practice). Both preserved and unpreserved core material is often infiltrated by drilling mud, and the core material must be cleaned in a proper way, followed by resaturation by an appropriate oil and/or brine. Extensive research by University of Stavanger has further stressed this, showing the influence of the chemical composition on the rock mechanical properties, as well as taking into account temperature effects when ageing and testing chalk (Nermoen, Korsnes et al. 2016).

6.4 Elastic state

6.4.1 Moduli in the elastic regime

The most basic modulus is the bulk modulus, which is determined as the mean stress divided by the volumetric strain. From a testing point of view, this is also the simplest test to do, as the stresses are the same in all directions throughout the test thus most old tests are hydrostatic. The bulk modulus for Danian (Ekofisk) formation chalk is presented in **Fig. 6.11**. The JCR 5 trend lines for oil and water saturated chalk are indicated.

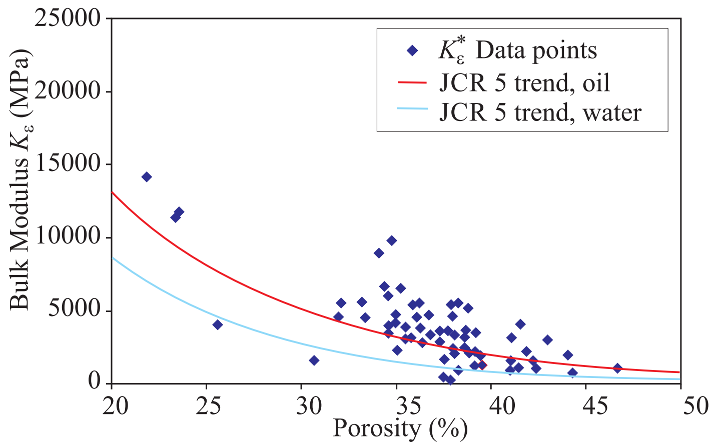

Figure 6.11: Bulk modulus, Danian (Ekofisk) fm. chalk.

The modulus of elasticity E (Young's modulus) for Danian (Ekofisk) formation is illustrated in **Fig. 6.12**. The modulus of elasticity E, Young's Modulus, is determined as the vertical stress divided by the vertical strain, in a stress state with zero or constant confining pressure. In the latest version of the JCR database, simple exponential functions are used for giving the relationship between porosity and the actual parameter. In Engstrøm (1992), it was suggested that the trend line should start at the theoretical modulus for pure calcite. However, this may not be the case, as low porosity chalk tends to have a significant amount of other minerals than calcite, e.g. quartz and various clay minerals. Another (and for the field more relevant) modulus is the

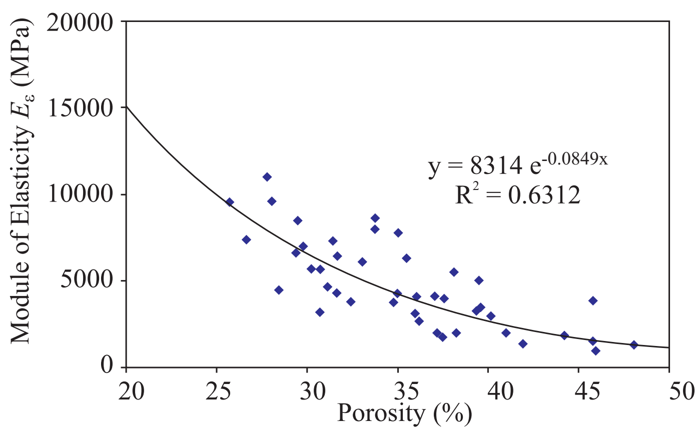

Figure 6.12: Modulus of elasticity, Danian (Ekofisk) fm. chalk.

modulus of uniaxial compaction. The modulus is determined as the vertical stress divided by the vertical strain, in the case where the horizontal strain is zero and thus the strain condition is uniaxial. Example of data and trend line for Maastrichtian (Tor) formation chalk is given in **Fig. 6.13**. It should be noted that very little data exists below 25 % porosity, and that the data scatter increases significantly with decreasing porosity. It should also be noted that part of the scatter in the high porosity range may be attributed to difference in test temperature, gas or fluid in the specimen, and the chemical composition of the pore fluid.

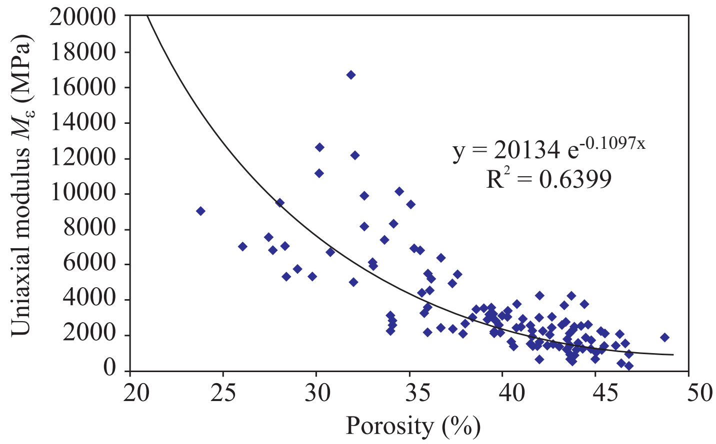

Figure 6.13: Uniaxial compaction modulus, Maastrichtian (Tor) fm. chalk.

6.4.2 Poisson's ratio and coefficient of earth pressure at rest

Poisson's Ratio is defined as the negative ratio between the horizontal and the vertical strain (under constant confining pressure conditions). As illustrated in **Fig. 6.14** for Maastrichtian (Ekofisk) formation chalk, there tend to be only a weak dependency of the porosity. The same goes for the coefficient of earth pressure at rest, K_0, as illustrated in **Fig. 6.15**. K0 is the ratio between the horizontal and the vertical stress (under uniaxial strain conditions). It should be noted that the modulus of elasticity, E, and Poisson's ratio, ν, form a pair of parameters and should be determined at the same stress level. The same goes for the uniaxial strain modulus and the K_0-ratio.

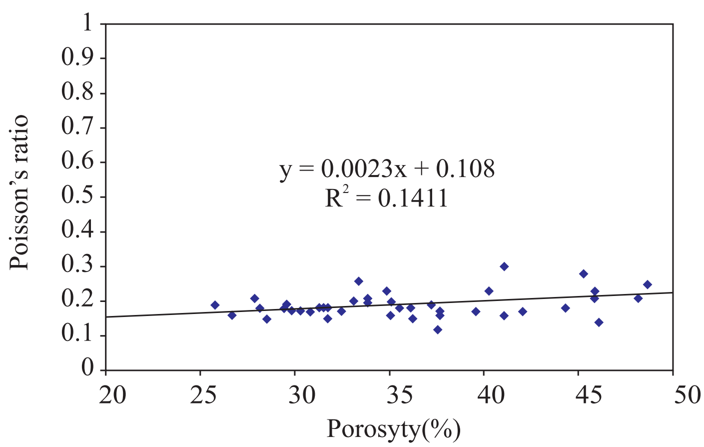

Figure 6.14: Poison's ratio, Danian (Ekofisk) fm.

6.4.3 Biot factor

The effective stress σ' is calculated by subtracting a factor α times the pore pressure P_p from the total stress σ, thus $\sigma' = \sigma - \alpha P_p$. The factor α is denoted the Biot factor and may be approximated from the bulk modulus as $\alpha = (1 - K_b/K_g)$, where K_b is the bulk modulus of the chalk matrix and K_g is the bulk modulus of the chalk grains (pure calcite has a bulk modulus of 74 GPa). Alternatively, the Biot factor can be determined from a specially designed test, where the effective stress or the pore pressure is kept constant(Alam, Hjuler et al. 2014). Finally, the Biot coeffcient may be estimated from acoustic velocity measurements. Determination of the Biot factor is complicated by the fact that it is both rate - and stress level dependent. Further, the stiffness of the test apparatus also affects the measurements (Nermoen, Korsnes et al. 2015; Omdal 2010).

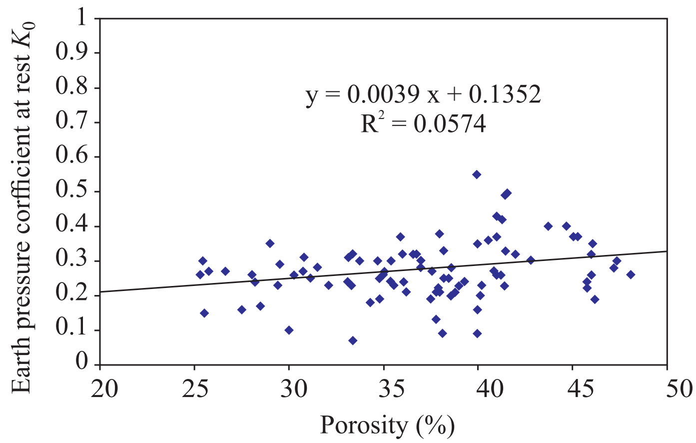

Figure 6.15: Coefficient of earth pressure at rest, Danian (Ekofisk) fm.

6.4.4 Strain rate effects in chalk and de Waal b factor

Most laboratory compaction tests are carried out at strain rates in the range 0.1 to 1 % strain per hour. However, the compaction rate in the field can be estimated to be in the range of 10^{-4} to 10^{-5} %/hour. This means that laboratory tests need to be converted to field rate in order not to underestimate compaction and pore collapse.

A simple and well-documented way of modelling the rate-type behavior of chalk is using the de Waal model, first described by (de Waal (1986)). The rate-type model addresses the fact that the loading rate affects the compaction curve - a slower loading rate results in more compaction at a given stress level.

The de Waal b factor is a sort of friction coefficient (e.g., for Valhall Tor chalk $b = 0.065$, for lower cretaceous chalk $b = 0.045$,). The b factor can be determined from a uniaxial compaction test, where the extent of the overconsolidated region σ_x after a creep phase at σ_{creep} is given by the strain rate at the end of the creep phase ε'_a and the applied strain rate ε'_{fc}. Further, b can be determined by matching a time curve from a uniaxial compaction test **Fig. 6.16**. Further details can be found in (Andersen, Foged et al. 1992a,b).

A simple and well-documented way of modelling the rate-type behavior of chalk is using the de Waal model, first described in (de Waal (1986)). The rate-type model addresses the fact that the loading rate affects the compaction curve - a slower loading rate results in more compaction at a given stress level. The de Waal b factor is a sort of friction coefficient (in example, for Valhall Tor chalk $b \sim 0.065$, for lower cretaceous chalk $b \sim 0.045$,). The b factor can be determined from a uniaxial compaction test, where the extent of the overconsolidated region σ_x after a creep phase at σ_{creep} is given by the strain rate at the end of the creep phase $\epsilon_a^{'}$ and the applied strain rate $\epsilon_{fc}^{'}$. Further, b can be determined by matching a time curve from a uniaxial compaction test **Fig. 6.16**. Further details can be found in (Andersen, Foged et al. 1992a,b).

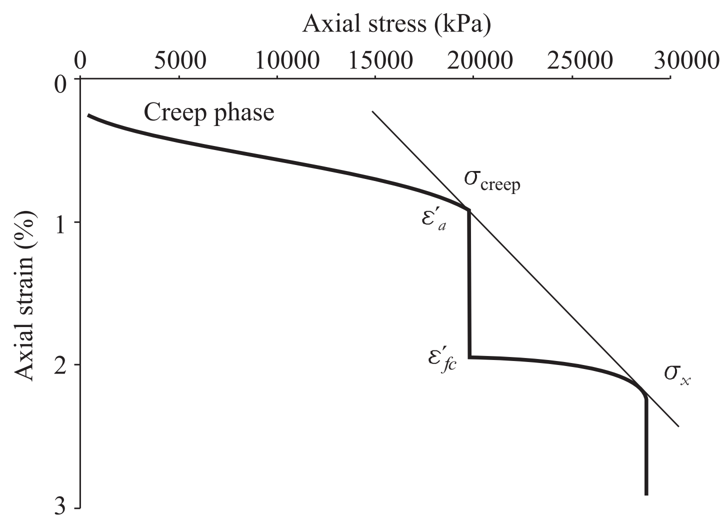

Figure 6.16: Illustration for how one can determine the de Waal b factor

6.5 Plastic state - pore collapse

6.5.1 Yield surface

The transition from elastic to elastoplastic behavior is occurring when the stress state exceeds the cap part of the yield surface. On a specific stress path (e.g. hydrostatic loading and uniaxial strain), the stress level where this transition occurs is also called the yield point or pore collapse. In the chalk literature you will also sometimes find the onset of this transitional phase called yield 1 and the end of the transition yield 2 (see **Fig. 6.17**). When the yield point is reached, the chalk specimen experiences permanent (irreversible) deformations. If the chalk specimen is unloaded and then reloaded, the new yield point is reached at the maximum stress of the previous phase - thus the location of the yield surface has been updated or moved outwards.

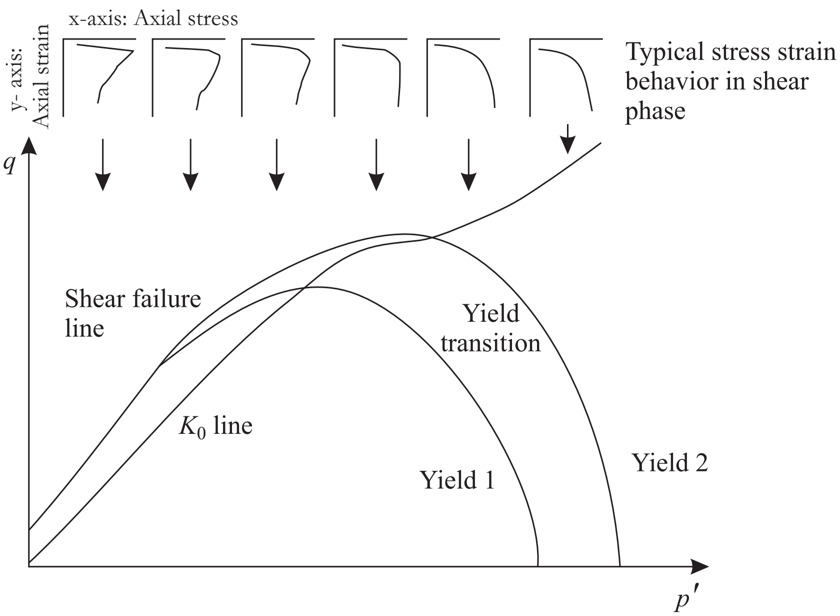

Figure 6.17: Shear failure, typical strain behavior.

6.5.2 Shear failure

Shear failure occurs in stress states where a fracture is formed through the specimen. As illustrated in Fig. 6.17, the stress-strain behavior changes depending on the confining pressure level. For low confining pressures, the failure is brittle and distinct. For higher confining pressures, the failure becomes more ductile and close to the end cap, the behavior resembles a compaction curve. Typical stress-strain responses of chalk are illustrated in Fig. 6.17. For both reservoir and outcrop chalk, the linear Mohr-Coulomb failure criterion is a good approximation to the shear failure line. The Mohr-Coulomb criterion is described by the friction angle and the cohesion.

The shear failure stresses for Maastrichtian chalk with porosity ranging from below 30 to 45 % is illustrated in a p', q-plot in **Fig. 6.18**. In order to determine the shear failure line, at least 2 triaxial tests at different confining stress are required. For reservoir chalk, it can be a challenge to find 2 comparable samples, thus multiple shear failure testing may be used. It should be noted that in a multiple shear failure test, only the first failure point represents the intact chalk, whereas the following shear failure stresses represent the strength of the already fractured material. For each porosity group, the tests at the highest confining stresses (and highest mean stress p', to the right in the diagram) shows lower deviatoric stress q than expected from a straight line failure criterion, indicating that failure occurs close to pore collapse.

6.5.3 Tensile strength

The tensile strength is determined indirectly from the brazilian test. The tensile strength for Maastrichtian chalk as function of porosity is illustrated in **Fig. 6.19** for oil and water saturated specimens, respectively.

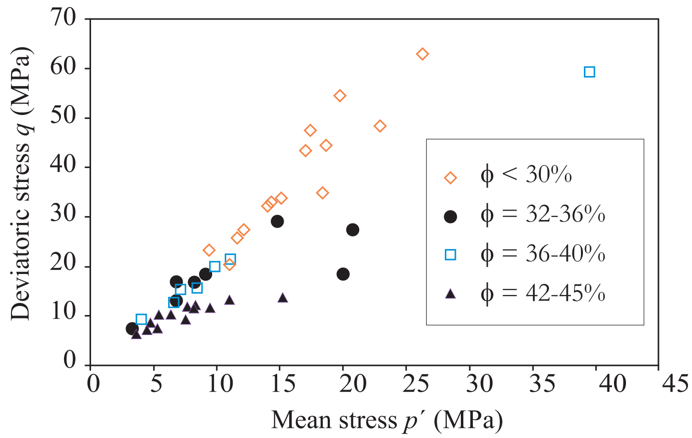

Figure 6.18: Shear failure stresses for Maastrichtian chalk.

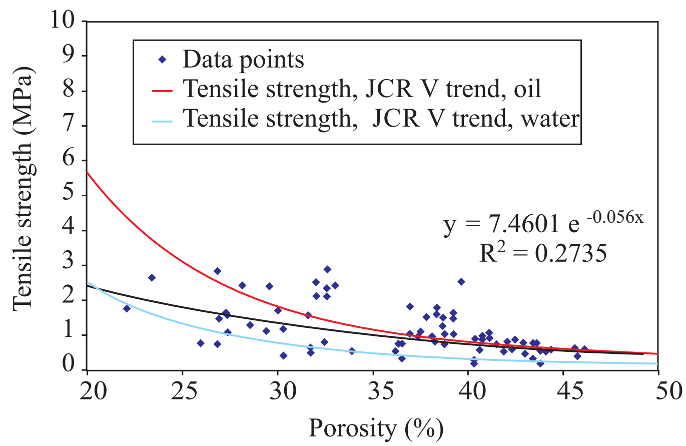

Figure 6.19: Tensile strength for Maastrichtian chalk.

6.5.4 Compaction

Compaction may be either hydrostatic (same stresses in all directions) or uniaxial (no horizontal strains). Uniaxial compaction is the more relevant boundary condition for the field condition. Both stress paths eventually leads to reduced porosity and pore collapse. Especially for high porosity chalk, rate-type behavior (time-dependent deformations/creep) is seen even in the elastic stress regime Risnes and Nygaard (1999). Close to pore collapse, the rate-type behavior becomes more and more dominating. The saturation fluid (e.g., oil or water), the temperature, and the chemical composition of the pore water affect the pore collapse stress level. When pore collapse is reached, permanent deformation is added to the elastic deformation of the chalk and porosity is reduced. When unloading and reloading, elastic behavior is observed until the new updated yield cap is reached and pore collapse continues.

Fig. 6.20 illustrates the pore collapse stress for Maastrichtian chalk under uniaxial strain compaction conditions. The red and blue curves show the significant difference in pore collapse stress between oil and water saturated chalk. The many green points represent older tests where the saturation fluid is unknown and illustrate the importance of knowing the chemical composition of the saturation fluid.

6.5.5 Water weakening

If the pore fluid in a rock is changed the chemical equilibrium may be disturbed, and a net dissolution or precipitation of minerals may occur (Fjær, Holt et al. 2008). This may have a strong effect on the rock properties, typically a reduction in strength of 30–100% is seen in many rocks due to deteriation of the cement (Broch 1974). A main uncertainty has been the magnitude of the water weakening in chalk. Water weakening of chalk has been known for a long time (Simon, Coulter et al. 1982; Newman 1983) and even earlier than these references. Similar chemical related water weakening effects have also been reported to take place in similar low permeable reservoir rocks with large grain surface area, the diatomite (Chase Jr and Dietrich 1989). The effect was brought

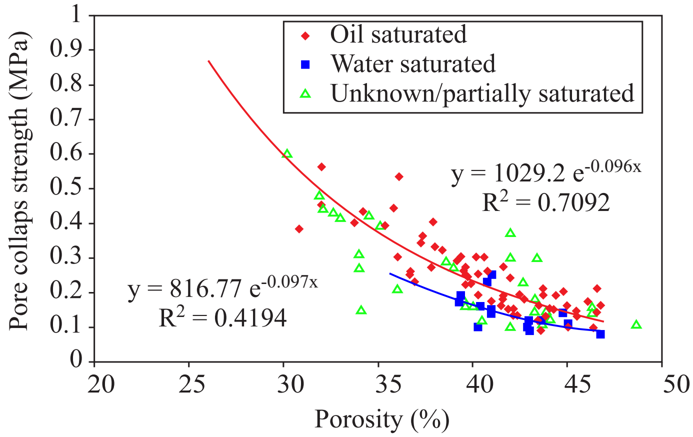

Figure 6.20: Pore collapse stress at uniaxial compaction, Maastrichtian chalk.

up again in relation to compaction during waterflood (Andersen, Foged et al. 1992a; Cook, Andersen et al. 2001). The quantitative mechanism has been investigated in a continuous effort the last decade (Risnes and Flaageng 1999; Risnes, Haghighi et al. 2003; Madland, Zangiabadi et al. 2009; Madland, Hiorth et al. 2011), but so far without the final conclusion.

The current understanding of water weakening seems to predict a degree of weakening that is dependent on the reservoir temperature. This can explain observations of different degrees of weakening between Ekofisk and Valhall (Kristiansen and Plischke 2010). It also indicate that the mechanism is strongly related to oil recovery from enhanced oil recovery (EOR) processes (Austad, Strand et al. 2008).

6.5.6 Simulating reservoir deformation during field life in the laboratory

A very interesting test program was executed by NGI Cuisiat, Grande et al. (2007) as part of JCR VI. In these experiments Liege outcrop of 42% initial porosity was used to simulate the expected reservoir deformation in the Valhall Tor reservoir. A comparison of a plug saturated with laboratory oil, one with synthetic seawater and one saturated initially with laboratory oil and then flooded with 2.7 pore volumes of synthetic seawater was performed. The tests were performed at reservoir temperature (93°C) and in situ pore pressure and total stresses. The oil saturated test was run for 30 days, the water saturated chalk for 50 days and the water flooded sample for 63 days. The results are shown in **Fig. 6.21**.

From the results, it is seen that the starting point for the initial water saturated sample is not a zero vertical strain as for the others. The reason being that the weaker chalk with water was deforming and creeping significantly as it was loaded to initial in-situ conditions. Although the vertical strain is slightly higher for the waterflooded sample, the overall volumetric strain for both tests are almost identical (around 190 microstrain mS). This indicates that the waterflooded sample is weakening to the same degree as the initial water saturated sample exposed to the same fluid and effective stress at this temperature.

Of interest from a field perspective is that the oil saturated specimen will deform around 115 mS (11.5%), meaning each meter of chalk will compact 11.5 cm. A 100 meter thick chalk column will compact 11.5 meters. The samples experiencing water flooding and then blowdown will experience between 155 to 175 mS vertical strain (15.5–17.5%). A 100 m thick chalk column will then compact between 15.5 and 17.5 meters.

Since the vertical strain and the volumetric strain is not exactly the same, a small difference indicating not perfect uniaxial strain conditions, we can use the volumetric strain (115 mS and 190 mS) to estimate the porosity in the chalk at the end of the blowdown. This gives a porosity at the end of the tests of around 35 and 28%.

If we look at the waterflooded sample the calculated change in porosity from the onset of water flooding until re-pressurisation and then blowdown is a porosity reduction from around 37–30%, i.e., a water induced compaction of around 7 porosity units reduction. From the vertical strain difference between start and end of waterflood this indicates 8 m compaction for a 100 m thick chalk.

So these experiments indicate that a 100 m chalk column of initial 42% porosity chalk at Valhall will first compact 7.5 meters due to depletion, then 8 meters due to water weakening and further 2 meters during extreme blowdown.

This is assuming waterflooding at constant reservoir pressure and overburden stress. This is never the case in the field. As Kristiansen and Plischke (2010) point out a re-pressurisation front will move ahead of the waterfront and unload the chalk. They present laboratory data from ambient conditions on field core which

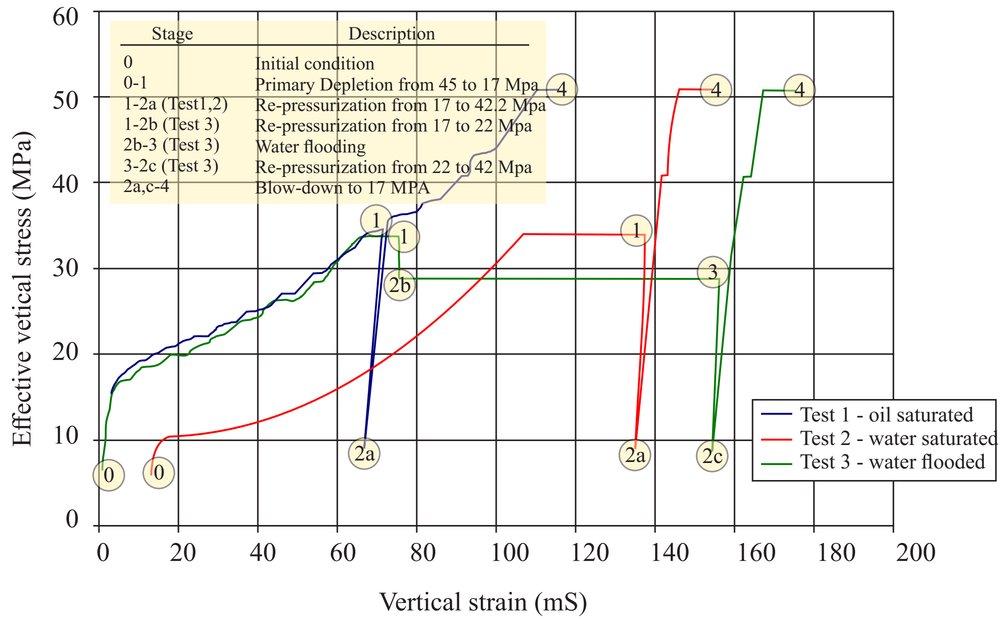

Figure 6.21: Simulation of vertical deformation (strain) in 42% Liege outcrop chalk exposed to in-situ fluids, temperature and stresses for a scenario with depletion, re-pressurisation and water flood and then blowdown. Blue curve oil saturated and depletion and re-pressurisation only; green curve denotes initially oil saturated, re-pressurized and then waterflooded followed by blowdown; red a water saturated sample exposed to same as previous (note the latter has already deformed at initial conditions).

indicate a maximum porosity loss of 6 porosity units for waterflooding at constant reservoir pressure, which is comparable to the 7 porosity units in the JCR 6 study. They indicate that a 1500 psi repressurisation ahead of the waterfront will only result in 0.5 porosity unit loss due to water weakening. For 3000 psi re-pressurisation ahead of the waterfront the water weakening contribution is zero. However, the weakening effect is then experienced during blowdown. In the laboratory experiment above there will exist a potential for 10 meters compaction during blowdown if the re-pressurisation has been that strong.

In reality some of the water weakening will be released during waterflooding depending on the local re-pressurisation and some will be released during blowdown, depending on what the pore pressure will be at the end of the blowdown.

Nomenclature

b = de Waal factor
C_0 = effective cohesion
E = Young's modulus, M/Lt^2, Mpa
G = shear modulus, share rigidity, M/Lt^2, MPa
L = length, L
K = bulk modulus, M/Lt^2, MPa
K_0 = ratio between horizontal and vertical stress (under uniaxial strain condition)
K_b = bulk modulus of chalk matrix, M/Lt^2, MPa
K_g = bulk modulus of chalk grains, M/Lt^2, GPa
L' = deformed length, L
M = compaction modulus
p' = $(\sigma_1' + \sigma_2' + \sigma_3')/3$, effective mean stress, m/Lt^2, MPa
P_p = pore pressure, m/Lt^2, Pa
q = deviatoric stress, m/Lt^2, MPa
S = total stress, m/Lt^2, MPa
T_0 = ultimate tensile strength
α = Biots coefficient
λ = Lamé's first parameter
ν = Poisson's ratio

$\phi =$ friction angle
$\sigma =$ stress, m/Lt^2
$\sigma_{1,2,3} =$ effective principal stresses, m/Lt^2
$\sigma' =$ effective stress, m/Lt^2
$\tau =$ shear stress, m/Lt^2
$\varepsilon =$ strain
$\varepsilon'_{fc} =$ applied strain rate

Subscripts

$0 =$ at 0
$1,2,3 =$ directions
$b =$ chalk matrix
$c =$ critical
$g =$ chalk grain
$i =$ directions (1,2,3), (ijk) or (xyz) = coordinate axes
$p =$ pore
$t =$ tensile

Abbreviation

GEO = Danish Geotechnical Institute
JRC = joint chalk research
GCP = good core practice
LVDT = linear variable displacement transducer
NGI = Norwegian Geotechnical Institute
UCS = unconfined compressive strength

References

Alam, M.M., Hjuler, M.L. et al., 2014. Petrophysical and rock-mechanics effects of CO 2 injection for enhanced oil recovery: Experimental study on chalk from South Arne field, North Sea. *Journal of Petroleum Science and Engineering*, **122**: 468–487. URL `http://dx.doi.org/10.1016/j.petrol.2014.08.008`.

Andersen, M.A., 1995. *Petroleum Research in North Sea Chalk.* RF-Rogaland Research. Joint Chalk Research Program Phase IV.

Andersen, M.A.A., Foged, N.A., and Pedersen, H.E.A., 1992a. The link between waterflood-induced compaction and rate-sensitive behavior in a weak North Sea chalk. In *Proceedings of 4th North Sea chalk symposium, Deauville*. a.

Andersen, M.A.A., Foged, N.A., and Pedersen, H.E.A., 1992b. The rate-type compaction of a weak North Sea chalk. In *The 33th US Symposium on Rock Mechanics (USRMS)*. American Rock Mechanics Association. b. URL `https://www.onepetro.org/conference-paper/ARMA-92-0253`.

Austad, T., Strand, S. et al., 2008. Seawater in Chalk: An EOR and Compaction Fluid. *SPE Reservoir Evaluation & Engineering*, **11** (04): 648–654. Society of Petroleum Engineers. doi:10.2118/118431-PA. August. URL `http://dx.doi.org/10.2118/118431-PA`.

Biot, M.A., 1941. General Theory of Three-Dimensional Consolidation. *Journal of Applied Physics*, **12** (2): 155–164. URL `http://dx.doi.org/http://dx.doi.org/10.1063/1.1712886`.

Biot, M.A., 1955. Theory of Elasticity and Consolidation for a Porous Anisotropic Solid. *Journal of Applied Physics*, **26** (2): 182–185. URL `http://dx.doi.org/10.1063/1.1721956`.

Biot, M.A., 1956. General solutions of the equations of elasticity and consolidation for a porous material. *J. appl. Mech*, **23** (1): 91–96.

Broch, E., 1974. The influence of water on some rock properties. In *Proceedings of the third congress of the International Society for Rock Mechanics, Themes*, 33–38.

Chase Jr, C.A. and Dietrich, J.K., 1989. Compaction Within the Belridge Diatomite. *SPE Reservoir Engineering*, **4** (04): 23–25. Paper SPE 17415 presented at the SPE California Regional Meeting, Long Beach, California. November. URL `http://dx.doi.org/10.2118/17415-PA`.

Chrisensen, H.F., Ditlevsen, F., and Hildegaard, K., 2007. Database update, standard curves and data input tod,. *Joint Chalk Research*. GEO report no 27493, Phase 6, Geomechanics project, Part 2, Task 2.12.

Cook, C.C., Andersen, M.A. et al., 2001. An Approach to Simulating the Effects of Water-Induced Compaction in a North Sea Reservoir (includes associated papers 73134 and 73135). *SPE Reservoir Evaluation & Engineering*, **4** (02): 121–127. URL `http://dx.doi.org/10.2118/71301-PA`.

Cuisiat, F., Grande, L., and Berre, T., 2007. Joint Chalk Research Phase 6 Geomechanics, Task 2.7 Laboratory testing. Tech. rep., Norwegian Geotechnical Institute. Re-pressurization tests, 2002 1002-2.

de Waal, J.A., 1986. *On the rate type compaction behaviour of sandstone reservoir rock*. Ph.D. thesis, Technische Hogeschool Delft. URL `https://www.researchgate.net/profile/Hans_De_Waal2/publication/35834162_On_the_Rate_Type_Compaction_Behavior_of_Sandstone_Reservoir_Rock/links/53e1d4630cf2235f352bda13/On-the-Rate-Type-Compaction-Behavior-of-Sandstone-Reservoir-Rock.pdf`.

Engstrøm, F., 1992. Rock mechanical properties of Danish North Sea chalk. In *Proceedings of 4th North Sea chalk symposium, Deauville*.

Fjær, E., Holt, R.M. et al., 2008. *Petroleum related rock mechanics*, vol. 53. 2nd ed., Elsevier. URL `http://store.elsevier.com/product.jsp?isbn=9780444502605`.

Havmøller, O. and Foged, N., 1996. Review of rock mechanics data for chalk. In *Fifth North Sea Chalk Symposium*. Reims Edinburgh, Scotland.

Kristiansen, T.G. and Plischke, B., 2010. History Matched Full Field Geomechanics Model of the Valhall Field Including Water Weakening and Re-pressurisation. Paper SPE-131505-MS presented at SPE EUROPEC/EAGE Annual Conference and Exhibition, Barcelona, Spain. 14–17 June. URL `http://dx.doi.org/10.2118/131505-MS`.

Madland, M.V., Hiorth, A. et al., 2011. Chemical Alterations Induced by Rock–Fluid Interactions When Injecting Brines in High Porosity Chalks. *Transport in Porous Media*, **87** (3): 679–702. January. URL `http://dx.doi.org/10.1007/s11242-010-9708-3`.

Madland, M.V., Zangiabadi, B. et al., 2009. Rock Fluid Interactions in Chalk with $MgCl_2$ and Na_2SO_4 Brines with Equal Ionic Strength. In *Presented at the IOR 2009 symposium (EAGE) in Paris, France*.

Nermoen, A., Korsnes, R.I. et al., 2015. Porosity and permeability development in compacting chalks during flooding of nonequilibrium brines: Insights from long-term experiment. *Journal of Geophysical Research - Solid Earth*, **120** (5): 2935–2960. May. URL `http://dx.doi.org/10.1002/2014jb011631`.

Nermoen, A., Korsnes, R.I. et al., 2016. How Stress and Temperature Conditions Affect Rock-Fluid Chemistry and Mechanical Deformation. *Frontiers in Physics*, **4**. Presented at IEA Collaborative Project, 36th EOR Workshop & Symposium. 2 February. URL `http://dx.doi.org/10.3389/fphy.2016.00002`.

Newman, G.H., 1983. The effect of water chemistry on the laboratory compression and permeability characteristics of some North Sea chalks. *Journal of Petroleum Technology*, **35** (5): 976–980. URL `http://dx.doi.org/10.2118/10203-PA`.

Omdal, E., 2010. *The mechanical behavior of chalk under laboratory conditions simulating reservoir operations*. Ph.D. thesis, Department of Petroleum Engineering, University of Stavanger, Norway. URL `http://idtjeneste.nb.no/URN:NBN:no-bibsys_brage_13330`.

Risnes, R. and Flaageng, O., 1999. Mechanical properties of chalk with emphasis on chalk-fluid interactions and micromechanical aspects. *Oil & Gas Science and Technology*, **54** (6): 751–758. URL `http://dx.doi.org/10.2516/ogst:1999063`.

Risnes, R., Haghighi, H. et al., 2003. Chalk–fluid interactions with glycol and brines. *Tectonophysics*, **370** (1): 213–226. URL `http://dx.doi.org/10.1016/S0040-1951(03)00187-2`.

Risnes, R. and Nygaard, V., 1999. Elasticity in high porosity outcrop chalk. *Second euroconference on rock physics and rock mechanics, Heriot-Watt University, Edinburgh, Scotland*.

Simon, D.E., Coulter, G. R. ND King, G.E., and Holman, G., 1982. North Sea Chalk Completions- A Laboratory Study. *Journal of Petroleum Technology*, **24** (11): 2531–2536. November. URL `http://dx.doi.org/10.2118/10395-PA`.

Springer, N., 1992. Preperation of chalk for petrophysical Experiments. *4th North Sea Chalk Symposium*. 21–23 September.

Chapter 7

Rock Properties

Ida Lykke Fabricius

7.1 Intoduction

Rock properties basically include the chalk mineralogical composition, the particle size and size distribution as reflected in sedimentary texture and the complementary size distribution of pores. These basic properties give rise to the mineralogy and nature of the solid fluid interface which is characterized by specific surface and wettability and which together with porosity controls the effect of capillary pressure, as well as the permeability and the electrical formation factor. The contact cementation and pore-filling cementation taking place during diagenesis of chalk are reflected in degree of induration and pore compressibility. The quality of a chalk reservoir is controlled by all these factors together with lithological and textural heterogeneity and degree of fracturing.

7.2 Mineralogical composition

A summary of some characteristic mineralogical properties of chalk is shown in **Table 7.1** and **Fig. 7.1**.

Calcite is the dominating mineral in chalk. It is generally found as crystals of low-magnesium calcite bounded by faces of the $\{10\bar{1}4\}$ rhombohedral form, although the crystals may have intricate shapes reflecting their biogenic origin (Black 1963). In newly deposited pelagic calcareous ooze, different calcite crystal forms are represented reflecting the preference of different calcareous planktonic organisms, but during the postdepositional early recrystallization, crystal surfaces representing non-rhombohedral forms will relatively quickly either dissolve or obtain overgrowth until stable rhombohedral faces are obtained (Neugebauer 1974). By contrast, rhombohedral faces grow slowly because of a strongly bound monomolecular layer of water molecules. Ca^{2+} ions or other divalent ions must thus adsorb on top of the water layer (Stipp 1999) and can only reach the mineral surface at crystal edges. The crystals thus grow by covering the surface from the edges so that the rhombohedral form is maintained or enhanced. Thermal energy caused by increasing burial facilitates the growth of rhombohedra, so that they become larger and more equant with burial (Scholle 1977).

Quartz is a typical minor constituent of chalk, either as detrital silt grains or as submicron size crystal aggregates of "nanoquartz". A straightforward explanation for the presence of nanoquartz is based on the fact that the chemically unstable opaline fossils (typically siliceous sponges) and volcanic glass dissolve during diagenesis and the readily formed opal CT precipitates based on local conditions either as flint beds or as dispersed sub micron size spherules (Wise Jr and Kelts 1972). The opal CT spherules will during progressing diagenesis transform to the chemically stable quartz, while to some extent maintaining the overall shape (Ehrmann 1986; Hjuler and Fabricius 2009). Based on the fact that quartz has a lower solubility than opal, Jakobsen, Lindgreen et al. (2000) proposed that nano-quartz might crystallize directly from sea water. A problem with this hypothesis is that there is no reported direct chemical route for the production of nanoscale quartz (Bertone, Cizeron et al. 2003).

Clay minerals in the chalk include mixed layer smectite-illite and illite-smectite-chlorite as well as kaolinite (Lindgreen, Fallick et al. 2012). Smectititic minerals can have detrital origin or can represent submarine altered volcanic ash. It can form sedimentary beds, pore-filling cement, overgrowths on detrital particles or sandsize glauconite (Pacey 1984; Deconinck and Chamley 1995; Wray and Wood 1998; Jeans 2006; Simonsen and Toft 2006; Wray and Jeans 2014). During burial diagenesis of deep sea chalk, smectite-illite-chlorite recrystallizes to

Mineral	**Formula**	**Point group**	**Refractive index**	**Mohs' hardness**	ρ_g **(g/cm^3)**	V_p **(km/s)**	V_s **(km/s)**
Calcite	$CaCO_3$	Trigonal -3m	n_ω=1.658 n_ε=1.486	3	2.711	6.26–6.64	3.24–3.44
Dolomite	$CaMg(CO_3)_2$	Trigonal -3	n_ω=1.679–1.698 n_ε=1.502–1.513	3½–4	2.86	6.93–7.34	3.96–4.23
Quartz	SiO_2	Trigonal 32	n_ω=1.5442 n_ε=1.5533	7	2.65	6.04–6.06	4.09–4.15
Opal-CT	$SiO_2 \cdot nH_2O$						
Kaolinite	$Al_2Si_2O_5(OH)_4$	Triclinic 1	n_α=1.553–1.565, n_β=1.559-–1.569, n_γ=1.560-–1.570	2–2½	2.60	1.44	0.93
Smectite: Mont-morillonite	$(Na,Ca)_{0.33}(Al,Mg)_2(Si_4O_{10})$ $(OH)_2 \cdot 4(H_2O)$	Monoclinic 2/m	n_α=1.475-–1.503, n_β=1.499-–1.533, n_γ=1.500-–1.534	1–2	2.0		
Illite (Hydro-muscovite)	$(K,H_3O)Al_2(OH)_2AlSi_3O_{10}$	Monoclinic 2/m	n_α=1.555-–1.575, n_β=1.577-–1.606, n_γ=1.580-–1.610	2	2.75	4.32	2.54
Pyrite	FeS_2	Cubic m-3	Opaque	6–6½	5.01	7.70–8.10	4.78–5.18
Apatite	$Ca_5(PO_4)_3(F,Cl,OH)$	Hexagonal 6/m	n_ω=1.634–1.667 n_ε=1.631–1.665	5	3.16–3.22	6.80–7.15	3.81–4.34
Clino-ptilolite	$(Na,K,Ca)_{2-3}Al_3(Al,Si)_2Si_{13}O_{36}\cdot 12H_2O$	Monoclinic		3½–4	2.17		
Baryte	$BaSO_4$	Orthorom--bic mmm	n_α=1.636 n_β=1.637 n_γ=1.648	3	4.480	4.29–4.49	2.22–2.30

Table 7.1: Minerals (formula, point group, Refraxtive index, Mohs' hardness, ρ_g, V_p and V_s), American Society for Testing and Materials (ASTM) Tröger (2017); Mavko, Mukerji et al. (2009).

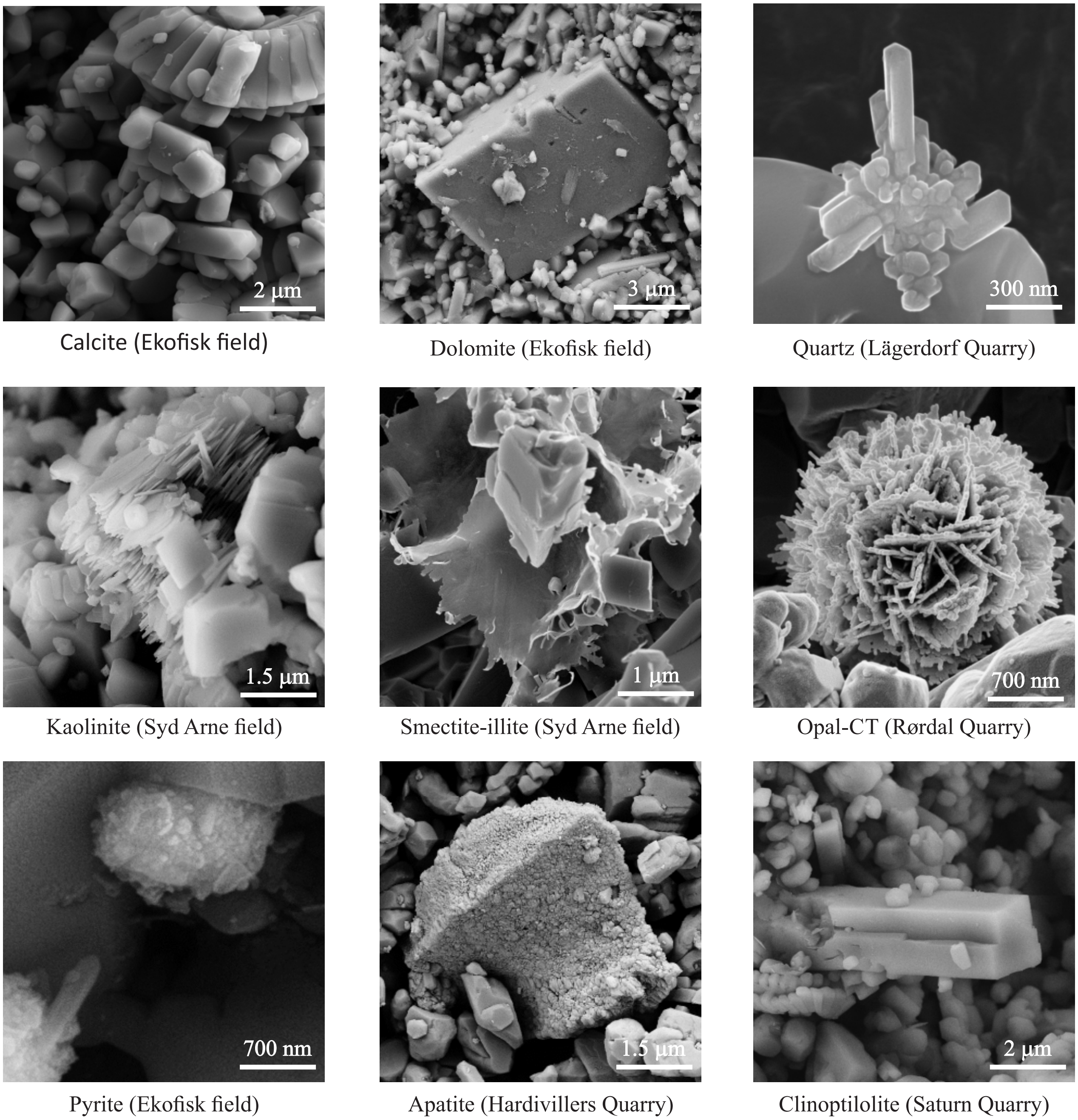

Figure 7.1: Minerals in chalk (SEM), by courtesy of Morten Leth Hjuler, GEUS.

illite-smectite via a dissolution–precipitation process thereby forming precursors for stylolites (Fabricius and Borre 2007). A similar process may well take place in North Sea chalk. Kaolinite can occur as part of lithoclasts (Fabricius, Høier et al. 2007) and can also occur as pore-filling cement probably sourced from diagenetically dissolved detrital feldspar. It is possible that the associated transport of aluminium in the pore water is facilitated by complexation with organic acids, which can form during maturation of organic matter (Maliva, Dickson et al. 1999).

Dolomite is present in some intervals of the Chalk, typically found as 10–30 micron size euhedral rhombohedra, in some places scattered along stylolites (Jørgensen 1983). A source of Mg can well be recrystallization of biogenic Mg-bearing calcite. Dolomite can form early after sediment deposition or after substantial burial. In some cases distinctly chemically zoned crystals are found reflecting variation in the pore water composition (Wolfe 1970; Maliva and Dickson 1994; Gély and Blanc 2004).

Apatite is a main component of phosphatic chalk. Massive phosphatic chalks are present in southern England, Belgium and Northern France (Jarvis 1992). In the chalks of the North Sea Basin apatite can be present as a minor component.

The zeolite, clinoptilolite is a typical minor component in chalk (Hjuler and Fabricius 2009).

Baryte and celestite can be found as authigenic crystals in chalk (Lind, Nykjaer et al. 1994; Madsen and Stemmerik 2009).

Organic matter is a constant component of chalk. Pacey (1989) found the white chalks from eastern England and northern France to contain 0.01% organic mater, 70% being intracrystalline in the calcite, the remaining probably being associated with clay.

7.3 Particle size and particle size distribution

Chalks are composed mainly of calcitic biogenic particles. The dominating components are nannofossil (coccollith) crystal elements 0.2–-1.0 μm in size, coccoliths of silt size, and microfossils of mm size (Håkansson, Bromley et al. 1974).

Macrofossils are rare in drill cores from the North Sea, but are visible and can be handpicked at outcrops (Hansen and Surlyk 2014). Non-carbonate particles are typically clay minerals and nanoquartz.

Jørgensen (1986) studied North Sea chalk down to a depth of 2.8 km and from SEM-studies found microspar to gradually replace crystal elements and grow with age and depth to a size around 3.5 μm. As noticed by Burns (1975) crystal elements of some nannofossil species tend to grow at the expense of elements from other species.

Due to the biogenic origin of the chalk, the grain size distribution is typically bimodal or trimodal. The relative proportion of grains of sand size (microfossils) is described as depositional texture (Dunham 1962) **(Fig. 7.2)**. North Sea chalks have mainly mudstone texture with less than 10% microfossils in cross section or wackestone texture with more than 10% microfossils in cross section, but where the sedimentary rock is supported by the finer fraction. Chalk with packstone texture, where the microfossils carry the load is rare. Depositional texture of chalk can be assessed visually after smoothing a chalk sample with a knife and using a hand lens.

Defining grain size distribution of chalk from laser-based methods is not recommendable. First, the chalk has to be disintegrated, and second, if the chalk is friable enough to make this unproblematic, the larger grains

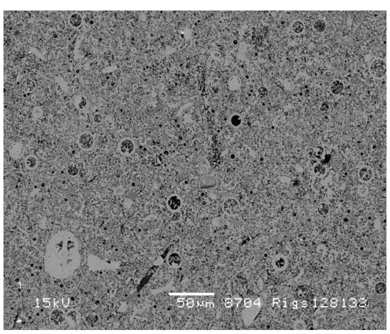

(a) Syd Arne field, Ekofisk Formation. Chalk wackestone with partly cemented moldic porosity and intrafossil porosity.

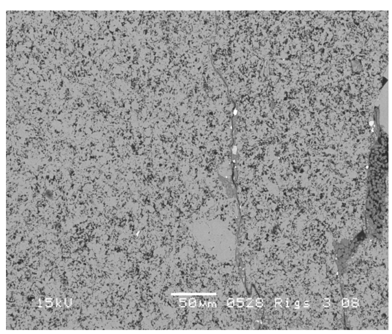

(b) Syd Arne field, Tor Formation. Chalk mudstone. Part of stylolite visible in right side of image with pyrite, apatite and authigenic kaolinite.

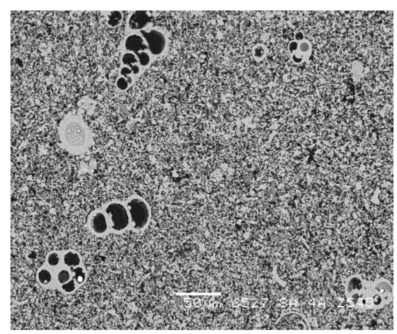

(c) Valhall field, Tor Formation. Chalk mudstone with intrafossil porosity.

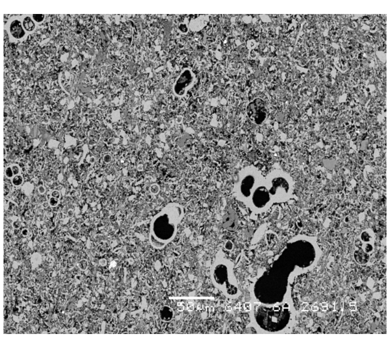

(d) Valhall field, Hod Formation. Argillaceous chalk wackestone with intrafossil porosity.

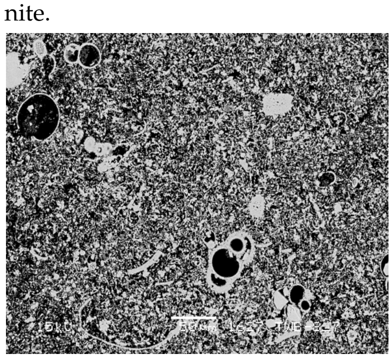

(e) Tyra field, Tor Formation. Chalk mudstone with intrafossil porosity.

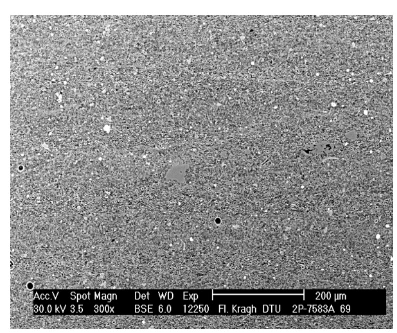

(f) Valdemar field. Tuxen Formation. Argillaceous chalk mudstone.

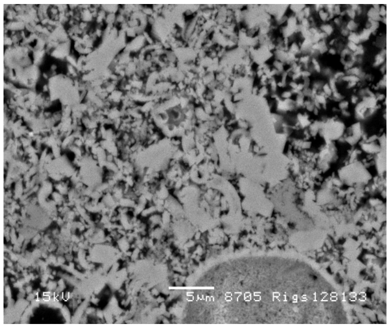

(g) Syd Arne field, Ekofisk Formation. 88% calcite, remains are quartz and kaolinite. Porosity 36%, gas permeability 0.9 mD.

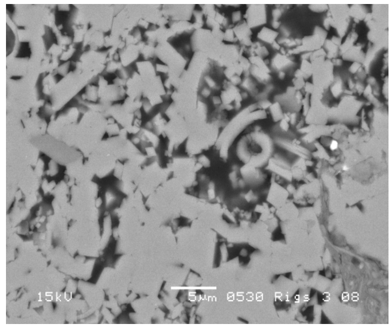

(h) Syd Arne field, Tor Formation. 97% calcite. Part of stylolite visible in right side of image. Porosity 22%, gas permeability 2.0 mD.

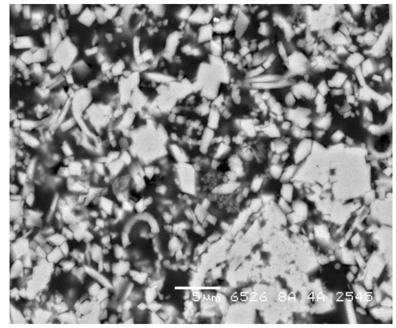

(i) Valhall field, Tor Formation. 97% calcite.

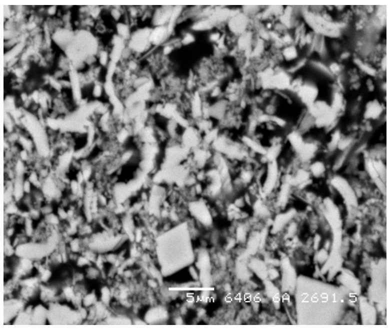

(j) Valhall field, Hod Formation. 70% calcite, remains are predominantly quartz. Porosity 30%., gas permeability 0.48 mD.

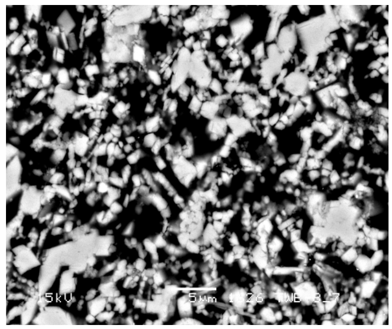

(k) Tyra field, Tor Formation. Porosity 39%, gas permeability 1.95 mD.

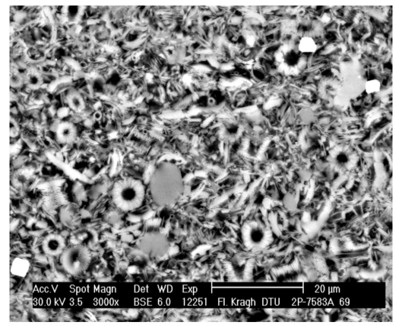

(l) Valdemar field, Tuxen Formation. 80% calcite. Porosity 38%, gas permeability 0.7 mD.

Figure 7.2: : Backscatter electron micrographs of chalk with different grain size distribution and degree of grain contact. The six upper images (a)–(f) depict samples at low magnification to illustrate texture. The six lower images (g)–(l) depict the same samples at high magnification to illustrate mineralogy and degree of cementation.

tend to be hollow fossils (Kerry, Rawlins et al. 2009). For a more quantitative grain size distribution, image analysis of backscatter electron micrographs can be done (Røgen, Gommesen et al. 2001).

7.4 Porosity and pore size distribution

Pore space in chalks comprises interparticle porosity among the fine-grained material and intra-fossil porosity (Fig. 7.2). It is characteristic of chalk that the relatively large intra-fossil porosity rarely exceeds 10% and that it is only connected through the fine interparticle porosity so that it's effect on permeability is insignificant (Fabricius, Røgen et al. 2007). Overall, the pore space is extremely well connected: Patsoules and Cripps (1982) prepared polyester resin casts of low-porosity/low permeability (ϕ= 13%–19%, k=0.005–0.09 mD) chalk from Yorkshire and found a high connectivity (14–17) between pores, a mean pore diameter of 3–5 μm, and a mean pore throat diameter of 1-2 μm. For chalk with mudstone texture, as is commonly the case in the Tor Formation, the pore size distribution is narrow as indicated by NMR and by Hg porosimetry **(Fig. 7.3)**.

The intrafossil porosity is in many reservoirs occluded by carbonate or silica cement. Where the intrafossil porosity is open, it has no significant net influence on porosity because the fossil shells are relatively thick; but when the intra-fossil porosity is occluded by cement, the presence of microfossils will tend to reduce porosity, so that wackestones obtain smaller porosity than mudstones (Borre and Fabricius 1998). A clear relation between depositional texture and porosity is rarely seen though, because the mixing of particle sizes takes place not only between calcareous microfossils and matrix, but also within the matrix. The fine-grained material comprises relatively large calcite particles and small particles of clay and nanoquartz. The degree of mixing of these components determines the inter-particle porosity (Maliva and Dickson 1992; Fabricius, Røgen et al. 2007). The nanoquartz can be a diagenetic product of dissolved siliceous microfossils, so the local

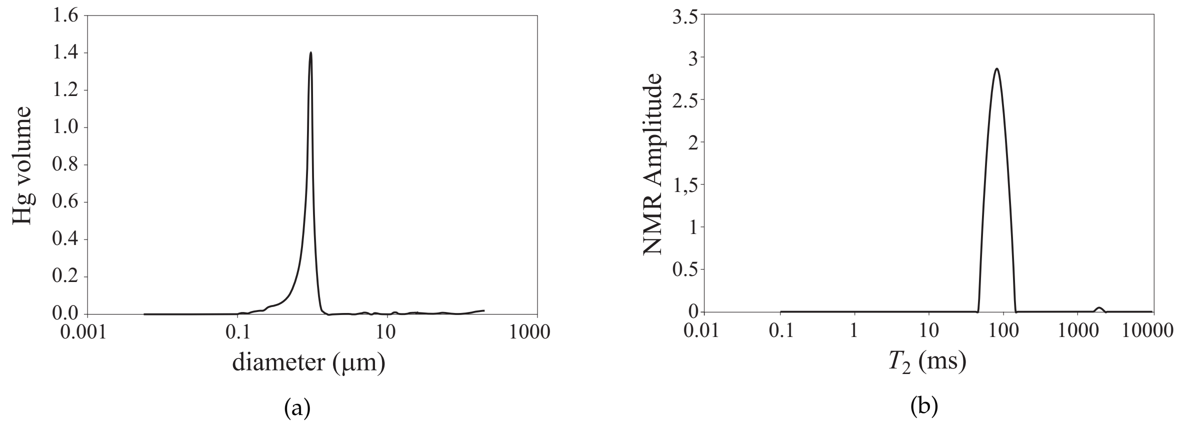

Figure 7.3: NMR curve and mercury injection curve. Gorm field, Tor Formation. Chalk mudstone. 97% calcite, porosity 35%, gas permeability 6.06 mD, BET 1.2 m^2/g. (a) Pore throat size distribution according to tube model from Hg porosimetry. (b) T2 distribution according to low field NMR spectrometry.

variations in porosity are in most cases determined by variations in the primary sediment composition, but in a complicated manner (Anderskouv and Surlyk 2012). Early seafloor cementation can cause local intervals of low porosity (hardgrounds).

Local porosity variations can be significant, but overall, porosity decreases with depth, and several attempts have been done to construct porosity-depth curves for the North Sea chalk (Scholle 1977; Mallon and Swarbrick 2002). Because the porosity reducing processes include stressgoverned processes as mechanical compaction and pressure dissolution sourced pore-filling cementation, it can make sense to construct porosity-effective stress trends or even porosity-elastic strain trends (Andersen 1995; Fabricius 2014). It is a general observation that presence of hydrocarbons in the pore space apparently prevents or retards the depth-related porosity decrease (D'Heur 1984).

7.5 Specific surface

The specific surface of a reservoir rock is the area of the interface between solid and liquid typically normalized to weight of the solid, but can also be normalized to bulk volume, solid volume or pore space. Newly deposited pelagic carbonate ooze has high specific surface but it decreases with time (Borre and Fabricius 1998) as a consequence of recrystallization. Recrystallization rate has been found to be 30–40%/Myr for freshly deposited ooze, but the rate decreases with time, so that 2-3 million old ooze recrystallize at a rate of ca. 2%/Myr (Fantle and DePaolo 2007). The recrystallization process continues in North Sea chalk and has been found to be associated with only little porosity loss (Maliva, Dickson et al. 1991).

When specific surface of chalk core samples is measured by N_2 adsorption, we find that Tor Formation samples have specific surface of ca. 1 m^2/g, whereas for samples from Hod- and Ekofisk formations the specific surface is higher. This high specific surface is mainly due to admixture of non-carbonates as clay and nanoquartz (Røgen and Fabricius 2002), so that the calcite crystals have roughly the same specific surface as in Tor Formation **(Fig. 7.4)**.

7.6 Wettability

Clean calcite has high affinity for water, but if part of the calcite surface is covered by remnants of coccolith biopolymers (Belova, Johnsson et al. 2012) or if clay and silica are present, polar hydrocarbons may adsorb and create oil-wet patches (Madsen and Lind 1998; Skovbjerg, Okhrimenko et al. 2013). Strand, Hjuler et al. (2007) found that only a small fraction of oil-wet surface could result in neutral Amott-Harvey wettability. When chalk cores are saturated with crude oil at irreducible water saturation and aged, Amott-Harvey wettability changes from water-wet to neutral wet (Graue, Viksund et al. 1999).

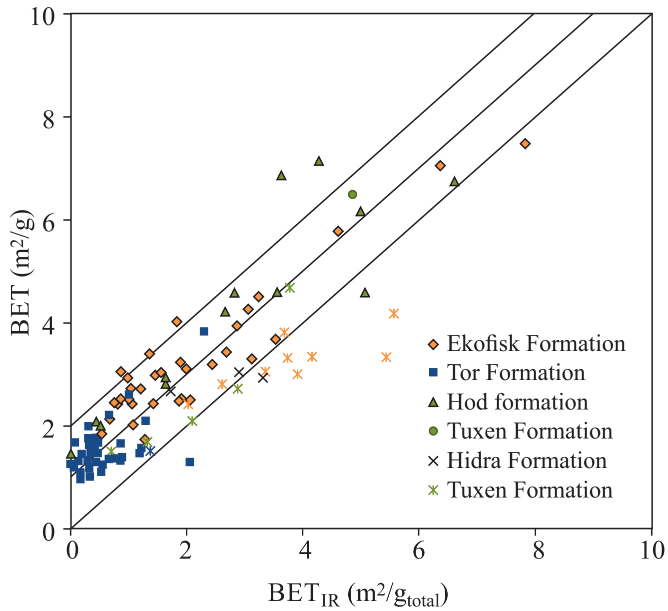

Figure 7.4: Specific surface of gently crushed samples measured by N_2 adsorption according to Brunauer, Emmett et al. (1938) (BET), versus specific surface of insoluble residue given with reference to total sample. Each formation is shown by a distinct color. Closed symbols indicate hydrocarbonbearing interval, open symbols indicate water zone samples.

7.7 Capillary pressure

A prerequisite for the common occurrence of hydrocarbon and water in a pore is that the two fluids have different pressure. The capillary pressure is then the difference between pressure in the wetting phase and in the nonwetting phase. In nature a chalk will be water saturated until hydrocarbons migrate up through fractures in the chalk. Pressure builds up in the hydrocarbons until the capillary entry pressure is overcome and hydrocarbons enter the pore space. In the samples studied by Røgen and Fabricius (2002) the capillary entry pressure is directly related to the measured specific surface with respect to pore volume. This indicates that the first pores entered are the interparticle pores. As capillary pressure builds up (the transition zone) more hydrocarbons enter, water drains out, and irreducible water saturation is reached. Also the irreducible water saturation is related to specific surface of the pore space in the sense that low irreducible water saturation is reached where specific surface is low. For this reason irreducible water saturation is typically lower in the Tor Formation than in the overlying Ekofisk Formation, and irreducible water saturation can vary significantly through a well (Fabricius and Rana 2010). The irreducible water saturation can be normalized to specific surface of pore space resulting in a calculated pseudo water film thickness which gradually diminishes as capillary pressure builds up (Larsen and Fabricius 2004). For production of hydrocarbons from a water-wet reservoir, a lowering of capillary pressure is required. Even where a neutral water-wet chalk reservoir is assumed, hydrocarbons can be produced by spontaneous imbibition of water (Yu, Evje et al. 2009).

7.8 Permeability

Permeability of sedimentary rocks depends on porosity, pore size distribution and pore connectivity. These properties can be estimated from 3D tomographic images or from 2D backscatter electron micrographs, and permeability can indeed be modelled although not without calibration the scale (Bekri, Xu et al. 2000; Talukdar and Torsæter 2002; Talukdar, Torsæter et al. 2002; Müter, Sørensen et al. 2014).

For estimating matrix permeability, especially where chalk is fractured, Kozeny's equation is useful, and it has been found that pores in North Sea chalk are so well connected, and pore space so homogeneous, that Kozenys equation can be used directly to calculate Klinkenberg permeability, k, from porosity, ϕ, and specific surface as measured from BET, S_g, and grain density ρ_g. Kozenys factor, c, can be estimated successfully from a simple model of pore space as perpendicular interpenetrating tubes, and no calibration is required (Mortensen, Engstrøm et al. 1998):

$$k = (c\phi^3)/((1-\phi)^2\rho_g^2 S_g^2), \tag{7.1}$$

$$c = (4\cos(\arccos(64\phi/\pi^3 - 1) + 4\pi)/3 + 4)^{-1}. \tag{7.2}$$

Fig. 7.5 illustrates the robustness of Kozeny's equation. Each type curve represents a constant specific surface of particles, and it can be seen how each formation, irrespective of porosity, can be assigned a specific, surface **(Fig. 7.5a)**. It can also be seen how specific surface to some extent is governed by carbonate content **(Fig. 7.5b)**. According to Mortensen, Engstrøm et al. (1998), Klinkenberg permeability may be estimated from air permeability k_a:

$$k = 0.52k_a^{1.083}, \tag{7.3}$$

where k and k_a are given in mD.

Because carbonate content also has a significant influence on velocity of elastic waves, elastic wave velocity can be a better predictor of permeability than porosity alone (Alam, Fabricius et al. 2011).

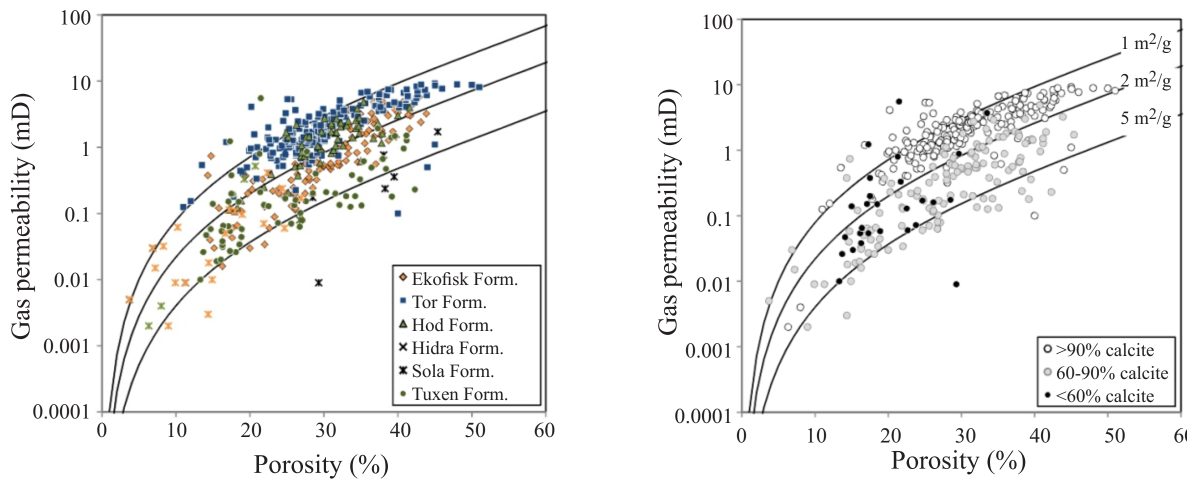

(a) (b)

Figure 7.5: Gas permeability vs. Helium porosity. (a) Data sorted by formation. Stars represent water zone data. (b) Data sorted by carbonate content calculated as calcite. The curves represent specific surface according to Kozeny's model as represented in Mortensen, Engstrøm et al. (1998).

7.9 Formation factor

In order to calculate water saturation, S_w, from porosity and electrical resistivity of the formation, R_t as well as of pore water, R_w, Archie's equation is used:

$$S_w^n = (aR_w)/(\phi^m R_t). \tag{7.4}$$

The petrophysical parameters a, m, n have default values 1, 2, 2, and especially n is difficult to estimate because it depends on the relative distribution of hydrocarbons and water in the pore space. If a is assumed equal to 1, m has been found to be related to specific surface (Olsen, Hongdul et al. 2008)

$$m = 0.09\log S + 1.97, \tag{7.5}$$

where "log" is the decal logarithm and S is specific surface with respect to bulk volume: $S = S_g\rho_g(1-\phi)$. The formation factor, F is derived from resistivity at 100% water saturation, R_o:

$$F = R_o/R_w. \tag{7.6}$$

7.10 Degree of induration

In chalk, particles are attached in a frame, which stiffens as particle contacts broaden by contact cementation, and further stiffens as pore space is filled by pore filling cementation. Degree of induration can easily be assessed on the fluid saturated chalk according to the scale of Bouma (1962):

H1 The material can without difficulty be remolded by fingers. Grain rich material falls apart in dry conditions.

H2 The material can easily be cut by a knife and scratched by a nail. For grain rich material, single grains can be detached using a fingernail.

H3 The material can be shaped by a knife but cannot be scratced by a nail. From grain rich material, grains can be detached with a knife.

H4 The material can be scratched by a knife, but single grains cannot be detached with a knife. Fractures follow the grain contacts.

H5 The material cannot be scratched by a knife. Fractures pass through the grains. North Sea chalk can have induration H2, H3 or H4.

H5 only applies to rocks composed of minerals harder than a knife, as for example sandstone, but are in chalk description typically used to designate flint.

7.11 Pore compressibility

For an isotropic porous rock at constant pore pressure, pore compressibility C_ϕ, can be calculated from porosity, the drained elastic bulk modulus, K_{dry} and the mineral bulk modulus, K_{min} (Zimmerman 1990):

$$C_\phi = (1/K_{\text{dry}} - 1/K_{\text{min}})/\phi. \tag{7.7}$$

For a discussion of elastic moduli, refer to Chapter 3 on Rock physics.

7.12 Heterogeneity

In cores and outcrop, chalks are typically bedded on a 0.2–1.0 m scale probably reflecting fluctuations in primary sediment composition possibly enhanced by diagenesis (Scholle 1977). In marly chalk, primary heterogeneity may be accentuated by pressure dissolution causing “dissolution seams” or “horse tails” to form (Scholle 1977). On a cm scale the chalk is typically thoroughly homogenized by burrowing organisms, and several types of trace fossils can be recognized (Ekdale and Bromley 1984). Large scale sedimentary structures have been observed in outcrop and from seismic investigations (Kennedy and Juignet 1974; Surlyk and Lykke-Andersen 2007).

Chalk may contain intraclasts and slump structures –clear signs of re-deposition by slumping and debris flows (Hatton 1986; Bromley and Ekdale 1987; Herrington, Pederstad et al. 1991). If sedimentation rate is low, exposure of the freshly deposited sediment on the sea floor and reaction with the sea water may lead to cementation of the sediment by phosphate, glauconite and carbonate leading to “hard grounds” (Bromley and Gale 1982).

Before petrophysical or rock mechanical testing it is advisable to check sample homogeneity by CT scanning.

7.13 Degree of fracturing

In outcrop, chalk has as a rule been found to be fractured near parallel to bedding and in two near orthogonal directions. Pumping tests in the English chalk aquifer indicate a joint spacing of 0.1 m with average aperture of 0.45 mm (Younger and Elliot 1996). With depth joints and factures tend to be closed.

In the central North Sea and in Jutland, fractures in chalk are typically associated with salt structures (Watts 1983; Jensenius 1987; Agarwal, Allen et al. 1997; Storti, Balsamo et al. 2011).

In relatively clean chalk with high porosity, shear deformation can lead to deformation bands. They are narrow zones of pore collapse - porosity reduction by grain reorganization (Wennberg, Casini et al. 2013). They occur along normal faults (Gaviglio, Bekri et al. 2009) and are typically pervasive and very visible in porous oil bearing intervals of the Tor Formation **(Fig. 7.6)** and should not be mistaken for sedimentary structures.

Figure 7.6: Deformation bands. Sample from Valhall field, Tor Formation.

Nomenclature

a = tortuosity factor
c = Kozenys factor
C_ϕ = pore compressibility
k = permeability klinkenberg, L^2, mD
k_a = permeability air, L^2, mD
K_{dry} = drained elastic bulk modulus, m/Lt^2, GPa
K_{min} = mineral bulk modulus, m/Lt^2, GPa
m = cementation exponent
n = saturation exponent
R_t = fluid saturated rock resistivity, mL^3/tq^2, Ωm
R_w = brine resistivity, mL^3/tq^2, Ωm
S_g = specific surface
S_w = water saturation
V_p = compression-wave velocity, L/t, km/s
V_s = share-wave velocity, L/t, km/s
ρ_g = grain density, m/L^3, g/cm^3
ϕ = porosity

Subscripts

dry = drained
g = grain
p = compression-wave
s = share-wave
w = water

References

Agarwal, B., Allen, L.R., and Farrell, H.E., 1997. Ekofisk Field Reservoir Characterization: Mapping Permeability Through Facies and Fracture Internsity. *SPE Formation Evaluation*, **12** (04): 227–234. SPE-35527-PA. Dec. URL `http://dx.doi.org/10.2118/35527-PA`.

Alam, M.M., Fabricius, I.L., and Prasad, M., 2011. Permeability prediction in chalks. *AAPG Bulletin*, **95** (11): 1991–2014. November. URL `http://dx.doi.org/10.1306/03011110172`.

Andersen, M.A., 1995. *Petroleum Research in North Sea Chalk.* RF-Rogaland Research. Joint Chalk Research Program Phase IV.

Anderskouv, K. and Surlyk, F., 2012. The influence of depositional processes on the porosity of chalk. *Journal of the Geological Society*, **169**: 311–325. May. URL `http://dx.doi.org/10.1144/0016-76492011-079`.

Bekri, S., Xu, K. et al., 2000. Pore geometry and transport properties in North Sea chalk. *Journal of Petroleum Science and Engineering*, **25** (3): 107–134. URL `http://dx.doi.org/10.1016/S0920-4105(00)00008-5`.

Belova, D., Johnsson, A. et al., 2012. The effect on chalk recrystallization after treatment with oxidizing agents. *Chemical Geology*, **291**: 217–223. 6 January. URL `http://dx.doi.org/10.1016/j.chemgeo.2011.10.025`.

Bertone, J.F., Cizeron, J. et al., 2003. Hydrothermal synthesis of quartz nanocrystals. *Nano Letters*, **3** (5): 655–659. URL `http://dx.doi.org/10.1021/nl025854r`.

Black, M., 1963. Function and fine-structure in protista: 2. The fine structure of the mineral parts of coccolithophoridae. *Proceedings of the Linnean Society of London*, **174** (1): 41–46. March. URL `http://dx.doi.org/10.1111/j.1095-8312.1963.tb00894.x`.

Borre, M. and Fabricius, I.L., 1998. Chemical and mechanical processes during burial diagenesis of chalk: An interpretation based on specific surface data of deep-sea sediments. *Sedimentology*, **45** (4): 755–769. August. URL `http://dx.doi.org/10.1046/j.1365-3091.1998.00178.x`.

Bouma, A.H., 1962. *Sedimentology of some flysch deposits: a graphic approach to facies interpretation*. Elsevier Pub. Co.

Bromley, R.G. and Ekdale, A.A., 1987. Mass transport in European Cretaceous chalk; fabric criteria for its recognition. *Sedimentology*, **34** (6): 1079–1092. URL `http://dx.doi.org/10.1111/j.1365-3091.1987.tb00593.x`.

Bromley, R.G. and Gale, A.S., 1982. The lithostratigraphy of the English chalk rock. *Cretaceous Research*, **3** (3): 273–306.

Brunauer, S., Emmett, P.H., and Teller, E., 1938. Adsorption of gases in multimolecular layers. *Journal of the American chemical society*, **60** (2): 309–319. February. URL `http://dx.doi.org/10.1021/ja01269a023`.

Burns, D.A., 1975. Changes in nannofossil morphology by diagenetic processes in cretaceous chalk deposits. *New Zealand Journal of Geology and Geophysics*, **18** (3): 469–476. URL `http://dx.doi.org/10.1080/00288306.1975.10421547`.

Deconinck, J.F. and Chamley, H., 1995. Diversity of smectite origins in Late Cretaceous sediments: example of chalks from northern France. *Clay Minerals*, **30** (4): 365–379. URL `http://dx.doi.org/10.1180/claymin.1995.030.4.09`.

D'Heur, M., 1984. Porosity and hydrocarbon distribution in the North Sea chalk reservoirs. *Marine and Petroleum Geology*, **1** (3): 211–238. URL `http://dx.doi.org/10.1016/0264-8172(84)90147-8`.

Dunham, R.K., 1962. Classification of carbonate rocks according to depositional texture. *Memoir -American Association of Petroleum Geologists Special Volumes*, 108–121. URL `http://archives.datapages.com/data/specpubs/carbona2/data/a038/a038/0001/0100/0108.htm`.

Ehrmann, W.U., 1986. *Zum Sedimenteintrag in das zentrale nordwesteuropäische Oberkreidemeer (Das Maastricht in Nordwestdeutchland, Teil 7)*. Schweizerbart Science Publishers, Stuttgart, Germany. ISBN 9783510963997. December. URL `http://www.schweizerbart.de//publications/detail/isbn/9783510963997/Geologisches_Jahrbuch_Reihe_A_Heft`.

Ekdale, A.A. and Bromley, R.G., 1984. Comparative ichnology of shelf-sea and deep-sea Chalk. *Journal of Paleontology*, **58** (2): 322–332. URL `http://www.jstor.org/stable/1304787`.

Fabricius, I.L., 2014. Burial stress and elastic strain of carbonate rocks. *Geophysical Prospecting*, **62** (6): 1327–1336. 18 September. URL `http://dx.doi.org/10.1111/1365-2478.12184`.

Fabricius, I.L. and Borre, M.K., 2007. Stylolites, porosity, depositional texture, and silicates in chalk facies sediments. Ontong Java Plateau–Gorm and Tyra fields, North Sea. *Sedimentology*, **54** (1): 183–205. February. URL http://dx.doi.org/10.1111/j.1365-3091.2006.00828.x.

Fabricius, I.L., Høier, C. et al., 2007. Modelling elastic properties of impure chalk from South Arne Field, North Sea. *Geophysical Prospecting*, **55** (4): 487–506. July. URL http://dx.doi.org/10.1111/j.1365-2478.2007.00613.x.

Fabricius, I.L. and Rana, M.A., 2010. Tilting oil-water contact in the chalk of Tyra Field as interpreted from capillary pressure data. In *Geological Society, London, Petroleum Geology Conference series*, vol. 7, 463–472. Geological Society of London, Geological Society of London. URL http://dx.doi.org/10.1144/0070463.

Fabricius, I.L., Røgen, B., and Gommesen, L., 2007. How depositional texture and diagenesis control petrophysical and elastic properties of samples from five North Sea chalk fields. *Petroleum Geoscience*, **13** (1): 81–95. February. URL http://dx.doi.org/10.1144/1354-079306-707.

Fantle, M.S. and DePaolo, D.J., 2007. Ca isotopes in carbonate sediment and pore fluid from ODP Site 807A: the Ca^{2+}(aq)–calcite equilibrium fractionation factor and calcite recrystallization rates in Pleistocene sediments. *Geochimica et Cosmochimica Acta*, **71** (10): 2524–2546.

Gaviglio, P., Bekri, S. et al., 2009. Faulting and deformation in chalk. *Journal of Structural Geology*, **31** (2): 194 – 207. February. URL http://dx.doi.org/http://dx.doi.org/10.1016/j.jsg.2008.11.011.

Gély, J.P. and Blanc, P., 2004. Evolution diagénétique dans la craie pélagique dolomitisée du crétacé supérieur du bassin de Paris (région de Provins, France). *Eclogae Geologicae Helvetiae*, **97** (3): 393–409. December. URL http://dx.doi.org/10.1007/s00015-004-1126-5.

Graue, A., Viksund, B.G. et al., 1999. Systematic wettability alteration by aging sandstone and carbonate rock in crude oil. *Journal of Petroleum Science and Engineering*, **24** (2): 85–97. URL http://dx.doi.org/10.1016/S0920-4105(99)00033-9.

Håkansson, E., Bromley, R., and Perch-Nielsen, K., 1974. Maastrichtian Chalk of North-West Europe—a Pelagic Shelf Sediment. *Pelagic Sediments: on Land and under the Sea*, 211–233. URL http://dx.doi.org/10.1002/9781444304855.ch9.

Hansen, T. and Surlyk, F., 2014. Marine macrofossil communities in the uppermost Maastrichtian chalk of Stevns Klint, Denmark. *Palaeogeography, Palaeoclimatology, Palaeoecology*, **399**: 323–344. URL http://dx.doi.org/10.1016/j.palaeo.2014.01.025.

Hatton, I.R., 1986. Geometry of allochthonous Chalk Group members, Central Trough, North Sea. *Marine and Petroleum Geology*, **3** (2): 79–98. URL http://dx.doi.org/10.1016/0264-8172(86)90022-X.

Herrington, P., Pederstad, K., and Dickson, J., 1991. Sedimentology and Diagenesis of Resedimented and Rhythmically Bedded Chalks from the Eldfisk Field, North Sea Central Graben (1). *AAPG Bulletin*, **75** (11): 1661–1674. November. URL http://archives.datapages.com/data/bulletns/1990-91/images/pg/00750011/0000/16610.pdf.

Hjuler, M.L. and Fabricius, I.L., 2009. Engineering properties of chalk related to diagenetic variations of Upper Cretaceous onshore and offshore chalk in the North Sea area. *Journal of Petroleum Science and Engineering*, **68** (3): 151–170. October. URL http://dx.doi.org/10.1016/j.petrol.2009.06.005.

Jakobsen, F., Lindgreen, H., and Springer, N., 2000. Precipitation and flocculation of spherical nanosilica in North Sea chalk. *Clay Minerals*, **35** (1): 175–184. March. URL http://dx.doi.org/10.1180/000985500546567.

Jarvis, I., 1992. Sedimentology, geochemistry and origin of phosphatic chalks: the Upper Cretaceous deposits of NW Europe. *Sedimentology*, **39** (1): 55–97. URL http://dx.doi.org/10.1111/j.1365-3091.1992.tb01023.x.

Jeans, C., 2006. Clay mineralogy of the Cretaceous strata of the British Isles. *Clay Minerals*, **41** (1): 47–150. March. URL http://dx.doi.org/10.1180/0009855064110196.

Jensenius, J., 1987. High-temperature diagenesis in shallow chalk reservoir, Skjold oil field, Danish North Sea: Evidence from fluid inclusions and oxygen isotopes. *AAPG Bulletin*, **71** (11): 1378–1386. URL http://archives.datapages.com/data/bulletns/1986-87/images/pg/00710011/1350/13780.pdf.

Jørgensen, N.O., 1983. Dolomitization in chalk from the North Sea central graben. *Journal of Sedimentary Research*, **53** (2): 557–564. URL http://archives.datapages.com/data/sepm/journals/v51-54/data/053/053002/pdfs/0557.pdf.

Jørgensen, N.O., 1986. Geochemistry, diagenesis and nannofacies of chalk in the North Sea Central Graben. *Sedimentary geology*, **48** (3): 267–294. July. URL http://dx.doi.org/10.1016/0037-0738(86)90033-3.

Kennedy, W. and Juignet, P., 1974. Carbonate banks and slump beds in the Upper Cretaceous (Upper Turonian-Santonian) of Haute Normandie, France. *Sedimentology*, **21** (1): 1–42. URL http://dx.doi.org/10.1111/j.1365-3091.1974.tb01780.x.

Kerry, R., Rawlins, B. et al., 2009. Problems with determining the particle size distribution of chalk soil and some of their implications. *Geoderma*, **152** (3): 324–337. September. URL http://dx.doi.org/10.1016/j.geoderma.2009.06.018.

Larsen, J.K. and Fabricius, I.L., 2004. Interpretation of water saturation above the transitional zone in chalk reservoirs. *SPE Reservoir Evaluation & Engineering*, **7** (02): 155–163. SPE-69685-PA. April. URL http://dx.doi.org/10.2118/69685-PA.

Lind, I., Nykjaer, O. et al., 1994. Permeability of stylolite-bearing chalk. *Journal of Petroleum Technology*, **46** (11): 986–993. SPE-26019-PA. November. URL http://dx.doi.org/10.2118/26019-PA.

Lindgreen, H., Fallick, A.E. et al., 2012. The tight Danian Ekofisk chalk reservoir formation in the south Arne field, North Sea: mineralogy and porosity properties. *Journal of Petroleum Geology*, **35** (3): 291–309. July. URL http://dx.doi.org/10.1111/j.1747-5457.2012.00531.x.

Madsen, H.B. and Stemmerik, L., 2009. Early diagenetic celestite replacement of demosponges in Upper Cretaceous (Campanian–Maastrichtian) chalk, Stevns, Denmark. *Geology*, **37** (4): 355–358. URL http://dx.doi.org/10.1130/G25254A.1.

Madsen, L. and Lind, I., 1998. Adsorption of carboxylic acids on reservoir minerals from organic and aqueous phase. *SPE Reservoir Evaluation & Engineering*, **1** (01): 47–51. SPE-37292-PA. February. URL http://dx.doi.org/10.2118/37292-PA.

Maliva, R.G. and Dickson, J., 1992. Microfacies and diagenetic controls of porosity in Cretaceous/Tertiary chalks, Eldfisk field, Norwegian North Sea (1). *AAPG Bulletin*, **76** (11): 1825–1838. November. URL http://archives.datapages.com/data/bulletns/1992-93/images/pg/00760011/0000/18250.pdf.

Maliva, R.G. and Dickson, J.A.D., 1994. Origin and environment of formation of late diagenetic dolomite in Cretaceous/Tertiary chalk, North Sea Central Graben. *Geological Magazine*, **131** (05): 609–617. September. URL http://dx.doi.org/10.1017/S0016756800012395.

Maliva, R.G., Dickson, J.A.D., and Fallick, A.E., 1999. Kaolin cements in limestones: potential indicators of organic-rich pore waters during diagenesis. *Journal of Sedimentary Research*, **69** (1): 158–163. January. URL http://archives.datapages.com/data/sepm/journals/v66-67/data/069/069001/pdfs/0158.pdf.

Maliva, R.G., Dickson, J.A.D., and Råheim, A., 1991. Modelling of chalk diagenesis (Eldfisk Field, Norwegian North Sea) using whole rock and laser ablation stable isotopic data. *Geological Magazine*, **128** (01): 43–49. January. URL http://dx.doi.org/10.1017/S0016756800018033.

Mallon, A.J. and Swarbrick, R.E., 2002. A compaction trend for non-reservoir North Sea Chalk. *Marine and Petroleum Geology*, **19** (5): 527–539. URL http://dx.doi.org/http://dx.doi.org/10.1016/S0264-8172(02)00027-2.

Mavko, G., Mukerji, T., and Dvorkin, J., 2009. *The Rock Physics Handbook*. 2nd ed., Cambridge University Press. Isbn: 9780521861366. URL http://dx.doi.org/10.1017/cbo9780511626753.

Mortensen, J., Engstrøm, F., and Lind, I., 1998. The relation among porosity, permeability, and specific surface of chalk from the Gorm field, Danish North Sea. *SPE Reservoir Evaluation & Engineering*, **1** (03): 245–251. SPE-31062-PA. June. URL http://dx.doi.org/10.2118/31062-PA.

Müter, D., Sørensen, H.O. et al., 2014. Resolution dependence of petrophysical parameters derived from X-ray tomography of chalk. *Applied Physics Letters*, **105** (4): 043108. July. URL http://dx.doi.org/10.1063/1.4891965.

Neugebauer, J., 1974. Some Aspects of Cementation in Chalk, In *Pelagic Sediments: On Land and under the Sea*, eds., K.J. Hsü and H.C. Jenkyns, , 149–176. Blackwell Publishing Ltd. ISBN 9781444304855. URL http://dx.doi.org/10.1002/9781444304855.ch7.

Olsen, C., Hongdul, T., and Lykke Fabricius, I., 2008. Prediction of Archie's cementation factor from porosity and permeability through specific surface. *Geophysics*, **73** (2): E81–E87. March. URL http://dx.doi.org/10.1190/1.2837303.

Pacey, N.R., 1984. Bentonites in the Chalk of central eastern England and their relation to the opening of the northeast Atlantic. *Earth and Planetary Science Letters*, **67** (1): 48–60. January. URL http://dx.doi.org/10.1016/0012-821X(84)90037-2.

Pacey, N.R., 1989. Organic matter in Cretaceous chalks from eastern England. *Chemical geology*, **75** (3): 191–208. March. URL http://dx.doi.org/10.1016/0009-2541(89)90118-6.

Patsoules, M. and Cripps, J., 1982. The application of resin impregnation to the three-dimensional study of chalk pore geometry. *Engineering Geology*, **19** (1): 15–27. December. URL http://dx.doi.org/10.1016/0013-7952(82)90003-5.

Røgen, B. and Fabricius, I.L., 2002. Influence of clay and silica on permeability and capillary entry pressure of chalk reservoirs in the North Sea. *Petroleum Geoscience*, **8** (3): 287–293. September. URL http://dx.doi.org/10.1144/petgeo.8.3.287.

Røgen, B., Gommesen, L., and Fabricius, I.L., 2001. Grain size distributions of chalk from image analysis of electron micrographs. *Computers & Geosciences*, **27** (9): 1071–1080. November. URL http://dx.doi.org/10.1016/S0098-3004(00)00159-X.

Scholle, P.A., 1977. Chalk diagenesis and its relation to petroleum exploration: oil from chalks, a modern miracle? *AAPG Bulletin*, **61** (7): 982–1009. July. URL http://dx.doi.org/10.1306/C1EA43B5-16C9-11D7-8645000102C1865D.

Simonsen, L. and Toft, J., 2006. Texture, composition and stratigraphy of volcanic ash beds in lower Palaeocene chalk from the North Sea Central Graben area. *Marine and Petroleum Geology*, **23** (7): 767–776. August. URL http://dx.doi.org/10.1016/j.marpetgeo.2006.06.003.

Skovbjerg, L.L., Okhrimenko, D.V. et al., 2013. Preferential adsorption of hydrocarbons to nanometer-sized clay on chalk particle surfaces. *Energy & Fuels*, **27** (7): 3642–3652. June. URL http://dx.doi.org/10.1021/ef301832b.

Stipp, S.L.S., 1999. Toward a conceptual model of the calcite surface: hydration, hydrolysis, and surface potential. *Geochimica et Cosmochimica Acta*, **63** (19): 3121–3131. October. URL http://dx.doi.org/10.1016/S0016-7037(99)00239-2.

Storti, F., Balsamo, F. et al., 2011. Sub-seismic scale fracture pattern and in situ permeability data in the chalk atop of the Krempe salt ridge at Lägerdorf, NW Germany: inferences on synfolding stress field evolution and its impact on fracture connectivity. *Marine and Petroleum Geology*, **28** (7): 1315–1332. July. URL http://dx.doi.org/10.1016/j.marpetgeo.2011.03.014.

Strand, S., Hjuler, M.L. et al., 2007. Wettability of chalk: impact of silica, clay content and mechanical properties. *Petroleum Geoscience*, **13** (1): 69–80. February. URL http://dx.doi.org/10.1144/1354-079305-696.

Surlyk, F. and Lykke-Andersen, H., 2007. Contourite drifts, moats and channels in the Upper Cretaceous chalk of the Danish Basin. *Sedimentology*, **54** (2): 405–422. April. URL http://dx.doi.org/10.1111/j.1365-3091.2006.00842.x.

Talukdar, M.S. and Torsæter, O., 2002. Reconstruction of chalk pore networks from 2D backscatter electron micrographs using a simulated annealing technique. *Journal of Petroleum Science and Engineering*, **33** (4): 265–282. May. URL http://dx.doi.org/10.1016/S0920-4105(02)00148-1.

Talukdar, M.S., Torsæter, O. et al., 2002. Stochastic reconstruction, 3D characterization and network modeling of chalk. *Journal of Petroleum Science and Engineering*, **35** (1): 1–21. July. URL http://dx.doi.org/10.1016/S0920-4105(02)00160-2.

Tröger, W.E., 2017. *Optische Bestimmung der gesteinsbildenden Minerale Teil I.: Bestimmungstabellen*. Schweizerbart Science Publishers, Stuttgart, Germany. ISBN 9783510651061. Hrsg.: Hans Ulrich Bambauer; Franz Taborszky; Hans Dieter Trochim. March. URL http://www.schweizerbart.de//publications/detail/isbn/9783510651061/Troger_Opt_Bestimmungen_Teil_1_Best.

Watts, N.L., 1983. Microfractures in chalks of Albuskjell Field, Norwegian Sector, North Sea: possible origin and distribution. *AAPG Bulletin*, **67** (2): 201–234. February. URL http://dx.doi.org/10.1306%2F03B5ACEB-16D1-11D7-8645000102C1865D.

Wennberg, O.P., Casini, G. et al., 2013. Deformation bands in chalk, examples from the Shetland Group of the Oseberg Field, North Sea, Norway. *Journal of Structural Geology*, **56**: 103 – 117. November. URL http://dx.doi.org/10.1016/j.jsg.2013.09.005.

Wise Jr, S.W. and Kelts, K.R., 1972. Inferred diagenetic history of a weakly silicified deep sea chalk. *GCAGS Transactions*, **22**: 177–203. URL http://archives.datapages.com/data/gcags/data/022/022001/0177.htm.

Wolfe, M., 1970. Dolomitization and dedolomitization in the Senonian chalk of Northern Ireland. *Geological Magazine*, **107** (01): 39–49. January. URL http://dx.doi.org/10.1017/S0016756800054686.

Wray, D. and Jeans, C., 2014. Chemostratigraphy and provenance of clays and other non-carbonate minerals in chalks of Campanian age (Upper Cretaceous) from Sussex, southern England. *Clay Minerals*, **49** (2): 327–340. May. URL http://dx.doi.org/10.1180/claymin.2014.049.2.10.

Wray, D.S. and Wood, C.J., 1998. Distinction between detrital and volcanogenic clay-rich beds in Turonian–Coniacian chalks of eastern England. *Proceedings of the Yorkshire Geological and Polytechnic Society*, **52** (1): 95–105. May. URL http://dx.doi.org/10.1144/pygs.52.1.95.

Younger, P.L. and Elliot, T., 1996. Discussion on 'Chalk fracture system characteristics: implications for flow and solute transport'. *Quarterly Journal of Engineering Geology and Hydrogeology*, **29** (1): 93–94. URL http://dx.doi.org/10.1144/GSL.QJEGH.1996.029.P1.07.

Yu, L., Evje, S. et al., 2009. Spontaneous imbibition of seawater into preferentially oil-wet chalk cores–Experiments and simulations. *Journal of petroleum science and engineering*, **66** (3): 171–179. June. URL http://dx.doi.org/10.1016/j.petrol.2009.02.008.

Zimmerman, R.W., 1990. *Compressibility of sandstones*, vol. 29. Elsevier, New York.

Chapter 8

Transport Equations

Hans Kleppe

8.1 Introduction

Reservoir simulation is a powerful prediction method for reservoir production performance. In early days engineering calculations consisted largely of analytical methods. Today sophisticated simulation tools are available. Using numerical solution detailed reservoir information is captured and complicated reservoir processes are modeled.

Chalk reservoirs represent special challenges regarding modeling. The reservoirs are fractured and fluid flow is largely governed by fracture network conductivity. To model such systems a dual porosity approach is frequently used, where two interconnected simulation cells are associated with each block in the geometric grid representing the matrix and fracture volumes. If a standard single continuum model is used for modeling of fractured reservoirs construction of effective flow parameters accounting for fractures are needed.

Conventional reservoir simulators calculate the effect of rock compaction on pore volume change through a time independent rock compressibility. This representation of compaction is normally not adequate for weak chalk reservoirs. Coupled analysis of geomechanics and fluid flow where flow properties vary with effective stress changes is required to obtain satisfactory simulation results.

In fractured preferentially oil-wet chalk reservoirs wetting changes during water injection will impact recovery. Studies of oil-wet chalk show that seawater may alter the wettability towards increased water-wetness. The result is increased imbibition of water from fractures to matrix rock resulting in higher oil recovery. To capture this effect a model allowing dynamic wetting alteration is needed.

Standard formulation of mass conservation equations for black-oil and compositional models is included in this exposition. Similar material can be found in numerous publications, for example SPOR Monograph (Skjæveland and Kleppe 1992) and Petroleum Engineering Handbook (Batycky, Thiele et al. 2007).

Equations for modeling of temperature effects are not included and instantaneous phase equilibrium is assumed. Special emphasis is put on formulation of equations to be used for modeling of fluid flow in fractured reservoirs, including dual porosity formulation, influence of stress changes on fluid flow and wetting alteration caused by seawater injection.

The differential equations for mass conservation are discretized using finite differences and solved numerically using IMPES, fully implicit or Adaptive Implicit Method (AIM). To avoid stability restrictions of IMPES solution, fully implicit or AIM methods are preferred. For most black-oil cases fully implicit solution is used. For problems with an extended set of components the AIM method is a convenient option since it represents an attractive compromise between fully implicit stability and IMPES low computer work. For coupled geomechanics and flow simulation finite element discretization is used for the geomechanics computations. Details regarding numerical solution are found in text books on reservoir simulation Batycky, Thiele et al. (2007) and are not included in this exposition.

8.2 Black oil models

Black oil equations are formulated using the assumption of three components; water, oil and gas at a reference level called standard conditions. There are three phases present, water phase, oil phase and gas phase. Water phase consists of water component only, oil phase consists of oil component and part of the gas component (dissolved gas) and gas phase consists of gas component only.

Conservation of mass is expressed in terms component balance. Using differential operators divergence $\nabla\cdot$ and gradient ∇ the black oil mass conservation differential equations are written

$$\text{water:} \quad \nabla \cdot \left[\frac{[k]k_{rw}}{\mu_w B_w} (\nabla p_w - \gamma_w \nabla d) \right] = \frac{\partial}{\partial t} (\phi \frac{S_w}{B_w}) + Q_w \tag{8.1}$$

$$\text{oil:} \quad \nabla \cdot \left[\frac{[k]k_{ro}}{\mu_o B_o} (\nabla p_o - \gamma_o \nabla d) \right] = \frac{\partial}{\partial t} (\phi \frac{S_o}{B_o}) + Q_o \tag{8.2}$$

$$\text{gas:} \quad \nabla \cdot \left[\frac{[k]k_{rg}}{\mu_g B_g} (\nabla p_g - \gamma_g \nabla d) \right] + \nabla \cdot \left[\frac{[k]k_{ro} R_s}{\mu_o B_o} (\nabla p_o - \gamma_o \nabla d) \right] = \frac{\partial}{\partial t} (\phi \frac{S_g}{B_g} + \phi \frac{R_s S_o}{B_o}) + Q_g \tag{8.3}$$

The equations consist of flow terms, source/sink terms Q and accumulation terms on the right hand side.

Tensor notation is used for absolute permeability$[k]$. Usually it is assumed that the principle axes of permeability coincide with the directions of the coordinate system. In this case $[k]$ is a diagonal tensor and three values of permeability are required for each point, one for each coordinate direction. However, in case fractured reservoirs are modeled using a single continuum model with effective properties to account for fractures, assuming that $[k]$ is diagonal may be too restrictive (Rodriguez, Klie et al. 2006). Also, assuming diagonal $[k]$ is not necessarily valid if modeling of fluid flow is coupled to geomechanics computations making absolute permeability dependent on stress changes (Bagheri and A. 2008).

Other symbols in Eqs. 8.1 – 8.3 denote phase properties, viscosities and volume factors μ_l, B_l, $l = w, o, g$, gravities γ_l, $l = w, o, g$, gas in oil solution ratio R_s and relative permeabilities $k_{rl}, l = w, o, g$. Finally, d is the vertical distance from a reference level and ϕ denotes porosity.

The Eqs. 8.1 – 8.3 are used to solve for phase pressures p_l and phase saturations S_l, $l = w, o, g$. Instructions on how to compute volume factors, viscosities and solution ratio as functions of phase pressures are supplied to the model in terms of tables or correlations. Relative permeabilities and capillary pressures are specified as functions of saturation distribution as well.

Three additional equations are required to obtain a well-posed problem. The additional equations are the capillary pressure and saturation constraints

$$p_o - p_w = P_{cow}(S_w), \quad p_g - p_o = P_{cgo}(S_g), \quad S_o + S_g + S_w = 1. \tag{8.4}$$

Finally, to obtain a unique solution boundary conditions are needed. Normally initial equilibrium state and no flow exterior boundaries are specified.

Black oil model finite difference equations for block i, j, k are written

$$\text{water:} \quad \Delta T_w \Delta \psi_w = \frac{V_{i,j,k}}{\Delta t} \Delta_t (\phi \frac{S_w}{B_w}) + q_{w,i,j,k} \tag{8.5}$$

$$\text{oil:} \quad \Delta T_o \Delta \psi_o = \frac{V_{i,j,k}}{\Delta t} \Delta_t (\phi \frac{S_o}{B_o}) + q_{o,i,j,k} \tag{8.6}$$

$$\text{gas:} \quad \Delta T_g \Delta \psi_g + \Delta T_o R_s \Delta \psi_o = \frac{V_{i,j,k}}{\Delta t} \Delta_t (\phi \frac{S_g}{B_g} + \phi \frac{S_o R_s}{B_o}) + q_{g,i,j,k}. \tag{8.7}$$

Finite difference time operator Δ_t is defined by $\Delta_t(A) = A^{n+1} - A^n$, n denotes old time step and $n + 1$ new time step. For 3D problems expanding the finite difference space operator $\Delta T_l \Delta \psi_l$ results in six terms for flow between block i, j, k and all neighbor blocks

$$\Delta T_l \Delta \psi_l = \Delta_x T_{lx} \Delta_x \psi_l + \Delta_y T_{ly} \Delta_y \psi_l + \Delta_z T_{lz} \Delta_z \psi_l.$$

To compute x-direction flow term $\Delta_x T_{lx} \Delta_x \psi_l$ grid parameters depicited in **Fig.** 8.1 are needed.

Flow between neighbor blocks i and $i + 1$ in the x-direction is given by

$$\left(\frac{k_x k_{rl}}{\mu_l B_l \Delta x} \right)_{i+1/2} A(\psi_{l,i+1} - \psi_{l,i})$$

where indices j and k for y- and z-directions are suppressed. Cross section area normal to x-direction flow is denoted A. This interblock flow term is a discretized version of Darcy's law for volumetric flow.

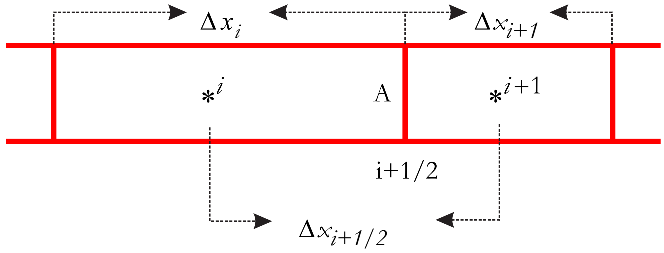

Figure 8.1: x-direction grid parameters.

Care must be taken in evaluating flow parameters at block boundary $i+1/2$. For absolute permeability harmonic mean is the standard choice. Inter block relative permeabilities are computed using upstream evaluation, i.e., the value in upstream block is used to represent block boundary value. For fluid properties arithmetic mean or upstream evaluation can be used.

All parameters appearing in the differential equations are also used in the difference equations. In addition time step length $\Delta t = t^{n+1} - t^n$ and grid block parameters including bulk volume $V_{i,j,k}$ is used. Phase potential ψ_l includes phase pressure and gravity.

Flow term in negative x-direction and flow terms for y- and z-directions are straightforward modifications of the x-term discussed above.

The finite difference Eqs. 8.5 – 8.7 express mass conservation for block i, j, k in terms of surface volumes of water, oil and gas. Change in fluid volumes during time step Δt is caused by flow between neighbor blocks and contribution from wells.

8.3 Compositional models

Compositional models are needed for simulation of gas injection where changes in fluid compositions play a crucial role. As for black-oil models three phases are present, water, oil, and gas. More than two hydrocarbon components are used in a compositional model. Let Nc be the number of hydrocarbon components and denote by $\{x_{ic}\}$ and $\{y_{ic}\}$ oil and gas phase compositions in terms of component mole fractions. Hydrocarbon phase density ρ_l and viscosity μ_l, $l = o, g$, depend on pressures and fluid compositions

$$\begin{aligned}\rho_o &= \rho_o(p_o, x_1, \ldots, x_{Nc}), \quad \rho_g = \rho_g(p_g, y_1, \ldots, y_{Nc}) \\ \mu_o &= \mu_o(p_o, x_1, \ldots, x_{Nc}), \quad \mu_g = \mu_g(p_g, y_1, \ldots, y_{Nc})\end{aligned}$$

Hydrocarbon fluid properties are calculated using a cubic equation of state like Peng-Robinson or Redlich-Kwong.

The water phase consists of water component only. The hydrocarbon components partition exclusively between oil and gas phases. Differential equations for component mass conservation are written

water:

$$\nabla \cdot \left[\frac{[k]k_{rw}}{\mu_w} \rho_w (\nabla p_w - \gamma_w \nabla d) \right] = \frac{\partial}{\partial t}(\phi \rho_w S_w) + Q_w \tag{8.8}$$

hydrocarbon component ic, $ic = 1, \ldots, Nc$:

$$\begin{aligned}\nabla \cdot \left[\frac{[k]k_{ro}}{\mu_o} \rho_o x_{ic} (\nabla p_o - \gamma_o \nabla d) \right] + \nabla \cdot \left[\frac{[k]k_{rg}}{\mu_g} \rho_g y_{ic} (\nabla p_g - \gamma_g \nabla d) \right] \\ = \frac{\partial}{\partial t}(\phi \rho_o x_{ic} S_o + \phi \rho_g y_{ic} S_g) + Q_{ic},\end{aligned} \tag{8.9}$$

where densities are mole densities.

Saturation dependent relative permeabilities k_{rl} and capillary pressures are specified in the same way as for the black oil model with one exception. For modeling of gas/oil multiple contact miscibility gas/oil saturation functions are modified using interfacial tension to obtain convergence towards straight lines as miscibility is approached.

The $Nc+1$ Eq. 8.8 and 8.9 are used to compute fluid compositions$\{x_{ic}\},\{y_{ic}\}$ and phase pressures and saturations. Additional equations are needed to obtain a well-posed problem. The capillary pressure and saturation constraints 8.4 are used. Two additional constraints are obtained using that mole fractions $\{x_{ic}\}$ and $\{y_{ic}\}$ add to one. The mole fractions for component ic in oil and gas phase are related by an equilibrium K-value

$$K_{ic} = \frac{y_{ic}}{x_{ic}}$$

This completes the set of equations needed to solve the $2Nc+6$ unknowns. Equilibrium K-values can be computed using fugacity relations. Another option will be to supply tables of K-values as part of the model input.

Similar to black oil models component finite difference equations for block i,j,k are written

water:

$$\Delta T_w \Delta\psi_w = \frac{V_{i,j,k}}{\Delta t}\Delta_t(\phi\rho_w S_w) + q_{w,i,j,k} \tag{8.10}$$

hydrocarbon component ic, $ic = 1,\ldots,Nc$:

$$\Delta T_o x_{ic}\Delta\psi_o + \Delta T_g y_{ic}\Delta\psi_g = \frac{V_{i,j,k}}{\Delta t}\Delta_t(\phi\rho_o x_{ic} S_o + \phi\rho_g y_{ic} S_g) + q_{ic,i,j,k}. \tag{8.11}$$

Finite difference operators are defined in the same way as for black oil difference equations.

The component finite difference Eq. 8.10 and 8.11 express mass conservation for block i,j,k in terms of number of moles. As for black oil models change in mass during time step Δt is caused by flow between neighbor blocks and contribution from wells.

8.4 Naturally fractured reservoirs

In naturally fractured reservoirs fluids exist in two interconnected systems

- the rock matrix usually providing the bulk of the reservoir volume
- the high permeable rock fractures where most of the flow takes place.

Fractures appear with varying spacing, orientation, length and aperture. To simulate matrix/fracture flow rigorously by sufficiently refining the computational grid to account for individual fractures is not practical. Dual continuum models are frequently used for simulating fluid flow in fractured reservoirs. Another option is to use a standard single continuum model where effective grid parameters and saturation functions are designed to account for fractures.

8.4.1 Dual porosity models

The basic assumption for dual porosity models is that fluid flow takes place in the fracture network only as shown in **Fig. 8.2**. The low permeability high storativity matrix is considered sink/source to the fractures. Two simulation grids with identical grid geometry are imposed on the reservoir. One simulation grid is given matrix properties. There is no communication between matrix grid blocks. The second simulation grid is given fracture properties with high permeability and small porosity reflecting that fracture volume accounts for a small fraction of the reservoir pore volume. A matrix/fracture mass exchange term is used for fluid transfer between matrix and fracture blocks.

There is one set of equations for the matrix system and one for the fracture system. For a black oil model discretized equations for fracture flow are

$$\text{water:}\qquad \Delta T_{wf}\Delta\psi_{wf} - \tau_{w,mf,i,j,k} = \frac{V_{i,j,k}}{\Delta t}\Delta_t(\phi_f\frac{S_{wf}}{B_{wf}}) + q_{wf,i,j,k} \tag{8.12}$$

$$\text{oil:}\qquad \Delta T_{of}\Delta\psi_{of} - \tau_{o,mf,i,j,k} = \frac{V_{i,j,k}}{\Delta t}\Delta_t(\phi_f\frac{S_{of}}{B_{of}}) + q_{of,i,j,k} \tag{8.13}$$

$$\text{gas:}\qquad \Delta T_{gf}\Delta\psi_{gf} + \Delta T_{of}R_{sf}\Delta\psi_{of} - \tau_{g,mf,i,j,k} = \frac{V_{i,j,k}}{\Delta t}\Delta_t(\phi\frac{S_{gf}}{B_{gf}} + \phi\frac{S_{of}R_{sf}}{B_{of}}) + q_{gf,i,j,k} \tag{8.14}$$

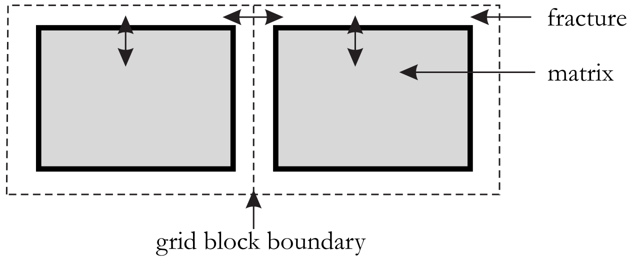

Figure 8.2: Dual porosity grid.

Subscripts f and mf denote fracture and matrix/fracture properties respectively. The τ terms are used to compute fluid transfer between matrix and fracture blocks and are given by

$$\begin{aligned}\tau_{l,mf,i,j,k} &= \xi_{i,j,k} V_{i,j,k} (\frac{k_{rl}}{\mu_l B_l})_{mf,i,j,k} (\psi_{lf} - \psi_{lm})_{i,j,k}, \quad l = o, w \\ \tau_{g,mf,i,j,k} &= \xi_{i,j,k} V_{i,j,k} [(\frac{k_{rg}}{\mu_g B_g})_{mf} (\psi_{gf} - \psi_{gm}) + (\frac{R_s k_{ro}}{\mu_o B_o})_{mf} (\psi_{of} - \psi_{om})]_{i,j,k}.\end{aligned} \tag{8.15}$$

Following the approach of Kazemi, Merrill Jr et al. (1976) the shape factor ξ is expressed as

$$\xi_{i,j,k} = 4K_{i,j,k} (\frac{1}{L_x^2} + \frac{1}{L_y^2} + \frac{1}{L_z^2})_{i,j,k},$$

where L_x, L_y, L_z are typical fracture spacing in x-, y4- and z-directions and $K_{i,j,k}$ is an effective matrix permeability.

The Eqs. 8.12–8.14 are identical to Eqs. 8.5–8.7 for the standard single continuum case except for the additional matrix/fracture mass exchange terms τ.

Conservation equations for matrix block i, j, k

$$\text{water:} \qquad \tau_{w,mf,i,j,k} = \frac{V_{i,j,k}}{\Delta t} \Delta_t (\phi_m \frac{S_{wm}}{B_{wm}}) + q_{wm,i,j,k} \tag{8.16}$$

$$\text{oil:} \qquad \tau_{o,mf,i,j,k} = \frac{V_{i,j,k}}{\Delta t} \Delta_t (\phi_m \frac{S_{om}}{B_{om}}) + q_{om,i,j,k} \tag{8.17}$$

$$\text{gas:} \qquad \tau_{g,mf,i,j,k} = \frac{V_{i,j,k}}{\Delta t} \Delta_t (\phi \frac{S_{gm}}{B_{gm}} + \phi \frac{S_{om} R_{sm}}{B_{om}}) + q_{gm,i,j,k} \tag{8.18}$$

The dual porosity model described above with no matrix-matrix flow is not adequate when gravity effects play a crucial role. Several authors including Gilman and Kazemi (1988), have modified dual porosity models to enhance the quality of gravity computations.

For compositional dual porosity models the Eq. 8.10 and 8.11 are modified in the same way as the black oil equations using a matrix/fracture exchange term.

8.4.2 Dual porosity dual permeability models

Dual porosity dual permeability models permit matrix - matrix flow as well as fracture – fracture flow as shown in **Fig. 8.3**. These models are suitable for moderately to poorly fractured reservoirs where the assumption of complete matrix discontinuity is not valid.

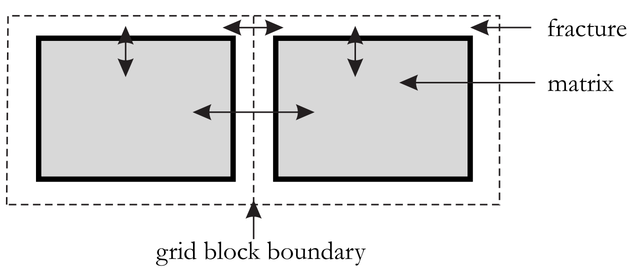

Figure 8.3: Dual porosity dual permeability grid.

The fracture flow equations for black oil dual porosity dual permeability models are identical to Eqs. 8.12–8.14 for dual porosity models. Equations for fluid flow between neighbor matrix blocks are obtained by including a matrix-matrix flow term in Eqs. 8.16–8.18

$$\text{water:} \quad \Delta T_{wm}\Delta\psi_{wm} + \tau_{w,mf,i,j,k} = \frac{V_{i,j,k}}{\Delta T}\Delta_t(\phi_m \frac{S_{wm}}{B_{wm}}) + q_{wm,i,j,k} \tag{8.19}$$

$$\text{oil:} \quad \Delta T_{om}\Delta\psi_{om} + \tau_{o,mf,i,j,k} = \frac{V_{i,j,k}}{\Delta T}\Delta_t(\phi_o \frac{S_{om}}{B_{om}}) + q_{om,i,j,k} \tag{8.20}$$

$$\text{gas:} \quad \Delta T_{gm}\Delta\psi_{gm} + \Delta T_{om}R_{om}\Delta\psi_{om} + \tau_{g,mf,i,j,k} = \frac{V_{i,j,k}}{\Delta T}\Delta_t(\phi \frac{S_{gm}}{B_{gm}} + \phi\frac{S_{om}R_{sm}}{B_{om}}) + q_{gm,i,j,k} \tag{8.21}$$

Dual porosity dual permeability models require considerably more computer time than dual porosity models.

Modifications needed to obtain the compositional dual porosity dual permeability equations are straight forward.

Comprehensive literature reviews on dual continuum models are found in research papers (Abushaikha and Gosselin 2008; Bossie-Codreanu, Bia et al. 1985; Hamidreza and Bruining 2009).

8.4.3 Single continuum models for fluid flow in naturally fractured reservoirs.

Improvements in reservoir characterization result in more detailed geological models. High resolution geological grid parameters need to be averaged to parameters for more manageable sized simulation grids. The construction of representative flow parameters for a coarse grid from fine grid representation is called upscaling. The upscaled parameters are referred to as effective parameters. A review of steady state upscaling techniques is presented by Jonoud and Jackson (2008).

When a standard single porosity model is used for fractured reservoirs special attention must be given to capture heterogeneities caused by fractures in the construction of effective properties. Hamidreza and Bruining (2009) applied a homogenization technique to derive effective properties for fractured reservoirs that combines dual porosity and dual permeability concepts simultaneously. Agarwal, Allen et al. (1997) presented a relation between fracture intensity and well test effective permeability to account for fractures in a fine grid geological model. To capture 3D geological model heterogeneities for use in a coarse grid simulation model upscaling is needed. Agarwal, Thomas et al. (1997) used a flow-based upscaling method for this purpose.

For multi-phase flow effective relative permeabilities and capillary pressures are needed for coarse grid reservoir simulation. Kyte and Berry dynamic pseudo functions are frequently used for this purpose (Kyte and Berry 1975). Agarwal, Hermansen et al. (2000) used a two-stage procedure to obtain effective relative permeabilities for the Ekofisk field to capture the effect of fractures. First, small scale mechanistic studies were conducted to construct effective relative permeabilities to account for fluid transfer between high permeability fracture blocks and low permeability matrix blocks. In the second stage dynamic pseudo functions for coarse grid numerical simulation were constructed using the Kyte and Berry approach.

8.5 Coupled geomechanics and reservoir flow simulation

The coupling of a reservoir simulator to geomechanics computations has many applications in petroleum production. With the aid of geomechanics, phenomena can be explained such as compaction, subsidence, wellbore stability, pore collapse as well as loss and gain in production.

In conventional numerical flow models porosity ϕ is computed as a function of fluid pressure p using correlations like $\phi = \phi_0[1 + c_r(p - p_0)]$, where ϕ_0 denotes porosity at reference pressure p_0 and c_r is a time independent rock compressibility. Absolute permeabilities are frequently treated as constants. Several studies show that for weaker formations with complicated rock compaction behavior, coupled geomechanics and multiphase fluid flow is required to capture important reservoir responses.

8.5.1 Fundamentals on coupling of fluid flow and geomechanics

In recent years theoretical and field studies of integrated geomechanics and flow simulation have been presented in the literature. Pressure computed by the flow simulator is passed to the geomechanics model and is used to compute new stresses and strains. This new geomechanics information is used to update porosities and permeabilities which are passed to the flow simulator for further computations. The coupling loop is shown in **Fig. 8.4**.

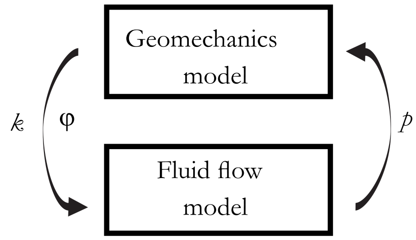

Figure 8.4: Coupling between geomechanics model and fluid flow model.

Fluid pressure p computed by the flow model is used to update effective stress state. Effective stress $\sigma^{'}$ is defined by

$$\sigma^{'} = \sigma - \alpha p \delta_{ij},$$

where δ_{ij} is the Kroenecker's delta, α Biot's constant and σ is total stress. A change in pressure p will result in a change of stress state. A geomechanics model uses appropriate constitutive stress-strain equations to relate stress (σ) state to strain (ε) state. Based on computed strains absolute permeabilities and porosities are updated.

The stress and strain tensors are written

$$\sigma = \begin{bmatrix} \sigma_x & \tau_{xy} & \tau_{xz} \\ \tau_{xy} & \sigma_y & \tau_{yz} \\ \tau_{xz} & \tau_{yz} & \sigma_z \end{bmatrix}, \quad \varepsilon = \begin{bmatrix} \varepsilon_x & \gamma_{xy} & \gamma_{xz} \\ \gamma_{xy} & \varepsilon_y & \gamma_{yz} \\ \gamma_{xz} & \gamma_{yz} & \varepsilon_z \end{bmatrix}.$$

Neglecting fluid and solid interaction steady state rock momentum balance equations in x-, y- and z-directions are written

$$\begin{aligned} \frac{\partial \sigma_x}{\partial x} + \frac{\partial \tau_{xy}}{\partial y} + \frac{\partial \tau_{xz}}{\partial z} + F_x = 0 \\ \frac{\partial \sigma_y}{\partial y} + \frac{\partial \tau_{xy}}{\partial x} + \frac{\partial \tau_{yz}}{\partial z} + F_y = 0 \\ \frac{\partial \sigma_z}{\partial z} + \frac{\partial \tau_{xz}}{\partial x} + \frac{\partial \tau_{yz}}{\partial y} + F_z = 0, \end{aligned}$$

where $\vec{F} = (F_x, F_y, F_z)$ denotes body force vector.

Strains are related to displacements u, v, w in the three coordinate directions

$$\varepsilon_x = \frac{\partial u}{\partial x}, \quad \varepsilon_y = \frac{\partial v}{\partial y}, \quad \varepsilon_z = \frac{\partial w}{\partial z}$$

$$\gamma_{xy} = \frac{\partial u}{\partial y} + \frac{\partial v}{\partial x}, \quad \gamma_{xz} = \frac{\partial u}{\partial z} + \frac{\partial w}{\partial x}, \quad \gamma_{yz} = \frac{\partial w}{\partial y} + \frac{\partial v}{\partial z}.$$

The equations for linear stress-strain relations are

$$\begin{aligned} \sigma_x &= 2G\varepsilon_x + \lambda(\varepsilon_x + \varepsilon_y + \varepsilon_z) \\ \sigma_y &= 2G\varepsilon_y + \lambda(\varepsilon_x + \varepsilon_y + \varepsilon_z) \\ \sigma_z &= 2G\varepsilon_z + \lambda(\varepsilon_x + \varepsilon_y + \varepsilon_z) \\ \tau_{xy} &= G\gamma_{xy} \\ \tau_{xz} &= G\gamma_{xz} \\ \tau_{yz} &= G\gamma_{yz}. \end{aligned}$$

Here λ is Poisson's ratio and G is defined by

$$G = \frac{E}{2(1+\lambda)},$$

where E denotes the Young's modulus.

After updating stresses using pressures computed by the flow simulator the geomechanics model computes new displacements and strains. Separate programs are normally used for geomechanics and flow computations. A finite element method is used for geomechanics computations. The finite element grid usually coincides with the grid used by the finite difference flow simulator.

Exterior boundary conditions are specified in terms of stresses and displacements. Frequently the bottom of the grid will have zero displacement condition while the sides and top will be given specific stresses. Sometimes an estimate of geomechanics behavior for formation outside of the target fluid reservoir is needed. This is accomplished by using an extended grid for the geomechanics computations. Initialization of the geomechanics model is specified in terms of an initial stress state. Usually an initial simulation step is required to establish the initial stress distribution.

Different suggestions for stress dependent flow simulator porosity ϕ and absolute permeability k are presented in the petroleum literature. The volumetric strain ε_v is calculated using diagonal terms of the strain tensor as

$$\varepsilon_v = \varepsilon_x + \varepsilon_y + \varepsilon_z,$$

and is frequently used to update porosities and permeabilities. Numerous strain dependent porosity formulas are suggested in the literature. A relation where porosity is given by

$$\phi = 1 - (1 - \phi_0)e^{\Delta\varepsilon_v},$$

where ϕ_0 is initial porosity and $\Delta\varepsilon_v$ is the difference between actual volumetric strain and initial volumetric strain is used by several authors (Thomas, Chin et al. 2003; Pettersen and Kristiansen 2009).

If permeability is a function of porosity only, a permeability-porosity relation

$$k = k_o e^{k_{ml}\left(\frac{\phi-\phi_0}{1-\phi_0}\right)},$$

where k_{ml} is a multiplier and k_0, ϕ_0 are initial permeability and porosity, is suggested by Tran et al. (Tran 2009) to compute stress dependent permeability.

Literature reviews of methods for stress-dependent porosities and permeabilities are included in research papers (Settari, Bachman et al. 2005; Thomas, Chin et al. 2003; Tran, Nghiem et al. 2009).

8.5.2 Water weakening.

Water weakening of chalk is a well-known phenomenon. For modeling of water weakening, water saturation is passed from the fluid flow model to the geomechanics model in addition to pressure.The coupling loop allowing for water weakening is depicted in **Fig. 8.5**.

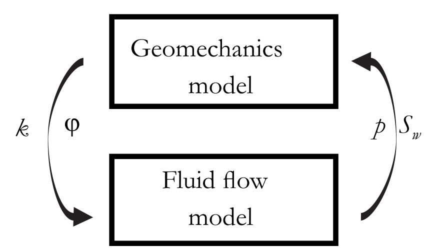

Figure 8.5: Coupling between geomechanics model and fluid flow model in case of water weakening.

Water induced compaction for the Ekofisk Field was modeled by Sylte, Thomas et al. (1999) based on field observations and laboratory data. Porosity was entered into the model as a function of initial porosity, effective stress and water saturation as a multi-dimensional table. Water weakening in the Valhall field was modeled by Kristiansen and Plischke (2010) using an elasto-plastic stress-strain relation with a water saturation dependent yield surface.

8.5.3 Stress dependent relative permeabilities.

Most of the approaches for coupling fluid flow and geomechanics have focused on the stress dependence of porosities and absolute permeabilities while changes in relative permeabilities due to geomechanics are ignored. On the other hand phase permeability computed as the product of relative permeability and absolute permeability is needed for fluid flow computations. Results from simulation studies show that the impact of geomechanics on relative permeabilities can be significant. To demonstrate this fact Ojagbohunmi, Chalaturnyk et al. (2012) used modified Brooks and Corey power law models for relative permeabilities with stress dependent end point values and saturation end points.

8.5.4 Geomechanics - fluid flow coupling methods.

The coupling of fluid flow simulation and geomechanics stress - strain computations results in a considerable increase in computing time. The computing time can easily increase by an order of magnitude over the time needed to solve reservoir flow equations only (Pettersen and Kristiansen 2009). Different degrees of coupling are described in the literature (Settari and Walters 1999). The degree of coupling will influence the accuracy of the solution as well as the computational efficiency. Trade-off between runtime and solution accuracy is required.

Explicit coupling is achieved by lagging geomechanics computations one or several time steps behind flow computations as shown in **Fig. 8.6**. Iterative coupling consists of repeated solution of the flow and stress equations at every Newton-Raphson iteration step as shown in **Fig. 8.7**. When iterative coupling scheme is run until complete convergence it is identical to fully coupled computations described below.

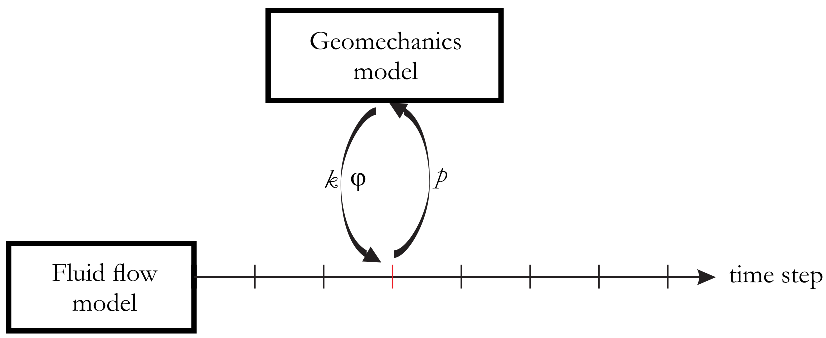

Figure 8.6: Explicit coupling, geomechanics computations at designated time steps.

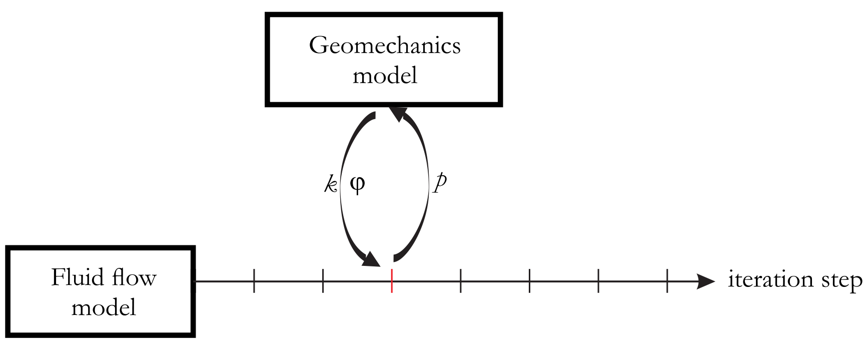

Figure 8.7: Iterative coupling, geomechanics computations at each Newton-Raphson iteration step.

In a fully coupled approach fluid flow equations and geomechanics equations are solved simultaneously. It results in an enlarged system of linear equations

$$\begin{bmatrix} \mathbf{KM} & \mathbf{LM} \\ \mathbf{LM^T} & \mathbf{EM} \end{bmatrix} \begin{bmatrix} \delta\vec{u} \\ \delta\vec{P} \end{bmatrix} = \begin{bmatrix} \vec{r}_1 \\ \vec{r}_s \end{bmatrix},$$

where **KM** is the stiffness matrix, **EM** is the flow matrix and **LM** is the coupling matrix geomechanics/flow. Moreover, $\delta\vec{u}$, $\delta\vec{P}$ denotes changes in displacements and flow unknowns (pressures and saturations) over a Newton-Raphson iteration, $\vec{r}_1$, $\vec{r}_2$ are right hand side residuals. Solving the enlarged system of equations is time consuming. Moreover, this approach requires a uniform solution procedure for fluid flow and geomechanics equations. Hence, the fully coupled approach is scarcely used in the industry.

8.5.5 Coupling of geomechanics and flow simulation for dual porosity models

The role of geomechanics becomes more crucial in the presence of fractures because fractures are more stress sensitive than the rock matrix. Disturbance in stresses will particularly effect fracture permeability due to opening, closure and reorientation of fractures.

The theory of coupling geomechanics and reservoir fluid flow published in the literature is usually built on single-porosity poroelastic theory. Bagheri and A. (2008) used a dual porosity approach to decompose geomechanics solution into fracture and matrix parts. Their main focus was to study the effect of stress changes on fracture permeability.

8.6 Wettability alteration

Spontaneous imbibition laboratory experiments with chalk cores indicate that seawater has the potential to improve oil recovery. A likely explanation is that salt ions adsorbs onto the chalk surface to cause changes in wettability.

A 1D model for simulation of dynamic wettability changes is reported by Yu, Evje et al. (2009). Equations for a 3D two-phase water/oil model with dynamic wettability capabilities are presented in this section. Changes in wettability are assumed to be caused by a wettability alteration (WA) agent. In addition to the water and oil equations a mass conservation equation for the WA agent is needed. WA agent exists in water phase only and volumes are not effected when WA agent is dissolved in water. The following modifications of the standard black oil model are used to model this type of dynamic wettability changes

$$
\begin{aligned}
&\nabla \cdot \left[\frac{[k]k_{rw}}{\mu_w}(1-c)\rho_w(\nabla p_w - \gamma_w \nabla d) \right] = \frac{\partial}{\partial t}((1-c)\rho_w S_w) + Q_w \\
&\nabla \cdot \left[\frac{[k]k_{ro}}{\mu_o}\rho_o(\nabla p_o - \gamma_o \nabla d) \right] = \frac{\partial}{\partial t}(\rho_o S_o) + Q_o \\
&\nabla \cdot \left[\frac{[k]k_{rw}}{\mu_w}c\rho_w(\nabla p_w - \gamma_w \nabla d) + D(S_w)\rho_w \nabla c \right] = \frac{\partial}{\partial t}(\phi c \rho_w S_w + (1-\phi)\rho_r a(c)) + Q_{wa},
\end{aligned}
$$

where c denotes concentration of the WA agent in water phase and Q_{wa} is a source/sink term for the WA agent. In the flow part of the equation for the WA agent a diffusion term is included where $D(S_w) = D_r \phi S_w$. In the diffusion term D_r is a constant diffusion coefficient and ρ_r is rock density. The term $a(c)$ on the right hand side in the last equation denotes the adsorption isotherm. The function $a(c)$ is part of the model input in terms of a correlation like Langmuir isotherm or as a table.

In addition the black oil constraint Eq. 8.4

$$
p_o - p_w = P_{cow}(S_w), \quad S_o + S_g + S_w = 1
$$

are used.

Concentration c is small and the approximation $1 - c \approx 1$ is introduced in the water equation. With this approximation conservation equations are written

$$
\text{water:} \quad \nabla \cdot \left[\frac{[k]k_{rw}}{\mu_w}\rho_w(\nabla p_w - \gamma_w \nabla d) \right] = \frac{\partial}{\partial t}(\rho_w S_w) + Q_w \tag{8.22}
$$

$$
\text{oil:} \quad \nabla \cdot \left[\frac{[k]k_{ro}}{\mu_o}\rho_o(\nabla p_o - \gamma_o \nabla d) \right] = \frac{\partial}{\partial t}(\rho_o S_o) + Q_o \tag{8.23}
$$

$$
\text{WA agent:} \quad \nabla \cdot \left[\frac{[k]k_{rw}}{\mu_w}c\rho_w(\nabla p_w - \gamma_w \nabla d) + D(S_w)\rho_w \nabla c \right] = \frac{\partial}{\partial t}(\phi c \rho_w S_w + (1-\phi)\rho_r a(c)) + Q_{wa}. \tag{8.24}
$$

The water and oil equations look like Eqs. 8.1–8.2 for the standard black oil model with the exception that densities are used instead of volume factors. However, there is a major difference because in Eqs. 8.22–8.24 saturation functions will depend on concentration c in addition to saturations

$$
k_{rl} = k_{rl}(S_w, c), \qquad P_{cow} = P_{cow}(S_w, c).
$$

Preferentially water-wet and preferentially oil-wet saturation functions are supplied as input to the model using correlations or tables. Intermediate wetting state properties are obtained by interpolation between preferentially water-wet (k_{rw}^{ww}, k_{ro}^{ww}, P_{cow}^{ww}) and preferentially oil-wet (k_{rw}^{ow}, k_{ro}^{ow}, P_{cow}^{ow}) saturation functions. Let $b(c)$ denote the scaled adsorption isotherm, $0 \leq b(c) \leq 1$. If the interpolation is assumed to be linear in $b(c)$ the saturation functions are computed as

$$
\begin{aligned}
k_{rl}(S_w, c) &= b(c)k_{rl}^{ww}(S_w) + [1 - b(c)]k_{rl}^{ow}(S_w) \\
P_{cow}(S_w, c) &= b(c)P_{cow}^{ww}(S_w) + [1 - b(c)]P_{cow}^{ow}(S_w).
\end{aligned}
$$

Starting with no adsorption, $b(c) = 0$, preferentially oil-wet properties are used by the model. At the other extreme if the matrix has adsorbed its maximal amount, $b(c) = 1$, preferentially water-wet properties are used.

Reservoir wettability and its effect on oil recovery have been subject to numerous studies. These studies address wettability behavior on a laboratory scale. However, major issues of oil recovery related to dynamic wettability alteration at a full-field reservoir scale remain poorly understood.

8.7 Concluding remarks.

This review is concerned with state-of-the-art for transport equations of fluid flow in chalk reservoirs. Important features like fractures, dynamic wetting changes, stress dependent compaction and water weakening are discussed. No attempt is made to present a comprehensive reference list of relevant literature.

Nomenclature

B =	volume factor
c =	WA component concentration
c_r =	rock compressibility, Lt^2/m
D =	diffusion, L^2/t
D_r =	diffusion coefficient, L^2/t
E =	Young's modulus, M/Lt^2
$\mathbf{EM}$ =	flow matrix
k =	absolute permeability, L^2
$[k]$ =	absolute permeability tensor
k_{rl} =	relative permeability, L^2
$\mathbf{KM}$ =	stiffness matrix
$\mathbf{LM}$ =	coupling flow/geomechanics matrix
Nc =	number of hydrocarbon components
p =	phase pressure, m/Lt^2
p_0 =	reference pressure, m/Lt^2
P_{cgo} =	gas/oil capillary pressure, M/Lt^2
P_{cow} =	oil/water capillary pressure, M/Lt^2
q =	source/sink term in difference equations
Q =	source/sink term in differential equations
R_s =	gas in oil solution ratio
S =	phase saturation
u, v, w =	displacements in x-, y- and z-directions
V =	grid block bulk volume, L^3
$\{K_{ic}\}$ =	K-values
$\{x_{ic}\}$ =	oil composition
$\{y_{ic}\}$ =	gas composition
Δ_t =	time difference operator
$\Delta T \Delta \psi$ =	space difference operator
Δt =	time step length
$\Delta x, \Delta y, \Delta z$ =	grid block lengths in x-, y- and z-directions
α =	Biot's constant
γ =	fluid gravity
δP =	change in fluid unknowns
δu =	change in displacements
ε =	strain
λ =	Poisson's ratio
μ =	fluid viscosity
ξ =	shape factor
ρ =	fluid density
ρ_r =	rock density
σ =	stress
σ' =	effective stress
ϕ =	porosity
ϕ_0 =	reference porosity
τ =	matrix/fracture transfer function

∇ = gradient
$\nabla\cdot$ = divergence

Subscripts

f = fracture
g = gas
m = matrix
mf = matrix/fracture
o = oil
w = water
wa = WA agent

Superscripts

ow = oil-wet
ww = water-wet

Abbreviations

AIM = adaptive implicit method
WA = wetting alteration
IMPES = implicit pressure explicit saturation

References

Abushaikha, A.S.A. and Gosselin, O.R., 2008. Matrix-Fracture Transfer Function in Dual-Medium Flow Simulation: Review, Comparison, and Validation. Presented at the SPE Europac/EAGE Annual Conference and Exhibition, Rome, Italy. URL `http://dx.doi.org/10.2118/113890-MS`.

Agarwal, B., Allen, L.R., and Farrell, H.E., 1997. Ekofisk Field Reservoir Characterization: Mapping Permeability Through Facies and Fracture Internsity. *SPE Formation Evaluation*, **12** (04): 227–234. SPE-35527-PA. Dec. URL `http://dx.doi.org/10.2118/35527-PA`.

Agarwal, B., Hermansen, H. et al., 2000. Reservoir Characterization of Ekofisk Field: A Giant, Fractured Chalk Reservoir in the Norwegian North Sea-History Match. *SPE Reservoir Eval. & Eng*, **3**: 534–543. SPE-68096-PA. URL `http://dx.doi.org/10.2118/68096-PA`.

Agarwal, B., Thomas, L.K. et al., 1997. Reservoir Characterization of Ekofisk Field: A Giant, Fractured Chalk Reservoir in the Norwegian North Sea-Upscaling. Presented at the SPE Annual Technical Conference and Exibition, San Antonis, Texas. 5–8 October. URL `http://dx.doi.org/10.2118/38875-MS`.

Bagheri, M. and A., S., 2008. Modeling of Geomechanics in Naturally Fractured Reservoirs. *SPE Reservoir Evaluation & Engineering*, **11** (01): 108–118. URL `http://dx.doi.org/10.2118/93083-PA`.

Batycky, R.P., Thiele, M.R. et al., 2007. Reservoir Simulation. In E. Holstein, ed., *Petroleum Engineering Handbook, Volum V: Reservoir Engineering and Petrophysics*, Chap. 17, 1399–1478. SPE Bookstore.

Bossie-Codreanu, D., Bia, P.R., and Sabathier, J.C., 1985. The 'Checker Model', An Improvement in Modeling Naturally Fractured Reservoirs With a Tridimensional, Triphasic, Black-Oil Numerical Model. *SPEJ*, **25** (05): 743–756. URL `http://dx.doi.org/10.2118/10977-PA`.

Gilman, J.R. and Kazemi, H., 1988. Improve Calculations for Viscous and Gravity Displacement in Matrix Blocks in Dual-Porosity Simulators. *Journal of Petroleum Technology*, **40** (01): 60–70. January. URL `http://dx.doi.org/10.2118/16010-PA`.

Hamidreza, S. and Bruining, J., 2009. Upscaling in Partially Fractured Oil Reservoirs Using Homogenization. Presented the SPE/EAGE Reservoir Characterization and Simulation Conference, Abu Dhabi. URL `http://dx.doi.org/10.2118/125559-MS`.

Jonoud, S. and Jackson, M.D., 2008. Validity of Steady-State Upscaling Techniques. *SPE Reservoir Evaluation & Engineering*, **11** (02): 405–416. URL `http://dx.doi.org/10.2118/100293-PA`.

Kazemi, H., Merrill Jr, L.S. et al., 1976. Numerical simulation of water-oil flow in naturally fractured reservoirs. *Society of Petroleum Engineers Journal*, **16** (06): 317–326. URL `http://dx.doi.org/10.2118/5719-PA`.

Kristiansen, T.G. and Plischke, B., 2010. History Matched Full Field Geomechanics Model of the Valhall Field Including Water Weakening and Re-pressurisation. Paper SPE-131505-MS presented at SPE EUROPEC/EAGE Annual Conference and Exhibition, Barcelona, Spain. 14–17 June. URL `http://dx.doi.org/10.2118/131505-MS`.

Kyte, J.R. and Berry, D.W., 1975. New Pseudofunctions To Control Numerical Dispersion. *Society of Petroleum Engineers Journal*, **15** (04): 269–276. URL `http://dx.doi.org/10.2118/5105-PA`.

Ojagbohunmi, S., Chalaturnyk, R., and Leung, J., 2012. Coupling of Stress Dependent Relative Permeability and Reservoir Simulation. Presented at SPE Improved Oil Recovery Symposium, 14-18 April, Tulsa, Oklahoma, USA. URL `http://dx.doi.org/10.2118/154083-MS`.

Pettersen, Ø. and Kristiansen, T.G., 2009. Improved Compaction Modeling in Reservoir Simulation and Coupled Rock Mechanics/Flow Simulation, With Examples From the Valhall Field. *SPE Reservoir Evaluation & Engineering*, **12** (02): 329–340. URL `http://dx.doi.org/10.2118/113003-PA`.

Rodriguez, A.A., Klie, H. et al., 2006. Porous Media Upscaling of Hydraulic Properties: Full permeability Tensor and Continuum Scale Simulations. Presented at SPE/DOE Symposium on Improved Oil Recovery, 22-26 April, Tulsa, Oklahoma, USA. URL `http://dx.doi.org/10.2118/100057-MS`.

Settari, A., Bachman, R.C., and Walters, D.A., 2005. How to Approximate Effect of Geomechanics in Conventional Reservoir Simulation. Presented at SPE Annual Technical Conference and Exhibition, Dallas, Texas. 9-12 October. URL `http://dx.doi.org/10.2118/97155-MS`.

Settari, A.T. and Walters, D.A., 1999. Advances in Coupled Geomechanical and Reservoir Modeling With Applications to Reservoir Compaction. Presenter at SPE Reservoir Simulation Symposium, 14-17 February, Houston, Texas. URL `http://dx.doi.org/10.2118/51927-MS`.

Skjæveland, S.M. and Kleppe, J., eds., 1992. *SPOR Monograph. Recent Advances in Improved Oil Recovery Methods for North Sea Sandstone Reservoirs*. Norwegian Petroleum Directorate, Stavanger.

Sylte, J.E., Thomas, L.K. et al., 1999. Water induced compaction in the Ekofisk Field. In *SPE Annual Technical Conference and Exhibition*. Society of Petroleum Engineers, Houston, Texas. SPE-56426-MS. 3-6 October. URL `http://dx.doi.org/10.2118/56426-MS`.

Thomas, L.K., Chin, L.Y. et al., 2003. Coupled Geomechanics and Reservoir Simulation. *SPE Journal*, **8** (04): 350–358. URL `http://dx.doi.org/10.2118/87339-PA`.

Tran, D., Nghiem, L., and Buchanan, L., 2009. Aspects of Coupling Between Petroleum Reservoir Flow and Geomechanics. Presented at the 43rd U.S. Rock Mechanics Symposium & 4th U.S. - Canada Rock Mechanics Symposium, 28 June-1 July, Asheville, North Carolina.

Yu, L., Evje, S. et al., 2009. Spontaneous imbibition of seawater into preferentially oil-wet chalk cores - Experiments and simulation, 2009. *Journal of Petroleum Science and Engineering*, **66**: 171–179.

Chapter 9

Multiphase Flow Parameters

Ole Torsæter and Ingebret Fjelde

9.1 Introduction

The chalk reservoirs below the North Sea are the largest and most important oil producing chalk reservoirs in the world (Li 2011). A few other chalk reservoirs with considerable amount of hydrocarbon production are in Texas (Martin, Baihly et al. 2011). The focus of this chapter will be flow of oil and water phases in fractured chalk reservoirs. Since most of the chalk reservoirs are naturally fractured, the multiphase parameters governing flow in chalk are both fracture parameters and rock matrix parameters (van Golf-Racht 1982). The degree of fracturing may vary in the oil reservoirs, from highly fractured reservoir parts dominated by spontaneous imbibition to less fractured reservoir parts dominated by viscous flooding. The rock matrix system contains most of the reservoir fluid and acts as a source of fluid for the fracture network. Since chalk reservoirs are described by both the fracture and rock matrix parameters, complexity is added to the fluid flow processes and affects all production stages of the reservoir. A fractured chalk reservoir will therefore behave fundamentally different from conventional non-fractured reservoirs. In numerical simulation models of flow in fractured chalk (dual continuum modelling), equations are written for both the fracture network and the matrix system at each spatial location, with a fluid exchange function that describes the transfer of fluid between the matrix and the fractures (Warren and Root 1963). The challenges for the reservoir engineering laboratories are to provide multiphase flow parameters that will describe actual flow mechanisms in fractured chalk reservoirs. In the following, water displacement parameters will be discussed in detail with emphasis on small scale matrix – fracture fluid exchange parameters, wettability, capillary pressure and relative permeability. The fundamentals of wettability, capillary pressure and relative permeability are first shortly presented before discussed more in detail.

9.2 Wettability fundamentals

Experience from waterflooding of several naturally fractured chalk reservoirs has shown the importance of a good understanding of the overall displacement mechanisms and the governing multiphase reservoir parameters. The literature survey by Anderson (1986a,b, 1987a,b,c) drew attention to the subject and emphasized the shortcoming of the knowledge of wettability, especially of carbonate reservoir rocks. The waterflooding process is especially affected by the wettability and the water imbibition mechanisms.

Wettability describes the preference of a solid to be in contact with one fluid rather than another. The balance of forces in the oil/water/solid system will result in a contact angle, θ, between the fluids at the solid surface **(Fig. 9.1)**.

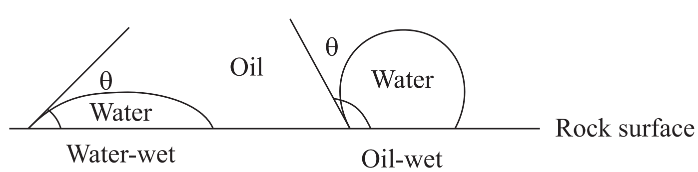

Figure 9.1: Contact angle θ for a water-wet and an oil-wet system (Raza, Treiber et al. 1968).

The wettability of a solid material (rock) is often estimated by measuring the contact angle, θ **(Table 9.1)**, and the concept of wetting is explained quantitatively by examining the force balances between two immiscible fluids on a solid surface (Cuiec 1987). At equilibrium, the sum of the forces acting must be zero. The Young-Dupré equation represents the force balance and relates the contact angle and the interfacial tensions (σ). For an oil-water-solid system the Young-Dupré equation is:

$$\sigma_{os} - \sigma_{ws} = \sigma_{ow} \cos\theta, \tag{9.1}$$

where σ_{os} is the surface tension between the oil and the solid, σ_{ws} the surface tension between the water and the solid, σ_{ow} the interfacial tension between the oil and the water, and θ the contact angle.

Contact angle, θ [degrees]	**Wettability preference**
0–80	Preferentially water-wet
80–100	Intermediate wettability
100–160	Oil-wet
160–180	Strongly oil-wet

Table 9.1: Wettability preference based on contact angle for an oil-water system (Chilingar and Yen 1983).

Contact angle measurements for wettability evaluation of reservoirs is not preferable (but the contact angle method is an important research tool) since the measurements are difficult to do on fluids inside the porous medium (Cuiec 1987). Most of the wettability studies on chalk have been performed by standard core analysis methods like the Amott-Harvey wettability test and the USBM (United States Bureau of Mines) test (Amott 1959; Donaldson, Thomas et al. 1969). See definition of capillary pressure (P_c) in next section. The Amott wettability index (WI_{Amott}) reflects the ease with which the wetting phase displaces the non-wetting phase from the pores, and the USBM wettability index (WI_{USBM}) is a measure of the amount of work required for one fluid to displace the other from the pores **(Fig. 9.2)**. The USBM method considers the system's free energy. The area under the capillary pressure curve involved measures the amount of work. Because of the favorable free energy change, it is expected that the work required for the wetting phase to displace the non-wetting phase is less than the work required for the reverse displacement. To a first approximation therefore, a quick look evaluation of the core wettability can be made from the rate of spontaneous imbibition and the amount of oil and water spontaneously imbibed.

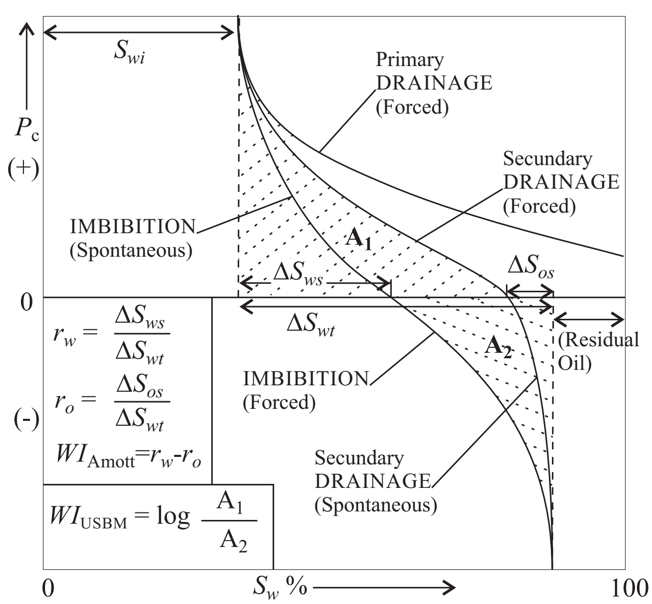

Figure 9.2: Wettability measurements by Amott-Harvey and USBM tests for a mixed wettability system (Morrow 1990).

9.3 Capillary pressure fundamentals

Capillary pressure versus saturation relationships are important information for evaluation of storage and production potential of an oil and gas producing chalk formation (Thomas, Dixon et al. 1987). When more than one fluid is present within a porous rock, there are at least three sets of acting forces affecting the capillary forces; namely, the interfacial tension between the fluids and the interfacial tension between each fluid and the solid surface (Collins 1976). The capillary pressure, P_c, is defined as the pressure difference between the non-wetting phase (P_{nw}) and the wetting phase (P_w):

$$P_c = P_{nw} - P_w. \tag{9.2}$$

The general expression for calculating the capillary pressure at any point on a curved interface is given by Eq. 9.3 (Laplace equation). This expression relates the capillary pressure to the interfacial tensions involved:

$$P_c = P_{nw} - P_w = \sigma(\frac{1}{r_1} + \frac{1}{r_2}), \tag{9.3}$$

where r_1 and r_2 are the principal radii of curvature.

Accurate determination of capillary pressure curves for chalk, especially for the imbibition process, is challenging (Spinler and Baldwin 1997). Since saturation may not change in the same direction for a particular point throughout the reservoir life, knowledge of the hysteresis of the capillary pressure functions is also important and the measurements are difficult. The capillary pressure of chalk can be measured by several methods, e.g. porous plate (Hammervold, Knutsen et al. 1998), centrifuge (Fernø, Treinen et al. 2007), mercury injection (Torsæter 1983), dynamic method (on low permability limestone, (Lombard, Gautier et al. 2006)) and standard flow tests (Nordtvedt, Urkedal et al. 1994).

9.4 Relative permeability fundamentals

When exposing a slight to medium water-wet reservoir rock to water, the water is spontaneously drawn into the rock while the oil is displaced (Amott 1959). The spontaneous imbibition process is determined by capillary forces and the relative permeability relationship. It is, however, difficult to obtain accurate estimates of the capillary pressure and relative permeability during an imbibition process in the relevant saturation range. Furthermore, saturations may increase and decrease locally, therefore knowledge of the relative permeability hysteresis is needed. In the following, the two-phase system oil-water is discussed.

Relative permeability is used to relate the absolute permeability of a porous medium to the effective permeability of a particular fluid in the system, when that fluid occupies only a fraction of the total pore volume (Leverett 1939). The following relationships are defined:

$$k_{ro} = \frac{k_o}{k}, \tag{9.4}$$

$$k_{rw} = \frac{k_w}{k}, \tag{9.5}$$

where k_{ro} and k_{rw} are the relative permeabilities of oil and water respectively, k_o and k_w are the effective permeabilities and k is the absolute permeability. The relative permeabilities depend on the following factors (Amyx, Bass et al. 1960): Saturation, saturation history, wettability, pore geometry, temperature and pressure, viscous, capillary and gravitational forces and interfacial tension

The main flooding experimental techniques for obtaining relative permeabilities are steady-state method (Osoba, Richardson et al. 1951), unsteady-state method (Welge 1952) and centrifuge method (Hagoort 1980).

9.5 Multiphase flow in chalk

9.5.1 Waterflooding in chalk reservoirs

Water has been injected into some chalk reservoirs. The Ekofisk and Valhall fields are examples on the Norwegian Continental Shelf and are described below.

Ekofisk:

Laboratory studies to evaluate waterflood potential of the Ekofisk field were started in 1979. Experiments conducted by Torsæter (1984) involved examination of about 100 core plugs from the Ekofisk and Tor formations. Wettability and imbibition studies revealed major differences between the formations. The Tor formation seemed to be completely water-wet, and no increase in the water saturation was obtained by applying a displacement pressure during the imbibition experiment. Concerning the Ekofisk formation, the wetting properties of the rock seemed to be very complex, and the imbibition recovery was more unpredictable. After further favorable results of laboratory analysis, a water injection pilot in the Tor formation was initiated in April 1981. The results were positive and a decision was made to waterflood the northern Tor formation with unheated North Sea water. A 30-slot water injection platform (2/4 K) was approved and water injection in the Tor formation commenced in 1987 (Hermansen, Thomas et al. 1997). Eventually, after positive results in the Tor formation, another pilot injection project was initiated in the Lower Ekofisk formation. Based on the results, it was decided to inject water into the Lower Ekofisk formation and to expand the Tor formation waterflooding field wide.

In 1990, based on the encouraging experiences of injecting water into Lower Ekofisk, evaluation of waterflooding the Upper Ekofisk formation was initiated. Subsequent to a major field study in 1992, the conclusion was to initiate water injection into the Upper Ekofisk formation as well as the rest of the field (Hermansen, Thomas et al. 1997). The current strategy is to waterflood the entire reservoir, both vertically and laterally. As illustrated in **Fig. 9.3**, the oil production from the Ekofisk field peaked at about 16 million Sm^3 oil per year in 1976 and thereafter a decline in the oil production was experienced until 1987 when the effects of waterflooding were observed. Oil production peaked again in 2002 and currently the oil production is around 6.4 million Sm^3.

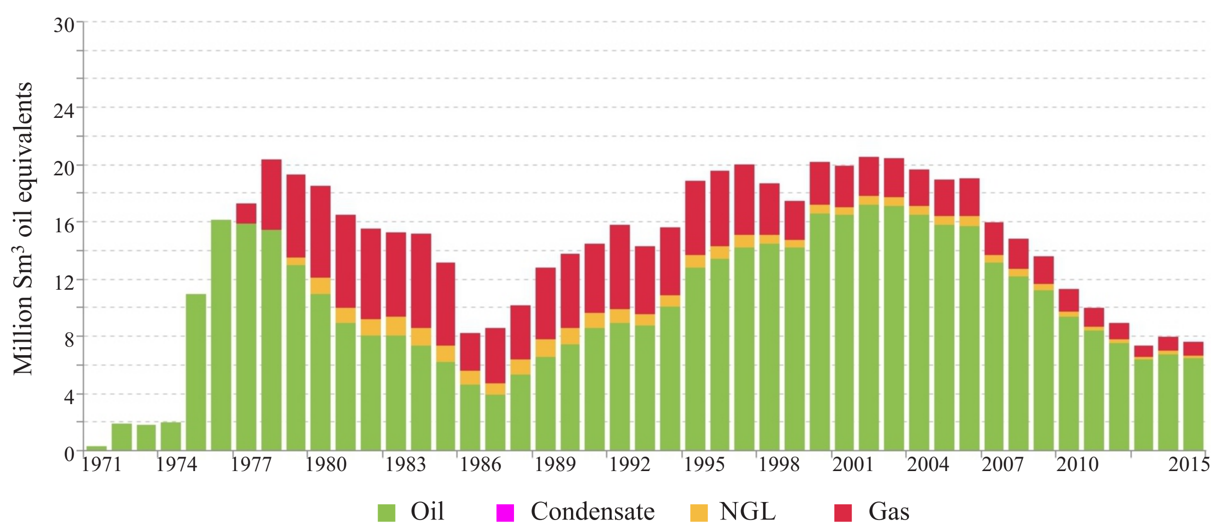

Figure 9.3: Ekofisk production profile, (Norwegian Petroleum Directorate 2016).

After concluding that the waterflooding of fractured chalk was successful, it was found that one of the dominating processes responsible for this was spontaneous imbibition of water into the chalk (Thomas, Dixon et al. 1987). Because of the intensely fractured nature of the chalk, the surface area subjected to imbibition is large. As the production of formation water was noticed, it was thought that this was the indication of viscous displacement. In addition, the effect of gravity is also considered as an important drive mechanism for imbibition.

A wide range of recovery processes have been evaluated to improve oil recovery beyond the waterflood scenario in Ekofisk. However, none of them have been implemented on the field scale. At the moment, water injection is the only recovery process applied. Since 1% enhanced recovery represents about 67 million barrels of oil, significant resources have been used for recovery efficiency studies. Among the processes assessed is water-alternating-hydrocarbon gas (WAG), and other WAG processes like water-alternating-nitrogen and water-alternating-carbon dioxide. Air injection, microbial EOR and surfactant flooding have also been considered (Jensen, Harpole et al. 2000). Extensive laboratory experiments, mechanistic simulations and even a pilot WAG test have been performed to appraise the incremental recovery potential. Still significant studies are ongoing to identify and mature a novel recovery process for Ekofisk.

Valhall:

The Valhall field was for a long time developed through primary depletion by solution gas drive. However, the high porosity chalk is compressible and this has provided significant reservoir energy (Barkved, Buer et al. 2003). After more than 30 years of production, a total of 110 million Sm^3 have been produced and additional 37 million Sm^3 remain to be produced of the original recoverable oil in place of 147 million Sm^3. This corresponds to a recovery factor of 35%. In fact, the initial estimate of primary recovery was very low, 24% OOIP (Ali and Alcock 1994). The pilot waterflood operation that began in 1990 (Ali and Alcock 1994) gave positive results and led to the initiation of water injection in 2004. Waterflooding of the Valhall reservoir has generally resulted in a good performance (Tjetland, Kristiansen et al. 2007).

9.5.2 Wettability studies of chalk

In the 1950s some low permeability reservoirs in the Spraberry sandstone and the Austin chalk in the US were planned for secondary recovery methods and knowledge of wettability was crucial. Especially spontaneous water imbibition experimental studies were initiated by Brownscombe and Dyes (1952); Graham and Richardson (1959); Mattax, Kyte et al. (1962). These researchers indicated that reservoir rocks could have various degrees of water wetness and even be oil-wet. Variations of wettability within reservoir formations were also discussed. However, also at that time it was considered that rock minerals that never had been in contact with crude oil are strongly water-wet. Later two comprehensive investigations on wettability of different reservoirs all over the world concluded that most carbonate reservoirs seem to be neutral to oil-wet (Chilingar and Yen 1983; Treiber and Owens 1972).

Results from investigations of wettability of chalk reservoirs indicate that they are preferentially water-wet, but the degree of water wetness is dependent on pH and composition of the equilibrium brine, reservoir temperature and crude oil properties (Standnes and Austad 2000). The pH in carbonate reservoirs is usually quite constant in the range 7–8 due to the great buffer capacity of the rock matrix itself. At this pH the chalk surface is positively charged (Zhang and Austad 2005). When crude oil containing surface active polar compounds migrates into a chalk reservoir the oil/brine interface will become negatively charged. This is mainly due to the partial dissociation of the carboxylic material of the crude oil in contact with the water phase (Puntervold 2008). Therefore, in chalk, the interface between brine/rock is positively charged and the interface between oil/brine is negatively charged. The disjoining pressure, which is the total pressure between interfaces close to each other, will in the case of chalk be negative and the interfaces will attract each other and a thinner wetting film is created. Eventually the film may rupture and oil will contact part of the rock (Buckley, Takamura et al. 1989). Formation waters in chalk reservoirs contain low concentration of sulphate. It has been shown that synthetic formation water with sulphate concentrations as low as 50ppm gave more water-wet chalk rock than formation water without sulphate (Fjelde and Asen 2015). Seawater was shown to accelerate the spontaneous imbibition also for the core plugs prepared with synthetic formation water containing low concentration of sulphate. It is therefore important to include the sulphate in the synthetic formation water. Higher concentration of sulphate in initial brine has also been reported to give more water-wet rock (Ahsan, Madland et al. 2012).

Crude oil composition may have great impact on chalk wettability, especially the acid number of the crude oil. A high value of the acid number corresponds to less water-wet chalk (Standnes and Austad 2000). However, an interesting aspect is that the acid number of the present oils may have decreased during geological time due to decomposition of carboxylic acids at high temperatures. The base number, which is more stable over geological time, may also be an important parameter but not much research has been performed on base number versus chalk wettability.

Measurement methods of core plug wettability have been the subject for research for a long time and various methods are presented in Anderson (1986a,b). However, Strand (2005) developed a method specially for measurements in chalk. This method is based on chromatographic separation between sulphate, SO_4^{2-}, and the tracer thiocyanate, SCN^-, during core flooding. SO_4^{2-} adsorbs on the water-wet surfaces of the chalk and SCN^- is a non-adsorbing agent. A wetting index is introduced which quantifies the fraction of water-wet area inside the core.

Measurements on chalk core plugs give usually wettability indices (WI_{Amott} and WI_{USBM}) larger than 0.7 indicating that at this scale chalk is preferentially water-wet in accordance with literature on surface interactions between chalk/brine/crude oil. However, research on micro- and nanoscale has shown that the wetting properties of the chalk constituents vary from strongly water-wet to oil-wet. Torsæter (1983) observed that some chalk material was less water-wet than others and suggested that this could be due to an organic surface coating of chalk particles. Baldwin (1988) performed thorough surface examination of both outcrop chalk and North Sea chalk and found that chalk particles contained sufficient extractable material to form multimolecular coatings. This coating is most likely remnants from algae and may have survived over geologic time. Hassenkam, Skovbjerg et al. (2009) investigated the wettability of a water-bearing chalk formation below the Danish North Sea at sub porescale. They measured the parameters adhesion and surface elasticity to define the relationship between surface forces and macroscopic wettability. Their results show that in chalk some surfaces are water-wet while other rock grains are hydrophobic due to organic coating. Their explanation is that some surfaces are freshly cleaved and water-wet while the hydrophobic grains have an organic coating. The researchers mention that the coccoliths in the sea today are protected from dissolution by an organic coating, and they suggest that this organic material remains attached on the coccolith fragments throughout geologic time.

Several research groups have studied chalk imbibition behavior and waterflood behavior in core plugs, other rock matrix-fracture systems and related the results to oil recovery. The results have given important knowledge about the relation between capillary and viscous forces in the various systems and thereby the understanding of the endpoint saturations in the multiphase flow functions (Pourmohammadi, Hetland et al. 2008; Graue, Moe et al. 2000).

9.5.3 Capillary pressure and relative permeability relationship of chalk

Two types of relative permeability curves are used for fractured reservoirs: Matrix relative permeability and pseudo relative permeability (van Golf-Racht 1982). The type of relative permeability curve to be used depends on the application of single porosity or dual porosity simulation model. Pseudo relative permeability curves are used in single porosity simulation models and describe the average flow of fluid through a particular region (matrix and fracture combine). Pseudo relative permeability curves will vary in a particular fractured reservoir from one location to another due to variation of number of fractures and wettability of the rock. Matrix relative permeability curves are strongly dependent on the wettability of the rock. Matrix relative permeability curves are also needed to generate pseudo relative permeability curves.

Large wettability variation within the Ekofisk field, which contains the formations Tor and Ekofisk, exists as confirmed by several authors (Torsæter 1984; Agarwal, Hermansen et al. 2000; Hamon 2004). The amount of spontaneous imbibition of water is generally used to characterize the wettability of a particular core. There exists no general correlation between wettability and porosity, permeability or initial water saturation for the Ekofisk Field. However, the wettability has a particular trend with respect to height above free water level (FWL). Water wetness increases as the distance from oil-water contact decreases. Bottom layers are strongly water-wet while top layers are very weakly water-wet. **Fig. 9.4** is the graph showing the wettability variation with elevation above FWL in both Ekofisk and Tor formation. From Fig. 9.4, it can be seen that Tor formation is preferably water-wet while the Ekofisk formation is less water-wet. However, the wettability of the lower Ekofisk formation is quite similar to that of Tor formation. This graph is helpful to determine the average wettability (average amount of spontaneous imbibition) of a particular depth. For example, between 200 ft and 400 ft interval above FWL, the average spontaneous imbibition for Tor formation is around 55% while between 400 ft and 600 ft above FWL, the average spontaneous imbibition is around 40%. As mentioned above, the matrix relative permeability strongly depends on wettability and therefore the relative permeability curves will be different for each of these intervals.

Hallenbeck, Sylte et al. (1991) have also reported laboratory results from Tor and Ekofisk formation and mentioned that imbibition values in Tor formation ranges from 41% to 61% with an average value of 51%. For Ekofisk formation, the imbibition value ranges from 2.5% to 61% with an average value of 33%. These values confirm that typical relative permeability curves for the Ekofisk formation should correspond to its moderate to weak water-wetness while for the Tor formation typical relative permeability curves should correspond to its strong water-wetness.

Hamon (2004) also performed pore network simulations to complement the matrix relative permeability curves and presented a useful graph for determination of residual oil saturation and maximum relative permeability of water at a particular amount of spontaneous imbibition as given in **Fig. 9.5**. This graph can be used in combination with the graph of the wettability variation with depth (Fig. 9.4) to determine the end points of relative permeability curve at each depth. As mentioned above, reservoir chalk core plugs prepared with synthetic formation water with similar low sulphate concentration as in real formation water, gave higher spontaneous imbibition of brine than core plugs prepared with synthetic formation water without sulphate. This means that the oil saturation at capillary pressure equal to zero was lower for the first core plugs than for the second core plugs. Seawater was found to improve the spontaneous imbibition for both types of core plugs, i.e. reduced the oil saturation at capillary pressure of zero. High concentration of sulphate in initial brine has also been reported to give more water-wet conditions than brines without sulphate (Ahsan, Madland et al. 2012). For the core plugs prepared without sulphate in initial brine, imbibition brine with high sulphate concentration altered the capillary pressure curve from the less water-wet curve to the more water-wet curve (Ahsan, Madland et al. 2012).

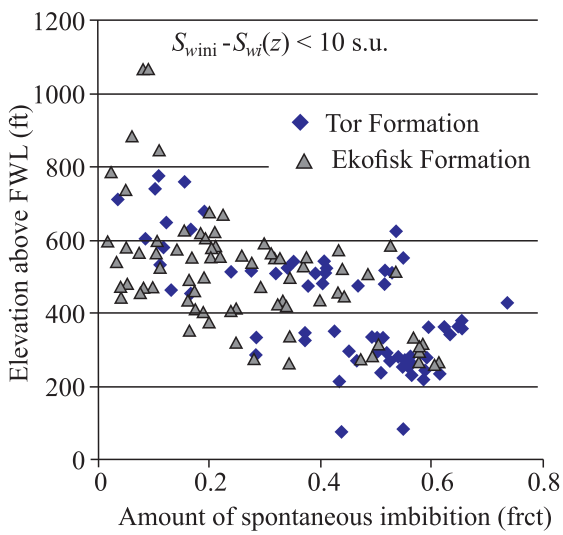

Figure 9.4: Wettability variation with respect to depth in Tor and Ekofisk formation (Hamon 2004).

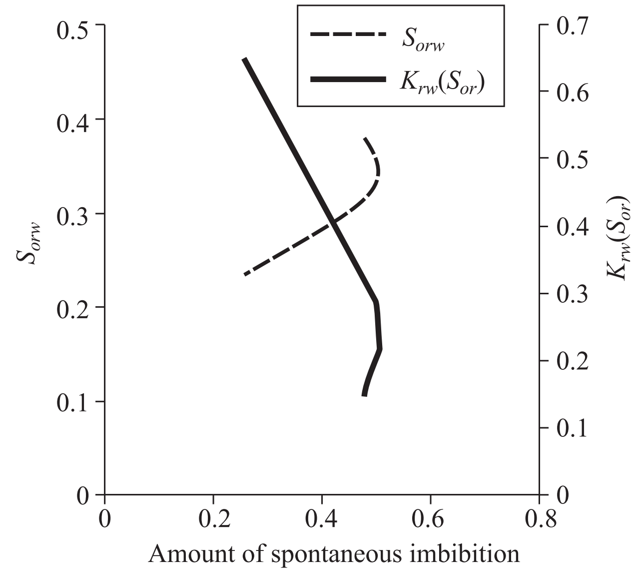

Figure 9.5: Residual oil saturation and water relative permeability at residual saturation for given wettability (Hamon 2004).

9.5.4 Matrix relative permeability and capillary pressure curves of a particular interval of formation

As different matrix relative permeability curves exists at different interval and different location because of the variation in wettability, the average spontaneous imbibition of that particular interval estimated from Fig. 9.4 is used to calculate the residual oil saturation and maximum water relative permeability of that particular region from Fig. 9.5. By combining these values of residual oil saturation and maximum water relative permeability with available data on chalk relative permeability it is possible to obtain appropriate relative permeability curves. For example, the typical matrix relative permeable curves for Tor formation and lower Ekofisk formation as given in **Figs. 9.6 and 9.7** are extracted from Talukdar (2002) PhD dissertation by using Figs 9.4 and 9.5. **Figs. 9.8 and 9.9** are the water-oil capillary pressure curves, also estimated from Talukdar (2002), for Tor and lower Ekofisk formation respectively.

Da Silva (1989) used different capillary pressure curves for different layers while simulating the pilot water flooding tests. As Tor and lower Ekofisk are more water-wet, a capillary pressure curve with higher spon-

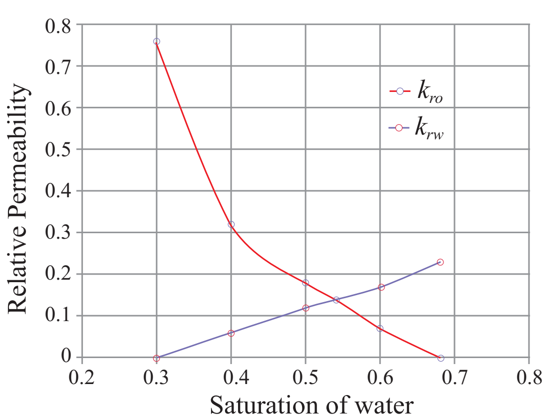

Figure 9.6: Water-Oil relative permeability for Tor formation (Talukdar 2002).

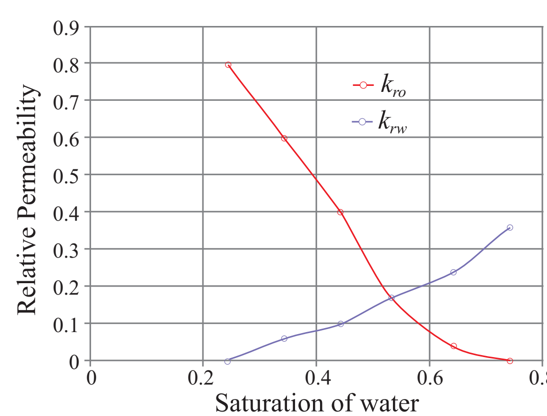

Figure 9.7: Water-Oil relative permeability for lower Ekofisk formation (Talukdar 2002).

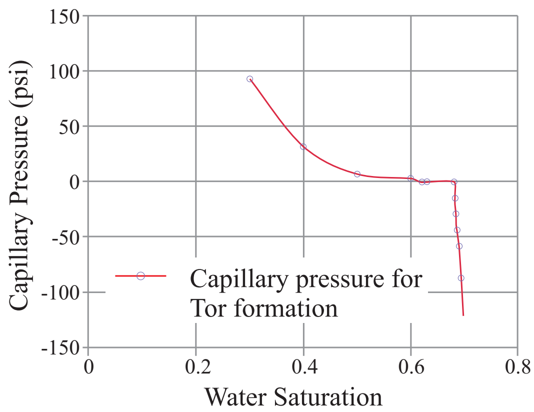

Figure 9.8: Water-Oil capillary pressure for Tor formation (Talukdar 2002).

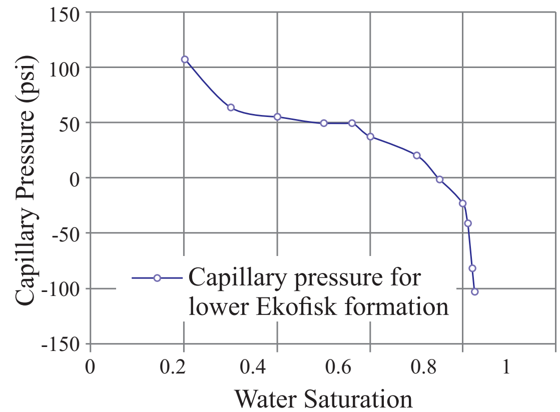

Figure 9.9: Water-Oil capillary pressure for Lower Ekofisk formation (Talukdar 2002).

taneous imbibition was used (around 50%). For upper and middle Ekofisk formation, the imbibition curve for low spontaneous imbibition recovery (around 25%) was used. The typical values of the negative capillary pressure curves for both formations are given in **Fig. 9.10**.

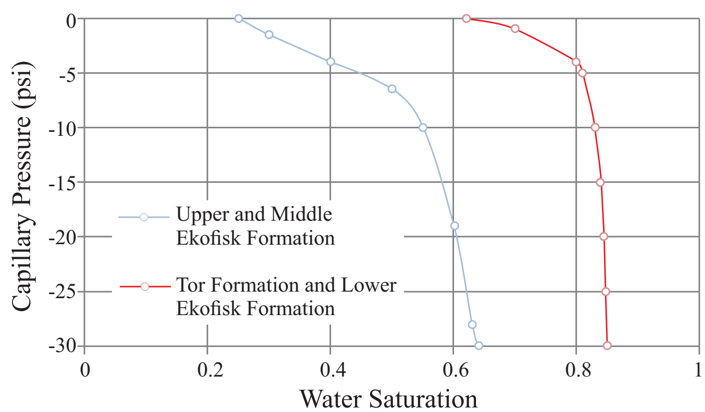

Figure 9.10: Water-Oil capillary pressure in forced imbibition region for Tor and Ekofisk formation (Da Silva 1989).

9.5.5 Matrix relative permeability and capillary pressure curves of the entire field

While performing the dual porosity numerical simulation of the entire field Da Silva (1989) used the following relative permeability and capillary pressure curves for oil-water system (see **Figs. 9.11 and 9.12**). Through history matching, he validated the use of relative permeability and capillary pressure data.

9.5.6 Oil-water pseudo relative permeability curves

Agarwal, Hermansen et al. (2000) have estimated oil-water pseudo relative permeability curves through mechanistic models while performing history matching of full field single porosity simulation model of the Ekofisk field. **Fig. 9.13** presents the typical pseudo relative permeability curves suggested by Agarwal, Hermansen et al. (2000) for highly fractured zone.

Da Silva (1989) mentioned that imbibition oil-water pseudo relative permeability does not change much with fracture spacing and fracture permeability and essentially depends on the wettability of the rock only. He also showed the effect of wettability on water pseudo relative permeability curves as given in **Fig. 9.14**. The pseudo relative permeability curve for 48% spontaneous imbibition is for Tor formation and Lower Ekofisk formation while 25% spontaneous imbibition is for lower and middle Ekofisk Formation. 38% spontaneous imbibition curve was used to history match GOR for upper and middle Ekofisk only during last year of production. When comparing this pseudo relative permeability curves with curves given by Agarwal, Hermansen et al. (2000), it is clear the curves of Agarwal et al. are given for spontaneous imbibition greater than 50%.

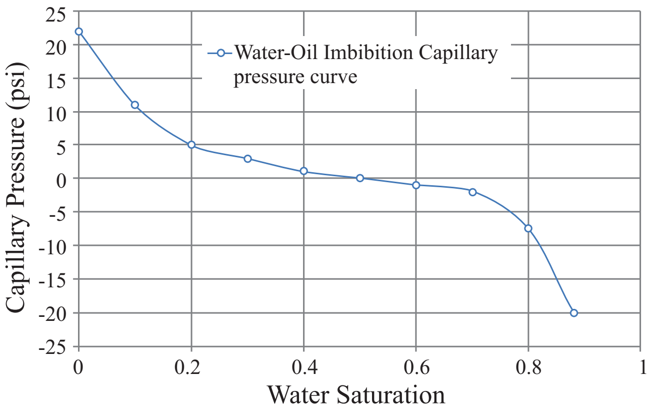

Figure 9.11: Water-Oil capillary pressure for the Ekofisk field used in dual porosity simulation model (Da Silva 1989).

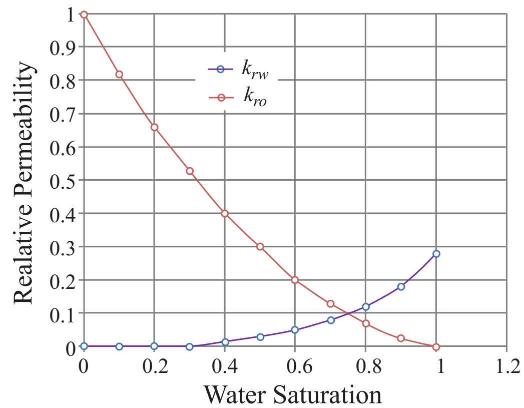

Figure 9.12: Matrix Water-Oil relative permeability for the Ekofisk field used in dual porosity simulation model (Da Silva 1989).

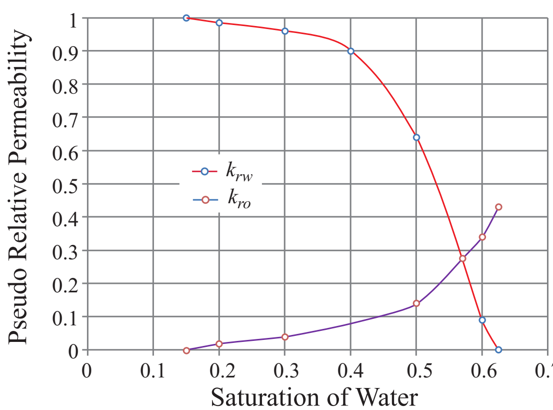

Figure 9.13: Water-Oil pseudo relative permeability estimated from history match (Agarwal, Hermansen et al. 2000).

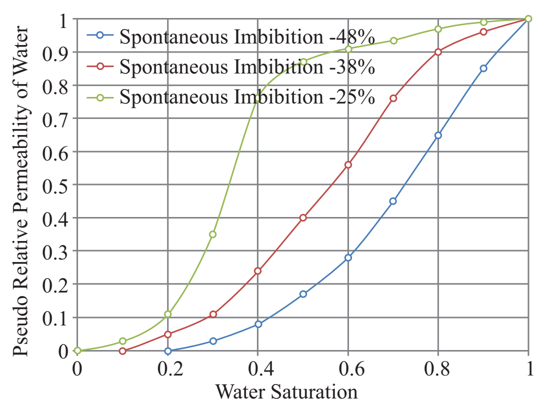

Figure 9.14: Effect of wettability on water-oil pseudo relative permeability (Da Silva 1989).

9.5.7 Qualitative comparison of relative permeability and capillary pressure curves from other sources

Feazel, Knight et al. (1990) presented matrix water-oil relative permeability curves that resembled the curves presented by Da Silva (1989). Thomas, Dixon et al. (1987) used the matrix imbibition capillary pressure curve from (Torsæter 1984) while simulating the water flooding performance during the pilot tests with three dimensional dual porosity simulation model. The curve resembles the curve presented by Da Silva (1989) and Talukdar (2002) for Tor and lower Ekofisk formation. Sulak and Danielsen (1989) studied the reservoir aspects of Ekofisk subsidence and used the water-oil capillary pressure curves for Tor and Ekofisk formation which also were quite similar as presented above.

Nomenclature

A_1 = area under the secondary water drainage curve, L^2
A_2 = area under the imbibition curve falling below the zero-P_c axis, L^2
k = absolute permeability, L^2
k_o = effective oil permeability, L^2
k_w = effective water permeability, L^2
k_{ro} = relative oil permeability
k_{rw} = relative water permeability
P_c = capillary pressure, m/Lt^3
P_{nw} = non-wetting pressure, m/Lt^3
P_w = wetting phase pressure, m/Lt^3

r_w = Amott wettability index to water
r_o = Amott wettability index to oil
r_1, r_2 = principal radii of curvature, L
S = saturation
S_{or} = residual oil saturation
S_{orw} = residual oil saturation to water
S_w = water saturation
S_{wi} = initial water saturation
WI_{Amott} = Amott wettability index
WI_{USBM} = USBM wettability index
ΔS_{ws} = change in water saturation by spontaneous imbibition
ΔS_{os} = change in oil saturation by spontaneous imbibition
ΔS_{wt} = overall change in water saturation
θ = contact angle
σ = interfacial tension, $\mathrm{m/t^2}$
σ_{os} = surface tension between oil and solid, $\mathrm{m/t^2}$
σ_{ws} = surface tension between water and solid, $\mathrm{m/t^2}$
σ_{ow} = interfacial tension between oil and water, $\mathrm{m/t^2}$

Subscripts

c = capillary
i = initial
n = non
o = oil
r = residual
s = spontaneous, solid
t = total (with saturation change ΔS)
w = water, wetting

Abbreviations

FWL = free water level
GOR = gas oil ratio
USBM = United States Bureau of Mines

References

Agarwal, B., Hermansen, H. et al., 2000. Reservoir Characterization of Ekofisk Field: A Giant, Fractured Chalk Reservoir in the Norwegian North Sea-History Match. *SPE Reservoir Eval. & Eng*, **3**: 534–543. SPE-68096-PA. URL `http://dx.doi.org/10.2118/68096-PA`.

Ahsan, R., Madland, M.V. et al., 2012. A study of sulphate ions–effects on aging and imbibition capillary pressure curve. In *International Symposium of the Society of Core Analysts held in Aberdeen, Scotland, UK*, 27–30. SCA2012-34. 27–30 August. URL `http://www.jgmaas.com/SCA/2012/SCA2012-34.pdf`.

Ali, N. and Alcock, T., 1994. Valhall field, norway-the first ten years. In J.O. Aasen, ed., *North Sea Oil and Gas Reservoirs — III*, 25–40. Kluwer Academic Publishers. URL `http://dx.doi.org/10.1007/978-94-011-0896-6_2`.

Amott, E., 1959. Observations relating to the wettability of porous rock. *Society of Petroleum Engineers*, **216**. SPE-1167-G. URL `https://www.onepetro.org/general/SPE-1167-G`.

Amyx, J.W., Bass, D.M., and Whiting, R.L., 1960. *Petroleum reservoir engineering: physical properties*, vol. 1. McGraw-Hill College.

Anderson, W., 1986a. Wettability literature survey-part 2: Wettability measurement. *Journal of Petroleum Technology*, **38** (11): 1–246. SPE-13933-PA. November. URL `http://dx.doi.org/10.2118/13933-pa`.

Anderson, W.G., 1986b. Wettability Literature Survey - Part 1: Rock/Oil/Brine Interaction and the Effects of Core Handling on Wettability. *Journal of Petroleum Technology*, **38** (10): 1125–1144. SPE-13932-PA. Octber. URL http://dx.doi.org/10.2118/13932-pa.

Anderson, W.G., 1987a. Wettability literature survey-part 4: Effects of wettability on capillary pressure. *Journal of Petroleum Technology*, **39** (10): 1–283. SPE-15271-PA. October. URL http://dx.doi.org/10.2118/15271-pa.

Anderson, W.G., 1987b. Wettability literature survey part 5: the effects of wettability on relative permeability. *Journal of Petroleum Technology*, **39** (11): 1–453. SPE-16323-PA. November. URL http://dx.doi.org/10.2118/16323-pa.

Anderson, W.G., 1987c. Wettability literature survey-part 6: the effects of wettability on waterflooding. *Journal of Petroleum Technology*, **39** (12): 1–605. SPE-16471-PA. December. URL http://dx.doi.org/10.2118/16471-pa.

Baldwin, B.A., 1988. Water Imbibition and Characterization of North Sea Chalk Reservoir Surfaces. *SPE Formation Evaluation*, **3** (01): 125–130. SPE-14108-PA. March. URL http://dx.doi.org/10.2118/14108-PA.

Barkved, O., Buer, K. et al., 2003. 4D Seismic Response of Primary Production and Waste Injection at the Valhall Field. 02 June. URL http://www.earthdoc.org/publication/publicationdetails/?publication=3102.

Brownscombe, E.R. and Dyes, A.B., 1952. Water-imbibition displacement-a possibility for the Spraberry. In *Drilling and Production Practice*. American Petroleum Institute. API-52-383.

Buckley, J.S., Takamura, K., and Morrow, N.R., 1989. Influence of electrical surface charges on the wetting properties of crude oils. *SPE Reservoir Engineering*, **4** (03): 332–340. SPE-16964-PA. August. URL http://dx.doi.org/10.2118/16964-pa.

Chilingar, G.V. and Yen, T.F., 1983. Some Notes on Wettability and Relative Permeabilities of Carbonate Reservoir Rocks, II. *Energy Sources*, **7** (1): 67–75. October. URL http://dx.doi.org/10.1080/00908318308908076.

Collins, R.E., 1976. *Flow of fluids through porous materials*. Petroleum Publishing Co., Tulsa, OK.

Cuiec, L., 1987. Wettability and oil reservoirs. In *North Sea Oil & Gas Reservoirs*. Graham & Trotman.

Da Silva, F.V., 1989. Primary and enhanced recovery of Ekofisk Field: A single-and double-porosity numerical simulation study. In *SPE Annual Technical Conference and Exhibition*. Society of Petroleum Engineers. SPE-19840-MS. URL http://dx.doi.org/10.2118/19840-ms.

Donaldson, E.C., Thomas, R.D., and Lorenz, P.B., 1969. Wettability determination and its effect on recovery efficiency. *Society of Petroleum Engineers Journal*, **9** (01): 13–20. SPE-2338-PA. March. URL http://dx.doi.org/10.2118/2338-pa.

Feazel, C.T., Knight, I.A., and Pekot, L.J., 1990. Ekofisk field—Norway Central graben, North Sea, In *AAPG Treatise of Petroleum Geology, Structural Traps IV: Tectonic and Nontectonic Fold Traps*, eds., E.A. Beaumont and N.H. Foster, , 1–25. AAPG Special Volumes. URL http://archives.datapages.com/data/specpubs/fieldst3/data/a018/a018/0001/0000/0001.htm.

Fernø, M.A., Treinen, R., and Graue, A., 2007. Experimental measurements of capillary pressure with the centrifuge technique—emphasis on equilibrium time and accuracy in production. In *Proceedings of the International Symposium of the Society of Core Analysts, paper SCA*, vol. 22. SCA2007-22. 10–13 September. URL http://www.jgmaas.com/SCA/2007/22.pdf.

Fjelde, I. and Asen, S.M., 2015. Effect of Initial Sulfate in Reservoir Chalks on the Spontaneous Imbibition of Sea Water. In *IOR 2015-18th European Symposium on Improved Oil Recovery*. EAGE Publications. April. URL http://dx.doi.org/10.3997/2214-4609.201412099.

Graham, J.W. and Richardson, J.G., 1959. Theory and application of imbibition phenomena in recovery of oil. *Journal of Petroleum Technology*, **11** (02): 65–69. SPE-1143-G. February. URL http://dx.doi.org/10.2118/1143-g.

Graue, A., Moe, R.W., and Bognø, T., 2000. Impacts of wettability on oil recovery in fractured carbonate reservoirs. In *Reviewed Proc.: 2000 International Symposium of the Society of Core Analysts, Abu Dhabi, United Arab Emirates*. SCA2000-25. 18–22 October. URL https://www.researchgate.net/profile/Arne_Graue/publication/266879533_IMPACTS_OF_WETTABILITY_ON_OIL_RECOVERY_IN_FRACTURED_CARBONATE_RESERVOIRS/links/5566b72908aefcb861d19f4a.pdf.

Hagoort, J., 1980. Oil recovery by gravity drainage. *Society of Petroleum Engineers Journal*, **20** (03): 139–150. SPE-7424-PA. June. URL `http://dx.doi.org/10.2118/7424-pa`.

Hallenbeck, L.D., Sylte, J.E. et al., 1991. Implementation of the Ekofisk field waterflood. *SPE Formation Evaluation*, **6** (03): 284–290. SPE-19838-PA. September. URL `http://dx.doi.org/10.2118/19838-PA`.

Hammervold, W.L., Knutsen, Ø. et al., 1998. Capillary pressure scanning curves by the micropore membrane technique. *Journal of Petroleum Science and Engineering*, **20** (3): 253–258. June. URL `http://dx.doi.org/10.1016/s0920-4105(98)00028-x`.

Hamon, G., 2004. Revisiting Ekofisk and Eldfisk wettability. In *SPE Annual Technical Conference and Exhibition*. Society of Petroleum Engineers. SPE-90014-MS. 26–29 September. URL `http://dx.doi.org/10.2118/90014-ms`.

Hassenkam, T., Skovbjerg, L.L., and Stipp, S.L.S., 2009. Probing the intrinsically oil-wet surfaces of pores in North Sea chalk at subpore resolution. *Proceedings of the National Academy of Sciences*, **106** (15): 6071–6076. March. URL `http://dx.doi.org/10.1073/pnas.0901051106`.

Hermansen, H., Thomas, L.K. et al., 1997. Twenty five years of Ekofisk reservoir management. In *SPE Annual Technical Conference and Exhibition*. Society of Petroleum Engineers, Society of Petroleum Engineers (SPE), San Antonio, Texas. SPE-38927-MS. 5–8 October. URL `http://dx.doi.org/10.2118/38927-MS`.

Jensen, T.B., Harpole, K.J., and Østhus, A., 2000. EOR Screening for Ekofisk. In *SPE European Petroleum Conference*. Society of Petroleum Engineers, Paris, France. SPE-65124-MS. 24–25 October. URL `http://dx.doi.org/http://dx.doi.org/10.2118/65124-MS`.

Leverett, M.C., 1939. Flow of oil-water mixtures through unconsolidated sands. *Transactions of the AIME*, **132** (01): 149–171. SPE-939149-G. December. URL `http://dx.doi.org/10.2118/939149-G`.

Li, G., 2011. *World atlas of oil and gas basins*. John Wiley & Sons. URL `http://dx.doi.org/10.5860/choice.48-6656`.

Lombard, J.M., Gautier, S. et al., 2006. Petrophysical parameter measurements: Comparison of semi-dynamic and centrifuge methods for water-wet and oil-wet limestone samples. SCA2006-09. 12–16 September. URL `http://www.jgmaas.com/SCA/2006/SCA2006-09.pdf`.

Martin, R., Baihly, J.D. et al., 2011. Understanding production from Eagle Ford-Austin chalk system. In *SPE Annual Technical Conference and Exhibition*. Society of Petroleum Engineers, Society of Petroleum Engineers (SPE). SPE-145117-MS. URL `http://dx.doi.org/10.2118/145117-ms`.

Mattax, C.C., Kyte, J. et al., 1962. Imbibition oil recovery from fractured, water-drive reservoir. *Society of Petroleum Engineers Journal*, **2** (02): 177–184. SPE-187-PA. June. URL `http://dx.doi.org/10.2118/187-pa`.

Morrow, N.R., 1990. Wettability and its effect on oil recovery. *Journal of Petroleum Technology*, **42** (12): 1–476. SPE-21621-PA. December. URL `http://dx.doi.org/10.2118/21621-pa`.

Nordtvedt, J., Urkedal, H. et al., 1994. Estimation of relative permeability and capilary pressure functions using transient and equilibrium data from steady-state experiments. In *SCA*, vol. 9418, 197–206. SCA-9418. 12–14 September. URL `http://www.jgmaas.com/SCA/1994/SCA1994-18.pdf`.

Norwegian Petroleum Directorate, 2016. NPD. URL `https://www.norskpetroleum.no/en/facts/field/ekofisk/`.

Osoba, J.S., Richardson, J.G. et al., 1951. Laboratory measurements of relative permeability. *Journal of Petroleum Technology*, **3** (02): 47–56. SPE-951047-G. February. URL `http://dx.doi.org/10.2118/951047-g`.

Pourmohammadi, S., Hetland, S. et al., 2008. Impact of petrophysical properties on water flood efficiency in Cretaceous and Tertiary chalk. SCA2008-27. 29 October – 2 November. URL `http://www.academia.edu/download/30910144/SCA2008-27.pdf`.

Puntervold, T., 2008. *Waterflooding of carbonate reservoirs: EOR by wettability alteration*. Ph.D. thesis, Univeristy of Stavanger. URL `http://hdl.handle.net/11250/183693`.

Raza, S.H., Treiber, L.E., and Archer, D.L., 1968. Wettability of reservoir rocks and its evaluation. *Prod. Mon.;(United States)*, **32** (4). April. URL `http://www.osti.gov/scitech/biblio/6093912`.

Spinler, E.A. and Baldwin, B.A., 1997. Capillary pressure scanning curves by direct measurement of saturation. In *SCA9705, International Symposium of the Society of Core Analysts*. 8–10 September. URL `http://www.jgmaas.com/SCA/1997/SCA1997-05.pdf`.

Standnes, D.C. and Austad, T., 2000. Wettability alteration in chalk: 2. Mechanism for wettability alteration from oil-wet to water-wet using surfactants. *Journal of Petroleum Science and Engineering*, **28** (3): 123–143. November. URL `http://dx.doi.org/10.1016/S0920-4105(00)00084-X`.

Strand, S., 2005. *Wettability alteration in chalk: a study of surface chemistry*. Ph.D. thesis, Univeristy of Stavanger.

Sulak, A.M. and Danielsen, J., 1989. Reservoir aspects of Ekofisk subsidence. *Journal of Petroleum Technology*, **41** (07): 709–716. SPE-17852-PA. 2–5 May. URL `http://dx.doi.org/10.2118/17852-PA`.

Talukdar, S., 2002. *Ekofisk Chalk: core measurements, stochastic reconstruction, network modeling and simulation*. Ph.D. thesis, Norwegian University of Science and Technology. URL `http://hdl.handle.net/11250/231141`.

Thomas, L.K., Dixon, T.N. et al., 1987. Ekofisk Waterflood Pilot. *Journal of Petroleum Technology*, **39** (02): 221–232. SPE-13120-PA. February. URL `http://dx.doi.org/10.2118/13120-PA`.

Tjetland, G., Kristiansen, T.G., and Buer, K., 2007. Reservoir management aspects of early waterflood response after 25 years of depletion in the Valhall Field. In *International Petroleum Technology Conference*. International Petroleum Technology Conference, Society of Petroleum Engineers (SPE), Dubai, U.A.E. IPTC-11276-MS. 4–6 December. URL `http://dx.doi.org/10.2523/IPTC-11276-MS`.

Torsæter, O., 1983. *An experimental study of water imbibition in chalk from the Ekofisk Field*. Ph.D. thesis, The Norwegian Inst. of Technology.

Torsæter, O., 1984. An Experimental Study of Water Imbibition in Chalk From the Ekofisk Field. SPE-12688-MS. 15–18 April. URL `http://dx.doi.org/10.2118/12688-MS`.

Treiber, L.E. and Owens, W.W., 1972. A laboratory evaluation of the wettability of fifty oil-producing reservoirs. *Society of petroleum engineers journal*, **12** (06): 531–540. SPE-3526-PA. December. URL `http://dx.doi.org/10.2118/3526-pa`.

van Golf-Racht, T.D., 1982. *Fundamentals of fractured reservoir engineering*, vol. 12. Elsevier. ISBN 9780444420466.

Warren, J.E. and Root, P.J., 1963. The behavior of naturally fractured reservoirs. *Society of Petroleum Engineers Journal*, **3** (03): 245–255. SPE-426-PA. September. URL `http://dx.doi.org/10.2118/426-pa`.

Welge, H.J., 1952. A simplified method for computing oil recovery by gas or water drive. *Journal of Petroleum Technology*, **4** (04): 91–98. SPE-124-G. April. URL `http://dx.doi.org/10.2118/124-g`.

Zhang, P. and Austad, T., 2005. The relative effects of acid number and temperature on chalk wettability. In *SPE International Symposium on Oilfield Chemistry*. Society of Petroleum Engineers, Society of Petroleum Engineers (SPE). SPE-92999-MS. 2–4 Ferbruary. URL `http://dx.doi.org/10.2118/92999-ms`.

Chapter 10

Geophysical Interpretation

Olav Inge Barkved, Ole Vejbæk, Anette Uldall, and Per Gunnar Folstad

10.1 Introduction

Calcareous algae accumulating as slow rain, draping pre-existing submarine morphology as a blanket of mainly laminated deposits formed the Upper Cretaceous to Lower Palaeogene Chalk Group. In the North Area, the Chalk Group may reach thicknesses higher than 2000 m. Chalk is a very clean form of calcium carbonate. Slow deposition combined with burrowing and pauses in the deposition resulted in early lithification. This resulted in an apparently well-defined Top Chalk Group, which in the seismic sections may appear as a continuous reflector, representing a strong acoustic impedance contrast to the overlying clastic Palaeogene sediments. The base of the chalk may not be as pronounced as the top, as the lithology of the underlying lower cretaceous sediments might vary and include marls and dense shale, although a marked doublet in some areas may be used as a signature.

A closer look of the seismic expression of the cretaceous chalk reveals a more complex and convoluted response. Significant thickness variations are observed at regional and local scales. Local thickness variations may be to due prevalent periods of monotonous deposition or periods of re-working and mass-flow redistributions linked to deep-water currencies and to tectonic events. There are also significant changes in the properties of the chalk, porosity may range from the lower tens to fifty percent, and very high porosity chalk could have lower acoustic properties than the overlying tertiary shales. The resulting porosities that we observe today are due to a complex combination of diagenesis, depositional effect and burial history.

Persisting fractures are well known from consolidated chalk. Softer chalk may also be intensively fractured due to overpressure and tectonic stresses, but the properties are of a more dynamic character.

During the fifty years of seismic interpretation the North West Europe's Chalk Group, the scope has changed from focusing on structural and depth-conversion issues to detailed analysis of stratigraphy and reservoir properties. Seismic quality, rather than interpretation technology has been the primary driver behind today's elaborate use of seismic for managing the North Seas chalk reservoirs.

In this section we will discuss in more details the seismic expressions of chalk and how the seismic data can be used, combined with geological insights to describe chalk reservoirs in more detail. We will illustrate the importance of seismic data to understand the regional structural development, recognize and delineate stratigraphic elements for detailed reservoir property characterization.

10.2 What is special with seismic in chalk?

Clastic sediments are typically sourced from highs, from which the sediments are eroded and transported away. Water is the dominant source of erosion and transport, but wind and ice may also play a role.

Chalk deposits are different in that the source of the sediments is organisms, coccoliths living in uppermost part of the sea. A chalk deposit may be autochthonous, meaning that the rock is formed where the remnants of the coccoliths landed on the seabed, or it may be allocthonous. In this case, the sediments have been redistributed by mass flow of seabed currents.

The diagenetic processes in chalk alter the initial mineralogical nature and the texture by recrystallization. The preservation and diagenesis of chalk are sensitive to climate changes and presence of terrigeneneous sediments being transported into the basin. Even small amounts of clay mineral may have significant impact on the diagenetic processes.

The present petrophysical and mechanical properties of the chalk are closely linked to the initial sedimentological settings and subsequent diagenesis during burial. Early diagenetic cementation may have taken place shortly after deposition, partly helped by bioturbation. Sedimentation rates and hydrodynamic conditions could result in subsequent thin and very tight layers exhibiting acoustic properties significantly higher than found in clastic rocks at similar depth of burial. Later sediment re-mobilization resulted in the destruction of these early diagenetic events, and only the topmost few meters of these new deposits appear to be subjected to alteration. As a consequence the resulting allochtonous sediments attained higher porosities than the initial deposits.

Chemical compaction in the chalk probably started after 800–1000 m of burial. At that depth the porosities probably were in the order of 40 %, e.g., Fabricius and Borre (2007); Fabricius (2007). The chemical cementation was probably linked to the presence of argillaceous clays that may have reduced the contact dissolution. Today the cleanest formations sometimes appear to be the most lithified and cemented.

Early inflow of hydrocarbons may retard diagenesis by preventing occlusion of porosity by externally derived carbonate cement (Brasher and Vagle 1996). The generally very small pore throats hampers the hydrocarbons ability to enter the pore space due to the large associated capillary entry pressure (Engstrøm 1995; Vejbaek, Bech et al. 2015). Minor differences in mineralogy and grain size may play a big role in whether the chalk sediments develop into an oil bearing reservoir or remain a water filled rock subjected to further diagenesis. In other cases, isolated re-worked sediments that have been isolated from water influx and reduced effective stress, the effect of diagenesis may be considerably reduced and the high porosity can have been maintained.

The relative high productivity of some of the North Sea producing oil wells is caused by natural or induced fracturing. Natural fracturing is believed to be linked to major episodic events. Initially, the tectonics associated with the early Tertiary epeirogenesis (inversion) probably resulted in the formation of the early joints and faults. Later, during burial, the external loads combined with low permeability and local overpressure may have caused a secondary phase of fracturing. This stage of fracturing affected the weakest and most porous chalk the most, and may locally have caused an intense brecciating of the rock (Watts 1983).

Many important chalk reservoirs are characterized by local high porosities effected anomalies and associated low acoustic impedance. Seismic data may provide direct identification of porosity and fracture developments in the chalk (Hall, Kendall et al. 2002; Mueller 1991).

Uses of seismic data to distinguish between pore-fills remains may be challenging. Preservation of high porosity in a typical north sea reservoir does is often linked to the presence of hydrocarbons. However, high porosity anomalies have also been found filled with water, indicating apparent lack of pressure communications. Significant amounts of remaining oil in producing and yet un-discovered chalk reservoirs remain important economic resources. To locate and define these resources, utilization of dedicated geological knowledge, understanding of the origin of the chalk, depositional processes and ability to identify burial effects, are needed. Seismic data remains an important source for deriving this information. The reflection patterns revealed in the seismic data and provides essential insights to the tectonic settings and can be indicative of the actual depositional process (Hatton 1986; Back, Van Gent et al. 2011).

Structurally trapped reservoirs within the Chalk Group range from inversion-generated anticlines, e.g. the Valhall, Roar, Tyra and South Arne fields , over salt domes with some degree of inversion overprint, e.g. the Dan, Ekofisk and Svend fields to salt diapirs, e.g. the Skjold and Harald fields.

More details on how the local tectonism affected the sedimentation and eventually the shape and extent of the reservoir container of the Valhall field can be found in Farmer and Barkved (1999). **Fig.10.1** from the Valhall field shows the forming of a local thinner Cretaceous Chalk Group above a thick upper Jurassic deposit. The local tectonics, faulting, i.e. during the apparent high tectonic activity periods in Maastrictian and Danian times, appear to control the presence of local thick and thin chalk during these stages. The settlement of pelagic skeletal debris at the seafloor forming the calcareous ooze is effected by topography of the seafloor and effected by water currents and storm waves. Snow may be useful analogue to the forming of a chalk deposition. Wind are sweeping snow away from the highest area where the icy and denser patches are formed, and move the snow drifts to lower, more sheltered areas.

The applications and analysis of the seismic reflections from chalk sequences are not without challenges. The hard and tight chalk interfaces are very good reflectors, sometimes so good that it may be difficult to illuminate the deeper layers properly. When the chalk deposit consists of alternating hard and less hard layers, we might get additional ringing effects and interferences that make it difficult to separate the primary seismic reflector from the reverberations.

To understand the development of a chalk deposit, we also need clear imaging of the sediments above and below. Due to the generally higher velocities in chalk, we typically get critical seismic reflections at low angles of incidence. Combined with the ray bending effects, the ranges of incidence angles available to image

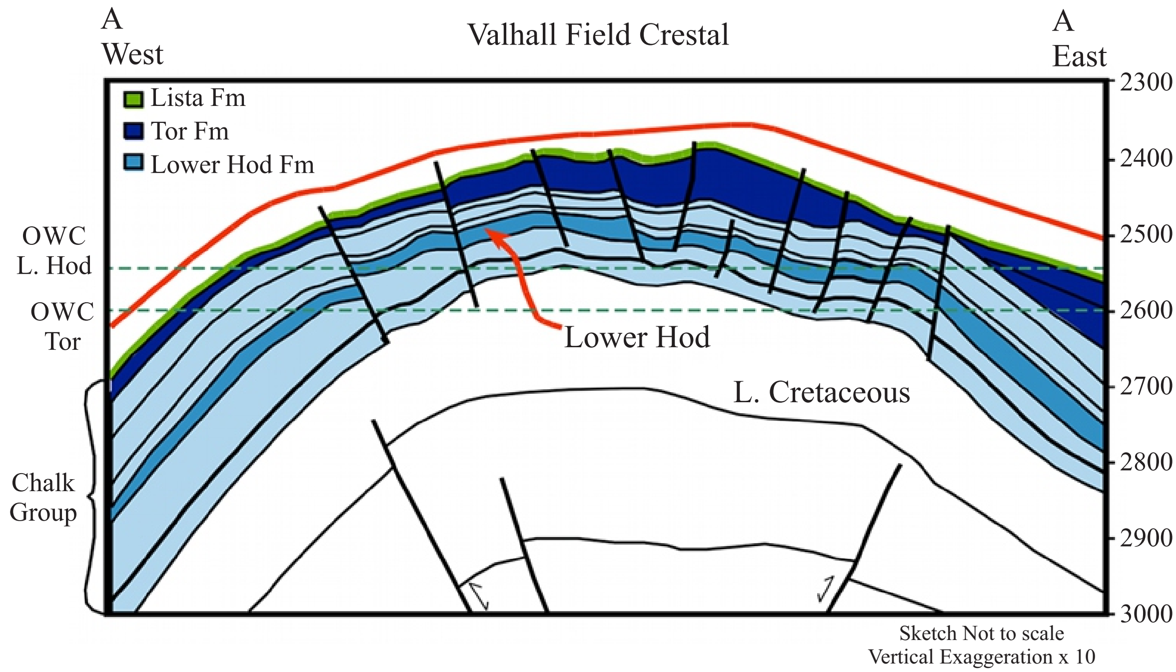

Figure 10.1: Example from the from The Valhall illustrating thinning of the Lower Hod Chalk formation due to inversion along the Lindesnes Ridge. During Mastrictian/Danian time a crestal collapse allowed for a thick Tor Formation to be developed.

the layers below the chalk very often are limited. Limited incidence angles affect our ability to determine the velocities uniquely and hamper multiple attenuations.

Seismic interpretation provides the basis for understanding the structural and tectonic framework, enable the spatial delineation of depositional features and help unraveling the compaction and burial effects as well as supporting direct porosity and fracture mapping.

10.3 Seismic interpretation

Continuous extensive seismic reflectors are commonly linked to stratal surfaces. Stratal surface are linked with a specific geological time, while the rock type above and below can vary. This first order tie to chronostratigraphy is often easily recognized in a regional seismic section. The link to lithology may be more subtle and linked to other seismic reflection attributes as changes in lithology often is gradual, varying laterally away from the sediment source. In chalk deposits, the presence of strong diagenetic effects may complicate linking the seismic reflectors to chronostratigraphy.

Seismic interpretation may be divided into three main methods: structural interpretation, seismic stratigraphic analysis and seismic inversion. In structural interpretation, we map the seismic horizons and evaluate the seismic velocities to define a geological structure and make maps or cross-sections that point out the shapes of the highs and lows of a geological layer or interface.

Structural maps depicting the main structural elements like faults and thick and thins of one or many geological layers are essential in providing the context for how a regional or local basin has developed. As such, seismic structural interpretation has merits at all geological scales from a regional basin down to understanding local reservoir compartments a few hundred meters across.

During the 1970s the seismic stratigraphy concept was introduced (Vail 1977). This methodology is based on that the geometry of seismic events appearing in a seismic section is as representing particular styles of sedimentation and depositional environments. The configuration of the local reflections may be used to infer bedding patterns, depositional properties, erosional features, paleo-topography, subsidence and eustasy. The continuity of the reflections may inform us about the lateral continuity of the geological layers and hence the depositional processes involved. The reflection amplitudes carry information about the contrast in densities and velocities between the individual layers and provide insights into the actual lithofacies, porosities or fluid. The frequencies of reflections may indicate fluid content, but are primarily due to variations in thin layers thicknesses.

In both the structural interpretation and seismic stratigraphic analysis, the fundamental challenges are to get rid of possible multiple reflections that may clutter the seismic images. Still the basis is the seismic reflection, where the seismic response is linked to the interaction between the interfaces between two acoustic layers and the seismic signal or wavelet used to image the subsurface.

The interpreter is not interested in the wavelet itself but in the geological information that it brings. One of the most important tasks for the seismic interpreter is to understand the characteristics of the wavelet and differentiate these from the geological information it reflects. In the third group of methodologies, alternative ways of removing the characteristics of the seismic wavelet to better delineate the properties of the layers rather than their interfaces. This process is often referred to as seismic inversion, **Fig.10.2**, simply because it's the inverse of the forward modelling we use to define the seismic response of sequence of geological layers with different acoustic properties observed in wells or a random geological scenario, see Fig.10.2 below. Seismic inversion may be used as a basis for structural and stratigraphic analysis, as well as being used directly in quantitative descriptions of the reservoir.

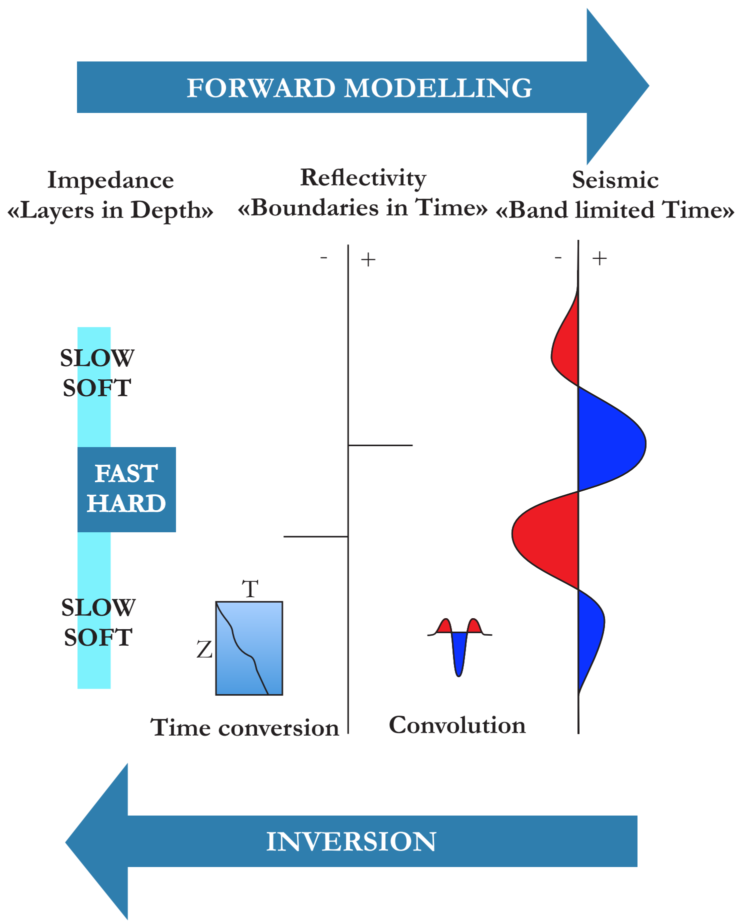

Figure 10.2: Illustrating the seismic inversion concept.

10.3.1 Regional structural interpretation

Our geological understanding of the North Sea chalk starts out with regional maps showing the high and lows of specific geological units, initially provided by seismic or other geophysical measurements.

The first seismic work carried out in the North Sea appears to be in 1953, when 3 refraction seismic lines were acquired by the US Hydrographic department, (cfr. Bungenstock, Closs and Hinz; in (Cook 1965)). These surveys unraveled about 3000 feet of sedimentary rocks including a few hundred meter of chalk. More geophysics work followed. In 1960, gas was found in the Groningen area in the Netherlands. When the potential of the Groningen field was realized in 1963, the seismic activities increased with a factor of 10 based on the speculation that a vast new gas province was lying under the North Sea. The base Permian was the main target of the early seismic surveys acquired in the Dutch and German sector of the North Sea (e.g. the SPBA atlas). Below was the Carboniferous coal, which was believed to be the source for the Rotliegendes Gas. Fair reflections were also observed from the base Tertiary, the base of the Upper Cretaceous and the base Zechstein, se **Fig.10.3**. In the early 1960s gravity maps were also available from most of the North Sea area reflecting the overall shape of the basin.

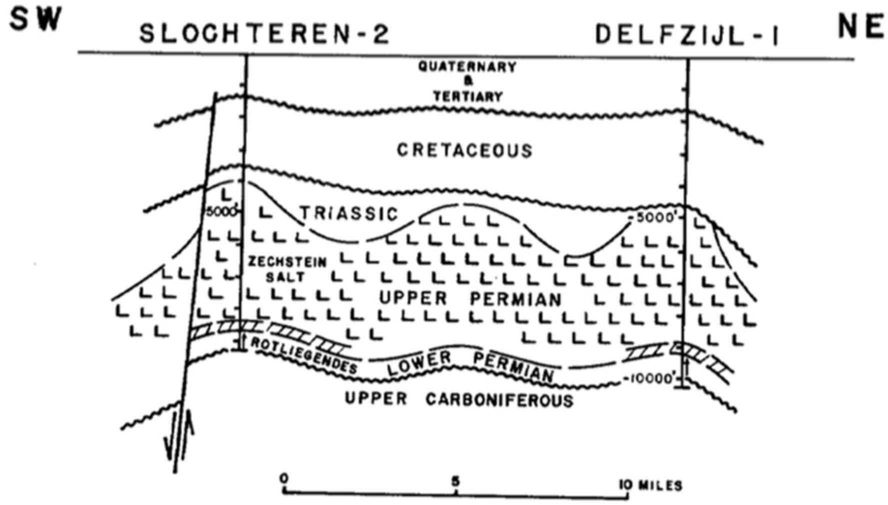

(a) Geologic section across the Groningen area.

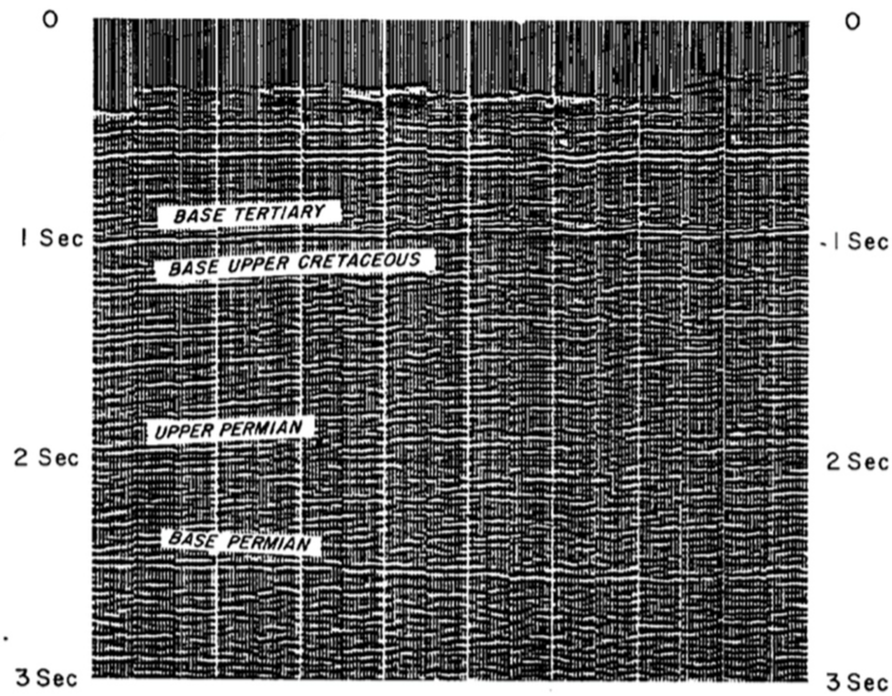

(b) Record section near Groningen.

Figure 10.3: Early Seismic section near Groningen, acquired in the early sixties and annotated with primary seismic reflector of interest Cook (1965).

In structural seismic interpretation, the travel time of the seismic reflections and the associated velocities are the primary information. The primary use of the velocities is to convert travel time to depth. At the same time, the overall understanding of the representative seismic velocities was also used for diagnostic purposes (Rockwell 1967).

Although deeper reflections were identified in the very early seismic data, proper imaging of the layers below the chalk constituted a challenge, due to the strong velocity contrast and the associated problem with removing multiple reflections originated from the chalk sequence. Some geophysicists will claim that it was not until recently, during the last ten years that decent data quality below chalk generally has been achieved, **Fig. 10.4**.

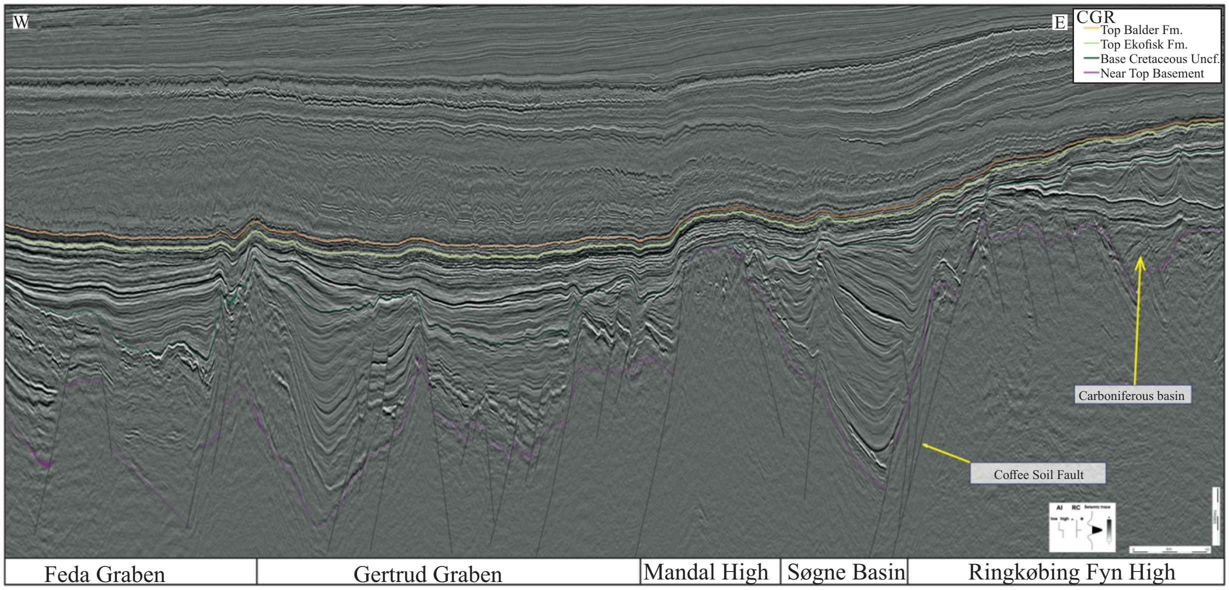

Figure 10.4: Modern broadband seismic data allow for high quality seismic imaging also below the Chalk Group, marked with orange (top) and green (base). The seismic is from the Southern North Sea, close to the border between Norway and Denmark. The main structural elements from this area are annotated at the bottom. Data example is by courtesy of PGS.

Today's maps of the North Sea Chalk Group, covering the stratigraphic interval from the Cenomanian to the Danian ages are almost entirely based on modern 3D seismic data. The understanding of the overall shape and the main features have not changed significantly since the early pioneering work in the late 1960s and seventies (Isaksen and Tonstad 1989), but the details and the level of insight that has been revealed has improved dramatically. The most complete North Sea Map published can be found in Vejbæk, Bidstrup et al. (2007), **Fig. 10.5**, and are based on available 2D and 3D reflection seismic, complemented by available maps and well data.

The late Jurassic rifting dies out during the Early Cretaceous. However, the regional subsidence of the sediments deposited during the strong rifting phase provides the backdrop for the late Cretaceous chalk deposition in the North Sea.

A closer look at the a North Sea isopach map of the Chalk Group reveals that there are significant irregularities in the thickness to what a regional subsidence model can explain. Anomalous thin Chalk Group deposits are found along the Lindesnes Ridge in the Norwegian sector, in the Sole Pit Basin, in the Danish part, and along the Sorgenfrei-Tornquist Zone in Dutch waters. These anomalies are surrounded by local thicker deposits, and are interpreted to be caused by inversion movements during the Late Cretaceous - Palaeogene times (Vejbæk and Andersen 2002).

Inversion of a sedimentary basin is the process by which a previous geographical low is inverted to become a geographical high. In this case late Jurassic lows were formed due to local or regional extension and were then uplifted due to the influence of local or regional compressional forces. The compressive forces results in folding, flexing and possible reversal and are often recognized by a dominance of reverse faulting.

Vejbæk and Andersen (2002), suggest that the structural inversion started in the Late early Cretaceous and persisted into the Paleogene. During this period there appear to be several periods with stronger tectonism, **Fig. 10.6**. Due to complex pre-existing structural settings it may be difficult to establish the orientation of the main compressional forces and they suggest an apparent NNE-SSW compression, resulting in mild NNW-SSE oriented dextral strike slip component. **Fig. 10.7** shows the location of chalk oil and gas reservoirs in the north sea.

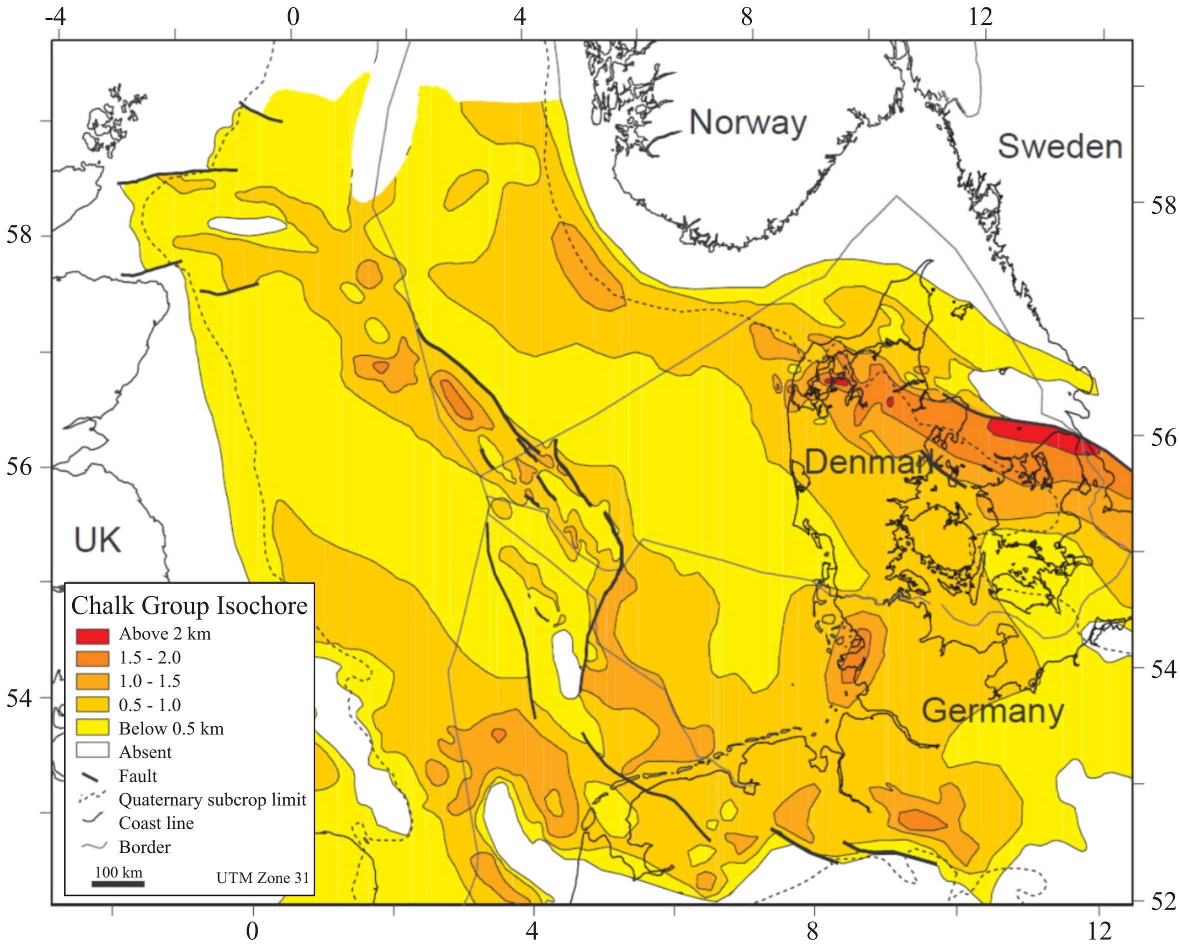

Figure 10.5: Chalk Group isopach from the North Sea Region, from Vejbæk and Andersen (2002).

10.4 Seismic Stratigraphic Interpretation

The development of 3D seismic allowed for complementary analysis of the structural and stratigraphic development of a rock unit. Seismic attribute maps extracted along mapped reflector or constant time of depth interval may reveal morphology or lineaments which are easily recognized and help concluding both the stratigraphic and the structural story.

Seismic stratigraphic interpretations are based on identifying unconformities. The unconformities and/or their correlative conformities are mapped with the intention of dividing a stratigraphic intervals into Chronostratigraphic context (Vail 1977).

Similar approaches have been applied to the Chalk Group. Nygaard, Andersen et al. (1990), subdivided the chalk offshore Denmark into six sequences, and Andersen, Clausen et al. (1990), identified eight. Vejbæk and Andersen (2002) suggested six seismic sequences based on their work, see **Fig. 10.8**.

Recent work by Van der Molen and Wong (2007) divided the Chalk Group in the Dutch sectors into eleven units. Larsen, Ineson et al. (2014) report on seismic stratigraphy work and the link to sedimentary architecture of the Chalk Group in south west Denmark and Gennaro (2011) reports on seismic stratigraphy of the Chalk Group in the Norwegian Central Graben. This paper identifies eight seismic sequence boundaries, which in turn define seven seismic stratigraphic sequences characterized by different seismic facies and well log signatures. Gennaro, Wonham et al. (2013) also conclude that the seismic sequences can be grouped into three sequence groups that link to the main tectonic phases active during the evolution of the chalk deposits in the Norwegian Central Graben.

Seismic sequence analysis of pelagic chalk deposits loses out on the common observations of landwards or seawards shifts in depositional environments, which are commonly observed in clastic sediments. The closest we get to linkages to fluctuation in sea levels are probably the decrease or increase of terrigeneous material in the autochtoneous sediments.

The seismic resolution represents a major challenge to and seismic sequence analysis as it is difficult to

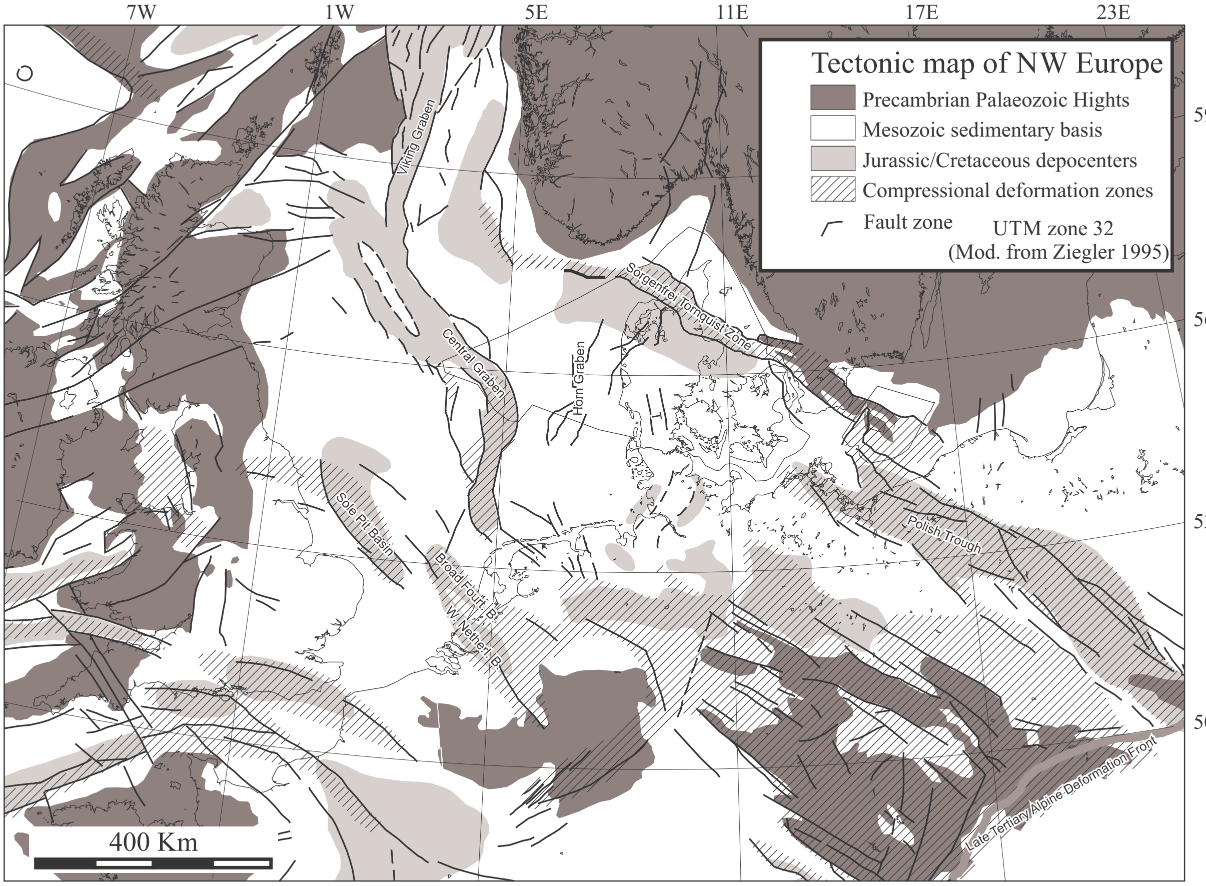

Figure 10.6: North Sea zones of Cretaceous to Paleogene inversion (modified from Ziegler), from Vejbæk and Andersen (2002).

delineate the individual unit. A significant amount of details are hidden within the seismic bandwidth where the signal/noise level does not support conclusive analysis.

A basic methodology in seismic stratigraphy is the definition on genetic reflection units. The bounding surfaces that define these units, seismic sequences or system tracts, are based on the continuity of the seismic reflectors or reflections terminating against the surfaces (reflectors) from below (toplap) or below (onlap).

Fig. 10.9 shows an example of seismic sequences analysis based on reflection configuration and terminations within the Chalk Group across the northern edge of the Lindesnes Ridge.

Seismic stratigraphy is founded on the explicit identification and characterization of reflection termination, while the structural interpretation the focus on identifying and characterizing structural elements. Both techniques rely on explicit mapping of seismic horizons, which are results but are also used to help facilitating the interpretation process. The paper of Gennaro, Wonham et al. (2013) contains several examples of application of seismic sequence analysis to the North Sea Chalk Croup, and also shows examples of various seismic facies. It is not possible to separate seismic sequence analysis from "conventional" structural interpretations completely, as there is significant overlap in the reasoning applied by the interpreter. It is useful though to distinguish between the structural development that set the scene for the resulting stratigraphy and the mapping of the stratigraphic units.

Complementary ways of visualizing the seismic data, in terms of acoustic impedances or other layer based properties are useful in the stratigraphic analysis, while various edge detection techniques, like coherency are useful in delineating structural elements as well as sediment logical morphology. In the next section we will review a number of field examples on the application of the techniques. We also refer to the chapter on Geophysics for some more details on the various technologies.

10.4.1 Seismic inversion

In the early days seismic interpretation was mainly a mental process but when seismic acquisition and processing progressed to the state where it is possible to recover true amplitudes that directly reflect changes in the

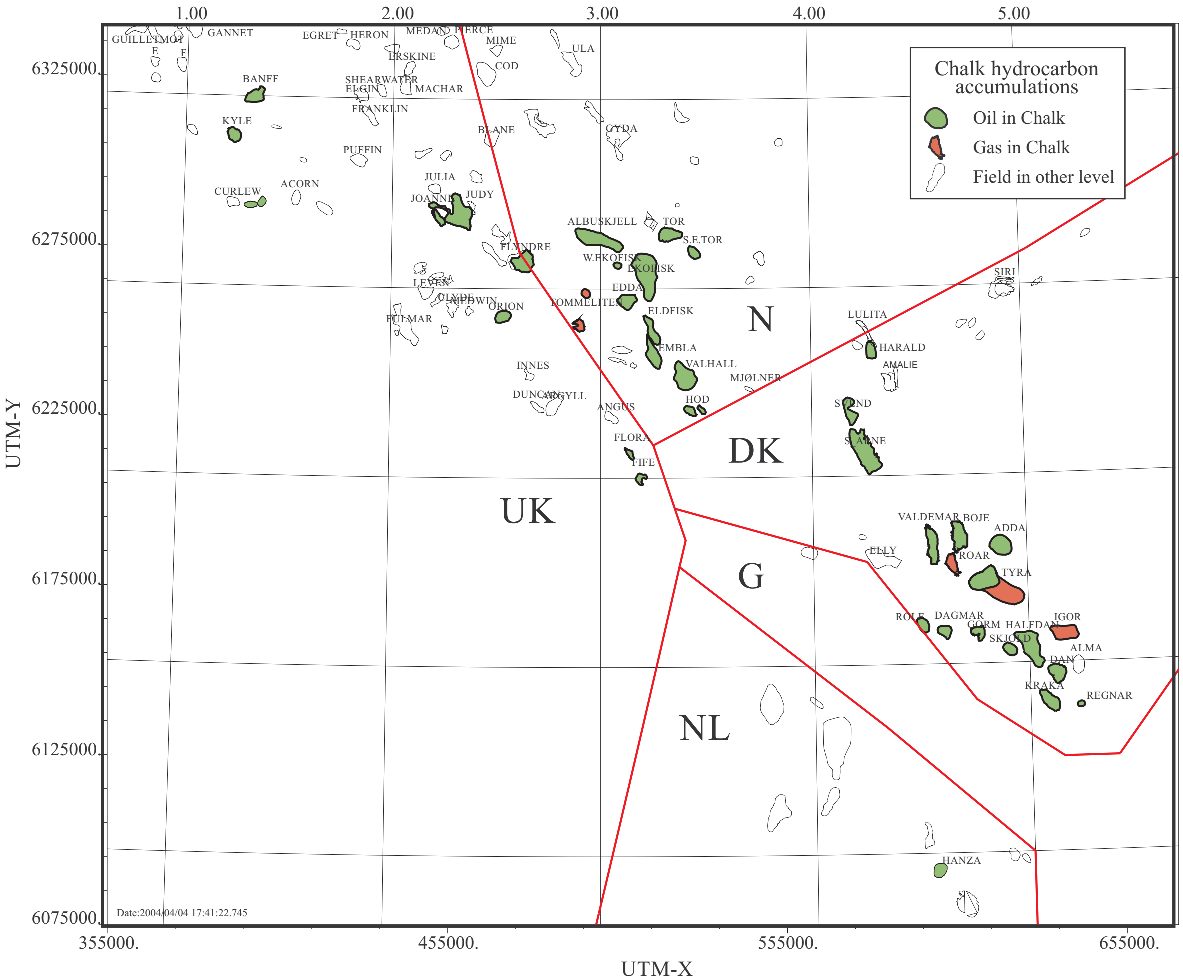

Figure 10.7: Oil and gas field in the Southern Nort Sea with chalk reservoirs (modified from from Vejbæk and Andersen (2002).

earths acoustic impedance (late 1980s), quantitative interpretation based on rock physics became possible.

The term inversion points to the close relation with forward modelling. Forward modelling includes the use of an adequate model, for the subsurface problem at hand. This can for instance be to construct the seismic response of a simple or complex subsurface definition. The inversion process may be done by matching the results of an initial "guessed" solution with an observed seismic data set. The differences or errors are calculated and distributed according to various optimization schemes, which are iterated to come up with a minimum error solution.

Seismic inversion in it broadest definition includes a number of techniques. Seismic migration aims at inverting for or reconstructing the geometry of the subsurface (Gardner 1985). Predictive deconvolution aims at inverting for the reflectivity of the subsurface (Peacock and Treitel 1969). Amplitude versus offset analysis aims at resolving the elastic properties of the subsurface (Castagna and Backus 1993). Other techniques may use alternative ways of translating the seismogram (or other geophysical data) into subsurface characteristics, these include in their simplest form various types of cross plotting techniques for lithological definition,(Connolly 2010), geostatistical techniques where established correlation are used (Xu, Tran et al. 1992), or use of geometrical attributes (Chopra and Marfurt 2008).

A simple but powerful model commonly used in seismic interpretation and inversion deploys a one dimensional layer cake model which may be a velocity model by assigning velocity to each layers sourced by well or data from seismic velocity analysis. This velocity model makes it possible to tie well observations (in depth) to seismic data (in Two Way Time). Well logs can be converted to Two Way Time and reflectivity based on well logs, preferably sonic and density logs, can be estimated. The reflectivity series can be convolved with an assumed relevant seismic wavelet and a synthetic seismogram that can be compared directly with the seismic data is thereby constructed. Given that our processing of the actual seismic recordings are sufficient, we could in fact invert this forward convolution model into a deconvolution technique that gives us an estimated

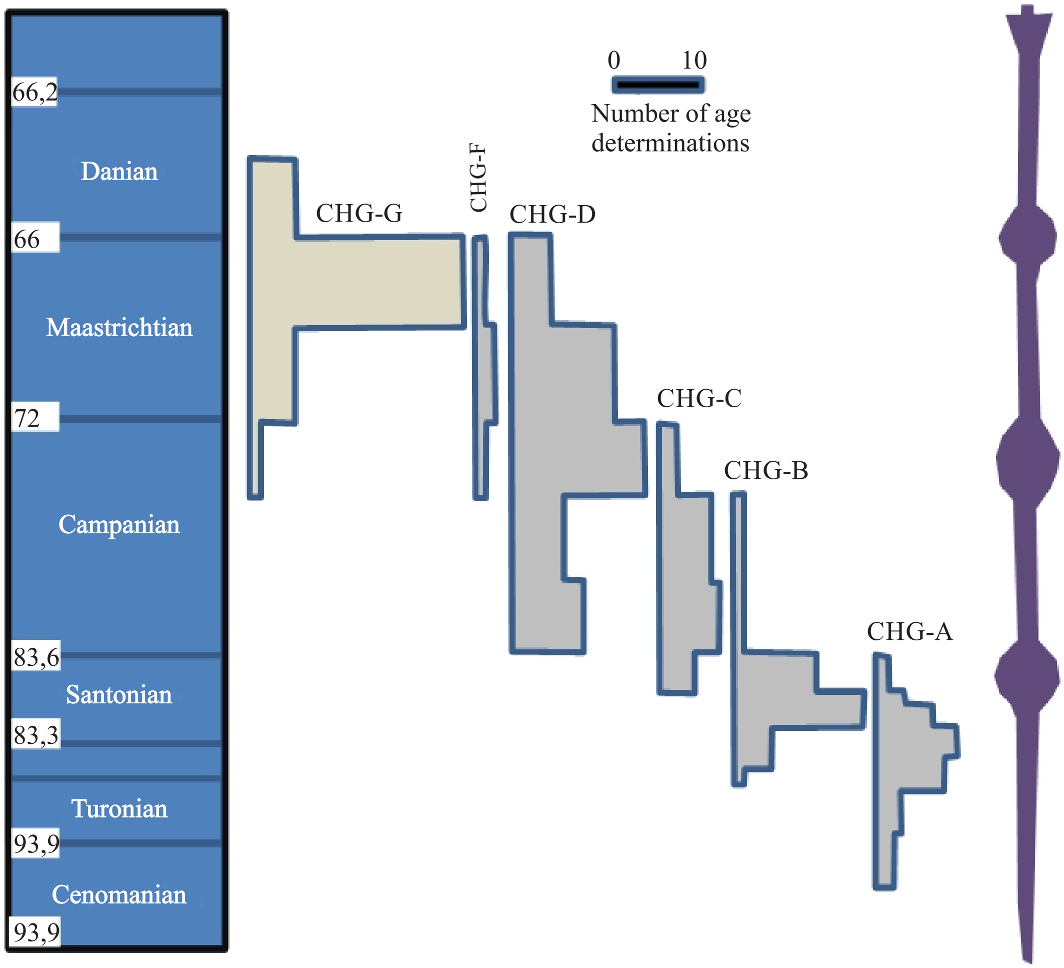

Figure 10.8: Dating of top of seismic sequences CHG-A through CHG-G based on industry reports. The Graph to the right indicates relative magnitude of tectonic activity. The tectonic activity is continuous, but with culminations. Modified fromVejbæk and Andersen (2002).

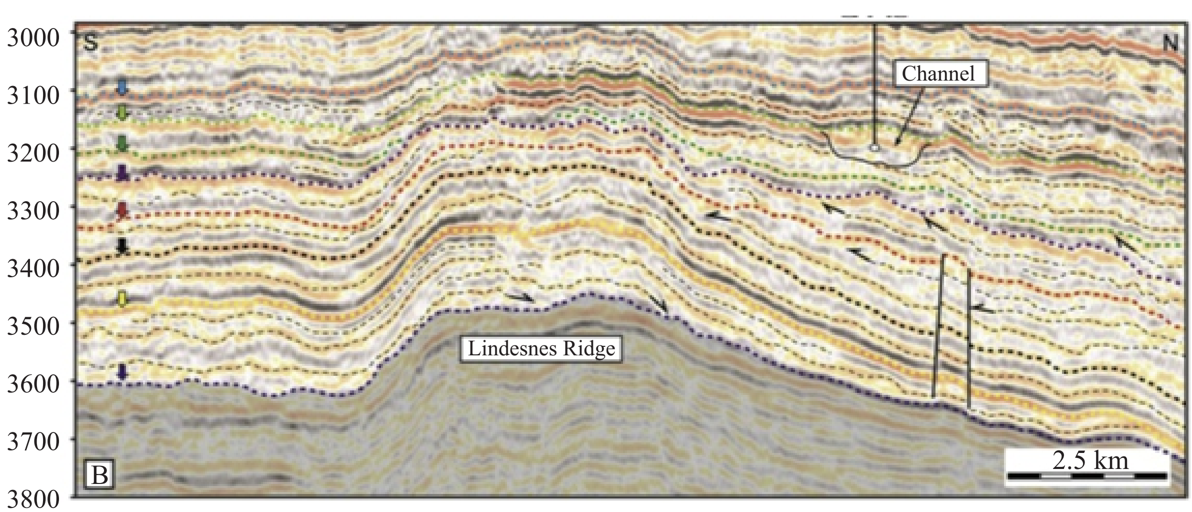

Figure 10.9: Seismic sequences defined based on reflection configuration and terminations within the Chalk Group across the northern edge of the Lindesnes Ridge. The arrow denotes the sequences as defined by Gennaro et al. Notice the channel features identified in the shallow most sequence. Modified from Gennaro, Wonham et al. (2013).

impedance log from an single zero-incidence seismic trace. One version based on this approach became very popular and was used across several North Sea chalk fields in the late seventies, early eighties. The technique was marketed under the name SeisLog^{TM}, as it provided the seismic traces in terms of sonic logs (Lindseth 1976).

The seismic data are bandlimited, which implies that it is only the relative impedance or velocity that can be calculated. To provide the absolute value the low frequencies or velocity trend functions have to be provided by other sources. In the case of Seislog^{TM}, the stacking velocities estimated from the seismic data were used. **Fig. 10.10** shows an example of a Seislog^{TM} section from the Valhall field. The results were presented in the same way as a conventional sonic log.

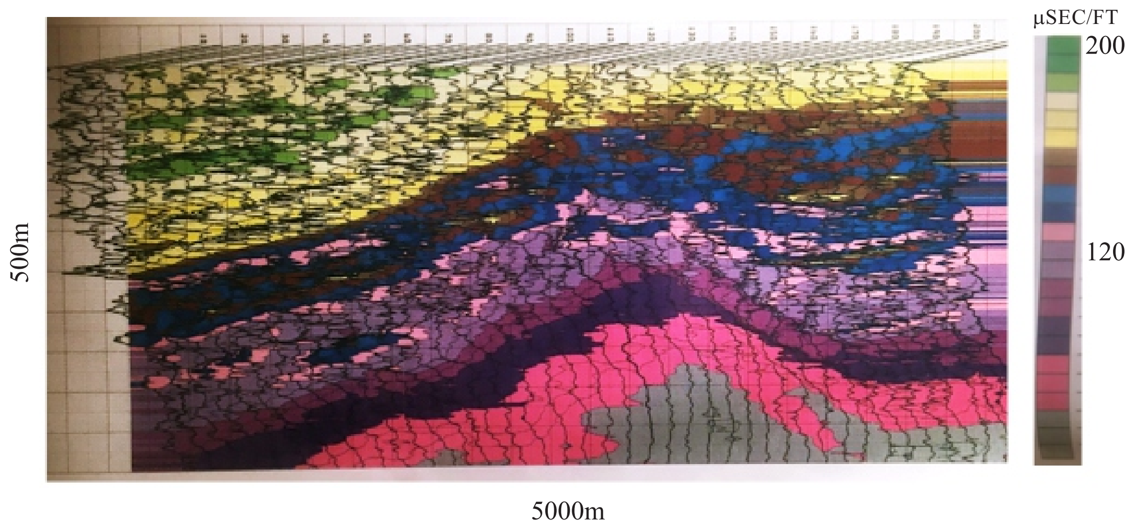

Figure 10.10: Example of early seismic inversion, Seislog^{TM} applied to the Valhall field.

The SeisLog^{TM} type of inversion helped the interpreter to build an apparent objective image pointing out the presence of low velocity and possible porous units within the chalk, which were primary exploration and development targets. The background velocity model were useful as it provided a low frequency model that compensated for the bandwidth limitation of the seismic data and rendered an inverted seismic trace with an appearance similar to a velocity log.

The risk of obtaining an erroneous absolute impedance value from a seismic inversion is more sensitive to the quality of the added low frequency information than the quality of bandlimited seismic inversion method itself, see Pedersen-Tatalovic, Uldall et al. (2008). Therefore significant effort has been put into developing methods for improving the quality of the required low frequency information by applying seismic attributes, seismic velocities, and other relevant geological information (Hansen, Mosegaard et al. 2008), as well as trying to acquire more low frequency data.

Many different inversion schemes have been applied. Neff and West (1993), tested a methodology referred to as incremental pay thickness (IPT) modeling, which were applied to some of the Chalk fields operated by Phillips (Hermansen, Thomas et al. 1997). This technique uses a convolutional modeling program to create thousands of alternative realization by combining variations in thickness, porosity and saturations observed in one or multiple fields, and create a catalog, which is used for matching with traces from 3D seismic surveys. When a good match was found, this was used to create pseudo map points for gross and net thickness and average porosities.

In the 1990s model driven post-stack inversion were made available either though dedicated software packages or as dedicated products. Due to the strong correlations between porosity and acoustic impedance, chalk prospects remain an interested application. 3D acoustic impedance volumes were generated and used directly through field based correlation schemes to estimate porosity (Pearse and Özdemir 1994; Campbell and Gravdal 1995; Barkved 1996; Rasmussen and Maver 1996). **Fig. 10.11** shows an example of post-stack seismic inversion, where the resulting acoustic impedance has been converted to porosities using acoustic and porosity logs from wells (Barkved 1996). Probably all relevant chalk reservoirs were subject to post-stack inversion in one way or another during the 1990s. The products were used in well planning and reservoir management, but not without pitfalls and always depending on the quality of the supplied low frequency model.

Acoustic impedance is also influenced by lithology (presence of clay mineral) and fluid effects which make direct porosity derivation difficult. Britze, Nielsen et al. (2000) looked into the possibility for including ad-

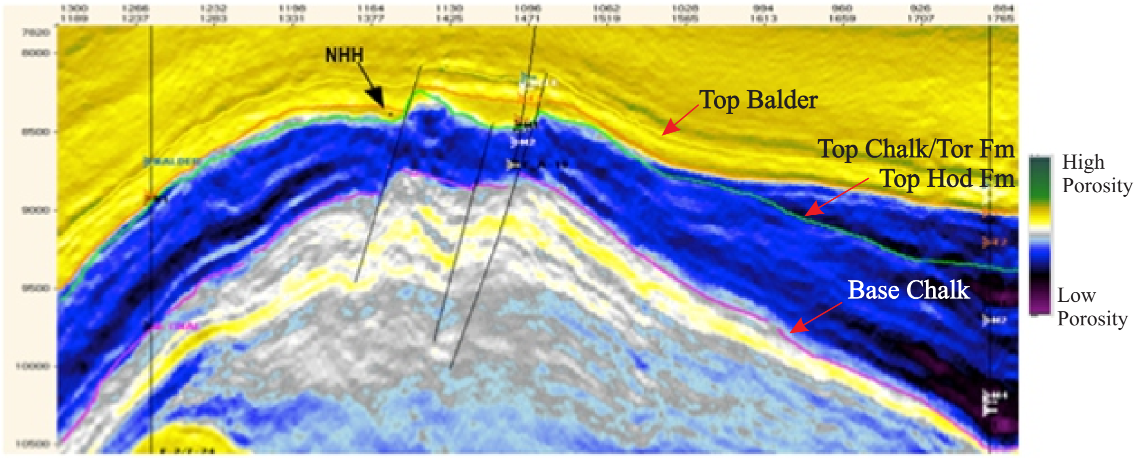

Figure 10.11: Example of least square post-stack seismic inversion. The example is from the Valhall field and the results are presented as porosities, using a linear correlation between porosities and acoustic impedance established using well logs. NHH indicate the position of a horizontal well drilled orthogonal to the seismic section. Modified from Barkved (1996).

ditional attributes, which could help address the lithology issues. And as alternatives to the direct porosity mapping, other workers used inverted seismic data to derive trends to support well based property modeling (Vejbaæk and Rasmussen 1996).

AVO Inversion was tested with the purpose of addressing shale and fluid effects. Since that chalk often exhibit a strong increase in seismic velocity compared to overlying rocks, critical angle reflections may occur at low offsets and result in distinct AVO character at pre-critical offsets. In one of the most successful cases of identifying a down-flank stratigraphic reservoir NE of the Hod East field, the critical angle effects impact on the AVO response were used as an additional diagnostic tool to post-stack inversions for locating presence of high porosity chalk (Landrø, Buland et al. 1995). The prospect was drilled and presence of hydrocarbon was confirmed.

The Edgar and Noekken chalk prospects were drilled around the same time as the NE Hod prospect (Andersen 1995). AVO analysis was not applicable for the Edgar prospect. The conventional seismic cable used was too short to allow reasonable offset ranges. Presence of porous reservoir was identified based on Incremental Pay Thickness and another model based inversion scheme. The predicted porosity was found, but the pores were water-filled. When drilling the Noekken prospect, Amoco found chalk of 29% porosity, but also this was water filled. The predicted porosity based on seismic inversion was in the range 28–33 %. The Noekken project was covered by long offset seismic data, but AVO analysis for fluid was not conclusive. Furthermore, the current geological model for both these prospect predicted significant diagenesis unless hydrocarbon was present. Unfortunately, most likely both these prospects had been isolated from circulating water, and the porosity were most likely a results of local overpressure effects (Øxnevad and Taylor 1999).

Early AVO inversion suffered from weak signal on the individual seismic traces. Current application of AVO inversion is based on the use of offset range stacks, which appears to help stabilizing the inversion, or more likely help addressing issues like stretching and attenuation somewhat better. AVO inversion is generally based on the assumption that the chalk and the surrounding rocks are isotropic. The overlying shales are clearly not isotropic (Brandsberg-Dahl and Barkved 2002). Furthermore, the chalk itself is most likely not anisotropic in general due to layering and fracturing. Finally the frame of the chalk rock is stiff which makes it more difficult to see the effect of the pore filling fluid. Thus it is relatively easy to recognize a chalk - shale interface due to the difference in shale and chalk bulk rock parameters. Porosity variations also have a strong effect because the bulk rock parameters change, but the effect of the pore-fill is generally dampened due to the stiffness of the chalk rock frame. Thus using AVO as a hydrocarbon indicator remains difficult.

Highly porous chalk may have the same or even lower acoustic impedance than the above-lying shale. At the same time there are a marked shear wave velocity contrast between shale and chalk (Mueller, Barkved et al. 1997; D'Angelo, Brandal et al. 1997; Gommesen, Fabricius et al. 2007). The net effect is that the ratio between compressional and shear velocities, the V_p/V_s ratios, in shale may range between 2.5–3.5, while in chalk it is very stable around 1.8–1.9, except for cases with very high porosity.

The introduction of the elastic impedance concept in the late 1990s (Connolly 1999), opened up for an improved use of AVO attributes in formulating estimates of angle independent quantities such as acoustic impedance, shear impedance, V_p/V_s ratios, and gradient impedance.

Several cases have been documented where elastic inversion for, V_p/V_s has made it possible to identify the top of the chalk, where there were no acoustic impedance contrast (Henriksen, Gommesen et al. 2009). Herbert, Escobar et al. (2013), brought this analysis a step forward to include fluid imaging as part of the inversion using elastic inversion. A combination the I_p and V_p/V_s is able to define lithological boundaries and map the fluid distribution making interpretation easier and more accurate. Recently stochastic inversion has increased in popularity, for a chalk related paper see Cherrett, Escobar et al. (2011).

It is possible to improve seismic inversion by inverting the seismic data with other geophysical such as CSEM for improved understanding of the Chalk. Vossepoel, Darnet et al. (2010), show an example where CSEM was used with the seismic inversion to map a hydrocarbon column in chalk.

10.4.2 Fractures

Understanding the natural or induced fractures are critical in optimal development of our chalk fields (Andersen 1995; Hermansen, Thomas et al. 1997; Barkved, Heavey et al. 2003; Bauer and Trice 2004).

Nelson (2001) remains one of the key references for evaluating naturally fractured reservoir. He mentions four main obstacles for proper fracture analysis. These are :

- General lack of in-depth quantitative approaches to describe and characterize highly anisotropic reservoirs
- Failure of geologist and engineers to recognize fractures and/or the regularity of their distribution
- Over-simplified approaches to the description of fracture distributions and morphologies
- The need for a deterministic solution to model fluid flow in fractured porous media, while understanding that our data limitations force us towards stochastic solutions at best

The effects of fractures have been studied in the lab (Graue, Moe et al. 2000), and conceptual geological models have been tested against dynamic data (Rogers, Enachescu et al. 2007).

The standard for integrating seismic data into the fracture modelling appears to be mainly through classic linkage with mapped faults (Casabianca, Jolly et al. 2007). P-wave amplitude variation with offset and azimuth (AVOA) can be used to determine fracture properties (Hall, Kendall et al. 2002). Shear wave anisotropy is another tool that may be used for fracture characterization. Olofsson, Kommedal et al. (2002), is an industry reference for shear wave splitting effects in the shallow overburden, across a compacting chalk reservoir. The primary objective which was to isolate S-wave splitting effects across the chalk reservoir turned out to be a challenging task as the methods currently used relies on a layer stripping approach where the effects of the layer above have to be removed, to estimate the effects from the layer below.

10.4.3 Use of seismic attributes

The strong reflectivity often associated with chalk, has resulted in many spectacular seismic attribute maps but maps delineating geometrical details.

Calculating the second derivative of a structural map of the Chalk Group was commonly used for detailed fracture analysis. As 3D seismic became generally available from most of the North Sea Chalk fields during the 1990s, coherency cubes and extraction of coherency maps at the various chalk levels revealed structural and depositional features an order of magnitude higher in detail.

While seismic attributes not generically are linked to 3D seismic, the ability to extract maps from a 3D cube opens up for a new way of interpreting seismic data. Amplitude based attribute maps revealed the later variation in seismic impedance, while layer based attributes like coherency, peak frequency and peak-to-though thickness maps were more sensitive to layer thickness (Bahorich and Farmer 1995; Chopra and Marfurt 2008). See also **Fig. 10.12** for examples of dip/azimuth, coherency and lineament maps from the same stratigraphic level (Barkved 1996).

The standard way of using seismic attribute of "any-kind" is to calibrate with well data. Presence of apparent "geological" lineaments or morphology may be used directly for either detailed fault mapping or to develop contextual geological models used as framework for detailed interpretation and mapping.

Seismic attributes include a wide range of more or less relevant derivatives from the seismic data. Some of these are onedimension and in nature while others are based on calculation from a small subvolume of seismic data. Spectral decomposition, where the seismic is analyzed based on the contribution from selected frequency ranges, may help delineating features of various size and scale, which when combined through blending helps

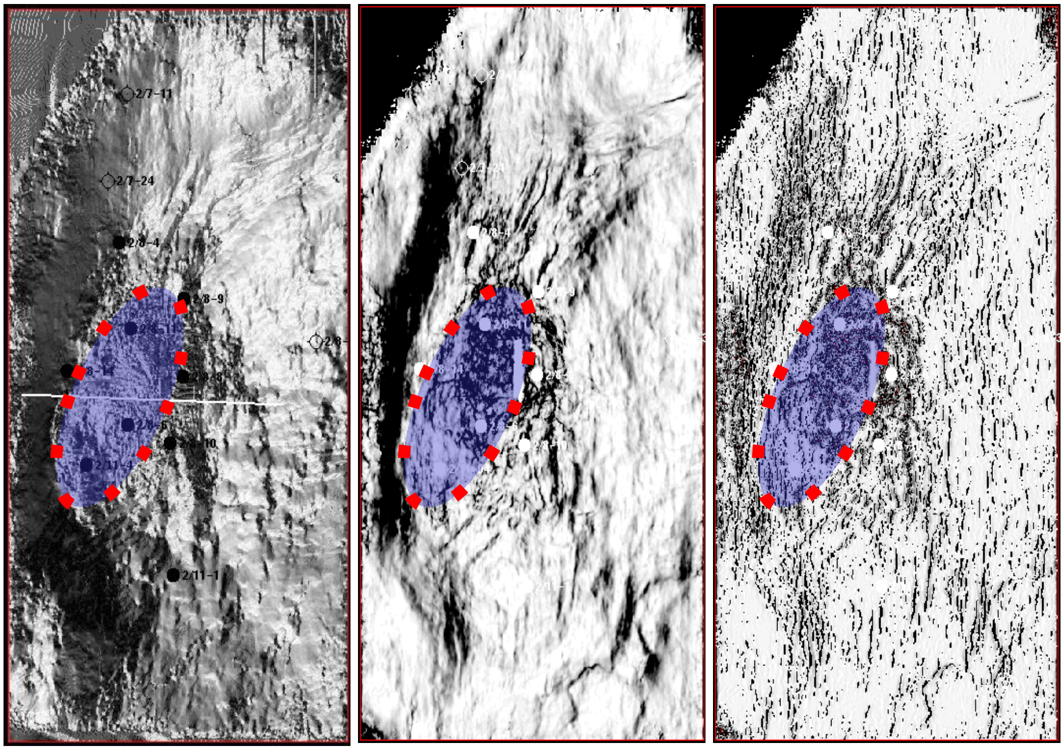

Figure 10.12: Dip/azimuth map, coherency and lineament extraction (Barkved 1996)

improving the understanding of the subsurface. This technique also helps the interpreter to appreciate that the earth has its own lenses that can mask or enhance features. Spectral decomposition allows for showing features at all frequencies with the same strength.

Curvature attributes are another family of useful geometrical attributes, see **Fig. 10.13**. Curvature is a measure for how deformed a surface is at a particular point in a 3D cube. These algorithms help delineate structural and stratigraphic features, extracted from the seismic data itself similar to how the coherence methods work.

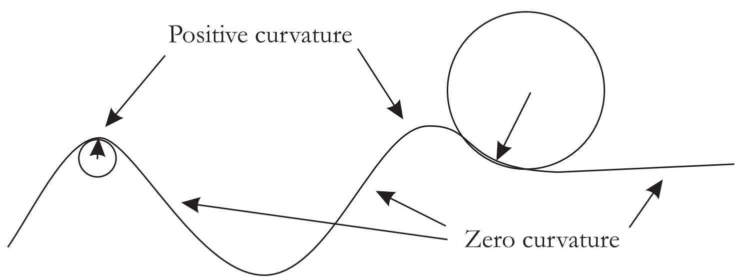

Figure 10.13: Illustrating the curvature concept in a 2D setting. Modified from Chopra and Marfurt (2008).

Attributes have become very useful and popular. It is however important to remember that the fundamental seismic laws still apply, and should be used both to qualify the results as well as guiding the selections of which attributes that may be applicable.

As mentioned above, it is beneficial for seismic inversion to acquire the seismic data as broad frequency band as possible, but specifically the recent advances in broadband seismic acquisition and processing will certainly have a positive impact on the seismic quality of the chalk interval. Better signal-to-noise levels and improved fault definition will help structural interpretation as the richer frequencies (and probably especially) the low end will improve the basis for seismic stratigraphic analysis.

10.5 Conclusion

The methodology used for seismic interpretation of the North Sea Chalk generally follows standard workflows. Chalk is special due to that the acoustic contrasts commonly stand out against the layers above or below. Strong overprint of post depositional digenesis occurs commonly in chalk and may reflect paleo fluid contacts, which may sometimes convolute the interpretation if not fully understood.

Seismic inversion is commonly used to characterize chalk reservoir, due to the strong correlation between acoustic impedance and porosity and can work well if the low frequency model is well controlled.

Classical amplitude versus offset analysis in chalk may be complicated as presence of preferred open fracture orientation may result in amplitude versus offset variation with azimuth.

Emerging technologies implemented to increase the bandwidth of the seismic signal are believed to make profound impact on the ability to better image chalk prospects. Lower frequency will contribute to make the seismic responses more unique and higher frequencies will add in resolving units and depositional features in more detail.

The continuous improvement in seismic quality, combined with improved tools for analysis will surely make seismic chalk interpretation an engaging and value adding activity in years to come.

Nomenclature

I_p = acoustic impedance
V_p = compressional velocity
V_s = shear velocity

Abbreviations

AVO = amplitude versus offset
AVOA = amplitude versus offset and azimuth
CSEM = controlled source electromagnetic
IPT = incremental pay thickness

References

Andersen, C., Clausen, C.K. et al., 1990. Intra-chalk Study, EFP-87: A Multidisciplinary Breakdown. *Geological Survey of Denmark (Copenhagen)*, 30. Copenhagen.

Andersen, M.A., 1995. *Petroleum Research in North Sea Chalk.* RF-Rogaland Research. Joint Chalk Research Program Phase IV.

Back, S., Van Gent, H. et al., 2011. 3D seismic geomorphology and sedimentology of the Chalk Group, southern Danish North Sea. *Journal of the Geological Society*, **168** (2): 393–406. February. URL `http://dx.doi.org/10.1144/0016-76492010-047`.

Bahorich, M. and Farmer, S., 1995. 3-D seismic coherency for faults andstratigraphic features. *The Leading Edge*, **60** (3): 1075–1082.

Barkved, O., 1996. Succesfull use of seismic attribute maps and poststack inversion in horizontal well planning. Paper presented at 58th EAGE Conference and Exhibition. 06 June. URL `http://dx.doi.org/10.3997/2214-4609.201409039`.

Barkved, O.I., Heavey, P. et al., 2003. Valhall field-Still on plateau after 20 years of production. In *Offshore Europe*, vol. 83957. Society of Petroleum Engineers (SPE). Paper SPE-83957-MS presnted at Offshore Europe, Aberdeen, United Kingdom. 2–5 September. URL `http://dx.doi.org/10.2118/83957-MS`.

Bauer, K. and Trice, R., 2004. Data integration and numerical fracture models for water flood management–a case study of the Valhall Chalk reservoir, North Sea. In *Fractured Reservoirs Conference, London, UK*, 16–17.

Brandsberg-Dahl, S. and Barkved, O.I., 2002. Anisotropic P-wave velocity derived from deviated wells at the Valhall field. In *64th EAGE Conference & Exhibition*.

Brasher, J.M. and Vagle, K.R., 1996. Influence of lithofacies and diagenesis on Norwegian North Sea chalk reservoirs. *AAPG Bulletin*, **80** (5): 746–769. URL http://archives.datapages.com/data/bulletns/1994-96/data/pg/0080/0005/0700/0746.htm.

Britze, P., Nielsen, E.B. et al., 2000. North Sea chalk porosity resolved by integration of seismic reflectivity and well data. Paper presented at EAGE Conference on Exploring the Synergies between Surface and Borehole Geoscience - Petrophysics meets Geophysics. 06 August. URL http://www.earthdoc.org/publication/publicationdetails/?publication=5197.

Campbell, S.J.D. and Gravdal, N., 1995. The prediction of high porosity chalks in the East Hod Field. *Petroleum Geoscience*, **1** (1): 57–69. February. URL http://pg.eage.org/publication/publicationdetails/?publication=36436.

Casabianca, D., Jolly, R.J.H., and Pollard, R., 2007. The Machar Oil Field: waterflooding a fractured chalk reservoir. *Geological Society, London, Special Publications*, **270** (1): 171–191. URL http://dx.doi.org/10.1144/gsl.sp.2007.270.01.12.

Castagna, J.P. and Backus, M.M., eds., 1993. *Offset-Dependent Reflectivity—Theory and Practice of AVO Analysis*. Society of Exploration Geophysicists. January. URL http://dx.doi.org/10.1190/1.9781560802624.

Cherrett, A.J., Escobar, I., and Hansen, H.P., 2011. Fast deterministic geostatistical inversion. Paper presented at 73rd EAGE Conference and Exhibition incorporating SPE EUROPEC. URL http://dx.doi.org/10.3997/2214-4609.20149359.

Chopra, S. and Marfurt, K.J., 2008. Emerging and future trends in seismic attributes. *The Leading Edge*, **27** (3): 298–318. URL http://dx.doi.org/10.1190/1.2896620.

Connolly, P., 1999. Elastic impedance. *The Leading Edge*, **18** (4): 438–452. April. URL http://dx.doi.org/10.1190/1.1438307.

Connolly, P.A., 2010. Robust Workflows for Seismic Reservoir Characterisation. *SEG Distinguished Lecture*.

Cook, E.E., 1965. Geophysical operations in the North Sea. *Geophysics*, **30** (4): 495–510. URL http://dx.doi.org/10.1190/1.1439614.

D'Angelo, R.M., Brandal, M.K., and Rørvik, K.O., 1997. 13. Porosity Detection and Mapping in a Basinal Carbonate Setting, Offshore Norway. In I. Palaz and K.J. Mafurt, eds., *Carbonate Seismology*, Chap. 13, 321–336. Society of Exploration Geophysicists. URL http://dx.doi.org/10.1190/1.9781560802099.ch13.

Engstrøm, F., 1995. A new method to normalize capillary pressure curves. Paper SCA 9535 presented at . International Symposium of the Society of Core analysts, San Francisco.

Fabricius, I.L., 2007. Chalk: composition, diagenesis and physical properties. *Geological Society of Denmark. Bulletin*, **55**: 97–128. URL http://www.forskningsdatabasen.dk/en/catalog/2282178759.

Fabricius, I.L. and Borre, M.K., 2007. Stylolites, porosity, depositional texture, and silicates in chalk facies sediments. Ontong Java Plateau–Gorm and Tyra fields, North Sea. *Sedimentology*, **54** (1): 183–205. February. URL http://dx.doi.org/10.1111/j.1365-3091.2006.00828.x.

Farmer, C.L. and Barkved, O.I., 1999. Influence of syn-depositional faulting on thickness variations in chalk reservoirs– Valhall and Hod fields. *Geological Society, London, Petroleum Geology Conference series*, **5**: 949–957. URL http://dx.doi.org/10.1144/0050949.

Gardner, G.H.F., 1985. *Migration of seismic data*. 4. Society of Exploration Geophysicists.

Gennaro, M., 2011. *3D seismic stratigraphy and reservoir characterization of the Chalk Group in the Norwegian Central Graben, North Sea*. Ph.D. thesis, University of Bergen. URL https://bora.uib.no/handle/1956/5396.

Gennaro, M., Wonham, J.P. et al., 2013. Characterization of dense zones within the Danian chalks of the Ekofisk Field, Norwegian North Sea. *Petroleum Geoscience*, **19** (1): 39–64.

Gommesen, L., Fabricius, I.L. et al., 2007. Elastic behaviour of North Sea chalk: A well-log study. *Geophysical Prospecting*, **55** (3): 307–322. May. URL http://dx.doi.org/10.1111/j.1365-2478.2007.00622.x.

Graue, A., Moe, R. et al., 2000. Comparison of numerical simulations and laboratory waterfloods with in-situ saturation imaging of fractured blocks of reservoir rocks at different wettabilities. In *SPE International Petroleum Conference and Exhibition in Mexico*. Society of Petroleum Engineers. 1–3 Febryary. URL `http://dx.doi.org/10.2118/59039-MS`.

Hall, S.A., Kendall, J.M., and Barkved, O.I., 2002. Fractured reservoir characterization using P-wave AVOA analysis of 3D OBC data. *The Leading Edge*, **21** (8): 777–781. August. URL `http://dx.doi.org/10.1190/1.1503183`.

Hansen, T.M., Mosegaard, K. et al., 2008. Attribute-guided well-log interpolation applied to low-frequency impedance estimation. *Geophysics*, **73** (6): R83–R95. URL `http://dx.doi.org/10.1190/1.2996302`.

Hatton, I.R., 1986. Geometry of allochthonous Chalk Group members, Central Trough, North Sea. *Marine and Petroleum Geology*, **3** (2): 79–98. URL `http://dx.doi.org/10.1016/0264-8172(86)90022-X`.

Henriksen, K., Gommesen, L. et al., 2009. Optimizing Chalk Reservoir Development Using Detailed Geophyiscal Characterization: The Halfdan Northeast Field, Danish North Sea. Paper SPE-123843-MS presentet at Offshore Europe, Aberdeen, UK. 8–11 September,. URL `http://dx.doi.org/10.2118/123843-MS`.

Herbert, I., Escobar, I., and Arnhild, M., 2013. Modelling Fluid Distribution in a Chalk Field Using Elastic Inversion. In *75th EAGE Conference & Exhibition incorporating SPE EUROPEC 2013*. EAGE Publications BV. URL `http://dx.doi.org/10.3997/2214-4609.20130878`.

Hermansen, H., Thomas, L.K. et al., 1997. Twenty five years of Ekofisk reservoir management. In *SPE Annual Technical Conference and Exhibition*. Society of Petroleum Engineers, Society of Petroleum Engineers (SPE), San Antonio, Texas. SPE-38927-MS. 5–8 October. URL `http://dx.doi.org/10.2118/38927-MS`.

Isaksen, D. and Tonstad, K., 1989. A revised Cretaceous and Tertiary lithostratigraphic nomenclature for the Norwegian North Sea. *Norwegian Petroleum Directorate, Stavanger, Norway*, 59.

Landrø, M., Buland, A., and D'Angelo, R., 1995. Target-oriented AVO inversion of data from Valhall and Hod fields. *The Leading Edge*, **14** (8): 855–861. August. URL `http://dx.doi.org/10.1190/1.1437171`.

Larsen, C., Ineson, J., and Boldreel, L.O., 2014. Seismic stratigraphy and sedimentary architecture of the Chalk Group in south-west Denmark. *Geological Survey of Denmark and Greenland Bulletin*, **31**: 23–26. URL `www.geus.dk/DK/publications/geol-survey-dk-gl-bull/31/Documents/nr31_p23-26.pdf`.

Lindseth, R., 1976. Seislog process uses seismic reflection traces. *Oil & Gas Journal*, **74**: 67–71.

Mueller, M.C., 1991. Prediction of lateral variability in fracture intensity using multicomponent shear-wave surface seismic as a precursor to horizontal drilling in the Austin Chalk. *Geophysical Journal International*, **107** (3): 409–415.

Mueller, M.C., Barkved, O.I., and Thomsen, L.A., 1997. Dipole sonic results (Valhall area)-implications for AVO and OBS interpretation. In *59th EAGE Conference & Exhibition*. URL `http://www.earthdoc.org/publication/publicationdetails/?publication=24678`.

Neff, D.B. and West, K.L., 1993. Integrated Interpreation of North Sea Carbonates using Automated seismic modelling. Paper presented at 55th EAEG Meeting. 9 June. URL `http://dx.doi.org/10.3997/2214-4609.201411420`.

Nelson, R., 2001. *Geologic analysis of naturally fractured reservoirs*. Gulf Professional Publishing.

Nygaard, E., Andersen, C. et al., 1990. Integrated multidisciplinary stratigraphy of the Chalk Group: an example from the Danish Central Trough. In *Chalk*, 195–201. Thomas Telford Publishing.

Olofsson, B., Kommedal, J. et al., 2002. Continuous Progress in Processing Multicomponent Data-a Case Study. In *64th EAGE Conference & Exhibition*. EAGE. 27 May. URL `http://www.earthdoc.org/publication/publicationdetails/?publication=5797`.

Øxnevad, I.E.I. and Taylor, M.S.G., 1999. An integrated approach to hydrocarbon emplacement in chalk, Norwegian North Sea Central Graben. *Geological Society, London, Petroleum Geology Conference series*, **5**: 1221–1230. URL `http://dx.doi.org/10.1144/0051221`.

Peacock, K.L. and Treitel, S., 1969. Predictive deconvolution: Theory and practice. *Geophysics*, **34** (2): 155–169. April. URL http://dx.doi.org/10.1190/1.1440003.

Pearse, C.H.J. and Özdemir, H., 1994. The Hod Field: Chalk Reservoir Delineation from 3D Seismic Data Using Amplitude Mapping and Seismic Inversion. Papre presented at the Norwegian Petroleum Society Geophysical Seminar.

Pedersen-Tatalovic, R., Uldall, A. et al., 2008. Event-based low-frequency impedance modeling using well logs and seismic attributes. *The Leading Edge*, **27** (5): 592–603. URL http://dx.doi.org/10.1190/1.2919576.

Rasmussen, K.B. and Maver, K.G., 1996. Direct inversion for porosity of post stack seismic data. Paper SPE-35509-MS preentet at European 3-D Reservoir Modelling Conference, Stavanger, Norway. 16–17 April. URL http://dx.doi.org/10.2118/35509-MS.

Rockwell, D.W., 1967. The digital computer's role in the enhancement and interpretation of North Sea seismic data. *Geophysics*, **32** (2): 259–281. April. URL http://dx.doi.org/10.1190/1.1439865.

Rogers, S., Enachescu, C. et al., 2007. Integrating discrete fracture network models and pressure transient data for testing conceptual fracture models of the Valhall chalk reservoir, Norwegian North Sea. *Geological Society, London, Special Publications*, **270** (1): 193–204. URL http://dx.doi.org/10.1144/GSL.SP.2007.270.01.13.

Vail, P.R., 1977. Seismic stratigraphy and global changes of sea level. *Bull. Am. Assoc. Petrol. Geol., Mem.*, **26**: 49–212.

Van der Molen, A.S. and Wong, T.E., 2007. Towards an improved lithostratigraphic subdivision of the Chalk Group in the Netherlands North Sea area-A seismic stratigraphic approach. *Netherlands Journal of Geosciences*, **86** (02): 131–143. URL http://dx.doi.org/10.1017/s0016774600023131.

Vejbaæk, O. and Rasmussen, K.B., 1996. Geostatistical reservoir characterization using inverted seismic data: Application to a chalk reservoir, Dan Field, Denmark. Paper SPE-35486-MS presentet at European 3-D Reservoir Modelling Conference, Stavanger, Norway. 16–17 April. URL http://dx.doi.org/10.2118/35486-MS.

Vejbæk, O.V. and Andersen, C., 2002. Post mid-Cretaceous inversion tectonics in the Danish Central Graben–regionally synchronous tectonic events. *Bulletin of the Geological Society of Denmark*, **49** (2): 93–204. URL http://www.academia.edu/download/16043078/bull49-2-129-144.pdf.

Vejbaek, O.V., Bech, N. et al., 2015. Modeling unequilibrated oil saturations in a chalk reservoir, the South Arne Field case. *SPE Reservoir Evaluation & Engineering*, **18** (02): 133–148. URL http://dx.doi.org/10.2118/174085-pa.

Vejbæk, O.V., Bidstrup, T. et al., 2007. Chalk depth structure maps, central to eastern North Sea, Denmark. *Geological Survey of Denmark and Greenland Bulletin*, **13**: 9–12.

Vossepoel, F., Darnet, M. et al., 2010. Detecting hydrocarbons in carbonates: joint interpretation of CSEM and seismic. In *2010 SEG Annual Meeting*. Society of Exploration Geophysicists. URL https://www.onepetro.org/conference-paper/SEG-2010-2391.

Watts, N.L., 1983. Microfractures in chalks of Albuskjell Field, Norwegian Sector, North Sea: possible origin and distribution. *AAPG Bulletin*, **67** (2): 201–234. February. URL http://dx.doi.org/10.1306%2F03B5ACEB-16D1-11D7-8645000102C1865D.

Xu, W., Tran, T.T. et al., 1992. lntegrating seismic Data in Reservoir Modeling: The Collocated Cokriging Alternative. Paper SPE-24742-MS presented at SPE Annual Technical Conference and Exhibition, Washington, D.C. 4–7 October. URL http://dx.doi.org/10.2118/24742-MS.

Part II

Reservoir Description

Chapter 11

Geomodelling

Michel-Bøgh Thomas

11.1 Forewords & geomodelling objectives

The following chapter will focus on the building of the reservoir model, often wrongly named geological model (reservoir earth model can also be found), which is a computer model of a reservoir representing the 3D distribution in space of the main reservoir characteristics which can either be qualitative (sedimentary facies, Gross Depositional Environments–GDEs–...) or quantitative (Net/Gross–N/G–, porosity– ϕ–...). In this chapter, reservoir model/modelling and geomodelling will be used alternatively with the same meaning.

Since it represents the geological setting and characteristics, both static and dynamic, of the reservoir, this model will integrate part of the geological concepts used for describing the reservoir, generally deduced from the knowledge of the regional setting and stratigraphy. Such integration of geological concepts need to be clearly detailed and explained in order to correctly understand their impacts on the input data and on the resulting reservoir model.

At another scale, the reservoir model, which mostly deals with static parameters, will also have to include important key parameters for further dynamic modelling (permeability, k, S_w, permeability barriers, faults...) whose characteristics and/or distribution may tightly depend upon either a few geological concepts or other static parameters.

It is of paramount importance to never forget that a reservoir model, as well indicated by its name, is just a model ("an analogy used to help visualize something that cannot be directly observed") and as such is mainly dedicated for representing "a" 3D model of a reservoir, or several different scenarios of it, and "in fine" be used as a test with regard to hard data, either static or dynamic, whose abundance, importance and viability will depend upon the project maturity.

Modelling the chalk is not as easy as modelling other silico-clastic reservoirs and this chapter will obviously focus on the particular issues related to the chalk geology and their impacts on the input data and methodology used for creating geomodels for chalk reservoirs. At first, the objectives of the modelling, as they need to be clearly defined and explained and understood by all actors of the modelling chain, are crucial in the further modelling workflow and methodology to be used and will be reviewed first before focusing on the chalk related issues.

11.1.1 Timing of the geomodelling vs. the discovery/field life

The objectives of a geomodelling will obviously first depend upon the maturity of the development project of the discovery and/or field and the reasons why the modelling is launched for. Following a discovery, a rather simplistic reservoir modelling can be needed for having a good enough illustration/description of the discovery for further internal decision to be made towards a development project or not. In such a case, the main important targets of such a modelling phase will be:

- the size of the accumulation and its distribution;
- the number of independent panels to be produced;
- the number of producer wells needed by panel;

At that stage, the reservoir model to be initiated for a chalk reservoir will not be very different from a reservoir model to be launched for a silico-clastic reservoir if one excepts, for a chalk discovery/field, the very often challenging appraisal stage of the external geometry and structural model when facing seismic disturbances such as a Seismic Obscured Area (SOA; due to gas dysmigration) as it is often the case in the Norwegian South North Sea.

In addition, another aspect to take into account when discovering/appraising a chalk accumulation is the limitation of the available data from the chalk formations, especially when looking at semi-regional scale since the chalk has been often drilled through as being part of the overburden and not a primary well objective. This aspect related to the data limitations will be developed even further in Sec. 11.2.1.

11.1.2 Different geomodelling objectives

Generally speaking, the main and more usual objectives which can be assigned to a reservoir model are:

- In Place determination: whose figures will essentially depend upon the external geometry of the accumulation together with some key parameters for the reservoir: thickness, N/G, porosity;
- Well placement: for location and further follow-up or even geo-steering of a development well;
- Dynamic reserves simulation: for an evaluation of the reserves to be produced once a development plan is defined;
- Predictive production: of the years to come generally thanks to a calibration from an initial development/production phase.

For most of these cases, the building of the geomodel for a chalk reservoir will have to follow the same methodology that for a silico-clastic reservoir, the main G&G&R (Geology & Geophysics & Reservoir) issues being very similar and the objectives of the model often driving the methodology used to build it.

As an example, building a reservoir model in complex structural settings for further dynamic simulation input will have to respect cell orthogonality in order to decrease flow issues as compared with a reservoir model dedicated for well placement where fault precise location will be crucial, independently of cell orthogonality (Spilsbury-Schakel 2006).

With regard to the geomodelling objectives and in addition of the classical infill well programme, production follow-up and prediction..., chalk reservoir model objectives can possibly be more specific, as compared to other reservoirs, focusing on, for example: water/gas injection management, sweep efficiency management, reservoir and overburden compaction follow-up... potentially to be performed only over parts of the field, due to structural compartmentalization for example, making the reservoir model building even more complicated.

11.1.3 Modelling the main reservoir heterogeneity

As for all other reservoir model, the recognition and identification of the main reservoir heterogeneity/ies is a crucial step before going further in the building of the reservoir model. Such identification has not only to be qualitative but also quantitative aiming at defining the size of the model layers and cells.

For chalk reservoirs, this step is a crucial one and special attention should be paid on:

- the structural setting and fault density, styles (fault corridors ?) and throws;
- the layering refinement:
  - from the Tor Fm to the Ekofisk Fm, for example;
  - for a good representation of the permeability barriers and/or conductive layers;
- the size of the cells for ensuring a good catch of the sedimentary packages (erosive “channels”, moats vs. drifts...) and heterogeneities;
- the “crest vs. flank” porosity decrease: a laterally and vertically depth dependent process.

During this reservoir model building phase, the step of recognizing and identifying the main reservoir heterogeneities has to be seen as a pre-requisite step, a kind of SOR0 (State Of Requirements) review meeting, to go through with all G&G&R actors working on the field since it will be of paramount importance in both the model building methodology and the uncertainty approach to be further applied to the static and dynamic simulations.

Another important, if not the most important heterogeneity in the chalk reservoirs, is the fault and fracture distribution which directly controls the fluid flow within the reservoir, and which is expressed through its resulting effective permeability (k_e), so difficult to assess in most of the cases, although crucial for ensuring a good match with the dynamic production data. Such a dynamic vs. static data matching issue has forced the G&G&R community to develop different adapted methodologies which will partly be reviewed later on Sec. 11.6.

11.1.4 Geomodel size

A geomodel size will essentially depend upon two main parameters which are the size of the accumulation and the size of the main reservoir heterogeneity. With regard to this last parameter and as a "rule of thumb", a correct reservoir model size should allow this main reservoir heterogeneity to be described by at least 3 consecutive cells, in order to well account for border effects during dynamical simulation, this, of course, depending upon the nature of the heterogeneity.

Another element when defining the size of the reservoir model cells is, depending upon the model objectives, the level of precision which is expected from the reservoir model for further dynamic simulation; level which could be implied by different elements such as:

- the mean and minimum thicknesses of the reservoir layers, knowing that again all important reservoir layers should be represent into the model by several layers;
- the heights of the different hydrocarbon columns within the reservoir and especially the Hydrocarbon (HC) Water Contact (HWC) location and/or proximity of the HC zones, in order to well account for all fluid phases;
- the development scheme, with/without gas and/or water injection.

Depending upon the precision of the static reservoir model, the next step will be to decide or not to up-scale that model before forwarding it to the dynamic simulation. More and more, and thanks to the always increasing CPU, the refined scale of the static reservoir model is kept as is into the dynamic model, which is definitely the best way of doing for well accounting of all heterogeneities and get a geomodel which will be, in the future, able to answer all kinds of needs.

If not possible due to the size of the model, the up-scaling has to be defined through successive tests in order to select the best methodology and scale of the up-scaling process which will, at the end, ensure the best representation of the main reservoir heterogeneities. In such a process, different detailed methodologies exist in the different reservoir modelling tools for verifying that the up-scaling of all important parameters is done a correct way and does not lose any important elements.

11.2 Chalk issues and their impacts on the geomodelling

The chalk is a carbonate low permeability reservoir with very special sedimentary, petrophysical and dynamic behaviors creating a lot of complex issues when studying and producing the chalk reservoir, especially in North Sea. Consequently, special attention will be paid to the chalk dedicated issues and complexities, especially when implying the use or development of adapted methodologies when building the static reservoir model or dynamically matching it with the acquired dynamic data all along the field history.

11.2.1 Data limitations

The data quality and availability will obviously be a crucial element in determining the methodology to apply for any reservoir modelling, whatever the reservoir is. There will not only have a strong impact on the methodology to be selected but also on the objectives of the reservoir modelling which will have to be adapted according to the data constraints.

What is true for all types of reservoirs is also true for the chalk but will be even more influential on the resulting reservoir model since the chalk, mainly due to its apparent homogeneity, demands more information/data than all other reservoir lithologies. As a consequence, in a case of limited data availability and/or quality, the resulting reservoir model, if forced to build it, will have to be considered and used with extreme caution.

The first and main data limitation which is characteristic of chalk reservoirs, as already mentioned in Sec. 11.1.1, is the SOA which is completely masking or altering the seismic data of the area just below it. Such

SOAs are quite well known in the Norwegian South North Sea above fields like Ekofisk, Eldfisk and Valhall, for example.

It has created huge uncertainties at the beginning of the life of these field and continues to locally create issues due to the lack of good seismic marker interpretation and lack of good seismic data set, even with new LOFS (Life Of Field Survey) technology **Fig. 11.1**. Limiting the uncertainties related to such SOAs could by the way only be done thanks to more well data, to be combined with the seismic data set out of the SOA itself.

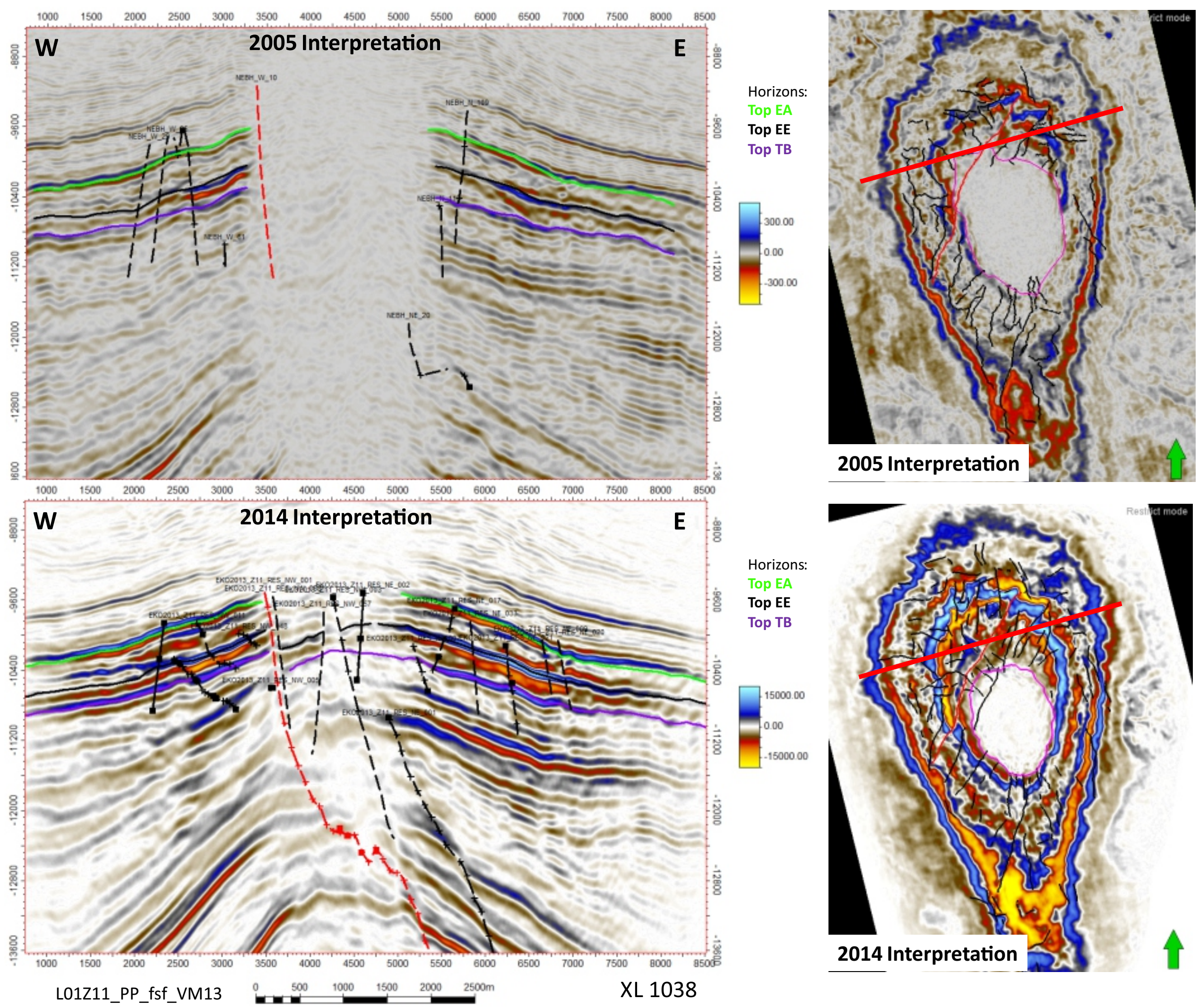

Figure 11.1: Ekofisk field: SOA evolution from 2005 to 2014 seismic data-sets → SOA reduced by 38% (from ConocoPhillips).

11.2.2 Regional setting & stratigraphy

Regional setting

The chalk sea was quite widely spread over the North Sea in very similar climatic conditions but potentially different palaeobathymetric, hydrodynamic and, not the least, tectonic conditions and/or environments. This is quite obvious when comparing the geological environment in the Netherlands with the one in Norway and United Kingdom, with palaeotopographical and present geometry strongly influenced by the onset of the compressive Alpine Africa-Europe convergence, not forgetting its consequent resulting effects on both the chalk sea hydrodynamic and chalk depositional processes.

Such different geological environments have been responsible for different lithostratigraphical sections and, more particularly, for development of unconformable and even erosional local features, obviously worth to take into account into further reservoir geomodelling. A good way to do so can be to build a burial curve of the considered reservoir for different structural locations of the discovery/field and thus better evidence possible differences in terms of the tectonosedimentary setting, potential local unconformities, burial and related diagenesis vs. HC charging phases,...

Regional stratigraphy

The regional stratigraphy, as previously defined by the Joint Chalk Research (Fritsen 1996) might seem quite easy as input data but can effectively be more complex if a sequence stratigraphy approach has been used in the reservoir description. In such a case, the regional stratigraphy to be used has to integrate all described sedimentary events and their geological meaning **Figs. 11.2 and 11.3** knowing that they will represent important sedimentary breaks and layer limits into the models, both static and dynamic.

The difference of methodology used can lead to two completely different reservoir layering/model: the flow unit vs. stratigraphic types.

Actually, less than 10 years ago, most if not all chalk reservoir models were flow unit types, mainly due to the fact that the porosity was seen as the main geological attribute and hence the porosity logs as the best tools for characterizing the chalk facies variations. In such flow unit type models, the matching with the dynamic data was generally good in early steps of the field life but became increasingly difficult with time, especially once either water injection or overburden and reservoir compaction started.

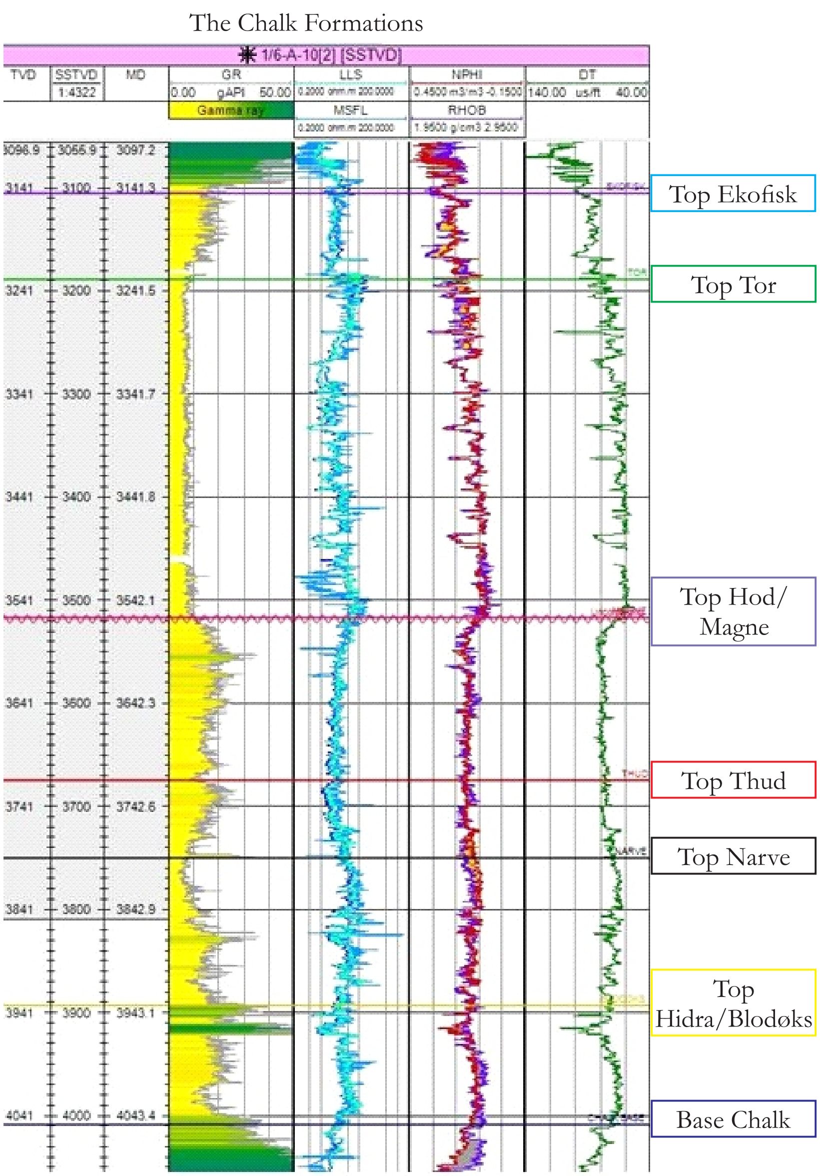

Ekofisk:
Mainly eustatic controlled pelagic laminated, interbedded & bioturbated chalk with relative high clay/silica content (abundant dense zones) and local resedimentation features

Tor:
Mainly eustatic controlled pelagic homogeneous & bioturbated chalk facies with a lot of resedimentation features

Hod/Magne:
Both tectonic/eustatic controlled rather argillaceous chalk

Hod/Thud:
Mainly tectonic controlled rather homogeneous & bioturbated chalk

Hod/Narve:
Mainly eustatic controlled pelagic homogeneous & bioturbated chalk

Hod/Hidra/Blodøks:
Eustatic controlled pelagic bioturbated, homogeneous & argillaceous chalk, evolving to marls towards the Lower Cretaceous

Figure 11.2: The chalk formations with indications of main lithology and geological controlling factors: eustatism vs. tectonism

The main issues of such flow unit models were:

- the far too simplistic "layer cake" representation of the reservoir;
- the absence of any description of the sedimentary packages and related sedimentary breaks as well described in cores of the Tor Fm, for example.

The first stratigraphic modelling started to be used and applied as soon as sequence stratigraphic framework was established at a field scale helping in more understandable geologic correlations accounting for the existence, location and distribution of either different sedimentary packages as the re-sedimented chalk in the Tor Fm, or sedimentary breaks as the dense zones. A good summary of what could be expected sedimentary packages and related sedimentary breaks in the North sea chalk section is well summarized on Fig. 11.3 (Gennaro 2011).

Geological concepts can also be underlined into either the layering method (erosive vs. on-lapping surfaces,...) or the ways parameters are in-filled into the model (regional GDE maps and/or accommodation

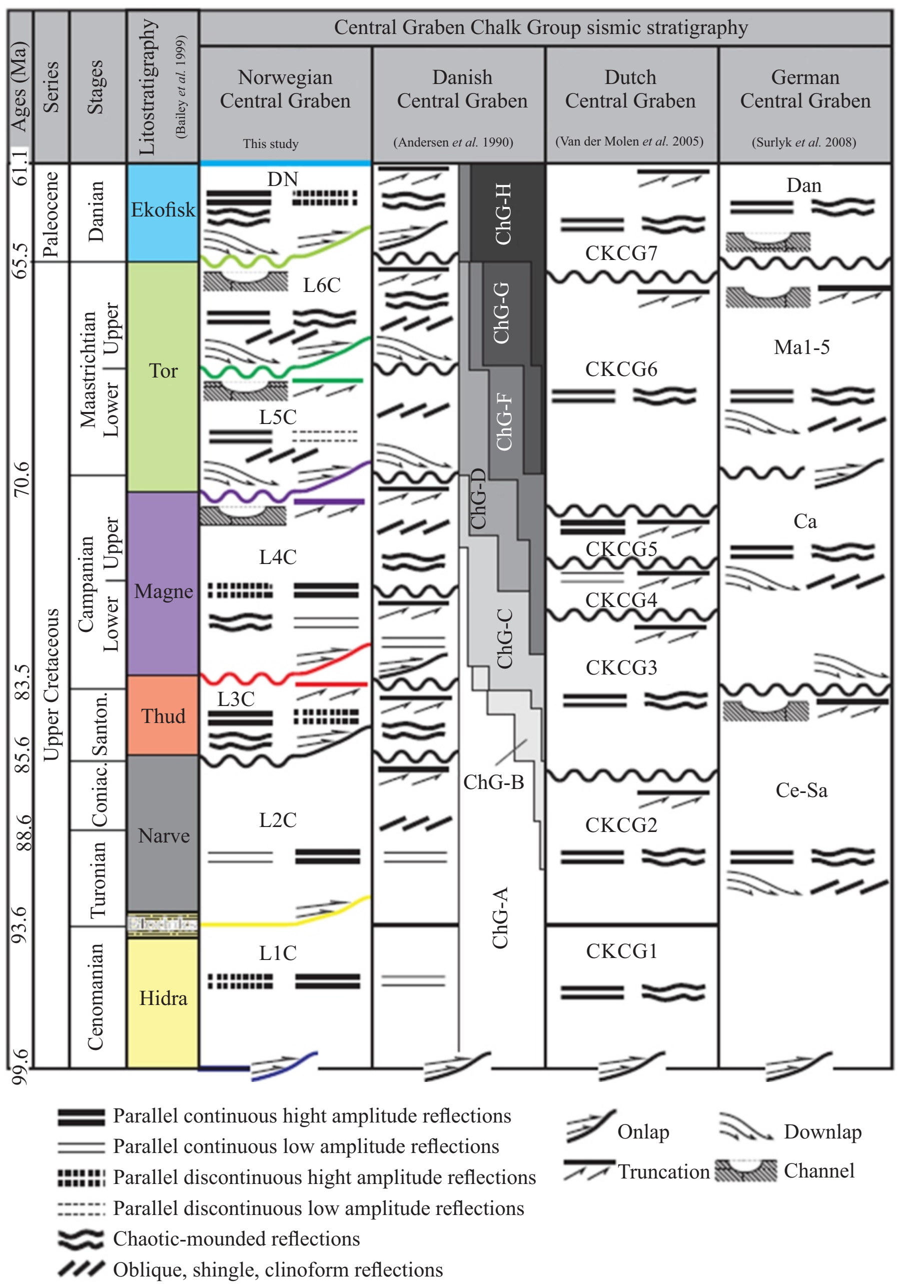

Figure 11.3: Overview of the seismic sequences and facies and their inferred sedimentary packages in the Central Graben, North Sea, Ma (megaannus, one million year) Gennaro (2011).

curves used as external drifts,...): whatever the way, the main goal will always be to integrate into a field reservoir model as much geology as possible. A practical example on how to use "geology as... the main wire" in building a reservoir model can be found in the work done by the Share Eldfisk Team, (SET1 2005) **Fig. 11.4**.

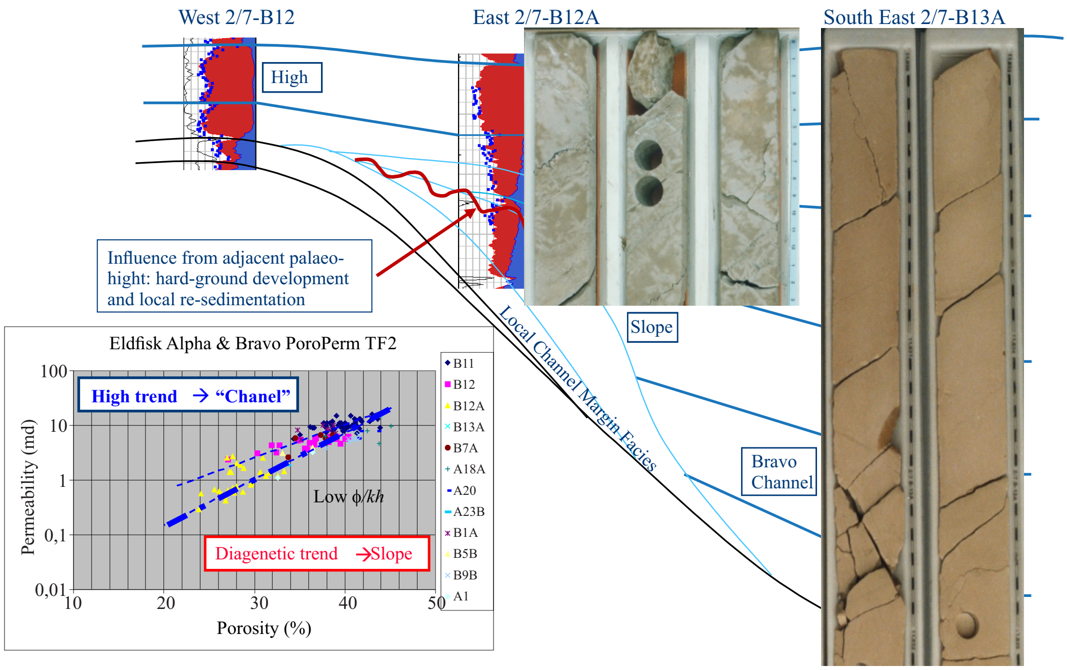

Figure 11.4: Geological Trend Maps as used in Eldfisk SET geomodel, (Thomas, Alexandersen et al. 2005).

Despite multiple attempts based on review of the core and log facies, of the biostratigraphical data and establishment of a sequence stratigraphy framework also supported by seismic interpretation, no clear detailed facies mapping or even GDE maps were possible to draw in order to populate petrophysical parameters.

Nevertheless, and mainly based on seismic isochore maps and detailed review of the relationships between chalk facies and petrophysical characterisitics (ϕ, k), a so-called Geological Trend Map (GTM) was drawn and then used for populating both the $k = f(\phi)$ laws and the 5 rock-types type J-functions defined on ϕ/k and P_c data.

11.2.3 Sedimentary facies & features

Once the chalk reservoir stratigraphy and associated layering are defined, another typical chalk issue appear which is the facies modelling upfront of any further petrophysical parameter in-filling. Chalk facies are rather easy to describe from cores, see Fig. 11.2, and then associated with either a rock-type or a porosity/permeability data but the main issue is then how to populate the reservoir model with these defined facies knowing that there is no easy way for building a GDE map for a chalk interval. An attempt was made on Eldfisk SET geomodel but it was quite a simplistic one Fig. 11.4.

In most of the other cases this step is just put aside and the reservoir model in-filling is then directly done by either the porosity or rather defined rock-types calibrated on well data where both the facies and the porosity/permeability/capillary pressure (P_c) data is well informed. Distributing these parameters into the reservoir model can then be done through either a "between wells" extrapolation or by using a Acoustic Impedance (AI) volume issued from a seismic inversion, as successfully used for the Eldfisk field a few years ago Haller and Knoth (2004).

Going from a flow unit reservoir model, with simple "between wells" extrapolation of the reservoir parameters, to a stratigraphic modelling based on sedimentary packages obviously raised an issue on the methodology to be used to correctly model the sedimentary packages and populate them within the reservoir model with a correct representation of their static parameters.

This issue has been locally solved thanks to the seismic data which can help in mapping a few sedimentary packages, as for example, the Eldfisk Bravo "channel" (see **Fig. 11.5**), which is by the way not a channel but much probably a local, almost circular drift deposit created by contourite currents as well evidenced in different areas by Surlyk and Lykke-Andersen (2007).

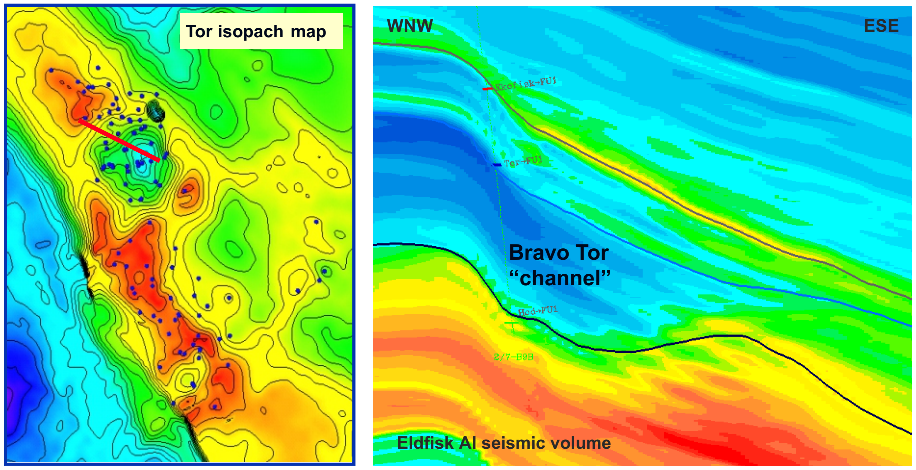

Figure 11.5: The Bravo Tor “channel” as seen on seismic AI volume in SET1 (2005).

But again, even such kind of seismic support can be difficult to use since an AI seismic volume, for example, will mostly react to porosity variations and hence not really express the discrete sedimentary breaks, as dense zones for example, far below the seismic resolution.

As a consequence and in most cases, the geomodelers' choice was to either be very deterministic, by extrapolating well data between wells following the stratigraphic architecture as defined by sedimentary packages, breaks and/or dense zones, or tentatively use the stochastic modelling proposed by the reservoir modelling tools Sequential Indicator Simulation, (SIS) based on a few basic sequence stratigraphical/sedimentological concepts.

Both approaches can be seen as usable so long the main sedimentary breaks defining the stratigraphic architecture of the reservoirs are respected and kept present in the model as potential barriers/conduits which can have a further important control on the fluid flow during production. A good example of heterogeneities to well recognize, identify and then populate into the reservoir model is the dense zones which have crucial impact on the fluid flow either as permeability barriers or conductive layers, if fractured.

The first phase of recognition and identification of these sedimentary features should imply getting an idea/proposing a tentative explanation about their distribution and lateral/vertical extent within the reservoir. An example of such an approach has been presented by (Walgenwitz, Caline et al. 2010; Gennaro, Wonham et al. 2013) on a few “dense zones” developed within the chalk reservoir and is summarized in **Table 11.1**:

11.2.4 Chalk compaction

Another drastic chalk-related issue is linked with the compaction of the chalk reservoir during production and all its related effects on:

- the sea bottom subsidence bowl, as well known over the Ekofisk field (ca 10m amplitude);
- the reservoir compaction itself to be balanced by the water injection pressure maintenance whose primary effect is to improve sweep/water flood efficiency but whose secondary effect can be to increase the subsidence due to water weakening (decrease of chalk rock strength) and chalk dissolution;
- the well integrity as severely damaged by the reservoir compaction;
- the reservoir and seal secondary fracturation creating risks of sealing efficiency;
- the chalk diagenesis and its differential behavior from crest to flank of a field;.

At the reservoir scale, the compaction as induced by mostly the Tertiary burial phase will be responsible for a diagenesis whose effects will be quite different from the crest to the flanks of the structure, as well seen in both the Ekofisk and Valhall fields. This compactional diagenesis can be reduced thanks to overpressure/hydrocarbon in-filling into the reservoir leading to a porosity preservation which can often be responsible for seismic amplitude anomalies. Practically, such a compactional diagenesis will imply the use of two different porosity $= f(\text{depth})$ trend to be applied into the reservoir model at both the crest and the flanks of the structure.

1. Stylolitized chalk	$\rightarrow$	Sedimentary/lithologic control + compaction	$\rightarrow$	Hectometric to pluri-hectometric scale
2. Silica-rich chalk:				
1) Clay-rich chalk	$\rightarrow$	Stratigraphic control, climatic cycle, global control	$\rightarrow$	Kilometric to field scale
2) Microsrystalline quartz	$\rightarrow$	Biogenic silica or seawater chemistry	$\rightarrow$	Pluri- hectometric scale?
3) Botryoidal silica crust	$\rightarrow$	Biogenic silica or seawater chemistry	$\rightarrow$	Pluri- hectometric scale?
4) Flint nodules/ beds	$\rightarrow$	Stratigraphic control and seawater chemistry	$\rightarrow$	Pluri- hectometric to kilometric scale
3. Hardgrounds	$\xrightarrow[\text{cementation}]{\text{inorganic calcite}}$	Sedimentation rate, currents	$\rightarrow$	Hectometric to pluri- hectometric scale
	$\xrightarrow[\text{calicite cementation}]{\text{organically-derived}}$	Sedimentation rate, currents	$\rightarrow$	Hectometric to pluri- hectometric scale
4. Dolomitized chalk	$\rightarrow$	Sedimentary control, depositionalenvironment	$\rightarrow$	Pluri- hectometric to kilometric scale

Table 11.1: Origin and extension of the dense zones in Walgenwitz, Caline et al. (2010).

At the dynamic modelling scale, the compaction of the reservoir through time implies to take into account this "living" process in order to be able to attach dynamic modelling results to the corresponding compaction stage of the reservoir at a particular time of the life of the field. At the field scale, these phenomena are today of paramount importance in the follow-up/management of the fields and have implied the need and development for use of geomechanical modelling which need to be calibrated to/integrated with both the static and dynamic reservoir models.

At the well scale, the chalk compaction during production of the field will be responsible for well collapses, especially taking place in sensitive areas of the field. This risk needs to be studied and monitored by use of geomechanical modelling to be applied before drilling to all wells in order to well assess that risk.

It is worth here mentioning that the chalk compaction/subsidence issue has been these last years greatly helped thanks to the recent 4D seismic data-sets obtained over both Valhall and Ekofisk fields, for example (Life Of Field Seismic, LOFS), whose repeatability of the data acquisition enables a much better follow-up and control/prediction. These new 4D data-sets now allow the reservoir behavior to be followed through time during production of the field, and are quite well adapted to the chalk thanks to its reactivity to fluid saturation and compaction during field life production. Practically speaking, the 4D data is generally managed into a dynamic reservoir model when focusing on the follow-up of the sweep efficiency of the reservoir fluids (HC and water), and by a new overburden earth model combining rock mechanics and 4D data when focusing on the follow-up of the compaction issues at both the reservoir and overburden levels and its impact on the well stability Kristiansen (2007).

11.2.5 Faults, fractures & effective permeability k_e

As it will be further developed (see Sec. 11.3), the faults and fracturation network of a chalk reservoir is definitely a particular issue mainly due to:

- the risk, as already seen earlier, of the presence of a SOA over the crest of the structure thus masking all faults in this area;
- the lithological homogeneity of the chalk reservoir not helping for a clear identification, recognition of the faults in the seismic data sets;
- the existence of more "faulted corridors" rather than well expressed normal faults;
- the diffuse network of fractures, mainly due to the chalk lithology itself, which reveals not easy neither to recognize nor to map and/or characterize.

In addition and due to the low permeability of the chalk, the faults & fractures will be the main permeable network in the chalk reservoir, hence the necessity to define and quantify a k_e which will be the best parameter for further dynamic test matching but which, as said, will not be easy neither to evaluate nor to distribute into the reservoir model (see Sec. 11.6).

11.2.6 HC contacts & transition zone Tz

The chalk being a low permeable reservoir, the HC contacts, such as GWC and/or OWC, will be very difficult to precisely identify from the logs due to the presence of a relatively thick transition zone Tz. As a result, the only and main informing data for the reservoir model will be the FWL (Free Water Level) as it can be deduced from the log interpretation (S_w saturation logs) and calibration with P_c (Capillary Pressure) data from cores.

11.3 Structural model "The container external geometry"

11.3.1 Horizons

The external geometry of a chalk reservoir will be defined, as for all other reservoirs, by its base and top, generally coming directly from a seismic interpretation after a time/depth conversion of the time horizons. Additional internal horizons can also be input for helping the definition of different zones into the model.

11.3.2 Faults

A chalk reservoir is very sensitive to tectonic constraints and will consequently be highly faulted with most of the faults well expressed on the seismic, if of good quality. As a consequence, the selection of the faults to be input into the model has to be made quite consciously respecting as much as possible:

- the hierarchy of the faults and their tectonic characteristics (style, direction and vertical extension);
- the characteristics of the faults in terms of throws, when easily computable;
- the real dip of the faults as interpreted on the seismic.

This process could also need, as when defining the main reservoir heterogeneity (see Sec. 11.1.3), a SOR0 meeting during which all actors could review and select the different fault models to be input into the geomodel not forgetting that this process can be highly challenged either by the presence of a SOA on the seismic data and the possible limitation of the well data

For the chalk reservoirs, and taking into account the importance of the effective permeability (k_e) in the control of the fluid flow during production, it will be of paramount importance to well assess not only the main faults as seen on seismic but also the secondary faults, the faulted corridors... and to match this data together with the fracturation data measured from cores and/or logs (see Sec. 11.6 for further development).

11.4 Sedimentary in-filling "The container internal geometry"

11.4.1 Direct between-wells extrapolation

If no chalk facies can be used as an input data into the reservoir model for further helping/controlling the distribution of any other static parameters such as Net/Gross (N/G), porosity..., the in-filling of static parameters has to be done more directly with one of the other of the following methods:

- simple extrapolation between wells, either directly for the porosity and permeability values or possibly via the identification of a cut-off parameter computed either directly from a porosity log or integrating the shaliness of the reservoir through the computation of a N/G equivalent;
- extrapolation between wells with control of an external drift which could be a depth structural map of the top of the reservoir, for example, or any other trend input into the reservoir model software;
- direct input into the reservoir model from a 3D seismic stochastically inverted cube for example.

Main static parameters to be modelled as such in these examples will be: N/G, possibly shaliness, porosity, permeability and for doing so a data blocking or zoning methodology should be used in order to well compute the average values per zones as defined for the reservoir model.

11.4.2 Facies modelling

In most of the field cases, it appears very challenging to create a facies distribution map for the chalk reservoirs mainly because of the high lateral and vertical variability of the chalk facies despite their apparent homogeneity and also the general scarcity of cored material.

From local core data, the 1st difficulty is then to be able to distribute the different chalk facies already at a 1D scale along the well sections. A way of doing such a distribution could be to use the log and core data, when available over the same sections, and based on an intelligent programme, interpret the log data in terms of facies thanks to a precise and detailed log-to-core calibration. This methodology works but often faces quite a few challenging issues as, for example: the detrimental fluid effect, the difficulty to recognize the shaliness component of the chalk, the difficulty to recognize/characterize the sedimentary elements of the different chalk facies and hence, at the end, the identification of more petro-log-facies than sedimentary log-facies behaviors.

At the end of the day, what most of the people is doing is to calibrate as much as possible a very simplistic interpretation of a combined "filled-in" GR-sonic curve (with/without the resistivity curves depending upon the data availability and quality) and then extrapolate such a log response to all non-cored intervals thus populating the different "GR-sonic" facies all along the well sections, at a 1D scale. The next step is then to constrain the 1D facies distribution thanks to well calibration generally using facies percentage distribution.

The 2nd difficulty will then to be able to extrapolate these 1D reference sections thanks to a few 2D maps such as facies, GDE, palaeogeographic maps, thus making possible the constant wish of integrating as much as geology as possible into a reservoir model, which is definitely the main goal of any geologist working on field reservoir model. For fulfilling this goal, an attempt was made on the Eldfisk field (Fig. 11.3) where geological trend maps were constructed for each of the different reservoir formations integrating both sedimentary and diagenetic data and used into the reservoir model for populating both the $k = f(\phi)$ laws and the P_c families/J-functions.

In absence of facies map distribution per formation and/or layer, another way is to build a conceptual GDE map based on either regional/local published papers or time thickness maps of the different formations/layers and use these maps as external drifts within a statistiscal cosimulation distribution of the facies from the referenced 1D well sections.

11.5 Petrophysical modelling "The contenant"

In-filling the geological model with reservoir petrophysics is one if not the main goal of any geological modelling and requires a robust preparation before going further. For chalk reservoirs, the preparation should focus on:

- the nature and type of available data (quality, quantity, vertical and lateral distribution...);
- the identification and geological knowledge, within each reservoir zone, of the main reservoir heterogeneity, the way it has been populated into the model and the impacts it might have on the petrophysical parameters of the reservoir;
- the existence or not of geological inputs potentially to be used as external constrains for the 3D in-filling of the model;
- the philosophy and related means to be used for achieving populating the 3D model with petrophysical data;
- the expected impacts of the static description of the reservoir on its dynamic behavior.

These different elements will help choosing the best adapted methodology, again depending upon the main objectives of the reservoir modelling.

11.5.1 Methodology

Among the different methodologies which can be used for populating chalk reservoir properties into a 3D reservoir model, the most commonly used are:

- well-to-well deterministic interpolation, generally based on either a simple kriging of the values or more sophisticated geostatistical interpolation defined thanks to computed variograms for each parameter and then applied within each of the reservoir zones;

- constrained methodologies using an external drift, either at well scale (1D as for example a N/G cut-off, facies distribution at well...) or in between wells (2D as GDE maps–see Sec. 11.4–or even 3D as an inverted seismic-deduced porosity);

- in case of use of rock-types, rock-types distribution, controlling a range of static and dynamic reservoir parameters (porosity, porosity-permeability laws, J-functions...) which will be populated according to the geological distribution of the different rock-types;

11.5.2 Petrophysical groups & rock-types

The identification of petrophysical groups, based on ϕ, k and P_c data, and the recognition then of their geological significance, thus leading to the definition of rock-types, starts to become one of the most used methodology but can be very difficult or even impossible to use for the chalk mainly because of the critical permeability parameter whose main effective component is controlled by the fracturation (effective permeability k_e) and not the pure matricial permeability (k_m). In addition, it is worth mentioning that the reliability of P_c data, which can be quite useful in defining different petrophysical groups, measured on chalk samples is quite questionable and very often not in agreement with the capillary behavior as deduced from calibration with the S_w logs.

It is probably why now quite a few geomodelers tend to be more practical and tentatively define their rock types through relatively simple petrophysical groups but also adding more information from the fracturation as seen by the seismic, the log and core data sets, as shown in **Table 11.2** for the Ekofisk field, de Lanlay, Thomas et al. (2010).

Mapping criteria for rocktyping (RT)				
RT	k_e		Porosity	
6	>15mD	Fractured	>32%	High Por
5			<32%	Low Por
4	<15mD & >5mD	Interm.	>32%	High Por
3			<32%	Low Por
2	<5mD or Frac. cont. <20%	Matricial	>32%	High Por
1	<5md		<32%	Low Por

Table 11.2: Ekofisk JET2 Rock-types, (de Lanlay, Thomas et al. 2010).

Whatever the methodology is, the main goal of the chosen methodology will be, depending upon the availability/quality of the data set and also the study objectives, to ensure a good and consistent way for first accounting for the static data sets, and second for establishing the best process to further forward the static geological modelling to the dynamic simulator.

11.5.3 Porosity and permeability

For most of the chalk reservoirs, the porosity modelling can be quite straightforward mainly thanks to several facts which are:

- that the porosity measurements obtained from the classical core analyzes are generally seen as quite reliable, which is definitely not the case for the permeabilities;

- that the chalk porosity variations are well recorded by quite a few logging tools such as: sonic, neutron and density, thus making possible an easy 1D evaluation and distribution;

- that the chalk porosity is, at a field scale and within each formation / layer, generally not varying a lot if one excepts what is due to differential burial and/or depth what is easy to recognize and to model thanks to porosity = f(depth) trends.

In addition, the porosity distribution issued from a seismic inversion has already been used and tested quite a few times (Haller and Knoth (2004), for example) and reveals an easy way for populating this parameter at a 3D scale within a field.

Distributing the permeabilities into a 3D geological modelling for chalk reservoirs is, on the contrary, one of, if not the most, challenging part of the job due to:

- the low permeability value range of the chalk reservoirs and hence the reliability of the measurements;
- the absence of any possible estimation and/or evaluation of the permeability values from log data;
- the impact of fracturation on the chalk reservoir behavior resulting in an effective permeability k_e, quite difficult to well assess, and often preventing any petrophysical groups and/or static rock-types to be easily defined, unless integrating into these groups/rock-types the fracture permeability.

Different methods for taking into account the fracturation impact on the effective permeabilities will be discussed in Sec. 11.6.

11.5.4 Hydrocarbon contacts & S_w

Both parameters are key parameters for calculating the HC In Place and their evaluation and understanding are consequently crucial. Unfortunately, in chalk reservoirs, there are quite a few issues for measuring, calculating or even evaluating both of them:

- The first issue deals with the Free Water Level (FWL) which is the first important input data in all reservoir models when starting calibrating S_w logs, especially using capillary pressure (P_c) data; it is generally deduced from pressure measurements in the water zone. Unfortunately, such information is very often missing in chalk low k reservoirs where, in addition, hydrocarbons are often found in either ODT or GDT (Oil/Gas Down To) positions.

  As a consequence, the selected FWL for most of the fields is then much more a matching parameter with S_w curves and this is generally done for the main porous facies of the Tor Fm often leading to complex situations with different FWLs for the Hod, Tor and Ekofisk formations, as induced by different reservoir properties (ϕ & k). In addition, local lateral porosity variations, due to either sedimentologic and/or diagenetic settings, are very often noticeable in chalk fields (*) and lead to the use of different P_c families distributed at the field scale and hence different FWLs from, for example, one part to the other part of a field, as it is the case for the Norwegian Tor, Albuskjell, Edda and Eldfisk fields (Evers 2014).

  > (*) Note: Such local variations of porosity/permeability have been noticed in a few chalk field examples and different interpretations have been proposed for tentatively explained them:

  - local primary reworked/re-sedimented chalk deposits as in the Tor Fm of the Eldfisk Bravo structure (the so-called "Bravo channel");
  - local porosity preservation thanks to early HC charge and/or overpressure in a part of a structure closer to the HC fetch area than the rest of the structure;
  - local diagenetic events either related to early syn-sedimentary processes such as condensed zones/hardgrounds or late due to compactional processes or fluid circulation (along faults for examples).

- Another main issue in chalk reservoirs is linked with the measured parameters from core material, such as ϕ/k and P_c measurements, since the core data is often of bad reservoir quality (low k), badly preserved, fractured... making these measurements quite difficult to use or even not reliable. It is worth mentioning that establishing best practices for core measurements are presently a big subject of the Joint Chalk Research Group #7 through one of their research project.

For evaluating S_w in chalk fields, different methods can be used depending upon data availability and knowledge of the FWL, as discussed above. On a theoretical basis, the best method would be to use core P_c data which present the advantage to account for the rock-types of the chalk reservoir, i.e. the primary and/or diagenetic facies, and hence varies either laterally or vertically thus allowing a mapping of the P_c families, as done on Eldfisk field in 2005 (Thomas, Alexandersen et al. 2005). Such an ideal situation would allow, thanks to a good knowledge of the facies distribution within the field, populating in space these P_c families, as it is done for silico-clastic and other carbonate reservoirs. But this is unfortunately very difficult or even impossible in chalk reservoirs mainly due to: (1) the difficulty of mapping the chalk facies distribution, and (2) the great similarity in terms of P_c behavior between the different facies (homogeneous, re-sedimented, laminated.... chalk). However, it is far easier to at least characterize the different formations, Ekofisk, Tor and Hod Fms, with individual P_c curves and hence populate this data vertically within the field.

On a most practical basis, a lot of reservoir geologists do prefer to use log-derived S_w allowing to easily deduce a FWL calibrated on well log data and thus well accounting for local variations, based on whatever computation methods to be selected by the petrophysicist: Leveret J-function, Thomeer model, Brooks-Corey equation.

An example of methodology for doing that is to define for each chalk formation, a S_w–ϕ–height function, being consistent with both P_c laboratory data and logged S_w profiles. But in doing so, some difficult situation can be encountered where log-derived S_w can be in disagreement with core data P_c curves as well shown by the Tor field example in **Fig. 11.6**.

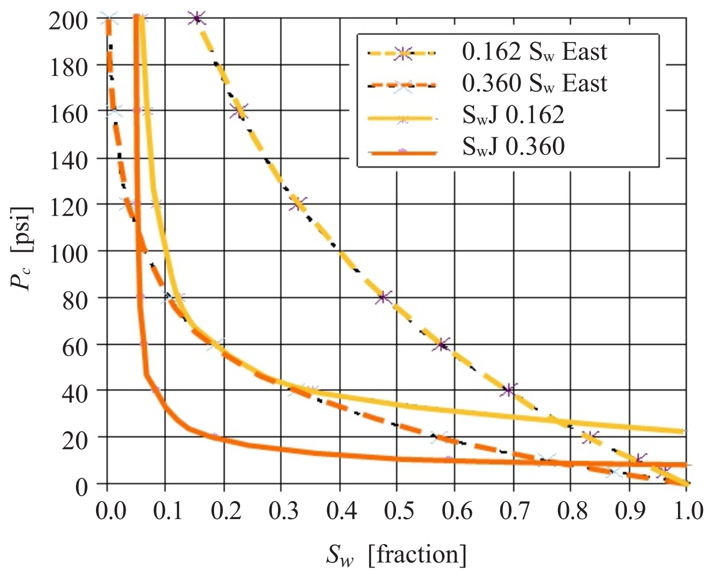

Figure 11.6: Tor field P_c vs. S_w - log (stippled) and core (full), (Internal ConcoPhillips document).

11.6 Fracturation modelling "The resulting effective permeability"

As already said in Sec. 11.5.2, the effective resulting permeability k_e controlling fluid flow in chalk reservoirs is the combination of the matrix permeability k_m and the fracture permeability k_f. If the matrix permeability is sometimes quite difficult to assess due to many reasons already discussed, evaluating the impact of the fracturation on the effective permeability is even more a challenge mainly due to the complexity of the matrix/fractures inter-actions via a complex network of vugs, fissures... as described in **Fig. 11.7**.

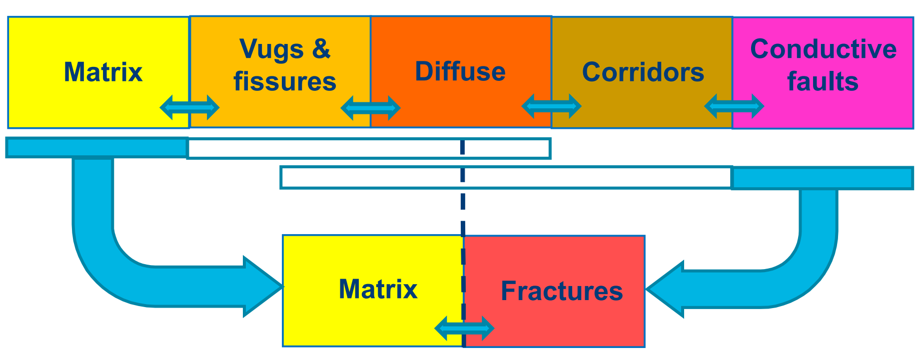

Figure 11.7: From the matrix to the fractured network into a chalk reservoir, (Internal Total document).

11.6.1 Methodology

Most well-known methodologies for establishing a field k_e are based on either establishing a fracture driver, generally issued from a fault and fracture statistical analysis made from core and/or seismic data-sets, or using a Discrete Fracture Network (DFN) from different softwares: FracMan® from Golders Associates, Petrel® DFN, Beicip FracaFlow®, Roxar RMS FracPerm®; (Rogers, Enachescu et al. 2007)), to be then combined to the matrix permeability.

This methodology aims at taking much better into account the impact of fracturation on the resulting k_e via a computation and then distribution of an "enhanced" k_m. The following phase of such a methodology is then the comparison with the dynamic well test and production history leading to back-and-forth adjustments of the k_e field distribution at the different steps of the process.

An attempt to summarize the methodology to be used and the back-and-forth calibration process depending upon results is presented on following **Fig. 11.8**:

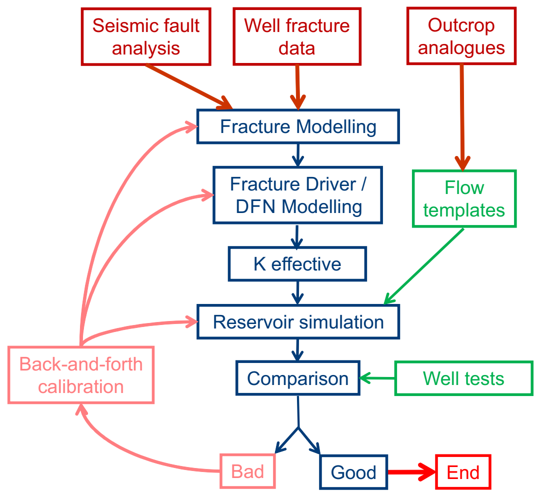

Figure 11.8: Methodology for k effective computation, (Total internal document)

11.6.2 Effective permeability modelling

For the resulting effective permeability modelling, as presented in the methodology here above, different fracture drivers issued from either core, log, seismic and well data sets, can be used for "multiplying" the matrix permeability as notably done for the Eldfisk field during the SET1 study **Fig. 11.9** and see also (Jenkins, Ouenes et al. 2009; Golder Associates 2002).

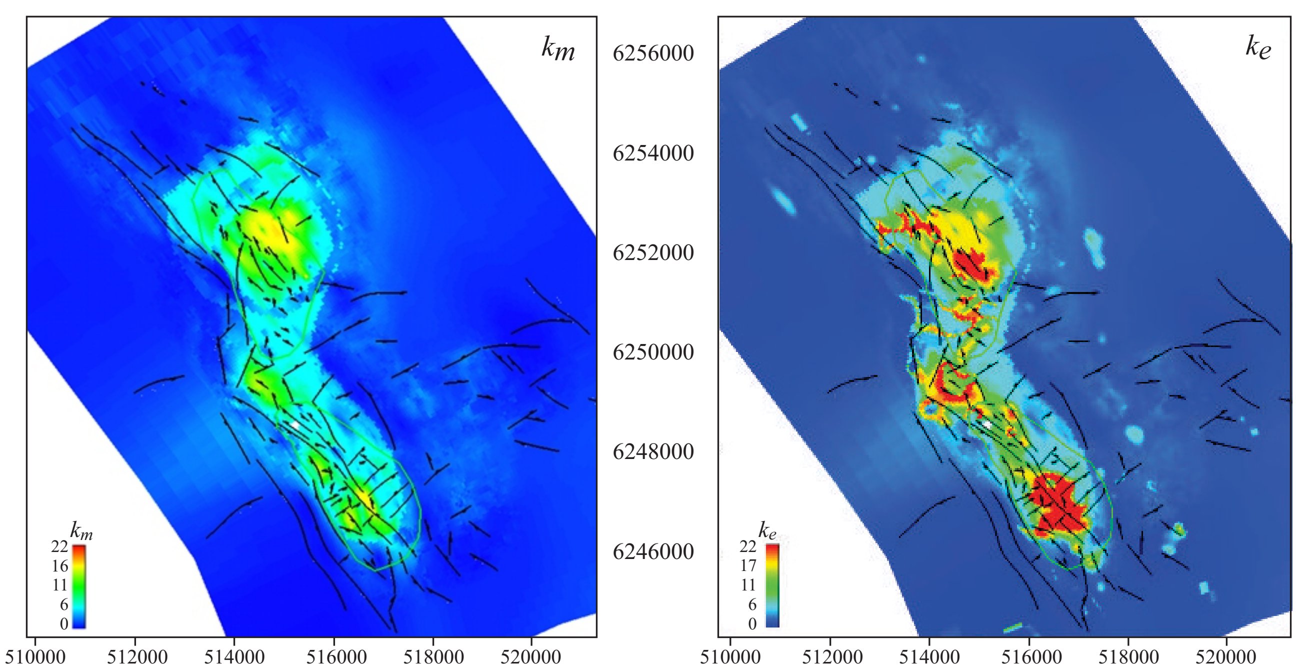

Figure 11.9: Eldfisk SET1 study: Upper Tor k_m & k_e maps, using a fracture driver mainly based on seismic curvature maps (SET1 2005).

The most commonly used fracture drivers are generally combined from different parameters issued from well and seismic data-sets, as listed here below:

- Core data:
  - Fracture orientation $\rightarrow$ fracture families;
  - fracture density and intensity in layers, from core and/or log measurements, differentiating the different types of fractures: tectonic (per families $\rightarrow$ spatial model), stylolites associated...;
  - fracture size and spacing;
  - fracture flow (k.h);
  - lithofacies volumes;
  - correlation framework;
- Seismic data:
  - amplitude- and/or impedance-, frequency-based attributes;
  - curvature (dip and slope attributes) maps, one of the most often used driver;
  - fault spacing and dilatation (taking into account the in-situ stress field);
  - fault spacing, distance to faults;
  - fault throws;
  - fault anisotropy mapping;
  - Structural Fault Enhanced Volumes (SFEV) or equivalent highways, motorways;
  - DFN, integrating both core and seismic data;
- Well / test data:
  - test derived permeability formulas / values;
  - reservoir pressure and temperature variations;
  - interference tests;
  - Production Logging Tool (PLT) kicks;
  - water breakthroughs;
  - tracers;
- mud losses.../...

Once well identified, layer per layer, this information can be then directly input into the reservoir model and used in the mapping of the different rock-types for in-fine distributing the final effective permeability and then calibrate the dynamic data, as done on Ekofisk during the JET2 model, shown on **Fig. 11.10**.

As such, the k_e parameter is becoming the calibrating parameter used by the reservoir engineers for matching their production/pressure evolution through time (well tests), often resulting, after a few years and a few new wells, in a bias of the final k_e field from the initial "geological mapping", requesting many and frequent reviews/up-dates often based on new technologies/methodologies. This has, for example, been the case for the Ekofisk field for which 2 different methodologies were recently used:

1. In 2001-2002, the Joint Ekofisk Team JET1 (2002) evaluates k_e by combining fracture data from core and borehole imaging tool (FMS, Formation MicroScanner) together with a geological "fracture driver" control deduced from a statistical analysis of the faults and fractures and evidencing relationships in between fracture families and their own characteristics (mainly orientation), and parameters mainly deduced from seismic interpretation such as fault density. And then, the resulting k_e was compared/calibrated to/with permeabilities as deduced from the well tests allowing back-and-forth adjustments.

2. In 2008-2010, the JET2 project de Lanlay, Thomas et al. (2010) applied a new innovative methodology where k_e evaluation was based on a full detailed review of dynamic well tests and production history using this data as a fracture network indicator through integration of both fracture-enhanced matrix, as seen by the dynamic data, and static fracture network, as seen by wells and seismic data using up to 12 different indicators leading to the recognition and mapping of SEFV regions Fig. 11.10.

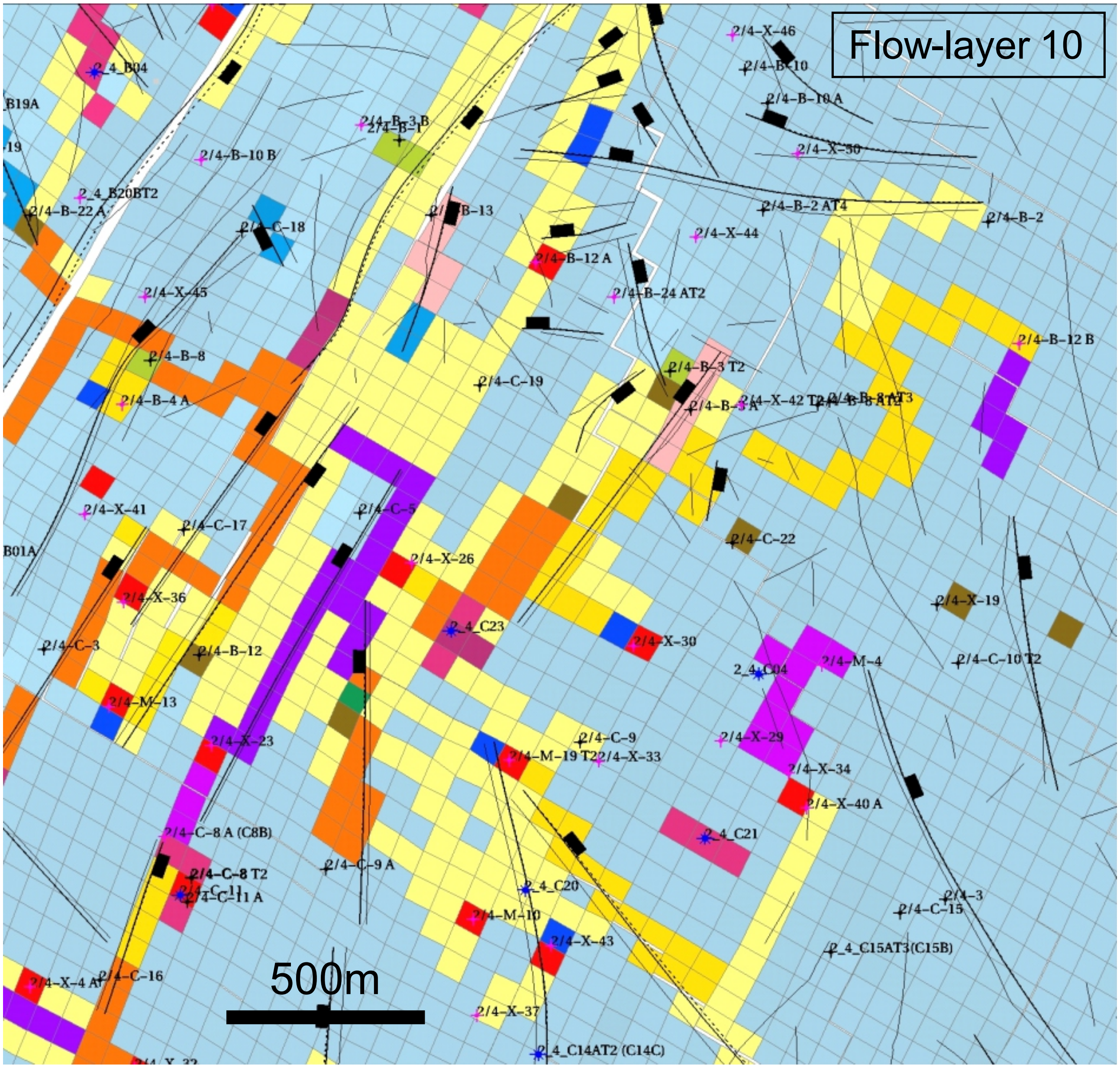

Figure 11.10: Ekofisk field: mapping of the fracture network indicators, (de Lanlay, Thomas et al. 2010).

Within that process, another challenge in the chalk fields is the effective permeability modelling within the Seismic Obscured Area (SOA) created by HC dysmigration over the structure itself mostly due to seal hydraulic fracturing and leading to the quasi absence of seismic information, as over Ekofisk, Eldfisk, Valhall..., In such a situation, well data modelling, kriging...using external drifts often appears to be the only solution, together with new seismic technologies such as 4D.

11.7 From static to dynamic

The link between static to dynamic data already started during the previous step of the k_e modelling, when calibrating static data with dynamic data from well tests for computing and distributing k_e, and it revealed being a crucial step in that process.

It will, from now on, be even more crucial and need in-depth back-and-forth reviews when starting the initial phase of dynamically testing the reservoir model. During that process, and as for other types of reservoirs, particular attention will be paid to:

- ensuring a good link in between the static rock-types and/or P_c families and the dynamic properties such as the relative permeability to fluids, k_r;

- the k_v/k_h ratio, quite difficult to assess without any precise and reliable measurements and which will, in addition, be affected by the stress regime, both vertical and horizontal;
- the reservoir connectivity, which can be first tested within the reservoir model thanks to tools such as streamlines in RMS, and then into the dynamic model with help from calibration of well dynamic data (well tests, interference tests, water breakthrough...);
- the up-scaling process, if needed, from the static reservoir model to the dynamic simulation model, paying as much attention as possible to the main geological heterogeneities of the reservoir to be well accounted for into the dynamic model;
- the history matching of the dynamic model which will need quite a few back-and-forth reviews of the static model, through much probably adjustments of the k_e parameter, in order to get the best match, crucial for any further use of the dynamic simulation model.

In addition to these steps, quite usual in all type of reservoirs, the chalk reservoirs will require additional static-to-dynamic reviews which will have to focus on:

- One of the major issue in chalk reservoirs, that is to say the sweep/water flood efficiency whose follow-up and understanding requires a good understanding of the reservoir connectivity especially through the fracture network controlling most if not all of the water breakthroughs observed in the fields. This has for example been the case in the Ekofisk field where a particular attention has been paid to that issue during the last up-date of the model, the JET2 study (de Lanlay, Thomas et al. 2010).

11.8 Uncertainty approach

Identifying and quantifying uncertainties is an important step in a field evaluation and monitoring process and should start as upfront as possible when building the reservoir model. As for the main reservoir heterogeneity identification, the identification and ranking of the main uncertainties have to be made very early knowing that they can later on drive the methodology to be used for building the reservoir model. This is especially true when facies modelling is used into the model for populating sedimentary packages.

The uncertainty approach will highly depend upon the field maturity and the amount of data availability, both as static (wells & seismic) and dynamic (well tests, production history...) data sets. Accordingly, two different approaches can be conducted:

1. In case of low maturity field: and as for all uncertainty study, the 1st step will be a SOR0 / review meeting where technicians will review and rank the main static and dynamic uncertainties, in order to highlight from this review the needs for additional works on these uncertainties, if any.

   On the static side, and based on historical review of many different fields, the main uncertainty is the STOIIP (Stock Tank Oil Initially In Place) mainly due to the seismic related uncertainties (picking, time/depth conversion) and the existence of the SOA over the crest of the fields. Other common uncertainties are: porosity and S_w.

   On the dynamic side, both the fluid dynamic parameters, such as S_o, S_g, k_r, and the k_e evaluation (also including the fault behavior: sealing/non-sealing for example) and distribution are, by far, the main uncertainties.

   The uncertainty approach then needs to work out the selected parameters, proposing different scenarios, and then produce different P10/P50/P90 static models using the modelling tool possibilities for further compare the deterministic Base Case, as built before any uncertainty approach, with the P50 aiming at getting two relatively close models ensuring a good representativity of the study and the other computed P10 and P90 cases.

   A good methodology of a "best practice" workflow, as established by Roxar, is presented on **Fig. 11.11**.

2. In case of high maturity fields: the amount of data is such that the main uncertainties are generally well known but, if still present, very difficult to be reduced. In such cases, people generally considers the input data, especially the static ones, as hard data and will develop, at the stage of the history matching, a quality assessment aiming at "fine-tuning" different dynamic parameters for getting the best wished match depending upon the objectives of the reservoir simulation. This has, for example, been the case of both the Ekofisk last modelling study (de Lanlay, Thomas et al. 2010).

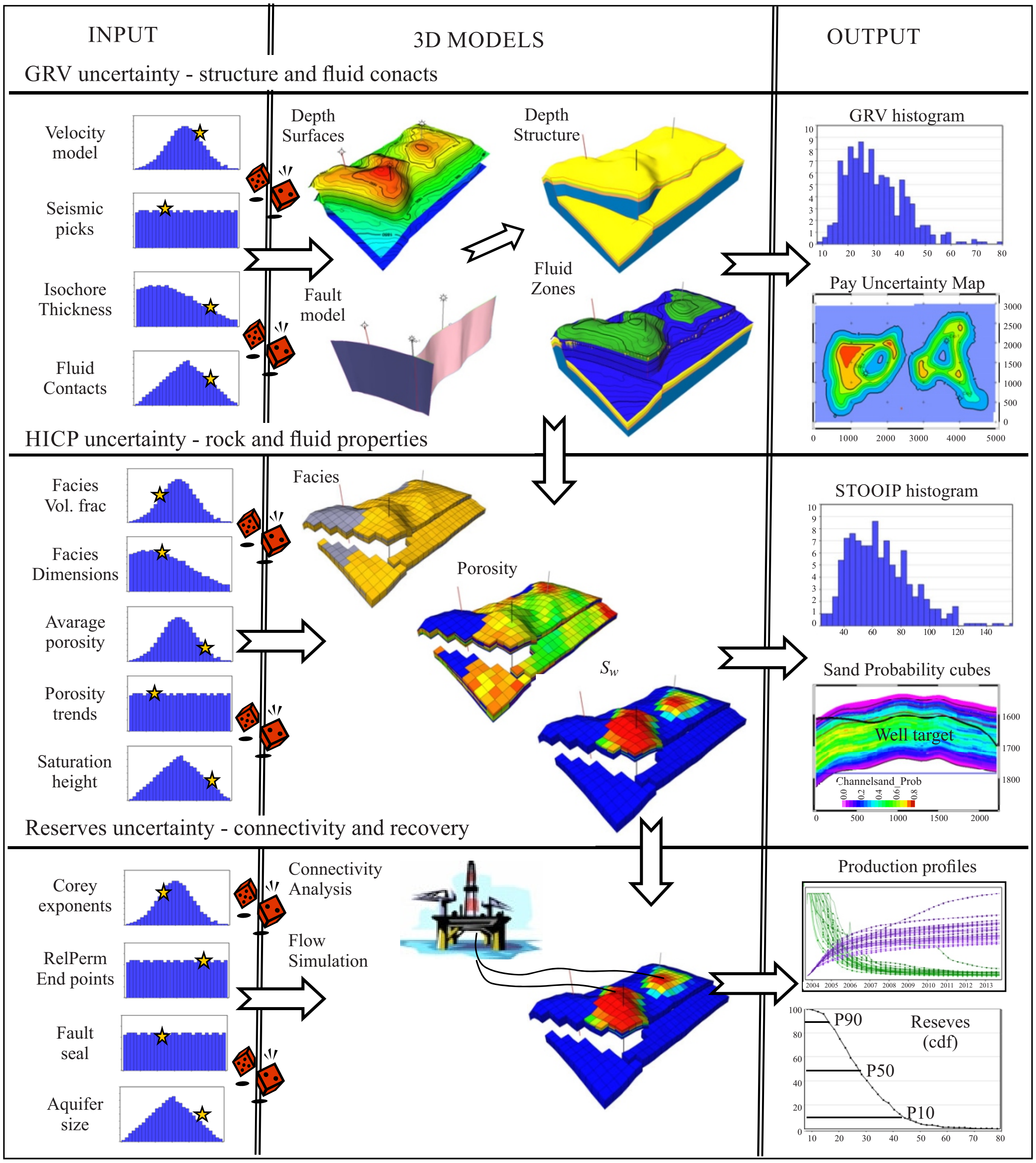

Figure 11.11: Schematic of a 3D uncertainty workflow, showing most common inputs, stages and outputs in process Mac Donald, Zhang et al. (2009).

As already said at the beginning of this chapter for the reservoir modelling, the type of uncertainty study to be launched will also depend a lot upon the objectives of the modelling at the time of its realization: well placement and integrity, improve sweep/water flood efficiency, predictive forecast....

Very typical of chalk fields, the compaction/subsidence effect can also drive, for obvious reasons of safety, the methodology to be used when approaching/processing uncertainties.

Nomenclature

k = permeability, L^2

k_e = effective permeability, L^2

k_f = fracture permeabillity, L^2

k_h = horizontal permeability, L^2
k_m = matrix permeability, L^2
k_r = relative permeability, L^2
k_v = vertical permeability, L^2
P_c = capillary pressure, m/Lt^3
S_g = gas saturation
S_o = oil saturation
S_w = water saturation
ϕ = porosity

Subscripts

c = capillary
e = effective
g = gas
h = horizontal
m = matrix
o = oil
r = relative
v = vertical
w = water

Abbreviations

AI = acoustic impedance
DFN = discret fracture network
FWL = free water level
FMS = formation microscanner
GDE = gross depositional environments
GDT = gas down to
GR = gamma ray
GTM = geological trend map
GWC = gas water contact
HC = hydrocarbon
HWC = hydrocarbon water contact
JET = joint Ekofisk team
LOFS = life of field survey
ODT = oil down to
OWC = oil water contact
N/G = net/gross
PLT = production logging tool
RMS = regression modelling strategies
SFEV = structural fault enhanced volumes
SIS = sequential indicator simulation
SOA = seismic obscured area
SOR0 = initial state of requirements
STOIIP = stock tank oil initially in place
Tz = transition zone

References

de Lanlay, J., Thomas, K. et al., 2010. JET2 Project – Ekofisk field reservoir characterization and flow simulation. Tech. rep., ConocoPhillips Norge. Joint ConocoPhillips, Total, Eni, Statoil JET2 project. Internal ConocoPhillips Norge report.

Evers, G., 2014. Review of the Free Water Levels in the main Norwegian chalk fields. Tech. rep., TEPN. TEPN internal study.

Fritsen, A., ed., 1996. *Description and Classification of Chalks North Sea Central Graben*. Joint Chalk Research Phase IV. Norwegian Petroleum Directorate, Stavanger.

Gennaro, M., 2011. *3D seismic stratigraphy and reservoir characterization of the Chalk Group in the Norwegian Central Graben, North Sea*. Ph.D. thesis, University of Bergen. URL `https://bora.uib.no/handle/1956/5396`.

Gennaro, M., Wonham, J.P. et al., 2013. Characterization of dense zones within the Danian chalks of the Ekofisk Field, Norwegian North Sea. *Petroleum Geoscience*, **19** (1): 39–64.

Golder Associates, 2002. Ekofisk enhanced matrix fracture model. Tech. rep., ConocoPhillips. Internal ConocoPhillips Norge report.

Haller, N. and Knoth, O., 2004. Challenges around Integration of Stochastic Inversion in the Eldfisk Geomodel. In *66th EAGE Conference & Exhibition*. 07 June. URL `http://www.earthdoc.org/publication/publicationdetails/?publication=2165`.

Jenkins, C., Ouenes, A. et al., 2009. Quantifying and predicting naturally fractured reservoir behavior with continuous fracture models. *AAPG bulletin*, **93** (11): 1597–1608. URL `http://dx.doi.org/10.1306/07130909016`.

JET1, J.E.R.C.T., 2002. Joint ConocoPhillips, Total, Eni, Statoil project. Tech. rep., ConocoPhillips Norge.

Kristiansen, T.G., 2007. Drilling wellbore stability in the compacting and subsiding Valhall Field: A case study. *SPE Drilling & Completion*, **22** (04): 277–295. URL `http://dx.doi.org/10.2118/87221-PA`.

Mac Donald, A., Zhang, K. et al., 2009. Introduction to reservoir uncertainty modeling. In *Frontiers+ Innovation, CSPG CSEG CWLS Convention*, 90171, 802–805. May 4–8. URL `http://www.searchanddiscovery.com/pdfz/abstracts/pdf/2013/90171cspg/abstracts/ndx_macd.pdf.html`.

Rogers, S., Enachescu, C. et al., 2007. Integrating discrete fracture network models and pressure transient data for testing conceptual fracture models of the Valhall chalk reservoir, Norwegian North Sea. *Geological Society, London, Special Publications*, **270** (1): 193–204. URL `http://dx.doi.org/10.1144/GSL.SP.2007.270.01.13`.

SET1, J.E.R.C.T., 2005. Joint ConocoPhillips, Total, Eni, Statoil project. Tech. rep., ConocoPhillips Norge.

Spilsbury-Schakel, J.A., 2006. Quality Control of Static Reservoir Models. In *SPE Asia Pacific Oil & Gas Conference and Exhibition*. Society of Petroleum Engineers. URL `http://dx.doi.org/10.2118/101875-MS`.

Surlyk, F. and Lykke-Andersen, H., 2007. Contourite drifts, moats and channels in the Upper Cretaceous chalk of the Danish Basin. *Sedimentology*, **54** (2): 405–422. April. URL `http://dx.doi.org/10.1111/j.1365-3091.2006.00842.x`.

Thomas, M., Alexandersen, H. et al., 2005. Modelling geology from static to dynamic in the Eldfisk chalk field (Southern Norwegian North Sea). Poster session at the AAPG International Conference 6 Exhibition, Paris. URL `http://www.searchanddiscovery.com/documents/abstracts/2005intl_paris/thomas.htm`.

Walgenwitz, F., Caline, B. et al., 2010. Characteristics of "dense zones" in the Chalk, Central Graben, North Sea. "From depositional systems to sedimentary successions on the Norwegian continental shelf". Norwegian Petroleum Society Conference, Stavanger. 4–6 May.

Chapter 12

Formation Evaluation

Ida Lykke Fabricius and Finn Engstrøm

12.1 Introduction

Petrophysical formation evaluation aims at quantifying reservoir properties such as porosity, permeability, pore fluid saturation, and pore compressibility from well logging data, typically detailed and calibrated by analysis of core samples. The aim is to obtain a one dimensional –along a borehole- representation of properties and their variation, typically at a 0.5 ft scale.

Modelling of petrophysical properties from 3D pore space representations has been attempted. For chalk most successfully from images generated by compiling closely spaced 2D high resolution sections generated by a focused ion beam (FIB) technology associated with scanning electron microscopy. This method is illustrative but data has to be calibrated with data from other petrophysical methods and resolution is not always sufficient (Tomutsa et al. 2007). In this chapter we focus on petrophysical analysis based on conventional and special core analysis (SCAL) as well as well logs **(Table 12.1)**.

12.2 Temperature

The temperature recorded while drilling will be the temperature of the drilling mud and thus lower than the formation temperature. In order to obtain a reliable formation-temperature we should in principle wait long enough for the mud temperature to equilibrate with the surrounding formation temperature. We can estimate this situation from temperature data obtained at time intervals after mud-circulation stopped by using Horner's method, where measured temperature is plotted versus dimensionless time ($(t + \Delta t)/\Delta t$). Δt is time since circulation stopped and t is circulation time. When dimensionless time is extrapolated to unity, it corresponds to "infinite time since circulation stopped", and the corresponding temperature is formation temperature. It is easiest done by plotting temperature versus $((t + \Delta t)/\Delta t)$ on a logarithmic scale and extrapolate to zero.

To obtain temperature data recorded at time intervals since circulation stopped, the temperature data recorded by the formation pressure tool are useful. Here temperature typically is recorded at each measuring point and the operation takes its time. For older wells, where several wireline tools were run in a hole section, the recorded bottom hole maximum temperatures may be used. Where these kinds of data are unavailable it is necessary to rely on the best estimate of geothermal gradient in the area.

12.3 Pore pressure and in-situ stress

Pore pressure is measured by the formation pressure tool either while drilling or after drilling. The principle of the tool is that one circular end of an open cylinder is squeezed through the mud cake onto the borehole wall and a negative pressure gradient is applied inside the cylinder by pulling back a piston. Provided the formation is permeable, fluid will now flow from the formation though the cylinder and into the logging tool until pressure equilibrium, and the pore pressure can be measured. It should be observed that it is the pressure in the movable fluid which is measured. In a water-wet hydrocarbon-bearing reservoir interval at irreducible water saturation, it is the pressure corresponding to the hydrocarbon phase which is measured. The pressure in the

Property	Laboratory	Well log
Temperature		Dedicated log or associated with other logging tools.
Pore pressure stress		Pressure in the movable fluid can be measured by a formation tester tool
Mineralogy	X-ray diffraction, grain density from He-expansion	Spectral GR, density/neutron, photo electrical effect, V_p-V_s, fast neutron
Fluid properties	Analysis of fluid samples	Neutron/density/resistivity logs/ SP log
Porosity	Grain density from He-expansion in combination with dry sample density. Low field Nuclear Magnetic Resonance spectrometry (NMR)	Density/neutron, Low field Nuclear Magnetic Resonance spectrometry (NMR)
Petrophysical parameters, a, m, n	SCAL: resistivity of core samples with well-defined fluid saturation, and well-defined fluid resistivity	
Fluid saturation	Dean-Stark distillation, NMR	Neutron/density/resistivity logs
Capillary pressure vs. fluid saturation	Mercury porosimetry, porous plate	
Wettability	Amott test	
Specific surface	N_2 adsorption (BET)	
Permeability, absolute	N_2 flow	NMR Logs
Pore compressibility	Ultrasonic wave velocities and density of dry sample	Sonic/density log interpreted porosity and water saturation
Biot's coefficient		

Table 12.1: Petrophysical properties

water phase can be measured in the water zone and in the hydrocarbon zone must be inferred by extrapolating the pressure trend from the water zone.

The pressure gradient with vertical depth, $\Delta P/\Delta h$, will provide the mass density of the movable fluid, ρ_{fl}, -the hydrocarbon in the hydrocarbon zone and of the water in the water zone: $\rho_{fl} = \Delta P/(\Delta h g)$, where g is the acceleration of gravity.

The total in-situ vertical stress can be obtained by integrating the bulk density to the required depth. Typically density logging data are not available all the way from the reservoir to the sea floor. For the interval above the density log, an empirical average density ρ_{av} = 1.98 g/cm^3 can be used (Japsen 1998). The total vertical stress, σ_v becomes: $\sigma_v = (\rho_{av} h_{\log} + \sum \Delta h \rho_b) g$, where $h_{\log}$ is the vertical depth to the top of the logged interval, Δh is the vertical interval between log data points, and $\rho_b$is the bulk density logging data.

The horizontal stress, σ_h, is difficult to estimate. One way is to assume the horizontal and vertical total stress to be similar (hydrostatic stress conditions). Another possibility is to assume the horizontal elastic strain is zero (lateral stress at rest -K_0 condition), so that $\sigma_h = K_0 \sigma'_v$, where K_0 can be estimated from sonic data $(K_0 = 1 - 2(V_S^2/V_P^2))$,

The elastic strain of the chalk corresponding to a given hydrostatic stress will be counteracted by a fraction of the pore pressure, so that an "effective stress, σ'" can be defined as:

$$\sigma' = \varepsilon K_{\text{dry}} = \sigma - \alpha P, \tag{12.1}$$

where, ε is the elastic strain, K_{dry} is the drained bulk modulus and α is Biot's coefficient (see chapter 3 on Rock Physics). Please observe that the term "effective stress" can have different definitions depending on context.

12.4 Mineralogical composition

Where cuttings samples or drill cores are available, mineralogical composition can be determined by X-ray diffraction analysis (XRD). For North Sea chalk, XRD of a powdered bulk sample will typically reveal only the presence of calcite and quartz. To identify minor components and especially clay minerals, it is necessary to remove the calcite by acid treatment. The recommended procedure is first to take a few gram of chalk and estimate the carbonate content by dissolution in hydrochloric acid and titration with an aqueous sodium hydroxide solution. Based on this value it can be estimated how big a chalk sample is needed for obtaining the necessary insoluble residue of 0.5 g of sample for XRD. The big sample is crushed and calcite removed by repeated treatment with acetic acid. The insoluble residue is then used for bulk XRD to determine the overall mineralogical content of the insoluble residue and a specific XRD procedure is applied to determine the type of clay minerals (Brindley and Brown 1980).

Grain density, ρ_g, is measured by He or N_2 expansion as a part of the conventional core analysis for porosity. The expected value for calcite is 2.71 g/cm^3, so lower grain density can be an indication of high content of quartz (ρ_g = 2.65 g/cm^3). By contrast, higher grain density can be an indication of the presence of (e.g. Fe-rich clay and/or pyrite).

Because clay minerals typically are radioactive, the clay content can be generalized from a few samples to a larger interval of the chalk by using the natural gamma ray log, GR **(Fig. 12.1)**. It should be noted that this generalization should not be done over wide distances and among formations. The reason is that not all clay is equally radioactive and that there are regional and stratigraphic variations in content of other radioactive minerals as for example the radioactive K-feldspar.

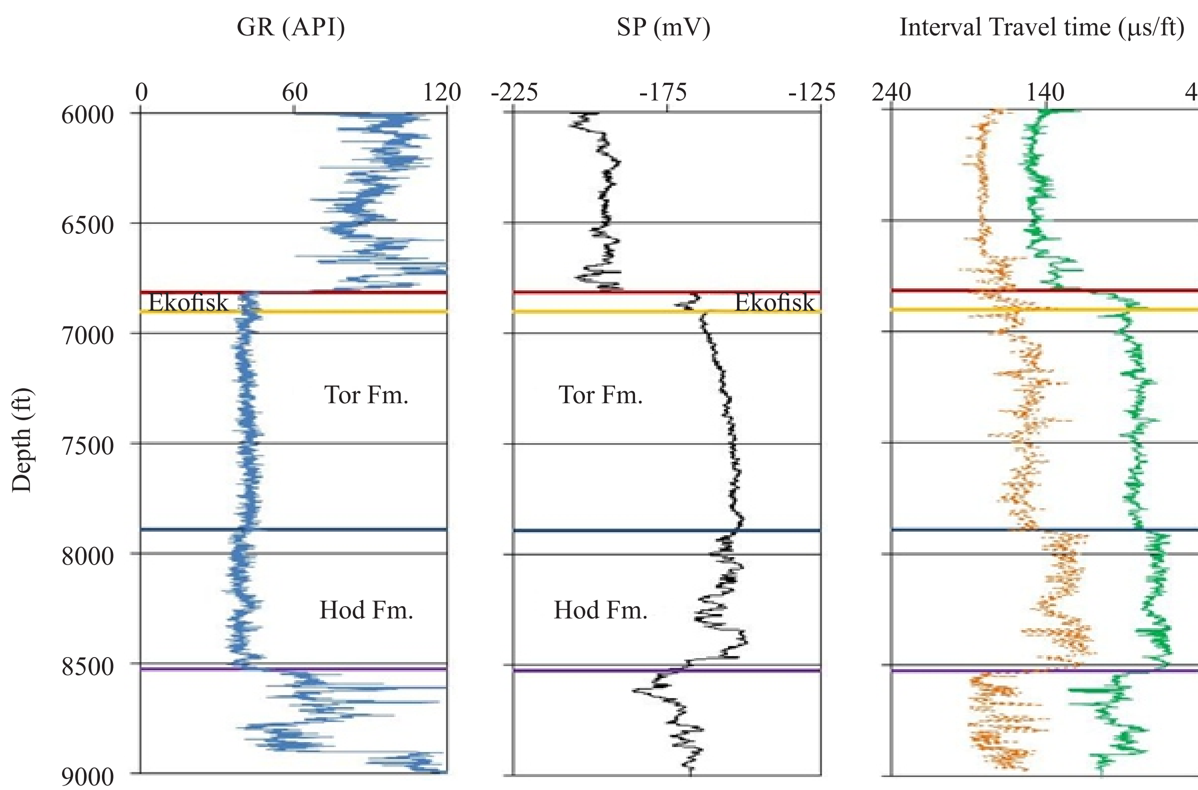

Figure 12.1: Natural gamma ray, spontaneous potential and array sonic logs for exploration well Nana-1XP. The orange stippled curve represents interval travel time for the shear log, whereas the green curve represents interval travel time for the P-wave log. The litho-stratigraphic units are based on Abramovitz, Andersen et al. (2010). The static spontaneous potential is estimated to be 33 mV. It is derived as the difference in SP between the SP-trendline for chalk and the SP-trendline for shale (shale base line). From log heading a mud filtrate resistivity of 0.02 Ωm at 77°C is estimated, so that a pore-water resistivity of 0.048 Ωm is found from Nernst's equation.

The GR log is in principle a scintillation counter which measures the background radiation at the location of the detector. It is a relatively cheap tool and widely used for lining up different logging runs. GR data are recorded in API (American Petroleum Institute) units and can in principle be calibrated. The absolute reading though, can be heavily influenced by radioactivity of the drilling mud, so for quantitative use it must be calibrated with core- or cuttings data. Traditionally a "shale point" could be chosen in the shale overlying the chalk, and used as a 100% basis value for quantifying "shale content" of the chalk. Because the shale radioactivity varies stratigraphically and with location and not necessarily has the same clay mineralogy as the chalk, this procedure is far from quantitative.

The spectral gamma ray log, where contributions from potassium, the uranium series and the thorium series are quantified is rarely used for the chalk. Due to the extremely low solubility of Th, the thorium signal quantifies the amount of detrital clay. The potassium signal gives overall clay content but includes a signal from other K-bearing minerals. The U-signals is not directly associated with clay content. The reason is that the soluble uranyl ion can be transported by diffusion and advection in the pore water and adsorb to negative sites on minerals, probably including calcite. Where a borehole crosses open fractures, an enhanced U-content may be detected, probably sourced by water flowing in fractures from U-rich layers. Uranium can also be enriched in glauconite and phosphorite-bearing chalk intervals.

X-plotting density and neutron logging data can also give an indication of mineralogical content, especially in intervals with no hydrocarbons **(Fig. 12.2)**. Both tools respond to the pore-water, but responds differently to minerals. If calcite is taken as the solid phase basis, the density log will respond to variations in grain density and the neutron log to variations in neutron stopping power, which varies among elements. From density logs where the amount of photoelectric effect is modelled, the presence of barite invaded into fractures may be detected. Geochemical logging tools based on gamma rays generated by interaction of fast neutrons and atomic nuclei are rarely used in chalk.

When linking petrophysics to rock physics, a method for assessing mineralogical variations among layers is to cross-plot the P-wave velocity, V_p, with shear wave velocity, V_s, from the array sonic log (Fig. 12.2). Because the V_p/V_s ratio varies among minerals, the effect on velocity of difference in porosity is largely evened out by cross-plotting.

12.5 Fluid properties

12.5.1 Hydrocarbons

An indication of hydrocarbon composition can be obtained from the ditch gas, cuttings gas and chromatographic analysis compiled on the mud log. In situ hydrocarbon density can be assessed from the formation pressure log, where available (see above). Pore fluid sampling associated with formation pressure logging is rarely attempted. More detailed information on the hydrocarbon phase requires a hydrocarbon sample from a production test or from hydrocarbon production.

12.5.2 Pore water

For formation evaluation, the salinity of the pore water is the central property. Probably due to the association between several chalk fields and underlying salt structures, the pore water of the North Sea chalk fields can be highly saline, but in other cases much less so. The pore water salinity varies among fields, and can even vary within a field. The salinity of the pore water is a main determinant of its electrolytic electrical conductivity and mass density.

A water sample for chemical analysis can be obtained by production testing the water zone or less expensively from water produced together with hydrocarbons. There is always a possibility that the water sample is contaminated with drilling or completion fluids. Electrical resistivity (inverse of conductivity) can be measured directly on a water sample at reservoir temperature. If salinity is known, pore water electrical resistivity can also be predicted from temperature by using published empirical relations (Schlumberger Log Interpretation Charts, available online), and the density of the water at a given temperature and pressure can also be predicted from empirical relations (Batzle and Wang 1992).

The in–situ density of the pore water can be calculated from formation pressure logging the water zone (see above).

SP-log. It is a part of classic log interpretation to evaluate electrical resistivity of the pore water from the spontaneous potential (SP) log (Fig. 12.1). By this method the contrast in salinity between pore water and aqueous mud filtrate gives rise to a spontaneous electrical potential between the invaded zone and the undisturbed zone in permeable rocks and to an oppositely directed electrical membrane potential between the drilling mud and impermeable shale. From the difference between these potentials and provided that mud filtrate salinity and temperature are known, pore water salinity can be calculated from the electrochemical Nernst's equation. Measurement of the potential requires a simple electrode, but for offshore application it can be a problem that

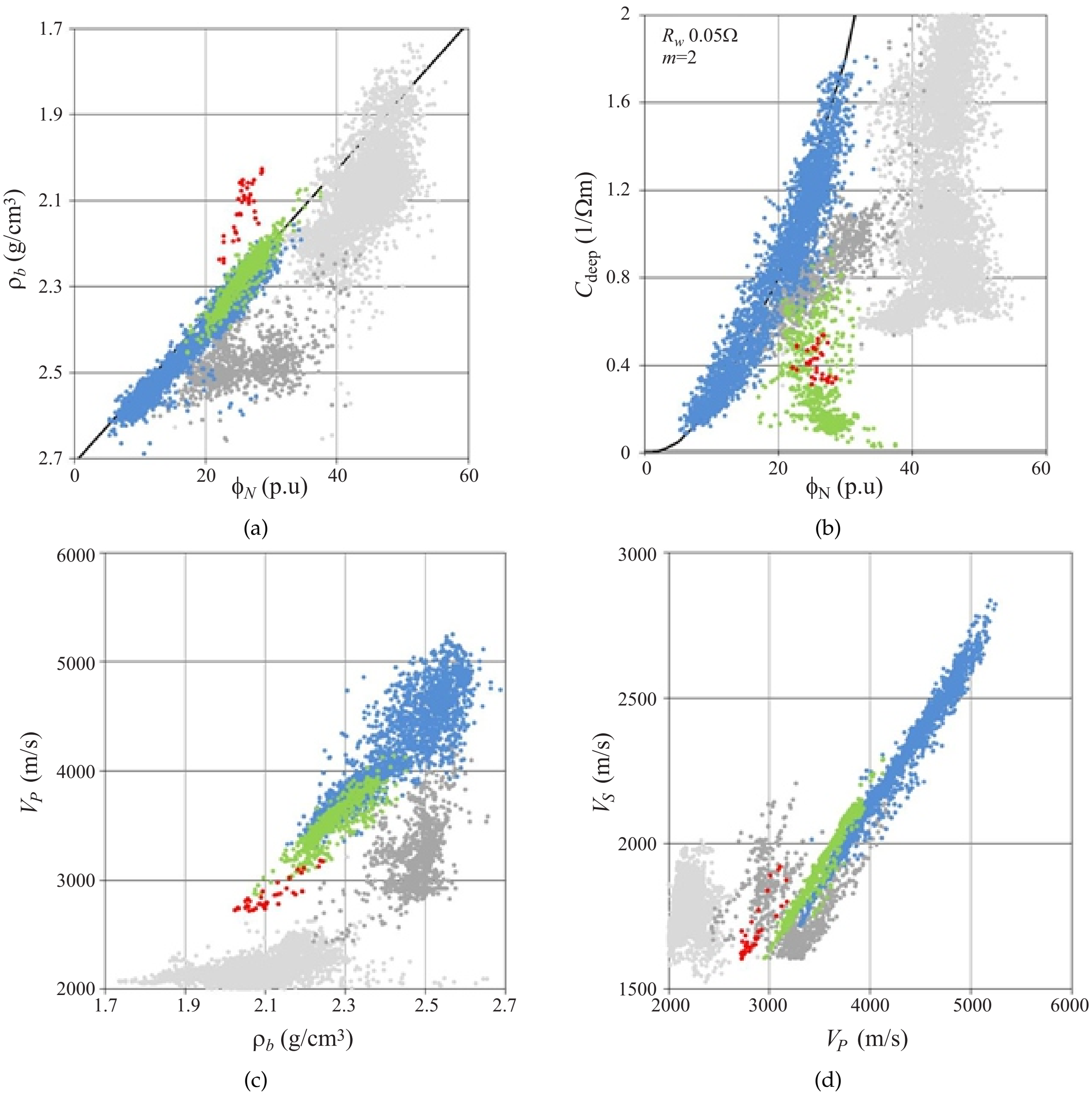

Figure 12.2: X-plots of (a) bulk density vs neutron porosity, (b) deep electrical conductivity vs neutron porosity, (c) P-wave velocity vs. bulk density, and (d) shear wave velocity vs P-wave velocity. Light gray represents Cenozoic shale, dark grey Cretaceous shale; blue is water saturated chalk, green is oil bearing chalk and red is gas bearing chalk. In (a) gas-bearing chalk has a clear low-density signature. In (b) water saturated chalk is separated from hydrocarbon-bearing chalk. The curve corresponds to a water resistivity of 0.05 Ωm and a cementation exponent, m = 2 in Archie's equation. In (c) shales are distinguished by low P-wave velocity for a given density. (d) illustrates the high V_s/V_p for hydrocarbon (especially gas) bearing chalk.

the corresponding electrode at the wellhead needs to be grounded. The method obviously does not work in (electrically insulating) oil-based mud. The big advantage of the log is that water resistivity can be assessed even in oil-bearing intervals.

Archie's method. Where a dry hole or the water leg of a hydrocarbon field is drilled and logged, it is common practice to find the pore water resistivity by Archie's method (Archie 1942). A water zone resistivity, R_o, log should be available, and it requires that porosity, ϕ, is determined by radioactive logs (density log and/or neutron log). Archie's equation simply states:

$$R_w = R_o \phi^{-m}, \tag{12.2}$$

where m for chalk can be assumed equal to 2, unless core data for m is available. The problem can also be solved graphically by fitting a curve through water zone data representing ϕ^m/R_w on a $C_o = (1/R_o)$ – porosity cross-plot, by adjusting R_w and m (Fig. 12.2).

12.6 Porosity

On cleaned, dry core samples it is common practice to measure porosity by expansion of helium or nitrogen. The gas expansion method is based on Boyle-Mariotte's law and strictly speaking measures the volume of the solid part of the sample, V_s. To obtain porosity, the bulk volume, V, of the regularly shaped (cylindrical) sample is calculated from sample dimensions measured by a caliper, and the porosity, ϕ, obtained:

$$\phi = (V - V_s)/V. \tag{12.3}$$

As a check of quality, the sample is weighed, and the grain density, ρ_g, is obtained. In the calcite rich Tor Formation grain density is practically equal to the mineral density of calcite (2.71 g/cm^3). This indicates that closed pores (mineral fluid inclusions) play no significant role in the porosity. Where the chalk is richer in silica, grain density can in intervals be as low as 2.69 g/cm^3 (mineral density of quartz is 2.65 g/cm^3). If the reported grain density is lower than expected, it can be a sign that the core sample is not sufficiently cleaned for hydrocarbons.

From well logs it is common practice to calculate porosity from the response of density and neutron porosity logs. They are typically both calibrated in water saturated limestone and are therefore easy to use in chalk.

The density log is based on emission of gamma rays from a source in the logging tool squeezed to the borehole wall. The source is chosen so that the subsequent attenuation in the chalk is in the energy interval where gamma ray attenuation is dominated by Compton scattering, so that the attenuation corresponds to the number of electrons per volume and thus mass density of a rock composed of elements as Ca, C, and O, where the mass number is the double of the number of electrons. A complication in principle arises because H only has a mass number equal to the number of electrons. This problem is overcome by calibration, and although the density log is calibrated in water saturated limestone, it will give accurate measurement (3 significant digits) of the bulk density, ρ_b, also in hydrocarbon bearing intervals. The majority of the gamma ray scattering and attenuation takes place within the first few centimeters of the borehole wall, so in permeable intervals, the response primarily arises from the zone invaded by mud filtrate. If the density of the fluid, ρ_f, in the invaded zone is known, porosity becomes:

$$\phi = \frac{\rho_g - \rho_b}{\rho_g - \rho_f}. \tag{12.4}$$

It is not always easy to know the fluid density of the invaded zone, especially in a gas bearing interval. It is in this case advisable to use porosity data from core samples for calibration **(Fig. 12.3)**.

The neutron porosity log is based on the energy loss during thermalization of medium energy neutrons generated by a radioactive source in the logging tool. The neutrons loose energy by collisions with the atomic nuclei in the formation. Due to a similar mass to that of the neutron, hydrogen nuclei give a very large contribution to the energy loss, but all element nuclei, especially the light carbon nucleus, contribute. The neutron porosity log is sometimes perceived as a "porosity log" because it is calibrated to give an accurate measure of the porosity in water saturated limestone (chalk). When the pore fluid is different from water, especially when the chalk is gas bearing, the log does not report porosity, but rather the porosity of a fictitious water saturated chalk with the same ability to slow neutrons as the chalk in question. The main function of the neutron log in chalk in the water zone is to provide a quality check on porosity measured by the density log, and to highlight gas bearing intervals where neutron attenuation will be low (and apparent porosity therefore also low, Fig. 12.2a, Fig. 12.3) due to the low mass density of gas. The low mass density of gas will at the same time cause low fluid density, and unless invasion dominates, consequently low (but correct) bulk density as measured by the density log. Provided a similar degree of invasion effect can be assumed for the neutron and the density log, the porosity in a gas-bearing interval can be obtained from the apparent porosity from density log, ϕ_d, and apparent porosity from neutron log, ϕ_n:

$$\phi = 2(\phi_d + \phi_n)/3. \tag{12.5}$$

If radioactive logs are unavailable, porosity can be estimated from the sonic log by Wyllie's equation (Wyllie, Gregory et al. 1956):

$$\phi = (\Delta t_g - \Delta t)/(\Delta t_g - \Delta t_f), \tag{12.6}$$

where $\Delta t = 1/V_P$ is the measured interval travel time (= slowness = inverse velocity) of elastic P-waves, Δt_g is the interval travel time for the mineral and Δt_f is the interval travel time for the pore fluid. P-wave velocity of calcite is 6.24-6.64 km/s (Table 7.1, Chapter 7), so interval travel time for the mineral calcite is c. 155 μs/m or

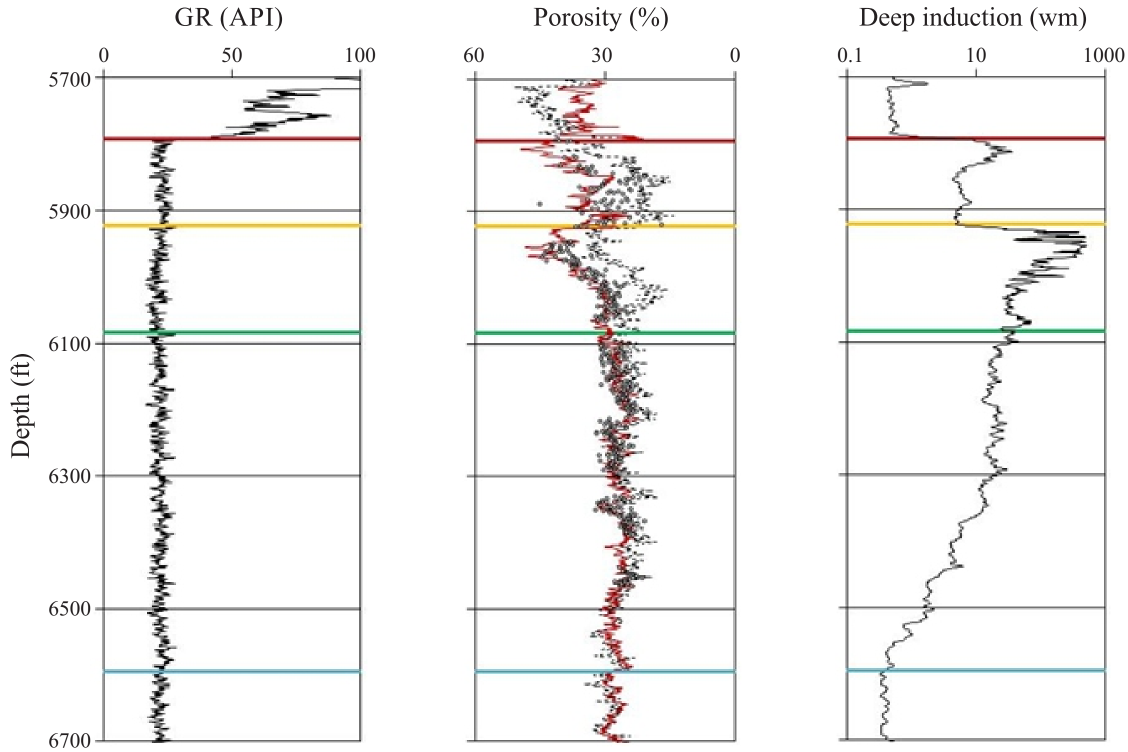

Figure 12.3: GR, neutron (stippled), density (red) and resistivity logs through reservoir interval of Dan field M-1X. Porosity from He-porosimetry of cores is also shown with circle signature. Red line is top Ekofisk Formation, yellow line is top Tor Formation of Cretaceous age, Green line is Gas-Oil contact, and blue line is Oil-Water contact (100% water saturation). The Cretaceous part of the reservoir is of Maastrichtian age (Kristensen, Dons et al. 1995). The core porosity data indicate that in the relatively high-permeability Maastrichtian part of the gas zone, porosity can be read directly from the density log. This is because drilling-mud filtrate invades the chalk and replaces the gas in the depth of investigation of the density tool.

47.5 μs/ft. whereas pore fluid travel time for water varies around 190 μs/m depending on salinity, temperature and pressure (Batzle and Wang 1992). It should be noted though, that there is no strict physical basis for Wyllie's equation and that it only gives a good guess in water or oil saturated chalk with porosity lower than 30%. An empirical, lithology-dependent relation between bulk density, ρ_b, and P-wave velocity, V_P, was proposed by Gardner, Gardner et al. (1974):

$$\rho_b = \alpha_g V_P^{\beta_g}, \tag{12.7}$$

where α_g and β_g are lithology-dependent parameters. By fitting these parameters for a given setting, sensible porosity data can be derived from the estimated bulk density.

Because the sonic logging tool responds to the elastic wave travelling as a refracted wave along the wellbore, the measured interval travel time depends heavily on the degree of mud filtrate invasion and thus the time passed between drilling and logging (Borre, Beales et al. 2004).

For boreholes from before radioactive logs became common, porosity in water zones can be estimated from electrical logs and Archie's equation, provided pore water resistivity is determined from SP logs.

12.7 Electrical Resistivity and Petrophysical parameters

The electrical conductance of chalk is controlled by the water content of the rock and the salinity of the water. There will be no contribution to conductance from the hydrocarbons or the solid insolating minerals calcite, quartz and clay constituting the rock. A contribution from surface conduction at the water-solid interface, mainly from cations adsorbed to clay, is only relevant for pore water salinity below that of seawater (Clara, Zelenko et al. 1998; Revil, Linde et al. 2007).

Because the conductivity of the chalk is given with reference to the rock sample geometry, the measured conductivity, C_o will be smaller than the conductivity of the pore water, C_w, and the formation factor, F , can be defined (Archie 1942):

$$F = C_w/C_o = R_o/R_w = \phi^{-m}. \tag{12.8}$$

For a fully saltwater-saturated chalk, Archie's equation apply, and it will be relevant to find the cementation exponent, m, from core analysis: A cleaned core sample of known porosity is saturated with salt water of one concentration and then with another concentration and so forth, and from a series of corresponding R_w and R_o, m can be determined. If for practical reasons a constant m is desired for a whole flow unit, it is possible to take a series of cleaned chalk plugs with different porosity and saturate them with the same saltwater with a given R_w, and measure R_o in all samples. An extra constant, a, must then be introduced, and Archie's equation gets the empirical form:

$$F = a\phi^{-m}. \tag{12.9}$$

The factor a rarely varies much from 1 and should be in the range $0.5 < a < 1.5$. A recommended alternative to introducing an a is to allow m to vary with porosity. The latter will ensure that the limes of conductivity goes toward the conductivity of the formation water when porosity goes towards unity. The porosity-dependent exponent, m, has been found to have no relation to degree of contact cementation or Biot's coefficient, (Gommesen, Fabricius et al. 2007), but it is related to the grain smoothening cementation (recrystallization) in that, m has been found to correlate with specific surface with respect to bulk volume, $S = (c\phi^3/k)$, where c is Kozeny's factor and k is Klinkenberg permeability (see section 12.12 on permeability, in m^2/cm^3) (Olsen, Hongdul et al. 2008):

$$m = 0.09 \log(c\phi^3/k)^{\frac{1}{2}} + 1.98, \tag{12.10}$$

where "log" is the base 10 logarithm. Olsen, Hongdul et al. (2008) thus found, that it is not the specific surface as measured by nitrogen adsorption (BET), but the specific surface as calculated from porosity and permeability, that is relevant for the electrical properties. It should be kept in mind that S not only depends on calcite recrystallization but also to a large extent on the content of tiny quartz and clay crystals in the chalk (see Fig. 7.2 2 in Chapter 7).

When some of the pore space is taken up by hydrocarbons, S_{hc}, and the remaining pore space, S_w, by formation water, it would be logical to expect Archie's equation to be modified as:

$$R_t/R_w = a(S_w\phi)^{-m}, \tag{12.11}$$

where R_t is the electrical resistivity of the chalk saturated with water and hydrocarbons. Hydrocarbons are unfortunately not distributed regularly like solid particles in the chalk, so in reality Archie's equation must be modified to:

$$\frac{R_t}{R_w} = aS_w^{-n}\phi^{-m} <=> S_w^n = \frac{aR_w}{R_t\phi^m} \tag{12.12}$$

The saturation exponent, n, can be estimated from laboratory experiments on samples with known S_w, but unfortunately n has been found to vary with S_w and to be different when a given water saturation is a result of drainage from when it is a result of imbibition (Howard, Fidan et al. 1999). In water-wet homogeneous chalk, n is typically close to 2; but when chalk is oil-wet, n can be much higher. In a fractured sample n can be found to be close to 1.

12.8 Fluid saturation

Drill cores of chalk will typically have been more or less invaded or flushed by mud filtrate during retrieval of the core, but an estimated S_{hc}, can be obtained by controlled heating of a core sample, where water and hydrocarbons are evaporated and then condensed in a cool measuring tube (Dean-Stark extraction, Dean and Stark (1920)).

From well logging of chalk, water saturation is typically found from porosity (based on density log) and resistivity logs by using Archie's equation **(Fig. 12.4)**. It is in this context a concern that the saturation exponent, n, generally is so poorly defined. It should also be noted that the entire porosity is typically effective, and that no correction for clay content should be made. This is because most clay and silica is dispersed in the pore space and only a minor part concentrated in distinct stylolites.

In water-wet chalk, saturation of water and hydrocarbons can alternatively be quantified from the Nuclear Magnetic Resonance (NMR) log. The chalk needs to be water-wet because the NMR T_2 peak for hydrocarbons then typically is clearly separated from the water peak. For logging while drilling data, Reppert, Akkurt et al. (2006) found that due to its higher resolution than the NMR T_2 distribution, the NMR T_1 distribution can give more accurate water saturation determination.

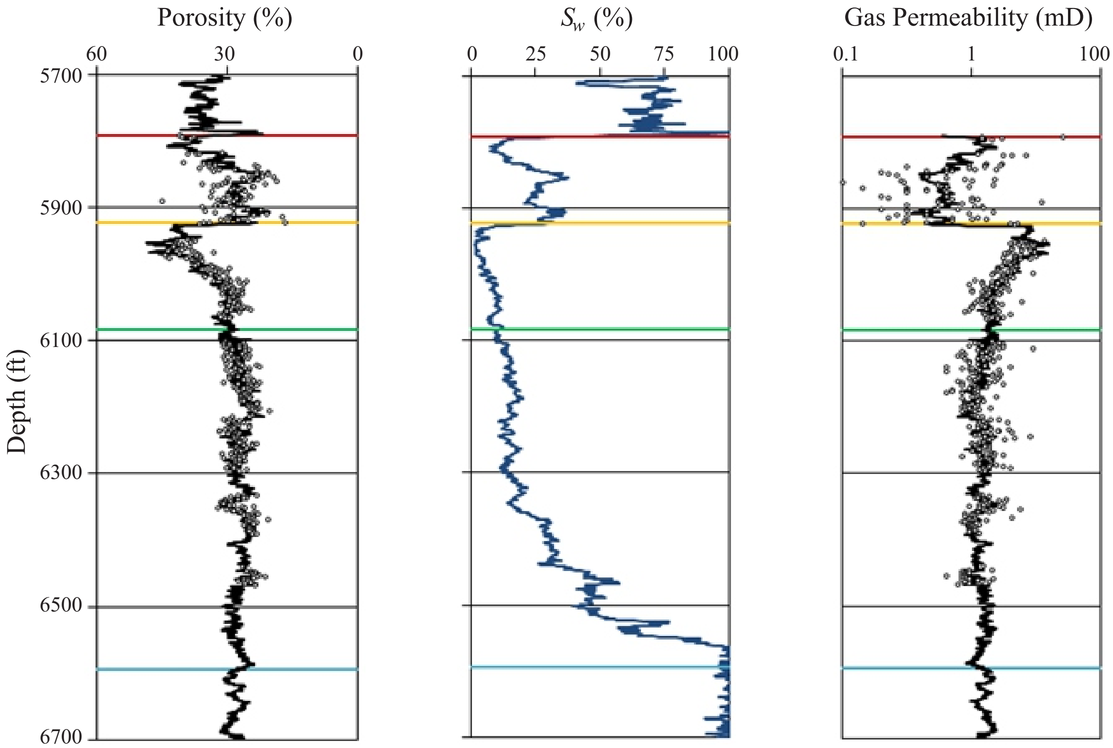

Figure 12.4: Interpreted logs: Porosity, water saturation, and permeability. Dan field M-1X. Circles represent He-porosity respectively Gas-permeability. Red line is top Ekofisk Formation, yellow line is top Tor Formation, green line is gas-oil contact, and blue line is oil-water contact (100% water saturation). In the Ekofisk Formation porosity is modelled as the average of density-porosity and neutron-porosity. In the Tor Formation, porosity is modelled directly as density-porosity. The water saturation was calculated by Archie's method by assuming that the interval below the supposed oil-water contact is 100% water saturated. Gas permeability was modelled from core data by (1) Calculate Klinkenberg permeability; (2) Calculate the average specific surface of solids for the Ekofisk Formation respectively the Tor Formation by using Kozeny's equation; (3) Using Kozeny's equation again to model Klinkenberg permeability from porosity and each of the two modelled specific surface of solids; (4) Convert from Klinkenberg permeability to gas permeability.

12.9 Capillary pressure

The capillary pressure, P_c, is defined as the difference between the pressure in the non-wetting phase and the pressure in the wetting phase. In water-wet chalk:

$$P_c = P_{hc} - P_w, \tag{12.13}$$

where for a given depth in a reservoir, P_{hc} can be obtained from the formation pressure log and P_w from extrapolation of the water zone pressure gradient. It should be noted that it is a precondition for two fluids being in equilibrium in the same pore space, that the pressure in each fluid is different.

Due to the lower density of hydrocarbons than of water, P_{hc} decreases less rapidly with distance above free water level (FWL, where $P_{hc} = P_w$) than P_w. For this reason, P_c increases with distance above free water level and more and more water is replaced by oil, so that S_w to a first approximation decreases with distance above FWL.

The relation between S_w and P_c is determined by the hydrocarbon-water surface tension, γ, porosity, ϕ, and fluid permeability, k; and was defined by Leverett (1941) as the J-function:

$$J(S_w) = P_c(S_w)(k/\phi)^{1/2}/\gamma. \tag{12.14}$$

The expression $(k/\phi)^{1/2}$ represents the radius of imaginary capillary tubes and can be understood as pore throat radius. Pore space in chalk is typically so homogeneous that $(\phi/k)^{\frac{1}{2}}$ is proportional to the specific surface of the chalk pore space, S/ϕ. It can now be understood that the relatively high water saturation found in some chalk intervals (typically in parts of the Ekofisk Formation, Fig. 12.4) is caused by high specific surface as a consequence of prevalence of tiny quartz and clay particles.

In spite of its simplicity, Leverett's J-function is not unique because the distribution of water and oil in the pore space is not defined. For this reason there is a marked hysteresis, and the relation between P_c and S_w is different under increasing water saturation (imbibition) than under decreasing water saturation (drainage). A typical capillary pressure curve **(Fig. 12.5)** can be described as: the chalk starts out being 100% water saturated, P_c increases and hydrocarbons are introduced in the pore space at a capillary entry pressure proportional to S/ϕ (Røgen and Fabricius 2002). In a homogeneous Tor Formation chalk, most of the pore space is then filled with oil under an only small increase in P_c, before the is met and P_c increases sharply causing only a small decrease in S_{wir}. In the less homogeneous chalk formations the relationship between P_c and S_w is more gradual. When the process is reversed and water is introduced, the hysteresis becomes obvious and S_w increases at a modest rate while P_c drops and consequently residual oil is left when $P_c = 0$ is met. The magnitude of S_{wir} depends on the specific surface of pore space, and a water film thickness can be defined (Larsen and Fabricius 2004).

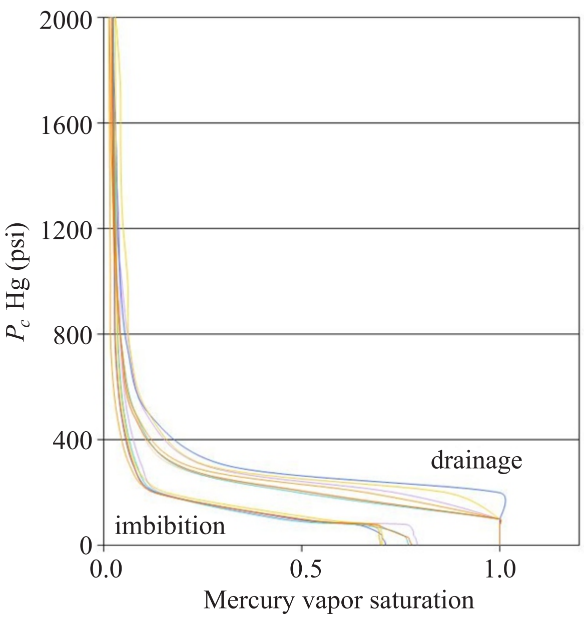

(a)

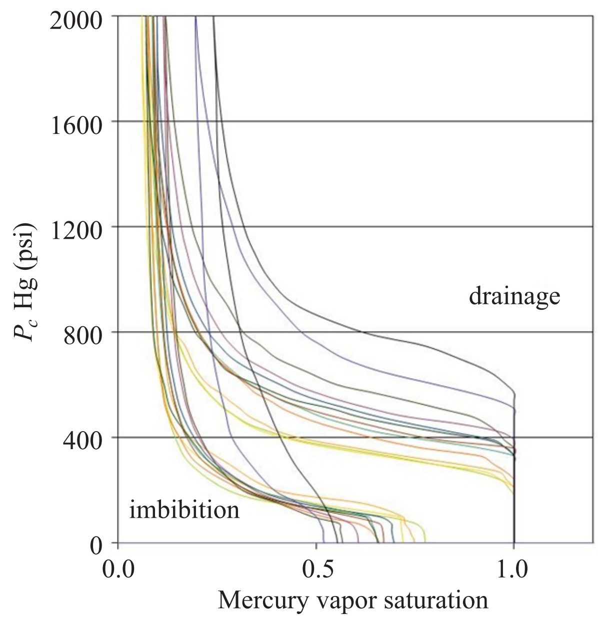

(b)

Figure 12.5: Mercury Capillary pressure curves from Tyra field. (a) Data from Maastrichtian chalk indicate high homogeneity. All curves follow same path and the low wetting phase irreducible saturation (c 0.02) indicate relatively low specific surface of pore space. (b) By contrast chalk from Ekofisk Formation is more variable. Data follows a range of paths and irreducible wetting fluid saturation ranges from 0.06 to 0.24 indicating higher and more variable specific surface of pore space.

Leverett's J-function is sometimes formulated where the denominator is a product between surface tension and cosinus of a contact angle, $\cos\theta$, between calcite, hydrocarbons and water, but in a water-wet chalk this contact is not to be found, and if wettability is mixed θ is ill defined. We expect that no big error is done by setting $\gamma \cos\theta = \gamma$.

An interesting property of Leverett's J-function is that if ϕ and k are given, the relation between P_c and S_w depends only on interfacial tension, so that if a capillary pressure curve is determined from one set of fluids, the capillary pressure curve can be modelled for another set of fluids. For this reason the capillary pressure curve is typically measured with mercury/mercury vapor (where the density contrast is very large and a relatively small experimental setup is needed) by so called mercury porosimetry, and the capillary pressure curve then recalculated for reservoir fluids.

12.10 Wettability

The wettability of chalk is a controversial issue in that some researchers assume that hydrocarbon bearing chalk is water-wet (Fabricius and Rana 2010) whereas other researchers assume that hydrocarbon bearing chalk is oil-wet (Austad and Standnes 2003). It should in this context be born in mind that calcite under reservoir conditions (high pH) typically is negatively charged and that polar hydrocarbons with functional groups can adsorb to the surface, so that a transition from water-wet to oil-wet is possible provided capillary pressure is high enough to render the irreducible water film very thin so that functional groups protruding from the oil phase can reach the mineral surface possibly via a cationic (Ca^{++}) bridge. The process is frequently assumed to be promoted by time, so that chalk samples for experiments with both water and oil in the pore space, typically are "aged" for some weeks before testing (Austad and Standnes 2003).

In the laboratory, three methods can give information on wettability:

Amott's method is based on the capillary behavior of chalk, and compares the saturations of oil and water during imbibition tests using porous plate (Amott 1959).

First a cleaned sample is saturated with water, and oil is intruded to irreducible water saturation, S_{wir}; then oil is produced and water imbibed to $P_c = 0$, and a water saturation of S_{spv}. Water saturation is now increased by forced imbibition to residual oil saturation, S_{or}, is reached, and oil subsequently reintroduced to $P_c = 0$ and an oil saturation of S_{spo} is reached. The Amott water index, I_w, and oil index I_o, can then be obtained:

$$I_w = \frac{(S_{spv} - S_{wir})}{(S_{or} - S_{wir})}, \tag{12.15}$$

$$I_o = \frac{(S_{or} - S_{spo})}{(S_{or} - S_{wir})}, \tag{12.16}$$

and the two indices combined to and Amott wettability index

$$AI = I_w - I_o. \tag{12.17}$$

The idea is that $S_{spv} - S_{wir}$ will be large and $S_{or} - S_{spo}$ small in a water-wet chalk; and vice versa. By this method chalk samples will typically get an AI in the range 0–1.0, corresponding to the neutral-wet or mixed-wet to water-wet. What the number signifies is a matter of discussion, but Strand, Hjuler et al. (2007) pointed to the latter option from comparison with data from flooding and ion exchange experiments. They also pointed out that only a small part of the internal surface needs to be oil-wet to obtain the typical AI. A mixed wet situation could arise from hydrocarbon adsorption a part of the specific surface. Madsen and Lind (1998) found evidence that it might be the silicate fraction of the surface.

Resistivity index, n, is expected to vary with wettability in the sense that a continuous water film covering the solids will give high connectivity and consequently low n (around $n = 2$); whereas an oil-wet situation causes a discontinuous water phase and consequent higher n.

The third method is based on **low field nuclear magnetic resonance spectrometry (NMR)** and could in principle also apply to logging data, although the method is not well established. The mechanism behind this method is that the hydrogen bearing fluid wetting the mineral has a fast surface-relaxation of the magnetic response, whereas the hydrogens of the non-wetting phase has a slow bulk relaxation of the magnetic response (Katika, Saidian et al. 2016).

In principle also the centrifuge based **USBM** wettability method could be used, but because the specifications of this standard method are based on the capillary behavior of permeable sandstone, **USBM** is not recommendable for chalk and is rarely used.

12.11 Specific surface.

The specific surface of a porous rock is the area of the internal surface and is together with porosity a key parameter defining the bulk reservoir properties of chalk. In the laboratory, the classical method for determining specific surface is N_2 adsorption BET (Brunauer, Emmett et al. 1938). Specific surface by BET is as a standard given with respect to solid mass (m^2/g), so for petrophysical use, it is recommended to recalculate BET to surface area per solid volume, S_s, bulk volume, S, or pore volume, S_ϕ:

$$S_s = \mathrm{BET}\,\rho_s \tag{12.18}$$

$$S = S_s(1-\phi) \tag{12.19}$$

$$S_\phi = S/\phi, \tag{12.20}$$

where ρ_s is grain density and ϕ is porosity.

In chalk, BET varies stratigraphically and with depth. The stratigraphic variation is due to varying amounts of nanoquartz and clay, whereas the depth-related change is caused by the temperature-controlled slow growth of calcite crystals (Fig. 7.2, Chapter 7). Some authors have discussed that the size of nanofossils as coccoliths might have an influence on specific surface (Hardman 1982), but the nanofossils is from a specific surface point of view an aggregate of crystals, and it is the size of the crystals, that controls the specific surface.

The surface relaxation time constant, T_2, of NMR is a measure of the specific surface of pore space, S_ϕ, so where surface relaxivity, ρ, of chalk is known the specific surface of water zone chalk can be calculated from an NMR log:

$$S_\phi = \rho / T_2 \tag{12.21}$$

The surface relaxivity, ρ, for chalk is not well established: From combining NMR and mercury porosimetry data for chalk plugs, a value of 23 μm/s was found by Liaw, Kulkarni et al. (1996), whereas a value of 2-3 μm/s was found by using BET and NMR on chalk powder (Alam, Katika et al. 2014).

The stratigraphic variation in S_ϕ is a primary reason for the stratigraphic variation in water saturation in a typical chalk hydrocarbon zone. S_{wir} becomes larger when there is more surface to be covered in a water-wet reservoir. For this reason a Sw-log can give an indication of specific surface (Fabricius and Rana 2010). S_ϕ not only is a major control on irreducible water saturation for a given P_c, it is also well correlated with the capillary entry pressure (Røgen and Fabricius 2002).

12.12 Permeability

Henry Darcy defined permeability to water from pressure drop, δP over a distance l, through a porous medium with cross sectional area, A. If the definition of permeability, k, is generalized to any Newtonian fluid (absolute permeability), fluid viscosity,ν, must be taken into account, and Darcy's law becomes:

$$Q = \frac{k \Delta P A}{\nu l}, \tag{12.22}$$

where Q is volumetric fluid production per time. In accordance with Poiseuille's law, liquid velocity at the fluid-solid interface is zero, so Darcy's law only applies to liquid permeability. In the case of the flow of a gas through a porous medium, the gas velocity at the gas-solid interface is larger than zero, so that a too high apparent "gas permeability", k_g will be measured. Permeability to gas is much cheaper and easier to measure than liquid permeability, so in order to find the absolute permeability from gas permeability data a Klinkenberg correction can be done by measuring gas permeability at three different average-pressures and extrapolate the measured gas permeabilities to infinite gas pressure. This is easiest done by inverting the numbers and extrapolating to zero. For chalk, the distance between measuring pressures is unfortunately relatively small as compared to the extrapolation, making this method uncertain, so it can be simpler and more accurate to use an empirical relation between gas permeability and absolute permeability (Mortensen, Engstrøm et al. 1998):

$$k = 0.52 k_g^{1.083}. \tag{12.23}$$

This pre-SI type formulation requires permeability to be in the units of mD. If permeability is given in square meters, the equation becomes:

$$.k = 9.15 k_g^{1.083} \tag{12.24}$$

When estimating permeability from logging data, simple correlations with porosity may be used, but a more precise prediction is obtained by using Kozeny's equation:

$$k = c\phi^3 / S^2 = c\phi^3 / (\mathrm{BET}^2 \rho_s^2 (1 - \phi^2)), \tag{12.25}$$

where c is the Kozeny's factor, which is close to 0.25, but for large and small porosities may be predicted from the porosity-based model of Mortensen, Engstrøm et al. (1998):

$$c = (4\cos(1/3 \arccos(\phi 64/\pi^{3\check{}} 1) + 4\pi/3) + 4)^{-1}. \tag{12.26}$$

When this information is unavailable, permeability can be estimated via a correlation with sonic log travel time, which may be more robust than a simple correlation with porosity (Alam, Fabricius et al. 2011). Alternatively, where both V_p, V_s, and porosity are available, permeability can be estimated from these properties (Fabricius, Baechle et al. 2007).

Prediction of permeability from NMR logging data has been attempted by using Coates equation (Coates, Xiao et al. 1999), but the formulation used by logging companies are not well suited for chalk, so it is recommended to rather use the formulation of Hossain, Grattoni et al. (2011):

$$k = c\phi\rho_2^2 \sum_{i=1}^{N} f_i (T_{2i})^2 \tag{12.27}$$

It should be noted that ρ must be assessed from representative core samples.

When pore space is narrow (k/ϕ is low) liquid permeability can be significantly lower than Klinkenberg-permeability. In this case prediction of liquid permeability, k_l, requires correction for the circa 5 nm thick immobile water film on the solid surface:

$$k_l = k\left(\frac{\phi - 5nm\sqrt{c\phi/k}}{\phi}\right). \tag{12.28}$$

12.13 Biot's coefficient and pore compressibility

Biots coefficient, α, is a measure of rock stiffness, where the effect of mineral stiffness, $K_{\min}$, is normalized out, so that it directly reflects the degree of contact cementation:

$$\alpha = 1 - K_{\text{dry}}/K_{\min}. \tag{12.29}$$

K_{dry} can be calculated or estimated from sonic and density logging data (see Chapter 3 on Rock Physics), $K_{\min}$ for calcite is c. 70 GPa, so α is simple to derive from logging data, and from α and porosity pore compressibility, C_f can be estimated by:

$$C_f = \alpha/(\phi K_{\text{dry}}). \tag{12.30}$$

It should be borne in mind though, that this purely elastic approach is not generally accepted, and that if plastic deformation is taking place, pore compressibility will be higher (Azeemuddin, Scott et al. 2001; Alam, Fabricius et al. 2012). Biot's coefficient is also needed for estimating effective stress for elastic deformation (see Section 12.3).

12.14 Heterogeneity effects

Chalk properties typically change gradually with degree of burial and consequent cementation, but they can fluctuate significantly with stratigraphy. Whereas specific surface of solids is relatively stable in a flow unit or formation in a given well, porosity can vary a lot depending on size distribution of sedimentary and diagenetic particles. For this reason the different sampling frequency of logging tools must be taken into account by a running averaging of the more frequently sampled data. This procedure unfortunately does not solve the heterogeneity problem because different tools do not sample the same volume of chalk, and thus include information from different ratios of the invaded zone and uninvaded zone (Frykman and Duetsch 2002). This must where possible be taken into account, for example by proper calibration with core data (Fig. 12.3). From a geostatistical study of logging and core data by calculating the Lorenz coefficient, Fitch, Davies et al. (2013) found that by contrast to the case for typical shallow carbonate reservoirs, reservoir quality of chalk deteriorates with increasing heterogeneity.

Nomenclature

a = constant
A = area, L^2
AI = Amott wettability index
c = Kozeny's factor
C_f = porosity pore compressibility, Lt^2/m
C_o = conductivity, tq^2/mL^3
C_w = conductivity of pore water, tq^2/mL^3
F = formation factor
g = acceleration og gravity, L/t^2
$h_{\log}$ = vertical depth to the top of the logged interval, L
I_o = Amott oil index
I_w = Amott water index
k = Klinkenberg permeability, permeability, L^2, mD
k_g = gas permeability, L^2, mD
k_l = liquid permabillity, L^2, mD
K_o = coefficient of lateral stress at rest
K_{dry} = drained bulk modulus, m/Lt^2

l = distance, L
m = cementation exponent
n = saturation exponent
P_c = capillary pressure, m/Lt^2, psi
P_{hc} = pressure in hydrocarbon phase, m/Lt^2
p_w = pressure in water phase, m/Lt^2
Q = volumetric fluid production per time, L^3
R_o = resistivity water zone, mL^3/tq^2, Ωm
R_t = resistivity of the chalk saturated with water and hydrocarbons, mL^3/tq^2, Ωm
R_w = resistivity water, mL^3/tq^2, Ωm
S = specific surface, saturation
S_{hc} = hydrocarbon saturation
S_{or} = residual oil saturation
S_{spv} = $S_w(P_c = 0)$ for imbibition
S_{spo} = $S_o(P_c = 0)$ for secondary drainage
S_w = water saturation
S_{wir} = irreducible water saturation, imbibition
t = circulation time, t
V = bulk volume, L^3
V_p = pore volume, L^3
V_p = P-wave velocity, L/t, m/s
V_s = solid volume, L^3
α = Biot's coefficient
α_g = lithology-dependent parameter
β_g = lithology-dependent parameter
γ = hydrocarbon-water surface tension, m/t^2
Δh = vertical interval between log data points, L, ft
ΔP = pressure gradient, m/Lt^2
Δt = time since circulation stopped, t
Δt = interval travel time, t
Δt_f = interval travel time for fluid, t, μs/m
Δt_g = interval travel time for mineral, t, μs/m
ε = elastic strain, L^2/t
θ = contact angle
ν = viscosity, L^2/t
ϕ = porosity
ϕ_d = porosity form density log
ϕ_n = porosity from neutron log
ρ = surface relaxivity
ρ_b = bulk density, m/L^3, g/cm^3
ρ_{av} = empirical average density, m/L^3, g/cm^3
ρ_f = fluid density, m/L^3, g/cm^3
ρ_{fl} = mass density of the movable fluid, m/L^3, g/cm^3
ρ_g = grain density, m/L^3, g/cm^3
ρ_s = grain density, m/L^3, g/cm^3
σ = normal stress, m/Lt^2
σ' = effective stress, m/Lt^2
σ_h = horizontal stress, m/Lt^2
σ_v = total vertical stress, m/Lt^2

Subscripts

av = average
b = bulk
c = capillary
d = density
dry = drained
f = fluid

fl = fluid
g = grain, gas, mineral
h = horizontal
hc = hydrocarbon
log = logged
n = neutron
o = oil
or = residual oil
p = pore
s = solid grain
t = true formation
v = vertical
w = water
wir = irreducible water

Abbreviations

API = American Petroleum Institute
BET = Brunauer-Emmet-Teller (specific apea measurement)
FIB = focused ion beam
FWl = free water level
GR = gamma ray
NMR = nuclear magnetic resonance
SCAL = special core analysis
SP = spontaneous potential
XRD = x-ray diffraction analysis
X-plots = crossplots

References

Abramovitz, T., Andersen, C. et al., 2010. 3D seismic mapping and porosity variation of intra-chalk units in the southern Danish North Sea. In *Petroleum Geology: From Mature Basins to New Frontiers—Proceedings of the 7th Petroleum Geology Conference*, 537–548. Geological Society of London. URL `http://dx.doi.org/10.1144/0070537`.

Alam, M., Katika, K., and Fabricius, I., 2014. Effect of Salinity and Specific Ions on Amount of Bound Water on Quartz, Calcite and Kaolinite, as Observed by NMR T2. In *Proceedings 76th EAGE Conference and Exhibition 2014*. EAGE Publications. URL `http://dx.doi.org/10.3997/2214-4609.20141013`.

Alam, M.M., Fabricius, I.L., and Christensen, H.F., 2012. Static and dynamic effective stress coefficient of chalk. *GEOPHYSICS*, **77** (2): L1–L11. March. URL `http://dx.doi.org/10.1190/geo2010-0414.1`.

Alam, M.M., Fabricius, I.L., and Prasad, M., 2011. Permeability prediction in chalks. *AAPG Bulletin*, **95** (11): 1991–2014. November. URL `http://dx.doi.org/10.1306/03011110172`.

Amott, E., 1959. Observations relating to the wettability of porous rock. *Society of Petroleum Engineers*, **216**. SPE-1167-G. URL `https://www.onepetro.org/general/SPE-1167-G`.

Archie, G., 1942. The Electrical Resistivity Log as an Aid in Determining Some Reservoir Characteristics. *Transactions of the AIME*, **146** (01): 54–62. SPE-942054-G. December. URL `http://dx.doi.org/10.2118/942054-g`.

Austad, T. and Standnes, D.C., 2003. Spontaneous imbibition of water into oil-wet carbonates. *Journal of Petroleum Science and Engineering*, **39** (3-4): 363–376. September. URL `http://dx.doi.org/10.1016/s0920-4105(03)00075-5`.

Azeemuddin, M., Scott, T.E. et al., 2001. Stress-Dependent Biot's Constant Through Dynamic Measurements On Ekofisk Chalk. In *DC Rocks 2001, The 38th US Symposium on Rock Mechanics (USRMS)*. American Rock Mechanics Association. 7–10 July. URL `https://www.onepetro.org/conference-paper/ARMA-01-1217`.

Batzle, M. and Wang, Z., 1992. Seismic properties of pore fluids. *GEOPHYSICS*, **57** (11): 1396–1408. November. URL `http://dx.doi.org/10.1190/1.1443207`.

Borre, M., Beales, V. et al., 2004. Fluid Substitution In Horizontal Chalk Wells And Its Effect On Acoustic Rock Properties? A Case Study Comparing Logging While Drilling And Wireline Acoustic Data. In *SPWLA 45th Annual Logging Symposium*. Society of Petrophysicists and Well-Log Analysts. SPWLA-2004-T. URL https://www.onepetro.org/conference-paper/SPWLA-2004-T.

Brindley, G.W. and Brown, G., eds., 1980. *Crystal structures of clay minerals and their X-ray identification*. Oxford Univ Press. URL http://dx.doi.org/10.1180/mono-5.

Brunauer, S., Emmett, P.H., and Teller, E., 1938. Adsorption of gases in multimolecular layers. *Journal of the American chemical society*, **60** (2): 309–319. February. URL http://dx.doi.org/10.1021/ja01269a023.

Clara, C., Zelenko, V. et al., 1998. Appraisal of the Horse Creek Air injection project performance. In *Abu Dhabi International Petroleum Exhibition and Conference*. Society of Petroleum Engineers. URL http://dx.doi.org/10.2118/49519-MS.

Coates, G.R., Xiao, L., and Prammer, M.G., 1999. *NMR logging: principles and applications*. Gulf Professional Publishing.

Dean, E.W. and Stark, D.D., 1920. A Convenient Method for the Determination of Water in Petroleum and Other Organic Emulsions. *Journal of Industrial & Engineering Chemistry*, **12** (5): 486–490. May. URL http://dx.doi.org/10.1021/ie50125a025.

Fabricius, I.L., Baechle, G. et al., 2007. Estimating permeability of carbonate rocks from porosity and $v_p?v_s$. *GEOPHYSICS*, **72** (5): E185–E191. September. URL http://dx.doi.org/10.1190/1.2756081.

Fabricius, I.L. and Rana, M.A., 2010. Tilting oil-water contact in the chalk of Tyra Field as interpreted from capillary pressure data. In *Geological Society, London, Petroleum Geology Conference series*, vol. 7, 463–472. Geological Society of London, Geological Society of London. URL http://dx.doi.org/10.1144/0070463.

Fitch, P., Davies, S. et al., 2013. Reservoir quality and reservoir heterogeneity: petrophysical application of the Lorenz coefficient. *Petrophysics*, **54** (05): 465–474. SPWLA-2013-v54n5-A5. October. URL https://www.onepetro.org/journal-paper/SPWLA-2013-v54n5-A5.

Frykman, P. and Duetsch, C.V., 2002. Practical application of geostatistical scaling laws for data integration. *PETROPHYSICS-HOUSTON*, **43** (3): 153–171. URL https://www.researchgate.net/profile/Peter_Frykman/publication/274955045_Practical_Application_of_Geostatistical_Scaling_Laws_for_Data_Integration/links/552d15070cf21acb09212b55.pdf.

Gardner, G.H.F., Gardner, L.W., and Gregory, A.R., 1974. FORMATION VELOCITY AND DENSITY—THE DIAGNOSTIC BASICS FOR STRATIGRAPHIC TRAPS. *GEOPHYSICS*, **39** (6): 770–780. December. URL http://dx.doi.org/10.1190/1.1440465.

Gommesen, L., Fabricius, I.L. et al., 2007. Elastic behaviour of North Sea chalk: A well-log study. *Geophysical Prospecting*, **55** (3): 307–322. May. URL http://dx.doi.org/10.1111/j.1365-2478.2007.00622.x.

Hardman, R.F.P., 1982. Chalk Reservoirs of the North Sea. *Bulletin of the Geological Society of Denmark*, **30** (3–4): 119–137. URL http://2dgf.dk/xpdf/bull30-03-04-119-137.pdf.

Hossain, Z., Grattoni, C.A. et al., 2011. Petrophysical properties of greensand as predicted from NMR measurements. *Petroleum Geoscience*, **17** (2): 111–125. April. URL http://dx.doi.org/10.1144/1354-079309-038.

Howard, J.J., Fidan, M. et al., 1999. Water saturation breakthrough intervals, Ekofisk Field, Norway. In *Society of Professional Well Log Analysts 40th Annual Logging Symposium*, vol. 30. SPWLA-1999-LL. 30 May – 3 June. URL https://www.onepetro.org/conference-paper/SPWLA-1999-LL.

Japsen, P., 1998. Regional velocity-depth anomalies, North Sea Chalk: a record of overpressure and Neogene uplift and erosion. *AAPG bulletin*, **82** (11): 2031–2074. URL http://dx.doi.org/10.1306/00aa7bda-1730-11d7-8645000102c1865d.

Katika, K., Saidian, M., and Fabricius, I.L., 2016. Wettability of chalk and argillaceous sandstones assessed from T1/T2 ratio. In *78th EAGE Conference and Exhibition 2016*. URL http://www.earthdoc.org/publication/publicationdetails/?publication=85130.

Kristensen, L., Dons, T. et al., 1995. A multidisciplinary approach to reservoir subdivision of the Maastrichtian chalk in the Dan Field, Danish North Sea. *AAPG bulletin*, **79** (11): 1650–1659. URL http://dx.doi.org/10.1306/7834de40-1721-11d7-8645000102c1865d.

Larsen, J.K. and Fabricius, I.L., 2004. Interpretation of water saturation above the transitional zone in chalk reservoirs. *SPE Reservoir Evaluation & Engineering*, **7** (02): 155–163. SPE-69685-PA. April. URL http://dx.doi.org/10.2118/69685-PA.

Leverett, M., 1941. Capillary Behavior in Porous Solids. *Transactions of the AIME*, **142** (01): 152–169. SPE-941152-G. December. URL http://dx.doi.org/10.2118/941152-g.

Liaw, H.K., Kulkarni, R. et al., 1996. Characterization of fluid distributions in porous media by NMR techniques. *AIChE Journal*, **42** (2): 538–546. February. URL http://dx.doi.org/10.1002/aic.690420223.

Madsen, L. and Lind, I., 1998. Adsorption of carboxylic acids on reservoir minerals from organic and aqueous phase. *SPE Reservoir Evaluation & Engineering*, **1** (01): 47–51. SPE-37292-PA. February. URL http://dx.doi.org/10.2118/37292-PA.

Mortensen, J., Engstrøm, F., and Lind, I., 1998. The relation among porosity, permeability, and specific surface of chalk from the Gorm field, Danish North Sea. *SPE Reservoir Evaluation & Engineering*, **1** (03): 245–251. SPE-31062-PA. June. URL http://dx.doi.org/10.2118/31062-PA.

Olsen, C., Hongdul, T., and Lykke Fabricius, I., 2008. Prediction of Archie's cementation factor from porosity and permeability through specific surface. *Geophysics*, **73** (2): E81–E87. March. URL http://dx.doi.org/10.1190/1.2837303.

Reppert, M.G., Akkurt, R. et al., 2006. Porosity and water saturation from LWD NMR in a North Sea chalk formation. *Petrophysics*, **47** (05). SPWLA-2006-v47n5a2. October. URL https://www.onepetro.org/journal-paper/SPWLA-2006-v47n5a2.

Revil, A., Linde, N. et al., 2007. Electrokinetic coupling in unsaturated porous media. *Journal of Colloid and Interface Science*, **313** (1): 315–327. September. URL http://dx.doi.org/10.1016/j.jcis.2007.03.037.

Røgen, B. and Fabricius, I.L., 2002. Influence of clay and silica on permeability and capillary entry pressure of chalk reservoirs in the North Sea. *Petroleum Geoscience*, **8** (3): 287–293. September. URL http://dx.doi.org/10.1144/petgeo.8.3.287.

Strand, S., Hjuler, M.L. et al., 2007. Wettability of chalk: impact of silica, clay content and mechanical properties. *Petroleum Geoscience*, **13** (1): 69–80. February. URL http://dx.doi.org/10.1144/1354-079305-696.

Wyllie, M.R.J., Gregory, A.R., and Gardner, L.W., 1956. ELASTIC WAVE VELOCITIES IN HETEROGENEOUS AND POROUS MEDIA. *GEOPHYSICS*, **21** (1): 41–70. January. URL http://dx.doi.org/10.1190/1.1438217.

Chapter 13

Reservoir Modeling

Henrik Olsen, Dimitrios Georgios Hatzignatiou and Ole Jørgensen

13.1 Abstract

Dynamic modelling of chalk reservoirs has been a natural element of development activities for the North Sea Chalk fields since these were first discovered and developed in the 1960's and 70's.

This section of the Monograph discusses some of the main aspects related to modelling of fluid flow and oil recovery processes of typical chalk field developments. Most of these processes can be handled adequately by commercial reservoir simulation software packages. Reference is made to a well-written overview of key principles of numericalmodeling, most of which also applies to commercial simulators used when simulating chalk reservoirs (Skjæveland and Kleppe 1992).

The authors wish to prioritise elements of simulation that are distinctly linked to chalk characteristics. The petrophysical properties of chalk (tightness, capillary pressure, relative permeability characteristics) have strong implications on (a) the definition of initial reservoir conditions, (b) how "simulation models are set up, (c) history matching and reservoir dynamics, and (d) designing and implementing an effective water flood strategy. The last point, water injection strategy, also has to include an element of poro-elasticity modelling because stresses are altered during production and injection, and because deliberate fracturing can be invoked for efficient pressure maintenance. This particular sub-item is less well understood in the industry, e.g., the physical causalities that make water injection under fracturing conditions a sound strategy in many chalk fields. It is seen as a natural opportunity to include such chalk specific aspects in this Monograph, while at the same time demonstrate the simplicity of reservoir simulation as a powerful tool to integrate data and concepts from multiple disciplines to stimulate physical intuition and reasoning.

In view of this, the contents of this chapter will focus on few key aspects related to the numerical modeling of North Sea Chalk formations. Topics selected include simulation model choice, model setup, drive mechanisms, and well completions. Furthermore, two examples are provided to illustrate how dynamic models for chalk fields can be used for (a) diagnostics and explanation of reservoir observations to improve understanding and reduce uncertainty in the field and (b) explore reservoir characteristics to guide choice and design of reservoir exploitation strategy.

Some of the chalk fields are naturally fractured and require different modelling approaches. Fractured reservoirs have received a lot of attention in the research communities, so an Appendix 13.A on page 203 is included which provides a literature survey on aspects related to naturally fractured reservoirs (NFRs) including characterization, modeling, upscaling, multiphase flow modeling, and geomechanics.

Finally, Appendix 13.B on page 207 provides further details on the geomechanical considerations related specifically to water injection with high pressure gradients in the tight chalk formations. In conclusion, this chapter is not meant to fully cover reservoir simulation or geomechanics modelling, but focus has been placed on key aspects that distinctly point back to chalk characteristics and the modelling considerations around these.

13.2 Modelling objectives

A key objective of dynamic reservoir modelling, also referred to as reservoir simulation, is to integrate formation, fluids and development data to evaluate the dynamic behavior of the combined system. As the simulation model is built to incorporate the anticipated drive and communication elements, it also serves to characterise the reservoir by comparing observed dynamic data to model output, thereby improving the understanding of the chalk characteristics and reducing uncertainty of key reservoir parameters. Field development support is another key modelling objective, provided a sound reservoir model and appropriate uncertainty definitions could be obtained.

Aiming at reservoir simulation, we are in particular keen on understanding the spatial distribution of porosity, permeability and capillarity/saturation. Coccolith chalk is in a class of its own when it comes to petrophysical properties. Wireline logs and core analysis provide quantitative measurements of petrophysical parameters on the 0.01 m to 1 m length scale, and integration of these data with a geological model gives the three dimensional distribution of properties, which is the goal of the static reservoir characterization. Parameters such as porosity and permeability are effective media properties, and as such they include an underlying statement of homogeneity. To this end, we note that homogeneity is not an absolute characteristic of matter, but a term applicable to properties averaged over a suitable volume. Hence, the term homogeneity indirectly implies a scale element.

In reservoir simulation, several scales can be considered depending on the phenomena under consideration. Typically, the critical linear dimension to resolve in the lateral direction relates to the distance between wells, size of any gas cap present, extent of the hydrocarbon accumulation, etc. In the vertical direction, reservoir height, hydrocarbon-leg height, thickness of reservoir sub units and the subdivision required to resolve saturations in the transition zone, affect the linear dimension we seek to resolve in simulation. Summarizing, an important objective of reservoir simulation studies is to provide a means of reservoir characterization on the kilometre scale and down to the height of the thinnest characteristic sub-unit, which is typically around a few feet for chalk reservoirs.

13.3 Choice of simulation model

Commercial black-oil reservoir simulation packages are generally three phase, three-dimensional modelling tools, which solve for pressures and saturations using finite difference or similar formulation schemes. The models offer a number of features to supplement the basic functionalities to support more advanced modelling related to reservoir type (e.g., naturally fractured, geomechanics), reservoir processes (thermal, tracer tracking, EOR processes) or development types (networks, segmented well models).

For chalk reservoirs, the matrix properties often lead to thick transition zones and tilting contacts reflecting very slow equilibration processes. This calls for options to cater for drainage/imbibition modelling in conjunction with options to enable model initialization in the absence of static equilibrium. Fields with natural fractures are often simulated with dual porosity/permeability models to account for the beneficial imbibition process between fractures and matrix resulting from the predominantly water-wet chalk.

In some chalk fields, the development relies on deliberate initiation and propagation of water injection fractures to improve reservoir contact. For such fields a simulation approach must be chosen that can answer critical questions pertaining to steering and planning of water injection fractures. Modelling of stress and the theory of elasticity become parts of the simulation objective, either as embedded elements in coupled geomechanical flow simulations, or as separate geomechanical evaluations appended to conventional flow simulations.

Streamline simulation models are mostly defined with reduced physics formulations to enable faster run times. The limitations of these models - in particular those related to capillarity representation - often exclude them for modelling tight chalk reservoirs.

13.4 Key modelling elements

13.4.1 Model setup

Tilting oil-water contacts (OWC) and transitional zones that are not in line with drainage processes are normally observed in low permeability chalk formations, which are generally characterized by high entry capillary pressures and large oil-water transition zones (Bech, Frykman et al. 2007). Albrechtsen, Andersen et al. (2001) reported EW tilted oil-water and gas-oil contacts across the Halfdan area as indicative of non-equilibrium conditions. The non-structural trapping was a combination of updip thinning of the hydrocarbon bearing section, late structural tilting, and slow re-adjustment caused by the low permeability. The authors discussed the mechanisms for oil trapping in the Halfdan area outside structural closure, the application of saturation modelling in the assessment of hydrocarbon in place, and how to handle the uncertainty associated with the complex fluid distribution.

Development of a robust static model and estimation of oil-in-place in such formations dictate information on reservoir history, capillary pressure behavior description, and Free Water Level (FWL) data. FWL is typically non-horizontal and FWL gradients of more than 100 m/km have been observed in the North Sea (Bech, Frykman et al. 2007). Bech, Frykman et al. (2005) presented a method for modeling initial saturations along vertical wells in two-phase water-wet reservoirs having a large transition zone and being in imbibition equilibrium. The authors stated that oil accumulations are formed through a drainage process resulting in a drainage equilibrium saturation distribution and a paleo FWL. In reservoirs that are not in drainage equilibrium, water influx affects fluids saturations indicated by frequently observed residual oil zones; water influx can also be the consequence of a burial and/or tectonic event. The new saturation distribution is therefore a result of both drainage and imbibition and cannot be described by a drainage equilibrium model. This methodology was applied by Bech, Frykman et al. (2007) to describe a technique, based on existing empirical drainage and imbibition capillary pressure correlations, for determining the FWL in low-permeability chalk reservoirs along slanted or horizontal wells from logged saturations and porosities. The method takes into account possible imbibition, which results in a FWL that is shallower than the original paleo FWL, and it was applied to North Sea Oilfield to demonstrate that it can capture a tilting FWL along a horizontal well.

Another implication of the low permeability chalk is frequently found in fluid property variations across the field, even without compartmentalization within the field. The oil fields typically display higher bubble point pressures at the crest while significant undersaturation can occur on the flank.

Tilting contacts and varying fluid properties can be modelled in commercial simulators, constructed with the mindset that "all fluid contacts are horizontal", by discretizing the contacts and e.g. bubble point pressure distribution using small discretization steps, thereby mimicking the varying properties by stair-stepping these variations across the field. This approach can lead to thousands of equilibration regions which serve to initialize the simulator to a non-equilibrium condition as observed in the field. The tilting contacts essentially represent flow of water and/or oil phases corresponding to a lateral pressure variation in the corresponding phase, in the order of 2–3 psi per 1000 feet. Once production wells are switched on in the model, the pressure gradients resulting from imposed drawdowns exceed the natural pressure gradients by several orders of magnitude, so the inherent non-equilibrium generally does not cause any problems in the simulator.

Solution gas drive is often a key drive mechanism in tight reservoirs, especially those with low compaction drive, since flank and bottom aquifers fail to keep up with depletion due to the low matrix permeability. The strength of the solution gas drive is directly related to the degree of undersaturation, which is why a rigorous modelling of bubble point pressure distribution can be essential for fields undergoing primary depletion. The multi-region equilibration technique applied for modelling of the tilting contacts is also well suited for this aspect.

Capillary pressure curves can be normalized into just a few shape curves representing different rock types or subunits. Since most chalk fields display long transition zones these reservoirs require extra attention to relative permeability characteristics, as the residual oil saturations and other relative permeability data are not just a function of porosity and rock type, but also depend strongly on the filling state and history of the reservoir. Transition zones have only been partly filled and have only experienced a partial drainage process. Therefore, the residual oil saturation to water flood varies down through the transition zone, and this phenomenon needs to be incorporated into the simulation model. End-point scaling and application of hysteresis models are useful features available to support modelling of these aspects.

13.4.2 Fractured reservoirs

Some of the chalk oil fields in the North Sea are naturally fractured reservoirs (NFR) with interplay between low permeabilities in the matrix and high permeabilities in the fracture system. Oil production in NFRs can be challenging due to large matrix/fracture transmissibility contrasts, which can lead to low primary recovery factors. Other fields can actually obtain very high primary recoveries resulting from an efficient imbibition process in the water-wet chalk associated with inflow of aquifer water into the fracture system.

Traditionally, the models used to describe NFRs can be classified into two main groups: the dual porosity (DP) and dual permeability (DK). The former, which are further subdivided into standard dual-porosity model (SDP), multiple interacting continua model (MINC), and vertical refinement model (VR), assume that the fracture network is the primary continuum for fluid flow (CMG, 2010). Difficulties in history matching NFR field behavior or desire for more detailed simulations has led to the development of alternative, more realistic models such as the discrete fracture network (DFN) and discrete fracture and matrix (DFM) models.

Discrete fracture network (DFN) flow modeling relies on 3D spatial mapping of fracture planes used to construct a network of interconnected fractures. Unstructured grids DFN are effective models for capturing fracture connectivity and scale dependent heterogeneity in NFRs compared to traditional dual continuum models

(Dershowitz and Miller 1995; Kiraly and Morel 1976; Dershowitz, LaPointe et al. 2000). DFN modeling can be employed to increase geological prior knowledge and therefore produce more geologically consistent models (Elfeel, Jamal et al. 2013).

Traditionally, the fracture domain relative permeability curves used in reservoir simulation are linearly proportional to the phase saturations, which result in the well-known x-shape relationships, essentially reflecting vertical phase separation in the fracture system. Several researchers found that this type of relative permeability curves is not fully correct, especially when addressing multiphase flow behavior in non-smooth fractures (Fourar, Bories et al. 1993; Nicholl and Glass 1994; Persoff and Pruess 1995).

Additional details on characterization and modelling of fractured reservoirs can be found in a comprehensive literature survey in Appendix 13.A.

13.4.3 Drive mechanisms

Many chalk fields developments have initially relied on the natural reservoir drive mechanisms, i.e., primary recovery process. Some chalk reservoirs having a very high porosity ($\sim$50%) have exhibited a substantial compaction, but in most fields the compaction drive is only modest such that fluid expansion may represent the dominating natural drive mechanisms. While compaction drive can provide very high recovery factors (20 to 40%) in a few fields, the majority of chalk fields can only yield primary recovery factors in the region of 5% to 10%.

Fluid expansion drive and compaction drive for low compressibility rocks are readily modelled in standard simulation software, whereas formations exhibiting heavy compaction require special attention. A simple implementation could apply tabulated pore volume and permeability modifiers on a region basis, but fields with strong rock deformation effects require support from, or even direct links to, geomechanical models. A natural consequence of the low primary recovery potential is to implement a secondary recovery scheme to boost oil recovery rates and ultimate recovery factors. Drilling and completion technology development now allows for long horizontal wells, which provide significant benefits from the increased reservoir contact compared to vertical or slanted wells, thereby draining much larger reservoir sections. Close well spacing and large pressure gradients between injectors and producers are required to sweep out the mobile oil within a reasonable time scale, e.g., 20 to 30 years. The impact of water injection in terms of pressure and saturation changes can be monitored by performing 4D seismic surveys.

A general 4D workflow, linking static and dynamic models along with the geomechanical model and time lapse seismic analysis, was applied by Gommesen, Dons et al. (2007) in the Dan oil reservoir. The authors presented field examples, which demonstrate (a) changes of the chalk reservoir formation due to the oil production and water injection captured by time lapse seismic; injected water into oil-bearing chalk formation yields hardening effects, whereas dissolved gas evolution results into softening effects; (b) changes in AVO response, which can be used to identify water induced fractures; and (c) pressure and compaction alterations observed in two-way travel time. Henriksen, Gommesen et al. (2009) discussed the use of optimized elastic inversion, which allowed the mapping of the continuous chalk reservoir and the base of the overburden shales through the use of the v_p/v_s ratio. This yielded improved placement of the long horizontal, multilateral wells for the development of the thin Halfdan NE chalk gas field. Similarly, Gommesen and Hansen (2012) provided practical insights, through examples, on how rock physics can support both short- and long-term development and production of chalk fields. Dons, Jørgensen et al. (2007) demonstrated a strong seismic response due to water injection in the Halfdan chalk oilfield. It was concluded that the fact that the injection signatures form parallel lines, which on the one hand align with injectors and on the other hand extend beyond the well and completion intervals, proves that the stress field generated by the well pattern controls injection fracture propagation.

Classical reservoir simulation does not predict acoustic impedance directly but modelling the underlying physical processes resulting in changes of saturations and pressures forms the basis for derivation of synthetic impedance evaluations such that the 4D responses can be used to validate and refine the reservoir models.

13.4.4 Well completions

Both production and injection wells for chalk fields are designed for increased reservoir contact associated either with the length of the horizontal sections or through acid or fracture stimulation.

Simulation models rely on well inflow models, which provide connection factors between a well and the intersected grid blocks in which the well has been perforated. Peaceman type inflow correlations Peaceman (1978) designed for radial inflow are adequate for both vertical and horizontal wells, provided the well stimulation effect does not extend outside the intersected grid blocks.

Hydraulically fractured wells pose special challenges to model the increased reservoir contact associated with the hydraulic fracture lengths. Static (e.g., sand propped) hydraulic fractures often have fracture half-lengths of 100 to 200 ft, meaning that they can extend several gridblocks away from the actual wellbore grid location. Local grid refinement (LGR) can be a solution to account for the high conductivity and narrow geometry of the induced fractures, particularly in models with only a limited number of fractures. In fields with several hundred hydraulic fractures, the LGR approach becomes impractical, so the hydraulic fractures are best modelled by adding well connections corresponding to all grid block cells which are traversed by the given fracture geometry. Note that the radial inflow PI derived from Peaceman equations are not applicable for inflow to a large fracture plane, so the connection factors have to be corrected to represent linear rather than radial flow.

13.5 Model support for reservoir diagnostics and choice of oil recovery strategy

History matching can provide the means of quantifying uncertainties related to static or dynamic properties, especially when integrated with 4D seismic surveys, and validating and/or improving an existing reservoir model. Effectiveness and quality of a history matching process are key to enable field predictions and design of appropriate field (re)development or well intervention plans for maximizing oil recovery factors. The main parameters for history matching chalk fields are wells productivity, calibration of reservoir drives, sustainability of fluid flow rates, amount and distribution of residual oil, breakthrough time of injected fluids, and oil recovery factor versus time (Matthäi and Nick 2009).

In NFRs, history matching results depend on reservoir geological model and reservoir (fracture and matrix) properties; uncertainties related to geological model are also affected by DFN upscaling errors (Elfeel, Jamal et al. 2013) since it provides information required for reservoir simulation and history matching. Results obtained in an onshore oil reservoir showed that various upscaling methods of the same DFN model yield different permeability fields even though the quality of the history matching was similar. The authors stated that DFN upscaling can enrich prior knowledge and assist in the development of more geologically consistent simulation models. They concluded that original DFN properties (fracture intensity, aperture, orientation) used in history matching should reserve geological consistency of the fracture model.

The following two subsections will present some practical cases to demonstrate the use of reservoir modelling as a tool to apply dynamic data for improving reservoir characterisation and understanding of key aspects of operating chalk fields. The reservoir models used in these examples were built along the lines discussed in previous sections to ensure rigorous integration and quantification of the individual drive and flow processes affecting field performance.

13.5.1 Reservoir diagnostics - primary drive mechanisms

The Dan field is a low permeability reservoir with matrix permeability in the order of 1 mD and comprising non- or mildly fractured chalk. The field was discovered in a state of an ongoing active migration; regional pressure gradients and tilted fluid contacts (oil/water, gas/oil) were clear proofs of active fluids migration. In the early 1990s the initial regional pressure distribution had been overlain by strong local pressure variations due to primary production; from the existing records of these pressure variations we can deduce information about the field dynamics when analysed with reservoir simulation models.

The Dan field is a dome-shaped structure with an oil column of six hundred feet at its thickest point, and overlain by up to two hundred fifty feet of gas; hence, free gas was present together with oil and water from the start of production, and until 1995 the predominant recovery mechanism was due to gas cap expansion and solution gas drive. The three fluid phases responded differently to pressure depletion, and significant lateral variations in formation pressure were developed due to differences in fluid compressibility and mobility.

The period from start of production in 1972–1995 provides an example of dynamic characterization using flow simulation. Reservoir pressure declined monotonically during this period, water injection was initiated, albeit at first only on a trial basis, and the period is therefore, from a reservoir dynamics point of view, considered as the Dan Field's primary production period.

The 1991 and 1995 development plans included long horizontal wells drilled in a radial pattern from the crest of the field. Formation pressures recorded in these wells have provided invaluable insights with regard to characterizing pressure communication and the overall field dynamics in the Dan field.

Pressures obtained along horizontal wells drilled from below the gas cap and extending beyond the GOC outline and further into the flank of the oil accumulation, revealed substantial lateral pressure gradients in the field, **Figs. 13.1 and 13.2.**

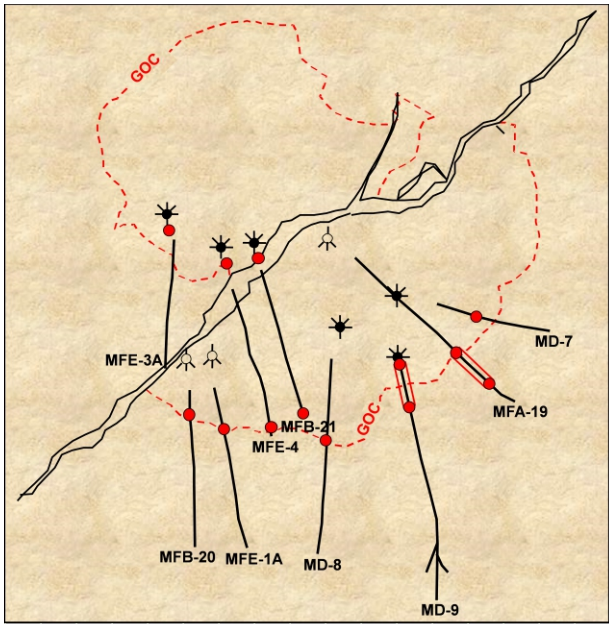

Figure 13.1: Nine infill wells drilled in the early- to mid-1990s showed distinct pressure minima (red dots) that could be correlated with the contour of the gas cap (GOC red stipulated line).

Fig 13.1 shows nine wells drilled in the early 1990's at infill positions between two producers (not shown). For the sake of simplicity, the full development as of 1990's is also not shown on the figure. Formation pressures recorded in these wells demonstrate the reservoir dynamics of Dan under pressure depletion. In all nine wells, formation pressures were recorded along the full horizontal sections, and the local pressure minima along each well are indicated with a red dot on the map.

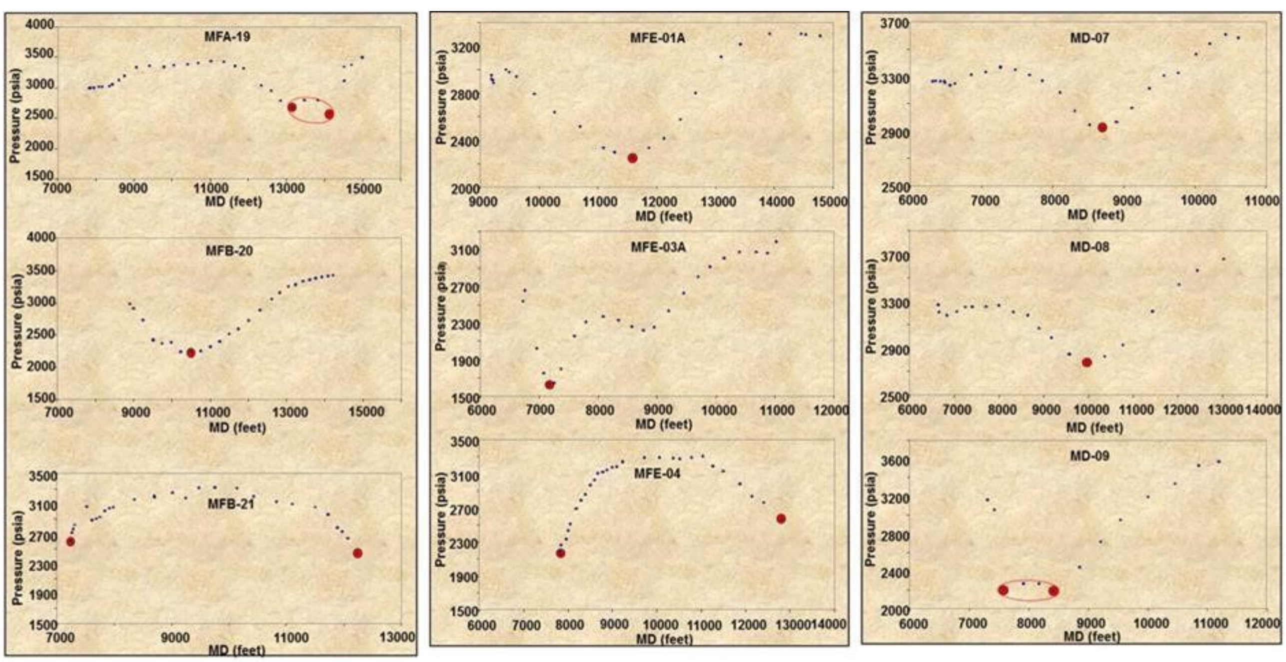

Figure 13.2: Formation pressure data recorded in nine infill wells drilled in the early- to mid-1990s in the Dan Field. Distinct pressure minima are indicated by red dots and the red dots are shown in map view in Fig. 13.1 in order to prove that the minima can be correlated with the contour of the gas cap (compare Fig 13.1).

The measured pressures versus depth in each well are shown in Fig. 13.2, where pressure variations of 1,000–2,000 psia along the respective horizontal sections, of typically 4,000 ft of length, are seen. The variation along these wells follow a general pattern: formation pressures recorded at the crest, where the gas column is thickest, are all around 3,000 psia, reflecting the gas cap pressure at the time of drilling. A significant lowering of the pressure follows as the wells approach the edge of the gas cap; further down dip, towards the flank of the field, pressure increases towards levels around 3,500 psia, which was the flank pressure at the time of drilling.

The pressure lows, which coincide with the outline of the GOC, Fig 13.1, may seem at first peculiar, but analysis of the interplay between drive and mobility in detailed numerical models built for the area provides the explanation and understanding of these observations. Such simulations demonstrate that in tight 1 mD chalk, pressure minima occur when a thin accumulation of attic gas, such as characterizes the zone where the free gas pinches out, is blown off. The local pressure drop occurs because the gas mobility is very high compared to that of oil and water, and it occurs where the attic gas volume per area is not large enough to sustain pressure, i.e., along the GOC contour. The low permeability is an important element in this explanation; the low permeability in the vertical direction delays the pressure equilibration. Hence, expansion of the oil underneath the gas - and expansion of water underneath the oil - cannot prevent the pressure drop in the high mobility gas phase. Laterally, the low permeability also prevents the shallow gas along the periphery of the gas cap from equilibrating with the greater gas cap. Hence, the modelled GOC outline, the volumes in place and the permeability in the reservoir column are all critical to achieving a history match of measured reservoir pressures. Due to this particular sensitivity, the recorded pressure variations in the nine infill wells Fig. 13.2 supplement key data for permeability characterization but they also provide an independent calibration source for the extent of the gas cap in the field. These findings come from a successful modelling effort where irregular and unexpected observations are fully explained through appropriate modelling of the reservoir responses, which differ across the field due to reservoir properties and configuration and initial fluid distribution.

13.5.2 Choice of oil recovery strategy - secondary drive mechanisms

Within the scope of describing the recent history of reservoir simulation and chalk fields, some areas which are distinguishing marks or trait related to the matrix properties of chalk and North Sea developments will be prioritized. One is the fluid compressibility and mobility phenomena discussed in the previous example and their effect on depletion dynamics; another is the whole prospect of water flooding. Pressure maintenance and displacement of oil with water are the two main objectives of water flooding. Due to the inherent wettability and relative permeability characteristics of chalks, the endpoint mobility ratio for oil displacement by water is favourable. This, together with constraints on flowing bottomhole pressures in wells, means that a water injector typically requires a larger reservoir contact area than its producing counterpart in order to balance the offtake. This is the key reason for pursuing injection above fracture propagation pressures. The tightness of the chalk matrix means that fracturing can be accommodated without causing short-circuiting. An example from the Halfdan field is used to demonstrate this observation.

The Halfdan field initial pressure was around 4,200 psia at a depth of ca. 6,900 ft below seabed. The upper bound on injection pressure was approximately 5,000–5,500 psia (fracturing pressure at initial conditions) and the producing bottomhole pressure was in the order of 1,000–1,500 psia depending on the watercut, GOR and lifting conditions. Hence, operating conditions involve large pressure differentials between wells. These pressure differentials in the fluid phase exert loading of the rock. Apart from the pressure differential between producer and injector, the geometry of the flow pattern determines this loading. This can be illustrated by considering a linear variation of pressure in a cross sectional strip of height, h, and well spacing, L, **Fig. 13.3.**

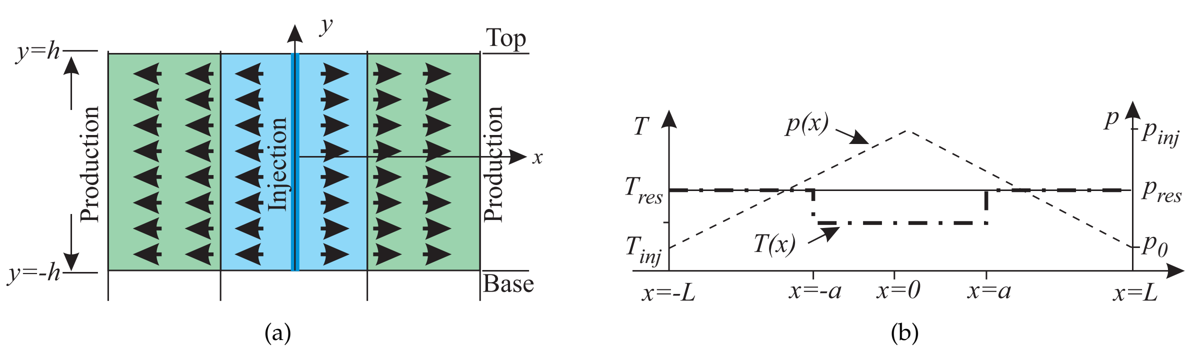

Figure 13.3: a) linear displacement of oil with water in cross-section; b) cooling and pressure gradients exert loading of the frame.

Everywhere in the strip, the local pressure gradients in the fluid phase are balanced by volume forces in the rock frame, (b_x, b_y, b_z), which are opposite in sign, and are defined as:

$$b_x = -\alpha\frac{\partial p}{\partial x}; \;\; b_y = -\alpha\frac{\partial p}{\partial y}; \;\; b_z = -\alpha\frac{\partial p}{\partial x} \tag{13.1}$$

In Eq. 13.1, p is the pore pressure, α denotes Biot's coefficient, b is a volume force and (x, y, z) are co-ordinates in a Cartesian co-ordinate system. Measurements on chalk with 25 % or higher porosity show that Biot's coefficient attains values in the range of 0.9–1.0, i.e., Biot's coefficient is close to unity in most chalk reservoir rock. This means that a variation in porosity caused by a variation in pressure is insignificant, which also implies that the fluid flow and elasticity problems can be decoupled. Hence, conventional reservoir simulators, such as for instance Eclipse, can be used for the flow and fluid pressure analysis, and the elasticity analysis can be carried out in parallel. In the present case the solution for stress on the symmetry plane $(x = 0; -h < y < h)$ shown in Fig. 13.3 can be derived analytically in three steps see Appendix 13.B. From the solution it may be seen that stress on the centre plane depends on pressure difference between injector and producer, on well spacing, on height of the strip, on thermal expansion, and on the elastic parameters of the rock.

In the following, we will apply parameters reflecting the Halfdan field conditions. That is thermal expansion coefficient, $\beta = 8 \times 10^{-6}$ $(°C)^{-1}$, Young's modulus, $E = 1.1 \times 10^6$ psi, and Poisson's ratio, $\nu = 0.2$. For well spacing $L = 600$ ft, producing bottomhole pressure, $p_p = 1,500$ psia, injection pressure, $p_{\text{inj}} = 5,000$ psia, initial pressure, $p_0 = 4,200$ psia, and formation cooling by 60 °C have been used. For these values, the effective stress distribution at the centre cross section can be calculated for $h/L = 1/24, 1/12, 1/8, 1/6$ **(Fig. 13.4)**.

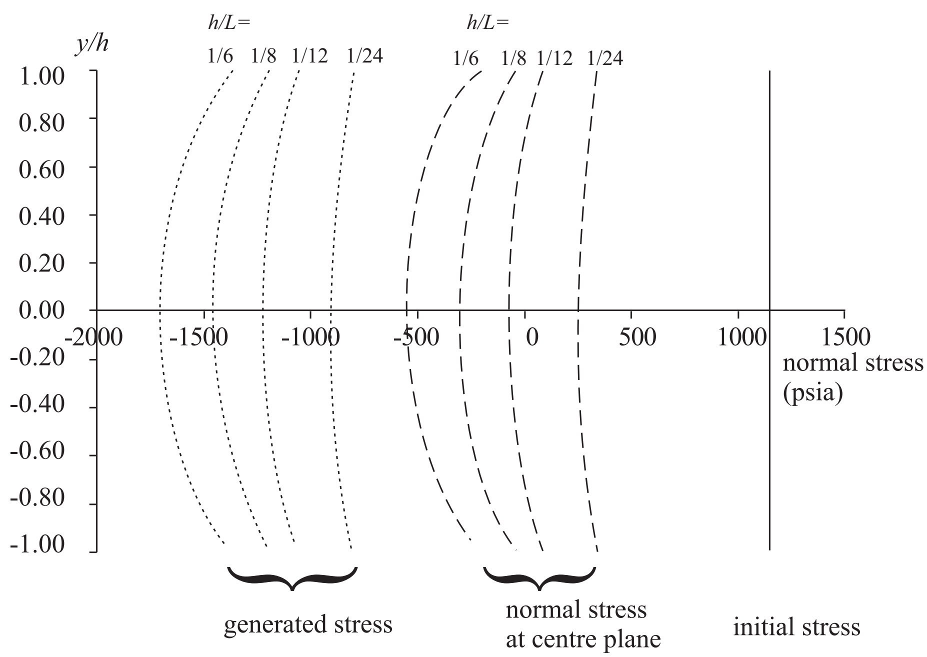

Figure 13.4: Stress on vertical centre plane. In thicker columns, h/L > 1/12, cooling and pressure gradients cause a tensile state of stress.

Importantly, a change in sign occurs for h/L around $1/12$, hence for larger values the calculated normal stress is tensile. For $L = 600$ ft, $h/L = 1/12$ corresponds to a flowing interval height of 100 ft ($2h = 100$ ft). Given that chalk has a very low tensile strength, opening of a fracture would result under the modelled conditions. Common for sound injection management are the three recognitions:

- Reservoir stress is under strong influence from production and injection;
- Fracturing is essential for pressure maintenance in most North Sea oil fields, because the mobility of water is low compared to oil and gas;
- Fractures can be placed along pre-determined injection lines in the reservoir, and thereby enhanced support to drainage areas on either side can be imposed.

The conversion of this knowledge into practice and field scale modelling may be carried out differently from one operator to the other. Maersk Oil has developed and patented the FAST concept (Fracture Aligned Sweep

Technology), and over the past 15 years published several papers about this method. The FAST technique is used in Maersk Oil operated DUC fields in the North Sea (Albrechtsen, Andersen et al. 2001; Jørgensen 2002; Rod and Jørgensen 2005).

13.6 Conclusions

Chalk reservoirs represent an important segment of the oil and gas fields in the North Sea. Though chalk reservoirs differ significantly from sandstone reservoirs in the region, the industry routinely uses similar simulation tools to perform dynamic modelling.

This chapter seeks to focus on some of the key characteristics of chalk fields relevant to reservoir simulation. Key topics discussed are typical model setup considerations, such as definition of initial reservoir conditions associated with tilting contacts, accounting for lateral fluid property variations and handling of transition zones and related fluid flow characteristics down through the oil column. The setup of the models also defines the reservoir drive and potential variation across the field, which leads naturally to the reflexions of primary versus secondary recovery schemes.

Naturally fractured chalk reservoirs add further aspects to the modelling considerations, out of which only a few have been included in the chapter. However, an appendix has been compiled to present industry experience on modelling, characterization, upscaling and flow models relating to fractured reservoirs. Practical use of dynamic modelling to support the analysis and understanding of chalk reservoir responses are discussed in two examples. The first one considers field observations resulting from primary development in a an oil field partly overlain by a gas cap, while the other example touches on some of the important engineering aspects associated with secondary recovery based on deliberate fracture propagation as part of the water injection scheme. Both examples illustrate the power of the dynamic reservoir modelling tools: to integrate reservoir and fluid characteristics; and to explore and gain insights into the physical behavior of chalk fields under development.

The priority for the authors has been to draw up some of the key considerations which are characteristic for chalk field modelling. Many other topics of a more general nature relating to both reservoir simulation and geomechanics modelling have thereby been omitted.

Appendix

13.A Natural fractured reservoirs

Several oil fields in the North Sea are fractured chalk formations containing a low matrix permeability. The implementation of secondary recovery or enhanced oil recovery (EOR) techniques is essential for effectively producing this type of oil fields and maximizing oil recovery. In general, oil production in NFRs is challenging due to matrix/fracture large transmissibility contrast, which often leads to low primary recovery factors. Significant oil reserves are located in oil-wet, fractured, carbonate formations and their recovery requires the proper formation characterization, as well as understanding and modeling of multiphase fluid flow in both fracture and matrix domains and the ability of their fluids to ”interact”.

13.A.1 Modeling

Over the years, several models have been introduced to describe physical processes which govern fluid and heat flow in NFRs. Viscous, capillary, gravitational and diffusive forces need to be properly quantified in order to model these processes effectively. In hydrocarbon bearing formations, the relative importance of these forces depends primarily on the fractured reservoir rock properties (matrix and natural fractures), fluid properties, and the implemented oil recovery technique.

Challenges in modeling fluid flow in NFR systems are many. Even single-phase fluid flow modeling in non-symmetric, rough-walled fractures is a challenge due to the variation of fracture transmissivity. Fracture-filling mineral veins indicate a compel distribution of fracture apertures (Matthäi, Mezentsev et al. 2005). Other factors, such as stress and thermal effects, may also contribute to fracture conductivity (Matthäi, Mezentsev et al. 2005); for example, fracture size enhances aperture stress sensitivity (Renshaw and Park 1997); dilation, due to fluid-flow-induced thermal variations in wells, occurs only in critically stressed fractures (Barton, Zoback et al. 1995). Crandall, Bromhal et al. (2010) correlated fracture wall-roughness with the joint roughness coefficient (JRC) and the fractal dimension, and developed relationships between the observed roughness properties of the fracture geometries and flow parameters that are of importance for modeling flow through fractures in field scale models.

Fracture size (aperture), orientation, degree of interconnectedness, and conductivity as well as matrix rock permeability and wettability, capillary pressure and relative permeability curves, as well as reservoir architecture, net/gross, type and well location will significantly impact the performance of a given reservoir. Natural fractures, normally encountered in carbonate formations, may present significant difficulties to address fluid production and formation sweep depending on their properties and their connectivity with a production/injection well (see for example (Hatzignatiou 1999; Hatzignatiou and McKoy 2000)). Oil and gas production associated with NFRs has become more pronounced in the case of horizontal wells; these wells have, in general, a higher degree of probability than the vertical ones of intersecting natural fractures (Hatzignatiou 1999; Hatzignatiou and McKoy 2000).

Traditionally, the models used to describe NFRs can be classified into two main group: the dual porosity (DP) and dual permeability (DK). The former, which are further subdivided into standard dual-porosity model (SDP), multiple interacting continua model (MINC), and vertical refinement model (VR), assume that the fracture network is the primary continuum for fluid flow CMG (2010). Difficulties in history matching NFR field behavior using traditional reservoir simulation models has led to the development of alternative, more realistic models such as the discrete fracture network (DFN) and discrete fracture and matrix (DFM) models.

13.A.2 Characterization

NFR characterization and development of a realistic, effective and representative geological model based on geological, geophysical, wellbore, analogue field, and dynamic data is of a vital importance in developing accurate reservoir simulation models for proper reservoir management. Use of outcrop, core, well log, and seismic data is normally the procedure followed in the development of the fracture network model. Increased seismic resolution, effective and accurate borehole imaging, and DFN modeling can benefit fracture characterization in NFRs.

NFRs are more challenging than conventional reservoirs mainly due to high uncertainty. Quantitative description of 3D fracture networks in NFR are vital in building robust static geological models, history-matching field production data, conducting required predictions, and performing accurate reservoir evaluations required for an effective reservoir management. This description normally incorporates information/characteristics of fracture connectivity, fracture types, fracture surface roughness and flow characteristics.

A comprehensive, comparison study conducted by Koestler and Reksten (1995) at the Lëgerdorf analogue fractured chalk field increased the understanding and improved the methods to make predictions of fracture networks and their influence on the flow behavior in complex deformed chalk reservoirs. The Lëgerdorf formation chalk fracture network was characterized and mapped at different scales during the wall scrape off, as chalk exploitation proceeded in the established quarry. The investigated chalk formation bulk volume was over 200k m^3. Three cored wells were drilled in order to establish methods to extrapolate fracture data from cores and wells into the surrounding rock volume. The wellbores were imaged with both the resistivity formation micro-scanner (FMS) and the sonic circumferential borehole image logger (CBIL), and packer tests were performed to investigate the flow behavior of the fracture network. Observations from the Lägerdorf chalk formation revealed that fracture-frequency variation was related to the proximity of the main structural features and lithology variations. With respect to potential fluid flow through the fractured volume, Koestler and Reksten (1995) placed emphasis on the 3D fracture connectivity, fracture surface characteristics, matrix deformation close to fractures, and aperture variation along fractures.

In addition to the core, well, and seismic survey data, chemical and radioactive tracers have been used extensively in the oil industry to investigate reservoirs fluid dynamics and obtain information for the tested field (Zemel 1995). Poulsen, Lafond et al. (2012) developed and applied a deuterium-based tracer technology in the Halfdan North Sea oilfield to obtain information about high conductivity fractures in tight reservoirs. The deuterium oxide tracer is completely miscible with water, does not dissolve in the oil phase, is environmentally friendly and safe to handle. The produced fluids tracer concentration was analyzed to determine breakthrough time, concentration profile, volume of tracer returned; with an injector-fracture-producer model these data to determine the number of fractures, their conductivity and their relative position in the wellbore.

Discrete fracture network (DFN) flow modeling relies on 3D spatial mapping of fracture planes used to construct a network of interconnected fractures. Unstructured grids DFN are effective models for capturing fracture connectivity and scale dependent heterogeneity in NFRs compared to traditional dual continuum models (Dershowitz and Miller 1995; Kiraly and Morel 1976; Dershowitz, LaPointe et al. 2000). DFN modeling can be employed to increase geological prior knowledge and therefore produce more geologically consistent models (Elfeel, Jamal et al. 2013)

Tamagawa, Matsuura et al. (2002) used both static (borehole images) to develop a DFN model and dynamic (pressure derivative curves) data to evaluate the model's fluid flow behavior for the Yufutsu fractured basement gas reservoir. The DFN model was constructed by applying fractal theory and geostatistics to define fracture size and fracture spatial distribution, respectively. The two model were merged and converted to a continuum model with equivalent permeable fine-grid blocks based on cubic law, which were subsequently upscaled into a continuum coarse grid model for fluid flow simulation. Araujo, Lacentre et al. (2004) described the dynamic behavior of DFN models and highlighted the need to calibrate these models against short- and long-term pressure transient test data. The authors demonstrated how the dynamic behavior of a DFN model of Margarita gas field compared against pressure transient measurements in a sidetrack delineation-well.

Characterization and modelling of NFR containing fracturing at different scales is challenging since it is difficult to isolate the specific response from each scale. Gouth, Toublanc et al. (2006) presented a workflow process which they applied to characterize fractures in a North African carbonate reservoir based on an extensive integration of static (FMI) and dynamic (well test, pressure buildup, mud losses) data. The authors then described the building of a dynamic DP/DK model using the DFN approach; the model integrated the intermediate scale fractures implicitly and the conductive faults explicitly, with the smallest scale fractures been discarded as having a negligible impact. Le Maux, Mattioni et al. (2007) used DFN to characterize and model the Venezuelan Orocual sandstone NFR field. Core analyses and borehole image logs revealed the presence of numerous open or partially-open tectonic fractures. The authors integrated geology (borehole image logs, cores and wireline logs), geophysics, and reservoir engineering (production, flowmeter, well-test) data to identify the main type of fractures, predict their occurrence, and determine the hydraulic properties of various fractures sets. The DFN approach was used to characterize the natural fractures at well scale, and to model the full field 3D fracture network. The model was calibrated by simulating and matching measured flowmeter log data, and by matching permeability-thickness product obtained from pressure transient testing.

Discrete Fracture Matrix (DFM) (see for example, Kim and Deo 2000; Juanes, Samper et al. 2002; Matthäi, Mezentsev et al. 2005) are used to model fluid flow behavior when both fractures and matrix contribute to fluid flow. Hatzignatiou (1999); Hatzignatiou and McKoy (2000) used a first generation single-phase DFM model in which the fracture network, generated from outcrop analog formations with the assistance of a DFN model, was explicitly defined and the matrix blocks contributing to the fluid flow into the fractures and subsequently into production wells. The model decoupled fluid flow in the fracture and matrix domains. The system of natural fractures was determined using a stochastic fracture-porosity model which generated fracture network realizations and provided the location, apertures, density, and clustering data of natural fractures. Hatzignatiou (1999) used the model to study the pressure behavior and recovery of natural gas from a tight gas formation in the Paludal Sands of the Rulison Field, Piceance Creek Basin in Colorado. Simulation results showed that horizontal well location, degree of clustering, fracture density, fracture aperture distribution, and degree of fracture interconnectedness are very important factors dictating gas recovery factors. Hatzignatiou and McKoy (2000) focused on quantifying uncertainties in gas recovery factor estimates due to network heterogeneity and variability in the connection between the well and the network.

Kim and Deo (2000) developed a discrete-fracture multiphase flow model that allows the explicit incorporation of fractures as an alternative to conventional DP/DK models. A standard Galerkin finite element method was used to discretize the domain. The model was applied to a waterflood simple case on a 2D random fracture network: the results showed that at high fracture-to-matrix permeability contrast, the fracture network was very important in the advancement of water flow and achieved oil recovery. Reduction of fractured medium capillary pressure in general yielded higher oil recovery. The major disadvantages of the DFM simulation are the computational cost associated with large simulation run times, the amount of data required, challenges in generating suitable finite element or volume grid system for the entire field; all these have limited its application to commercial reservoir simulators even though DFM models provide a more-accurate representation of fractured reservoirs than dual-continuum models.

13.A.3 Upscaling

Accurate effective fracture permeability tensors are one of the most important parameters for an accurate reservoir history matching and successful prediction of ultimate oil recovery in NFRs. Since only the main fractures can be incorporated into a full field-scale model, upscaling of the natural fracture's integral effects on multiphase flow are required (Matthäi and Nick 2009); for example upscaling of matrix permeability (Oda 1985) or derivation of parameters for dual-continua simulations (see for example Sarda, Jeannin et al. 2002).

DFN modeling and analytical or flow-based methods can be used to upscale fracture permeabilities. Although analytical methods, such as the Oda (1985) one, can be used the upscale fracture permeabilities can be inaccurate for poorly connected fracture networks. On the other hand, flow-based methods, in addition to being computationally expensive, are heavily dependent on the employed boundary conditions, and the employed grid size (Elfeel and Geiger 2012).

Gong, Karimi-Fard et al. (2008) presented a systematic upscaling procedure to construct a DP/DK model from detailed discrete fracture characterizations. Multiple Subregion (MSR) model, the subregions were constructed for each coarse block using the isopressure curves obtained from local pressure solutions of a DFM over the block. These subregions account for the fracture distribution and can represent accurately the matrix-matrix and matrix-fracture transfer. The matrix subregions were connected to matrices in vertically adjacent blocks (as in DK model) to capture phase segregation caused by gravity. The proposed method was used to simulate 2D and 3D fracture models, with viscous, gravitational, and capillary pressure effects.

Matthäi and Nick (2009) presented an upscaling workflow and semi-analytical model to compute multiphase flow properties from NFR field data for use in conventional reservoir simulators in which sub-seismic fractures cannot be represented explicitly. The upscaling method presented based on three-dimensional DFM model of two-phase flow revealed that grid-block-scale relative permeability, water breakthrough time, and water cut depend mainly on the fracture-to-rock matrix flux ratio. The authors proposed upscaling the capillary-driven fracture-matrix transfer using the fraction of the fracture-matrix interface that is in contact with water as a function of the grid-block average water saturation.

Elfeel and Geiger (2012) explored the uncertainties arising from upscaling of DFN model an investigated the scale dependency issue by comparing different DFN upscaling methods and using a DFM to find the optimum coarse scale model. The authors compared Oda's analytical method and DFN based fluid flow methods to obtain upscaled effective permeabilities. The two methods provided similar upscaled effective permeability values, but prediction of oil production depended heavily on the employed grid size and degree of connectivity of natural fractures. The authors proposed a new methodology to test the average permeability values around a well obtained from DFN upscaling and the DFM model, which represents the true formation permeability. Elfeel, Jamal et al. (2013) highlighted DFN upscaling errors stating that geometrical (semi-analytical) methods overestimate fracture permeability, whereas fluid flow based (numerical) approaches, despite the fact that they are more accurate, are expensive and model size restrictive. In the latter, boundary conditions do also play a role in the DFN upscaling process uncertainties.

13.A.4 Multiphase flow and simulation models

Strong non-linear coupling of viscous, gravity, and capillary forces as well as variation of how these forces manifest themselves in the two continua complicate the modeling of multiphase flow in NFRs compared to non-fractured porous media. Compositional models are required for describing accurately light oil or gas condensate reservoirs. Special oil processes such as gravity drainage in NFRs require specific models to address this process affectively with the reservoir block matrix and interaction with natural fractures. EOR processes, including waterflooding, require knowledge of rock matrix wettability in order to model effectively the imbibition process, rock wettability alterations, and their impact on oil recovery. In large thickness formations, the modeling of the transition zone becomes extremely important as well as variation of fluid properties along the vertical fluid column. Finally, specialized issues such as tilting oil/water or oil/gas interfaces are also important in low permeability chalk formations.

Injection of either gas or water in fractured carbonate reservoirs requires the identification of factors, and understanding of mechanisms, which control both microscopic and macroscopic sweep efficiencies. Lateral reservoir quality, vertical reservoir quality, dynamic fluid flow parameters, and geography and economics are the main parameters which affect oil recovery in chalk formations (Horikx, Timmermans et al. 2013). Many naturally fractured carbonate fields are oil-wet and wettability favors gas rather than water injection. Formation wettability can be very important in the oil drainage processes applied in chalk reservoirs, especially when there is lack of capillary continuity. Wettability variations across the reservoir the oil column need to be properly accounted for in the development and design of an oil recovery process.

Kazemi, Merrill Jr et al. (1976) presented a 3D simulation model for two-phase (oil/water) flow in NFRs. The model accounted for relative fluid mobilities, gravity forces, imbibition, and variation in reservoir properties, and handled uniformly and non-uniformly distributed fractures. An implicit compositional simulation model for simulating single porosity and dual porosity oil or gas condensate reservoirs was introduced by Coats (1989). The author used a three-component equation-of-state compositional approach to extend black oil modelling. A new matrix-fracture transfer formulation including matrix-fracture diffusion was presented for the DP description. The author presented and discussed results from a 3D simulation of a highly fractured, near-critical volatile oil reservoir.

Firoozabadi and Hauge (1990) proposed a phenomenological model for fracture capillary pressure to address the modeling and impact of capillary pressure in fractured porous media. Computed capillary-pressure/saturation results displayed a porous-medium behavior for fracture capillary pressure. Fung (1991) examined the mechanisms involved in NFR gas/oil gravity drainage in terms of the block-to-block process, and proposed an approach through the computation of pseudo capillary potentials, in which these mechanisms can be represented properly in field-scale simulations. Luan (1992) discussed that the capillary pressure end effects may be important in a drainage process in NFRs. The saturation distribution at the end-face of the blocks is dependent on the wetting conditions and the properties of the fractured medium. Experimental studies (Suffridge and Renner 1991) showed that the end effects (caused by saturation discontinuity) can be reduced by increased contact areas between blocks. Catalan and Dullien (1992) demonstrated that semi-permeable membranes are able to prevent gas breakthrough and eliminate capillary end effects. Cuiec, Bourbiaux et al. (1994) described various experimental studies of spontaneous imbibition of oil by water in a low-permeability outcrop chalk samples. At constant and high interfacial tension, the importance of capillary forces and the existence of a predominant countercurrent mechanism were established. The importance of capillary pressure when simulating multiphase flow in NFRs was highlighted by Monteagudo and Firoozabadi (2004); neglecting capillary pressure effects may affect significantly predictions of flow pattern and oil recovery. A Control-Volume Discrete-Fracture (CVDF) method for water injection in fractured media with strong-water-wettability state, and homogeneous matrix and rock and fluid properties was presented. Monteagudo and Firoozabadi (2007) extended that CVDF model to incorporate rock heterogeneity and heterogeneity in rock-fluid properties, and presented a novel algorithm to model strong water-wetting with zero capillary pressure in the fractures.

Bertels, DiCarlo et al. (2001) developed an experimental technique that uses CT scanning to obtain high-resolution measurements of aperture distribution and in-situ saturation along with capillary pressure and relative permeability in rough-walled fractures. The authors measured atypical, non-monotonic capillary pressure curves with the capillary pressure to increase initially and then decrease with decreasing water saturation; saturation maps suggest local rearrangement of fluids under gravity and capillary forces, which led to the observed decrease of capillary pressure with increasing gas saturation.

Traditionally, the fracture domain relative permeability curves used in reservoir simulation are linearly proportional to the phase saturations, which result to the well-known x-shape relationships. Several researches found that this type of relative permeability curves is not correct, especially when addressing multiphase flow behavior in non-smooth fractures (Fourar, Bories et al. 1993; Nicholl and Glass 1994; Persoff and Pruess 1995). Chen, Horne et al. (2004), based on laboratory studies of air/water relative permeability behavior in a smooth-walled fracture, concluded that the x-shape curves cannot be used to describe two-phase flow in fractures even if the surfaces were smooth. An alternative approach that lumps the micro-scale physical mechanisms of viscous and capillary forces into a channel tortuosity parameter was proposed to model two-phase relative permeability behavior in rough-walled fractures based on two-phase flow structure (Chen and Horne 2005). Although an empirical tortuous-channel model was developed for the given fracture heterogeneities considered in their study, Chen and Horne (2005) highlighted both the complexity and variability of natural fractures heterogeneity, and concluded that more robust relationships tortuosity and fracture geometry are required to obtain rigorous models for predicting fracture relative permeabilities.

Geiger, Matthäi et al. (2009) presented a discrete-fracture modeling and simulation of two-phase flow in realistic representations of fractured reservoirs for the design of IOR/EOR strategies. The proposed black-oil model for three-component, three-phase flow used a finite-element/finite-volume discretization generalized to unstructured hybrid element meshes, employed higher-order accurate representations of the flux terms, and carried flash calculations with an improved EOS allowing for a more realistic treatment of phase behavior.

Moortgat, Firoozabadi et al. (2013) modeled capillarity in fully compositional three-phase flow, with higher-order finite-element methods. The authors stated that capillary pressure gradients may be important in formations which exhibit sharp discontinuities in permeability such as layered or NF reservoirs. The authors presented both core- and large-scale three-phase flow examples illustrating the capillary end effect, capillary-driven crossflow in layered media, and the importance of capillarity in fractured media. Moinfar, Varavei et al. (2014) presented the development of an efficient embedded discrete fracture model for 3D compositional reservoir simulation in NFR. In contrast to dual-continuum models, fractures have arbitrary orientations and can be oblique or vertical, honoring the complexity of a typical NFR. Based on their simulations the authors stated that in order to achieve accurate results, the embedded DFM may only require moderate mesh refinement around the fractures, and hence it may offer a computationally efficient approach. Waterflooding, gas injection, and primary depletion examples were also presented to demonstrate the performance and applicability of the developed method for simulating fluid flow in NFRs.

13.B Geomechanics considerations related to water flooding

The solution for stress on the symmetry plane ($x = 0; -h < y < h$) shown in Fig. 13.3 in the main text, can be derived analytically in three steps, i.e., a contribution from lateral gradients in pressure; a contribution from redistribution of over- and under-burden loads; and finally the temperature effect.

13.B.1 Contribution to horizontal stress from lateral flow

$$
\begin{aligned}
\sigma'_{x,L}(y) = &\\
& -\frac{(p_{\text{inj}}-p_p)}{2\pi}\left((1-\overline{\nu})\left(\tan^{-1}\left(\frac{h-y}{L}\right)-\frac{1}{2}\sin\left(2\tan^{-1}\left(\frac{h-y}{L}\right)\right)\right)-(3+\overline{\nu})\tan^{-1}\left(\frac{h-y}{L}\right)\right)\\
& -\frac{(p_{\text{inj}}-p_p)(h-y)}{2\pi L}\left((3-\overline{\nu})\ln\left|\sin\left(\tan^{-1}\left(\frac{h-y}{L}\right)\right)\right|+(1-\overline{\nu})\left(1-\sin^2\left(\tan^{-1}\left(\frac{h-y}{L}\right)\right)\right)\right)\\
& -\frac{(p_{\text{inj}}-p_p)}{2\pi}\left((1-\overline{\nu})\left(\tan^{-1}\left(\frac{h+y}{L}\right)-\frac{1}{2}\sin\left(2\tan^{-1}\left(\frac{h-y}{L}\right)\right)\right)-(3+\overline{\nu})\tan^{-1}\left(\frac{h+y}{L}\right)\right)\\
& -\frac{(p_{\text{inj}}-p_p)(h-y)}{2\pi L}\left((3-\overline{\nu})\ln\left|\sin\left(\tan^{-1}\left(\frac{h+y}{L}\right)\right)\right|+(1-\overline{\nu})\left(1-\sin^2\left(\tan^{-1}\left(\frac{h+y}{L}\right)\right)\right)\right)
\end{aligned}
\tag{13.2}
$$

In Eq. 13.2, ν is Poisson's ratio, $\overline{\nu} = \frac{\nu}{1-\nu}$, p_{inj} and p_p denote injecting and producing bottomhole pressures, respectively. Subscript,L refers to impact of lateral flow on stress. From the above equation, it can be seen that h/L and the pressure difference $(p_{\text{inj}} - p_p)$ are the key parameters to the problem. If h/L approaches zero the induced stress at the center plane approaches zero as well. For a typical reservoir rock, $\overline{\nu}$ values range between 0.1 and 0.3; therefore, Poisson's ratio is of second order significance to the problem.

13.B.2 Contribution to horizontal stress from over- and under-burden

When pressures are distributed not uniformly in the reservoir, over- and under-burden loadings will be distributed unevenly as well. For the case under consideration, we are interested in the resulting normal stress on the center plane $x = 0$ (Fig. 13.3). This can be obtained by integrating the influence function expressing the influence on stress of a distributed force of magnitude

$$(p_0 - p(x))dx = \left[(p_0 - p_{\text{inj}}) + \frac{(p_{\text{inj}} - p_p)}{L}x\right]dx \tag{13.3}$$

along the top and bottom ($y = h$ and $y = -h$) of the reservoir. In Eq. 13.3 p_0 is the pore pressure (datum corrected) in the over- and under-burden, which is assumed equal to the initial reservoir pressure ($p_0 = p_{\text{res}}$). Integration gives the following closed form solution:

$$\begin{aligned}
\sigma'_{x,v}(y) = \\
&- \frac{(1-\overline{v})}{2\pi}\left[(p_{\text{inj}} - p_0)\left(\tan^{-1}\left(\frac{L}{h-y}\right) + \tan^{-1}\left(\frac{L}{h+y}\right)\right)\right] \\
&+ \frac{(1+\overline{v})}{2\pi}\left[(p_{\text{inj}} - p_0)\left(\tan^{-1}\left(\frac{L}{h-y}\right) - \frac{1}{2}\sin\left(\tan^{-1}\left(\frac{L}{h-y}\right)\right)\right)\right] \\
&+ \frac{(1+\overline{v})}{2\pi}\left[(p_{\text{inj}} - p_0)\left(\tan^{-1}\left(\frac{L}{h+y}\right) - \frac{1}{2}\sin\left(\tan^{-1}\left(\frac{L}{h+y}\right)\right)\right)\right] \\
&+ \frac{(1+\overline{v})}{2\pi}\left[(p_{\text{inj}} - p_0)\frac{(h-y)}{L}\left(\ln\left|\cos\left(\tan^{-1}\left(\frac{L}{h-y}\right)\right)\right|\right)\right] \\
&+ \frac{(1+\overline{v})}{2\pi}\left[(p_{\text{inj}} - p_0)\frac{(h+y)}{L}\left(\ln\left|\cos\left(\tan^{-1}\left(\frac{L}{h+y}\right)\right)\right|\right)\right] \\
&+ \frac{(1+\overline{v})}{2\pi}\left[(p_{\text{inj}} - p_0)\frac{(h-y)}{L}\left(1 - \cos^2\left(\tan^{-1}\left(\frac{L}{h-y}\right)\right)\right)\right] \\
&+ \frac{(1+\overline{v})}{2\pi}\left[(p_{\text{inj}} - p_0)\frac{(h+y)}{L}\left(1 - \cos^2\left(\tan^{-1}\left(\frac{L}{h+y}\right)\right)\right)\right]
\end{aligned} \tag{13.4}$$

Subscript, v refers to impact of vertical load.

13.B.3 Contribution to horizontal stress from thermal stress

The contribution to normal stress $\sigma'_{x,T}$ from cooling can be assessed by considering the stresses generated due to cooling of a finite volume of rock embedded in an infinite homogeneous elastic body. The normal stresses within the reservoir volume cooled from the original temperature T_{res} to T_{inj} are

$$\sigma'_{x,T} = \frac{E\beta(T_{\text{res}} - T_{\text{inj}})}{2(1-\nu)} \tag{13.5}$$

where E is the Young's modulus, β is the linear thermal expansion coefficient, T_{res} and T_{inj} denote reservoir and injected-water temperature, respectively, and ν is the Poisson's ratio.

Nomenclature

a = length, L, ft
b = volume force, m/L^{2}t^{2}T, psi/ft°C
E = Young's modulus,m/Lt^2, psi
h = height, L, ft
L = well spacing, L, ft
p = pressure, m/Lt^2, psia
T = temperature, T, °C
v_p = P-wave velocity, L/t
v_s = S-wave velocity, L/t
x = length x-axis, L, ft
y = length y-axis, L, ft

α = Biot's coefficient, dimensionless
β = thermal expansion coefficient, 1/T, 1/°C
ν = Poisson's ratio, dimensionless
$\overline{\nu}$ = $\nu/(1-\nu)$
σ = stress, m/Lt^2, psi
σ'_p = effective external hydrostatic stress, m/Lt^2, psi

Subscripts

0 = initial
inj = injection
p = pressure, bottomhole production
res = reservoir
s = share, secondary
T = temperature
x, y, z = Cartesian coordinates

Superscripts

$'$ = effective stress

Abbrevations

AVO = amplitude versus offset
CBIL = circumferential borehole image logger
CT = computer tomography
CVDF = control-volume discrete-fracture
DFM = discrete fracture matrix
DFN = discrete fracture network
DK = dual permeability
DP = dual porosity
DUC = Dansk Undergrunds Consortium
EOR = enhanced oil recovery
EW = east-west
FAST = fracture aligned sweep technology
FMI = formation micro imager
FMS = formation micro scanner
FWL = free water level
GOC = gas oil contact
JRC = joint roughness coefficient
LGR = local grid refinement
MINC = multiple ineracting continua
MSR = multiple subregion
NRF = natural fractured reservoirs
OWC = oil water contact
PF = productivity index
SDP = standard dual-porosity
VR = vertical refinement

References

Albrechtsen, T., Andersen, S.J. et al., 2001. Halfdan: Developing Non-Structurally Trapped Oil in North Sea Chalk. Paper SPE 71322 presented at SPE Annual Technical Conference and Exhibition, New Orleans, Louisiana. 30 September–3 October. URL `http://dx.doi.org/10.2118/71322-MS`.

Araujo, H., Lacentre, P. et al., 2004. Dynamic Behavior of Discrete Fracture Network (DFN) Models. Paper SPE 91940 presented at SPE International Petroleum Conference in Mexico, Puebla Pue., Mexico. 7–9 November. URL `http://dx.doi.org/10.2118/91940-MS`.

Barton, C.A., Zoback, M.D., and Moos, D., 1995. Fluid flow along potentially active faults in crystalline rock. *Geology*, **23** (8): 683–686. URL http://dx.doi.org/10.1130/0091-7613(1995)023<0683:FFAPAF>2.3.CO;2.

Bech, N., Frykman, P., and Vejbæk, O.V., 2005. Modeling of Initial Saturation Distributions in Oil/Water Reservoirs in Imbibition Equilibrium. Paper SPE 95365 presnted at SPE Annual Technical Conference and Exhibition, Dallas, Texas. 9–12 October. URL http://dx.doi.org/10.2118/95365-MS.

Bech, N., Frykman, P., and Vejbæk, O.V., 2007. Determination of Free Water Levels in Low-Permeability Chalk Reservoirs from Logged Saturations. Paper SPE 105622 presented at Latin American & Caribbean Petroleum Engineering Conference, Buenos Aires, Argentina. 15–18 April. URL http://dx.doi.org/10.2118/105622-MS.

Bertels, S.P., DiCarlo, D.A., and Blunt, M.J., 2001. Measurement of aperture distribution, capillary pressure, relative permeability, and in situ saturation in a rock fracture using computed tomography scanning. *Water Resources Research*, **37** (3): 649–662. URL http://dx.doi.org/10.1029/2000WR900316.

Catalan, L. and Dullien, F.A.L., 1992. Applications of Mixed-Wet Pastes in Gravity Drainage Experiments. *Journal of Canadian Petroleum Technology*, **31** (05). May. URL http://dx.doi.org/10.2118/92-05-02.

Chen, C.Y. and Horne, R.N., 2005. Multiphase Flow Properties of Fractured Geothermal Rocks. PROCEEDINGS, Thirtieth Workshop on Geothermal Reservoir Engineering Stanford University, Stanford, California SGP-TR-176. January 31-February 2. URL http://www.geothermal-energy.org/pdf/IGAstandard/SGW/2005/chen.pdf.

Chen, C.Y., Horne, R.N., and Fourar, M., 2004. Experimental study of liquid-gas flow structure effects on relative permeabilities in a fracture. *Water Resources Research*, **40** (8). W08301. URL http://dx.doi.org/10.1029/2004WR003026.

CMG, 2010. *User's Guide of STARS: Advanced Process and Thermal Reservoir Simulator Version 2010*. Computer Modeling Group Ltd, Calgary, Alberta, Canada. URL http://www.cmgl.ca/software/stars2014.

Coats, K.H., 1989. Implicit Compositional Simulation of Single Porosity and Dual Porosity Reservoirs. Paper SPE 18427 presented at SPE Symposium on Reservoir Simulation, Houston, Texas. 6–8 February. URL http://dx.doi.org/10.2118/18427-MS.

Crandall, D., Bromhal, G., and Karpyn, Z.T., 2010. Numerical simulations examining the relationship between wall-roughness and fluid flow in rock fractures. *International Journal of Rock Mechanics and Mining Sciences*, **47** (5): 784–796. URL http://dx.doi.org/http://dx.doi.org/10.1016/j.ijrmms.2010.03.015.

Cuiec, L.E., Bourbiaux, B., and Kalaydjian, F., 1994. Oil Recovery by Imbibition in Low-Permeability Chalk. *SPE Formation Evaluation*, **9** (03): 200–208. September. URL http://dx.doi.org/10.2118/20259-PA.

Dershowitz, B., LaPointe, P. et al., 2000. Integration of Discrete Feature Network Methods with Conventional Simulator Approaches. *10.2118/62498-PA*, **3** (02): 165–170. April. URL http://dx.doi.org/10.2118/62498-PA.

Dershowitz, W. and Miller, I., 1995. Dual porosity fracture flow and transport. *Geophysical Research Letters*, **22** (11): 1441–1444. URL http://dx.doi.org/10.1029/95GL01099.

Dons, T., Jørgensen, O., and Gommesen, L., 2007. Seismic Observation and Verification of Line Drive Water Flood Patterns in a Chalk Reservoir, Halfdan Field, Danish North Sea. Paper SPE 108531 presented at Offshore Europe, Aberdeen, Scotland, U.K. 4–7 September. URL http://dx.doi.org/10.2118/108531-MS.

Elfeel, M.A. and Geiger, S., 2012. Static and Dynamic Assessment of DFN Permeability Upscaling. Paper SPE 154369 presented at SPE Europec/EAGE Annual Conference, Copenhagen, Denmark. 4–7 June. URL http://dx.doi.org/10.2118/154369-MS.

Elfeel, M.A., Jamal, S. et al., 2013. Effect of DFN Upscaling on History Matching and Prediction of Naturally Fractured Reservoirs. Paper SPE 164838 presnted at EAGE Annual Conference & Exhibition incorporating SPE Europec, London, UK. 10–13 June. URL http://dx.doi.org/10.2118/164838-MS.

Firoozabadi, A. and Hauge, J., 1990. Capillary Pressure in Fractured Porous Media. *Journal of Petroleum Technology*, **42** (06): 784–791. June. URL http://dx.doi.org/10.2118/18747-PA.

Fourar, M., Bories, S. et al., 1993. Two-phase flow in smooth and rough fractures: Measurement and correlation by porous-medium and pipe flow models. *Water Resources Research*, **29** (11): 3699–3708. URL `http://dx.doi.org/10.1029/93WR01529`.

Fung, L.S.K., 1991. Simulation of Block-to-Block Processes in Naturally Fractured Reservoirs. *SPE Reservoir Engineering*, **6** (04): 477–484. November. URL `http://dx.doi.org/10.2118/20019-PA`.

Geiger, S., Matthäi, S.K. et al., 2009. Black-Oil Simulations for Three-Components, Three-Phase Flow in Fractured Porous Media. *SPE Journal*, **14** (02): 338–354. June. URL `http://dx.doi.org/10.2118/107485-PA`.

Gommesen, L., Dons, T. et al., 2007. 4D Seismic Signatures of North Sea Chalk - The Dan Field. Paper SEG-2007-2847 presented at SEG Annual Meeting, San Antonio, Texas. 23–28 September. URL `https://www.onepetro.org/conference-paper/SEG-2007-2847?sort=&start=0&q=4D+Seismic+Signatures+of+North+Sea+Chalk+-+The+Dan+Field.&from_year=&peer_reviewed=&published_between=&fromSearchResults=true&to_year=&rows=10#`.

Gommesen, L. and Hansen, H.P., 2012. Chalk Reservoir Management through Rock Physics Diagnostics - Field Examples from the Danish North Sea. Paper SPE 154670 presented at SPE Europec/EAGE Annual Conference, Copenhagen, Denmark. 4–7 June. URL `http://dx.doi.org/10.2118/154870-MS`.

Gong, B., Karimi-Fard, M., and J., D.L., 2008. Upscaling Discrete Fracture Characterizations to Dual-Porosity, Dual-Permeability Models for Efficient Simulation of Flow with Strong Gravitational Effects. *SPE Journal*, **13** (01): 58–67. March. URL `http://dx.doi.org/10.2118/102491-PA`.

Gouth, F., Toublanc, A., and Mresah, M.H., 2006. Characterisation and Modelling of a Fractured Reservoir Using a Novel DFN Approach. Paper SPE 102165 presented at Abu Dhabi International Petroleum Exhibition and Conference, Abu Dhabi, UAE. 5–8 November. URL `http://dx.doi.org/10.2118/102165-MS`.

Hatzignatiou, D.G., 1999. Reservoir Engineering Aspects of Horizontal Wells in Stochastic Naturally Fractured Gas Reservoirs. Paper SPE 54626 presented at SPE Western Regional Meeting, Anchorage, Alaska. 26–27 May. URL `http://dx.doi.org/10.2118/54626-MS`.

Hatzignatiou, D.G. and McKoy, M., 2000. Probabilistic Evaluation of Horizontal Wells in Stochastic Naturally Fractured Gas Reservoirs. Paper SPE/CIM 65459 presented at SPE/CIM Horizontal Well Technology Conference, Calgary, Canada. 6–8 November. URL `http://dx.doi.org/10.2118/65459-MS`.

Henriksen, K., Gommesen, L. et al., 2009. Optimizing Chalk Reservoir Development Using Detailed Geophyiscal Characterization: The Halfdan Northeast Field, Danish North Sea. Paper SPE-123843-MS presentet at Offshore Europe, Aberdeen, UK. 8–11 September,. URL `http://dx.doi.org/10.2118/123843-MS`.

Horikx, J., Timmermans, P. et al., 2013. A Specific Way of Assessing Target Recovery Factor (Chalk Oil Fields). Paper IPTC 16925 presented at International Petroleum Technology Conference, Beijing, China. 26–28 March. URL `http://dx.doi.org/10.2523/IPTC-16925-MS`.

Jørgensen, O., 2002. Using flow induced stresses for steering of injection fracturesUsing flow induced stresses for steering of injection fractures. In *SPE/ISRM Rock Mechanics Conference*. Society of Petroleum Engineers. Paper SPE 78220 presented at SPE/ISRM Rock Mechanics Conference, Irving, Texas. 20–23 October. URL `http://dx.doi.org/10.2118/78220-MS`.

Juanes, R., Samper, J., and Molinero, J., 2002. A general and efficient formulation of fractures and boundary conditions in the finite element method. *International Journal for Numerical Methods in Engineering*, **54** (12): 1751–1774. URL `http://dx.doi.org/10.1002/nme.491`.

Kazemi, H., Merrill Jr, L.S. et al., 1976. Numerical simulation of water-oil flow in naturally fractured reservoirs. *Society of Petroleum Engineers Journal*, **16** (06): 317–326. URL `http://dx.doi.org/10.2118/5719-PA`.

Kim, J.G. and Deo, M.D., 2000. Finite element, discrete-fracture model for multiphase flow in porous media. *AIChE Journal*, **46** (6): 1120–1130. URL `http://dx.doi.org/10.1002/aic.690460604`.

Kiraly, L. and Morel, G., 1976. Remarques Sur l'hydrogramme des Sources Karstiques Simule par Modeles Mathematiques. *Bulletin du Centre d'Hydrogeologie*, **1**: 37–60. URL `ftp://ftp.unine.ch/Kiraly/Papers/KiralyL76a.pdf`.

Koestler, A.G. and Reksten, K., 1995. 3D Characterization of the Fracture Network in a Deformed Chalk Reservoir Analogue: The Lagerdorf Case. *SPE Formation Evaluation*, **10** (03): 148–152. URL http://dx.doi.org/10.2118/28728-PA.

Le Maux, T., Mattioni, L. et al., 2007. Use of Discrete Fracture Network "DFN" to Characterize and Model a Naturally Fractured Sandstone Reservoir: A Case Study of Orocual Field, San Juan Formation, Venezuela. Paper SPE 108052 presented at Latin American & Caribbean Petroleum Engineering Conference, Buenos Aires, Argentina. 15–18 April. URL http://dx.doi.org/10.2118/108052-MS.

Luan, Z., 1992. Oil Recovery Mechanisms in Naturally Fractured Reservoirs. Tech. rep., RUTH Project Report, NTH, November.

Matthäi, S.K., Mezentsev, A.A. et al., 2005. A high-order TVD transport method for hybrid meshes on complex geological geometry. *International Journal for Numerical Methods in Fluids*, **47** (10–11): 1181–1187. URL http://dx.doi.org/10.1002/fld.901.

Matthäi, S.K. and Nick, H.M., 2009. Upscaling Two-Phase Flow in Naturally Fractured Reservoirs. *AAPG Bulletin*, **93** (11): 1621–1632. November. URL http://dx.doi.org/10.1306/08030909085.

Moinfar, A., Varavei, A. et al., 2014. Development of an Efficient Embedded Discrete Fracture Model for 3D Compositional Reservoir Simulation in Fractured Reservoirs. *SPE Journal*, **19** (02): 289–303. URL http://dx.doi.org/10.2118/154246-PA.

Monteagudo, J.E.P. and Firoozabadi, A., 2004. Control-volume method for numerical simulation of two-phase immiscible flow in two- and three-dimensional discrete-fractured media. *Water Resources Research*, **40** (7). W07405. URL http://dx.doi.org/10.1029/2003WR002996.

Monteagudo, J.E.P. and Firoozabadi, A., 2007. Control-Volume Model for Simulation of Water Injection in Fractured Media: Incorporating Matrix Heterogeneity and Reservoir Wettability Effects. *SPE Journal*, **12** (03): 355–366. URL http://dx.doi.org/10.2118/98108-PA.

Moortgat, J.B., Firoozabadi, A. et al., 2013. Three-phase compositional modeling with capillarity in heterogeneous and fractured media. *SPE Journal*, **18** (06): 1–150. URL http://dx.doi.org/10.2118/159777-PA.

Nicholl, M.J. and Glass, R.J., 1994. Wetting Phase Permeability in a Partially Saturated Horizontal Fracture. In *High Level Radioactive Waste Management:*, vol. 4, 2007–2019. Proceedings of the fifth annual international conference. 22–26 May. URL http://fluidflowvisualization.sandia.gov/pdf_text/Papers%20in%20Conference%20Proceedings%20and%20Sand%20reports/23_1994_ICHLRWM_NG.pdf.

Oda, M., 1985. Permeability Tensor for Discontinuous Rock Masses. *Geotechnique*, **35** (4): 483–495. URL http://dx.doi.org/10.1680/geot.1985.35.4.483.

Peaceman, D.W., 1978. Interpretation of Well-Block Pressures in Numerical Reservoir Simulation. *SPE Journal*, **18** (03): 183–194. URL http://dx.doi.org/10.2118/6893-PA.

Persoff, P. and Pruess, K., 1995. Two-Phase Flow Visualization and Relative Permeability Measurement in Natural Rough-Walled Rock Fractures. *Water Resources Research*, **31** (5): 1175–1186. URL http://dx.doi.org/10.1029/95WR00171.

Poulsen, A.K., Lafond, K.B. et al., 2012. Characterization of Direct Fractures Using Real Time Offshore Analysis of Deuterium Tracer Technology. Paper SPE-154878-MS presented at SPE Europec/EAGE Annual Conference, Copenhagen, Denmark. 4–7 June. URL http://dx.doi.org/10.2118/154878-MS.

Renshaw, C.E. and Park, J.C., 1997. Effect of mechanical interactions on the scaling of fracture length and aperture. *Nature*, **386** (6624): 482–484. Apr. URL http://dx.doi.org/10.1038/386482a0.

Rod, M.H. and Jørgensen, O., 2005. Injection Fracturing in a Densely Spaced Line Drive Waterflood–The Halfdan Example. Paper SPE-94049-MS presented at SPE Europec/EAGE Annual Conference, Madrid, Spain. 13–16 June. URL http://dx.doi.org/10.2118/94049-MS.

Sarda, S., Jeannin, L., and Bourbiaux, B., 2002. Hydraulic Characterization of Fractured Reservoirs: Simulation on Discrete Fracture Models. *SPE Reservoir Evaluation & Engineering*, **5** (02): 154–162. URL http://dx.doi.org/10.2118/77300-PA.

Skjæveland, S.M. and Kleppe, J., eds., 1992. *SPOR Monograph. Recent Advances in Improved Oil Recovery Methods for North Sea Sandstone Reservoirs*. Norwegian Petroleum Directorate, Stavanger.

Suffridge, F.E. and Renner, T.A., 1991. Diffusion and Gravity Drainage Tests to Support the Development of a Dual Porosity Simulator. Paper presented at 6th European Symposium on Improved Oil Recovery , Stavanger. 21–23 May. URL `http://dx.doi.org/10.3997/2214-4609.201411278`.

Tamagawa, T., Matsuura, T. et al., 2002. Construction of Fracture Network Model Using Static and Dynamic Data. Paper SPE-77741-MS presented at SPE Annual Technical Conference and Exhibition, San Antonio, Texas. 29 September–2 October,. URL `http://dx.doi.org/10.2118/77741-MS`.

Zemel, B., ed., 1995. *Tracers in the Oil Field*, vol. 43 of *Developments in Petroleum Science*. Elsevier. URL `http://dx.doi.org/http://dx.doi.org/10.1016/S0376-7361(06)80013-0`.

Chapter 14

Geomechanical Modeling

Tron Golder Kristiansen and Marte Gutierrez

14.1 Introduction

This chapter will focus on geomechanical modeling of chalk as it has been developed within Joint Chalk Research (JCR) and in the industry in general. Geomechanical modeling of chalk means that we numerically will model how the chalk material is deforming as it is exposed to changes in the loads in the subsurface as reservoir pressure changes during production and injection. We will build on the earlier chapter on geomechanical properties of chalk. We also refer to Andersen (1995) for a detailed summary of work up until 1994. This chapter will provide an overview of the elements that needs to be included in a geomechanical model of chalk. We will not cover all the theoretical background needed to understand everything in detail, but do include some background information that will help the reader understand the concepts presented. For more detailed theory there are several petroleum related textbooks that can be used. We will also review some of the most used models for chalk as described in the literature for various applications. The main focus will be on the Unified Chalk Model which was developed as part of Joint Chalk Research Phase V and VI.

The main applications of a numerical geomechanical model are compaction and subsidence modeling, production modeling, injection modeling, chalk production prediction, wellbore stability, tubular deformation assessment and coupled geomechanics and reservoir modeling.

14.2 A simple analytical compaction and subsidence model

The most famous application of geomechanical modeling is probably the prediction of compaction and subsidence of the chalk fields in the North Sea. Fields like Ekofisk and Valhall have experienced larger subsidence than most other offshore and onshore fields, approaching 10 and 7 meters respectively. As an introduction to the topic in this chapter we will illustrate some of the concepts by an analytical model to predict compaction and subsidence of Ekofisk and Valhall. We will use an analytical model for subsidence prediction published by Geertsma (1973). Geertsma worked on the large onshore gas field Groningen, set on production in the late 1950's, where small amounts of subsidence could have huge impact on the above ground infrastructure in the area. Groningen inspired some of the geologists look at fields outside Norway and Denmark. As for the chalk fields, Groningen is still producing and subsiding. Subsidence was first observed above Ekofisk in 1984 after start production in 1971. Subsidence was discovered in 1985 above Valhall, 3 years after first production.

Chalk cores had already been recovered from the fields in the late 1960's and traditional laboratory tests to assess the petrophysical properties have been performed in the oil companies' laboratories. They observed that chalk deformed more easily than rocks from reservoirs they had developed earlier. There was a lot of in-house discussion around what this large compressibility could mean and if one could use these high values to estimate recovery. The first publication dealing with the large deformations and nonlinear behavior of North Sea chalks is by Blanton (1981), see **Fig. 14.1**.

For a core plug with an initial porosity of 43%, when tested to an anticipated depletion level, this would result in a volumetric strain, ε_v, of around 8%, resulting in a porosity decrease of around 5%, using the relationship:

$$\varepsilon_v = \frac{\phi_0 - \phi}{1 - \phi}, \tag{14.1}$$

where ϕ_0 is initial porosity and ϕ is porosity as the confining pressure has increased. Volumetric strain was probably not measured but rather the porosity as a function of increase in confining pressure. The apparatus was a Hassler cell with a rubber membrane around the chalk specimen, a standard way of measuring porosity change as a function of increased hydrostatic stress. This test would result in a porosity versus confining pressure curve that would show a very non-linear behavior. An early published example from Ekofisk is shown by Johnson and Rhett (1986). Their plot indicates a porosity reduction closer to 10%, i.e. a volumetric strain closer to 15%. The difference may be the strain rate applied in the experiment, i.e. that the latter experiment is performed at much slower loading rate, an effect for chalk we will return to. In the early phase of the compaction diagram, fig. 14.1, a fairly linear trend is seen providing the bulk modulus:

$$K = \frac{\Delta \sigma_c}{\varepsilon_v}, \tag{14.2}$$

where K is the bulk modulus and $\Delta\sigma_c$ is the change in confining pressure. Using the databases and trendlines

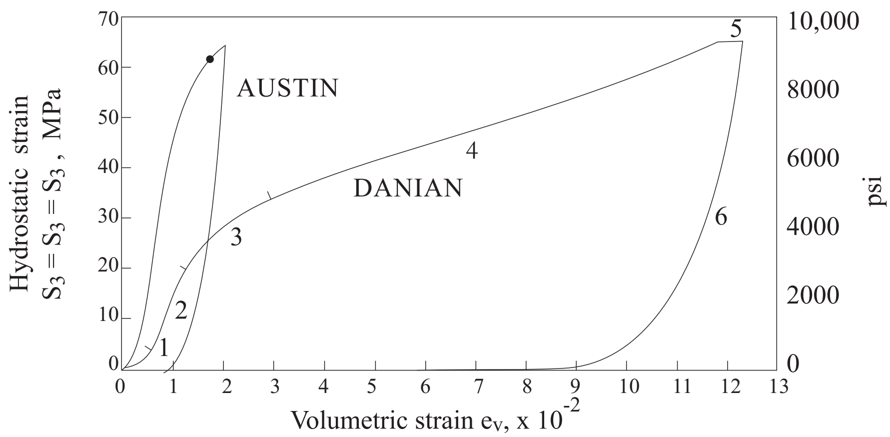

Figure 14.1: Laboratory data of a hydrostatic test on dry high porosity chalk comparing Austin chalk to Danian (around 43% porosity) from Blanton (1981).

developed over the years in JCR, a 40% porosity chalk should have a bulk modulus of around 2 to 2.5 GPa (300 to 350,000 psi). As the confining pressure is increased, the linear compaction trend would start to curve. The slope of the stress-strain curve will be lower than in the initial phase, indicating a lower bulk modulus. From the JCR database, the new slope would be around 0.25 GPa (35,000 psi). The increased compaction would not be seen for other more competent reservoir rocks. This is a result of the open pore structure in the chalk and pore collapse with increased reduction of volume, i.e., increased compaction. Although an uncommon behavior of reservoir rocks in the oil and gas industry at the time, it was normal behavior for soft clays as encountered in geotechnical engineering

As mentioned earlier, Geertsma (1957, 1973) presented his analytical work on subsidence at the time as production started from a number of the major chalk fields in the North Sea. Geertsma's analytical equation for subsidence, u_z, at a point at the surface above the center of a disc shaped compacting reservoir is:

$$u_z = -2c_m(1-\nu)\Delta p h \left(1 - \frac{\eta}{\sqrt{1+\eta^2}}\right), \tag{14.3}$$

where c_m is the uniaxial compaction coefficient, h is the thickness of the productive interval (reservoir), Δp is change in pore pressure, u_z is vertical displacement at the surface (i.e., subsidence), $\eta = D/R$ is the ratio of the depth, D, to the radius, R, of a disc-shaped reservoir, and ν is Poisson's ratio. Given an estimate of vertical strain we can replace c_m and Δp in Eq. 14.3 with the vertical strain, since

$$\varepsilon_v = c_m \Delta p. \tag{14.4}$$

If the reservoir deformation just is uniaxial strain, i.e., only deformation in the vertical direction and no deformation allowed laterally, not an unreasonable assumption for a wide reservoir at depth, the volumetric strain measured in the hydrostatic test discussed above can be transformed into vertical strain of 8% as a simplification and entered into Eq. 14.3. Poisson's ratio 0.2 for chalk and 0.4 for shale, and a value of 0.3 can be assumed for the uniform elastic half-space. If we use 250 million m^2 for areal extent of the reservoir, a depth of 3000 m, and effective reservoir thickness of 100 m, this will result in a seafloor subsidence above the chalk fields of around 7.6 m. The seafloor subsidence was 2.5 m at Ekofisk in 1984 and is now around 10 m, while at Valhall it is 6.5 m. Gutierrez, Barton et al. (1995) discussed the applicability of Geertsma's equation to the subsidence in North Sea fields.

There has also been efforts to make more accurate predictions of subsidence for the North Sea chalk fields. This has resulted in laboratory testing of chalk, and development of numerical, geomechanical models. These models have also been applied to other types of engineering problems than just compaction and subsidence. Numerical models use mathematical equations to calculate changes in deformation and stress in the chalk and the surrounding rock mass. These equations specify a constitutive model for the chalk.

14.3 A constitutive model.

The simplest form of a constitutive model is Eq. 14.2. for elastic volumetric deformation. This expression is linking the change in stress to the change in strain for a hydrostatic loading path. The strain dependens on the stiffness of the chalk determined by the bulk modulus, K. Another relationship used is for a triaxial loading path where the confining stress on the sample is kept constant and the axial stress is increased,

$$\Delta\sigma = E\varepsilon, \tag{14.5}$$

where E is the Young's modulus. Both Eq. 14.2 and 14.5 are based on the generalized Hooke's law which states that for loading in axial directions 1, 2, and 3, the stresses and strain are related by:

$$\begin{aligned} E\varepsilon_1 &= \Delta\sigma_1 - \nu(\Delta\sigma_2 + \Delta\sigma_3), \\ E\varepsilon_2 &= \Delta\sigma_2 - \nu(\Delta\sigma_1 + \Delta\sigma_3), \\ E\varepsilon_3 &= \Delta\sigma_3 - \nu(\Delta\sigma_1 + \Delta\sigma_2). \end{aligned} \tag{14.6}$$

Another relationship that is quite useful and can be derived from the generalized Hooke's law, often called the burial equation, and links the effective horizontal and vertical stresses, σ_h and σ_v:

$$\sigma_h = K_0\sigma_v = \left(\frac{\nu}{1-\nu}\right)\sigma_v, \tag{14.7}$$

where K_0 is the coefficient of lateral earth pressure at rest. Eq. 14.7 is developed for uniaxial strain conditions, i.e. no horizontal strains or $\varepsilon_2 = \varepsilon_3 = 0$. Eq. 14.7 is expressed in terms of effective stresses that are calculated from the total stress and pore pressure. The effective stress is an important and central concept in geomechanics. It was first suggested by Terzaghi (1943) based on observations in experiments during his work on deformation in porous media like rocks and cement:

$$\sigma = S - p_p, \tag{14.8}$$

where σ is effective stress, S is total stress and p_p is the pore pressure. The effective stress law was later extended (Biot 1941, 1955, 1956) to account for the deformability of the rock grain and for three-dimensional deformation,

$$\sigma = S - \alpha p_p \tag{14.9}$$

here α is often referred to as the Biot-Willis poroelastic coefficient. The poroelastic parameter α determines the split of the total stress between the pore pressure and the solid grains of the material.

These equations give a framework for calculating elastic deformations, i.e., if the increase in load is released the volume of rock returns to its initial dimensions. Rocks can normally be approximated as linear elastic material if the change in stress is small. If the stress state in the rock becomes too high, the rock can fail in shear and micro-cracks can develop in the rock and coalesce into shear bands that can be observed by the naked eye. In Chapter 6 we discussed how the chalk sample loaded under hydrostatic conditions failed in a pore collapse mode under high hydrostatic compression. In this compressive failure mode the micro-cracks are developing more uniformly through the rock volume and result in a homogenous failure of the pore structure. If the rock is suffering too much tension the micro-crack development will result in a tensile fracture that will split the rock. The different failure modes are shown in **Fig. 14.2**.

The next step to model chalk behavior is to develop expressions to decide if the rock being loaded is still behaving elastically or if the load has induced significant permanent deformations. To do so, we need to develop what is called a failure criterion or a yield surface. This yield surface is a mathematical expression

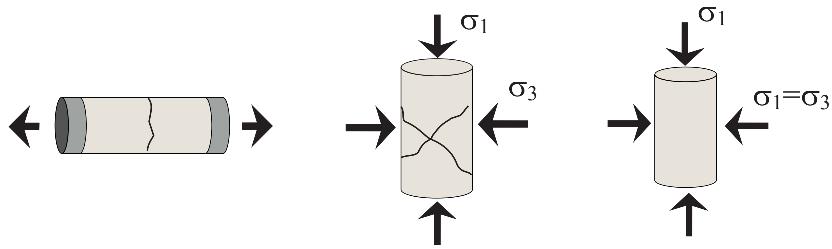

Figure 14.2: Illustration of the 3 most common failure modes of rock, tensil failure, shear and pore collapse.

showing if the material is still elastic or has started to fail. One of the most famous yield surfaces or failure criteria is the Mohr-Coulomb criterion. This criterion is only applicable for shear failure and is expressed as

$$\sigma_1 - \sigma_3 = (\sigma_1 + \sigma_3)\sin\phi + 2c_o\cos\phi. \tag{14.10}$$

Here σ_1 is the maximum principal stress, σ_3, is the minimum principal stress, c_0 is the cohesion and ϕ the internal friction angle. If the stress differential $(\sigma_1 - \sigma_3)$ reaches the failure surface then the rock has failed in shear and shear bands may start to form. Failure does not occur when the stress differential is below the failure surface. The rock is then behaving elastically.

In tension, assuming compressive stresses are positive, the failure criterion is expressed by a tensile cut-off:

$$|-\sigma_3| > T_o, \tag{14.11}$$

where T_o is the tensile strength of the rock. Eq. 14.11 states that negative stresses in a rock mass cannot exceed the tensile strength.

A simple failure criterion for hydrostatic compression or "pore collapse" is

$$\sigma_c > P_c, \tag{14.12}$$

where σ_c is the confining stress, and P_c is the hydrostatic yield strength or pore collapse parameter of the material.

In general, if one tests rocks and porous materials using any imaginable combination of the three principal stresses σ_1, σ_2 and σ_3 on the rock volume, the failure points in shear, tension and pore collapse will form a composite three-dimensional failure surface in principal stress space. An example of a full three-dimensional model is shown in **Fig. 14.3a** for the Sandia Geomodel Fossum, Brannon et al. (2004). The composite yield/failure surface has the general mathematical form of This yield surface has in general three main parts. At the negative side of the origin of the σ_1, σ_2, and σ_3 axes is the zone for tensile failure. At the more linear conical portion of the surface in the positive stress region is the zone for shear failure. At high compressive stresses, the failure surface rounds off and closes the cone, and this is the zone of pore collapse. This rounded end of the yield surface is often referred to as the end-cap.

Another feature of the composite yield surfaces of rocks is the shape as one looks through the hydrostatic $\sigma_1 = \sigma_2 = \sigma_3$ axis towards the origin, as shown in Fig. 14.3a. The non-circular shape in the plane perpendicular to the hydrostatic axis is because rocks are stronger in triaxial compression than in triaxial extension in terms of shear stress. The plane perpendicular to the hydrostatic axis is also referred to as the π-plane or the deviatoric plane. An illustration of this plane is given in **Fig. 14.3b**.

$$f = f(\sigma_1, \sigma_2, \sigma_3). \tag{14.13}$$

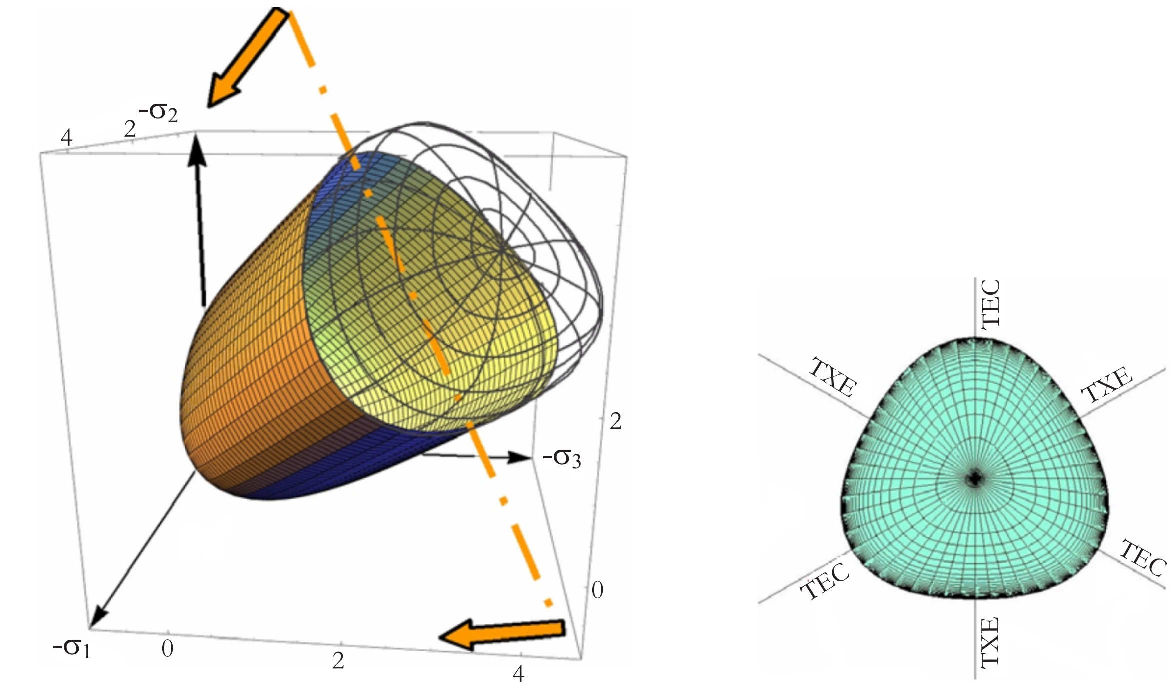

(a) (b)

Figure 14.3: (a) A typical 3D yield surface for rocks in principal stress space, (b) A typical view down the hydrostatic axis inside a yield surface of a rock. The asymmetry is because the rock has a lower strength in triaxial extension (TXE) compared to triaxial compression (TXC) (courtesy of Fossum, Brannon et al. (2004)).

As mentioned, rocks undergo permanent deformation once loaded to yield or failure. If unloaded, the material recovers some of the deformations, which are the elastic strains, but retains some permanent deformations, which are the plastic strains. A class of material is one that continues to deform under constant stresses once the loads have reached the failure surface. These are called perfectly plastic materials. However, there is a class of materials that continue to gain strength as plastic deformation occurs. These are called strain hardening elastoplastic materials where the yield surface expands with the stress state. The yield surface continues to expand, usually uniformly which is the case for isotropic hardening, until the failure surface is reached. Yet another class is where the yield surface shrinks with deformation and the material undergoes strain softening with loading. This strain softening phenomenon is associated with instability due to strain localization leading to the creation of shear bands in the material. How the yield surface evolves during loading will dictate the stress-strain behavior of the rock. The evolution of the yield surface during loading is prescribed by a "hardening rule".

Finally, one needs to have rules of how plastic deformation in the material will evolve once the stress state has reached the yield surface. This requires a "plastic potential surface" or a "plastic flow rule". For certain modes of deformation such as a pore collapse and tensile failure, the plastic potential coincides with the yield surface. This means that the plastic strain increment vectors are normal to the yield surface. In this case, the flow rule is said to be "associative". In some cases, particularly for shear deformation, the plastic potential is different from the yield surface and the plastic strain increment vectors are not normal to the yield surface. This flow rule is called "on-associative". For the case of the Mohr-Coulomb criterion (Eq. 14.10), a non-associative flow rule is given by the plastic potential

$$(\sigma_1 - \sigma_3) = (\sigma_1 + \sigma_3) \sin \psi, \tag{14.14}$$

where ψ is the dilation angle which prescribes how much shear-induced volume increase the rock will undergo during shearing. Typically, $\psi < \phi$, which is the reason why in shear, the flow is non-associative. Using the yield surface as the plastic potential or assuming $\psi = \phi$ will yield too high dilative strains when the material yields or fails in shear.

There are many ways of formulating a constitutive model, but a normal way of doing this is to use stress invariants which are independent of the choice of the reference axes for the model. One of the most famous constitutive models for soils and rocks is the Cam-Clay model developed by Roscoe, Schofield et al. (1958), and Schofield and Wroth (1968) based on Critical State Soil Mechanics. This model was developed using the

"Cambridge" stress invariants p and q which have also been used widely in the modeling of chalk. The stress invariant p is the effective mean stress is

$$p = (\sigma_1 + \sigma_2 + \sigma_3)/3, \tag{14.15}$$

where $\sigma_i = S_i - \alpha p_p$ is the effective principal stresses, as discussed earlier. The stress invariant q is the deviatoric shear stress

$$q = \frac{1}{\sqrt{2}}\sqrt{(\sigma_1 - \sigma_2)^2 + (\sigma_1 - \sigma_3)^2 + (\sigma_2 - \sigma_3)^2}. \tag{14.16}$$

Fig. 14.4 shows how a yield surface typically looks in $p - q$ space. A $p - q$ diagram is often used to present laboratory data from chalk.

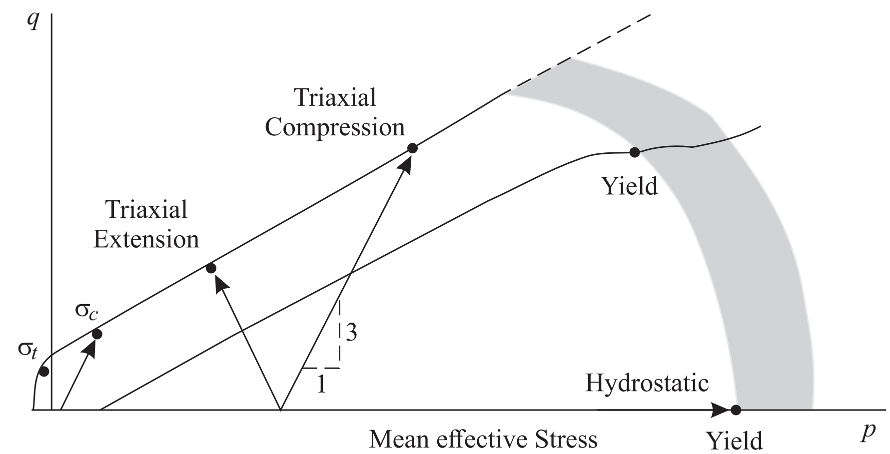

Figure 14.4: Yield surfaces in the $p - q$ diagram including examples of laboratory tests used to define the yield surface.

What we have reviewed now are the components needed for establishing a constitutive model for rocks. What one will need to do is to fit this general model to the rock type that needs to be modeled. What one will typically do as a minimum is to perform a suite of laboratory tests with loads that are probing the yield surfaces at different locations. In this way the shapes of the yield and failure surfaces can be confidently established. Typical tests are tensile strength test (often Brazilian split tension test), triaxial tests at varying levels of confining stresses to penetrate the shear surface and the end cap. Uniaxial strain tests (or K_0-compaction tests) will also penetrate the end cap. A hydrostatic test will penetrate the end-cap at the intercept with the hydrostatic axis. To establish the shape of the yield surface in the π-plane, cubical true triaxial testing is needed, where different magnitudes of the three principal stresses σ_1, σ_2 and σ_3 can be applied independently.

A three-dimensional version of the $p - q$ diagram where the third axis represents porosity is a useful way of visualizing how the various yield surfaces evolve with loading. This three-dimensional plot provides the basis for establishing the plastic hardening rules for the different yield and failure surfaces. Finally, the plastic strain increment vectors can be plotted superimposed on the established yield and failure surfaces to deduce the plastic potential surfaces or the flow rules. Extensive experimental study has now shown that the plastic flow is typically associative for tensile failure and pore collapse, but non-associative for shear failure. Also, plastic flow is associative in the π-plane leading to what is called "deviatoric normality".

When the surface and their required parameters are fitted to the laboratory data, one can start to implement the model in the framework of elastoplasticity theory to predict the behavior of the rock type in question. The next section will go through some of the specific elements of constitutive models for chalk based on the framework just described.

14.4 A constitutive model for chalk

The early chalk models were based on a geotechnical framework, particularly the Cam-Clay model Plischke (1994). Modified Drucker Prager with an elliptical end-cap was also used (Pattillo, Kristiansen et al. (1998), as well as was single surface models with continuous yield surfaces composed of a slightly curved Mohr-Coloumb shear surface and curved end cap (Papamichos, Brignoli et al. 1997; Plischke 1994). Share experience from modeling several chalk fields. His model had roots in the Cam-Clay model. In JCR V, the work on a dedicated chalk model was started by (Gutierrez 1998, 1999) . This work was continued in JCR VI by Gutierrez and Hickman (2006) and Hickman and Gutierrez (2007), and reviewed by Lade (2004). This model was programmed in FORTRAN by Chin (2006) and implemented in a finite element code by Plischke (2006).

The main objective when developing a constitutive model is to have a numerical way of predicting what the stress-strain response will be of the specific material in question. The following is a short summary of the work by Gutierrez and Hickman (2006) to develop the Unified Chalk model in JCR Phase VI. Please consult the original JCR report for all the details.

As we have already discussed the chalk material response to load is highly nonlinear. The first task is then to determine what type of nonlinear constitutive model is most applicable to model chalk. The choice is between nonlinear elastic, elastoplastic, and elastoviscoplastic models. Of these options, a rate-dependent elasto-viscoplastic model was chosen. Prior to this work most models applied on chalk had been rate independent elastoplastic. However, extensive experimental studies have conclusively shown the time and rate dependency of chalk response, requiring elasto-viscoplasticity model.

Rate-independent mechanical behavior of chalk is typically described by a multi-mechanism elastoplastic model which consists of a composite yield surface. The composite yield surface contains regions which activate the pore collapse, shear failure, and tensile failure mechanisms as shown in the **Fig. 14.5**. It is important to keep in mind that the properties needed to produce the yield surface of chalk can be predicted from initial porosity of the chalk plugs as illustrated in the previous section on rock mechanics of chalk in this book.

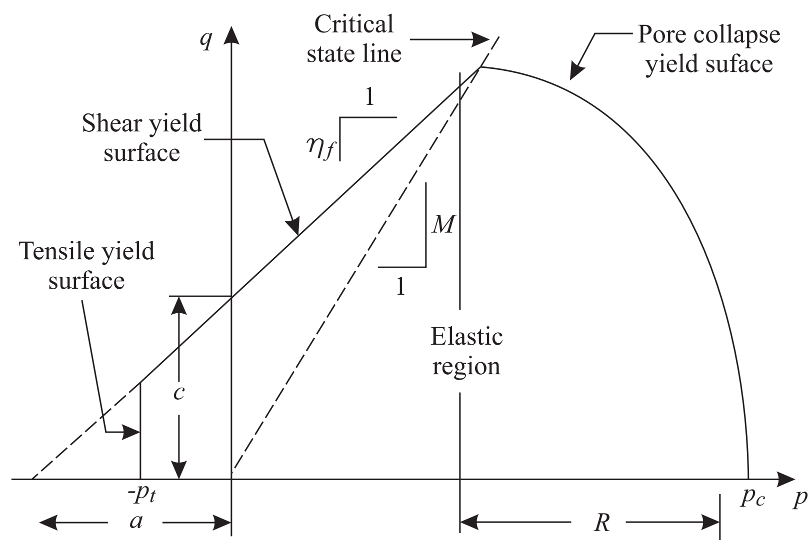

Figure 14.5: Illustration of the main components of an elastoplastic model of chalk (redrawn from Gutierrez and Hickman (2006)). The yield surface is divided into a tensile part, a shear part and a pore collapse part. The other parameters are $\breve{}p_t$ which is the tensile strength, q_0 is linked to cohesion of the material, n_f is linked to the internal friction of the material, p_c is the hydrostatic yield and R is a parameter that dictates the transition between shear failure and pore collapse, and the shape of the cap surface.

To model three-dimensional loading conditions, an associative William and Warnke (1975) yield criterion is used in the π-plane, the shape of which is shown in **Fig. 14.6**.

Rate-dependent elastoviscoplastic constitutive models for chalk are similar to the rate-independent elastoplastic models (i.e., they have the same shapes for the composite surface) but also have the capability to simulate rate-dependent behavior. Rate dependency typically occurs only during pore collapse, and shear and tensile failures are assumed to be rate independent. An example of a rate-dependent constitutive model with such a viscoplastic potential surface follows from the model of Gutierrez (1999) . The next section will go bit deeper into the time dependence of chalk.

14.5 Creep, strain rate and time-dependent behavior

Sec. 6.4.4 provides an introduction to strain rate effects in chalk and the de Waal b factor, (de Waal 1986). This section will elaborate on the topic as well and discuss how creep has been implemented in numerical chalk models. Laboratory measurements are briefly discussed in terms of chalk models.

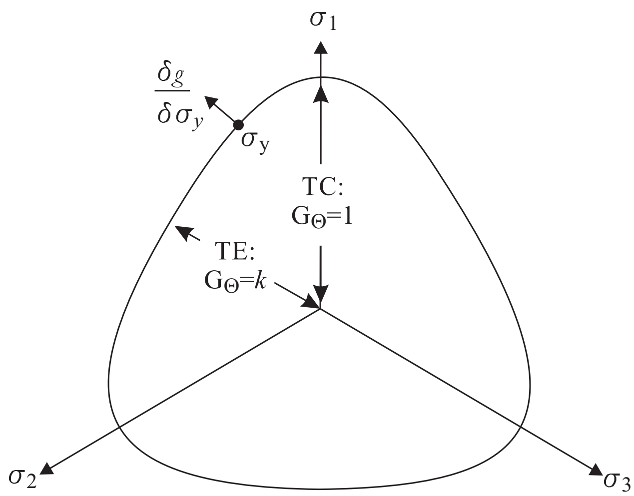

Figure 14.6: Shape of the yield surface in the π-plane for the UCM, redrawn from Gutierrez and Hickman (2006). Note that the plastic increment vectors are normal to the yield surface (i.e., the π-plane yield surface and plastic potential coincide resulting in deviatoric normality).

Rocks typically show a delayed response to changes in load. This is related to the time it takes to adjust the grain structure to the new load and involves grain sliding, grain rotation, microcracking and redistribution of load from areas experiencing volume reduction in the grain structure to surrounding grain structure that then may fail and result in volume reduction, repeating the process. This has been referred to as the nucleus of strain failure process by Andersen (1995).

This type of behavior is also observed as the sample is loaded faster and faster, and the rock stiffness will increase proportionally. The same is true if the rock is loaded slower and slower, then the stiffness will be reduced. The deformation process is often referred to as a strain rate dependence. Creep is a related phenomenon, but usually observed as continued deformation after the loading is stopped and held constant. The continued deformation is typically decaying with time in a logarithmic or powerlaw fashion. These phenomena are also referred to as time-dependent deformation or viscous deformation in some cases.

Creep deformation has also been used a lot to understand the weakening impact of various pore fluids on the chalk. That the replacement of one fluid with another is most often impacting the creep behavior. The properties impacting creep seems to be altered due to the water weakening. The weakened chalk, with altered grain contact properties, is seeking a new equilibrium through load and creep.

Johnson and Rhett (1986) point out that the North Sea reservoir chalk strain at a certain stress level is time-dependent and includes creep. They suggest predicting the ultimate strain at a given stress level by plotting the inverse cumulative volume change $(1/\varepsilon_{\text{vol}})$ versus theinverse of time $(1/t)$, see **Fig. 14.7**.

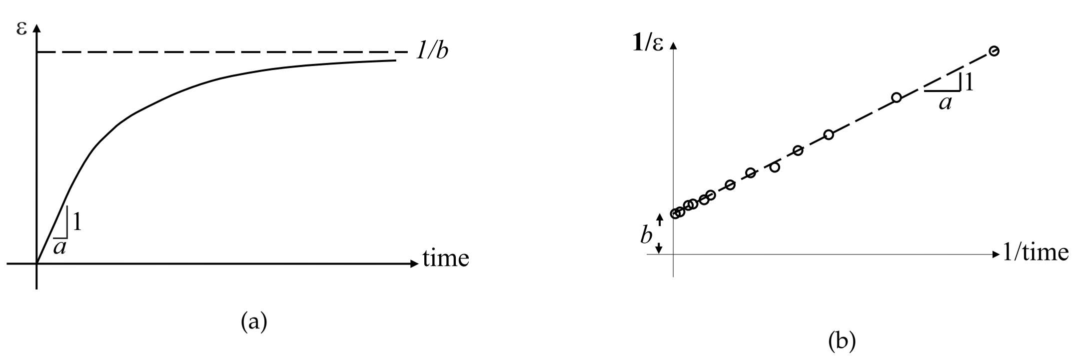

Figure 14.7: The hyperbolic time-dependent model is characterized by a limiting strain value shown in (a). Model parameters are found from creep test data by plotting (1/time) versus (1/creep strain) as shown in (b). (Redrawn)

Other rate-dependent models for soft rocks have been suggested with a variety of formulations. The first discussion of creep in chalk with reference to the Bjerrum (1967) and de Waal (1986) creep models was by Ruddy, Andersen et al. (1989) for Valhall chalk. The creep behavior of chalk has been modeled by Andersen, Foged et al. (1992) using the logarithmic rate-type model of de Waal (1986) which was developed for soft reservoir rocks (mostly sand). This model is very similar to that of Bjerrum (1967), but is formulated differently. Use of de Waal's model produces the similar behavior as Bjerrum's model, but makes no reference to material age as an example (Gutierrez 1999). The de Waal model (1986) has been implemented in a constitutive model for chalk and used on field scale problems by Kristiansen and Plischke (2010).

The unified chalk model (UCM) was based on the Bjerrum (1967) concept originally used to describe the behavior of soft Norwegian clays. Gutierrez (1999) selected this concept after a careful comparison of Bjerrum (1967), de Waal (1986) and a viscoplastic model. Gutierrez (1999) concludes that a viscoplastic model will not be able to model geomaterials satisfactorily and will be complicated to implement numerically in a finite element code. Gutierrez (1999) also concluded that the UCM model based on Bjerrum (1967) has many similarities to the de Waal (1986) model, with some advantages.

14.6 Water and chalk

Pore fluid composition has been known for many years to greatly affect the mechanical behavior of high-porosity chalk. The stiffness, pore collapse yield strength, shear strength, tensile strength, and creep rate have all been shown to be affected by the pore fluid, as summarized in the chapter on Rock Mechanics, Chapter 6. The strength of water-saturated English outcrop chalk in unconfined compression was reported by Meigh and Early (1957) to be two to three times less than that of corresponding air-dry or oven-dry chalk. Numerous experimental studies performed in the intervening 50 years have confirmed that dry chalks are stronger than oil-saturated chalks, which are in turn stronger than water-saturated chalks, (Carter and Mallard 1974; Simon, Coulter et al. 1982; Newman 1983; Andersen, Foged et al. 1992; Matthews and Clayton 1993; Schroeder and Shao 1996; Risnes, Kristensen et al. 1996; Risnes and Flaageng 1999; Gutierrez 1999; Hickman and Gutierrez 2007; Hickman, Gutierrez et al. 2008; Homand and Shao 2000; Talesnick, Hatzor et al. 2001; Collin, Cui et al. 2002; Risnes, Haghighi et al. 2003; Risnes, Hole et al. 2004; Schroeder 2003; Madland 2005; Korsnes 2007; Madland, Hiorth et al. 2011).

As to the effects of saturating pore fluid, several different models have been proposed to describe this behavior. The various models are described in the following paragraphs.

The pore fluid-dependent model of de Gennaro, Delage et al. (2003); Collin, Cui et al. (2002) is the Barcelona Basic Model (BBM) proposed by Alonso, Gens et al. (1990) for unsaturated soils. The BBM is formulated using suction, which is related to the capillary pressure or the difference between oil and water pressures in chalk, as an independent variable. The BBM separates irreversible strains into mechanical and suction-based components. The model of de Gennaro, Delage et al. (2003); Collin, Cui et al. (2002) is formulated such that that both cohesion and preconsolidation stress vary with suction, but friction angle is independent of suction.

The pore fluid-dependent model of Homand and Shao (2000) is formulated so that irreversible strains are generated if the water saturation increases from a value less than the critical value to a value greater than the critical value. In contrast to the BBM, the variation in yield surface is not continuous but instead is abrupt, occurs at some critical value of water saturation, and does not depend on suction. The yield surfaces contract when water saturation increases to a critical value. If the force on a sample remains constant during a decrease in suction, large irreversible strains are produced. In the model of Homand and Shao, the cohesion, friction angle, and pre-consolidation stress all change when water saturation increases to the critical value (**Fig. 14.8**).

Gutierrez (1999); Gutierrez, Øino et al. (2000) formulated the pore fluid-dependent model only as a modification to time-dependent behavior. This model is formulated so that the creep parameter ψ increases as water saturation increases. Since the age of the chalk depends on the creep parameter in the time-dependent model of Gutierrez, the viscoplastic strain rate increases when ψ increases, even though the yield surface undergoes no instantaneous change. Only the pore collapse yield mechanism is a function of the pore fluid-dependent model; the shear yield behavior is not affected by pore fluid composition in this model. This model was later extended by Hickman and Gutierrez (2007); Hickman, Gutierrez et al. (2008) to allow for effects of pore fluid changes on other model parameters. Of the 13 model parameters required in the UCM, it was found that nine parameters were dependent on pore fluid composition. Examples of the dependency of some the parameters are shown in (**Fig. 14.9**).

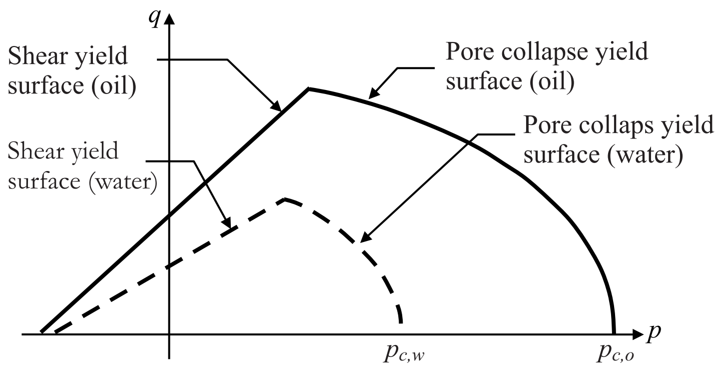

$$d\varepsilon_{ij} = d\varepsilon^{e}_{ij} + d\varepsilon^{p}_{ij} + \Delta\lambda_w \frac{\partial g}{\partial \sigma_{ij}}, \tag{14.17}$$

$$\Delta\lambda_w > 0 \text{ for } S_{wi} < S_{wc} < S_{wf},$$
$$\Delta\lambda_w = 0 \text{ for } S_{wi} > S_{wc} \text{ or } S_{wf} < S_{wc}, \tag{14.18}$$

where λ_w is water-induced plastic multiplier, S_{wi} is initial water saturation and S_{wf} is final water saturation.

Figure 14.8: Pore fluid-dependent model of Homand and Shao (2000) differs from the Barcelona Basic Model because the yield surface changes abruptly when water saturation increases to the threshold value redrawn (after Homand and Shao (2000)).

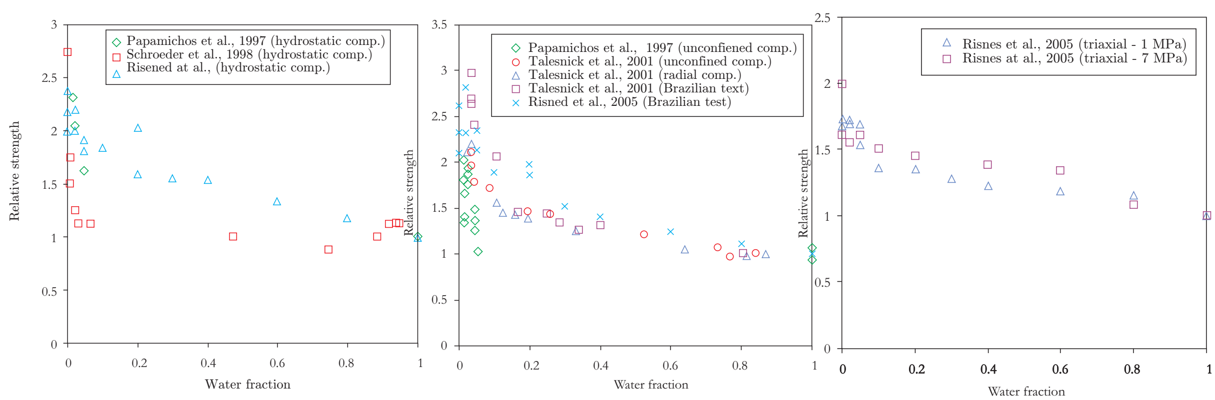

(a) (b) (c)

Figure 14.9: Relative strength values for (a) reference pore collapse yield stress; (b) unconfined compressive strength and tensile strength; (c) shear strength decrease as water saturation increases in chalk Hickman, Gutierrez et al. (2008).

It can be seen for all pore fluid dependent parameters, the value of each parameter drops significantly as water displaces oil for water saturations below about 25%. Above this saturation, the parameter becomes nearly constant and equal to the value for water-saturated chalk. The changes in the different parameter values as function of water saturation S_w may be filled by the same "water-weakening" function

$$N = N_{\text{oil}} + (N_{\text{oil}} - N_{\text{water}})(1 - S_w)^b, \tag{14.19}$$

where N is any of the model parameters that vary as a function of pore fluid composition, N_{oil} is the parameter value for oil-saturated chalk or $S_w = 0$, N_{water} is the parameter value for water-saturated chalk or $S_w = 100\%$, and b is an empirical exponent. The parameters in eq. 14.19 can be obtained for different chalk types from the JCR database, or from laboratory data, while it is recommended to use a value of 20 to 30 for the exponent b.

Fig. 14.10 depicts the variation of the pore fluid dependent parameters with fluid saturation. Implementation of the pore fluid dependent materials properties used a Damage Mechanics formulation as presented in Hickman, Gutierrez et al. (2008) to account for the water weakening. Pore fluid dependence is included in the model of

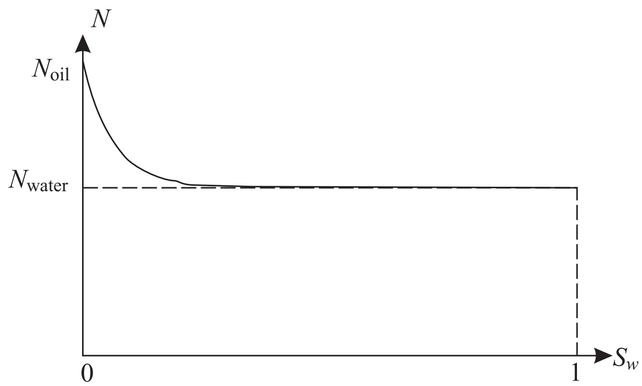

Figure 14.10: Variation in model parameter N as function of water saturation Hickman, Gutierrez et al. (2008).

Papamichos, Brignoli et al. (1997) in much the same way as for the models of de Gennaro, Delage et al. (2003); Collin, Cui et al. (2002). Both the tension cut-off (which acts as a surrogate for cohesion) and pre-consolidation stress vary as a function of water saturation. While the weakening mechanism is attributed to changes in capillary forces, the model is not formulated in terms of suction. The elastic modulus also decreases as water saturation increases, while the Poisson's ratio is not affected.

The pore fluid-dependent model of Piau, Bois et al. (1998); Maury, Piau et al. (1996); Piau and Maury (1994, 1995) is formulated using the concept of the "yield surface jump at the waterfront" (YSJW). This concept is much like the model of Papamichos, Brignoli et al. (1997) in that the yield surface changes continuously as a function of water saturation. Both the shear yield surface and pore collapse surface are affected by water saturation in this formulation. The friction angle, critical shear stress ratio, and pre-consolidation stress all change with water saturation, **Fig. 14.11**.

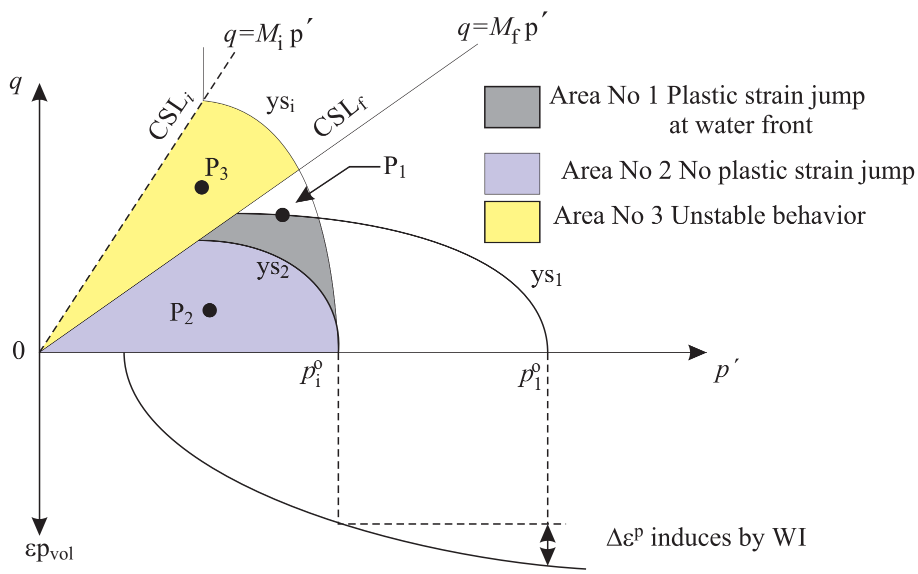

Figure 14.11: The pore fluid-dependent model of Piau and Maury changes the size of the yield surfaces as a function of water saturation, including changes in pre-consolidation stress, friction angle, and critical shear stress ratio. Instantaneous change in yield surface produces a "yield surface jump at the waterfront" (Maury, Piau et al. 1996).

Plischke (1994, 1996) includes a pore fluid-dependent component in simulating the effects of waterflooding. In this model, the pre-consolidation stress decreases gradually as water saturation increases. An explicit function which relates water saturation to pre-consolidation stress is not given.

The majority of models vary the size of the initial yield surface as a function of the water saturation or of the suction, such that changing the pore fluid causes an instantaneous change in the position of the yield surface. The UCM of Gutierrez considers the effects of saturating fluid in a different way, as a set of parameters which vary and depend on water saturation.

The basic approach used in the model by Kristiansen and Plischke (2010) is that pore collapse strength is a function of water saturation for a given strain rate.

14.7 Temperature effects

Temperature can impact deformation in many ways. Most obvious in geomechanics is the thermo-elastic effect that is, in its simplest form, given by

$$\Delta\sigma = \frac{E}{1-\nu}\alpha_T \Delta T, \tag{14.20}$$

where $\Delta\sigma$ is change in stress due to change in temperature ΔT, E is Young's Modulus, ν is Poisson's Ratio and α_T is the thermal expansion coefficient of the rock.

This effect can also be coupled to the pore pressure, which is maybe more important for material with even lower permeability than chalk. In this case, the effect can be modeled as porothermoelastic or porothermoelastoplastic materials.

These effects are important around injection of fluids with other temperature than the in-situ formation. Cooling around water injections will reduce the stresses in the cooled region and hence promote thermal fracturing that will increase injectivity. Tjetland, Kristiansen et al. (2007) quantifies the thermoelastic and the poroelastic effects for the soft Tor formation at Valhall and concludes that due to the low permeabillity and resulting high pore pressures in the matrix around injectors combined with a low Young's Modulus due to the soft high porosity chalk, there would, in that case, not be possible thermally to fracture the water injectors. At lower porosities, this may be more favorable, but will depend on the magnitude of the thermoelastic versus poroelastic effect.

The thermal expansion coefficient of chalk has not reached any wide interest. In general, the thermal expansion coefficient of a rock is dominated by one of the minerals.

In recent years, the importance of temperature on the chemical aspects of water weakening of the chalk has been demonstrated. Hence it is belived that modeling of coupled thermal effects in geomechanical models will be important in the future. Ther will be a need for thermo-chemico-poroelastoplastic models.

14.8 Constitutive models used for field studies of chalk currently

The constitutive models that are currently or frequently used to model chalk behavior on the reservoir scale are:

14.8.1 UCM

The first version of the UCM model was developed by Gutierrez (1998); Gutierrez and Lewis (1998) as part of JCR V and was later improved in JCR VI by Gutierrez and Hickman (2006); Hickman and Gutierrez (2007). The preliminary version was implemented in VISAGE for performing coupled modeling and micro-seismic studies at Valhall (Barkved, Buer et al. 2003; Pettersen and Kristiansen 2009; Zhang, Koutsabeloulis et al. 2011). VISAGE was acquired by Schlumberger in 2007 and has since been used to model fields like Syd-Arne (Herwanger, Schiøtt et al. 2010) and Valhall (Han, Vaughn et al. 2013) by Hess. The model has also been used by ConocoPhillips on Ekofisk and Eldfisk.

14.8.2 ISAMGEO

The ISAMGEO constitutive model has been developed over time for chalk and used in several JCR phases from the early 1990's. From the late 1990s, the constitutive model in ISAMGEO was based on the work by Papamichos, Brignoli et al. (1997). Through the 2000s, the model was enhanced to account for the strain rate dependence and water weakening in order to model Valhall for BP (Kristiansen and Plischke 2010). The model was also compared to the UCM model as part of the JCR VI on a Valhall full field model. The model results agreed well, considering that no efforts were made to adjust the parameters in the model to give the exact same stress-response for the same chalk. As expected, considering the UCM model was a very newly developed model, the ISAMGEO model was more computational effective. The model has also been extended to include shear localization in chalk by the use of the Cosserat approach in a project with GEO and sponsored by BP, ConocoPhillips and Mærsk. The Cosserat approach used was originally presented by Statoil for the Troll field multi-lateral project in sandstones (Plischke, Kageson-Loe et al. 2004). The constitutive model, excluding the strain localization part, is currently also implemented in a near wellbore simulation tool under development by a small Norwegian numerical company, Petrell, sponsored by BP and ConocoPhillips. It has also been implemented in VISAGE by Schlumberger.

14.8.3 SR3

The first application of the Soft Rock 3 (SR3) model by Rockfield in their finite element code ELFEN on chalk was published by Crook, Yu et al. (2008). The SR3 model has many similarities to the other models discussed. The application was reproducing the chalk liquefaction experiments performed by Flatebø (2005) . The model has been used to model fault re-activation, micro-seismic modeling and 4D seismic modeling Angus, Verdon et al. (2011). The model is available as an explicit finite element model and can therefore run very fast with tight coupling between the geomechanical finite element model and the finite difference reservoir flow model. The model is currently in use for reservoir and geomechanical coupling of the Valhall and Hod fields by BP as illustrated in a paper by Angus, Verdon et al. (2011).

14.9 Effects of stress on permeability

As the chalk compacts, the porosity and permeability is reduced. This is a normal observation in porous media. Many studies in JCR up through the years have focused demonstrated this fact.

In geomechanical modeling, permeability does not play any significant role for some types of chalk models. For example, a one-way coupled model is usually applied when the porosity and permeability changes are handled in the flow model. With a more accurate two-way coupled system, the permeability decline can be handled in the flow model or the geomechanics model, the most important iteration between the two model is on pore pressure (in the flow model) and the pore volume change in the geomechanics model.

In both cases of coupling approach, one will need to use a function to convert pore volume changes to changes in the permeability. This is typically done with a general form of the Kozeny-Carman equation

$$k = C\frac{\phi^3}{(1-\phi)^2}, \tag{14.21}$$

where k is absolute permeability, ϕ porosity and C a function of grain diameter and tortuosity.

The pore volume deformations are then converted to absolute permeabillity that will decrease for depletion and increase for re-pressurisation.

In the chalk literature there have been different field observations reported in terms of permeabillity variation with depletion. Powley, Peng et al. (1992) report permeability decline with depletion. Teufel and Rhett (1991) report permeabillity increase during depletion at Ekofisk.

The reason for this difference is probably not related to the matrix behavior as discussed above, but more related to the mechanical properties in the very weak Tor formation versus the more competent Tor and Ekofisk formation in Ekofisk. We will discuss some of these aspects in the next section on fracture permeability.

14.10 Fracture permeability

Fracture characterization has been on the agenda since the chalk fields were discovered. Much work has also been dedicated to this topic in JCR. Many efforts have been dedicated to the geologic mapping of fractures, less to the multiphase flow aspects required for implementation in a field model. The geoemchanical aspect of fracture permeability is to determine how the changes in stress impact the fracture permeability. The fracture permeability depends on the aperture of the fracture as shown by Witherspoon, Wang et al. (1980),

$$k = \frac{a^2}{12}, \tag{14.22}$$

where a is the fracture aperture. Fracture flow is not a phenomenon only of interest to the oil and gas industry, but also in hydrology and nuclear waste disposal. There are fracture models that handle the geomechanical aspects of flow in fractures, or more correctly how stress changes are impacting the aperture of fractures. In the work on the UCM model in JCR Phase VI, Gutierrez (2007) developed a model to address this point. A smeared crack formulation (Rots and De Borst 1987) is used as the modeling framework for the fractured chalk in combination with the Barton-Bandis model for rock joints (Bandis, Lumsden et al. 1983; Barton, Bandis et al. 1985). However, the modeling of fracture chalk hydro-mechanical behavior was not a priority in the development of the UCM in JCR Phase VI, since it was felt that more development was needed in the characterization of input for such a model and also to link and couple such a geomechanical model to the flow model.

What a geomechanical model of fracture deformation can offer depends on the chalk input parameters to calculate how much the aperture will decrease or increase with the stress in the rock and the pressure in the fracture. If the fracture is re-activated it can also be determined if the fracture permeability will increase or decrease since this also depends on the geomechanical properties of the chalk. The fracture permeability will increase if the re-activation results in dilation of the fracture. The fracture permeability will decrease if the re-activation results in contraction and hence closure of the fracture. Fracture behavior is an important mechanism to understand to optimize waterfloods as shown by the experiment presented by Tjetland, Kristiansen et al. (2007) that a 6 mm shear displacement of a fracture in the chalk resulted in a fracture permeability lower than the matrix permeability in a waterflooded chalk.

Procedures exist to develop fracture rock mass models if the appropriate input from the geologic characterization is available and reservoir models can in theory handle permeability tensors and changes in them that could be predicted by a geomechanical model. This is still a potential future project for JCR. Currently the changes in fracture permeability are often handled through manual changes in transmissibility factors versus pressure in the reservoir flow model.

14.11 Modeling of the overburden

To predict compaction and subsidence in chalk fields, properties and behavior of the overburden also need to be modeled. Kristiansen (1998); Nagel (1998) addressed these topics for Valhall and Ekofisk. The overburden rock is mainly mudstones, claystones and shales, but may also contain sandstones, diatomites and carbonates, (Barkved, Buer et al. 2003). In JCR IV, there was a dedicated project on shale characterization, which tested shale cores from the Sele formation at Valhall (Berre, Gutierrez et al. 1994). The results were summarized in the JCR paper by Berre, Gutierrez et al. (1996).

Characterizing the overburden formations is also an important part of wellbore stability analysis needed to predict what mud weight one should use to drill wells with different inclinations and azimuths. The difference between predicting properties needed for a wellbore stability model and a compaction and subsidence model is mainly scale. In the compaction and subsidence model we need to capture the large scale stiffness of the grid blocks, while in the wellbore stability models we need to predict the rock strength and mechanical properties on a foot by foot basis.

The properties estimated from core to log correlations as the one for shales by Horsrud (2001) may need to be uspcaled to account for the stiffness anisotropy, plane of weakness, fractures and faults in the overburden. Kristiansen and Plischke (2010) refer to procedures developed for subsidence prediction above mines by Wittke (1990). How to appropriately upscale is an area of uncertainty. But with seiemics the increased use of 4D seismics in the chalk fields, one can start to get a bit more confident with this part of the models as well. As an example Kristiansen and Plischke (2010) also refer to 4D seismics to support the anisotropic elastic model used for the overburden.

Other aspects (Kristiansen and Plischke 2010) is the use of drained or undrained conditions in the overburden layers. They conclude that undrained is probably the preferred condition, but also that the impact of drainage condition is fairly small. The results from modelling drainage of the caprock from the reservoir are shown in **Fig. 14.12**. The figure to the left (a) is showing how pressure is changing at different locations in the caprock. At around 28 m above the top reservoir there is little change in pore pressure after 20 years of production, and 1 m above the top of the reservoir the pressure change is almost as large as in the top of the reservoir. These changes can impact the fracture gradient and the mud weight needed to avoid borehole collapse when wells are drilled through the section, as observed in the field. The impact of deformation (compaction) is only 40 cm. This is in line with a simplistic semi-analytical estimate reported by Kristiansen (1998).

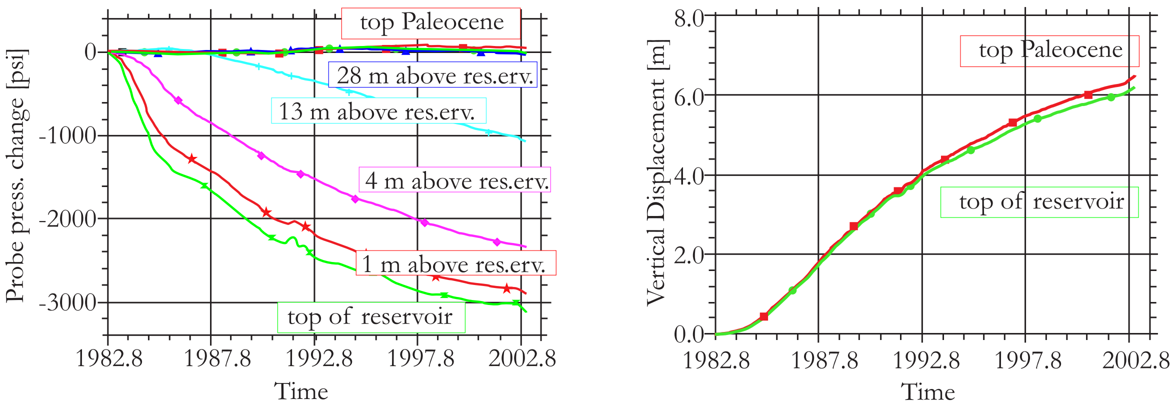

(a) (b)

Figure 14.12: Results from modelling drainage of the caprock from the reservoir.

Another aspect, which is not unique for the overburden, is the modeling of faults. This is linked to the point above about upscaling. Faults were not introduced into the full field models for chalk fields, on a regular basis, before the 2000s. There is a lot of challenges with odelling faults. Their uncertain presence and geometry are mapped from the seismics. The approaches on how to model these can be found in papers by Zhang, She et al. (2010); Kristiansen and Plischke (2010); Angus, Verdon et al. (2011). The methods vary from dedicated fault elements, elasto-plastic constitutive models for the fault elements, and use of contact elements. Each method has positive and negative aspects, but allows fault modelling and fault re-activation for chalk fields.

14.12 Initial conditions for field models

It is worthwhile to briefly discuss the initialization of the full field models of the chalk fields. This procedure seems to vary some and is somewhat determined by the modeling software applied. The objective of the initialization is to start the model close to equilibrium and replicate field conditions before production. This may sound trivial, but there are a lot of input parameters that are required for the geomechanics model. First it should produce the same geometry and initial chalk properties as in the geologic model. One should not accept a lot of compaction before the modeling starts after the initialization. This could be expected since the exact stress state, exact deformation properties and exact boundary condition for each cell in the model is not known very precisely. The issue of upscaling and faults also plays a role in the initialization of the reservoir part, as well as the overburden.

The most typical boundary conditions used for the geomechanical modeling are to anchor the bottom of the deepest underburden layer. The sides or edges are often modeled as so called "roller boundaries", i.e., this provides free movement of the edge of the model vertically, but no lateral deformation. This is the same as uniaxial strain conditions. One can also impose a larger horizontal stress in one direction than in other, to reproduce breakout patterns from caliper and image log data.

There is probably no single "right wa" to perform an initialization, but it is important to be consistent with observed data available at initial conditions and avoid issues that could make the forward prediction less accurate. The goal is to produce initial in situ stresses that are consistent and in equilibrium with the weights of the overburden materials, tectonic loads if any, the pore pressures, and heterogeneities.

14.13 Summary

This chapter covers methods to numerically model chalk, how they have evolved over time and what the current status is. One could predict the subsidence of the chalk fields based on simple hand calculations and standard oilfield core measurements already in the 1970's with fair accuracy. We have reviewed the components needed to construct a constitutive model to numerically model chalk behavior, mainly through a review of how the Unified Chalk Model (UCM) was developed in JCR. New features needed to be added to a standard elasto-plastic model is strain rate dependence and waterweakening. We review the main constitutive models in use today for modeling chalk behavior. We discuss how permeability changes can be modeled by geomechanics models, how the overburden and how faults are included in the models. We discuss aspects of the initialization process and the applications of full field geomechanics models to manage the chalk fields.

Nomenclature

a = fracture aperture
b = empirical exponent
c_m = uniaxial compaction coefficient
c_0 = cohesion
C = grain diameter function
D = depth, l
E = Young's modulus,M/Lt^2
G_θ = William-Warnke (1975) third invariant scaling factor
h = thickness of productive interval, L
k = absolute permeability, L^2
K = bulk modulus, m/Lt^2
K_0 = coefficient of lateral earth pressure at rest
M_f = Slope of critical state line after failure
M_i = initial slope of critical state line
N = model parameter that vary as a function of pore fluid saturation
N_{oil} = parameter value for oil-saturated chalk
N_{water} = parameter for water-saturated chalk
p_c = hydrostatic yield
p = stress invariant, effective mean stress, m/Lt^2
p_t = tensile strength
p_p = pore pressure, m/Lt^2
P = pressure, m/Lt^2
P_c = hydrostatic yield strength or pore collapse parameter
q = stress invariant, deviatoric share stress
R = radius, transition between shear failure and pore collapse, L
S = total stress, saturation
S_w = water saturation
S_{wc} = critical water saturation
S_{wi} = initial water saturation
S_{wf} = final water saturation
t = time, t
T_o = tensile strength of rock
u_z = vertical displacement, L
α = Biot-Willis coefficient
α_T = thermal expansion coefficient
Δp = pressure change, m/Lt^2
ΔT = temperature change
$\Delta\sigma$ = stresses change, m/Lt^2
$\Delta\sigma_c$ = change in confining pressure, m/Lt^2
ε = strain
ε_v = volumetric strain
ε_{vol} = cumulative volume change
$\dot{\varepsilon}^p_{ij}$ = directional visoplastic strain rate
η = ratio of depth to radius
η_f = stress ratio at failure
λ_w = water-induced plastic multiplier
ν = Poisson's ratio
π = porosity, internal friction angle, deviatoric plane
σ = effective stresses[†]
$\sigma_1, \sigma_2, \sigma_3$ = principal stresses
$\sigma_{h,v}$ = stresses horizontal, vertical
ψ = dilation angle, creep parameter

[†] We adopt the convention that σ usually means effective stress, see text below Eq. 14.7. In those cases where σ means total (normal) stress, it will be made clear from the content.

Subscripts

0 =	initial
c =	confining
h =	horizontal
p =	pore
t =	tensile
T =	temperature
v =	volumetric, vertical
vol =	volume
z =	z-direction
w =	water
wi =	initial water
wf =	final water

Superscripts

e =	elastic behavior
p =	plastic behavior
vp =	viscolplastic behavior

Abbreviations

BBM =	Barcelona basic model
ISAMGEO =	trademark of ISAMGEO GmbH
SR3 =	soft rock 3
UCM =	unified chalk model
VISAGE =	trademark of Schlumberger

References

Alonso, E.E., Gens, A., and Josa, A., 1990. A constitutive model for partially saturated soils. *Géotechnique*, **40** (3): 405–430. URL `http://dx.doi.org/10.1680/geot.1990.40.3.405`.

Andersen, M.A., 1995. *Petroleum Research in North Sea Chalk.* RF-Rogaland Research. Joint Chalk Research Program Phase IV.

Andersen, M.A.A., Foged, N.A., and Pedersen, H.E.A., 1992. The link between waterflood-induced compaction and rate-sensitive behavior in a weak North Sea chalk. In *Proceedings of 4th North Sea chalk symposium, Deauville*.

Angus, D.A., Verdon, J.P. et al., 2011. Integrated fluid-flow, geomechanic and seismic modelling for reservoir characterisation. *Focus Article coordinated by Kurt Wickel, UK*, 27–35. URL `http://csegrecorder.com/assets/pdfs/2011/2011-05-RECORDER-Integrated-fluid-flow.pdf`.

Bandis, S.C., Lumsden, A.C., and Barton, N.R., 1983. Fundamentals of rock joint deformation. *International Journal of Rock Mechanics and Mining Sciences & Geomechanics Abstracts*, **20** (6): 249–268. URL `http://dx.doi.org/http://dx.doi.org/10.1016/0148-9062(83)90595-8`.

Barkved, O., Buer, K. et al., 2003. 4D Seismic Response of Primary Production and Waste Injection at the Valhall Field. 02 June. URL `http://www.earthdoc.org/publication/publicationdetails/?publication=3102`.

Barton, N., Bandis, S., and Bakhtar, K., 1985. Strength, deformation and conductivity coupling of rock joints. *International Journal of Rock Mechanics and Mining Sciences & Geomechanics Abstracts*, **22** (3): 121–140. URL `http://dx.doi.org/http://dx.doi.org/10.1016/0148-9062(85)93227-9`.

Berre, T., Gutierrez, M., and Høeg, K., 1994. Norwegian Geotechnical Institute: Laboratory Testing of an Overburden Shale,. *Joint Chalk Research Phase IV*. JCR Phase IV, Project VI Compaction, Subsidence and Horizontal/Deviated Well Stability in Chalk Fields. October 14.

Berre, T., Gutierrez, M. et al., 1996. Laboratory testing of an overburden shale. In *Proceedings of the 5th North Sea Chalk symposium, Reims, France*.

Biot, M.A., 1941. General Theory of Three-Dimensional Consolidation. *Journal of Applied Physics*, **12** (2): 155–164. URL http://dx.doi.org/http://dx.doi.org/10.1063/1.1712886.

Biot, M.A., 1955. Theory of Elasticity and Consolidation for a Porous Anisotropic Solid. *Journal of Applied Physics*, **26** (2): 182–185. URL http://dx.doi.org/10.1063/1.1721956.

Biot, M.A., 1956. General solutions of the equations of elasticity and consolidation for a porous material. *J. appl. Mech*, **23** (1): 91–96.

Bjerrum, L., 1967. Engineering Geology of Norwegian Normally-Consolidated Marine Clays as Related to Settlements of Buildings. *Géotechnique*, **17**: 83–118. URL http://www.icevirtuallibrary.com/content/article/10.1680/geot.1967.17.2.83.

Blanton, T.L., 1981. Deformation of chalk under confining pressure and pore pressure. *Society of Petroleum Engineers Journal*, **21** (01): 43–50. February. URL http://dx.doi.org/10.2118/8076-PA.

Carter, P.G. and Mallard, D.J., 1974. A study of the strength compressibility and density trends within the chalk of south east England. *Quarterly Journal of Engineering Geology*, **7** (1): 43–55. URL http://trid.trb.org/view.aspx?id=38964.

Chin, 2006. Development and Implementation of the JCR 6 Unified Chalk Model into a FORTRAN Code. Tech. rep., JCR VI report.

Collin, F., Cui, Y.J. et al., 2002. Mechanical behaviour of Lixhe chalk partly saturated by oil and water: experiment and modelling. *International Journal for Numerical and Analytical Methods in Geomechanics*, **26** (9): 897–924. URL http://dx.doi.org/10.1002/nag.229.

Crook, A.L., Yu, J.G. et al., 2008. Computational Modelling of the Rate Dependent Deformation and Liquefaction of Chalk. *American Rock Mechanics Association*. Paper presented at The 42nd U.S. Rock Mechanics Symposium (USRMS), San Francisco, California. 29 June – 2 July. URL https://www.onepetro.org/conference-paper/ARMA-08-176.

de Gennaro, V., Delage, P. et al., 2003. Time-dependent behaviour of oil reservoir chalk: a multiphase approach. *Soils and Foundation*, **43** (4): 131–147. URL http://dx.doi.org/10.3208/sandf.43.4_131.

de Waal, J.A., 1986. *On the rate type compaction behaviour of sandstone reservoir rock*. Ph.D. thesis, Technische Hogeschool Delft. URL https://www.researchgate.net/profile/Hans_De_Waal2/publication/35834162_On_the_Rate_Type_Compaction_Behavior_of_Sandstone_Reservoir_Rock/links/53e1d4630cf2235f352bda13/On-the-Rate-Type-Compaction-Behavior-of-Sandstone-Reservoir-Rock.pdf.

Flatebø, R., 2005. *Stability and Flow of Chalk Near Production Wells*. Ph.D. thesis, Department of Petroleum Engineering, University of Stavanger, Norway.

Fossum, A.F., Brannon, R.M. et al., 2004. The Sandia GEOMODEL: Theory and UserÃ¢â‚¬â„¢s Guide. Tech. rep., Sandia National Laboratory, Report no. SAND2004-3226. URL http://dx.doi.org/http://citeseerx.ist.psu.edu/viewdoc/summary?doi=10.1.1.363.4082.

Geertsma, J., 1957. The effect of fluid pressure decline on volumetric changes of porous rocks. *Petroleum Transactions*, **210**: 331–340. SPE-728-G. URL https://www.onepetro.org/general/SPE-728-G.

Geertsma, J., 1973. Land subsidence above compacting oil and gas reservoirs. *Journal of Petroleum Technology*, **25** (6): 734–744.

Gutierrez, M., Barton, N., and Makurat, A., 1995. Compaction and subsidence in North Sea hydrocarbon fields. *Proc Int Worksh Rock Foundation*, **30**: 57–64. 25–30 September.

Gutierrez, M. and Hickman, R.J., 2006. Constitutive Modeling of Chalk Time-Dependent Behavior and Chalk-Water Interaction. In *Geomechanics II: Testing, Modeling, and Simulation*, 169, 269–284. URL http://dx.doi.org/10.1061/40870(216)19).

Gutierrez, M. and Lewis, R.W., 1998. The Role of Geomechanics in Reservoir Simulation. Paper SPE-47392-MS presened at SPE/ISRM Rock Mechanics in Petroleum Engineering, Trondheim, Norway. 8–10 July. URL http://dx.doi.org/10.2118/47392-MS.

Gutierrez, M., Øino, L.E., and Høeg, K., 2000. The Effect of Fluid Content on the Mechanical Behaviour of Fractures in Chalk. *Rock Mechanics and Engineering, Rock*, **33** (2): 93–117. May. URL `http://dx.doi.org/10.1007/s006030050037`.

Gutierrez, M.S., 1998. Formulation of a basic chalk constitutive model. Tech. rep., NGI.

Gutierrez, M.S., 1999. Modelling of Time-Dependent Chalk Behavior and Chalk-Water Interaction. *NGI Report No. 541105*, **4**.

Gutierrez, M.S., 2007. Formulation of a Constitutive Model for Fractured Chalk. Tech. rep., NGI. Project Report Submitted to the Joint Chalk Research Phase VI (JCR VI) Program.

Han, G., Vaughn, B. et al., 2013. Development and Calibrations of a Coupled Reservoir Geomechanic Model for Valhall Field. *American Rock Mechanics Association*. Paper presented at 47th U.S. Rock Mechanics/Geomechanics Symposium, San Francisco, California. 23-26 June. URL `https://www.onepetro.org/conference-paper/ARMA-2013-163`.

Herwanger, J.V., Schiøtt, C.R. et al., 2010. Applying time-lapse seismic methods to reservoir management and field development planning at South Arne, Danish North Sea. In *Geological Society, London, Petroleum Geology Conference series*, vol. 7, 523–535. Geological Society of London. URL `http://dx.doi.org/10.1144/0070523`.

Hickman, R.J., Gutierrez, M. et al., 2008. Modeling of pore fluid-rock interaction as a weathering process. *Intl. J. Num. Analy. Meth. Geomech*, **32**: 1927–1953.

Hickman, R.J. and Gutierrez, M.S., 2007. Formulation of a three-dimensional rate-dependent constitutive model for chalk and porous rocks. *International Journal for Numerical and Analytical Methods in Geomechanics*, **31** (4): 583–605. URL `http://dx.doi.org/10.1002/nag.546`.

Homand, S. and Shao, J.F., 2000. Mechanical behaviour of a porous chalk and effect of saturating fluid. *Mechanics of Cohesive-frictional Materials*, **5** (7): 583–606. URL `http://dx.doi.org/10.1002/1099-1484(200010)5:7<583::AID-CFM110>3.0.CO;2-J`.

Horsrud, P., 2001. Estimating mechanical properties of shale from empirical correlations. *SPE Drilling & Completion*, **16** (02): 68–73. URL `http://dx.doi.org/10.2118/56017-PA`.

Johnson, J.P. and Rhett, D.W., 1986. Compaction behavior of Ekofisk chalk as a function of stress. In *European Petroleum Conference*. Society of Petroleum Engineers. URL `http://dx.doi.org/10.2118/15872-MS`.

Korsnes, R.I., 2007. *Chemical Induced Water Weakening of Chalk by Fluid-rock Interactions: A Mechanistic Study*. Ph.D. thesis, Department of Petroleum Engineering, University of Stavanger, Norway.

Kristiansen, T.G., 1998. Geomechanical characterization of the overburden above the compacting chalk reservoir at Valhall. In *SPE/ISRM Rock Mechanics in Petroleum Engineering*. Society of Petroleum Engineers. URL `http://dx.doi.org/10.2118/47348-MS`.

Kristiansen, T.G. and Plischke, B., 2010. History Matched Full Field Geomechanics Model of the Valhall Field Including Water Weakening and Re-pressurisation. Paper SPE-131505-MS presented at SPE EUROPEC/EAGE Annual Conference and Exhibition, Barcelona, Spain. 14–17 June. URL `http://dx.doi.org/10.2118/131505-MS`.

Lade, P.V., 2004. Critical Evaluation of the JCR V Unified Chalk Model Task 1.1. Tech. rep., JCR VI report, Task 1.1.

Madland, M.V., 2005. *Water weakening of chalk. A mechanistic study*. Ph.D. thesis, Department of Petroleum Engineering, University of Stavanger, Norway.

Madland, M.V., Hiorth, A. et al., 2011. Chemical Alterations Induced by Rock–Fluid Interactions When Injecting Brines in High Porosity Chalks. *Transport in Porous Media*, **87** (3): 679–702. January. URL `http://dx.doi.org/10.1007/s11242-010-9708-3`.

Matthews, M.C. and Clayton, C.R.I., 1993. Influence of intact porosity on the engineering properties of a weak rock. In A. Anagnostopoulos, N. Kalteziotis, and R. Frank, eds., *Geotechnical engineering of hard soils - soft rocks. International symposium*, 693–702. Balkema. URL `http://eprints.soton.ac.uk/74832/`.

Maury, V., Piau, J.M., and Halle, G., 1996. Subsidence induced by water injection in water sensitive reservoir rocks: the example of Ekofisk. *Society of Petroleum Engineers*. Paper presented at European Petroleum Conference, Milan, Italy. 22–24 October. URL http://dx.doi.org/10.2118/36890-MS.

Meigh, A.C. and Early, K.R., 1957. Some physical and engineering properties of chalk. In *Proceedings of 4th International Conference on Soil Mechanics and Foundation Engineering*, 68–73.

Nagel, N.B., 1998. Ekofisk Field Overburden Modelling. *Society of Petroleum Engineers*, paper presented at SPE/ISRM Rock Mechanics in Petroleum Engineering, Trondheim, Norway. 8–10 July. URL http://dx.doi.org/10.2118/47345-MS.

Newman, G.H., 1983. The effect of water chemistry on the laboratory compression and permeability characteristics of some North Sea chalks. *Journal of Petroleum Technology*, **35** (5): 976–980. URL http://dx.doi.org/10.2118/10203-PA.

Papamichos, E., Brignoli, M., and Santarelli, F.J., 1997. An experimental and theoretical study of a partially saturated collapsible rock. *Mechanics of Cohesive-frictional Materials*, **2** (3): 251–278. URL http://dx.doi.org/10.1002/(SICI)1099-1484(199707)2:3<251::AID-CFM33>3.0.CO;2-#.

Pattillo, P.D., Kristiansen, T.G. et al., 1998. Reservoir compaction and seafloor subsidence at Valhall: SPE 47274. *Society of Petroleum Engineers*. SPE/ISRM, presented at Rock Mechanics in Petroleum Engineering, Trondheim, Norway. 8–10 July. URL http://dx.doi.org/10.2118/47274-MS.

Pettersen, Ø. and Kristiansen, T.G., 2009. Improved Compaction Modeling in Reservoir Simulation and Coupled Rock Mechanics/Flow Simulation, With Examples From the Valhall Field. *SPE Reservoir Evaluation & Engineering*, **12** (02): 329–340. URL http://dx.doi.org/10.2118/113003-PA.

Piau, J.M., Bois, A.P. et al., 1998. Water/Chalk (Or Collapsible Soil) Interaction: Part I. Comprehensive Evaluation of Strain and Stress Jumps at the Waterfront. In *SPE/ISRM Rock Mechanics in Petroleum Engineering*. Society of Petroleum Engineers. URL http://dx.doi.org/10.2118/47390-MS.

Piau, J.M. and Maury, V., 1994. Mechanical effects of water injection on chalk reservoirs. *Society of Petroleum Engineers*. Paper presented at Rock Mechanics in Petroleum Engineering, Delft, Netherlands. 29–31 August. URL http://dx.doi.org/10.2118/28133-MS.

Piau, J.M. and Maury, V., 1995. Basic mechanical modelisation of chalk/water interaction. *Unsaturated Soils*, 775–783.

Plischke, B., 1994. Finite element analysis of compaction and subsidence-Experience gained from several chalk fields. *Society of Petroleum Engineers*. Presented at Rock Mechanics in Petroleum Engineering, Delft, Netherlands. 29–31 August. URL http://dx.doi.org/10.2118/28129-MS.

Plischke, B., 1996. Some aspects of numerical simulation of water-induced chalk compaction. In *Proc. 5th North Sea Chalk Symp., Reims, France*.

Plischke, B., 2006. Development and Implementation of the JCR 6 Unified Chalk Model Tasks 1.7 and 1.8: Numerical Validation against Test Cases and Model Optimization,. Tech. rep., JCR VI report.

Plischke, B., Kageson-Loe, N. et al., 2004. Analysis of MLW open hole junction stability. *American Rock Mechanics Association*. Paper presented at Gulf Rocks 2004, the 6th North America Rock Mechanics Symposium (NARMS), Houston, Texas. 5–9 June.

Powley, K.D., Peng, C.P., and Ali, N., 1992. Simulation of a North Sea chalk reservoir with dynamic rock and natural fracture properties: Case study of the Valhall Field. *Society of Petroleum Engineers*. Paper presented at SPE Annual Technical Conference and Exhibition, Washington, D.C. 4–7 October.

Risnes, R. and Flaageng, O., 1999. Mechanical properties of chalk with emphasis on chalk-fluid interactions and micromechanical aspects. *Oil & Gas Science and Technology*, **54** (6): 751–758. URL http://dx.doi.org/10.2516/ogst:1999063.

Risnes, R., Haghighi, H. et al., 2003. Chalk–fluid interactions with glycol and brines. *Tectonophysics*, **370** (1): 213–226. URL http://dx.doi.org/10.1016/S0040-1951(03)00187-2.

Risnes, R., Hole, M., and Kwabiah, N.K., 2004. Chalk-fluid interactions with water-glycol mixtures. In *Proceedings of Workshop on Chalk Mechanical Behavior, Stavanger, Norway*, 3–4. 3–4 February.

Risnes, R., Kristensen, C.N., and Andersen, M.A., 1996. Triaxial tests on high porosity chalk with different saturating fluids. In *Fifth North Sea Chalk Symposium*, 12.

Roscoe, K.H., Schofield, A.N., and Wroth, C.P., 1958. On the yielding of soils. *Geotechnique*, **8** (1): 22–53. URL `http://dx.doi.org/10.1680/geot.1958.8.1.22`.

Rots, J.G. and De Borst, R., 1987. Analysis of mixed-mode fracture in concrete. *Journal of Engineering Mechanics*, **113** (11): 1739–1758.

Schofield, A. and Wroth, P., 1968. *Critical state soil mechanics*. McGraw-Hill London. URL `http://users.skynet.be/fc001349/files/CSSM.pdf`.

Schroeder, C., 2003. Mechanical behaviour of partially and multiphase saturated chalks and fluid-skeleton interaction: Main factor of chalk oil reservoirs compaction and related subsidence. *Final report of the EU project (PASACHALK2)*. EC Contract no. ENK6-2000-00089. URL `http://cordis.europa.eu/documents/documentlibrary/77480211EN6.pdf`.

Schroeder, C. and Shao, J., 1996. Plastic deformation and capillary effects in chalks. In *5th North Sea Chalk Symposium*, 1–14.

Simon, D.E., Coulter, G.R. et al., 1982. North Sea Chalk Completions-A Laboratory Study. *Journal of Petroleum Technology*, **34** (11): 2–531. URL `http://dx.doi.org/10.2118/10395-PA`.

Talesnick, M.L., Hatzor, Y.H., and Tsesarsky, M., 2001. The elastic deformability and strength of a high porosity, anisotropic chalk. *International Journal of Rock Mechanics and Mining Sciences*, **38** (4): 543–555. June. URL `http://dx.doi.org/http://dx.doi.org/10.1016/S1365-1609(01)00024-7`.

Terzaghi, K., 1943. *Theoretical soil mechanics*. JohnWiley & Sons.

Teufel, L.W. and Rhett, D.W., 1991. Geomechanical evidence for shear failure of chalk during production of the Ekofisk field. In *SPE Annual Technical Conference and Exhibition*. Society of Petroleum Engineers. URL `http://dx.doi.org/10.2118/22755-MS`.

Tjetland, G., Kristiansen, T.G., and Buer, K., 2007. Reservoir management aspects of early waterflood response after 25 years of depletion in the Valhall Field. In *International Petroleum Technology Conference*. International Petroleum Technology Conference, Society of Petroleum Engineers (SPE), Dubai, U.A.E. IPTC-11276-MS. 4–6 December. URL `http://dx.doi.org/10.2523/IPTC-11276-MS`.

William, K.J. and Warnke, E.P., 1975. Constitutive model for the triaxial behavior of concrete. ISMES Seminar on Concrete Structures Subjected to Triaxial Stress, Bergamo. URL `http://www.google.no/url?sa=t&rct=j&q=&esrc=s&source=web&cd=2&ved=0CC4QFjAB&url=http%3A%2F%2Fretro.seals.ch%2Fcntmng%3Fpid%3Dbse-re-001%3A1974%3A19%3A%3A40&ei=R6MyVfPdIoKQsAG3uoDAAQ&usg=AFQjCNH1sBWQl9Y8UiJdM3K6yn7ZmXzUGQ&sig2=FuXfuxwKywQ9SuNTnN8N1w&bvm=bv.91071109,d.bGg&cad=rja`.

Witherspoon, P.A., Wang, J.S.Y. et al., 1980. Validity of Cubic Law for fluid flow in a deformable rock fracture. *Water Resources Research*, **16** (6): 1016–1024. URL `http://dx.doi.org/10.1029/WR016i006p01016`.

Wittke, W., 1990. *Rock Mechanics -Theory and Applications with Case Histories*. 1st ed., Springer. URL `http://www.springer.com/gp/book/9783642881114`.

Zhang, F., She, Y. et al., 2010. Response of microbial community structure to microbial plugging in a mesothermic petroleum reservoir in China. *Applied Microbiology and Biotechnology*, **88** (6): 1413–1422. URL `http://dx.doi.org/10.1007/s00253-010-2841-7`.

Zhang, X., Koutsabeloulis, N. et al., 2011. Modelling of depletion-induced microseismic events by coupled reservoir simulation: application to Valhall field. Paper SPE-143378-MS presented at SPE EUROPEC/EAGE Annual Conference and Exhibition, Vienna, Austria. 23–26 May. URL `http://dx.doi.org/10.2118/143378-MS`.

Chapter 15

Surveillance & Monitoring

Olav Inge Barkved, Hardy Hartmann Nielsen, Anette Uldall, Harald Johansen, and Adrian Zett

15.1 Introduction

North Sea Chalk reservoirs are unique and possess unique properties. The porosities are generally high while matrix permeability is low and fractures may play an important role for fluid flow. The chalk reservoir is often complex with abundant heterogeneities, whose impact on reservoir flow may vary during depletion. Initial oil recovery due to pressure depletion is commonly low. Active reservoir management is critical for increasing the recovery and water injection schemes and continues infill drilling has been used successfully.

Precise knowledge about fluid flow and impact of reservoir heterogeneities are critical for economic and effective development of a chalk reservoir. The reservoir complexities and the dynamic behavior of the chalk make reservoir management more challenging than most clastic reservoirs. At the same time ample opportunities may exist for significant increases in recovery, which justifies the additional resources needed managing and developing chalk reservoirs towards the recovery seen in clastic reservoir.

Surveillance is an essential activity in applied reservoir management. The production engineer's main focus is to optimize production and injection rates. The essential tools are analytical and empirical techniques and include decline curve analysis, material balance calculation, and flow modeling. Reservoir simulation models are built and run to understand the potential of the reservoir and forms the basis for short-term production decisions and long-term reservoir management strategies.

A broad variety of production data may be acquired to understand sweep efficiency, production optimization, well and reservoir integrity, compartmentalization, formation strength and fluid effects. Data acquisition that requires well intervention has significant associated cost and may include lost production/injection, operational risk and risk of not getting the planned data or the quality needed. As a result production surveillance programs are subject to significant scrutiny and most producing reservoirs suffer from shortage in detailed production data, which makes it hard to develop the field optimally.

Typical reservoir surveillance programs include production/injection volumes, well head/down-hole pressure/temperature, fluid composition, water cut, rates, water chemistry and may in addition also cover tracers, fluid gravity, and zonal contribution along the production/injection zones. In heterogeneous reservoirs, understanding which area or zone that contributes to production or where injected fluid is moving into may be difficult to predict based on the static measurements made before the field is put on production. Production logging tools have historically been the only option to acquire such data, but running these tools is costly and is typically used at best in very few wells and even less to understand the dynamic behavior in the wells over time. Recent development of fiber-optic, distributed, temperature and acoustic sensing tools made it possible to do real time data gathering without well intervention, but adds cost and complicate completion. More details on the importance reservoir surveillance data may be found in Grose (2007).

Monitoring of reservoir compaction and related subsidence has for long been one of the key activities for many of the chalk reservoirs. While compaction and associated subsidence due to oil and gas production have been known to the industry since early days, the importance of this effect was fuelled by a single local event, the sinking of the Ekofisk tank. Better understanding of the reservoir behaviors beyond fluid flow suddenly became a multi-billion dollar issue, and highlighted the need for improved understanding of reservoir rock dynamics. Measurements of changes in distances between radioactive bullets have since been used routinely performed to determine the reservoir compaction and the potential stretch/compaction response in the overburden across the most important chalk fields.

Time-lapse bathymetric seabed surveys combined with GPS subsidence measurements at platform installations have also been used to obtain the subsidence rates and determination of the seafloor subsidence volumes. When time-lapse or 4D seismic was first introduced across producing oil fields, the compaction and subsidence effects turned out to be a dominating effect on the seismic travel times. These observations from the Ekofisk and Valhall fields around the turn of the millennium have made material impact on modern use of 4D seismic analysis.

Well performance monitoring using step rate and well interference testing of producers and/or producer injector pairs provide valuable information about lateral reservoir connectivity. Such techniques are used with success in several chalk reservoirs. However, well-based monitoring techniques in the relatively low permeable and complex North Sea chalk reservoirs do not fully capture the reservoir dynamic flow pattern details away from and in between the wells. Due to the compaction and associated loading/unloading effects made 4D/time-lapse seismic surveying very applicable for reservoir monitoring of most producing chalk reservoirs.

The seismic acquisition techniques used, span from marine towed streamers through retrieval seabed system and permanently installed sensor systems. Towed air gun arrays are used to generate the reflection source signals for all the offshore active seismic monitoring systems.

The use of passive seismic methods has been on the agenda for the chalk reservoirs since the mid 1980s, when it was realized that the compaction and associated subsidence could be results of episodic deformations of the reservoir and over-/under-burden formations. These deformations generated recordable microseismic events, which were recorded in wells or at seabed with deployed seismic monitoring systems. High quality seismic emission events, not only provide information about where the deformation takes place, but also the associated changes in stress state. Recently, the use of faint natural background seismic noise as a microseismic a source signal generator has been considered and studied. These signals are typically low frequency and the result of interaction between the seawater column wave motion and seafloor sediments. Intriguing images of shear wave splitting effects that may be linked to seabed subsidence have been derived from recordings of these waves.

While seismic surveillance has become a key tool enabling detailed understading of the production and injection effects, production logging remains the local reference and calibration tool for compaction induced density changes and fluid monitoring of chalk reservoirs.

15.2 Petrophysical surveillance in chalk

Petrophysical surveillance is a key component of field management and optimization. The ability to monitor changes in reservoir performance, fluid contacts and well productivity become even more significant towards the end of field life.

Highly porous chalk is weak and limits the practical drawdown that can be applied in the wells without risking the chalk to start flowing. Rock compactions are generally high and may be accelerated when exposed to seawater. Compaction represents additional energy in the reservoir, but represent challenges to wells and reservoir integrity. The low permeability may require long horizontal wells, which are stimulated by fracking to produce economic rates. The variations in properties laterally or vertically result in practical challenges to optimize production from the individual wells. Dedicated startup scheme and close monitoring during production of the individual wells are often needed to avoid rock failures and to ensure stable production. A detailed petrophysical definition is essential for optimal completion and production planning, but petrophysical in well measurement plays an important role in monitoring changes in petrophysical properties, geomechanical effects and well integrity (cement bond/cap rock integrity, corrosion) during production.

15.2.1 Challenges with petrophysical surveillance in chalk reservoirs

Well access:

- Production/injection losses during logging
- Subsea completion limits the duration of the operation and sensor selection
- Highly deviated and long horizontal well sections requires complex conveyance methods and operation risks

Wellbore conditions:

- Borehole size

- Quality of cement/unknown fluids in annulus
- Change of borehole fluid with time (affects saturation data)
- Unstable flow regime (affects production logging)

Reservoir characteristics:

- Porosity change due to
  - Acid stimulation
  - Reservoir compaction
- Mixed / variable water salinity (seawater injection, presence of salt diapirs)

15.2.2 Traditional methods for petrophysical surveillance

A combination of production logs and pulsed neutron technologies are used for petrophysical surveillance of various recovery mechanisms in chalk reservoirs. The techniques involved are reservoir specific and take into account the completion design as well as the fluid displacement mechanisms (Zett, Mukerji et al. 2011).

While production logging is targeting conformance and production allocation, the pulsed neutron technologies are used to monitor saturation behind casing for further use in wells and reservoir management. Reconciliation of Petrophysical Surveillance with reservoir models is a key objective. Comparing the Cased Hole (CH) logging results with the dynamic model may provide answers to:

- Does CH saturation match the saturation forecast from the dynamic model?
- Do endpoints derived from CH agree with core and model data?

Figs. 15.1 shows an example from Machar field (Central North Sea, UK Sector) (Zett, Webster et al. 2010)

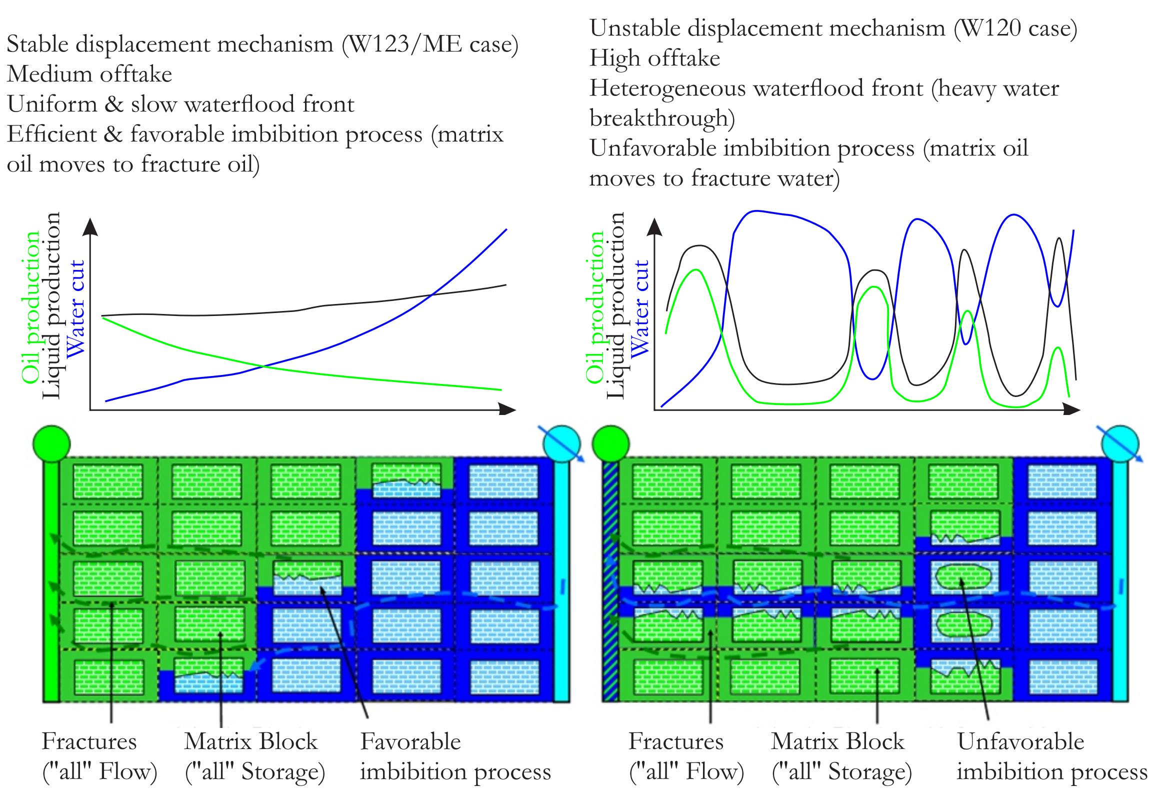

Figure 15.1: Waterflood recovery mechanism in the Machar Field, redrawn.

New technologies for saturation monitoring emerged in the recent years. Generically called multi detector pulsed neutron technologies (MDPN), do offer a larger spectrum of nuclear attributes for further use in complex recovery mechanisms. The evolution and applications of MDPN technologies were described by (Zett, Riley et al. 2008; Zett, Webster et al. 2011, 2012). **Fig. 15.2** illustrates the response of a MDPN attribute from a Valhall well.

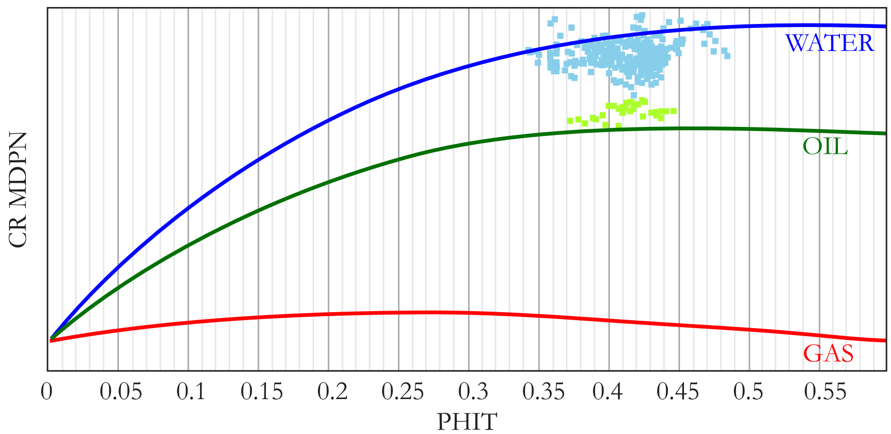

Figure 15.2: The nuclear model for a MDPN attribute (CR MDPN) as a function of Total Porosity for Tor Formation in Valhall. Points represented in light blue are affected by imbibition, redrawn.

15.3 Subsidence and compaction monitoring

Since the mid 1980s, seafloor subsidence and compaction monitoring have been important activities for most of the producing North Sea chalk fields. The sinking of the Ekofisk tank triggered widespread renewed interest in reservoir compaction and associated overburden subsidence. Reservoir compaction and surface subsidence is not unique for chalk reservoirs. The effects were first observed above unconsolidated clastic oil reservoirs in Texas, Venezuela and in California (Andersen 1995) . The subsidence across the Groningen Field offshore the Netherlands is also a well-known case. The sea-floor/surface subsidence is directly coupled to change in pore volume due to changes in effective stress changes (for example pressure depletion) and the ability for the overburden to withstand the stress changes associated with the resulting compaction. Fig. 15.3 shows a typical North Sea chalk plot of compaction induced porosity changes as functions of increases in the effective reservoir stress during pressure depletion production.

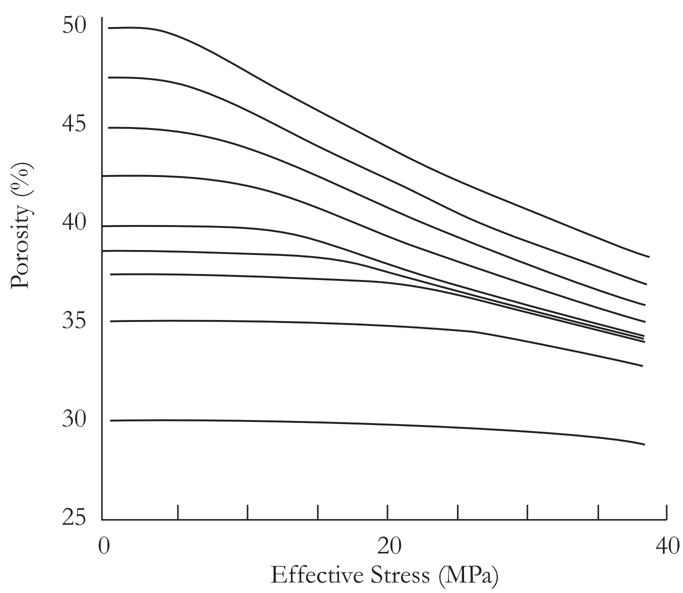

Figure 15.3: Compaction type curves from the Valhall Field indicate the generalized behavior of a number of porosity classes, Andersen (1995) redrawn.

The chalk fields in the Southern North Sea was characterized by high initial pore pressure and hence low effective reservoir stress prior to start of the production through pressure depletion. The reduction in porosity as function of increased effective reservoir stress is not reversible for example through high-pressure water or gas injection. The compaction curves are therefore only valid for the depletion scenario. Re-pressurization by high-pressure water injection has displayed a different stress pattern due water weakening effects of the chalk hence the porosity stress relationship is different from Fig. 15.3. Re-pressurization by water injection has been shown to reduce the compaction induced subsidence rates in for example the Ekofisk area but the compacted volume and subsidence process is not reversed.

15.3.1 Compaction monitoring

Direct measurements of the compaction are difficult to obtain. One way is to place radioactive bullets into the formation outside the wellbore. The relative movements of the bullets may then be measured using repeated radioactive logging runs though time. The interpretation of the results may be complicated if the wells differ too much from vertical. The results may also be affected by presence of local heterogeneities, resulting in non-linear deformation during the compaction or subsidence. The compaction may also be estimated be by repeated porosity measurements through casing as the compaction is resulting in a reduced porevolume. A consistent analysis of the measurements includes and assessment of the full stress state time-lapse history at the observation point. It is difficult to estimate the compaction effects from dynamic measurements (acoustic & density log derived mechanical modulus), since the static (rock mechanical modulus) and the dynamic modulus differ. The static uniaxial compressibility is much larger than the dynamic compressibility that may be read from acoustic logs. Use of very low frequency measurements using the tidal effects has been suggested and tested (Dean, Hardy et al. 1994).

High degree of compaction / subsidence may results in rock failure both in the reservoir and the overburden. Micro-seismic measurements may be used to detect events linked to pore collapse or fault movement. Reservoir compaction, seafloor and overburden subsidence modeling is essential to perform correct analysis and conclusions based on reservoir monitoring data. Jones and Mathiesen (1993) provide a brief review of subsidence monitoring and modeling for Ekofisk.

15.3.2 Subsidence monitoring

Seafloor subsidence monitoring is significantly simpler than compaction monitoring. The technology applied includes bathymetry surveying, air gap measurements at the platforms and the use of Global Positioning (GPS) systems on platforms installed on the seafloor. Changes in the lateral and vertical antenna positions of the permanent GPS installations on a supported by the seafloor can be measured down to millimeters precisions which are directly linked to the movement of the seabed where the platform are positioned. Today bathymetry surveys are routinely run whenever seismic data are acquired and provide seabed depth data with a resolution around one foot. Dedicated time lapse repeated high-resolution bathymetric surveys are acquired at for examples Ekofisk, Eldfisk and Valhall to estimate the volumetric changes of at the seabed and used to historymatch spatial subsidence volumes for geomechanical and reservoir flow simulation. Several of the larger fields have high-end GPS system installed, which continuously records satellite data. The raw GPS data are processed and referenced to provide regular positional update with an accuracy of a few mm. The GPS data are used as additional calibration points for bathymetric time-lapse surveys to provide improved subsidence volumes determinations.

15.3.3 Use of compaction and subsidence monitoring data

The possible impact on wells and field installations is the main driver for monitoring of compaction and subsidence. The monitoring data helps to predict economical impact and to ensure safe operations. A minimum distance, an air gap, is needed between the sea and the lowest cellar deck of a platform and overburden strain and reservoir compaction may cause wellbore failures and limits the well life. Stress redistribution over time in the overburden and the reservoir causes constant changes in wellbore stability and may be a challenge when new replacement wells or sidetracks have to be drilled.

Geomechanical modeling is a principal tool for managing a highly porous chalk reservoir (see Chapter 14). The models are built using all available geomechanical subsurface data. Surveillance data are used to perform historymatching, which includes the matching of reservoir compaction and seafloor subsidence. The surveillance data may be of different accuracy and quality and the geomechanical model are therefore important for validating the consistency of these data. Information from formation integrity tests, leakoff tests or extended leakoff test done during drilling will provide complementary information at this stage.

The geomechanical model, conditioned using available surveillance, well-log and drilling data are then used to predict future subsidence/compaction rates and to inform whether and when mitigating actions are necessary to implement at the fields. The consequences may invoke large investments in order to increase the lifetime of the infrastructure by jacking up the platform as was done at Ekofisk (Sulak 1991; Nagel 2001) or replacing the platforms by new ones, as was the case at Valhall after 30 years of production. In other cases the information about the compaction and subsidence process may impact choice of trajectory for a new well, or even impact the drainage strategy. As much as 50 % of the recovery from a highly porous chalk field may be attributed to the extra energy that follows from compaction (Tjetland, Kristiansen et al. 2007).

15.3.4 Seismic time-lapse / 4D seismic monitoring

"4D seismic does not work in carbonates!" This view in the mid 1990s was based on a generalized view of Middle East carbonate reservoirs, which often exposed a high rigidity of the rock matrix and small contrast between the elastic properties and pore fluid. In addition, several of the larger North Sea chalk reservoirs had P-wave seismic imaging problems over the crest of the fields due to overburden gas/ complex overpressure patterns. These were initial barriers to overcome to perform expensive 4D seismic reservoir monitoring experiments.

In the mid/late 1990s the first serious lab testing and analysis started to qualify the feasibility of using 4D seismic for chalk reservoir monitoring. Phillips Petroleum Company was probably one of the first operators seriously to qualify a project across a chalk field, (Key, Søiland et al. 1996). Rigorous log analysis and corestudies were conducted to establish the sensitivity of elastic properties (Walls, Dvorkin et al. 1998). The studies concluded that seismic based reservoir monitoring hold significant promises for adding value to some of the producing chalk reservoirs. In 1999 a repeat 3D seismic survey was acquired across the Ekofisk field to demonstrate the 4D seismic reservoir monitoring feasibility. The 1989 3D seismic survey was used as the base survey, acquired at the start of the waterflooding program of Ekofisk when the field peaked pressure depletion production.

The rock physics work had concluded that compaction-induced porosity reduction probably would be the main seismic time-lapse contributor, while saturation, pressure and temperature also could result in significant measurable seismic changes over time (Key, Pederson et al. 1998). The 1989 and 1999 3D seismic surveys were processed through identical flow and they found significant time shifts at key reservoir horizons between the two surveys, linked to the reservoir compaction. To quantify the compaction from the 4D seismic images, the team working the data developed a depth conversion approach, which took into the account the subtle changes in the overburden, see **Fig. 15.4**, (Guilbot and Smith 2002).

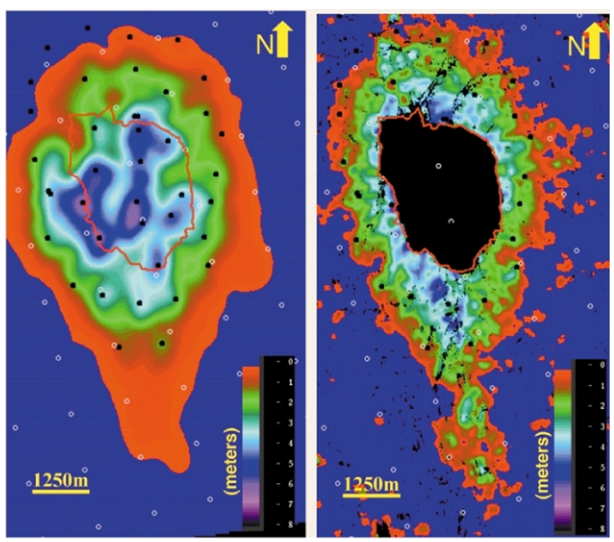

Figure 15.4: Left: Ekofisk field: Compaction from geomechanical modeling, with water injection wells displayed as black dots. Right: Seismic-derived compaction map. The black hole in the middle of the field is within the seismic obscured area where P-wave monitoring is not feasible (Guilbot and Smith 2002).

At Ekofisk the subsequent repeat towed streamer dataset was acquired in 2003, 2006 and 2008 with various attempts to repeat the acquisition configurations (Haugvaldstad, Lyngnes et al. 2011).

The first 4D seismic survey across the Valhall field was acquired in 2002, ten years after the baseline survey (Barkved, Gaucher et al. 2002). However, this was not the first attempt to do a seismic time-lapse analysis at Valhall. A 3D seismic OBC data set had been matched with the 1992 3D marine towed streamer survey, and showed some intriguing time shifts effects at the reservoir level Hall, Kendall et al. (2002), **Fig. 15.5**. These results revealed the sensitivity to even very small time shifts on 4D images, see also Hall (2006).

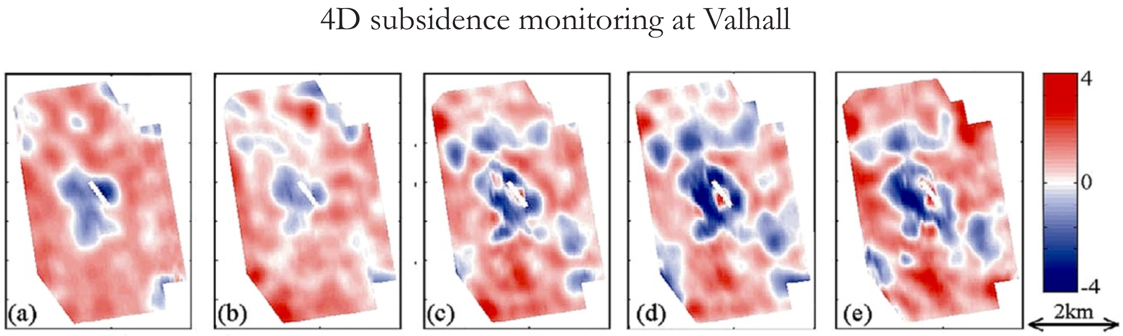

Figure 15.5: Matching OBC and marine towed streamer data for time-lapse effects.

Fig. 15.5 shows the z-component of the warp vectors derived at nodes placed on the main horizons but distributed evenly in x and y. Warping is a three-dimensional analogue to time-shifts analysis, where a small volume of data are compared between two 3D volumes to estimate possible lateral and vertical movement or deformations. The horizons are: (a) Early Miocene at about 1700 ms; (b) Middle Eocene event at about 2000 ms; (c) Balder at about 2700 ms; (d) Top hard chalk at about 2800 ms; (e) Base chalk at about 2900 ms. The reservoirs are located between the Balder and Top hard Chalk. Values are in number of samples (sample rate=4ms) and negative values indicate a downshift from legacy to repeat (1992 to 1998). The white rectangle in the center of each figure is the zone muted out in the streamer data due to the presence of the platform; artifacts exist in the lower horizons due to this mute zone, (Hall, Kendall et al. 2002).

The later repeat marine streamer 4D results from matching a 2002 towed streamer monitor to a 1992 baseline at Valhall revealed even more detailed results from the velocity changes outside the reservoir, **Fig. 15.6**. Individual perforations were possible to image along a horizontal well, see **Fig. 15.6e** (Barkved, Gaucher et al. 2002). For more extensive studies separating and reservoir changes and velocity changes above see Corzo Mojica (2009); Corzo, MacBeth et al. (2013).

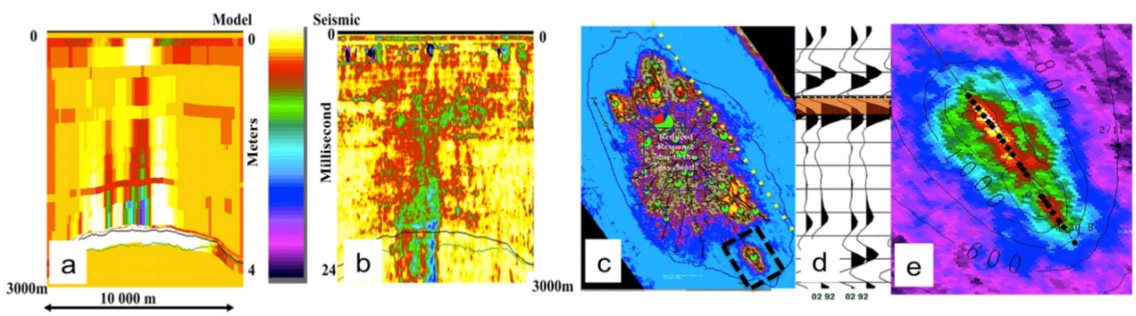

Figure 15.6: Modeled and observed Seismic time-lapse effects as seen by matching towed streamer data from 2002 with 1992 at Valhall. a) Modeled changes in volumetric strain, b) Time-shift analysis along seismic section indicated by stippled line in c), c) rms changes in a window of 160 msec around the reservoir, includes time shift and amplitude changes, d) seismic traces in a 500 msec window showing typical differences between 1992 and 2002, reservoir shown as light brown box, e) detailed from c) along a 1800 m horizontal well, perforations are shown as black dots.

At South Arne field a towed streamer monitor survey was acquired in 2005 and matched with the original 1995 3D survey. Hess Corporation acquired a second monitor in 2011 (Vejbæk, King et al. 2012). The seismic time-lapse attributes derived at South Arne are a combination of a time shift and amplitude changes. Production induced changes outside the reservoir results in a decrease in velocity in the overburden, while the velocity changes in the reservoir may both decrease and increase. Hess Corporation includes AVO inversions in their analysis of the 4D response, and uses this in combinations with an established rock property template to invert for saturation and compaction changes, see **Fig. 15.7** (Corzo Mojica 2009; Corzo, MacBeth et al. 2013).

In 2005 Maersk acquired a marine towed streamer seismic monitor survey across the Dan field. The baseline was acquired in 1998, using two streamers while the 2005 survey included 8 streamers. The repeatability was reported to be satisfactory. The resulting 4D seismic images reflected a hardening due to the production-induced compaction and to water injection. Softening effects were observed were gas breakouts had occurred

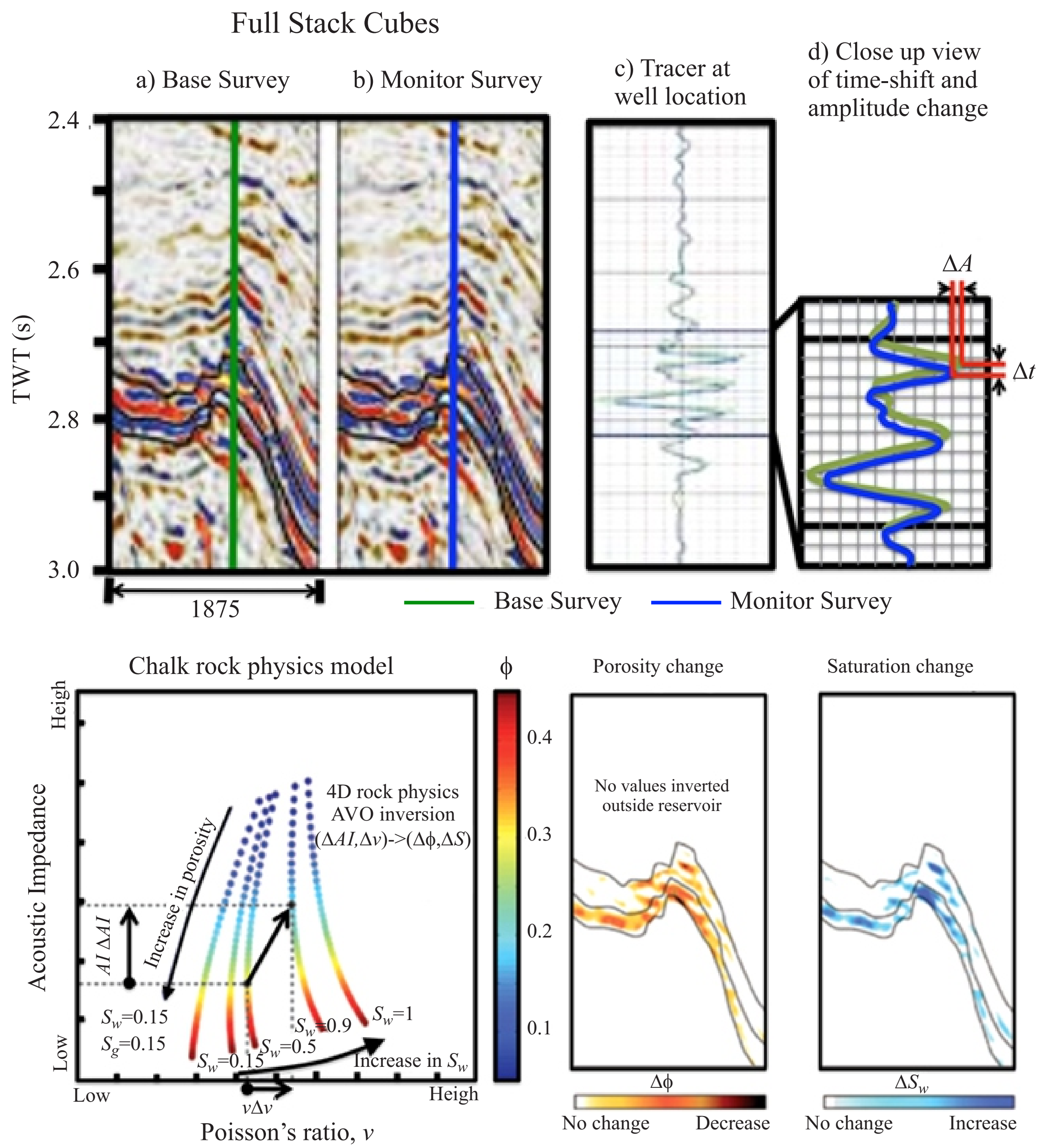

Figure 15.7: a) Base and Monitor survey are processed using the same flow, b) a rock physics template is used in combination with AVO inversion to estimate compaction and fluid changes. c) and d) shows the 4D effects fora single seismic trace. Redrawn from Kosco, Rau Schøtt et al. (2010).

due to pressure reduction. Time-lapse AVO analysis revealed the presence of a fracture that aligned with two water injectors, see **Fig. 15.8** (Gommesen, Dons et al. 2007).

The 4D seismic history from the Dan field also includes an early field trial. A 3D seismic survey was acquired in 2000 that covered part of the 1988 3D seismic survey. The two surveys were acquired in almost orthogonal orientation, which normally does not favor high degree of repeatability. Still the results "succeeded in identifying areas for possible development, identifying possible barriers or baffles to flow, and highlighted cases of possible sweep pattern skew. Information useful for production optimization was identified and possible effects of porosity reduction and reservoir compaction were recognized" (Rod and Jørgensen 2005).

One of the most intriguing 4D seismic case stories is about the Halfdan field, where the depletion strategy was to drill alternating 10,000–15,000ft long horizontal production and water injection wells at a spacing of 600ft between the wells to develop the field. Enhanced productivity is achieved by acid stimulation of the wells. To maintain voidage replacement and pressure maintenance in the low permeable reservoir, water needs to be injected above the fracture propagation pressure (Jørgensen 2002). A new seismic survey was acquired across the field in 2005, with the intention of using it for 4D seismic imaging by matching to the previous seismic survey acquired prior to production/injection starting. It turned out that the new 3D seismic reflected

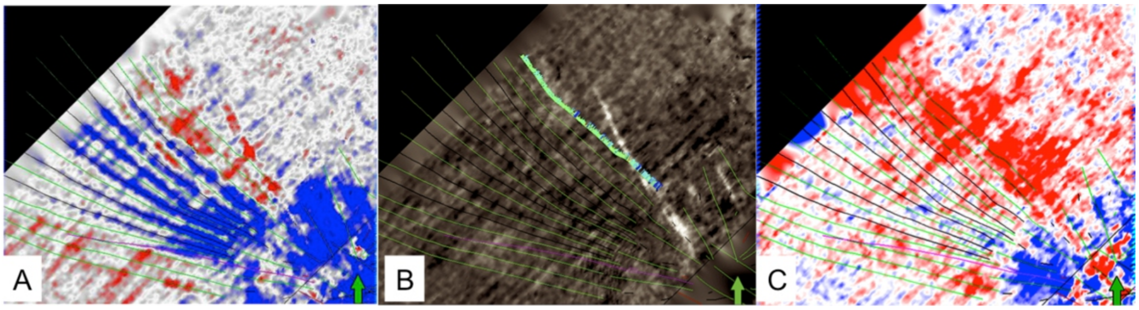

Figure 15.8: A) 4D seismic example from the west flank of the Dan Field.Seismic hardening is observed along the injectors (black or purple, if inactive) and seismic softening due to gas break out is observed along the rim where the producers (green) are not pressure supported. B) Example of a fracture induced by water injection. The map shows the time-lapse difference of the AVO response (left). A well was drilled through and shows low oil saturation in the fractured interval. C) On both sides of the fracture stress relief patterns from the high the pore pressure are observed from changes in two-way-travel time measured across the reservoir (right). From Gommesen, Dons et al. (2007).)

the sweep pattern without any 4D seismic processing. The amplitude difference between a production and an injection well was as high as 50%, **Fig. 15.9**, Dons, Jørgensen et al. (2007). The Halfdan case proves an

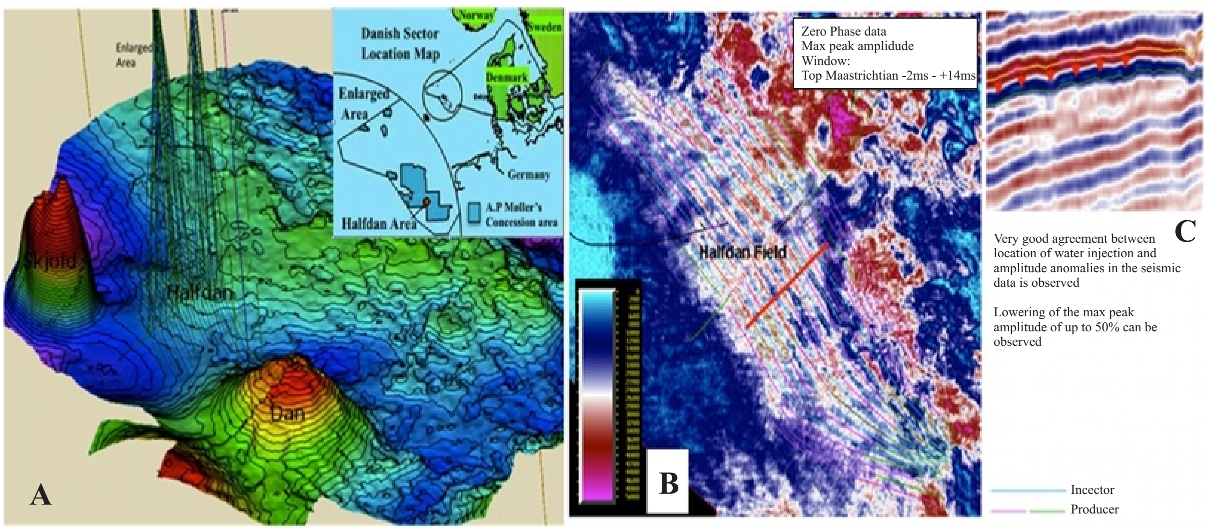

Figure 15.9: From the Halfdan field. A) The Halfdan field is located in the Danish part of the North Sea. The trap is dynamic, structural and stratigraphic. B) The map shows the top Maastrichtian. Seismic attribute map showing the presence of the injectors and planned and existing producers. C) The caption to the right shows how the pairs of injectors and producers are affecting the seismic response, from (Dons, Jørgensen et al. 2007)

injection/production management strategy and demonstrates how such strategies are related to fluid and rock mechanics considerations. These observations also prove that it is possible to use seismic techniques to monitor production-induced effects in relatively low porous chalk. The porosity is less than 30% and the permeability is 0.5–2.0 mD. The seismic response observed in Fig. 15.9 is a combined effect of fluid substitution and compaction of the rock, both increasing the acoustic impedance, and from increasing the pore pressure leading to lower acoustic impedance.

A new repeat time-lapse seismic survey was acquired in 2012 over the Halfdan oil field, and the 800 km^2 surrounding area, located in the Danish North Sea Central Graben, approximately 250 km west of the Danish west coast. The main objectives of the repeat 4D were to understand the lateral and vertical sweep, identify unswept areas, and guide future well interventions and to clarify the reservoir model (Calvert, Roende et al. 2013). The first 3D tow streamer survey was acquired across the Hod field in 1990, as a part of a multiclient project. In 2011 PGS acquired a 3D geostreamer survey across the field. The two datasets was processed for 4D, and with reasonable results despite large differences in the acquisition geometries **Fig. 15.10**, Gil (2012).

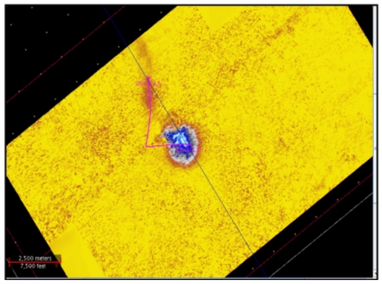

Time-shift volume slice, 2680ms

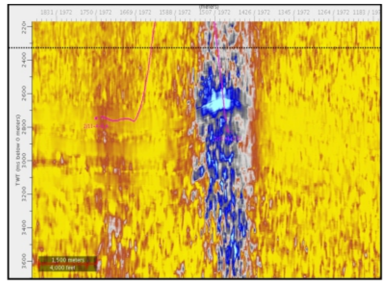

Time-shift section, Xline 1972

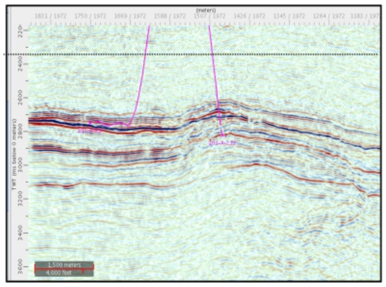

CGR-2010 final PSDM stack (4D), Xline 1972

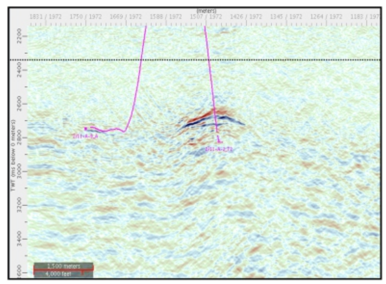

CI 4D difference, time shift removed, Xline 1972

Figure 15.10: Hod 4D seismic results, top left is a time shift map derived above the reservoir, and a corresponding resection from the same time shift dataset to the right. The stipple lines shows the location of the section/map. Light blue corresponds to around 16 msec time shift. Below is the same cross-section shown amplitude data (left) and amplitude difference (right), Gil (2012)

15.4 4D Seismic analysis

The two essential attributes of any reflection seismic experiments are travel time and amplitude. These attributes also form the basis for all 4D seismic analysis, which are focused on the changes in these parameters between two time-lapse seismic surveys. Until the millennium change, literally all 4D seismic work focused on isolating the changes across the producing reservoir. Acoustic change outside the reservoir was initially not compensated for and the seismic processing was very much focused on making the best match using reference intervals or reflectors outside the reservoir. Time-shift changes or amplitude changes were considered to be the results of pressure and fluid changes within the reservoir solely, (Biondi, Mavko et al. 1996; Landrø, Solheim et al. 1999).

In the case of production induced reservoir compaction, it was known that subsidence at surface could be a consequence. The geomechanical community working with compaction of reservoirs also knew that the mechanism outside the reservoir would lead to possible velocity changes in the overburden. The magnitudes of these changes were not known, until the early results from field like Ekofisk and Valhall came across (Guilbot and Smith 2002; Hall, Kendall et al. 2002; Barkved, Buer et al. 2003). These ”new” observations of changes outside the reservoir lead immediately to some changes in how the 4D seismic time-lapse surveys were processed, for example were statics corrections performed to compensate for subsidence changes over this type of producing fields.

Detectable differences in seismic arrival times were also observed above the reservoir interval in some of the North Sea high-pressure fields by geophysicists from Shell. As it turned out, the observations had impact beyond academic interest. The travel-time difference was linked to stress/strain changes in the overburden. These stress/strain changes could in certain cases be coupled directly to specific wells, which suffered from deformations and tubing collapses. Significant efforts were put into understanding the link between the strain effects and the seismic time differences. Some of the chalk field, like Valhall and Ekofisk had advanced geomechanical models built, and consequently reasonable understanding of what the strains above the reservoir would be. These insights could be used to match the seismic time shift observations to the changes in the mechanical stress state of the overburden rock. The realization that the strain and velocity changes would impact the seismic travel time as function of offset differently lead Martin Landrøe to formulate an approach for direct estimation of compaction and velocity changes (Landrø and Janssen 2002). A further development of the method incorporated the seismic amplitude changes into strain analysis using 4D seismic data (Landrø and Stammeijer 2004).

It had been noticed that crossplotting traveltime difference and modeled strains, revealed a linear correlation. Based on a linear assumption between travel time difference and strain Hatchell, Kawar et al. (2005) proposed a constant R that denotes the ratio between travel time changes and travel path changes, strain,

$$\frac{\Delta t}{t} = \frac{\Delta z}{z} - \frac{\Delta v}{v} = (1+R)\varepsilon_{zz}, \tag{15.1}$$

here t denotes the travel time, v the P-wave velocity, z strain, and Δt, Δz and Δv small local changes. The term ε_{zz} is the average strain estimate over the interval where the Δt, Δz and Δv are measured. The R term is a global constant. By introducing the R term the, ”timeshift” community had a single parameter model that could be derived for any field and used for comparison. Hatchel and Bourne suggested theoretic values for R to be in the range 4–6. As it turned out, relevant R are in the range values 3–7 (Herwanger, Palmer et al. 2007). Another single parameter model was suggested by Røste, Stovas et al. (2005), at the same time as Hatchell, Kawar et al. (2005).

This single parameter model has worked well for practical applications, and has been reported to be used regularly both at the Ekofisk field (Janssen, Byerley et al. 2006), and at the Valhall field (van Gestel, Best et al. 2011). It needs to be kept in mind that the single parameter model Eq.15.1 is based on a ”mean stress” assumption, which is not adequately describing stress and strain changes over a compacting reservoir. To validate the assumption geomechanical modeling needs to be done. SINTEF, together with BP developed a modeling flow and relevant functionality for testing of conceptual or field specific model for the simulation of elastic properties changes, including traveltime shift effects connected to a depleting reservoir, Fjær and Kristiansen (2009). Stress state changes are easiest to pick up by using traveltime changes, however, especially across the top reservoir interface the changes is so large that amplitude differences are noticeable (Pettersen, Barkved et al. 2006). Also worth noting is the fact that thickness variation, permeability contrast and lateral pressure variation, might impact the orientation of the horizontal minimum and maximum stresses. This implies that time-lapse Amplitude Versus Offset (AVO) measurements might be affected by changes in stress orientation. **Fig. 15.11** which shows the AVO Azimuthal effects (AVOA), in one of the sub-basins of the Valhall field. The conclusion is that a full AVOA analysis is needed to separate fluid and pressure effects. The earlier shown results from South Arne Field, see Fig. 15.7, might be biased by this effect.

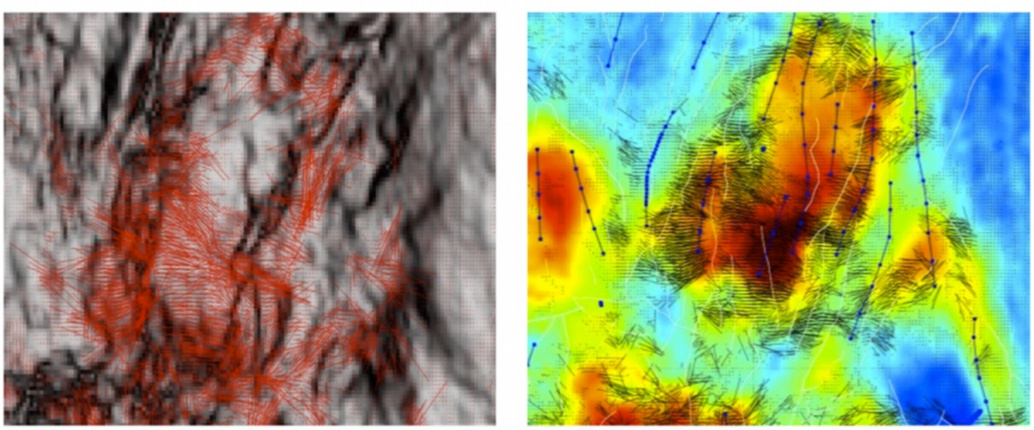

Figure 15.11: Left: Results of AVOA analysis of Valhall LoFS data. Red sticks, align to some degree with the implied fracture density and orientation at the top hard chalk horizon, as seen in the black to white coherency map, which agreed well with a previous study. Right: the 4D difference map shows strong correlation with changes in the production induced time-lapse. The blue-green-yellow-red, small-large, map reflects changes in acoustic impedance in the reservoir for the 10 years prior to the LoFS survey. The figure is from internal BP report, used with permission. AVOA analysis courtesy of O.J. Askim in Barkved (2012).

15.5 Seismic surveillance options

Any seismic survey represents a snapshot of the subsurface acoustic state at specific point in time, which implies that literally all type of seismic recordings beyond reflection seismic surveying may be used for surveillance purposes. In general daily variation linked to tidal effects, industrial and weather effects, weekly effects linked to lunar effects and seasonal effect like water temperature impacts the seismic images and are seismic sources that may generate seismic recordable signals. The most significant short-term variations, which are not production induced, are likely to occur in the water column due to seawaves. Variation in stress state linked to subsidence effects as demonstrated by passive recordings of microseismic effects (see below), are typically ignored and probably rightfully accepted as ”noise” in our standard 4D seismic analysis.

The NRMS attribute, defined as Normalized Root Mean Square (NRMS) of the difference between two datasets, is used routinely as a quality control measurement of similarity or repeatability of time-lapse seismic data (Kragh and Christie 2002). Differences in transducer positions (either the source emitting the seismic signal or the hydrophone/geophone receiving the seismic signal after it has travelled through the earth) are known to have an effect on the quality and resolution of a time-lapse survey. This is linked to the fact that acoustic description of the inhomogeneous earth is far from detailed enough to properly compensate for small variations in the seismic rays travel paths. The total disposition in source and receiver position between a monitor and the base line in the cases described above could be several 100 meters. Today’s acceptable difference in a standard time-lapse survey for the North Sea is less than 100 meter for repeated seismic streamer conveyed surveys.

Most of the 4D seismic examples listed above are based on the use of repeated marine streamer conveyed seismic surveys. The rationale behind this is linked to fact that most baseline surveys were towed streamer surveys. However, for proper line planned modern 4D seismic surveys the geometrical repeatability is impressive, and below 100 meters between pairs of repeated source and receiver positions. Repeated ocean bottom nodes and retrievable cable systems have reported even better repeatability, and the corresponding NRMS measures are reported to be in the lower tens, and sometimes below. As discussed is the spatial time-lapse changes outside the reservoir important for most the compacting chalk fields. This causes significant limitations to perform signal-matching processes between repeated seismic surveys, without risking deteriorating the 4D signal desired measured. The degree of geometrical repeatability that is needed for a high quality 4D seismic response, and to what extend geometric repeatability can be compensated for in processing is subject for discussions. However, its has been shown beyond doubt that use of permanent sensor installed at the seabed, results in nominal position errors in source/receiver repeatability less than 5 meters and provides NRMS values as low as 3-4% (Folstad, Morgan et al. 2015). This obviously results in a significant uplift in the 4D seismic signal quality and was one of the drivers for selecting permanent sensors at seabed for the Ekofisk field (Folstad 2011). The same paper illustrates very well how improved 4D seismic signal impact the business decision to be made based on the 4D seismic images.

15.5.1 Permanent seabed installations - LoFS

The Ekofisk permanent seismic installation was put in place in 2010, seven years later than the Valhall permanent installation in 2003 (Barkved, Buer et al. 2003). **Figs. 15.12 and 15.13** show the outline of the cable system installed at the seabed at the Valhall and the Ekofisk field.

15.5.2 Passive microseismic monitoring

Passive microseismic acquisition offers a non-invasive method for monitoring deformation and changes in the stress distribution inside the earth. Recently there has been significant focus to utilize such monitoring techniques to study hydraulic fracturing stimulation in shale gas and oil reservoir. This technology primarily makes use of geophones installed in wells (Maxwell, Rutledge et al. 2010), but utilities of surface installations are emerging (Duncan and Eisner 2010).

Passive seismic monitoring is not new to the chalk field players. The uses of installations launched in wells have been tested several times. Long-term deployment for monitoring of an operational oil field has not been implemented due to operational cost, logistic issues and acoustic interference problems with the production and injection priorities. Temporary and permanent in well systems that continuously records seismic emissions or microseismicity has been tested at Ekofisk, Valhall and the Dan field. Some of the recorded data sets have been offered to academia and there exist several PhD theses, supervised by Dr. Michael Kendall at University of Leeds and later at University of Bristol that address this work in great details, i.e. (Jones 2010; Meersman 2005).

The permanent seismic ocean bottom (OBC or LoFS) recording system installed at the Valhall and the Ekofisk fields do have the capability to record passive data in the bandwidth of interest, typically between 2–60 Hz. Long wavelength microseismic signals as low as 0.18–2 Hz (100–3000 meters wavelength) are observed. Recent studies have shown that it is possible to invert for shear wave properties in the shallow overburden (Dellinger and Yu 2009).

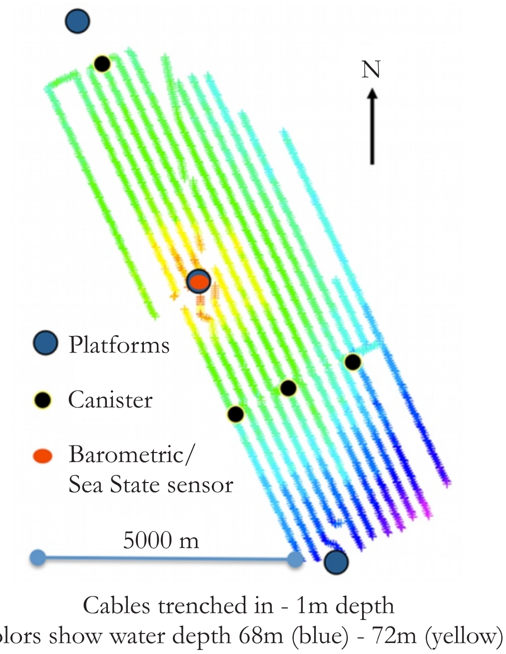

Figure 15.12: Valhall LoFS System: The cables were trenched 1 meter into the seabed. The cables end in seismic array terminators (SATs), which are located in 4 canisters that have been dug into the seabed. The SATs are connected to the Valhall IP.

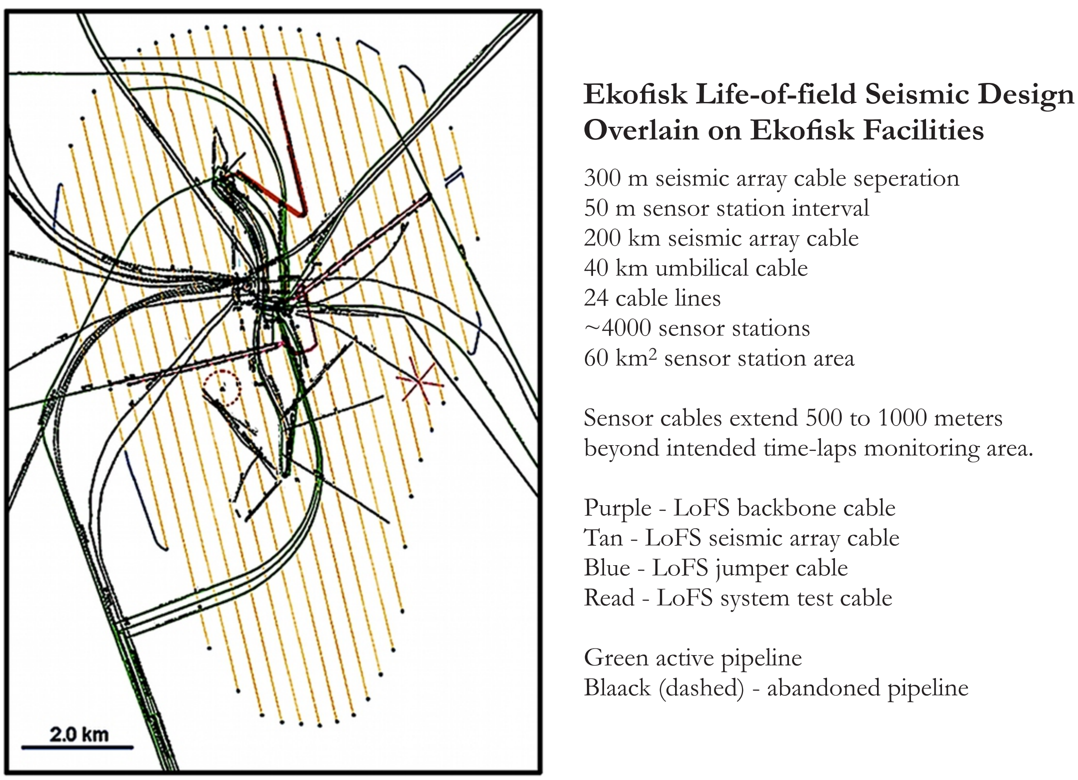

Figure 15.13: The Ekofisk Life of Field Seismic design overlain on existing Ekofisk facilities

Seven seismic subarrays of the Ekofisk LoFS array, each consisting of four 4 components sensors, are switched to passive recording mode when active seismic is not shooting at the field. The passive recorded data are in real time send onshore, where the data is distributed to the Norwegian National Seismic Network at university in Bergen. They integrate the data with the onshore national seismological network data for earthquake monitoring. Ekofisk is the first oil field on NCS with such data integration. ConocoPhillips also distribute real time passive data to a contractor that do the real time microseismic data analysis for fracturing surveillance. They are working with the feasibility to use the low magnitude microseismic events to calibrate the Ekofisk overburden and reservoir mechanical property changes resulting from the compaction and subsidence processes. The entire Ekofisk LoFS array has successfully been used to accurate passive detection of for example perforation shots as a source threshold and location calibration tests.

In the following some of the relevant passive seismic studies done across some of the North Sea Chalk fields will be discussed.

15.5.3 Early testing of in well passive seismic recordings

The realization that the observed subsidence at surface may be driven by shear failure in addition to pore collapse lead to the first installation of borehole seismometer at the Ekofisk field. Episodic shear failure would result in events that could be detected as micro earthquakes.

In 1993 (Rutledge, Fairbanks et al. 1994) a single three-component geophone was installed at 2985 m depth, in the Ekofisk C-11 vertical observation well, which was designed for making strain measurements across the reservoir at the crest of the field. The C-11 is situated in the P-wave Seismic Obscured Area (SOA) in the central parts of the Ekofisk field. The SOA is caused by gas concentration and high variable pressure in the overburden formations. During the passive experiment the well was not initially pressurized when the geophone was launched and significant noise was recorded. The noise was most likely due to gas bubbles rising and creating tube wave energy guided by the fluid /tubing interface. It was decided to pressurize the well, which resulted in reduction of the noise. The system recorded almost continuously for 106 days, but unfortunately the signal/noise level deteriorated, and only 104 hours of data were recorded within a useable noise level. Still 572 clear P&S wave events were identified as likely real microseismic sourced signals. The majority of these events were within 400 m radius from the well, but events as far as 1000 m away were detected. The event locations were determined using the differences in P and S wave arrival times. The azimuthal direction of the seismic event can be determined by P-wave polarization, although there will be an ambiguity of ± 180 degree when a single 3 component geophone station is used. Attempt was made to orient the receivers using an air gun source. This failed, however, and only a relative orientation was estimated. The experiments proved that significant microseismicity is caused by mechanical (shear) failure in the reservoir and possible outside the reservoir. The single level tool and the significant noise problems limited the quantitative use of the recordings, but resulted in a subsequent attempt in recording more comprehensive and better quality data set.

In April 1997, a six level three-component geophone array was deployed in the Ekofisk C-11 monitoring well and recorded passively for 18 days. The three component geophone groups had 20 m spacing and were positioned within the producing Ekofisk formation. Over 4400 micro-seismic events were detected during the experiment, of these 2000 events had computable hypocenters (Maxwell, Bossu et al. 1997; Oye and Roth 2003). The events source locations appear in map view as diffuse line elements, which have been interpreted as evidence for production induced movement of pre-existing faults (Maxwell, Bossu et al. 1997; Oye and Roth 2003).

During June/July the same equipment as used at Ekofisk was deployed in a deviated well at Valhall. The Valhall recordings were conducted for 57 days. Unlike the Ekofisk field trial the geophones were deployed approximately 250 m above the top of the deforming reservoir. A total of 572 microseismic events were detected. The De Meersman, Kendall et al. (2009) study was based on the acquired passive data and able to locate 303 events. These events formed two clusters, see **Fig. 15.14**, within the reservoir overburden. The location of these clusters matched seismic mapped faults (De Meersman, Kendall et al. 2009). A cyclical failure / stress build up model was proposed based on the passive seismic data analysis and the systematic repeating behavior of earthquakes intensity and measurements of anisotropic parameters from re-located source locations (De Meersman, Kendall et al. 2009; Zoback and Zinke 2002). The temporal variation in seismic anisotropy and source mechanism reflected a deformation process in the overburden, which appeared to be strongly linked to production.

The Ekofisk microseismic dataset reflects passive microseismic activity linked directly to the productioninduced compaction, as most of the events are appearing within the reservoir. The Valhall dataset consist of events that appear to originate from similar locations and limited ray paths, and as such reflect the production induced stress re-distribution and failure mechanism above the reservoir. **Fig. 15.15** shows an example of a seismic events as recorded by the seismic sensors, there are three sensors in every station which are oriented such that they are sensitive to movement in three orthogonal directions. A microseismic event is caused by instantaneous geomechanical deformations. Strain or slip creates seismic waves, which are captured by the seismic sensors. The magnitude of the events is of primary interest as this is linked to the size of the deformation, and may therefore be linked to the volumes of rock or fluids being impacted. Subsequent analysis make use of the

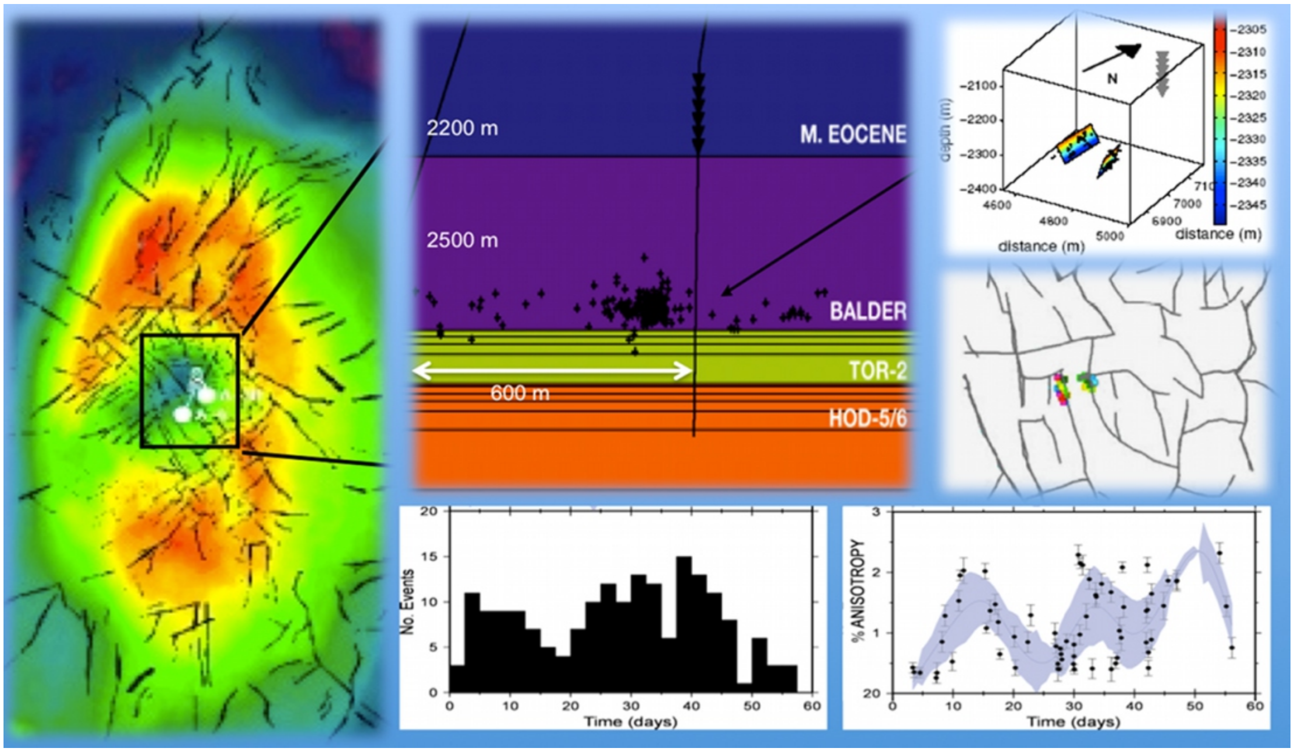

Figure 15.14: Valhall microsseismic recordings

polarization and radiation characterization of the seismic waves which then may be linked the failure mode, i.e. the amount of slip or strain, but also provide indication of stress/fracture anisotropy which may indicate preferred flow orientations, **Fig. 15.16**.

Based on studying the Valhall dataset a number automated procedures and algorithms were proposed by the microseismic industry (De Meersman, Kendall et al. 2009). Today, there are systems and workflows in place that support real time source location and characterization based on the microseismic recordings (Jones 2010).

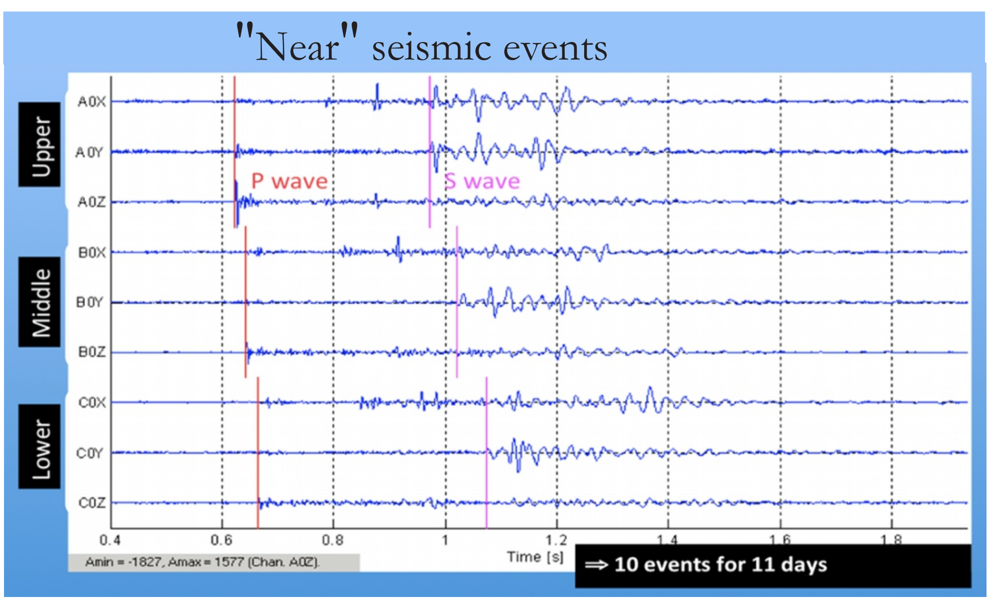

Figure 15.15: A passive seismic event recorded at three different stations

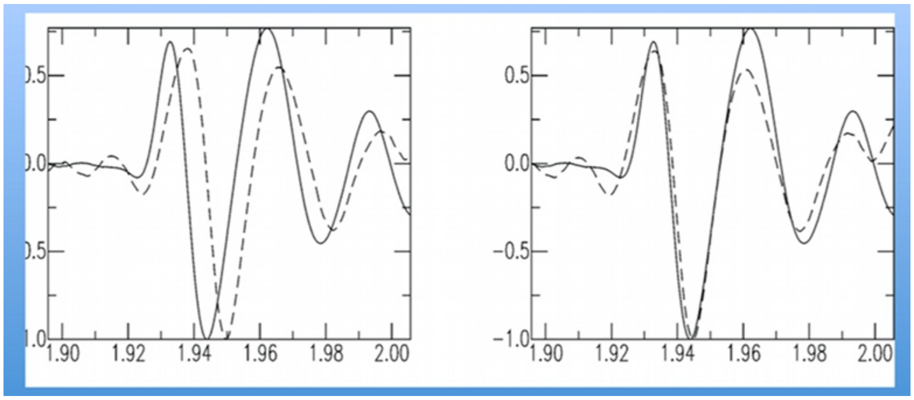

(a) S-wave window

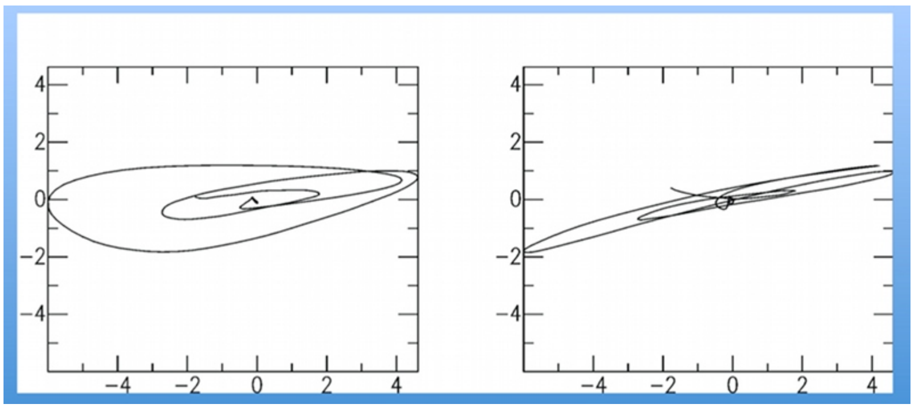

(b) Polarization window

Figure 15.16: Show an example of how shear wave polarization can be used to delineate the orientation of fast and slow S-velocity, which may be linked to anisotropy caused by stress/faults and hence provide indication of preferred flow orientations in the reservoir.

15.6 Microseismic monitoring of hydraulic fracturing

Microseismic monitoring can be used during hydraulic fracturing and high-pressure water injection above fracture pressure to image the orientation, height, length, complexity and thermal growth of the induced fractures (Maxwell and Urbancic 2001).

A permanent microseismic monitoring array was installed in a horizontal well at the Danish Halfdan field with the objective of imaging the propagation of an acid and water injection fractures in neighboring wells (Rod, Zyweck et al. 2005). The array consisted of 16 stations of three component geophones, placed at 500 ft interval in a horizontal well. The system was deployed inside a pre-perforated liner. Coupling between liner/reservoir formation and the geophones was based on gravity. The system has been operated during production and shut-in. The noise from the production reduced the sensitivity of the system such that on average one event was detected per week, while during shut-in one to two events were recorded every day.

The Halfdan field is developed with a line drive waterflood arrangement with alternating horizontal injectors and producers. The wells are drilled in the direction of maximum horizontal stress. Multiple acid fracking are placed in the producers while fractures are induced by water injection in the injection wells. It is critical to align the fractures along the well, to avoid early breakthrough in the producers (Rod, Zyweck et al. 2005). The technique for alignment of the injection fractures along the horizontal wells, are referred to as Fracture Aligned Sweep Technology (FAST)[2,4,5]. FAST is based on the principle that fluid flow in low permeability rocks affects the pore pressures and reservoir stresses. By active manipulation and control of the pressure field it is anticipated that the reservoir stress field direction can be controlled and hence the fracture growth direction.

The purpose of the microseismic monitoring was to independently validate the FAST development concept, and to image orientation and geometry of the acid stimulation fracturing. Around 450 microseismic events were identified from 13 acid fracture treatments in two offset wells, which were around 1200 ft away **Fig. 15.17**. Conclusive fracture orientations were found for 8 of the acid stimulations, showing that the fractures had propagated orthogonally rather than parallel to the wells. As a result this completion methodology was changed.

The water injection induced fractures were not imaged (Rod, Zyweck et al. 2005), probably due to weak energy release during the fracturing processes.

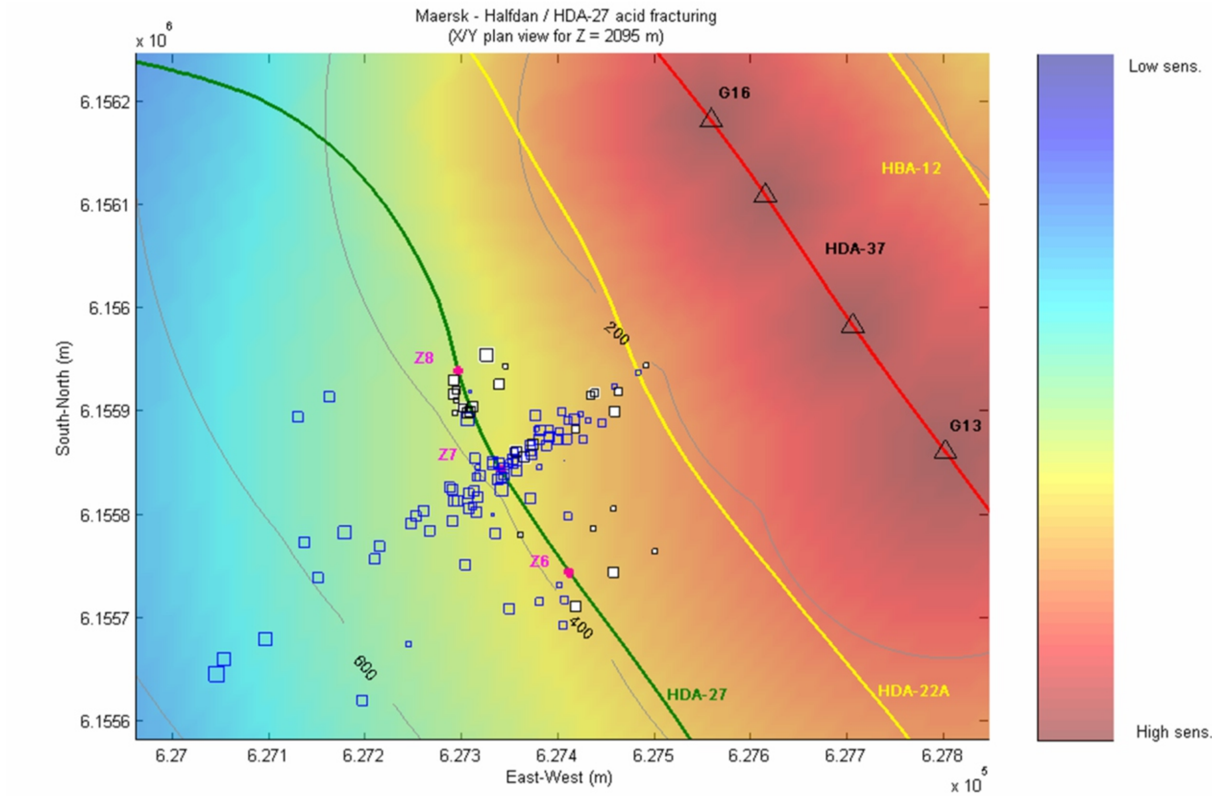

Figure 15.17: Plan view of Halfdan HDA-27 acid fracturing microseismicity (blue squares). The sizes of the squares are proportional to the microseism magnitude. White squares show microseisms with main location uncertainty smaller than ± 50 m. The colored background represents the average detection sensitivity of the network during the stimulations. The iso-distance to one geophone is plotted as grey lines. Locations were computed within a homogeneous velocity model of V_s=1900 m/s.

The Halfdan installation confirmed a number of issues:

- Microseismicity can be detected using a gravity coupling technique.
- Use of real time noise filter made it possible to detect events while producing with rates in excess of 5,000 stb/d.
- S-wave detections proportionally outweigh P-wave detections.
- Location uncertainty is driven by the linear array of sensors in the formation all nearly at the same depth. An alternative geometry of sensors, including a mix of horizontal and vertical arrays could eliminate symmetry and more uniquely define event locations.
- Sensitivity of the microseismic monitoring array seems to be the limiting factor for imaging water injection fractures.

15.6.1 Permanently installed downhole seismic system systems

To our knowledge there are very few permanently installed down-hole system in North Sea chalk fields. At Valhall a 3 level three components (electrical) geophone system was installed in well A-25 B while re-completing the well for drilled cuttings re-injection (Barkved, Gaucher et al. 2002). This system failed after a few weeks, and a more extensive system based on the same type of geophones was installed at the Halfdan field in 2002, as described above. A full five level 3 components optical system was installed in the G-24 well at Valhall in 2005

(Hornby, Barkved et al. 2007). This system was tested in 2012, and appeared to be recording relevant data. In the Ekofisk area have 3 level three- component geophones been installed in a couple of the most recently drilled new cuttings and waste re-injection wells. At Ekofisk the data are used to monitor the domain growth passively in combination with the passive surface array monitoring system and the frequent time-lapse LoFS shooting, while at Eldfisk it is the only seismic monitoring system beyond irregular time-lapse seismic shooting.

15.7 Passive seismic monitoring of hydraulic fracturing from the surface

Data from the Valhall permanent full field array (LoFS) has been used in conjunction with a migration style approach to locate microseismic events in Valhall Field during 6.5 hours of hydraulic fracturing. An event distribution that extends roughly 300 m vertically and 200 m horizontally was defined based on this analysis. Sources were located within the reservoir and within the overburden. However, the temporal distribution of the events was not consistent with the induced fracturing extending into the overburden, **Fig. 15.18**. Instead, the synchronous increase in event activity with down-hole pressure could be interpreted as evidence that elastic wave-fronts originating from well activity trigger movement on faults where the in-situ stress already was very close to failure (Chambers, Kendall et al. 2010).

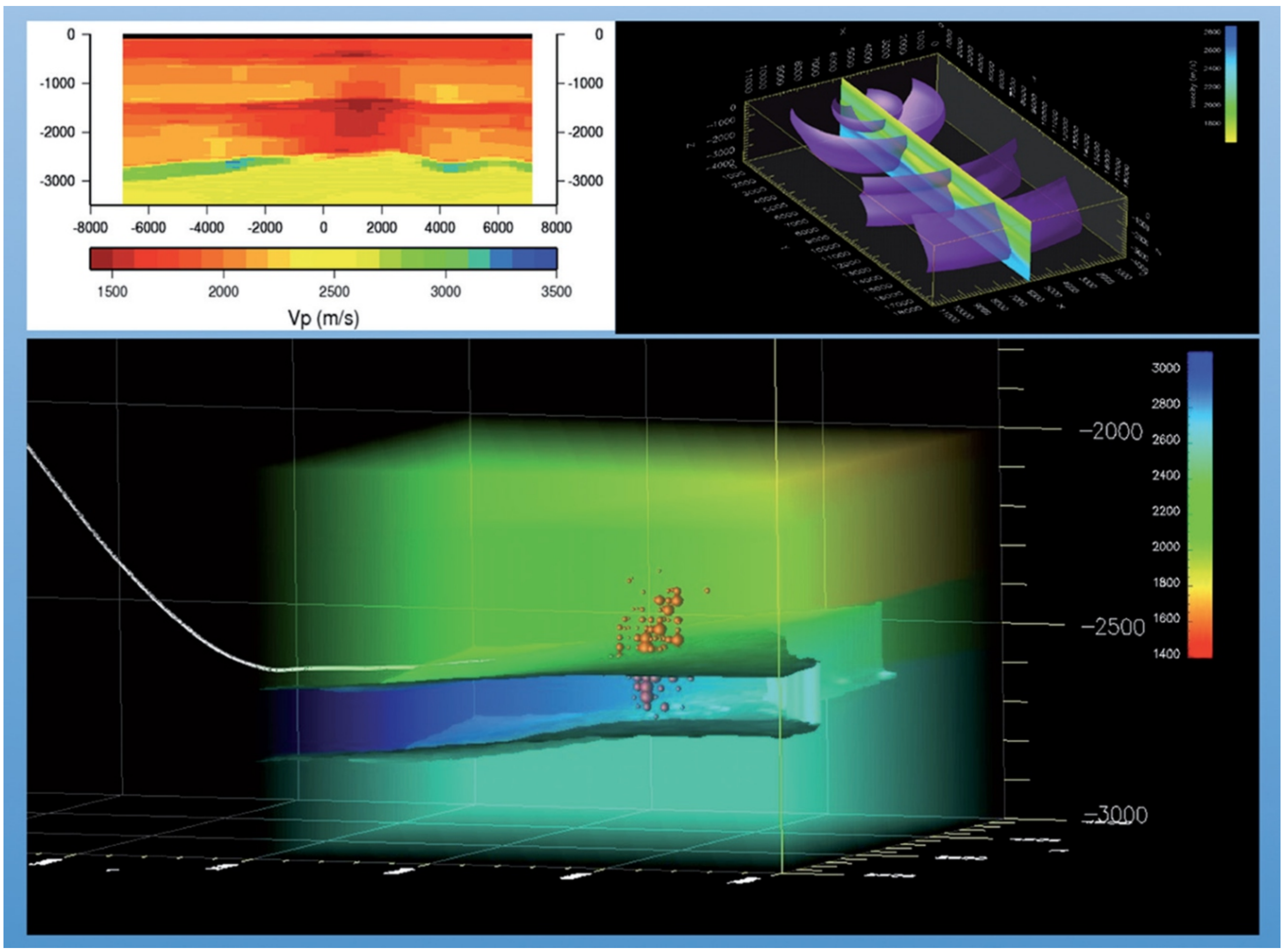

Figure 15.18: Top left shows a cross-section though the P-wave velocity model for the area covered by the Valhall LoFS array. Top right is the corresponding travel time iso-surfaces (wave fronts) for four time steps for a wave-field propagating through the velocity field. Initiating wave fronts from each sensor position and interpolating travel times throughout the sub surface construct travel timetables. The travel timetables are used to align and stack passive recordings resulting in images that identify the position and time of sources in the sub surface. The bottom figure shows the position of events identified using the imaging procedure, (Chambers, Kendall et al. 2010).

Nomenclature

R = time shift, t
t = time, t
V_s = homogeneous velocity, L/t
v = velocity, L/t
z = strain
Δv = velocity change, L/t
Δt = time change, t
Δz = strain change
ε_{zz} = average strain

Abbreviations

AVO = amplitude versus offset
AVOA = AVO azimuthal effects
BP = Beyond Petroleum, former name, British Petroleum
CH = cased hole
FAST = fracture aligned sweep technology
GPS = global position system
LoFS = Life of field seismic (permanent seabed installation)
MDPN = multi-detector pulsed neutron
NCS = Norwegian Continental Shelf
NRMS = normalized root mean square
OBC = ocean bottom cable
PLT = production logging tool
PHIT = total porosity
PGS = Petroleum Geo Services
SAT = seismic array terminator
SINTEF = Norsk forskningskonsern
SOA = seismic obscured area
WBT = water breakthrough

References

Andersen, M.A., 1995. *Petroleum Research in North Sea Chalk.* RF-Rogaland Research. Joint Chalk Research Program Phase IV.

Barkved, O., Buer, K. et al., 2003. 4D Seismic Response of Primary Production and Waste Injection at the Valhall Field. 02 June. URL `http://www.earthdoc.org/publication/publicationdetails/?publication=3102`.

Barkved, O.I., 2012. *Seismic Surveillance for Reservoir Delivery: From a Practitioner's Point of View*. EAGE publications. April. URL `http://dx.doi.org/10.3997/9789073834248`.

Barkved, O.I., Gaucher, E. et al., 2002. Analysis of Seismic Recordings during Injection Using In-Well Permanent Sensors. In *64th EAGE Conference & Exhibition*. May. URL `http://www.earthdoc.org/publication/publicationdetails/?publication=6171`.

Biondi, B., Mavko, G. et al., 1996. Reservoir Monitoring - a Multi-Disciplinary Feasibility Study in 3D. 27 October. URL `http://dx.doi.org/10.3997/2214-4609.201406847`.

Calvert, M., Roende, H. et al., 2013. Quick Impact of New 4D over the Halfdan Field, Danish North Sea. In *75th EAGE Conference & Exhibition incorporating SPE EUROPEC 2013*. 10 June. URL `http://dx.doi.org/10.3997/2214-4609.20130852`.

Chambers, K., Kendall, J.M., and Barkved, O.I., 2010. Investigation of induced microseismicity at Valhall using the Life of Field Seismic array. *The Leading Edge*, **29** (3): 290–295. URL `http://dx.doi.org/10.1190/1.3353725`.

Corzo, M., MacBeth, C., and Barkved, O., 2013. Estimation of pore-pressure change in a compacting reservoir from time-lapse seismic data. *Geophysical Prospecting*, **61** (5): 1022–1034. URL http://dx.doi.org/0.1111/1365-2478.12037.

Corzo Mojica, M.M., 2009. *Pressure estimation using time-lapse seismic in compacting reservoirs*. Ph.D. thesis, Heriot-Watt University. URL http://hdl.handle.net/10399/2318.

De Meersman, K., Kendall, J.M., and Van der Baan, M., 2009. The 1998 Valhall microseismic data set: An integrated study of relocated sources, seismic multiplets, and S-wave splitting. *Geophysics*, **74** (5): B183–B195. September. URL http://dx.doi.org/10.1190/1.3205028.

Dean, G., Hardy, R., and Eltvik, P., 1994. Monitoring compaction and compressibility changes in offshore chalk reservoirs. *SPE Formation Evaluation*, **9** (01): 73–76. SPE-23142-PA. March. URL http://dx.doi.org/10.2118/23142-PA.

Dellinger, J.A. and Yu, J., 2009. Low-frequency virtual point-source interferometry using conventional sensors. In *71st EAGE Conference & Exhibition*. 08 June. URL http://dx.doi.org/10.3997/2214-4609.201400529.

Dons, T., Jørgensen, O., and Gommesen, L., 2007. Seismic Observation and Verification of Line Drive Water Flood Patterns in a Chalk Reservoir, Halfdan Field, Danish North Sea. Paper SPE 108531 presented at Offshore Europe, Aberdeen, Scotland, U.K. 4–7 September. URL http://dx.doi.org/10.2118/108531-MS.

Duncan, P. and Eisner, L., 2010. Reservoir characterization using surface microseismic monitoring. *GEOPHYSICS*, **75** (5): 75A139–75A146. September. URL http://dx.doi.org/10.1190/1.3467760.

Fjær, E. and Kristiansen, T.G., 2009. An Integrated Geomechanics, Rock Physics and Seismic Model. In *71st EAGE Conference and Exhibition incorporating SPE EUROPEC 2009*. EAGE Publications. June. URL http://dx.doi.org/10.3997/2214-4609.201400078.

Folstad, P., 2011. Ekofisk - Justification for a Permanent Monitoring System. In *EAGE Workshop on Permanent Reservoir Monitoring (PRM) - Using Seismic Data 2011*. EAGE Publications. February. URL http://dx.doi.org/10.3997/2214-4609.20145242.

Folstad, P., Morgan, P. et al., 2015. Keynote Speech-Ekofisk Permanent Seismic Monitoring-Results After first 4 years. In *Third EAGE Workshop on Permanent Reservoir Monitoring 2015*. EAGE Publications. 16 March. URL http://dx.doi.org/10.3997/2214-4609.201411958.

Gil, J., 2012. Reservoir Modeling to Assess the Value of the Re-Development of the Hod Field. No public reference available., OTD 2012, Bergen.

Gommesen, L., Dons, T. et al., 2007. 4D Seismic Signatures of North Sea Chalk - The Dan Field. Paper SEG-2007-2847 presented at SEG Annual Meeting, San Antonio, Texas. 23–28 September. URL https://www.onepetro.org/conference-paper/SEG-2007-2847?sort=&start=0&q=4D+Seismic+Signatures+of+North+Sea+Chalk+-+The+Dan+Field.&from_year=&peer_reviewed=&published_between=&fromSearchResults=true&to_year=&rows=10#.

Grose, T.D., 2007. Surveillance-Maintaining The Field From Cradle To Grave. In *Offshore Europe*. Society of Petroleum Engineers, Aberdeen, Scotland, U.K. SPE-108498-MS. 4–7 September. URL http://dx.doi.org/10.2118/108498-MS.

Guilbot, J. and Smith, B., 2002. 4-D constrained depth conversion for reservoir compaction estimation: Application to Ekofisk Field. *The Leading Edge*, **21** (3): 302–308. March. URL http://dx.doi.org/https://doi.org/10.1190/1.1463782.

Hall, S.A., 2006. A methodology for 7D warping and deformation monitoring using time-lapse seismic data. *Geophysics*, **71** (4): O21–O31. July. URL http://dx.doi.org/10.1190/1.2212227.

Hall, S.A., Kendall, J.M., and Barkved, O.I., 2002. Fractured reservoir characterization using P-wave AVOA analysis of 3D OBC data. *The Leading Edge*, **21** (8): 777–781. August. URL http://dx.doi.org/10.1190/1.1503183.

Hatchell, P.J., Kawar, R.S., and Savitski, A.A., 2005. Integrating 4D seismic, geomechanics and reservoir simulation in the Valhall oil field. In *67th EAGE Conference & Exhibition*. URL http://www.earthdoc.org/publication/publicationdetails/?publication=1476.

Haugvaldstad, H., Lyngnes, B. et al., 2011. Ekofisk time-lapse seismic–a continuous process of improvement. *first break*, **29** (9): 113–120. URL `http://www.slb.com/~/media/Files/westerngeco/resources/articles/2011/201109_fb_ekofisk.pdf`.

Herwanger, J., Palmer, E., and Schiøtt, C.R., 2007. Field Observations and Modeling Production-Induced Time-Shifts in 4D Seismic Data at South Arne, Danish North Sea. In *69th EAGE Conference & Exhibition*. URL `http://dx.doi.org/10.3997/2214-4609.201401716`.

Hornby, B., Barkved, O.I. et al., 2007. Reservoir Monitoring Using Permanent In-Well Seismic. In *International Petroleum Technology Conference*. International Petroleum Technology Conference, Dubai, U.A.E. IPTC-11789-ABSTRACT. 4–6 December. URL `http://dx.doi.org/10.2523/IPTC-11789-ABSTRACT`.

Janssen, A., Byerley, G. et al., 2006. Simulation-driven seismic modeling applied to the design of a reservoir surveillance system for Ekofisk Field. *The Leading Edge*, **25** (9): 1176–1185. September. URL `http://dx.doi.org/10.1190/1.2349823`.

Jones, G.A., 2010. *Microseismicity in the Ekofisk Field:Faulting and fracturing in a compacting*. Ph.D. thesis, University of Bristol.

Jones, M. and Mathiesen, E., 1993. Pore pressure change and compaction in North Sea chalk hydrocarbon reservoirs. *International Journal of Rock Mechanics and Mining Sciences & Geomechanics Abstracts*, **30** (7): 1205–1208. December. URL `http://dx.doi.org/10.1016/0148-9062(93)90095-u`.

Jørgensen, O., 2002. Using flow induced stresses for steering of injection fracturesUsing flow induced stresses for steering of injection fractures. In *SPE/ISRM Rock Mechanics Conference*. Society of Petroleum Engineers. Paper SPE 78220 presented at SPE/ISRM Rock Mechanics Conference, Irving, Texas. 20–23 October. URL `http://dx.doi.org/10.2118/78220-MS`.

Key, S.C., Pederson, S.H., and Smith, B.A., 1998. Adding value to reservoir management with seismic monitoring technologies. *The Leading Edge*, **17** (4): 515–519. April. URL `http://dx.doi.org/10.1190/1.1438002`.

Key, S.C., Søiland, G.V. et al., 1996. Ekofisk field-reservoir characterization to reservoir monitoring on a giant chalk reservoir. In *58th EAGE Conference and Exhibition*. 06 June. URL `http://dx.doi.org/10.3997/2214-4609.201409047`.

Kosco, K., Rau Schøtt, C. et al., 2010. Integrating time-lapse seismic, reservoir simulation and geomechanics. *World oil*, **231** (3). URL `http://cat.inist.fr/?aModele=afficheN&cpsidt=22560862`.

Kragh, E. and Christie, P., 2002. Seismic repeatability, normalized rms, and predictability. *The Leading Edge*, **21** (7): 640–647. July. URL `http://dx.doi.org/10.1190/1.1497316`.

Landrø, M. and Janssen, R., 2002. Estimating Compaction and Velocity Changes from Time-Lapse near and far Offset Stacks. In *64th EAGE Conference & Exhibition*. 27 May. URL `http://www.earthdoc.org/publication/publicationdetails/?publication=5562`.

Landrø, M., Solheim, O.A. et al., 1999. The Gullfaks 4D seismic study. *Petroleum Geoscience*, **5** (3): 213–226. August. URL `http://dx.doi.org/10.1144/petgeo.5.3.213`.

Landrø, M. and Stammeijer, J., 2004. Quantitative estimation of compaction and velocity changes using 4D impedance and traveltime changes. *Geophysics*, **69** (4): 949–957. URL `http://dx.doi.org/10.1190/1.1778238`.

Maxwell, S., Bossu, R. et al., 1997. Microseismic logging of Ekofisk borehole C11a during April 1997. Tech. rep., Internal report Phillips Petroleum.

Maxwell, S.C., Rutledge, J. et al., 2010. Petroleum reservoir characterization using downhole microseismic monitoring. *GEOPHYSICS*, **75** (5): 75A129–75A137. URL `http://dx.doi.org/10.1190/1.3477966`.

Maxwell, S.C. and Urbancic, T.I., 2001. The role of passive microseismic monitoring in the instrumented oil field. *The Leading Edge*, **20** (6): 636–639. URL `http://dx.doi.org/10.1190/1.1439012`.

Meersman, K.D., 2005. *Passive Seismic Monitoring: Event Location And Anisotropy Estimation*. Ph.D. thesis, University of Leeds.

Nagel, N.B., 2001. Compaction and subsidence issues within the petroleum industry: From wilmington to ekofisk and beyond. *Physics and Chemistry of the Earth, Part A: Solid Earth and Geodesy*, **26** (1–2): 3–14. URL http://dx.doi.org/10.1016/S1464-1895(01)00015-1.

Oye, V. and Roth, M., 2003. Automated seismic event location for hydrocarbon reservoirs. *Computers & Geosciences*, **29** (7): 851–863. August. URL http://dx.doi.org/10.1016/S0098-3004(03)00088-8.

Pettersen, R.S.H., Barkved, O.I., and Haller, N., 2006. Time-lapse seismic inversion of data from a compacting chalk reservoir. In *2006 SEG Annual Meeting*, 3225–3229. Society of Exploration Geophysicists. URL http://dx.doi.org/10.1190/1.2370200.

Rod, M.H. and Jørgensen, O., 2005. Injection Fracturing in a Densely Spaced Line Drive Waterflood–The Halfdan Example. Paper SPE-94049-MS presented at SPE Europec/EAGE Annual Conference, Madrid, Spain. 13–16 June. URL http://dx.doi.org/10.2118/94049-MS.

Rod, M.H., Zyweck, M. et al., 2005. Permanent Microseismic Monitoring System in a Long Horizontal Well. In *SPE Annual Technical Conference and Exhibition*. Society of Petroleum Engineers. SPE-97075-MS. 9–12 October. URL http://dx.doi.org/10.2118/97075-MS.

Røste, T., Stovas, A., and Landro, M., 2005. Estimation of layer thickness and velocity changes using 4D prestack seismic data. In *Expanded Abstracts C*, vol. 10. 67th Meeting, EAGE. 13 June. URL http://www.earthdoc.org/publication/search?pubsummary=&pubparenttype=all&pubpublicationtype=0&pubtitle=&pubauthor=R%C3%B8ste&pubsession=&pubdoi=&pubedition=1&puborganisation=0&publanguage=0&pubstartdate=&pubenddate=&search=Search.

Rutledge, J.T., Fairbanks, T.D. et al., 1994. Reservoir microseismicity at the Ekofisk oil field. In *Rock Mechanics in Petroleum Engineering*. Society of Petroleum Engineers, Delft, Netherlands. SPE-28099-MS. 29–31 August. URL http://dx.doi.org/10.2118/28099-MS.

Sulak, R.M., 1991. Ekofisk Field: the First 20 years. *JPT*, **43** (10): 1265–1271. SPE-20773-PA. October. URL http://dx.doi.org/10.2118/20773-PA.

Tjetland, G., Kristiansen, T.G., and Buer, K., 2007. Reservoir management aspects of early waterflood response after 25 years of depletion in the Valhall Field. In *International Petroleum Technology Conference*. International Petroleum Technology Conference, Society of Petroleum Engineers (SPE), Dubai, U.A.E. IPTC-11276-MS. 4–6 December. URL http://dx.doi.org/10.2523/IPTC-11276-MS.

van Gestel, J.P., Best, K.D. et al., 2011. Integration of the life of field seismic data with the reservoir model at the Valhall Field. *Geophysical Prospecting*, **59** (4): 673–681. July. URL http://dx.doi.org/10.1111/j.1365-2478.2011.00946.x.

Vejbæk, O.V., King, A. et al., 2012. Repeat time lapse 4D seismic monitoring as a tool for South Arne field development. In *74th EAGE Conference and Exhibition incorporating EUROPEC 2012*. 4 June. URL http://dx.doi.org/10.3997/2214-4609.20148255.

Walls, J., Dvorkin, J., and Smith, B., 1998. Modeling seismic velocity in Ekofisk chalk. In *SEG Technical Program Expanded Abstracts 1998*, 1016–1019. Society of Exploration Geophysicists. SEG Annual Meeting, New Orleans. January. URL http://dx.doi.org/10.1190/1.1820055.

Zett, A., Mukerji, P. et al., 2011. Reservoir Surveillance and Successful Infill Well Delivery in a Mature Asset. In *Offshore Europe*. Society of Petroleum Engineers, Aberdeen, UK. SPE-145242-MS. 6–8 September. URL http://dx.doi.org/10.2118/145242-MS.

Zett, A., Riley, S. et al., 2008. An Integrated Data Acquisition And Analysis Approach Decreases Saturation Uncertainty And Provides Valuable Secondary Information In Difficult Conditions. In *SPWLA 49th Annual Logging Symposium Paper QQQ*. SPWLA-2008-QQQ. 25–28 May. URL https://www.onepetro.org/conference-paper/SPWLA-2008-QQQ.

Zett, A., Webster, M., and Jehanno, Y., 2010. Production Petrophysics-Preserving Program Flexibility to Ensure Successful Infill Delivery In a Mature Field Environment. In *SPWLA 51st Annual Logging Symposium*. Society of Petrophysicists and Well-Log Analysts. SPWLA-2010-46513. URL https://www.onepetro.org/conference-paper/SPWLA-2010-46513.

Zett, A., Webster, M. et al., 2012. Application of new generation multi detector pulsed neutron technology in petrophysical surveillance. In *SPWLA 53rd annual logging symposium*. Society of Petrophysicists and Well-Log Analysts, Cartagena, Colombia. SPWLA-2012-094. 16–20 June. URL `https://www.onepetro.org/conference-paper/SPWLA-2012-094`.

Zett, A., Webster, M.J. et al., 2011. Extending production petrophysics applications in monitoring complex recovery mechanisms. In *SPE Annual Technical Conference and Exhibition*. Society of Petroleum Engineers, Denver, Colorado, USA. SPE-146662-MS. 30 October – 2 November. URL `http://dx.doi.org/10.2118/146662-MS`.

Zoback, M.D. and Zinke, J.C., 2002. Production-induced Normal Faulting in the Valhall and Ekofisk Oil Fields. In C. Trifu, ed., *The Mechanism of Induced Seismicity*, Pageoph Topical Volumes, 403–420. Birkhäuser Basel. ISBN 978-3-7643-6653-7. URL `http://dx.doi.org/10.1007/978-3-0348-8179-1_17`.

Part III

Improved Oil Recovery Methods

Chapter 16

Gasflooding

Erling Stenby and Wei Yan

16.1 Introduction

The history of gas injection can be traced back to the 1930s when lean hydrocarbon gas was used for the purpose of reservoir pressure maintenance (Warner and Holstein 2007). In the 1960s, injection of liquefied petroleum gas (LPG) as slugs with chasing gas was tried but turned out economically unattractive (Lake 1989). It was until the 1970s that large commercial scale gas injections took place. Most of these projects are CO_2 injection thanks to the low cost CO_2 sources. Increased oil price and maturity of the technology are also behind the acceptance of the gas injection technology in the 1970s. Gas injection is now widely used to improve oil recovery with most projects implemented in the United States. A variety of gases can and have been used for gas injection, such as hydrocarbon gas (lean or rich gas, LPG, liquefied natural gas), CO_2, N_2 and flue gas. Injection of liquid solvents like organic alcohols and ketones shares a lot of similarity with injection of gaseous solvents but our discussion here focuses on gas injection in its narrow sense. Gas injection can be considered whenever there is a convenient gas supply, which can be produced gas or a relatively close gas field. For low permeable and deep reservoirs with light oil, gas injection can be a good EOR choice. Gas injection is usually classified into immiscible gas injection and miscible gas injection. Complete immiscibility is rarely seen since there is always exchange of components between the injection gas and the in-situ oil. The mass transfer between the gas and oil phases is described as extraction, dissolution, vaporization, and condensation depending what the major effect is. This chapter is intended to suffice to understand the fundamentals of gas injection by focusing on basic concepts, major experimental and modeling tools, and the latest development in the theory of gas injection processes. The chapter covers miscibility mechanisms, major findings from the theory of gas injection processes, experimental and modeling phase behavior topics related to gas injection, and basic treatment of the flow functions. A brief review of field cases is presented as a quick guide to typical gas injection examples.

16.2 Miscibility mechanisms and theory of gas injection processes

The major recovery mechanisms in a gas injection process include oil swelling, oil viscosity reduction, and development of miscibility. It requires mainly phase behavior knowledge to understand the first two mechanisms whereas the last mechanism is a result of the interplay of phase equilibrium and multiphase flow. The theory of one-dimensional multicomponent, multiphase flow of gas/oil displacements (Orr Jr. 2007) provides a basis for understanding gas injection processes, just as the Buckley-Leverett theory does for waterflooding processes.

16.2.1 Mechanisms of miscibility

It has long been recognized that displacements of oil by gas are either immiscible or miscible, with the miscible displacements further classified into first contact miscible (FCM) and multicontact miscible (MCM). In miscible displacements, a miscible zone is formed somewhere along the displacement path. Higher pressure usually favors formation of miscibility and the threshold pressure to develop miscibility is known as the minimum miscibility pressure (MMP). At the MMP, the local gas and oil phases in the miscible zone have essentially the same density and composition, and zero interfacial tension between them. No residual oil is left at and above the MMP and a 100% theoretical displacement efficiency can be obtained at the microscopic scale. If the injected gas and the initial oil can be mixed at any proportion to form a single phase at the injection pressure, it is known as first contact miscible. Even if the gas and oil do not form FCM, it is possible to develop miscibility through multiple contacts where gas and oil change their composition along the flow path as a result of vaporization of light components and condensation of heavy components. The final miscibility is achieved with at least one phase with altered composition. First contact miscibility is a more stringent miscibility condition and usually corresponds to a higher MMP than that for multicontact miscibility. Most miscible injections belong to the MCM category.

Pseudoternary diagrams are traditionally used to explain the recovery mechanisms of gas injection. The multicomponent system is grouped into three pseudo components: light, intermediate, and heavy ones as in **Fig. 16.1**. Recovery mechanisms including FCM, and vaporizing drive and condensing drive in MCM can be illustrated by the diagram. The critical tie-line divides the diagram into two parts: Part I containing only the single phase region and Part II containing the two-phase region. For FCM, there is no requirement on the locations of the injection gas and the initial oil in the diagram except that the connecting line between gas and oil, known as the dilution line, is always in the single phase region. As a result, the gas and oil are miscible with any mixing ratio. Three different combinations (Gas1 and Oil1, Gas2 and Oil2, and Gas1 and Oil2) shown in **Fig. 16.1a** are all FCM, but injection of Gas2 into Oil1 is not FCM. For vaporizing drive, the gas originally in Part II will be enriched with the intermediate and heavy components by the oil in Part I and finally reach miscibility in the front of the displacement. In **Fig. 16.1b**, the oil happens to be at the border where miscibility can form. For condensing drive, the oil originally in Part II will be enriched with the light and intermediate components by the gas in Part I and finally reach miscibility in the rear of the displacement. In **Fig. 16.1c**, the gas happens to be at the border where miscibility can form. However, pseudoternary phase diagrams cannot be applied to

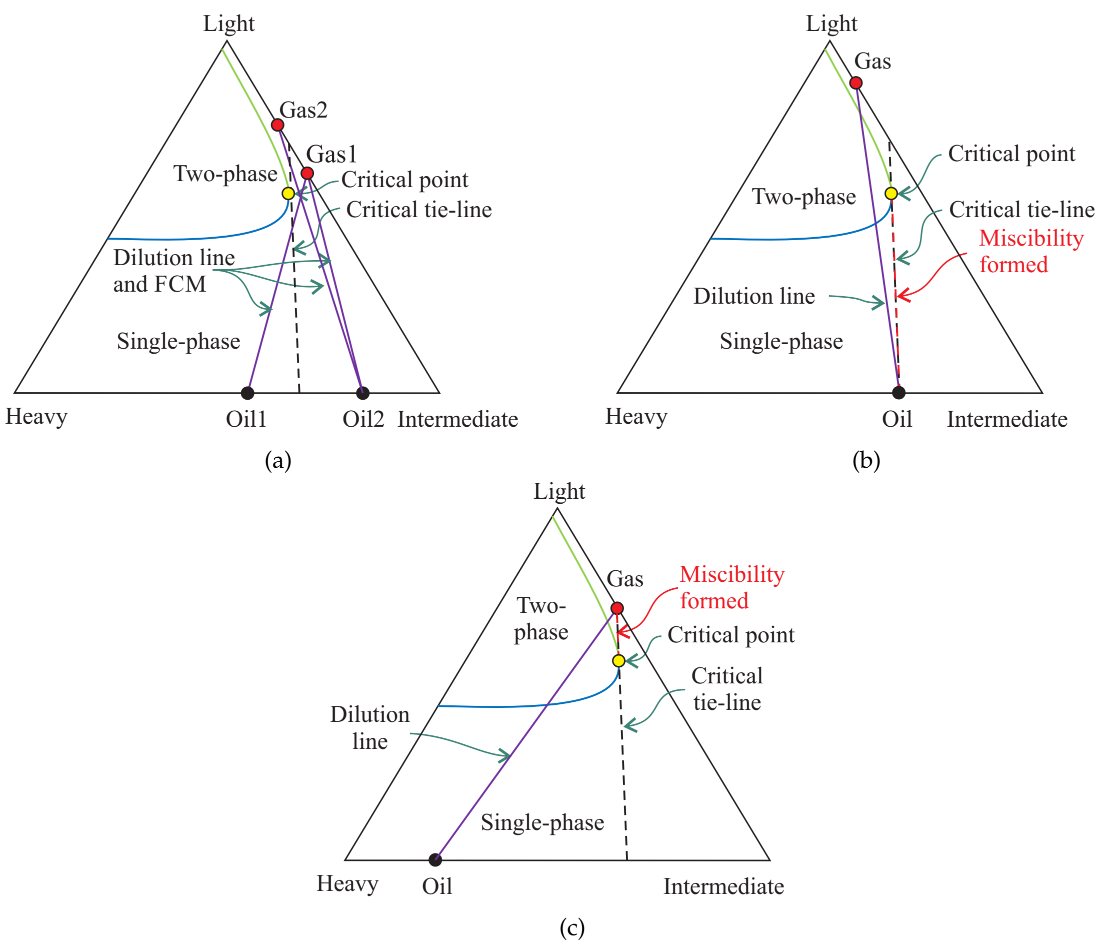

Figure 16.1: Pesudotenary phase diagrams for different miscibility mechanisms: (a) FCM: Gas1-Oil1, Gas2-Oil2 and Gas1-Oil2 are miscible in any proportion; (b) Vaporizing drive: Gas becomes more enriched and finally misicible with the initial oil; (c) Condensing drive: Oil becomes lighter and finally miscible with the injection gas.

combined condensing/vaporizing drive in MCM, which is perhaps the most common miscibility mechanism in multicomponent gas/oil displacements. The combined mechanism was first analyzed by Zick (1986) with both experimental evidence and simulation results. One way to understand the combined mechanism is to further distinguish between light intermediates and middle intermediates (Zick 1986). The light intermediates refer to components like ethane, propane, and butane, which are the enriching components present in the injection gas; the middle intermediates refer to the vaporizable components present in the oil but not significantly in the gas. For injection of enriched gas into a real reservoir oil, in the rear of the displacement where fresh gas comes into contact with the oil, the light intermediates condense into the oil but the middle intermediates are stripped to the gas. The oil will soon be rich in light intermediates but lean in middle intermediates. Such oil cannot form condensing drive miscibility with the fresh gas containing no middle intermediates. This is why condensing drive rarely happens in the real displacements. Farther downstream, the gas is enriched more with middle intermediates. If the original oil is sufficiently rich in intermediates, a vaporizing drive miscibility is likely to happen. But if not, the gas has accumulated enough intermediates from this vaporizing segment to form a condensing segment farther downstream. **Fig. 16.2** shows the typical simulation results of a 15-component gas/oil displacement with a combined drive mechanism. In the two-phase region, there is a leading condensing segment and a trailing vaporizing segment. The variations of K-values, (molar composition ratios between gas and liquid phases) and phase densities in these two segments are similar to those in vaporizing and condensing drive, respectively. The narrow neck where two segments join is the place with *K*-values close to 1 and gas and oil phase densities approaching each other. This is the place where miscibility will form. Miscibility for combined drive forms in the middle of the displacement, which is in contrast with vaporizing drive (in the front) and condensing drive (in the rear). If the pressure is higher than MMP, the narrow neck will in principle shrink to a point, and the two phase region will shrink to zero width. The near miscible gas saturation curve in Fig. 16.1 will develop to a single front corresponding to a piston-like displacement.

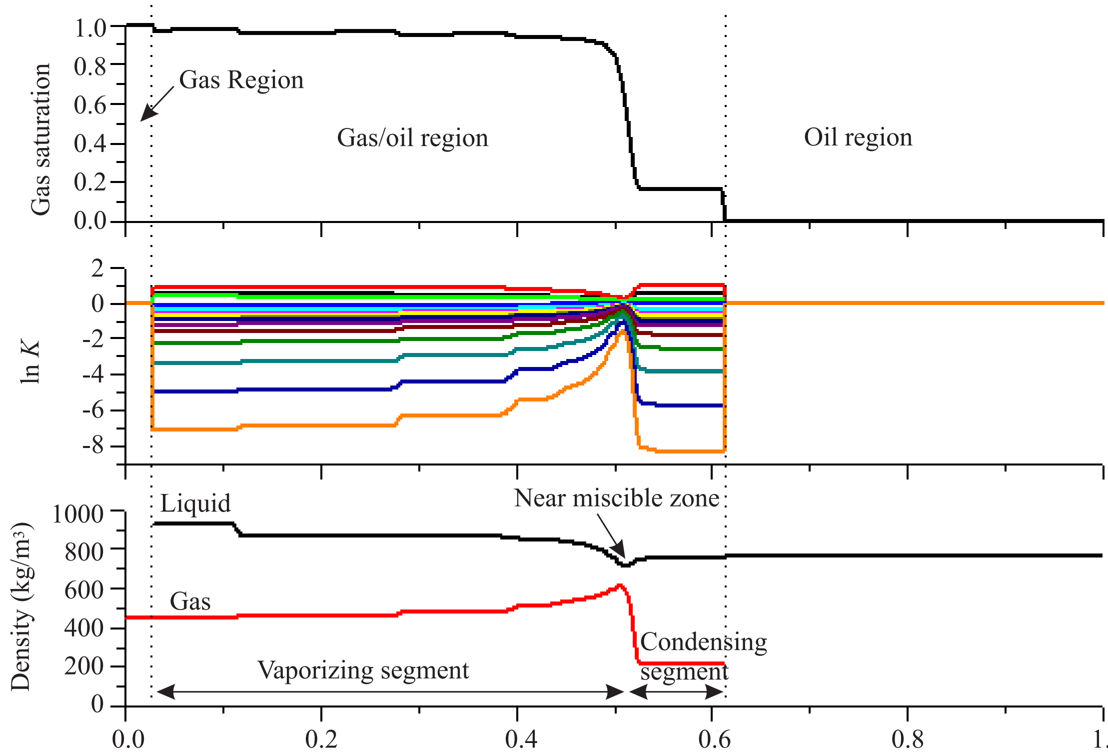

Figure 16.2: EoS calculated slim tube profiles for a condensing/vaporizing gas drive process for a 15-component system (curves in the $\ln K$ profile are for N_2, C_1, CO_2, C_2, C_3, iC_4, nC_4, iC_5, nC_5, C_6 and five C_{7+} fractions respectively from top to the bottom.)

16.3 Theory of gas injection processes

The theory of gas injection is closely linked to the theory of chromatography, (Helfferich and Klein 1970). In the area of enhanced oil recovery, it is closely linked to the theoretical descriptions of polymer flooding and surfactant flooding. (Larson 1979; Helfferich 1982; Hirasaki 1981) developed the theory for three-component systems for applications in surfactant flooding. The fundamental ideas in these early pioneering studies were later extended by Orr Jr. (2007) and his coworkers to multicomponent gas injection processes which are more complicated in terms of phase equilibrium, fluid flow, and the number of components involved.

The theory of gas injection is built upon the conservation equations for one-dimensional, multiphase, multicomponent flow and the phase equilibrium equations between gas and oil phases. The conservation equations for one-dimensional, n_c-component, two-phase flow is as follows:

$$\frac{\partial}{\partial \tau}\left(\sum_{j=1}^{2} x_{ij}\rho_j S_j\right) + \frac{\partial}{\partial \xi}\left(v_D \sum_{j=1}^{2} \chi_{ij}\rho_j f_j\right) = 0, \qquad i = 1, \dots n_c \tag{16.1}$$

The flow is assumed to be purely convective with negligible diffusion and dispersion mixing. In Eq. 16.1, ρ_j, x_{ij}, S_j and f_j are the phase density, mole fraction of component i, phase saturation, and fractional flow of phase j, respectively. The dimensionless time τ, the dimensionless distance ξ, and the dimensionless velocity v_D are given by

$$\tau = \frac{v_{\text{inj}} t}{\phi L} \tag{16.2}$$

$$\xi = \frac{x}{L} \tag{16.3}$$

$$v_D = \frac{v}{v_{\text{inj}}} \tag{16.4}$$

where t is the time, x the distance, L the length, ϕ the porosity, v the velocity, and v_{inj} the injection velocity. The theory assumes instantaneous equilibrium between gas and oil phases. The phase equilibrium can be described by constant K-values for simplicity of analysis. The results with constant K-values are reasonable approximations when displacements are far from miscibility. For a general situation including miscible displacements, more rigorous thermodynamic description with equations of state must be employed.

Orr's book (Orr Jr. 2007) presents a comprehensive and detailed review of the theoretical aspects of gas injection processes. The method of characteristics is extensively used to construct the solution to the conservation equations coupled with phase equilibrium relationships. The solution construction is far from trivial even for simple three-component and four-component displacements. In principle, combined drive can happen for systems with $n_c \geq 4$. The solutions for four-component displacements (Monroe, Silva et al. 1990; Dindoruk 1992; Johns 1992; Dindoruk, Johns et al. 1992; Dindoruk, Orr Jr. et al. 1997; Johns, Dindoruk et al. 1993; Johns and Orr Jr. 1996) actually reveal all the essential features of gas injection with various MCM mechanisms. For real reservoir oil systems, solutions to multicomponent displacements are needed. A practical approach for constructing such solutions was first provided by (Wang 1998; Wang and Orr Jr. 1997). Later, (Jessen 2000; Jessen, Wang et al. 2001) further developed efficient algorithms for automatic solution of problems with an arbitrary number of components in the oil or injection gas. Some important findings about the solution to 1D, two-phase displacement with uniform initial condition and constant injection condition are summarized below:

1. The self-similar solution can be constructed by finding the composition route in the composition space from the initial oil to the injection gas. The path consists of tie-line path and non tie-line path. In general, the solution consists of shocks and spreading waves. If the path between tie-lines are connected only by shocks, the solution is known as self-sharpening.

2. The solution is controlled by $n_c - 1$ tie-lines called the key tie-lines, including the the injection tie-line passing through the injection gas composition, the initial tie-line passing through the initial oil composition, and $n_c - 3$ crossover tie-lines.

3. Miscibility is developed if any of the key tie-lines becomes critical. A critical initial tie-line corresponds to vaporizing drive, a critical injection tie-line to condensing drive, and a critical crossover tie-line to combined drive. At miscibility, the solution collapses to a single front and the displacement is piston like.

4. The key tie-lines intersect pairwise if the solution is self-sharpening. For non self-sharpening solutions, pairwise intersection is a good approximation.

5. The theory suggests that MMP does not depend on fractional flow.

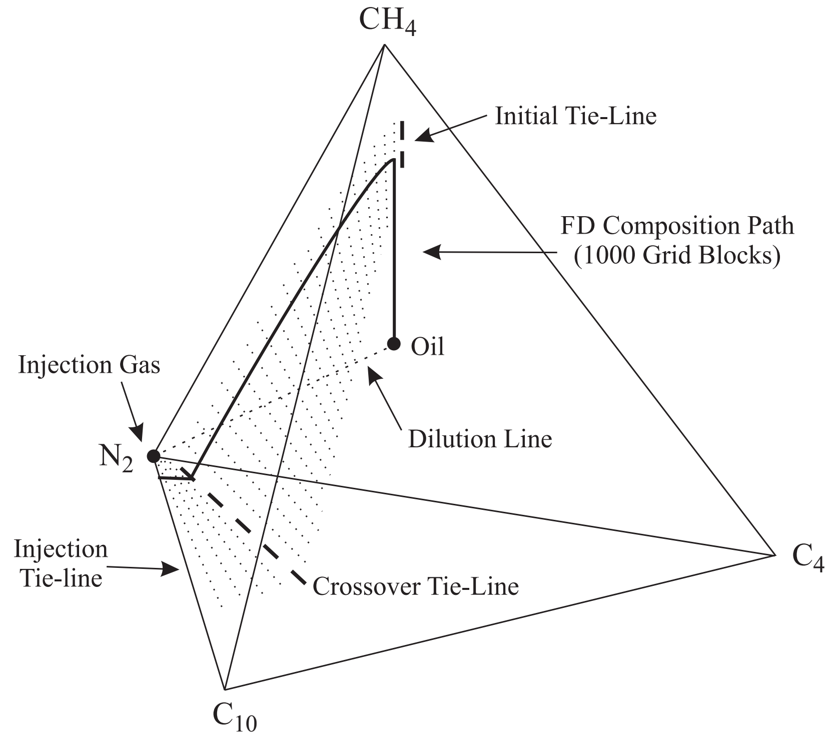

Figure 16.3: Displacement of a 3-component oil of CH_4, C_4 and C_{10} by N_2 (Jessen, Stenby et al. 2004).

Fig. 16.3 shows the composition route for the displacement of 3-component oil of CH_4, C_4 and C_{10} by N_2. The key tie-lines are intersecting pairwise. The composition route in this figure is generated by finite difference simulation and does not pass the key tie-lines exactly due to numerical dispersion. For a dispersion-free analytical solution, it should pass them strictly.

The theory of gas injection processes provides a rigorous approach to construct the detailed solution for one-dimensional gas injection. Apart from its theoretical significance , it has led to several useful tools for practical applications. First, a global approach for MMP calculation was developed based on the intersecting key tie-lines (Jessen, Michelsen et al. 1998), with more details described in Sec. 16.4.3 . Second, a semi-analytical solution for dispersion-free one dimensional gas injection can be constructed in an efficient manner (Jessen, Wang et al. 2001). The semi-analytical solution can be used as a benchmark for 1D numerical simulation results. It can also be extended to 3D applications when combined with compositional streamline simulation, providing a fast forecast of gas injection in real heterogeneous reservoirs. Finally, one useful concept built upon the theory of gas injection is dispersive distance. Finite difference simulation of gas injection suffers from numerical dispersion, which is particularly a concern when a limited number of grid blocks are used between injectors and producers in large scale simulations. Dispersive distance provides a quantitative estimate of the numerical dispersion tendency for a certain displacement system. It is defined as the perpendicular distance from the critical point where the MMP forms to the dilution line, thus characterizing the difference between the convection-dominated path and the dispersion-dominated path (the dilution line). **Fig. 16.4** shows that how the error in simulated recovery factor increases with dispersive distance.

16.4 Phase behavior related to gas injection

Enhanced oil recovery through miscible gas injection depends directly on how the oil properties change after exchange of components between the oil and gas. Both experimental measurement and model description of the relevant phase behavior are crucial to gas injection processes.

16.4.1 PVT tests for gas injection

Apart from the routine PVT tests, several extended ones, including swelling test, multiple-contact experiment, and slimtube experiment, are recommended for evaluation of gas injection.

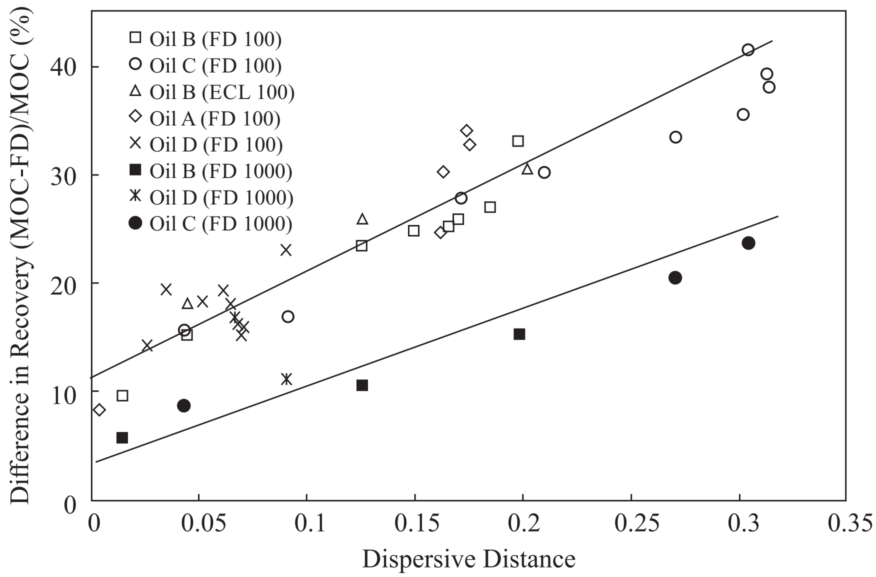

Figure 16.4: Difference in recovery predicted by the analytical theory and FD simulations using 100 and 1000 grid blocks as a function of dispersive distance (Jessen, Stenby et al. 2004).

Swelling test

This simple test mimics a single contact process. The injection gas is added to the reservoir oil in a PVT cell stepwise. At each addition, the saturation pressure and volumetric data of the resulting fluid are measured. The results typically include a saturation pressure-solvent concentration diagram, the swelling factors and viscosities of the oil/solvent mixtures. The maximum of the saturation pressure-concentration curve corresponds to the FCMP. This pressure can be too high and many swelling tests stop at a concentration before this pressure is reached. Multiphase equilibrium may be observed at high solvent concentrations.

Multiple-contact experiment

This experiment mimics the repeated contacts between gas and oil in the displacement. In the forward contact experiment, gas is moved forward to equilibrate with fresh oil repeatedly, thus corresponding to vaporizing drive. In the backward/reverse contact experiment, oil is moved forward to equilibrate with injection gas repeatedly, thus corresponding to condensing drive. Although this complex experiment still cannot account for combined drive, it provides valuable phase equilibrium and volumetric data for model tuning.

Slimtube experiment

The experiment physically simulates gas injection in a 1D reservoir. This classical MMP determination technique is deemed as the most reliable one but the experiment is not standardized. Basic design and variations of the experimental apparatus can be found in Yellig, Metcalfe et al. (1980) and Orr Jr, Silva et al. (1982). Its main part is a long steel tube packed with uniform sand or glass beads. Tubes with various types, lengths and packing material can be found in the literature (Orr Jr, Silva et al. 1982) but most are longer than 10 m. The whole tube is housed in an air or oil bath and usually connected with a sight glass in the outlet for gas breakthrough monitoring. During the experiment, the slim tube saturated with the reservoir oil is displaced by the injection gas at various pressures. The recovery at 1.2 pore volume injection versus pressure is plotted, and the pressure corresponding to the “break point” on the curve is considered to be the MMP. There are other definitions of experimental MMP (Orr Jr, Silva et al. 1982). It is important to keep the consistency for evaluation of a particular field application. Since the experiment is relatively time consuming, some quick MMP measurement techniques, such as the rising bubble method (Christiansen and Haines 1987) and the vanishing interfacial tension (VIT) method, (Rao 1997), have been suggested. However, the rising bubble method is only suitable to determine MMP with vaporizing mechanism, (Zhou and Orr Jr. 1995), and the VIT method is theoretically problematic for MMP determination, (Jessen and Orr Jr. 2008).

16.4.2 Modeling of properties

Prediction of miscible gas injection processes relies largely on equations of state (EoS) based compositional reservoir simulation. The simulation must be able to describe both microscopic displacement and macroscopic sweep. The former requires an accurate phase equilibrium description and the latter requires accurate physical properties such as density and viscosity. Empirical engineering correlations (Whitson and Brulé 2000) are often used for quick estimation but the importance of EoS-related models is more pronounced due to the large composition variation, and we cover only the EoS-related models here.

Equations of state and oil characterization

The Soave-Redlich-Kwong (SRK) EoS (Soave 1972) and the Peng-Robinson (PR) EoS (Peng and Robinson 1976) are the most widely used EoS in gas injection related calculations. An EoS provides the relationship between pressure, volume, temperature, and composition. Through rigorous thermodynamic relationships, one can express various thermodynamic properties and calculate phase equilibrium by use of an EoS. SRK and PR belong to cubic EoS due to their cubic function form. Simpler to use than other advanced EoS models, they generally provide enough accuracy for most engineering calculations. However, phase equilibrium calculation using a cubic EoS is not a trivial task. Details on robust and efficient phase equilibrium calculations can be found in Michelsen, Mollerup et al. (2007).

Oil characterization is a necessary step when SRK and PR are used for reservoir fluids with ill-defined heavy fractions. Characterization generally addresses three concerns: description of the molar composition in the heavy end of oil; estimation of model parameters; and lumping of detailed fluid description into a limited number of components. Pedersen's method (Pedersen, Thomassen et al. 1989; Pedersen, Fredenslund et al. 1989) and Whitson's method (Whitson, Anderson et al. 1989; Whitson and Brulé 2000) are the two commonly used characterization methods in the upstream. The two methods are similar in general PVT calculations. The difference is insignificant especially if tuning is to be made. Jessen and Stenby (2007) used an extensive database of detailed fluid descriptions with experimental PVT and MMP data to evaluate these two methods. For prediction calculation without any regression, Whitson's method predicts a better saturation pressure whereas Pedersen's method predicts a better MMP. Jessen and Stenby (2007) also investigated various regression strategies and found that using standard PVT and swelling data alone is often not sufficient for EOR performance evaluation, and inclusion of the MMP is recommended.

Other physical properties: viscosity, IFT and diffusion

EoS can provide results of density and phase equilibrium directly. Several other physical properties important to gas injection, including viscosity, interfacial tension (IFT), and diffusion coefficients, need their own models which are usually used together with EoS. The traditional model for viscosity is the Lohrenz-Bray-Clark (LBC) model (Lohrenz, Bray et al. 1964). It is simple to use but also very sensitive to errors in density. The corresponding states method is another way to calculate viscosity (Aasberg-Petersen, Knudsen et al. 1991). A promising approach is the friction theory viscosity model (Quiñones-Cisneros, Zéberg-Mikkelsen et al. 2001). Its computation cost is similar to the LBC model but its accuracy is much better. Interfacial tension is used as a scaling parameter for the oil and gas relative permeabilities. The Macleod-Sugden parachor method (Macleod 1923) and its variations are widely used. Several variations of the gradient theory for interfacial tension have been tried (Zuo and Stenby 1996; Zuo, Stenby et al. 1998). The comparative study made by Christensen (1998) suggests that the gas injection simulation results are not so sensitive to the IFT model. Molecular diffusion is considered important mainly for gas injection into fractured reservoirs (Hoteit and Firoozabadi 2009). The common engineering practice to model diffusion is to use empirical correlations for effective diffusion coefficients in Fick's law (Whitson and Brulé 2000), which are developed based on binary diffusion coefficients. For multicomponent diffusion, the Maxwell-Stefan framework instead of Fick's law should be used (Krishna, Wesselingh et al. 1995; Shojaei and Jessen 2014) but Fick's law is almost exclusively used in practice. It should be noted that precaution is needed to interpret diffusion experiments (Potsch, Toplack et al. 2013). There are several recent attempts (Moortgat, Firoozabadi et al. 2009; Alavian and Whitson 2012) to simulate laboratory experiments of CO_2 diffusion into cores.

16.4.3 EoS based MMP calculation

The multicell approach and the intersecting key tie-lines approach are the only two methods that can account for all types of miscibility mechanisms, including combined condensing/vaporizing drive.

Multicell approach

This approach simulates the slimtube experiment using either a multicell simulator or a 1D compositional simulator. Cook, Walker et al. (1969); Metcalfe, Fussell et al. (1973) are the first ones using multiple cells as a simplified 1D reservoir model. Stalkup et al. (1990) proposed to study 1D displacements with a compositional simulator. He also suggested extrapolating the recovery to infinite small grid block size to remove numerical dispersion. The multiple cell simulation and the 1D compositional simulation are actually based on the same formulation for 1D gas injection. The former emphasizes on the physical interpretation whereas the latter on the mathematical solution. Some representative multiple cell simulation methods include Zick's code, (Høier and Whitson 2001), the algorithm of Jaubert, Wolff et al. (1998); Jaubert, Arras et al. (1998), and the method of Ahmadi, Johns et al. (2011). Yan, Michelsen et al. (2012) presented an efficient slimtube simulation method for MMP determination. They suggested that the computation efficiency can be improved by a comprehensive strategy addressing several aspects, including flash algorithm, flash approximation, higher order numerical schemes, extrapolation of recovery, and MMP search strategy.

Intersecting key tie-lines approach

The theory of 1D gas injection shows that the key tie-lines of the analytical solution intersect pairwise, and at the miscibility condition is actually one of the key tie-lines becoming critical. If all the intersecting key tie-lies are determined, by monitoring their change with pressure, it is possible to determine the MMP. Early attempts of the intersecting key tie-lines include Dindoruk, Johns et al. (1992). Wang and Orr Jr. (1997) proposed the first general algorithm for multi-component systems which also allows injection gas with more than one component. Jessen, Michelsen et al. (1998) substantially increased the speed of MMP calculation for gas injection systems with an arbitrary number of components in either oil or gas. The intersecting key tie-lines approach is fast and free from numerical dispersion, but less intuitive than the multicell approach. Two methods give similar results if implemented properly (Jessen 2000; Yan, Michelsen et al. 2012).

16.5 Treatment of flow functions

Gas injection processes usually involve the flow of gas, oil and water phases. The role of water is particularly important in gas flood after water flood and WAG flood. Three-phase relative permeability models are apparently needed for the flow description in these processes. A unique feature to account for is the trapping of gas or solvent by advancing water. As a result of the trapping, the relative permeability exhibits hysteresis when switching between drainage and imbibition processes. In addition, miscible gas injection also needs to account for the variation of relative permeability as the miscibility is approached.

Trapping of gas by advancing water is somewhat similar to trapping of residual oil in a waterflood. The study of Chatzis, Morrow et al. (1983) on the trapping of residual oil is useful for understanding general trapping mechanisms and trapping behavior. Jerauld (1997) flooded Prudhoe Bay cores first with solvent to establish a maximum initial solvent saturation and then flooded the cores with either water or oil. He found that the final trapped-solvent saturation is strongly dependent on the maximum solvent saturation, but nearly independent of the trapping liquid phase. Trapping of gas results in hysteresis, where the gas relative permeability is usually much smaller during imbibition than during primary drainage. The hysteresis must be described quantitatively in a WAG simulation.

The work of Land (1968) provides the basis for most trapping and hysteresis models. Land distinguished between trapped gas and mobile gas: the former participates in phase equilibrium but not flow whereas the latter is the actual flowing portion in the gas phase. He further related the the trapped gas saturation S_{gr} to the initial gas saturation S_{gi} by an empirical equation

$$\frac{1}{S_{gr}} - \frac{1}{S_{gi}} = C \tag{16.5}$$

where C is Land's constant. S_{gi} is the saturation at the "reversal" point where drainage is swicthed to imbibition on the relative permeability and capillary pressure curve. For two-phase hysteresis, Killough's method (Killough 1976) and Carlson's method (Carlson 1981)) are probably the most prevalent models used in numerical simulation. Both methods can determine the intermediate scanning curves for saturation paths which are not primary drainage or primary imbibition. Killough's method calculates the end point of of the imbibition curve by Land's relation. Carlson's method adopts a simple geometric interpretation where the scanning curves are assumed to be parallel to the primary imbibition curve. In both methods, a switch from drainage to imbibition follows a specific scanning curve towards decreasing non-wetting phase saturation; when it switches back to drainage, the scanning curve is traced backwards until the inflection point from where the primary drainage curve will be followed, **Fig. 16.5**.

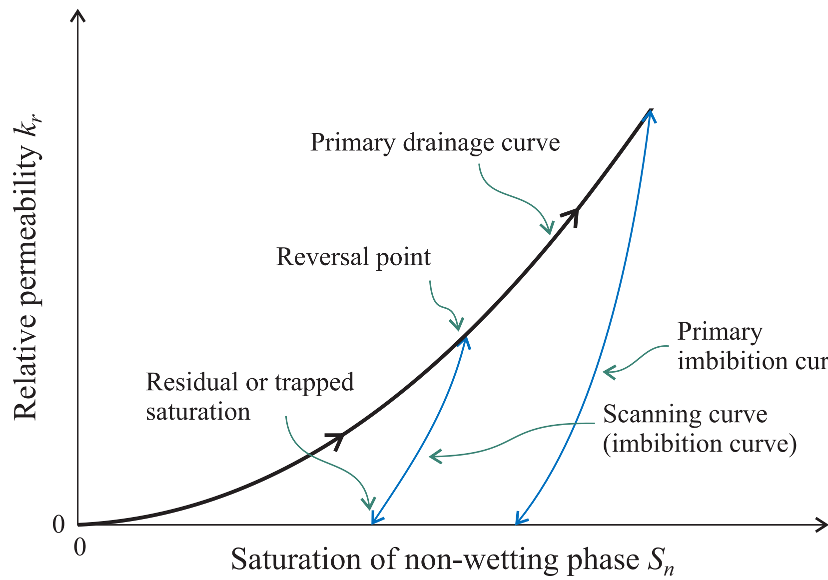

Figure 16.5: Hysteresis of relative permeability of the non-wetting phase (after (Killough 1976).

Three-phase hysteresis models are needed for WAG processes. Larsen and Skauge (1998) presented an approach to account for the spatial gas mobility variation within the reservoir, e.g., the gas mobility in the three-phase area near WAG injection wells is significantly different from that in other two-phase areas of the reservoir. Their model predicts non-reversible hysteresis loops for the non-wetting phase. The gas and water permeability typically reduce with each saturation cycle for increasing trapped gas saturations. The model requires estimation of three parameters: Land's constant, a reduction exponent that accounts for the reduced mobility of gas in the presence of mobile water, and a constant that describes the dependency of trapped gas saturation on the residual oil saturation. The model needs two relative premeability curves (two-phase and three-phase) for the water phase and one drainage curve for the gas phase. All these data must be provided from the laboratory. Other three-phase hysteresis models include Egermann, Vizika et al. (2000); Blunt (2000); Spiteri, Juanes et al. (2005).

At the location where miscibility is developed, the displacement is piston like and the relative permeability curves become straight lines. A proper scaling of the relative permeability is therefore required to reflect its change when the miscibility is approached. The IFT between gas and oil provides a convenient measure for such scaling since it vanishes at the miscibility point and is relatively cheap to calculate. The relative permeability for oil and gas can be calculated as weighted average between a curve at the immiscible conditions and a strainght line corresponding to the miscible conditions.

16.6 Field cases

Warner and Holstein (2007) discussed both successful and unsuccessful immiscible gas injection projects. They concluded that the most successful immiscible gas injection projects are the vertical gravity drainage projects. Gas is injected into the crestal primary or secondary gas cap, and the oil is produced from as far downdip as possible to keep a large distance from the gas cap. There are a few successful immiscible gas injection projects which are not the vertical gravity drainage type, such as the Swanson River field in Alaska. Other typical immiscible gas injection examples given by Warner and Holstein (2007) include the Hawkins Field (East Texas), the Prudhoe Bay field (North Slope, Alaska), the Empire Abo field (New Mexico), the Heft Kel field (Iran), and the Kuparuk River field (North Slope, Alaska). Holstein and Stalkup (2007) reviewed some typical miscible gas injection examples. Most of them are CO_2 projects such as the SACROC four-pattern flood, the Means San Andres unit (the Permian Basin), and the Denver unit. Other miscible gases include enriched-hydrocarbon gas (miscible WAG injection at the Prudhoe Bay) and nitrogen (the Jay field at the Florida-Alabama border). They concluded that miscible injection has been applied successfully in general and the resulting experience has made it possible to predict the economic viability of new projects in other reservoirs.

CO_2 injection has a unique importance in gas injection not only because it is easily miscible compared to many other gases and relatively inexpensive compared to propane or solvents for gas enrichment, but also because it can store anthropogenic CO_2 underground and act as an enabler for the CO2 sequestration technology. According to the Oil & Gas Journal's biennial survey in 2014, production from US miscible CO_2 floods totals 292,735 b/d vs. 284,725 b/d for steam. The production rate is 5% below its level of the previous survey in 2012, but still accounting for 38% of US output from EOR. Apart from the aforementioned miscible CO_2 examples, other important CO_2 cases in the US include the miscible injections in the Salt Creek field (Wyoming), the Rangely Weber Sand unit (Colorado) and Seminole San Andres Unit (the Permian Basin, Texas), and the immiscible one in the Yates oil field (the Permian Basin, Texas). It is worth mentioning that independent producers such as Occidental, Kinder Morgan and Denbury Resources are the dominant operators in CO_2 injection in the US today which is a dramatic change from the picture before the early 1990s. The large CO_2 projects outside the US include the miscible injection in the Weyburn unit (Canada) and the immiscible injection in the Bati Raman field (Turkey).

The WAG injection was originally proposed as a method to improve sweep of gas injection. In many situations the residual oil saturation to gas displacement is significantly lower than the residual oil saturation to water displacement but gas injection suffers from high mobility of gas. Injecting water and gas alternately reduces the gas mobility, gives a more favorable mobility ratio, and stabilizes the front. Christensen, Stenby et al. (2001) reviewed 59 field cases of WAG applications, most of which are reported to be successful among the first field applications of WAG injection. The WAG process was almost always applied as a tertiary recovery method. Only in newer applications in the North Sea has the WAG injection been initiated early in the field life. Around 80% of the reviewed WAG applications was planned to be miscible and the majority of the applications are in the high-permeability reservoirs. However, it should be noted that the WAG process has been applied to rocks from very low-permeability chalk (Daqing) up to high permeability sandstone (Snorre). The Injection gases used include CO_2, hydrocarbons, and other nonhydrocarbons (CO_2 excluded), with the first two types accounting for around 90%. Most reviewed WAG cases (88%) are onshore where the five-spot injection pattern with a fairly close well spacing is widely adopted. The ratio between water and gas is important since too much water will result in poor microscopic displacement, and too much gas will result in poor vertical, and possibly horizontal, sweep. The WAG ratio used is initially 1 in most cases, but varies up to 3 and 4. The slug sizes of the gas volume are mostly in the range of 0.1 to 3 pore volume. The average improved recovery over water flooding is calculated to be 9.7% for miscible WAG injection and 6.4% for immiscible WAG injection. The main problems connected with the operation of a WAG injection process seem to be corrosion, mainly of injection facilities but also of production equipment after gas breakthrough when using CO_2 as a gas phase; and loss of water injectivity. In addition, it is important to have a good understanding of the phase behavior of reservoir oil, injected gas mixtures, and reservoir heterogeneities to avoid early breakthrough of injection gas. Tapering has proved to be an efficient tool to optimize the recovery from WAG processes.

Awan, Teigland et al. (2008) made a survey of the EOR projects initiated in the North Sea in the period from 1975 until beginning of 2005. Among the 19 reviewed projects, only one project (microbial EOR) is not gas injection. The gas injection projects are classified into hydrocarbon (HC) miscible gas injection, water-alternating-gas (WAG) injection, simultaneous water-and-gas (SWAG) injection, and foam-assisted WAG (FAWAG) injection. All the projects have been applied successfully except WAG at Ekofisk and FAWAG at Snorre central fault block. HC miscible gas injection and WAG injection can be considered mature technologies in the North Sea. The most commonly used EOR technology in the North Sea has been WAG, and it is recognized as the most successful EOR technology. The main problems associated with WAG, SWAG and FAWAG applications are injectivity, injection system monitoring, and reservoir heterogeneities. Brodie, Jhaveri et al. (2012) reviewed BP's experience in gas injection with several BP examples in different regions. In the North Sea, BP operates offshore miscible gas floods in Magnus and Ula. Both projects are tertiary and successful. The authors attributed the success of the North Sea projects partly to BP's experience of operating the world's largest miscible gas flood at Prudhoe Bay (Alaska).

16.7 Summary

Gas injection is traditionally classified into immiscible injection and miscible injection. Immiscible injection is usually an inefficient oil displacement process due to the high mobility of gas and limited component exchange between oil and gas. Vertical gravity drainage provides a remedy for these problems. Vaporization of intermediate hydrocarbon components, oil swelling and oil viscosity reduction are the common mechanisms for immiscible injection. Miscible injection is a proven technology with a great number of successful examples. The economic viability of new miscible injection projects can be reasonably evaluated. Gas injection processes involve complex mass transfer and fluid transport. The mathematical theory for gas injection processes is largely established and relatively well understood although challenges still exist with its extension to more complex situations such as multiphase behavior and dissolution of CO_2 in brine. The theory has led to useful tools for reliable MMP calculation and analysis of gas injection processes in both 1D and 3D. Because the complex phase behavior and large compositional effects involved in gas injection processes, compositional reservoir simulations are generally recommended to evaluate gas injection projects. Special considerations for compositional simulation of gas injection can be found in Holstein and Stalkup (2007). The challenges of compositional simulation include the poor understanding and description of some underlying mechanisms like diffusion and the limitation of the size of the reservoir model. The latter can be handled by upscaling (Christie and Clifford 1998; Barker, Fayers et al. 1994; Thibeau, Barker et al. 1995) but the existing compositional upscaling methods are less matured than their black oil counterparts.

Nomenclature

C = Land's constant
f_j = fractional flow
k_r = relative permability, L^2
L = length, L
n_c = number of components
S = saturation
S_{gi} = initial gas saturation
S_{gr} = trapped gas saturation
S_j = phase saturation
S_n = saturation non-wetting phase
t = time, L
v = velocity, L/t
v_D = dimensionless velocity
v_{inj} = injection velocity
x = distance, L
x_{ij} = mole fraction of component i and phase j
ϕ = porosity
τ = dimensionless time
ρ_j = phase density
ξ = dimensionless distance

Subscripts

D = dimensionless
gi = gas initial
gr = trapped gas
i = component
inj = injection
j = phase
n = non-wetting
r = relative

Abbreviations

EOR = enhanced oil recovery
EoS = equation of state
FAWAG = foam assisted WAG
FCM = first contact miscible
FCMP = first contact miscible pressure
FD = finite difference
IFT = interfacial tension
LBC = Lohrenz-Bray-Clark
LPG = liquefied petroleum gas
MCM = multicontact miscible
MMP = minimum miscible pressure

PR = Peng-Robinsom
SRK = Soave-Redlich-Kwong
SWAG = simultaneous water and gas
VIT = vanishing interfacial tension
WAG = water alternate gas

References

Aasberg-Petersen, K., Knudsen, K., and Fredenslund, A., 1991. Prediction of viscosities of hydrocarbon mixtures. *Fluid phase equilibria*, **70** (2-3): 293–308. 30 December. URL http://dx.doi.org/10.1016/0378-3812(91)85041-R.

Ahmadi, K., Johns, R.T. et al., 2011. Multiple-mixing-cell method for MMP calculations. *SPE Journal*, **16** (04): 733–742. SPE-116823-PA. URL http://dx.doi.org/10.2118/116823-PA.

Alavian, S.A. and Whitson, C.H., 2012. Modeling CO2 Injection Including Diffusion in a Fractured-Chalk Experiment with Initial Water Saturation. Carbon Management Technology Conference, Orlando, Florida, USA. 7–9 February. URL http://dx.doi.org/10.7122/149976-MS.

Awan, A.R., Teigland, R., and Kleppe, J., 2008. A Survey of North Sea Enhanced-Oil-Recovery Projects Initiated During the Years 1975 to 2005. *SPE Reservoir Eval. & Eng*, **11**: 497–512. URL http://dx.doi.org/http://dx.doi.org/10.2118/99546-PA.

Barker, J., Fayers, F. et al., 1994. Transport coefficients for compositional simulation with coarse grids in heterogeneous media. *SPE Advanced Technology Series*, **2** (02): 103–112. SPE-22591-PA. URL http://dx.doi.org/10.2118/22591-PA.

Blunt, M.J., 2000. An empirical model for three-phase relative permeability. *Spe Journal*, **5** (04): 435–445. SPE-67950-PA. URL http://dx.doi.org/10.2118/67950-PA.

Brodie, J.A., Jhaveri, B.S. et al., 2012. Review of gas injection projects in BP. In *SPE Improved Oil Recovery Symposium*. Society of Petroleum Engineers. SPE-154008-MS. URL http://dx.doi.org/10.2118/154008-MS.

Carlson, F.M., 1981. Simulation of relative permeability hysteresis to the nonwetting phase. In *SPE Annual Technical Conference and Exhibition*. Society of Petroleum Engineers. SPE-10157-MS. URL http://dx.doi.org/10.2118/10157-MS.

Chatzis, I., Morrow, N.R., and Lim, H.T., 1983. Magnitude and detailed structure of residual oil saturation. *Society of Petroleum Engineers Journal*, **23** (02): 311–326. SPE-10681-PA. URL http://dx.doi.org/10.2118/10681-PA.

Christensen, J.R., 1998. *Thermodynamics in compositional reservoir simulation*. Ph.D. thesis, Technical University of Denmark.

Christensen, J.R., Stenby, E.H., and Skauge, A., 2001. Review of WAG field experience. *SPE Reservoir Evaluation & Engineering*, **4** (02): 97–106. SPE-71203-PA. April. URL http://dx.doi.org/10.2118/71203-PA.

Christiansen, R.L. and Haines, H.K., 1987. Rapid measurement of minimum miscibility pressure with the rising-bubble apparatus. *SPE Reservoir Engineering*, **2** (04): 523–527. SPE-13114-PA. URL http://dx.doi.org/10.2118/13114-PA.

Christie, M.A. and Clifford, P.J., 1998. Fast procedure for upscaling compositional simulation. *SPE Journal*, **3** (03): 272–278. SPE-50992-PA. September. URL http://dx.doi.org/10.2118/50992-PA.

Cook, A.B., Walker, C. et al., 1969. Realistic K values of C7+ hydrocarbons for calculating oil vaporization during gas cycling at high pressures. *Journal of Petroleum Technology*, **21** (07): 901–915. SPE-2276-PA. July. URL http://dx.doi.org/10.2118/2276-PA.

Dindoruk, B., 1992. *Analytical Theory of Multiphase, Multicomponent Displacement in Porous Media*. Ph.D. thesis, Stanford University.

Dindoruk, B., Johns, R.T., and Orr, F.M., 1992. Analytical solution for four component gas displacements with volume change on mixing. In *ECMOR III-3rd European Conference on the Mathematics of Oil Recovery*. Delft, Holland. 17 June. URL `http://dx.doi.org/10.3997/2214-4609.201411071`.

Dindoruk, B., Orr Jr., F.M. et al., 1997. Theory of multicontact miscible displacement with nitrogen. *SPE Journal*, **2** (03): 268–279. SPE-30771-PA. September. URL `http://dx.doi.org/10.2118/30771-PA`.

Egermann, P., Vizika, O. et al., 2000. Hysteresis in three-phase flow: experiments, modeling and reservoir simulations. In *SPE European Petroleum Conference*. Society of Petroleum Engineers. SPE-65127-MS. URL `http://dx.doi.org/10.2118/65127-MS`.

Helfferich, F.G., 1982. Generalized Welge construction for two-phase flow in porous media in system with limited miscibility. In *SPE Annual Technical Conference and Exhibition*. Society of Petroleum Engineers. SPE-9730-MS. URL `http://dx.doi.org/10.2118/9730-MS`.

Helfferich, F.G. and Klein, G., 1970. *Multicomponent chromatography: Theory of Interference*. Chromatographic Science Series. M. Dekker. ISBN 0824713060.

Hirasaki, G.J., 1981. Application of the theory of multicomponent, multiphase displacement to three-component, two-phase surfactant flooding. *Society of Petroleum Engineers Journal*, **21** (02): 191–204. SPE-8373-PA. URL `http://dx.doi.org/10.2118/8373-PA`.

Høier, L. and Whitson, C.H., 2001. Miscibility variation in compositionally grading reservoirs. *SPE Reservoir Evaluation & Engineering*, **4** (01): 36–43. SPE-69840-PA. Februar. URL `http://dx.doi.org/10.2118/69840-PA`.

Holstein, E.D. and Stalkup, F.I., 2007. Miscible Processes. In E.D. Holstein, ed., *Petroleum Engineering Handbook, Volum V: Reservoir Engineering and Petrophysics*, Chap. 14, 1261–1308. Society of Petroleum Engineers. URL `http://petrowiki.spe.org/PEH%3AMiscible_Processes`.

Hoteit, H. and Firoozabadi, A., 2009. Numerical modeling of diffusion in fractured media for gas-injection and-recycling schemes. *Spe Journal*, **14** (02): 323–337. SPE-103292-PA. June. URL `http://dx.doi.org/10.2118/103292-PA`.

Jaubert, J.N., Arras, L. et al., 1998. Properly defining the classical vaporizing and condensing mechanisms when a gas is injected into a crude oil. *Industrial & engineering chemistry research*, **37** (12): 4860–4869. 13 November. URL `http://dx.doi.org/10.1021/ie9803016`.

Jaubert, J.N., Wolff, L. et al., 1998. A very simple multiple mixing cell calculation to compute the minimum miscibility pressure whatever the displacement mechanism. *Industrial & engineering chemistry research*, **37** (12): 4854–4859. 12 November. URL `http://dx.doi.org/10.1021/ie980348r`.

Jerauld, G.R., 1997. Prudhoe Bay gas/oil relative permeability. *SPE Reservoir Engineering*, **12** (01): 66–73. SPE-35718-PA. February. URL `http://dx.doi.org/10.2118/35718-PA`.

Jessen, K., 2000. *Effective algorithms for the study of miscible gas injection processes*. Ph.D. thesis, Technical University of Denmark, Lyngby, Denmark. URL `http://orbit.dtu.dk/en/publications/effective-algorithms-for-the-study-of-miscible-gas-injection-processes%288eb44a75-b5dc-41ec-904a-a07eb39ce2cf%29.html`. March.

Jessen, K., Michelsen, M.L., and Stenby, E.H., 1998. Global approach for calculation of minimum miscibility pressure. *Fluid Phase Equilibria*, **153** (2): 251–263. URL `http://dx.doi.org/10.1016/S0378-3812(98)00414-2`.

Jessen, K. and Orr Jr., F.M., 2008. On interfacial-tension measurements to estimate minimum miscibility pressures. *SPE Reservoir Evaluation & Engineering*, **11** (05): 933–939. SPE-110725-PA. October. URL `http://dx.doi.org/10.2118/110725-PA`.

Jessen, K. and Stenby, E.H., 2007. Fluid characterization for miscible EOR projects and CO2 sequestration. *SPE Reservoir Evaluation & Engineering*, **10** (05): 482–488. SPE-97192-PA. October. URL `http://dx.doi.org/10.2118/97192-PA`.

Jessen, K., Stenby, E.H., and Orr Jr, F.M., 2004. Interplay of Phase Behavior and Numerical Dispersion in Finite Difference Compositional Simulation. SPEJ 9 (2): 193–201. *SPE Journal*, **9** (02): 193–201. SPE-88362-PA. June. URL `http://dx.doi.org/10.2118/88362-PA`.

Jessen, K., Wang, Y. et al., 2001. Fast, Approximate Solutions for 1D Multicomponent Gas-Injection Problems. *SPE Journal*, **6** (04): 442–451. SPE-74700-PA. December. URL `http://dx.doi.org/10.2118/74700-PA`.

Johns, R., Dindoruk, B. et al., 1993. Analytical theory of combined condensing/vaporizing gas drives. *SPE Advanced Technology Series*, **1** (02): 7–16. SPE-24112-PA. July. URL `http://dx.doi.org/10.2118/24112-PA`.

Johns, R.T., 1992. *Analytical theory of multicomponent gas drives with two-phase mass transfer*. Ph.D. thesis, Stanford University, Stanford, CA, USA.

Johns, R.T. and Orr Jr., F.M., 1996. Miscible gas displacement of multicomponent oils. *SPE Journal*, **1** (01): 39–50. SPE-30798-PA. March. URL `http://dx.doi.org/10.2118/30798-PA`.

Killough, J.E., 1976. Reservoir simulation with history-dependent saturation functions. *Society of Petroleum Engineers Journal*, **16** (01): 37–48. SPE-5106-PA. February. URL `http://dx.doi.org/10.2118/5106-PA`.

Krishna, R., Wesselingh, J.A., and Taylor, R., 1995. The Maxwell-Stefan approach to mass transfer. *Chemical engineering journal*, **57** (6): 77–246. URL `http://hdl.handle.net/11245/1.114343`.

Lake, L.W., 1989. *Enhanced oil recovery*. Old Tappan, New Jersey, Prentice Hall Inc. URL `http://www.osti.gov/scitech/biblio/5112525`.

Land, C.S., 1968. Calculation of imbibition relative permeability for two-and three-phase flow from rock properties. *Society of Petroleum Engineers Journal*, **8** (02): 149–156. PE-1942-PA. June. URL `http://dx.doi.org/0.2118/1942-PA`.

Larsen, J. and Skauge, A., 1998. Methodology for numerical simulation with cycle-dependent relative permeabilities. *SPE Journal*, **3** (02): 163–173. SPE-38456-PA. June. URL `http://dx.doi.org/10.2118/38456-PA`.

Larson, R.G., 1979. The influence of phase behavior on surfactant flooding. *Society of Petroleum Engineers Journal*, **19** (06): 411–422. SPE-6774-PA. URL `http://dx.doi.org/10.2118/6774-PA`.

Lohrenz, J., Bray, B.G. et al., 1964. Calculating viscosities of reservoir fluids from their compositions. *Journal of Petroleum Technology*, **16** (10): 1–171. SPE-915-PA. October. URL `http://dx.doi.org/10.2118/915-PA`.

Macleod, D.B., 1923. On a relation between surface tension and density. *Trans. Faraday Soc.*, **19**: 38–41. URL `http://dx.doi.org/10.1039/TF9231900038`.

Metcalfe, R.S., Fussell, D.D., and Shelton, J.L., 1973. A multicell equilibrium separation model for the study of multiple contact miscibility in rich-gas drives. *Society of Petroleum Engineers Journal*, **13** (03): 147–155. SPE-3995-PA. June. URL `http://dx.doi.org/10.2118/3995-PA`.

Michelsen, M.L., Mollerup, J., and Breil, M.P., 2007. *Thermodynamic Models: Fundamental & Computational Aspects*. Tie-Line Publications, Holte, Denmark. ISBN 87-989961-3-4.

Monroe, W.W., Silva, M.K. et al., 1990. Composition paths in four-component systems: effect of dissolved methane on 1D CO2 flood performance. *SPE Reservoir Engineering*, **5** (03): 423–432. SPE-16712-PA. August. URL `http://dx.doi.org/10.2118/16712-PA`.

Moortgat, J., Firoozabadi, A. et al., 2009. A new approach to compositional modeling of CO2 injection in fractured media compared to experimental data. In *SPE Annual technical conference and exhibition*. Society of Petroleum Engineers, New Orleans, Louisiana. SPE-124918-MS. 4–7 October. URL `http://dx.doi.org/10.2118/124918-MS`.

Orr Jr., F.M., 2007. *Theory of gas injection processes*. Tie-Line Publications, Holte, Denmark. ISBN 87-989961-2-5.

Orr Jr, F.M., Silva, M.K. et al., 1982. Laboratory experiments to evaluate field prospects for CO2 flooding. *Journal of Petroleum Technology*, **34** (04): 888–898. SPE-9534-PA. April. URL `http://dx.doi.org/10.2118/9534-PA`.

Pedersen, K.S., Fredenslund, A., and Thomassen, P., 1989. *Properties of oils and natural gases*. Contributions in petroleum geology & engineering. Gulf Pub. Co., Book Division, Huston. ISBN 9780872015883. URL `https://books.google.no/books?id=PtNTAAAAMAAJ`.

Pedersen, K.S., Thomassen, P., and Fredenslund, A., 1989. C_{7+} Fraction Characterization. In L. Chorn and G. Mansoor, eds., *Advances in thermodynamics*, vol. 1, 137–152. Gulf Pub. Co., Book Division, Taylor & Francis, New York.

Peng, D.Y. and Robinson, D.B., 1976. A new two-constant equation of state. *Industrial & Engineering Chemistry Fundamentals*, **15** (1): 59–64. URL `http://dx.doi.org/10.1021/i160057a011`.

Potsch, K., Toplack, P. et al., 2013. A new Interpretation of CO Diffusion Experiments. In *EAGE Annual Conference & Exhibition incorporating SPE Europec*. Society of Petroleum Engineers. SPE-164933-MS. URL `http://dx.doi.org/10.2118/164933-MS`.

Quiñones-Cisneros, S.E., Zéberg-Mikkelsen, C.K., and Stenby, E.H., 2001. One parameter friction theory models for viscosity. *Fluid phase equilibria*, **178** (1): 1–16. March. URL `http://dx.doi.org/10.1016/S0378-3812(00)00474-X`.

Rao, D.N., 1997. A new technique of vanishing interfacial tension for miscibility determination. *Fluid phase equilibria*, **139** (1–2): 311–324. December. URL `http://dx.doi.org/10.1016/S0378-3812(97)00180-5`.

Shojaei, H. and Jessen, K., 2014. Diffusion and Matrix-fracture Interactions during Gas Injection in Fractured Reservoirs. In *SPE Improved Oil Recovery Symposium, Tulsa, Oklahoma, USA*. Society of Petroleum Engineers, Tulsa, Oklahoma, USA. SPE-169152-MS. 12–16 April. URL `http://dx.doi.org/10.2118/169152-MS`.

Soave, G., 1972. Equilibrium constants from a modified Redlich-Kwong equation of state. *Chemical Engineering Science*, **27** (6): 1197–1203. URL `http://dx.doi.org/10.1016/0009-2509(72)80096-4`.

Spiteri, E., Juanes, R. et al., 2005. Relative-permeability hysteresis: trapping models and application to geological CO2 sequestration. In *SPE Annual Technical Conference and Exhibition*. Society of Petroleum Engineers, Dallas, Texas, USA. SPE-96448-MS. 9–12 October. URL `http://dx.doi.org/10.2118/96448-MS`.

Stalkup, F.L. et al., 1990. Effect of gas enrichment and numerical dispersion on enriched-gas-drive predictions. *SPE Reservoir Engineering*, **5** (04): 647–655. SPE-18060-PA. November. URL `http://dx.doi.org/10.2118/18060-PA`.

Thibeau, S., Barker, J. et al., 1995. Dynamical upscaling techniques applied to compositional flows. In *SPE Reservoir Simulation Symposium*. Society of Petroleum Engineers, San Antonio, Texas. SPE-29128-MS. 12–15 February. URL `http://dx.doi.org/10.2118/29128-MS`.

Wang, Y., 1998. *Analytical calculation of minimum miscibility pressure*. Ph.D. thesis, Stanford University, Stanford, CA, USA.

Wang, Y. and Orr Jr., F.M., 1997. Analytical calculation of minimum miscibility pressure. *Fluid Phase Equilibria*, **139** (1): 101–124. December. URL `http://dx.doi.org/10.1016/S0378-3812(97)00179-9`.

Warner, H.R.J. and Holstein, E.D., 2007. Immiscible gas injection in oil reservoirs. In E.D. Holstein, ed., *Petroleum Engineering Handbook, Volum V: Reservoir Engineering and Petrophysics*, Chap. 12, 1103–1147. Society of Petroleum Engineers. URL `http://petrowiki.spe.org/PEH%3AMiscible_Processes`.

Whitson, C.H., Anderson, T.F., and SøreideI., ., 1989. C_{7+} Fraction Characterization. In *Advances in Thermodynamics*, vol. 1, 35–56. Gulf Pub. Co., Book Division, Taylor & Francis, New York.

Whitson, C.H. and Brulé, M.R., 2000. *Phase behavior*. SPE Monograph Series Vol. 20, Richardson, Texas.

Yan, W., Michelsen, M.L., and Stenby, E.H., 2012. Calculation of minimum miscibility pressure using fast slimtube simulation. In *SPE Improved Oil Recovery Symposium*. Society of Petroleum Engineers. SPE-153758-MS. URL `http://dx.doi.org/10.2118/153758-MS`.

Yellig, W., Metcalfe, R. et al., 1980. Determination and Prediction of CO2 Minimum Miscibility Pressures (includes associated paper 8876). *Journal of Petroleum Technology*, **32** (01): 160–168. SPE-7477-PA. January. URL `http://dx.doi.org/10.2118/7477-PA`.

Zhou, D. and Orr Jr., F.M., 1995. An analysis of rising bubble experiments to determine minimum miscibility pressures. In *SPE Annual Technical Conference and Exhibition*, 883–892. Society of Petroleum Engineers. SPE-30786-MS. URL `http://dx.doi.org/10.2118/30786-MS`.

Zick, A.A., 1986. A combined condensing/vaporizing mechanism in the displacement of oil by enriched gases. In *SPE annual technical conference and exhibition*. Society of Petroleum Engineers, New Orleans, Louisiana. SPE-15493-MS. 5–8 October. URL `http://dx.doi.org/10.2118/15493-MS`.

Zuo, Y.X. and Stenby, E.H., 1996. A linear gradient theory model for calculating interfacial tensions of mixtures. *Journal of colloid and interface science*, **182** (1): 126–132. 1 September. URL http://dx.doi.org/10.1006/jcis.1996.0443.

Zuo, Y.X., Stenby, E.H. et al., 1998. Prediction of Interfacial Tensions of Reservoir Crude Oil and Gas Condensate Systems. *SPE Journal*, **3** (02): 134–145. SPE-38434-PA. June. URL http://dx.doi.org/10.2118/38434-PA.

Chapter 17

Rock Fluid Interaction in Chalk at Pore-, Core-, and Field-Scale – Insight From Modeling and Data

Mona Wetrhus Minde and Aksel Hiorth

Fluids may occupy a significant fraction of the total volume of a porous rock, and in many cases the chemical composition of the fluids is important for the macroscopic behavior of the rock. The pore fluids support the grains and affect mechanical properties. Ions in the brine affect the friction between the fluid layers and grain surfaces and change the fluid extraction rate. In this chapter we draw some correlations between pore-, core- and field-scale studies. We show why it is important to consider both theoretical and experimental studies, and highlight why insight from the smaller scale is important to reduce the uncertainty at larger scales. Our main focus is the strength of chalk, and the slow deformation at constant effective stress (creep). Reservoir compaction is a source of natural energy, and it might be relevant to utilize this energy in a producing reservoir. There are many observations on how different fluids affect pore collapse and the compaction rate at lab scale. In this chapter we review many of the experimental studies on chalk, combine it with additional insight from pore-scale studies, add some additional analysis, and discuss how the chemical effects might be relevant on a much larger scale.

17.1 Introduction

For quite some time it has been recognized by researchers that the physical properties of a porous rock are dependent on the pore fluids. An example is when a sandstone core is exposed to a low salinity brine, the surface energy and adhesion forces change (Hilner, Andersson et al. 2015). Direct measurements on cores also confirm that the streaming potential and therefore the surface charge are dependent on the brine chemistry (Vinogradov, Jaafar et al. 2010). The practical consequence of this is that one can to some extent control the fluid chemistry inside the pores, and thereby change the surface properties of the rock, thus impact the oil recovery. This has been the topic of numerous publications over the last decades, which we will come back to in the next section. In the lab it is quite easy to change the pore fluid chemistry, simply because the boundary conditions are set by the experimentalist and the core samples usually are small. Unfortunately, this is not the case in the reservoir, where pressure and temperature are changing, the pore water chemistry changes as minerals dissolve and precipitate, ions adsorb and desorb, and the mineralogical composition of the reservoir rock changes throughout the reservoir. In contrast to the effect of pore water chemistry on wettability and oil production, where field observations are subtle and affected by model interpretations, there are some quite spectacular field observations that clearly demonstrate fluid effects on reservoir compaction. Perhaps the most well-known example is the Ekofisk chalk field. The Ekofisk field is one of the largest oil fields in Norway. Due to reservoir compaction, the seafloor subsidence has accumulated over time to close to 10 m. Part of the reservoir compaction (50%) is due to a decline in pore pressure and an increase in the effective stress, but the effect of replacing oil and gas with water is assumed to be of equal importance (Doornhof, Kristiansen et al. 2006). The latter effect is known as water induced compaction or water weakening of chalk.

In the next sections we will discuss lab studies performed to investigate how the composition of the pore fluids affects the strength of chalk, and the rate of deformation of chalk cores exposed to constant stress (creep). The interesting question is if these observations also can explain the water induced compaction observed at the Ekofisk field? What kind of support do we have from lab studies to conclude that strength of the chalk cores is dependent on the fluid in contact with the grains?

Water induced compaction and the strength of the chalk must of course be seen in relation to Enhanced Oil Recovery (EOR). Optimising the composition of injected brines to change surface forces and wettability, could eventually lead to release or a speed up of the extraction of oil. If a brine is proven effective in an EOR context, it is important not only to understand the effect on wettability, but equally important, if not more, to evaluate how the brine affects the reservoir quality with respect to permeability, porosity, surface energy and forces, and unquestionably compaction of the reservoir rock. To understand the underlying mechanisms of these effects, a good starting point is the pore scale, where physical alterations in the rock can be observed, interpreted and incorporated into numerical modelling.

17.2 Insight from rock mechanical core scale experiments

In this section we will review and discuss parts of the rock mechanical aspects that have been observed in the lab which may be attributed to rock-fluid interactions. We will divide the discussion into three parts:

1. Fluid effects or the effect of saturating chalk with air, oil or water
2. Chalk surface chemistry
3. Chalk texture changes, dissolution and precipitation

We will focus on hydrostatic loading experiments. The reason for this is that there is a lot of data available. Although hydrostatic experiments are not representative for the stress state of a typical reservoir, the hydrostatic tests are simpler to perform, and are to a very large degree reproducible. The hydrostatic tests are usually performed in triaxial cells, where the axial and to some degree the radial strain can be monitored continuously during the experimental test. The axial strain is calculated by recording the change in length of the core normalized to its original length. Fluids are passed through the core during the experimental program, allowing for continuous measurement of permeability and sampling of effluent (Nermoen, Korsnes et al. 2015). During the test a back pressure is applied to keep a more or less uniform pore pressure in the sample and avoid boiling of the pore fluid at elevated temperatures. A pressure difference of the order of kPa is needed to drive fluids through the sample. The back pressure ensures that the pore pressure cannot increase during the compression, thus the stress-strain development is mainly dictated by the properties of the solid (matrix) framework. In a hydrostatic test, there are usually two sets of results reported: 1) the hydrostatic loading phase, where the confining pressure and pore pressure is increased to the test level beyond yield, while the axial strain is continuously measured. 2) The creep phase, which is the slow deformation of a material when it subjected to a constant small load over a longer time (Griggs 1939). In **Fig 17.1**, an example is shown where an Aalborg chalk core was heated to 130°C, loaded up to 12 MPa, and then left to creep at a constant creep stress of 12 MPa. In the creep phase 0.657M NaCl was flooded through the core at a flooding rate of 1PV per day (Andersen, Wang et al. 2018).

From the hydrostatic loading period, the yield point and bulk modulus can be determined. The yield point is the point where the material deviates from the elastic behavior. As can clearly be seen from Fig. 17.1, the deviation from the elastic behavior (the black solid line) is not a single point, but rather a zone of transition between the elastic and plastic phase (black dotted line). The Yield "point" is thus located somewhere between 7.5–8.5 MPa. The bulk modulus is defined as the ratio between the hydrostatic stress and the volumetric strain (Fjær, Holt et al. 2008), and if we assume that the material compresses equally in all directions the bulk modulus can be calculated from the slope of the lines to the left in Fig. 17.1. The axial strain is converted to volumetric strain by multiplying with a factor of 3. In this context, it makes sense to use the word "strength" or "compaction strength" to characterize the rock according to the yield point. If a rock has higher yield, it is said to be stronger.

During the creep phase the rock deforms continuously, and in the continuum limit one might use the word "viscosity" to describe the time-dependent behavior, and an effective viscosity can be defined as the ratio between the stress and strain rate ($\eta_{\text{eff}} = \frac{\sigma}{d\varepsilon_V/dt}$) (Fjær, Holt et al. 2008). Another interesting feature of the material in the creep phase is that the time dependent creep behavior usually follows a trend that is close to a log t behavior (to the right in Fig 17.1). De Waal (de Waal 1986) published a particularly interesting creep model:

$$\varepsilon_V(t) = B \log\left(1 + \frac{\dot{\varepsilon_V}(0)t}{B}\right). \tag{17.1}$$

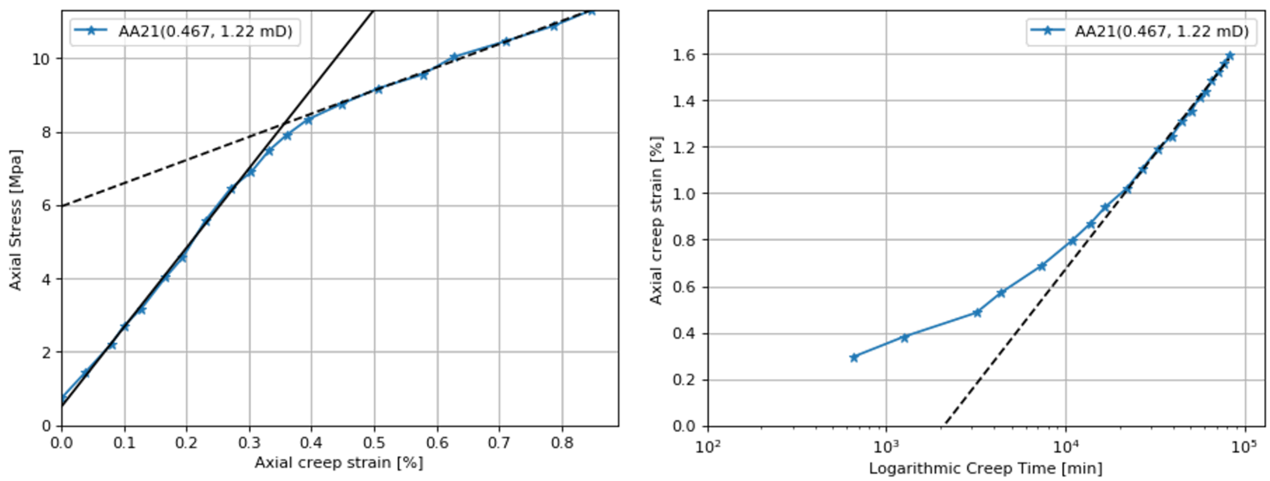

Figure 17.1: (Left) Hydrostatic loading, the Bulk modulus is 720 MPa and 210 MPa in the elastic and plastic phase respectively (right) The creep phase, the strain rate is 0.012%/hour, data are from (Andersen, Wang et al. 2018)

$\dot{\varepsilon_V}(0)$ is the initial strain rate, which can be seen by differentiating the above equation with respect to t:

$$\frac{d\varepsilon_V(t)}{dt} = \frac{\dot{\varepsilon_V}(0)}{1 + \frac{\dot{\varepsilon_V}(0)t}{B}} \xrightarrow{t \to 0} \dot{\varepsilon_V}(0). \tag{17.2}$$

The model suggested by de Waal was derived from the basis of an earlier work by (Dieterich 1978), where it was shown that the friction coefficient between rocks, μ, followed the empirical law:

$$\mu = \mu_0 + C \log(1 + Dt). \tag{17.3}$$

C, D and μ_0 are constants. t is the time at which the materials are in stationary contact. In (Dieterich 1972, 1978) experiments were conducted over a time period of up to one day, where the materials were kept in contact at a constant normal and shear stress. When the desired time t was reached, the shear stress was rapidly raised to the level required to produce a slip. They were then able to match the observations with the formula above. The reason for the time dependence is an increase in the contact area between the surfaces (Dieterich 1978). De Waal argues (de Waal 1986) that this is similar to what takes place during creep. The time in the equation above is replaced with a time constant t_a that describes the average lifetime of grain-grain contacts. The time constant is further related to the inverse strain rate. The physical explanation for the macroscopic time-dependent creep of rocks is thus, according to this model, the average lifetime of contact points and the number of contact points (i.e. the real contact area). As a side note (Westwood, Goldheim et al. 1967; Macmillan, Huntington et al. 1974) pointed out that the friction coefficient is dependent on the fluid chemistry. They argued that ion interactions modify the surface micro hardness. In particular they found that the maximum surface micro hardness was when the zeta potential was close to zero for MgO, which implies that the friction is at its lowest level close to zero zeta potential. Thus, a low value of the zeta potential would increase the strain rate.

Translating lab results to field is a huge challenge. In the next sections we will investigate in more detail the chemical effects and how they might propagate at field scale, but before that we would like to mention some important advances made with respect to strain rates in the field compared to the lab. For a producing reservoir, the reservoir pressure usually decreases over time due to the extraction of fluids. The reservoir rock then need to support more of the overburden weight. This results in a steady increase in loading rate and strain rate over the fields life time. In the lab it is well known that the loading rate affects the strain rate (Andersen, Foged et al. 1992a). If the rock is loaded very slowly, it will have more time to deform (creep) before reaching the final stress level. The observed strain rate in a typical lab experiment is usually, due to practical considerations, much larger compared to the field. The challenge is to translate the higher strain rates observed in the lab to the lower field strain rates. Based on the de Waal model (de Waal 1986), Andersen, Foged et al. (1992b) was able to develop a scaling law to translate the observed lab results to field scale. They did this by introducing a friction factor, which was estimated for the Valhall field. The friction factor was found to be more or less constant over the stress range of interest, thus partly confirming the validity of the proposed model and reducing the amount of tests to be performed in order to estimate compaction at field depletion rates.

17.3 Fluid effects or the effect of saturating chalk with air, oil or gas

(Homand, Shao et al. 1998; Homand and Shao 2000) demonstrated experimentally that chalk saturated with different fluids had different mechanical properties. Models were developed to take into account the fact that the mechanical properties of chalk change with the saturating fluid. The modelling was done by assigning different properties (constitutive equations) to water saturated chalk with respect to oil saturated chalk. The physical mechanism for the water weakening effect was explained through capillary and differences in "wettability" between the two fluids (Homand, Shao et al. 1998). In (Homand and Shao 2000) the model was refined by assuming that the chalk presents a jump between two material states when flooded with water. From a modelling point of view, it makes sense to do this simplification, but it is hard to capture time dependent effects, and upscaling to field conditions might be questionable without a proper understanding of the underlying mechanisms. (Gutierrez, Øino et al. 2000) proposed and discussed the following mechanisms for water weakening of chalk: 1) physical, 2) chemical 3) physio-chemical. Experiments were also performed where water was injected into oil saturated fractures, and an immediate deformation was observed. (Gutierrez, Øino et al. 2000) highlight that calcite dissolution at grain contacts, and modification of the surface properties of calcite crystals require further studies. In (Risnes 2001) a thorough study of fluid saturated chalk was performed. The full elastic region was determined for chalk saturated with water, methanol, oil & glycol, and dry chalk. As an example, the hydrostatic yield increased with 50%, 70%, 80% with respect to water saturated chalk for methanol, oil & glycol and dry chalk, respectively. To gain more insight into the mechanism behind the fluid effects this paper was followed up by a study where the activity of water was changed systematically by changing the fraction of glycol mixed into water (Risnes, Madland et al. 2005). These findings clearly demonstrated an increase in the strength as the water activity decreased. Even if it is possible to assign different material properties to saturated chalk, and construct constitutive equations that makes it possible to history match experiments, it is unsatisfying to not have some insight into what happens at micro scale, e.g. grain-grain contacts. Core scale experiments are great in order to perform experiments at realistic conditions, but of limited value in order to pinpoint the exact mechanisms. A recent study (Røyne, Bisschop et al. 2011) gives further insight into the water weakening effect, using a completely different approach. In (Røyne, Bisschop et al. 2011) they used a double torsion method, where a calcite crystal with an initial crack was immersed in a fluid. By bending the calcite sample, it was possible to estimate the crack velocity. The crack velocity was used to estimate the surface energy, a lower surface energy increases the crack velocity. Immersing the sample in a mixture of glycol and water, they were able to estimate the surface energy of calcite for different water activities. If one assumes that the hydrostatic yield is related to pore collapse and bond breaking between the individual grains in the sample, it makes sense that the bonds are easier to break if the surface energy is lowered. In (Risnes 2001) hydrostatic yield was estimated to be 18 MPa and 10 MPa for oil (glycol) and water saturated chalk, respectively. In (Røyne, Bisschop et al. 2011) the surface energy was 0.32 J/m^2 and 0.15 J/m^2 for fully glycol and water saturated calcite samples. The reduction in surface energy of a factor of 2 is very close to the reduction in hydrostatic yield. In **Fig. 17.2.**, the data from three different test series (square points) are shown, and the hydrostatic yield is normalized such that the yield point for fully water saturated samples is equal to one, and the surface energy for water wetted calcite surfaces is equal to one. The fact that not only the trend, but also the relative values of the measurements match is a support for the original hypothesis by (Risnes, Madland et al. 2005) that the water weakening effect is related to decreased cohesion between chalk grains.

17.4 Water chemistry effect on the hydrostatic yield

(Risnes, Haghighi et al. 2003) pointed out that the activity of water could also be changed by changing the concentration of salts. They were able to reduce the activity of water to as low as 0.48 by the addition of $CaCl_2$ in excessive amounts. The hydrostatic yield in those experiments are shown in Fig 17.2 as circular points, and follows the trend observed for chalk cores where the activity of water was changed by mixing fractions of glycol and water. These results are particularly interesting as they show that the mechanical properties could be changed by changing the brine chemistry, meaning that they could also be useful in management of a producing reservoir. An important step towards such application was made in (Heggheim, Madland et al. 2005; Korsnes, Strand et al. 2006), where it was observed that seawater at 130°C reduced the yield point compared to seawater depleted of sulphate at 130°C. If the amount of sulphate was replaced with an equivalent amount of NaCl to keep the total dissolved solid constant, the yield point was increased by 35%.

Can the water activity hypothesis discussed in (Risnes, Madland et al. 2005) explain these experiments? The activity of water for a brine is given by (Garrels and Christ 1965):

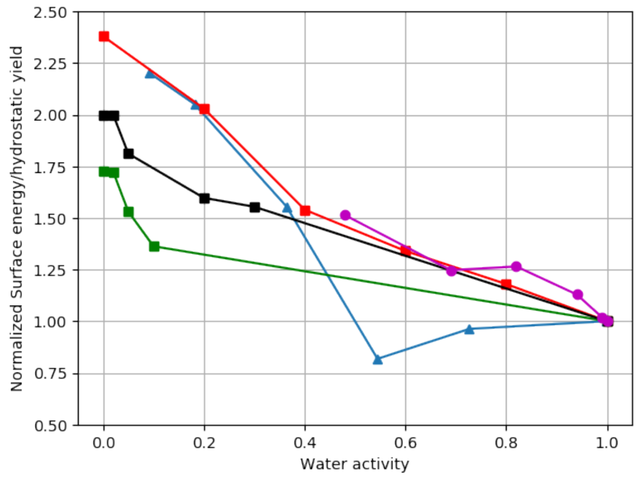

Figure 17.2: Plot of normalized surface energy of calcite crystals (triangular points), and normalized hydrostatic yield (square points) for different values of water activity. Data are taken from (Røyne, Bisschop et al. 2011) and (Risnes, Madland et al. 2005), the experimental uncertainties are not included in the figure. Circular points are from (Risnes, Haghighi et al. 2003) (see next section).

$$a_w = 1 - 0.018 \sum_i m_i, \tag{17.4}$$

where m_i is the molality of ions in the solution. Seawater would have an activity of ∼0.98 according to this formula. Thus, the minor reduction in water activity could not explain the effect sulphate had on the yield point. In (Megawati, Hiorth et al. 2012), the results of (Korsnes, Madland et al. 2006) were addressed in a systematic manner, where the seawater brine was replaced with Na_2SO_4 or NaCl brine with similar ionic strength as seawater. Both the temperature effect and ionic effect were varied systematically, and investigated for three different chalk types, Liège, Kansas, and Stevns Klint chalk. A total of 28 cores were tested in triaxial cells. Absorption tests were performed to quantify the amount of sulphate retained in the cores. In **Fig 17.3**, results from Liège outcrop cores are shown. In Fig 17.3, to the left, the effect of temperature is shown. The weakest core is the core saturated with 0.219 M Na_2SO_4 at 130°C. Cores saturated with NaCl behaves more or less similar regardless of temperature. To the right, all the cores are tested at the same temperature, but with different concentrations of Na_2SO_4. The ionic strength was kept constant by adjusting the amount of NaCl. Note that the plastic bulk modulus for all cores is almost unchanged after yield (0.15±0.01 GPa), whereas before yield it varies from (0.59–1.12 GPa).

In (Megawati, Hiorth et al. 2012) it was hypothesized that the electrostatic interactions that gives rise to an osmotic pressure (disjoining pressure) near the grain contacts could be an explanation for the enhanced weakening. Sulphate adsorb onto the calcite grains, and thereby change the surface and zeta potential. As more sulphate is added to the brine, the surface potential becomes more and more negative. The ionic strength, surface charge and temperature were varied and it was found that the variation in hydrostatic yield for all the chalk samples was proportional to the maximum peak of the disjoining pressure. This study was followed up by (Nermoen, Korsnes et al. 2018) in a recent paper, where additional experiments was performed. The authors argues that the electrochemical interactions that give rise to the disjoining pressure can be incorporated into an effective stress equation. In addition, they introduce a modified bulk modulus to handle the reduction of the slope in the stress strain curves induced by sulphate.

17.5 Water chemistry effect on the time dependent compaction

The water chemistry effect on the creep rate at elevated temperatures was first discussed in detail by (Korsnes, Madland et al. 2006; Korsnes, Strand et al. 2006). Stevns Klint chalk cores was loaded beyond yield to a constant hydrostatic stress level of 9.8–10.5 MPa. The temperature was kept constant at 130°C, while brines with a similar composition as seawater were flooded at one pore volume per day. Increased compaction, by a factor of 2.7 was observed for cores flooded with seawater compared to cores flooded with seawater where sulphate was removed. A mechanism for the enhanced compaction was suggested to be induced by potential determining

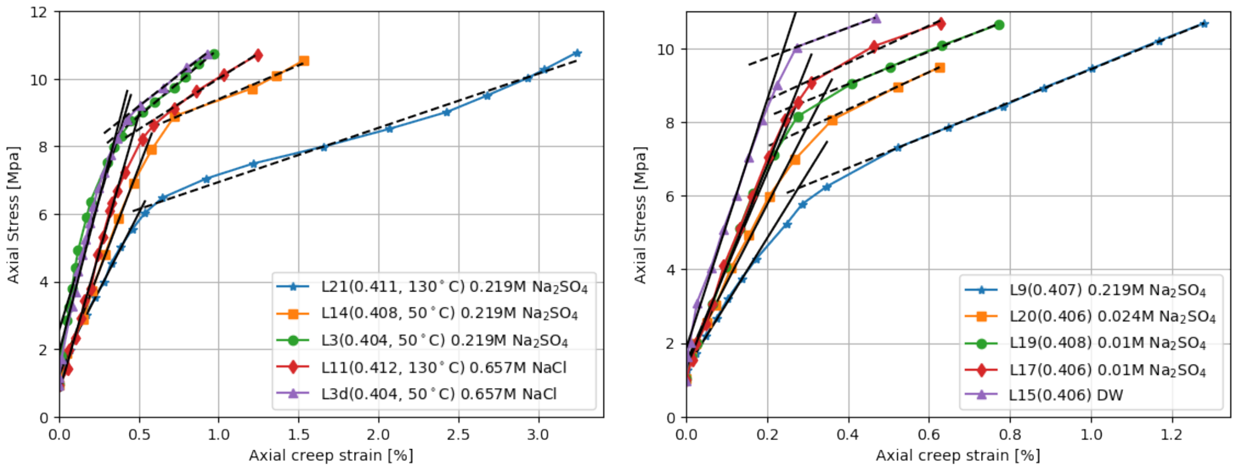

Figure 17.3: Hydrostatic yield for Liège cores saturated with different fluids and tested at different temperatures, data from (Megawati, Hiorth et al. 2012). The porosity of each core is given in the parenthesis. (Right) sulphate concentration is varied while the amount of NaCl is adjusted to keep a constant ionic strength of 0.657 M, with the exception of distilled water (DW). All the cores were tested at 130°C (Left). Effect of temperature at constant ionic strength.

ions, Ca^{2+}, Mg^{2+}, and SO_4^{2-}, and in particular it was suggested that magnesium substituted calcium at the intergranular contacts. The substitution of calcium by magnesium was believed to be catalysed by the presence of sulphate in the brine, which explained why sulphate had to be present in the water in order to induce an enhanced creep. The substitution of calcium with magnesium was supported by chemical analyses of the effluent, where a one to one correspondence between loss of magnesium and gain in calcium was observed. In light of more recent results discussed in the previous section (Megawati, Hiorth et al. 2012), an alternative explanation is possible. As already mentioned, sulphate affects the yield point of chalk cores. The cores that were exposed to sulphate in the brine, had a yield point that was 24% lower than cores without sulphate (Korsnes, Madland et al. 2006). Thus, the cores flooded with sulphate containing brines were left to creep at a stress level that was 60% above the yield point, whereas the cores flooded without sulphate were left to creep at a level that was 24% higher than the yield point. A possible explanation for the additional deformation of 2.7 could be that the cores containing sulphate were left to creep at a higher stress level relative to the yield point, and not because of chemical interactions with the rock.

As there seemed to be several ions that interacted with the rock when seawater was flooded through the cores, a set of experiments was performed where the effect of the individual ions was investigated. The ionic strength was kept constant and equal to that of seawater, the brines were 0.657 M NaCl, 0.219 M Na_2SO_4 and 0.219 M $MgCl_2$, all with an ionic strength of 0.657 M. The sulphate results have been discussed in (Megawati, Hiorth et al. 2012). In (Megawati, Hiorth et al. 2012) Liège and Stevns Klint chalk cores were loaded above yield, and flooded with $MgCl_2$ and NaCl brine at 130°C. The yield point for the different cores was similar for both NaCl and $MgCl_2$ brine. The Liège chalk cores contains ∼2wt% non-carbonate minerals whereas Stevns Klint has about 0.2wt% non-carbonate content (Hjuler and Fabricius 2009). For the $MgCl_2$ flooded cores a deviation from the typical log-creep behavior was observed, as expected from the de Waal model. The cores experienced an additional creep that was dependent on the amount of pore volumes flooded through the cores, and had a higher creep rate than the Liège cores flooded with NaCl. The core material was investigated by the use of Scanning Electron Microscopy (SEM) comparing unflooded and flooded material, and after flooding, newly precipitated minerals were discovered, both magnesium carbonates and magnesium bearing clay minerals. These results were also supported by geochemical models. In (Madland, Hiorth et al. 2011) it was observed that Stevns Klint cores flooded with $MgCl_2$ brine initially deformed less than Stevns Klint cores flooded with NaCl, however towards the end of the test (-10 days), the creep rate increased significantly. Based on this work it was concluded that chemical effects related to magnesium are time dependent, most likely related to mineralogical alterations, and that the initial mineralogy of the cores was of importance. The effect of initial mineralogy was further investigated in (Megawati, Madland et al. 2015), where five different chalk types (Stevns Klint, Aalborg, Liège, Mons (Trivières Fm), and Kansas) were investigated. The creep tests at 130°C were performed over much longer periods of time than in (Madland, Hiorth et al. 2011), some of them up to 63 days. The findings for the cores flooded with $MgCl_2$ were: Cores with a calcite content higher than 99.7% (Stevns Klint and Mons, Trivières Fm) experienced a lag in the creep. After 7 and 21 pore volumes flooded, the Stevns Klint and Mons cores, respectively, experienced enhanced creep. The chalk types with lower carbonate content (Aalborg, Liège, and Kansas) experienced an almost immediate enhanced creep. The additional creep was correlated with the amount of calcium produced. It was also speculated that the reduction in creep observed in the high calcite cores, could be due to an increased friction between the grains due to the formation of magnesium carbonate. The enhanced compaction observed in cores with a higher content of non-carbonate minerals could be due to a rapid dissolution of non-carbonate minerals.

The creep tests performed clearly showed that it was important to run tests for an extended period of time, both to observe the effect of chemical interactions and also to induce interactions that could be observed visually after testing. In (Nermoen, Korsnes et al. 2015) a Liège chalk core was flooded for almost 3 years (1072 days), see **Fig. 17.4**. The flooding rate was changed three times during the test (1PV/day $\rightarrow$ 3PV/day $\rightarrow$ 1PV/day $\rightarrow$ 3PV/day).

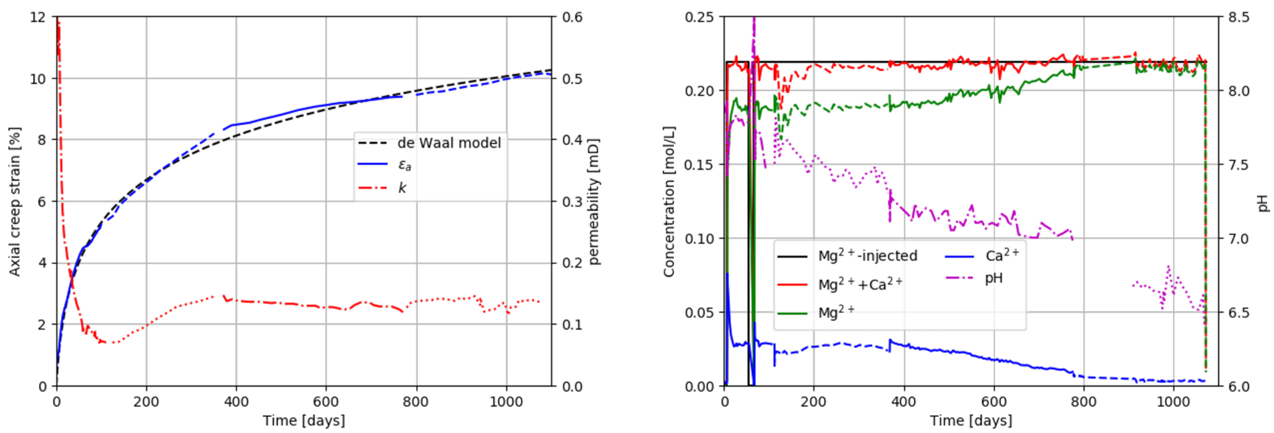

Figure 17.4: Data from (Nermoen, Korsnes et al. 2015), the change in line style indicates a change in flooding rate from 1 PV/day to 3 PV/day. (Left) The axial strain, and permeability development. (Right) Ion concentrations out of the core, solid black line is the injected $MgCl_2$ concentration.

The shift in flooding rate is indicated in the graphs by a change in the line style. $MgCl_2$ brine was injected for almost the entire period, except for 0.657 M NaCl from day 1 to 7, and distilled water from day 56 to 67 (Nermoen, Korsnes et al. 2015). We have fitted the de Waal model, equation (17.1), to the data and found $\varepsilon_a(0) = 0.0097\%/\text{hour}$ and $B = 2.14\%$. A significant flux of calcium out of the core was observed (see the blue line in the figure to the right in Fig. 17.4). The flux of calcium tails off towards the end of the experiment. Assuming that the calcium production is due to calcite dissolution, and the magnesium loss is due to magnesite precipitation, it was estimated that 93–98% of the initial amount of calcite was replaced with magnesite (Nermoen, Korsnes et al. 2015). These findings was backed up by density measurements (magnesite is denser than calcite) and SEM investigations. The porosity of the core before testing was $\sim$41%, after testing the porosity was calculated to more or less unchanged, $\sim$40%. The explanation for this unexpected behavior is the mineralogical alterations in the core. The pore volume was conserved even if the core experienced more than 10% axial (25% volumetric) strain. Thus, the compression of the pore volume was balanced by a decrease in matrix volume due to mineralogical alterations. The permeability development is particularly interesting, see Fig. 17.4. The permeability is significantly lower after testing than before, and stays more or less constant from 400–1072 days. This behavior cannot be explained by the porosity development and is most likely due to an increase in surface area caused by textural re-working of the primary mineral surfaces. Later in this chapter we will present more details about textural investigations, which are absolutely necessary in order to develop models that can capture these chemical effects.

17.6 Some recent results and additional analyses

In the following, we will take a closer look at some of the data presented in the previous section. Changes in the texture of the pore surface due to rock-fluid interactions, will impact the surface area of the grains. The surface area of the grains is in turn related to the permeability, thus the measured permeability may be inverted to give in-situ information about the specific surface area development and hints about the rock fluid interactions. This can be understood from a Carman-Kozeny (CK) type of equation, which can be derived as follows: Assuming that the porous medium is replaced by a bundle of tubes, with equal radii r, and a fully developed Poiseuille flow, it can be shown quite easily that the permeability of this medium would be $k_{CK} = \frac{r^2\phi}{8\tau^2}$ (see e.g. (Bear 2013)). ϕ is porosity, τ is the tortuosity, defined as the ratio between the tube length and the length of the porous medium. A cylindrical pore has a specific surface area of $S = 2/r$, combining these two equations we arrive at:

$$k_{\mathrm{CK}} = 987\frac{\phi}{2S^2\tau^2}, \tag{17.5}$$

the factor in front is a conversion factor to give the permeability in units of mD. The specific surface area (S) is measured in m^2/ml pore volume. Note that this equation is different from the one used in (Nermoen, Korsnes et al. 2015). If one would like to use the specific surface area measured in m^2/g rock (S_g), one has to use the following version:

$$k_{\mathrm{CK}} = 987\frac{\phi^2}{2(1-\phi)^2\rho^2 S_g^2\tau^3}, \tag{17.6}$$

where ρ is the density of the rock. How well does this equation work? In (Nermoen, Korsnes et al. 2015) the porosity, density, specific surface area were measured on untested and tested material, while the permeability was measured continuously by monitoring the pressure drop, ϕ=0.41, 0.40, $\rho \simeq$2.69,2.9 g/ml, $S_g \simeq$ 3.56–3.84, 8.85–9.92 m^2/g, $k \sim$ 1.05, 0.15mD before and after testing, respectively. Inserting these values in the equation above, we get k_{CK}= 0.97, 0.12mD, before and after testing, respectively, which is very close to the observed values. The fact that this simple analysis gives such good match, indicates that permeability for chalk cores can be modelled by a CK type model. The underlying reason is probably that the pore distributions of chalk is relative narrow (Megawati, Madland et al. 2015).

If we make the following assumptions:

1. Changes in the pore volume is due to a reordering of the grains and mineral dissolution/precipitation
2. The grains are incompressible, i.e. changes in grain volume is only due to mineral dissolution/precipitation

Then we can determine the evolution of the porosity as:

$$\phi(t) = 1 - \frac{V_m(t)}{V_b(t)}, \tag{17.7}$$

$$V_b(t) = V_b(0)(1-\varepsilon_V(t)) = V_b(0)(1-\xi\varepsilon_a(t)), \tag{17.8}$$

$$V_m(t) = V_m(0) + 10^{-3}\sum_i M_{V_i}\sum_j \nu_{ij}\int q(t)\Delta C(t)_j, \tag{17.9}$$

where ξ is a conversion factor from volumetric to axial strain (put equal to 2.5), M_{V_i} is the molar volume of mineral i, $\Delta C(t)_j$ is the difference in ion concentration between inlet and outlet, ν is a stoichiometric matrix that relates ion fluxes to mineral fluxes, and $q(t)$ is the flooding rate. V_b and V_m, refers to the bulk and matrix volume, respectively. This means that the specific surface area during the experiment can be predicted from measured quantities as:

$$S(t) = \sqrt{987\frac{\phi(t)}{2\tau^2 k(t)}} = 22.2\sqrt{\frac{\phi(t)}{k(t)}}, \tag{17.10}$$

in the last equation, we assumed that the tortuosity is equal to 1. In **Fig. 17.5**, the result of the calculation is shown. Note that the pore volume stays more or less constant during the whole experiment, even if the rock is compacting (see Fig. 17.4). The reason is that mineral dissolution is competing with the compaction and the net effect is that the pore volume is kept constant. The specific surface area has a very interesting development, it has a maximum value after 100 days. Assuming that our analyses are correct, this could indicate that there are minerals being formed with a high surface area that are being dissolved at a later stage. Another explanation can be that at this stage of flooding the state of equilibrium changes such that it goes to a stage which favours high growth rates as opposed to high nucleation rates. This means that one may envision a transition from a state where several new grains are nucleated to a state where crystals now rather grow in size instead, yielding a lower specific area. The degree of super-saturation in the rock – fluid system governs whether it is the nucleation or growth rate that is favoured (Myerson 2002). The processes taking place in the core during testing may likely be a combination of the two mechanisms.

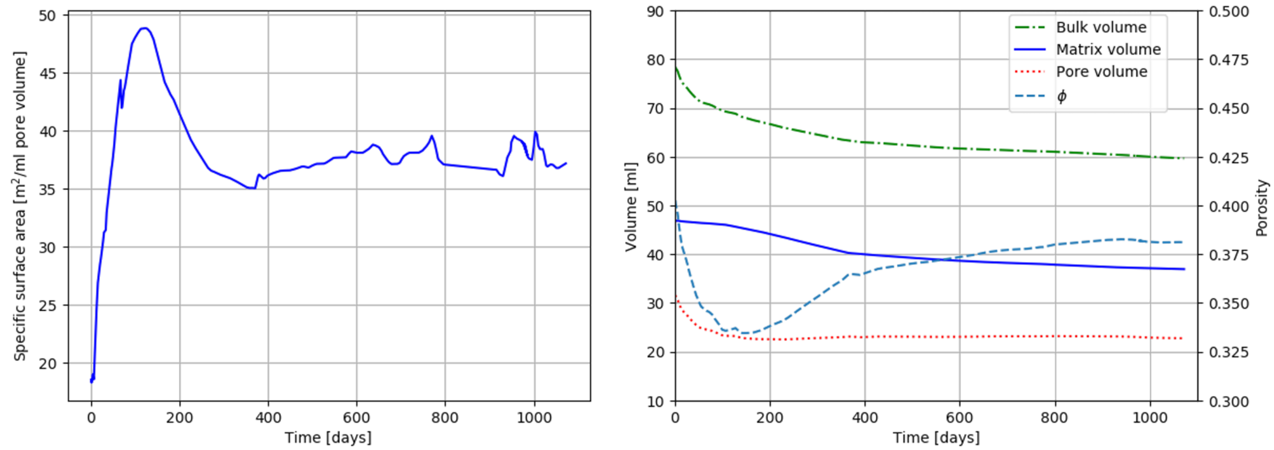

Figure 17.5: (left) The specific surface area development estimated from the CK equation. (Right) the corresponding development in bulk, matrix, pore volume, and porosity.

17.7 Additional creep induced by magnesium rich brine

In (Andersen, Wang et al. 2018) a comprehensive dataset was published, where five outcrop chalks were tested hydrostatically and analysed geochemically before and after flooding. The strength of this study is that several types of outcrop chalk cores were flooded, that the chalk cores were flooded for a sufficient long time to quantify the geochemical effects, and that reference cores flooded with a more or less inert brine was included. The hydrostatic loading and creep phase for the inert brines (NaCl) are shown in **Fig. 17.6**. These cores behave according to the de Waal model, equation (17.1), which can be observed from the log plot. As the yield point for the different chalk cores vary quite a lot, from ∼14 MPa for the Kansas cores to ∼6 MPa for the Stevns Klint cores, the cores were left to creep at different levels above the yield point. In Fig. 17.6 and **Fig. 17.7** the data are shown, and we have fitted the de Waal model to the creep data. It is quite apparent that the de Waal creep model works well for the cores flooded with NaCl brine[1]. The $MgCl_2$ data presented in Fig.17.7, shows a

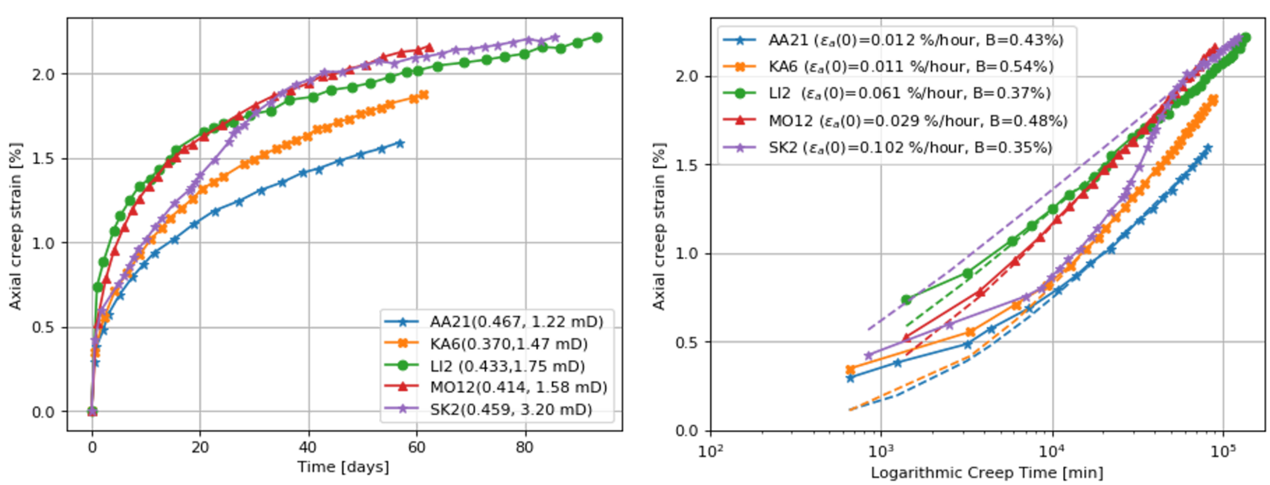

Figure 17.6: Creep data from (Andersen, Wang et al. 2018). The flooding fluid is 0.657 M NaCl. (left) The symbol gives the type of core AA=Aalborg, KA=Kansas, LI=Liège, MO=Mons, SK=Stevns Klint. The numbers in the parenthesis gives the porosity and permeability. (right) A direct fit to the de Waal model, equation (17.1), using the axial creep data. The values in the parenthesis gives the values of the parameters in the de Waal model.

remarkably different behavior. We have made an attempt to fit these data to the de Waal model (see the figure to the right), however by visual inspection it is quite clear that the behavior is not captured by this model. The Stevns Klint and Mons cores shows a bimodal behavior, with an accelerating creep after 20 days. In order to

[1] The data for the SK2 core are of poor quality before 30 days as the piston to measure axial strain was not in full contact with the core

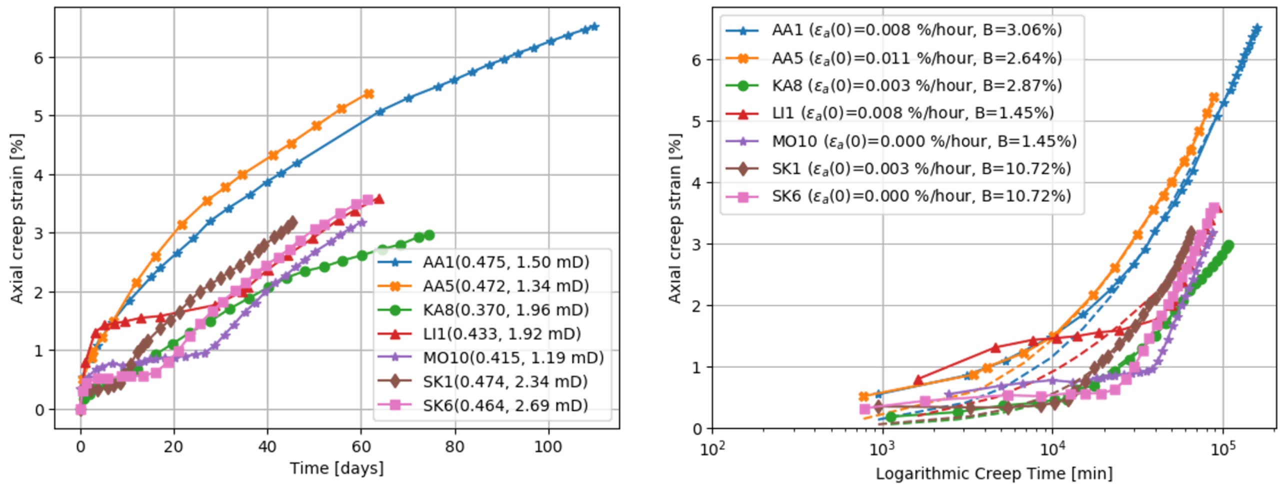

Figure 17.7: Creep data from (Andersen, Wang et al. 2018). The flooding fluid is 0.219 M MgCl2 (left) The symbol gives the type of core AA=Aalborg, KA=Kansas, LI=Liège, MO=Mons, SK=Stevns Klint. The numbers in the parenthesis gives the porosity and permeability. (right) A direct fit to the de Waal model, equation (17.1), using the axial creep data. The values in the parenthesis gives the values of the parameters in the de Waal model.

analyse these data in more detail, we have quantified the excess creep of the $MgCl_2$ cores. We define the excess creep as $\Delta\varepsilon(t) = \varepsilon^{\mathrm{MgCl_2}}(t) - \varepsilon^{\mathrm{NaCl}}(t)$, which is shown for each core in **Fig. 17.8**. The behavior is quite striking, as it seems that there is a pure linear additional creep induced by the $MgCl_2$ fluid. In the figure to the right in Fig 17.8, the development of the creep rate is shown, and after about 20–30 days, the creep rate stabilize around 0.04%/day. Thus, we might suggest that the creep development follows a modified de Waal model:

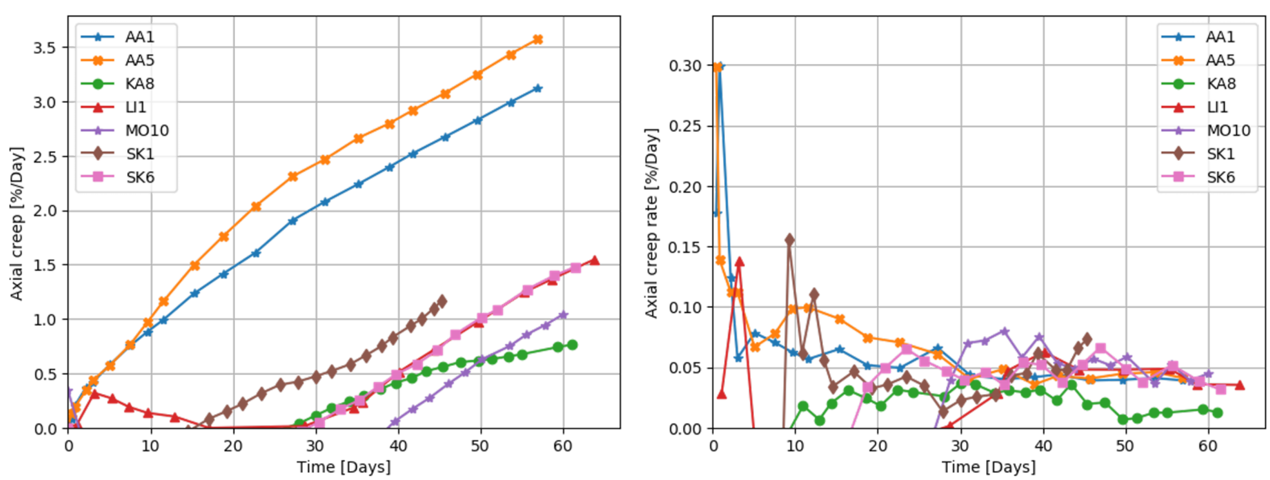

Figure 17.8: (left) Estimated excess $MgCl_2$ creep rate. (Right) Estimated excess creep rate.

$$\varepsilon_V^{\mathrm{MgCl_2}}(t) = B_{\mathrm{NaCl}} \log\left(1 + \frac{\dot{\varepsilon}_V^{\mathrm{NaCl}}(0)t}{B_{\mathrm{NaCl}}}\right) + Ct, \tag{17.11}$$

where C$\sim$0.04%/day. This model is similar to a creep model, first discussed by Griggs (Griggs 1939), where the following formula was suggested:

$$\varepsilon_V(t) = A + B\log t + Ct. \tag{17.12}$$

The term $B\log t$ is associated with elastic flow and Ct with pseudo viscous flow. This model was developed to discuss the creep of materials below the elastic limit and is therefore not directly applicable for the creep behavior discussed here. In our model, we can view C as an additional chemical creep. Most likely, it is more correct to use the pore volumes as a time scale, and not time directly. The mechanical creep rate in the de Waal model will slowly disappear after a time, and at some point the chemical creep will dominate the rock mechanical behavior.

17.8 Pore scale investigations of rock fluid interactions

Pore scale investigations can crudely be divided into two types 1) quantification of forces on microscale, and 2) quantification of chemical and textural changes. Both approaches are needed, and both have their strengths and weaknesses. Let us consider investigations that tries to evaluate the forces on microscale: Clearly the strength of this approach is that one gets a value of the forces between interfaces, such as grain-grain surfaces and grain-fluid surfaces. The values for the interaction forces can fairly easy be upscaled using the Young-Dupre equation to obtain values for contact angles and information about wettability changes (Hassenkam, Pedersen et al. 2011). A particular interesting study was performed by Røyne, Bisschop et al. (2011) as described previously in the section "Fluid effects or the effect of saturating chalk with air, oil or gas". They studied subcritical crack growth of calcite crystals and were able to estimate the surface tension of calcite exposed to mixtures of glycol and water. The surface energy was more than halved when the water concentration was increased from zero to one. These values are consistent with the decrease in strength observed by (Risnes 2001), as an example, the hydrostatic yield point was reduced from 17 MPa to 10 MPa by replacing glycol with water. The challenge with these microscale studies are that they are very hard to perform, and that one often has to make compromises regarding the type of samples used and the external conditions. As an example one usually use single mineral phases, while temperature and pressure conditions are limited to ambient (Hassenkam, Pedersen et al. 2011). Typical instrumentation for these studies can be Atom Force Microscopy (AFM), Surface Force Apparatus (SFA) and instrumentation for measuring stress, strain and zeta potential at micro- and nano-scale. The experiments and analyses are therefore best suited to study fundamental mechanisms and understanding of the exact physical and chemical reactions that take place at the rock - fluid interface. They are difficult to apply on real rock samples, but may be used to form a basis for the understanding of processes in samples tested under more realistic reservoir conditions, where the various reactions are not so easily distinguished.

Chemical and textural investigations have their clear strength in that they can be performed on samples that have been exposed to realistic flooding conditions. The weakness is of course that the observed alterations are not easily up scaled, and it is a challenge to extract quantitative measurements of the forces on micro- and nano-scale. Another challenge is to understand which alterations take place at which times during flooding. The alterations observed in the samples after flooding will be a sum of the alterations over time. However, the upside is that the results from these analyses can be very valuable in understanding which chemical and textural alterations take place, and where in the sample they preferentially take place. Alterations observed at pore-scale are important at field-scale, but how to implement these changes in a field-scale model with large grid blocks, is not straight forward.

One may, based on analyses of effluent water samples from core experiments or from a producing reservoir, estimate fluxes in ionic composition due to rock – fluid interaction (Fig. 17.6), thus the expected changes that have taken place in mineralogy. The changes in water composition and results from computational modelling should be confirmed by observations of chemical and textural changes in tested rock material. This allows for confirmation or refutation of the assumed processes that take place during flooding of non-equilibrium brines and can be used to constrain simulation and models.

The observable changes in rock samples are mostly related to dissolution and precipitation of mineral phases. Adsorption processes are not easily measured because of the small amounts of alterations, but may be detected by changes in other physical properties, e.g. zeta-potential. Dissolution and precipitation processes are governed by the state of equilibrium in the rock – fluid system and can be rather easily modelled following the rules of thermodynamics. However, most geochemical solvers and the rates given in thermodynamic databases cannot exactly match all reactions and rates observed in laboratory experiments. Therefore, post-experimental analyses are needed to study how much of the sample material has been altered, i.e. dissolved or precipitated, how the changes are distributed along the flooding axis, and if these changes can be matched by the given rates for dissolution and precipitation. Stoichiometric calculations can anticipate which mineral phases should dissolve and precipitate, however, formation of certain phases are in nature seen to be dependent on other factors or catalysts. One example of this is dolomite $CaMg(CO_3)_2$: Based on models and calculations, dolomite should precipitate in the given lab-experiments, however, after the experiments are finished, after months, or even years, the presence of dolomite cannot be confirmed (Borromeo, Egeland et al. 2018; Minde 2018). This may be because precipitated dolomite is dissolved again during flooding or that dolomite does not form in these type of laboratory experiments over the time lengths tested. Anyhow, this is an example of input that is needed to optimise pore- and core-scale modelling, which can be seen as the first step towards upscaling to field-scale.

By combining the two described types of pore-scale investigations one may be able to understand which alterations take place, where, when and how they take place. A continuous interaction between experimental work and modelling is needed to understand which of these factors are important at which scales, and which factors that need further in-depth investigation.

17.9 What have we learned from pore scale investigations?

In rock–fluid interaction, the composition of the rock, together with the composition of the injected brine, are the most important factors governing the thermodynamic processes under the given conditions. Typical reservoir rocks are most commonly divided into carbonates and sandstones, which have different mineralogy and different affinity towards ions in the pore water. This applies both for sorption processes and dissolution and precipitation of mineral phases. Sandstones are in general considered to have a negative surface charge and carbonates to have a positive surface charge. Carbonates are also more reactive and more soluble than sandstones, which make them more exposed to dissolution and precipitation of mineral phases.

However, the knowledge of type of rock is far from enough to predict the effects of rock–fluid interaction. Several other factors play important roles. Carbonates, for example, may be divided into several different groups of carbonates, dependent on properties such as grain-size and amount of matrix (Dunham 1962; Embry and Klovan 1971). Even though carbonate rocks mostly consists of carbonate minerals, such as calcite and dolomite, different amounts of impurities in the form of non-carbonate minerals, e.g. as clay, are found. These minerals could potentially be very important for rock–fluid interaction, the rocks strength and the recovery of oil.

When considering rock–fluid interaction and equilibrium states, all ions present in solution or in solid phase, in this case the minerals, has to be accounted for. This means that the minerals present in the rock before injection, together with the composition of the fluid, will define which minerals are under- or over-saturated in the fluid, i.e. which minerals will dissolve and which will precipitate. If we use chalk as an example, a clean chalk-type, mainly consisting of calcite, will, when flooded with $MgCl_2$, largely induce dissolution of calcite ($CaCO_3$) and precipitation of magnesite ($MgCO_3$) (**Fig. 17.8**). If the chalk contains a lot of primary non-carbonate minerals in the form of silicates, some of these may dissolve and together with the ions in the brine, in this case Mg^{2+}, form magnesium-silicate phases (**Fig. 17.10**) in addition to magnesite.

Changing the composition of the brine while keeping the composition of the rock the same, can also alter the type of minerals which will dissolution and precipitation in a system.

In several studies, also in the previous discussed example, brines have been simplified to enable the study of specific reactions and the effect of varying ions (Madland, Hiorth et al. 2011). However, to be able to link core scale experiments with field scale results, the conditions at core scale have to be as similar as possible to reservoir conditions. To understand changes due to injection of seawater at e.q. the Ekofisk field, seawater should be used as flooding agent. This has been performed in several experiments e.g. (Madland, Hiorth et al. 2011; Megawati, Madland et al. 2015; Heggheim, Madland et al. 2005; Korsnes, Strand et al. 2006) and the mineralogical alterations are similar to what is observed in chalk flooded with $MgCl_2$. Nevertheless, there are several differences which may be very important for fluid-flow and changes in mechanical parameters. In seawater, SO_4^{2-} is present, and together with Ca^{2+} this ion can form anhydrite ($CaSO_4$) which may, in the same way as clay-minerals (Fig. 17.10), significantly reduce the permeability if it precipitates in pore-throats or –spaces (Madland, Hiorth et al. 2011). Such precipitation is frequently observed during flooding with seawater, which hampers the execution of flow-through triaxial experiments because of clogging of tubes and subsequent pressure build-up. As when flooding with $MgCl_2$, changes in the carbonate mineralogy takes place, primarily through dissolution of calcite and precipitation of magnesium bearing carbonates.

The texture of the rock also plays a role dictating the mineralogical replacement and where these changes preferentially takes place. By texture, one can include the size of grains, pore-size distribution, the amount of cement and matrix, fossil-types and the preservation of these. The diagenetic history of the rock, including fluid-flow and burial depth will effect these factors. In general, mineralogical alterations seem to take place in favoured positions, such as in larger pore-spaces or fractures where there is room to grow, and stress and equilibrium states may differ from the rest of the rock. A good example of this is the growth of magnesite ($MgCO_3$), which takes place in chalk-cores flooded with $MgCl_2$ (Madland, Hiorth et al. 2011; Andersen, Wang et al. 2018; Minde, Wang et al. 2018). μm-sized magnesite crystals can quite rapidly be observed (after only months of flooding) precipitated in pore-spaces formed by large micro-fossils (Fig. 17.9a and 17.9b) or as smaller crystals or clusters within the matrix (Fig. 17.9c). The size and amount of precipitated crystals can be correlated

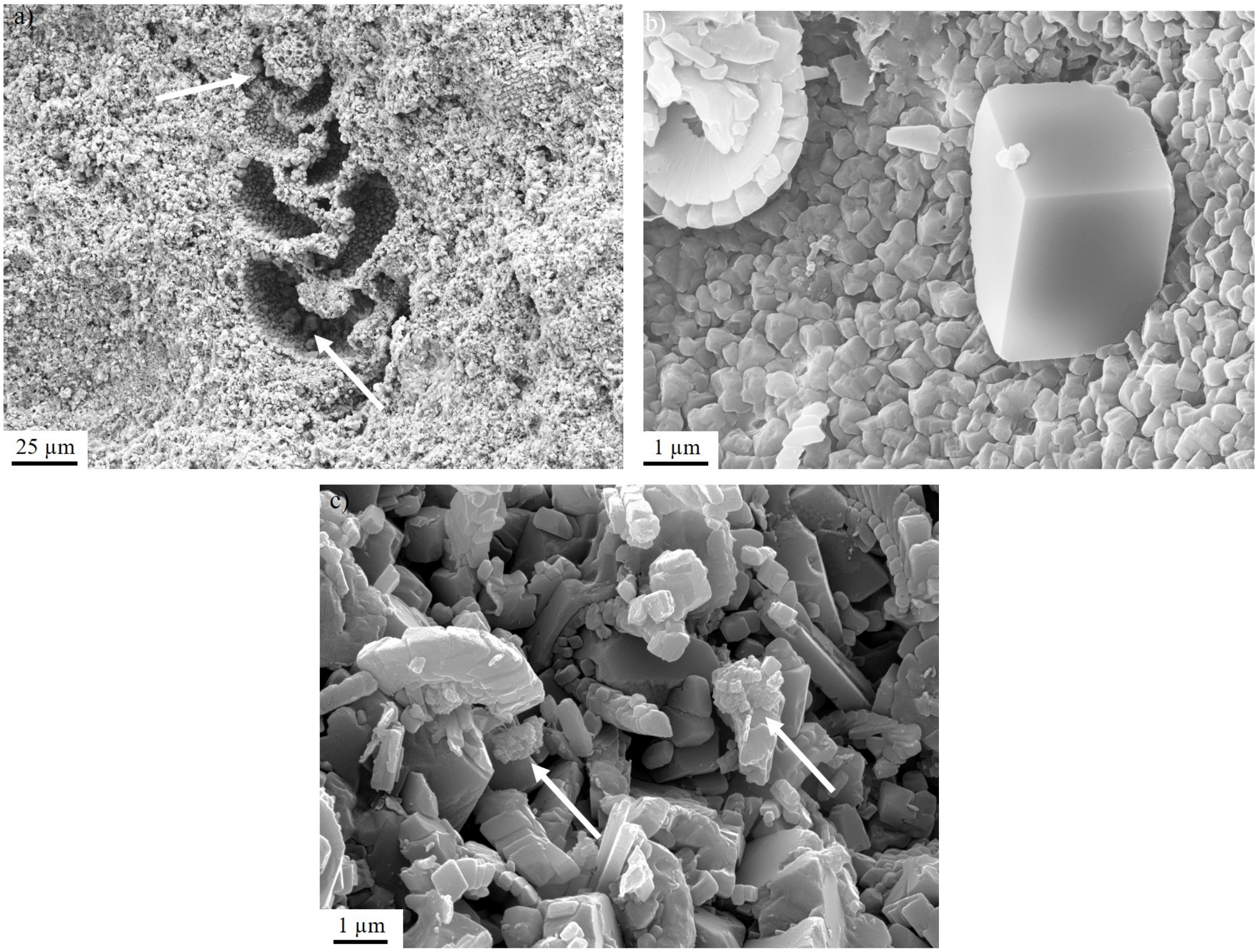

Figure 17.9: Examples of newly precipitated magnesite crystals in a) and b) large pore-spaces and as c) smaller clusters of crystals within the matrix. From (Minde 2018)(Minde, Madland et al. 2018).

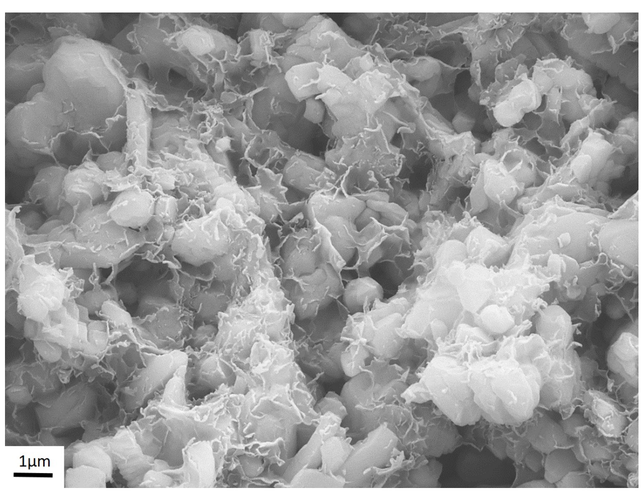

Figure 17.10: Precipitates of magnesium-bearing clay minerals in Aalborg chalk, which contains large amounts of primary opal-CT. From (Minde 2018).

to the room to grow and the distance from the fluid inlet.

In long-term tests of outcrop chalk from Liège, mineralogical alterations have been observed to take place in fronts progressing through the cores during flooding (Minde, Haser et al. 2017). The core was flooded for 516 days with 0.219 M $MgCl_2$, at conditions close to reservoir conditions of the Ekofisk field (Zimmermann, Madland et al. 2015). **Fig. 17.11** shows mapping by Energy Dispersive Spectroscopy (EDS) of the core from inlet to outlet, covering half of the diameter of the core, where the core centre is at the top of the image. After flooding, there are two regimes of mineralogy. The part towards the outlet of the core is only partly altered. The material still mainly consists of calcite (red pixels) in the form of microfossils commonly observed in chalk, but precipitates of clay (green pixels) and magnesite (blue pixels) are found within the calcite matrix. At the inlet part of the core, a total transformation from calcite to magnesite is observed. In this part of the core, only magnesite and clay are found, and no calcite is left. For cores flooded for an even longer period, the transition between the two regimes has moved further into the core, to the right in Fig. 17.11, indicating that this transformation of mineralogy moves like a front through the cores.

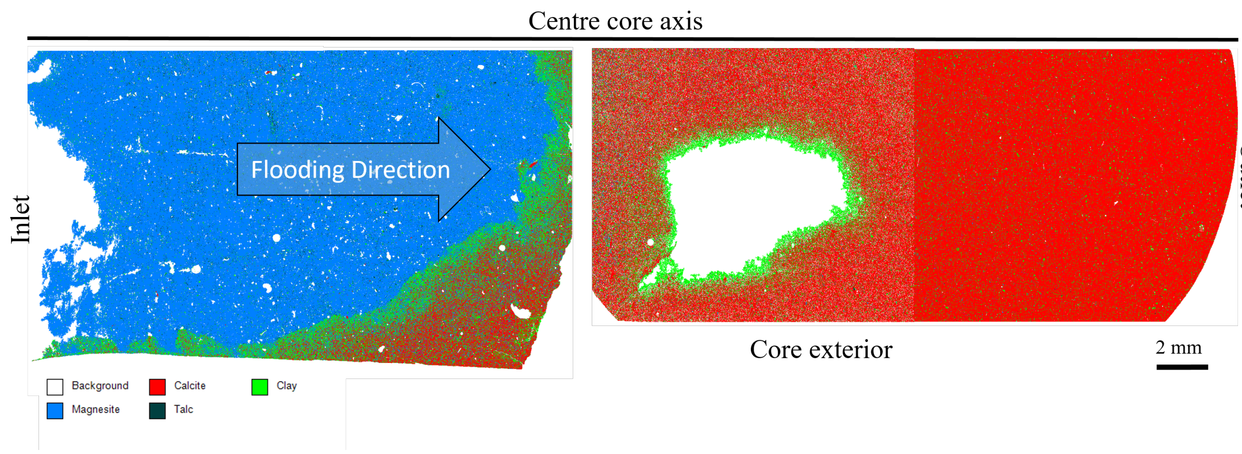

Figure 17.11: From Minde, Haser et al. (2017). EDS mapping of Liège chalk flooded with $MgCl_2$ for 516 days. The flooding direction is from left to right, and two fronts of alterations are observed in the core. The minor blue and green pixels inside the calcite (red) indicates a clay and magnesite precipitate front, while the blue area displays a front of complete transformation of the mineralogy from calcite dominated to magnesite. Legend below. Note: Towards the outlet, a hole (white) can be observed as an artefact of the sample preparation.

Even though this is an extreme example, with large amounts of magnesium injected into the core, the experiments still shed light on how the process of alteration takes place and seem to also match the front-like behavior found in modelling of geo-chemical reactions at field-scale.

Differences in available space, stress and equilibrium states may, as mentioned, also be encountered in fractures of the rock. Fractures play an important role for fluid-flow in a reservoir (Snow and Brownlee 1989), and precipitation of new mineral phases or closing of fractures due to compaction could therefore potentially have severe effects of the production of oil. On one hand, fractures are in many cases the main pathway for oil or fluids towards a producing well, and clogging of fractures may therefore reduce the recovery. On the other hand, fractures have high permeability compared to the matrix, and injected water or IOR-fluids may in these cases have difficulties in penetrating into the matrix and only flow in the open fractures (Graue, Moe et al. 2000; Hirasaki and Zhang 2004; Nielsen, Olsen et al. 2000). If this is the case, reducing the permeability in the fractures may increase the effect of the injected water and enhance the recovery of oil. Similarly, the effect the injected water has on the *geomechanical* properties of the rock, will also in large amount be affected by the amount of fractures and the permeability of these fractures. The effect fractures have on the oil-recovery and compaction based on rock – fluid interaction is therefore difficult to predict in general terms, and should be evaluated from case to case.

17.10 Modeling of rock fluid interactions

To model how fluids interact with the subsurface, the natural starting point is geochemistry. As explained by W. White: "in geochemistry, we use the tools of chemistry to solve geological problems, that is, we use chemistry to understand the Earth and how it works" (White 2013). In petroleum exploration, geochemistry has been an important tool to understand the thermal evolution of sedimentary basins. Geochemistry can also be used to understand what happens to the oil during generation, expulsion and migration, and to correlate between different fields and wells. For a producing reservoir, streamlines from different parts of the reservoir mixes in the producers. The individual streamlines might be in equilibrium with the rock, but when they mix, minerals may precipitate and lead to complete plugging of the producers. Therefore, geochemical calculations are a valuable tool to estimate the risk of mineral precipitation in the producers. By taking regular water samples, a computer program such as PHREEQC (Parkhurst 2017) can be used to estimate when scale-inhibiting measures should be taken.

Although geochemical interactions have been appreciated, and valued by the geologists and chemists dealing with e.g. scaling and souring issues, reservoir engineers have to a large degree ignored it. However, there are more and more evidence from lab experiments and field data, which demonstrates that the water chemistry affects both compaction and oil production. How can we make use of the geochemical models for a producing oil reservoir? In a producing reservoir, there will be large pressure variations, and temperature variations due to the cold water injected. One of the great advances the last century related to geochemical modelling is the development of thermodynamic databases. Thermodynamic databases are used to predict which minerals are stable under certain pressures; temperatures and fluid composition, for a review see Oelkers, Bénézeth et al. (2009).

17.11 Geochemistry of Ekofisk formation water

It is generally believed that for temperatures above 50°C most formation waters are in equilibrium with the rock, and before complete hydrocarbon filling of the reservoir, the pore water tends to equilibrate with the rock. If one knows the stability of minerals, one can use this information to reconstruct the in-situ formation water (Bazin, Brosse et al. 1997a,b). It is also possible to use the information about formation water to predict the presence of reservoir minerals. This information can be very valuable as the reservoir quality is dependent on the reservoir minerals (Bjørlykke, Aagaard et al. 1995). Clearly, this information is of interest in identifying poor reservoirs, but also of great interest for identifying the minerals present in a producing reservoir. This is because if we introduce a new brine into the reservoir, such as seawater, the seawater will react with the reservoir. As the injection fluid moves from the injector to the producer, it will interact with the reservoir, and lead to textural and chemical alterations. To quantify these changes we need information about minerals present. The quantification of the induced changes is a starting point to identify if the injected brine may affect the physical properties of the rock.

In **Table 17.1**, a measurement of produced water from the Ekofisk Formation at the Ekofisk field is listed (Hiorth, Bache et al. 2011). Clearly, this composition will not be identical to the actual composition of the pore water in the reservoir, as the samples have been depressurized and CO_2 has been released. In addition there might be some precipitation and dissolution. The thermodynamic databases tell us which minerals are expected to be stable at Ekofisk conditions. This information along with investigations of reservoir core material, e.g. (Hjuler 2007) are important information to construct a reasonable buffer for the Ekofisk formation. Usually when using the word "buffer" one refer to pH-buffer, but in reality minerals in the formation buffers the individual ions. Thus, if there are the same number of minerals in the formation as ions in the formation water, the chemistry and pH is completely determined. The calculation is performed by requiring that the minerals are in equilibrium with the rock, and that we know the chlorine concentration. Chlorine is usually not buffered by any mineral, and the pH is determined by requiring that the solution is charge neutral. This approach is quite standard, and described in the book by Garrels and Christ (Garrels and Christ 1965). We determine the equilibrium and dissociation constants using the HKF equation of state (Helgeson and Kirkham 1974a,b; Helgeson, Kirkham et al. 1981; Aagaard and Helgeson 1982) and the SUPCRT thermodynamic data (Johnson, Oelkers et al. 1992). In **Table 17.2**, the result of our calculations are shown. The match is quite good, many of the species are predicted within 10-15% of the measured values, with the exception of barium, strontium, bicarbonate and potassium. It is natural to expect that the bicarbonate concentration is higher in the reservoir, due to degassing of the sample, however, In this case, the prediction of the carbonate content in Table 17.2 is in the lower range of what is expected for clastic reservoirs Smith and Ehrenberg (1989). The potassium concentration is too low, but this can be explained by lack of aluminium (Bjørlykke, Aagaard et al. 1995), which we do not know from the analyses.

17.12 Chemistry of seawater and seawater like brines

In our view, there are two important sides to the story, one deals with the bulk chemistry and the other deals with the surface chemistry. Both from an experimental and modelling point of view the surface chemistry aspect is immensely more complicated. First, we will discuss the bulk chemistry of seawater, and how the bulk chemistry of seawater might change in contact with minerals.

Table 17.1: Measurement of produced water from the Ekofisk field, Ekofisk Formation

Ion	Measured Conc. [mmol/L]
Cl^-	1423.10
Na^+	1142.80
Ca^{2+}	99.90
Mg^{2+}	21.89
Sr^{2+}	8.50
Ba^{2+}	1.84
K^+	7.30
HCO_3^-	3.90

Table 17.2: Predicted ion composition at 200 bar and 130°C, assuming equilibrium with Smectite, Kaolinite, Mica (paragonite and muscovite), Dolomite, Calcite, Quartz, Talc, Witherite, and Strontianite. pH=5.4 and p_{CO_2}=0.29 atm

Ion	Predicted Conc. [mmol/L]
Cl^-	1423.10
Na^+	1179.63
Ca^{2+}	91.84
Mg^{2+}	18.17
Sr^{2+}	5.97
Ba^{2+}	0.13
K^+	3.46
HCO_3^-	21.77
SiO_2	1.62
Al^{3+}	3.48E-04

The chemistry of high salinity brines, such as the Ekofisk formation water described in the previous section, and seawater are different from the chemistry of low salinity brines such as the water in lakes and rivers. The main reason for this is that ions make complexes, which have the effect that e.g. calcite is much more soluble in seawater compared to distilled water. To make this point clearer we have made a calculation where seawater is assumed to be in equilibrium with calcite and a partial pressure of CO_2 equal to the atmospheric conditions $10^{-3.5}$ atm. **Table 17.3** are for ambient conditions and **Table 17.4** for 130°C and 200 bars (close to Ekofisk conditions).

Tables 17.3 and 17.4 show the total amount of the major species, and the distribution between the major species. The free ion column is related to the thermodynamic activity. Multiplying the concentration with an activity coefficient gives us the thermodynamic activity. It is the thermodynamic activity of the individual species that determines if minerals will dissolve or precipitate, not the total concentration. As an example the fluids above are in equilibrium with calcite ($CaCO_3$), but if we were to remove magnesium from the fluid, much more carbonate will be available in the fluid (due to the removal of the $MgCO_3$ complex), hence calcite would precipitate. The important point is that it is not only the pH or the total concentration of the individual ions that that determine the solubility. The system is like a game of musical chairs, if one ion is removed, all the other ions needs to reshuffle and the thermodynamic equilibrium might change. To make the picture more complete, we can also use the calculated thermodynamic activities to calculate saturation indices. The saturation index tells us if a mineral is thermodynamic stable; if the saturation index is larger than 0 the mineral might precipitate and if the saturation index is negative it might dissolve. It does not tell us the time scale of the process, only that it is eventually expected to be formed or dissolved.

17.13 Injection of seawater

When seawater is injected into a reservoir, it will displace oil, but also interact with the formation. We can quantify these interactions, or at least quantify the potential for interaction, by the use of thermodynamic models. As already indicated in the previous sections, we can use equilibrium chemistry to determine which minerals are expected to be formed or dissolved. The effect of the chemical alterations on physical properties such as wettability, and rock mechanical properties (e.g. compaction rate) is a different story, and the rock mechanics will be discussed in subsequent sections. In **Table 17.5**, the saturation indices are shown for some minerals when seawater is in equilibrium with calcite and a CO_2 buffer. The saturation index is shown for seawater at ambient conditions, core flooding conditions (130°C and 8 bar), and reservoir conditions (130°C and 200 bar). We clearly see that seawater at ambient conditions are close to equilibrium with magnesium carbonate minerals. Some variants of dolomite are supersaturated at ambient conditions. Even if the thermodynamic calculations shows that some minerals are supersaturated, it does not mean that they will form easily or in

Table 17.3: Distribution of major dissolved species in seawater, equilibrium with calcite and p_{CO_2}=$10^{-3.5}$ atm is assumed, pH=7.87 at 1 atm and 25°C

Ion	Molality (Total)	Free Ion (%)	Me-SO_4 Pair (%)	Me-HCO_3 Pair (%)	Me-CO_3 Pair (%)	Me-Cl Pair (%)
Na^+	0.4500	95.8	1.1	-	-	3.1
K^+	0.0100	98.3	1.6	-	-	0.1
Mg^{2+}	0.0445	81.3	9.8	0.2	0.0	8.7
Ca^{2+}	0.0124	87.8	6.4	0.1	0.1	5.6

Ion	Molality (Total)	Free Ion (%)	Ca-anion Pair (%)	Mg-anion Pair (%)	Na-anion Pair (%)	K-anion Pair (%)
SO_4^{2-}	0.024	56.9	3.3	18.3	20.9	0.7
HCO_3^-	0.00065	86.9	2.5	10.5	-	-
CO_3^{2-}	0.000028	26.7	25.3	48.0	-	-
C^-	0.525	96.4	0.1	0.7	2.7	0.0

Table 17.4: Distribution of major dissolved species in seawater, equilibrium with calcite and p_{CO_2}=$10^{-3.5}$ atm is assumed, pH=7.67 at 200 bar and 130°C

Ion	Molality (Total)	Free Ion (%)	Me-SO_4 Pair (%)	Me-HCO_3 Pair (%)	Me-CO_3 Pair (%)	Me-Cl Pair (%)
Na^+	0.4500	92.5	1.6	-	-	5.9
K^+	0.0100	97.5	2.1	-	-	0.4
Mg^{2+}	0.0445	70.8	10.7	0.0	0.0	15.7
Ca^{2+}	0.0128	76.5	6.5	0.0	0.1	16.5

Ion	Molality (Total)	Free Ion (%)	Ca-anion Pair (%)	Mg-anion Pair (%)	Na-anion Pair (%)	K-anion Pair (%)
SO_4^{2-}	0.024	46.1	3.5	19.9	29.7	0.9
HCO_3^-	0.00010	74.2	4.8	21.1	-	-
CO_3^{2-}	0.000014	11.6	46.8	41.6	-	-
Cl^-	0.525	93.2	0.4	1.3	5.0	0.0

a practical time span. Dolomite is found in numerous geological settings, but the formation of dolomite at ambient condition has been a challenge for researchers, and is known as the dolomite problem (Gregg, Bish et al. 2015). In Table 17.5, we have included a column for higher temperature, one at 8 bar pore pressure which is used in most experimental (core) settings, and one at higher (reservoir) pressures at 200 bar. As expected, the saturation indices do not change much from 8 to 200 bar, with the exception of anhydrite (Blounot and Dickson 1969).

In Table 17.2, we used equilibrium calculations to construct a mineral buffer that was consistent with the Ekofisk formation. We can now use this mineral buffer to predict what kind of mineralogical alterations could potentially happen when seawater is injected. The results of the calculations are shown in **Fig. 17.12**. The only difference between the "core" and "field" calculation is the pressure. The figure to the left shows the change in the ion concentrations, a positive change means that the concentration in solution drops and a negative change means that the concentration in the solution increases. The figure to the right shows the corresponding mineral fluxes: calcite, kaolinite, quartz, and paragonite (mica) is dissolved and Mg-beidellite (smectite), dolomite, muscovite (mica), and anhydrite is precipitated.

As we clearly see that if aluminium and quartz is present, injection of seawater is expected to cause precip-

Table 17.5: Saturation index of some carbonate minerals, brucite and anhydrite for seawater composition, at different pressures and temperatures.

Mineral	Saturation index		
	Ambient 25°C, 1 bar	Core 130°C, 8 bar	Reservoir 130°C, 200 bar
Dolomite			
$CaMg(CO_3)_2$	1.81	2.16	2.17
Dolomite(ordered)			
$CaMg(CO_3)_2$	1.81	2.16	2.17
Dolomite(disord.)			
$CaMg(CO_3)_2$	0.00	1.18	1.19
Huntite			
$CaMg_3(CO_3)_4$	0.27	1.97	1.99
Brucite			
$Mg(OH)_2$	0.18	1.77	1.84
Magnesite			
$MgCO_3$	-0.14	1.00	1.01
Anhydrite			
$CaSO_4$	-2.51	0.12	-0.04
Calcite			
$CaCO_3$	0	0	0

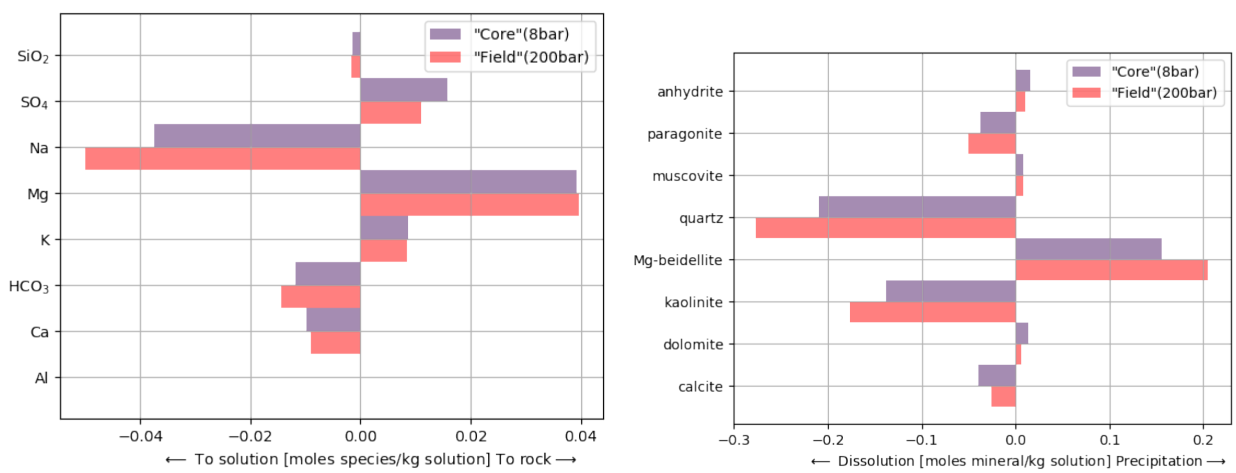

Figure 17.12: (left) ion flux when seawater is equilibrated with the rock, and to the right is the corresponding mineral fluxes when 1 kg of seawater equilibrates with the rock. pH = 5.7 for high and low pressure

itation of clay minerals such as smectite, as observed in chemical and textural investigations of flooded chalk from the laboratory. A signature of this should be seen in produced water or in the effluent of core floods. The figure to the left shows the ion fluxes, and generally one would expect increase in calcium, sodium, and quartz and a decrease in potassium, magnesium and sulphate. A couple of things should be noted:

- The thermodynamic calculations are equilibrium calculations, meaning that there is no time scale involved. We have already pointed out that dolomite is not easily formed in the lab.
- A CO_2 buffer might be present in the reservoir as a gas or oil phase. If much carbonate is formed by dissolution of calcite, some of this carbonate might dissolve into a gas and oil phase and thereby change

the equilibrium chemistry.

We have assumed that aluminium is present, if that is not the case, the picture is different and the results are shown in **Fig. 17.13**. It is interesting to note that the ion fluxes are not that different from Fig. 17.12. The general trends hold, calcium (and carbonate) should increase, whereas magnesium and sulphate decrease. However, in this case, without the aluminium silicates, the stoichiometry is such that $\Delta_{Mg} = \Delta_{SO_4} - \Delta_{Ca}$. This is simply because magnesium is replacing calcium to form dolomite, and then some calcium is lost due to anhydrite precipitation.

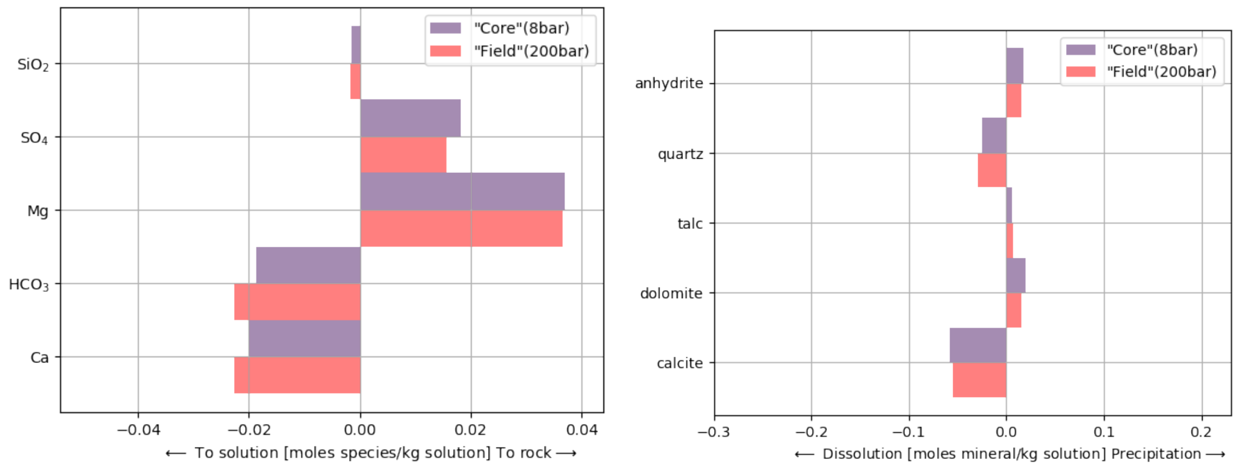

Figure 17.13: (left) ion flux when seawater is equilibrated with the rock, and to the right is the corresponding mineral fluxes when 1kg of seawater equilibrates with the rock. pH=5.5 for high and low pressures.

17.14 Streamline simulations

In order to gain insight and to understand part of the complexity of upscaling geochemical reactions, we have included some streamline simulations that are based on simple potential flow models (Hiorth, Bache et al. 2011; Hiorth, Jettestuen et al. 2013). The model assumptions are quite strong: a homogeneous reservoir with constant thickness (essentially a 2D flow problem), and constant injection rates. The flow lines are predicted from the velocity field involving a single phase only, and then they are frozen in time. The total resistance of all the streamlines are calculated, and subsequently the flow rate in each streamline is calculated from the total injected flow rate, times the resistance in each stream line, divided by the total resistance in the system, very similar to the method described in (Higgins and Leighton 1962). In **Fig. 17.14**, the flow lines are shown for the system described in more detail in (Hiorth, Bache et al. 2011; Hiorth, Jettestuen et al. 2013). The injection rates and well distances are comparable with a sector of the Ekofisk field. If more geological realism was included, the streamlines would have a different from, but the snap shots after five years of seawater injection in **Fig. 17.14 and 17.15** capture some of the important effects that would take place anyway. First of all, the results show that there is a temperature gradient that lags behind the injected water front. This is because the water only moves in the pore space, whereas the temperature moves in the total volume (matrix and pore space). Second, due to the temperature dependence (activation energy) of the mineral reactions, the chemical alterations travel at a totally different speed than the water and the temperature front, see Fig. 17.15 where some of the wt-fraction of mineral precipitation and dissolution is shown. From Fig. 17.15 it is quite clear that much of the magnesium carbonate alteration happens close to the injector, and we have found that 1.5wt% of calcite is dissolved and 1.5wt% of dolomite is precipitated near the injection well, after 40 years of simulated seawater injection (Hiorth, Bache et al. 2011). The calcite to magnesium carbonate transition may extend ∼400 m from the injection well with an activation energy of 65 kJ/mol. The sulphate bearing mineral anhydrite precipitate at high temperatures and dissolves at low temperatures, thus the simulations predict a sulphate wave that travels at the same speed as the temperature front, where anhydrite is precipitated and dissolved again throughout the reservoir.

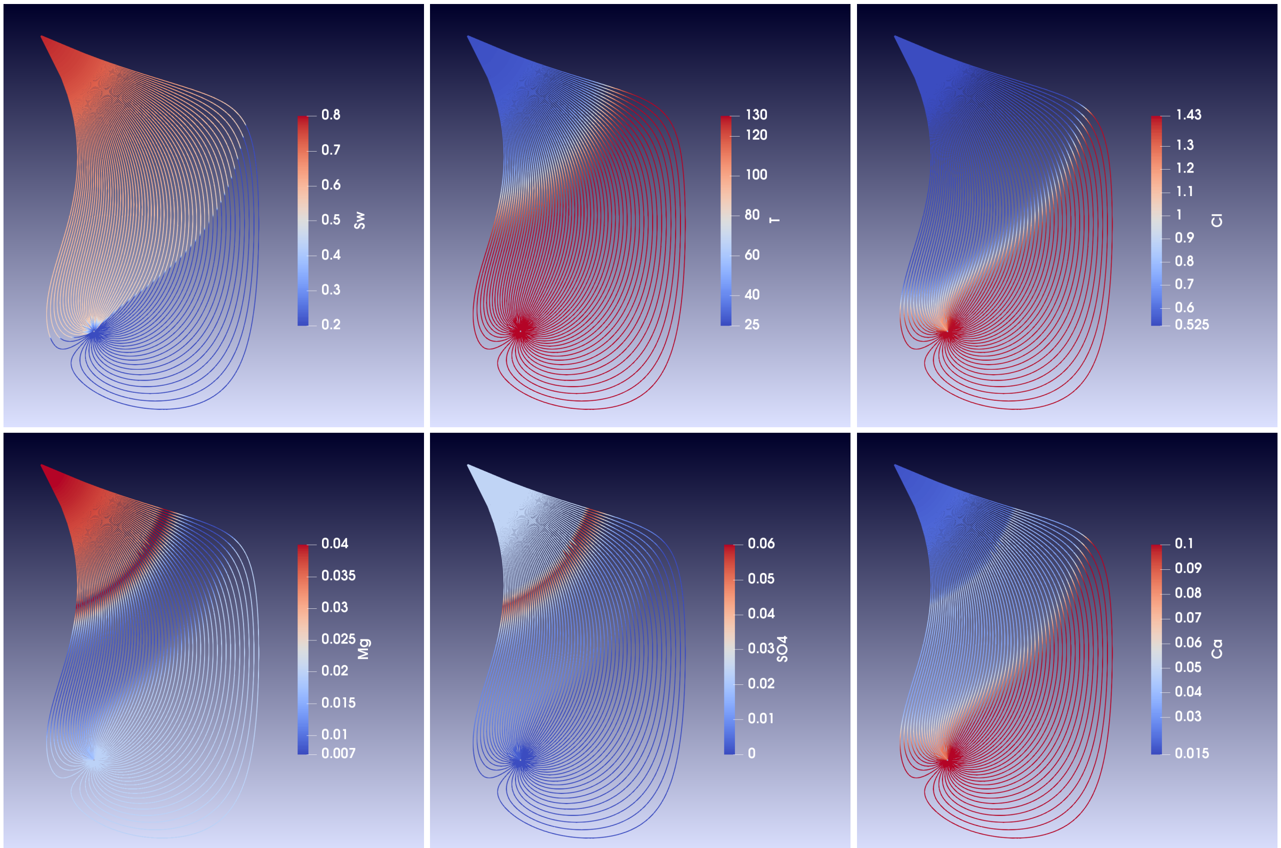

Figure 17.14: Streamlines with profiles of water saturation, temperature and ion concentration at water injection breakthrough (approximately 5 years of seawater injection).

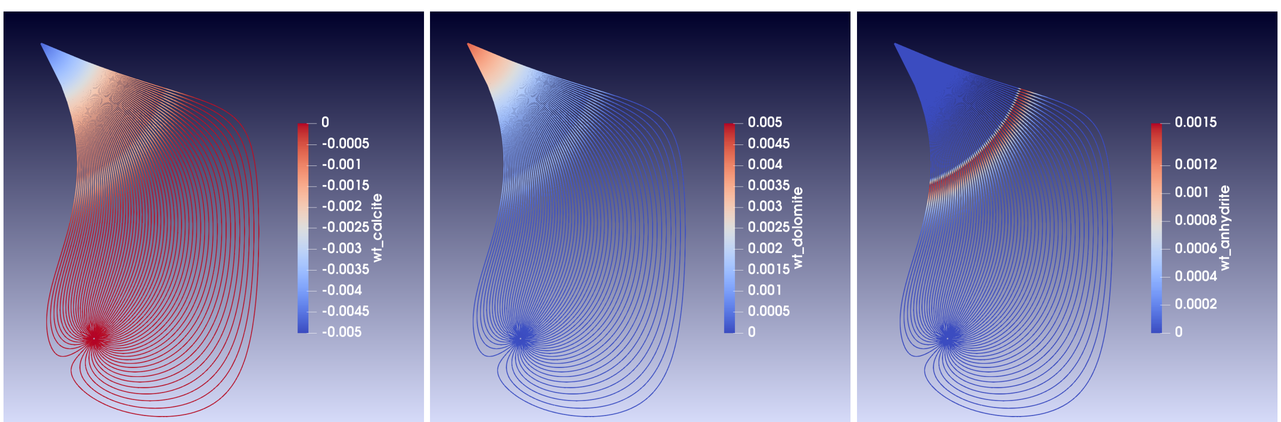

Figure 17.15: Streamlines showing the wt-fraction in the reservoir at water injection breakthrough (approximately 5 years of seawater injection).

17.15 Field scale observations

In (Hiorth, Bache et al. 2011) a particular interesting data set was published from the Ekofisk field. The data are produced water analyses from a producer located approximately 300–400 m from the nearest injector. In 2001 the well experienced seawater breakthrough, the composition of the produced water after seawater break through is shown in Fig. 17.15. The streamline picture discussed in the previous section is a very good conceptual model to understand these data. The streamlines have varying length, and because of this the arrival time in the producer differs. The concentrations measured in the well are the volume average of the concentrations from the different streamlines. In order to test if the ion profiles are consistent with the thermodynamic calculations presented in Fig. 17.12, and Fig. 17.13, we need some way of quantifying chemical interactions in the reservoir. This can be done by making the assumption that chlorine is inert and does not participate in any chemical reactions. The amount of chlorine in the produced water will then be an estimate of the fraction of seawater in the produced water compared to seawater. As an example, the concentration of chlorine in formation water is given in Table 17.1 (1.4 mol/L), and close to the measured concentration of chlorine in the produced water at year 0 in **Fig. 17.16**. Following the development of chlorine in Fig. 17.16, we see that during a period of 5–6 years the chlorine concentration drops to 0.63 mol/L, which is closer to the seawater concentration of 0.525 mol/L, but higher. Thus, the water in the producer is almost pure seawater, estimated to be 92%. Using the chlorine concentration as a tracer for seawater, we can then predict what the concentration of all the other ions should be if no chemical reactions were to take place in the reservoir. In Fig. 17.16, the solid line represents the expected amount of e.g. calcium, magnesium etc. that should be present if there were no chemical interactions in the reservoir. Any deviation between the observations (points) and solid line is an indication of interactions between the ions and the minerals in the formation-rock, or in the well.

Fig 17.17 shows the average of the net fluxes of the ions in Fig. 17.16, and the corresponding standard deviations. Fig 17.17 can be directly compared with Fig. 17.12 and 17.13. The similarities are quite striking, which is a strong indication that seawater injection on the Ekofisk field induces mineralogical alterations in the field.

17.16 Concluding Remarks

The mechanical behavior of chalk is dependent on the pore fluids. Apart from the apparent scientific rewarding challenge to understand this phenomenon, it might also have a direct practical use. Reservoir compaction is beyond any doubt a great source of natural energy to produce an oil reservoir, and capitalizing on this resource might be a very environmentally friendly method of improving oil recovery. In order to do so a multiscale understanding is needed. Most of the experimental data reviewed here are hydrostatic tests. A hydrostatic stress regime is usually not representative for a reservoir. Thus, is should be further investigated

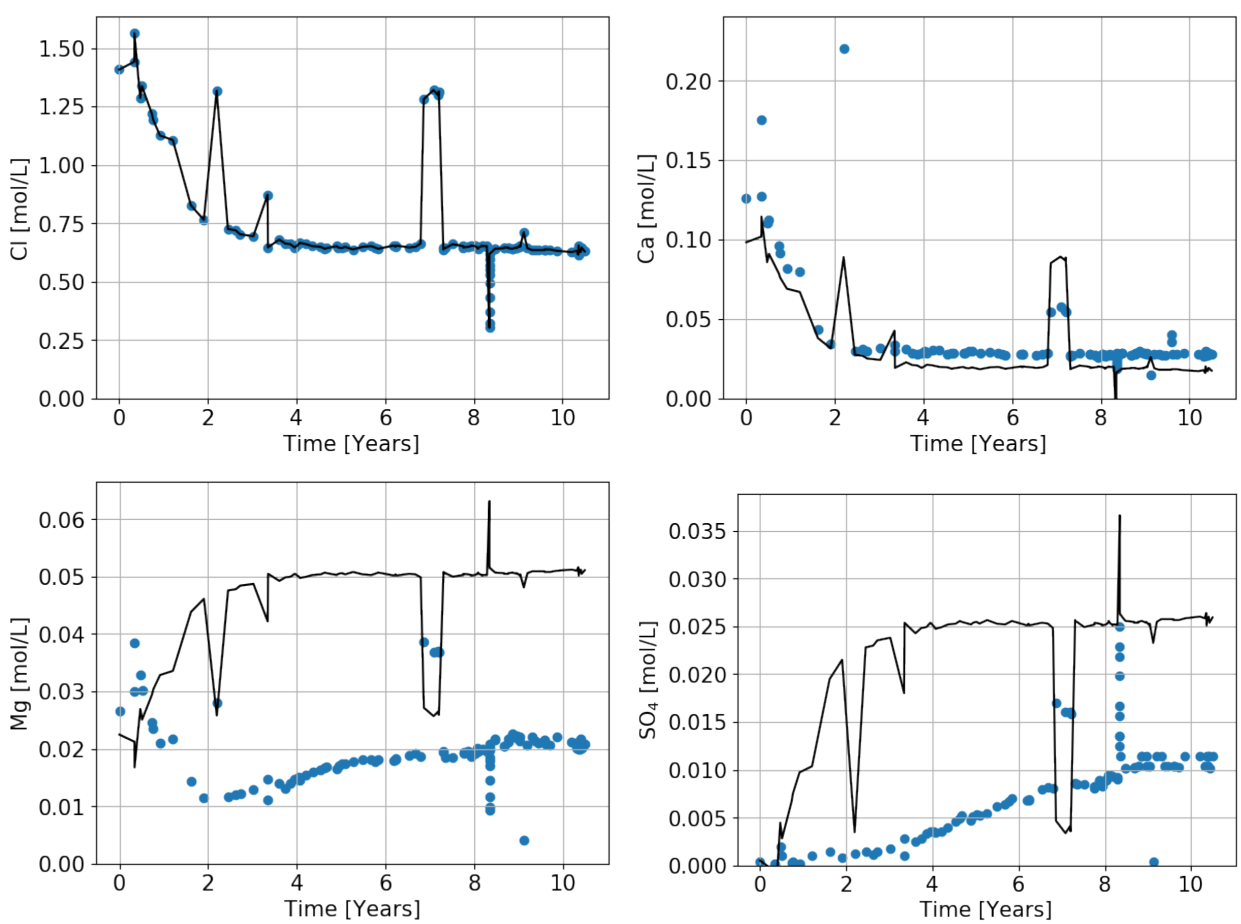

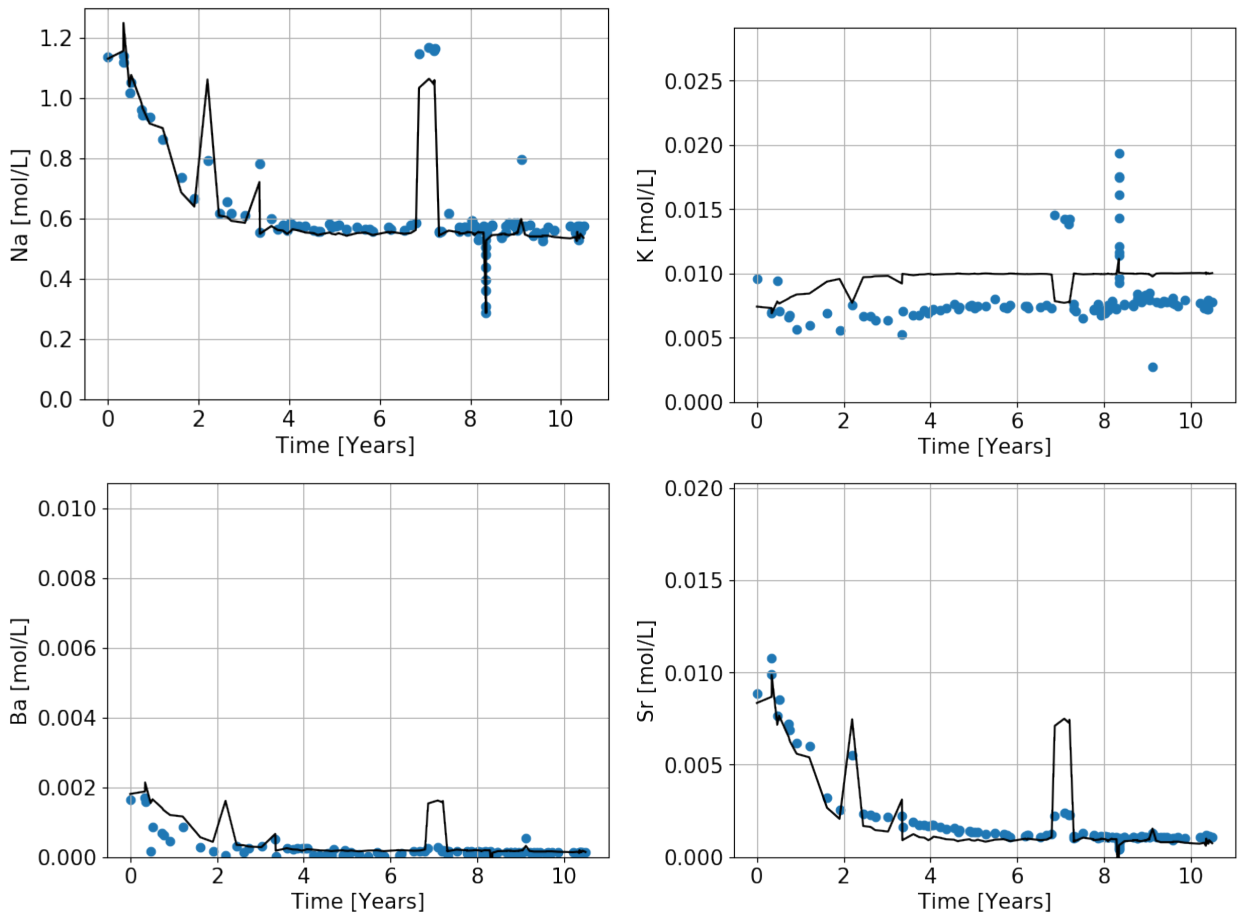

Figure 17.16: Analyses of produced water (points), the solid lines are the predicted initial ion concentrations assuming that chlorine is a conservative (ideal) tracer, and that the drop in chloride concentration is solely due to mixing between Ekofisk formation water and seawater. Note that the Y-axes in the various graphs have different scales.

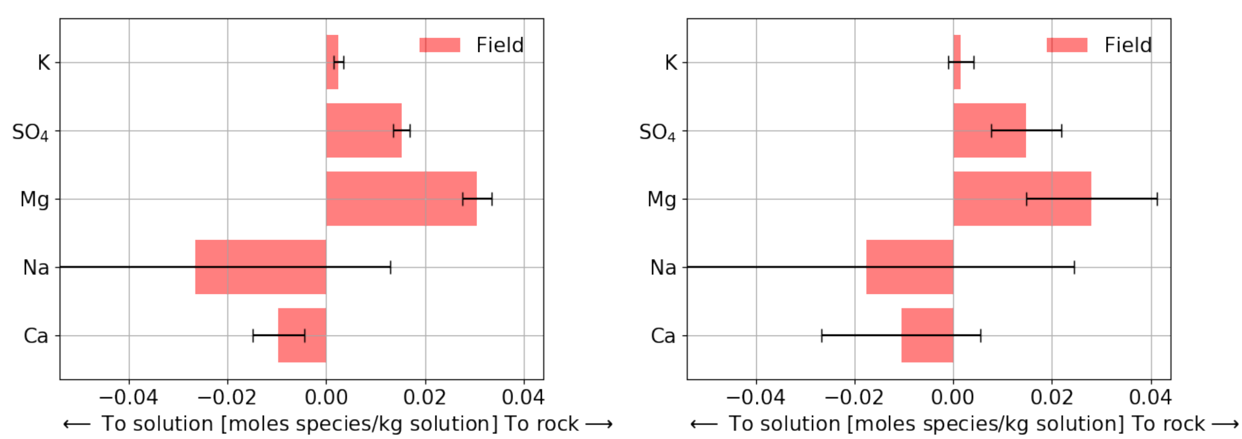

Figure 17.17: Estimated fluxes of ions from the Ekofisk well. In the figure to the left, the data from 1.5 latest year of production has been used to calculate the average value, and the standard deviation, whereas in the figure to the right all the historical data has been used.

how the stress-strain history of a producing reservoir would impact the chemical effects on compaction (Omdal, Madland et al. 2010). The reservoir is of course much larger than the core samples used in the lab, and has experienced a complicated stress history, but as we have tried to highlight, the chemistry affects the interaction forces between grains. By changing the interactions between the grains there is no reason why similar effects, but most likely of different magnitude, should not be observed on the field scale. Some aspects of the water weakening phenomena are probably only important in the lab, whereas other aspects might be more important at field scale. Below we list what we think are the most important aspects of rock- fluid interactions, relevant for chemical water weakening, at field scale:

- Compaction rate: The compaction rate in the field is different than in the data we have focused our attention on in this paper. Our analysis shows that the data fits the de Waal model when there are no (or little) chemical interactions. Due to the log-type behavior of the de Waal model, the creep rate will die off over time. We find that the chemical compaction rate follows a linear behavior, meaning that it does not disappear over time. Thus, at some point the chemical creep will dominate the pure mechanical creep.

- Core and field chemical fluxes: The chemical fluxes observed in core scale experiments are comparable to what is observed on field scale. In the core experiments, we can investigate the material before and after flooding, and determine the alteration speed. This is not currently possible on the field scale. It might be a long stretch, but there could be advances in 4D seismic which makes it possible to observe changes in the seismic signal due to mineralogical alterations in the reservoir.

- Surface forces vs textural alterations: Using models, data from core and pore investigations, we have tried to make the argument that water weakening is due to (at least) three different processes: 1) fluid effect, e.g. changing from water to oil. The effect is fast, almost immediate. It is questionable how transferrable it is to field scale. We have already argued that the fluid effect is most likely due to changes in surface energy. In a multi-phase system it is the wettability that controls which fluid is closest to the grain surface. When oil is displaced by water, the fraction of grain surface covered by water will not change if the wettability is unaltered. 2) Dissolution/precipitation, this effect is the slowest of the three effects, i.e. it usually requires several pore volumes to be observed on the core scale. It is time dependent and will dominate over the mechanical creep given enough time. 3) Changes in surface forces, this effect is fast on core scale, and should also be present at reservoir scale if potential determining ions are adsorbed in the reservoir.

- Field scale velocity of chemical alterations are different from core scale. The streamline calculations show that much of the dissolution and precipitation takes place near the injector, and close to the temperature front. Adsorption of sulphate slows down the sulphate front in the reservoir, but as the field data clearly shows, it breaks through in the producer, meaning that in a relative short time frame, sulphate is able to contact a large part of the reservoir and change the surface forces.

- The effect of field scale temperature front. The temperature front moves not only in the pore space but in the rock matrix as well, therefore it lags behind the seawater front. Clearly the temperature front impacts the thermal properties of fluid and matrix, which lead to additional stresses. In addition to this effect, we have seen from the streamline simulations that the temperature front is accompanied by chemical alterations. These alterations lead to dissolution and precipitation that might be an additional source of chemical compaction.

- Effect of wettability change. We have chosen to not include the effect of brines on the wettability on rock, because it requires a separate paper to be treated properly. However, we would like to point out that it is reasonable to expect that the primary mineral phases have a different wettability, than freshly made secondary minerals. A change in wettability towards more water wet leads to an increase in water wetted surface and a decrease in surface energy and increased chemical compaction.

- Field scale distribution of minerals: The chemical alterations are dependent on the primary mineral phases. We suggest using the composition of formation water and thermodynamic databases to back calculate which minerals are probably present in the reservoir. The permeability, and porosity field in the reservoir simulator might be used to estimate the relative fraction of the mineral phases.

- Effect of surface area: The mineralogical alterations are accompanied by a corresponding alteration in specific surface area. The specific surface area impacts permeability and porosity. For the case we have investigated, the specific surface area increases by a factor of two, which reduces the permeability by a factor of four. This could have an additional positive effect by diverting the flow of water, and improve the sweep.

Acknowledgements

The authors would like to thank Reidar Inge Korsnes, Merete Vadla Madland, Udo Zimmermann, Ida Lykke Fabricius, Helle Foged Christensen and Anders Nermoen for fruitful discussions and input to this chapter. The authors acknowledge the Research Council of Norway and industry partners, ConocoPhillips Skandinavia AS, AkerBP Norge AS, Eni Norge AS, Maersk Oil Norway AS, DONG Energy A/S, Denmark, Equinor AS, ENGIE E&P NORGE AS, Lundin Norway AS, Halliburton AS, Schlumberger Norge AS, and Wintershall Norge AS, for their support of the National IOR Centre of Norway

Nomenclature

B = constant
C = constant
D = constant
k = permeability, L, mD
m_i = molality of ions in solution
p = partial pressure, m/Lt^2
q = rate, L^3/t
r = radii, L
t = time, t
M_{V_i} = molar volume, L^3
S = surface area, L^2/V, m^2/ml
V = volume, L^3
ΔC = the difference in ion concentration
$\dot{\varepsilon}_V$ = strain rate
$\dot{\varepsilon}_V(0)$ = initial strain rate
η_{eff} = effective viscosity
μ = friction coefficient between rocks
μ_0 = constant
ν = stoichiometric matrix
ρ = density, m/L^3, g/ml
ϕ = porosity
σ = stress, M/Lt^2
τ = tortuosity
ξ = conversion factor

Subscripts

0 = initial
a = axial
b = bulk
eff = effective
g = gram
i = index
m = matrix
CK = Carman-Kozeny
V = volumetric

Abbreviation

AA = Aalborg
AFM = Atom Force Microscopy
CK = Carman-Kozeny
EDS = Energy Dispersive Spectroscopy
EOR = Enhanced Oil Recovery
KA = Kansan
LI = Liège
MO = Mons
SEM = Scanning Electron Microscopy
SFA = Surface Force Apparatus
SK = Stevns Klint

References

Aagaard, P. and Helgeson, H.C., 1982. Thermodynamic and kinetic constraints on reaction rates among minerals and aqueous solutions; I, Theoretical considerations. *American Journal of Science*, **282** (3): 237–285. March. URL http://dx.doi.org/10.2475/ajs.282.3.237.

Andersen, M., Foged, N., and Pedersen, H., 1992a. The rate-type compaction of a weak North Sea chalk. In *The 33th US Symposium on Rock Mechanics (USRMS)*. American Rock Mechanics Association. a.

Andersen, M.A.A., Foged, N.A., and Pedersen, H.E.A., 1992b. The link between waterflood-induced compaction and rate-sensitive behavior in a weak North Sea chalk. In *Proceedings of 4th North Sea chalk symposium, Deauville*. b.

Andersen, P.Ø., Wang, W. et al., 2018. Comparative Study of Five Outcrop Chalks Flooded at Reservoir Conditions: Chemo-mechanical Behaviour and Profiles of Compositional Alteration. *Transport in Porous Media*, **121** (1): 135–181. URL http://dx.doi.org/10.1007/s11242-017-0953-6.

Bazin, B., Brosse, É., and Sommer, F., 1997a. Chemistry of oil-field brines in relation to diagenesis of reservoirs 1. Use of mineral stability fields to reconstruct in situ water composition. Example of the Mahakam basin. *Marine and Petroleum Geology*, **14** (5): 481–495. August. a. URL http://dx.doi.org/10.1016/S0264-8172(97)00004-4.

Bazin, B., Brosse, É., and Sommer, F., 1997b. Chemistry of oil-field brines in relation to diagenesis of reservoirs—2. Reconstruction of palaeo-water composition for modelling illite diagenesis in the Greater Alwyn area (North Sea). *Marine and Petroleum Geology*, **14** (5): 497–511. August. b. URL http://dx.doi.org/10.1016/S0264-8172(97)00005-6.

Bear, J., 2013. *Dynamics of fluids in porous media*. Courier Corporation. ISBN 0486131807.

Bjørlykke, K., Aagaard, P. et al., 1995. Geochemical constraints from formation water analyses from the North Sea and the Gulf Coast Basins on quartz, feldspar and illite precipitation in reservoir rocks. *Geological Society, London, Special Publications*, **86** (1): 33–50. URL http://dx.doi.org/10.1144/gsl.sp.1995.086.01.03.

Blounot, C.W. and Dickson, F.W., 1969. The solubility of anhydrite ($CaSO_4$) in NaCl-H_2O from 100 to 450°C and 1 to 1000 bars. *Geochimica et Cosmochimica Acta*, **33** (2): 227–245. February. URL http://dx.doi.org/10.1016/0016-7037(69)90140-9.

Borromeo, L., Egeland, N. et al., 2018. Quick, Easy, and Economic Mineralogical Studies of Flooded Chalk for EOR Experiments Using Raman Spectroscopy. *Minerals*, **8** (6): 221. May. URL http://dx.doi.org/10.3390/min8060221.

de Waal, J.A., 1986. *On the rate type compaction behaviour of sandstone reservoir rock*. Ph.D. thesis, Technische Hogeschool Delft. URL https://www.researchgate.net/profile/Hans_De_Waal2/publication/35834162_On_the_Rate_Type_Compaction_Behavior_of_Sandstone_Reservoir_Rock/links/53e1d4630cf2235f352bda13/On-the-Rate-Type-Compaction-Behavior-of-Sandstone-Reservoir-Rock.pdf.

Dieterich, J.H., 1972. Time-dependent friction in rocks. *Journal of Geophysical Research - Solid Earth*, **77** (20): 3690–3697.

Dieterich, J.H., 1978. Time-dependent friction and the mechanics of stick-slip. *Pure and Applied Geophysics*, **116** (4–5): 790–806. URL http://dx.doi.org/10.1007/bf00876539.

Doornhof, D., Kristiansen, T.G. et al., 2006. Compaction and subsidence. *Oilfield Review*, **18**: 50–68.

Dunham, R.K., 1962. Classification of carbonate rocks according to depositional texture. *Memoir -American Association of Petroleum Geologists Special Volumes*, 108–121. URL http://archives.datapages.com/data/specpubs/carbona2/data/a038/a038/0001/0100/0108.htm.

Embry, A.F. and Klovan, J.E., 1971. A late Devonian reef tract on northeastern Banks Island, NWT. *Bulletin of Canadian Petroleum Geology*, **19** (4): 730–781. URL http://archives.datapages.com/data/cspg/data/019/019004/0730.htm.

Fjær, E., Holt, R.M. et al., 2008. *Petroleum related rock mechanics*, vol. 53. 2nd ed., Elsevier. URL http://store.elsevier.com/product.jsp?isbn=9780444502605.

Garrels, R.M. and Christ, C.L., 1965. *Solutions, Minerals and Equilibria*. Freeman, Cooper & Company, San Fransisco.

Graue, A., Moe, R.W., and Bognø, T., 2000. Oil Recovery in Fractured Reservoirs. URL http://www.ipt.ntnu.no/nordic/Papers/6th_Nordic_Graue.pdf. 6th Nordic Symposium on Petrophysics, Trondheim.

Gregg, J.M., Bish, D.L. et al., 2015. Mineralogy, nucleation and growth of dolomite in the laboratory and sedimentary environment: A review. *Sedimentology*, **62** (6): 1749–1769. April. URL http://dx.doi.org/10.1111/sed.12202.

Griggs, D., 1939. Creep of Rocks. *The Journal of Geology*, **47** (3): 225–251. URL http://dx.doi.org/10.1086/624775.

Gutierrez, M., Øino, L.E., and Høeg, K., 2000. The Effect of Fluid Content on the Mechanical Behaviour of Fractures in Chalk. *Rock Mechanics and Engineering, Rock*, **33** (2): 93–117. May. URL http://dx.doi.org/10.1007/s006030050037.

Hassenkam, T., Pedersen, C.S. et al., 2011. Pore scale observation of low salinity effects on outcrop and oil reservoir sandstone. *Colloids and Surfaces A: Physicochemical and Engineering Aspects*, **390** (1-3): 179–188. October. URL http://dx.doi.org/10.1016/j.colsurfa.2011.09.025.

Heggheim, T., Madland, M.V. et al., 2005. A chemical induced enhanced weakening of chalk by seawater. *Journal of Petroleum Science and Engineering*, **46** (3): 171–184. URL http://dx.doi.org/https://doi.org/10.1016/j.petrol.2004.12.001.

Helgeson, H. and Kirkham, D., 1974a. Theoretical prediction of the thermodynamic behavior of aqueous electrolytes at high pressures and temperatures; I, Summary of the thermodynamic/electrostatic properties of the solvent. *American Journal of Science*, **274** (10): 1089–1198. December. URL http://dx.doi.org/10.2475/ajs.274.10.1089.

Helgeson, H., Kirkham, D., and Flowers, G., 1981. Theoretical prediction of the thermodynamic behavior of aqueous electrolytes by high pressures and temperatures; IV, Calculation of activity coefficients, osmotic coefficients, and apparent molal and standard and relative partial molal properties to 600 degrees C and 5kb. *American Journal of Science*, **281** (10): 1249–1516. December. URL http://dx.doi.org/10.2475/ajs.281.10.1249.

Helgeson, H.C. and Kirkham, D.H., 1974b. Theoretical prediction of the thermodynamic behavior of aqueous electrolytes at high pressures and temperatures; II, Debye-Huckel parameters for activity coefficients and relative partial molal properties. *American Journal of Science*, **274** (10): 1199–1261. December. URL http://dx.doi.org/10.2475/ajs.274.10.1199.

Higgins, R.V. and Leighton, A.J., 1962. Computer Prediction of Water Drive of Oil and Gas Mixtures Through Irregularly Bounded Porous Media Three-Phase Flow. *Journal of Petroleum Technology*, **14** (09): 1048–1054. September. URL http://dx.doi.org/10.2118/283-pa.

Hilner, E., Andersson, M.P. et al., 2015. The effect of ionic strength on oil adhesion in sandstone – the search for the low salinity mechanism. *Scientific Reports*, **5** (1): 9933. April. URL http://dx.doi.org/10.1038/srep09933.

Hiorth, A., Bache, Ø. et al., 2011. A Simplified Approach to Translate Chemical Alteration in Core Experiments to Field Conditions. In *Paper SCA2011-09 presented at the International Symposium of the Society of Core Analysts*. Austin, Texas, USA. 18–21 September. URL https://www.researchgate.net/profile/Aksel_Hiorth/publication/267707675_A_SIMPLIFIED_APPROACH_TO_TRANSLATE_CHEMICAL_ALTERATION_IN_CORE_EXPERIMENTS_TO_FIELD_CONDITIONS/links/5608fe5a08aea25fce3b8be1/A-SIMPLIFIED-APPROACH-TO-TRANSLATE-CHEMICAL-ALTERATION-IN-CORE-EXPERIMENTS-TO-FIELD-CONDITIONS.pdf.

Hiorth, A., Jettestuen, E. et al., 2013. Thermo-Chemistry Reservoir Simulation for Better EOR Prediction. In *Stavanger, Norway: IEA EOR 34th Annual Symposium*, 1–15. Stavanger, Norway. September.

Hirasaki, G. and Zhang, D.L., 2004. Surface Chemistry of Oil Recovery From Fractured, Oil-Wet, Carbonate Formations. *SPE Journal*, **9** (02): 151–162. June. URL `http://dx.doi.org/10.2118/88365-pa`.

Hjuler, M.L., 2007. *Diagenesis of upper cretaceous onshore and offshore chalk from the North Sea area.* Ph.D. thesis, Technical University of Denmark. URL `http://www.er.dtu.dk/publications/fulltext/2007/MR2007-134.pdf`. August.

Hjuler, M.L. and Fabricius, I.L., 2009. Engineering properties of chalk related to diagenetic variations of Upper Cretaceous onshore and offshore chalk in the North Sea area. *Journal of Petroleum Science and Engineering*, **68** (3): 151–170. October. URL `http://dx.doi.org/10.1016/j.petrol.2009.06.005`.

Homand, S. and Shao, J.F., 2000. Mechanical Behaviour of a Porous Chalk and Water/Chalk Interaction. Part I: Experimental Study. *Oil & Gas Science and Technology*, **55** (6): 591–598. November. URL `http://dx.doi.org/10.2516/ogst:2000044`.

Homand, S., Shao, J.F., and Schroeder, C., 1998. Plastic Modelling Of Compressible Porous Chalk and Effect of Water Injection. URL `http://dx.doi.org/10.2118/47585-MS`. January.

Korsnes, R., Strand, S. et al., 2006. Does the chemical interaction between seawater and chalk affect the mechanical properties of chalk? In *Eurock 2006: Multiphysics Coupling and Long Term Behaviour in Rock Mechanics*, 427–434. Taylor & Francis. ISBN 978-0-415-41001-4. URL `http://dx.doi.org/10.1201/9781439833469.ch61`. April.

Korsnes, R.I., Madland, M.V., and Austad, T., 2006. Impact of brine composition on the mechanical strength of chalk at high temperature. In *EUROCK 2006 - Multiphysics Coupling and Long Term Behaviour in Rock Mechanics*, 133–140. CRC Press. ISBN 9780415410014.

Macmillan, N.H., Huntington, R.D., and Westwood, A.R.C., 1974. Chemomechanical control of sliding friction behaviour in non-metals. *Journal of Materials Science*, **9** (5): 697–706. May. URL `http://dx.doi.org/10.1007/bf00761789`.

Madland, M.V., Hiorth, A. et al., 2011. Chemical Alterations Induced by Rock–Fluid Interactions When Injecting Brines in High Porosity Chalks. *Transport in Porous Media*, **87** (3): 679–702. January. URL `http://dx.doi.org/10.1007/s11242-010-9708-3`.

Megawati, M., Hiorth, A., and Madland, M.V., 2012. The Impact of Surface Charge on the Mechanical Behavior of High-Porosity Chalk. *Rock Mechanics and Rock Engineering*, **46** (5): 1073–1090. October. URL `http://dx.doi.org/10.1007/s00603-012-0317-z`.

Megawati, M., Madland, M.V., and Hiorth, A., 2015. Mechanical and physical behavior of high-porosity chalks exposed to chemical perturbation. *Journal of Petroleum Science and Engineering*, **133**: 313–327. September. URL `http://dx.doi.org/10.1016/j.petrol.2015.06.026`.

Minde, M.W., 2018. *Mineral Replacements in Flooding Experiments Linked to Enhanced Oil Recovery in Chalk*. Ph.D. thesis, University of Stavanger. URL `https://uis.brage.unit.no/uis-xmlui/bitstream/handle/11250/2578165/Minde_MonaW_OA.pdf?sequence=1`.

Minde, M.W., Haser, S. et al., 2017. Comparative Studies of Mineralogical Alterations of Three Ultra-long-term Tests of Onshore Chalk at Reservoir Conditions. April. URL `http://dx.doi.org/10.3997/2214-4609.201700308`.

Minde, M.W., Wang, W. et al., 2018. Temperature effects on rock engineering properties and rock-fluid chemistry in opal-CT-bearing chalk. *Journal of Petroleum Science and Engineering*, **169**: 454–470. October. URL `http://dx.doi.org/10.1016/j.petrol.2018.05.072`.

Myerson, A.S., 2002. *Handbook of Industrial Crystallization*. Elsevier. URL `http://dx.doi.org/10.1016/b978-0-7506-7012-8.x5000-9`.

Nermoen, A., Korsnes, R.I. et al., 2015. Porosity and permeability development in compacting chalks during flooding of nonequilibrium brines: Insights from long-term experiment. *Journal of Geophysical Research - Solid Earth*, **120** (5): 2935–2960. May. URL `http://dx.doi.org/10.1002/2014jb011631`.

Nermoen, A., Korsnes, R.I. et al., 2018. Incorporating electrostatic effects into the effective stress relation — Insights from chalk experiments. *Geophysics*, **83** (3): MR123–MR135. March. URL `http://dx.doi.org/10.1190/geo2016-0607.1`.

Nielsen, C.M., Olsen, D., and Bech, N., 2000. Imbibition Processes in Fractured Chalk Core Plugs with Connate Water Mobilization. In *SPE Annual Technical Conference and Exhibition*. Society of Petroleum Engineers. URL http://dx.doi.org/10.2118/63226-ms.

Oelkers, E.H., Bénézeth, P., and Pokrovski, G.S., 2009. Thermodynamic databases for water-rock interaction. *Reviews in Mineralogy and Geochemistry*, **70** (1): 1–46.

Omdal, E., Madland, M.V. et al., 2010. Deformation Behavior of Chalk Studied Close to In Situ Reservoir Conditions. *Rock Mechanics and Rock Engineering*, **43** (5): 557–580. URL http://dx.doi.org/http://dx.doi.org10.1007/s00603-010-0087-4.

Parkhurst, D., 2017. PHREEQC. URL https://www.usgs.gov/software/phreeqc-version-3.

Risnes, R., 2001. Deformation and yield in high porosity outcrop chalk. *Physics and Chemistry of the Earth, Part A: Solid Earth and Geodesy*, **26** (1-2): 53–57. January. URL http://dx.doi.org/10.1016/S1464-1895(01)00022-9.

Risnes, R., Haghighi, H. et al., 2003. Chalk–fluid interactions with glycol and brines. *Tectonophysics*, **370** (1): 213–226. URL http://dx.doi.org/10.1016/S0040-1951(03)00187-2.

Risnes, R., Madland, M.V. et al., 2005. Water weakening of chalk -Mechanical effects of water-glycol mixtures. *Journal of Petroleum Science and Engineering*, **48** (1): 21–36. URL http://dx.doi.org/10.1016/j.petrol.2005.04.004.

Røyne, A., Bisschop, J., and Dysthe, D.K., 2011. Experimental investigation of surface energy and subcritical crack growth in calcite. *Journal of Geophysical Research*, **116** (B4). April. URL http://dx.doi.org/10.1029/2010JB008033.

Smith, J. and Ehrenberg, S., 1989. Correlation of carbon dioxide abundance with temperature in clastic hydrocarbon reservoirs: relationship to inorganic chemical equilibrium. *Marine and Petroleum Geology*, **6** (2): 129–135. May. URL http://dx.doi.org/10.1016/0264-8172(89)90016-0.

Snow, S.E. and Brownlee, M.H., 1989. Practical and Theoretical Aspects of Well Testing in the Ekofisk Area Chalk Fields. In *SPE Annual Technical Conference and Exhibition*. Society of Petroleum Engineers. URL http://dx.doi.org/10.2118/19776-ms.

Vinogradov, J., Jaafar, M.Z., and Jackson, M.D., 2010. Measurement of streaming potential coupling coefficient in sandstones saturated with natural and artificial brines at high salinity. *Journal of Geophysical Research-Solid Earth*, **115**. URL http://dx.doi.org/10.1029/2010jb007593.

Westwood, A.R.C., Goldheim, D.L., and Lye, R.G., 1967. Rebinder effects in MgO. *The Philosophical Magazine: A Journal of Theoretical Experimental and Applied Physics*, **16** (141): 505–519. URL http://dx.doi.org/10.1080/14786436708220861.

White, W.M., 2013. *Geochemistry*. John Wiley & Sons.

Zimmermann, U., Madland, M.V. et al., 2015. Evaluation of the compositional changes during flooding of reactive fluids using scanning electron microscopy, nano-secondary ion mass spectrometry, x-ray diffraction, and whole-rock geochemistryCompositional Changes during Flooding. *AAPG Bulletin*, **99** (5): 791–805.

Chapter 18

Waterflooding – Some Laboratory Experiments at UiB

Arne Graue, Martin Anders Fernø, and Geir Ersland

18.1 Introduction

This chapter emphasizes research achievements related to waterflooding fractured chalk reservoirs. The cooperative effort reported here has been sustained for twenty seven years as it brings together the detailed research, typically associated with academia, with the required information on reservoir recovery processes that the oil industry needs. The first step toward developing methods to increase oil recovery was to improve the fundamental understanding of the oil recovery mechanism(s). This was done by accurately mimicking the relevant reservoir properties in the laboratory under controlled and reproducible conditions. The second step was to systematically investigate the role of wettability and fractures on fluid flow and oil recovery mechanisms and correctly interpret the laboratory results from the viewpoint of the physics and chemistry of the field. This involved confidence in the experimental measurements and the ability to achieve representative reservoir conditions, even on a molecular level, which are representative of the native wettability, saturation distribution and petrophysical characteristics. The research results on waterflooding fractured chalk have provided a fundamental understanding of oil recovery mechanisms in fractured chalk at various wettabilities.

18.2 Wettability studies in outcrop chalk

18.2.1 Initial imbibition tests

An important recovery mechanism in producing oil by injecting water in fractured chalk is through spontaneous imbibition of water into matrix blocks surrounded by fractures. The capillary pressure in the water-wet matrix block will induce imbibition of water and produce oil to drive the system to capillary equilibrium ($P_c = 0$). For a less water-wet system, the capillary pressure will be lower for the same saturation, and therefore the driving force and potential for oil recovery will be lower. The wettability is therefore crucial for oil recovery in fractured reservoirs where the dominating mechanism is spontaneous imbibition. The potential for oil-recovery by water injection would generally be lower in neutral-wet or oil-wet fractured reservoirs.

One of the first objectives for Ekofisk was to determine whether differences in wettability and spontaneous imbibition endpoint were artifacts of sample preservation (Graue, Baldwin et al. 1986). Samples were cored with oil-based mud and sealed on-site in plastic for preservation. Care was taken to make the measurements as rapidly as possible, store the samples under an inert gas and avoid any process that could possibly alter the wettability. The imbibition and relative displacement index (RDI) trends, particularly as a function of core depth and formation, from preserved core samples, agreed with the previously observed trends from unpreserved samples. The absolute values of the oil produced, however, differed between sets of samples and may be the result of the oil-based mud making the core less water-wet, hence reducing oil recovery by spontaneous imbibition. This agreement in the trends between the formations indicated that the observed differences between the Upper- and Lower- Ekofisk and Tor formations were not an artifact of sample preservation, but real differences between the formations. The Tor samples were found to be strongly water-wet while the Ekofisk samples were found to be slightly to moderately water-wet. Although the Ekofisk formation plugs imbibed less than the highly water-wet Tor formation plugs, the Ekofisk plugs contained considerable mobile oil at the imbibition endpoint, which could be removed by viscous displacement. Previous correlations between porosity and imbibition in the Tor formation and the lack of a similar correlation in the Ekofisk formations were corroborated, further suggesting a difference between the formations. Elevated temperature imbibition of re-aged samples was not significantly different from ambient temperature imbibition of restored state samples, (Graue and Baldwin 1995a,b).

Fig. 18.1 shows an initial long term imbibition test for early cores sampled from North Sea chalk; four from the Tor formation, one from the Ekofisk formation and one outcrop sample. These tests ran for one year, a much longer time than previously measured. The objective was to determine whether the imbibition time used

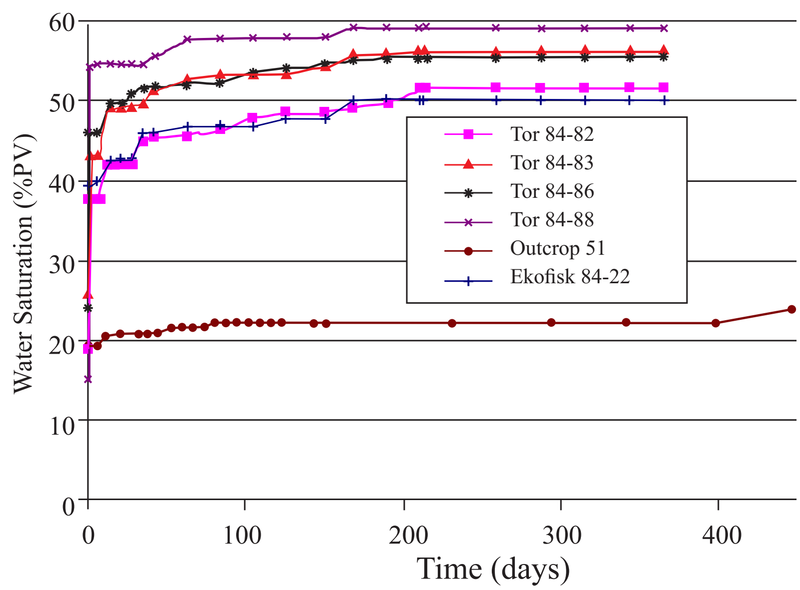

Figure 18.1: Long term spontaneous imbibition in North Sea Chalk. Water saturation versus time (days).

for most laboratory tests was adequate to predict the total spontaneous imbibition in chalk samples over the lifetime of the reservoir. A typical laboratory imbibition time is two days. From the plots in Fig. 18.1, it can be seen that most of the imbibition occurred within two days, however, additional oil, up to 30% PV, was obtained after the two days. This is a significant amount and would in many cases determine the economic assessment of oil recovery.

18.2.2 Outcrop chalk as a reservoir analog

The need for more and larger sized laboratory models motivated a search for outcrop chalk quarries with easy access to representative samples for North Sea chalk. Pore structure and pore-scale flow networks similar to those in the Ekofisk field core were screened to find the best reservoir analogue. The properties of four candidate outcrop chalks (Lie 1995) are shown in **Tab. 18.1**. The Beer samples were obtained from a quarry near Beer, England, the Stevns samples came from Denmark and the Dania and Rørdal samples, the latter sometimes called Portland, are both from Alborg, Denmark. All the samples had porosities and permeabilities similar to the Ekofisk reservoir. The Stevns samples had a slightly higher porosity, but produced an irreducible water saturation S_{wi} that was too low, when oilflooded. In addition, these plugs were too fragile for extensive handling. The Dania and Rørdal samples were easy to obtain and petrophysical and SEM examination showed a close resemblance to the Tor formation, Ekofisk reservoir core (Graue and Baldwin 1990). This indicated that the microscopic environment, including pore shape, pore throat size and extent of diagenesis was similar between these outcrop chalks and Ekofisk reservoir core. The Dania and Rørdal outcrop chalks have later extensively been used. Liege chalk was considered, but only a few plugs were obtained. However, this chalk has extensively been used for rock mechanics studies.

Core #	Outcrop	Porosity [%]	Permeability [mD]	S_{wi} [% PV][1]	S_{wf} [% PV][2]
E1	Beer	36	3.0	15	59
E2	Beer	35.1	2.9	16	57
E3	Beer	37.5	3.1	18	63
D1	Stevns	46.6	8.6	0	67
D2	Stevns	46.5	8.3	0	58
D3	Stevns	47.0	8.4	1	67
D4	Dania	42	4.4	34	56
D7	Dania	41.7	5.3	13	55
CHD-1	Dania	43	67	38	66
CHP-4	Rørdal	45	1.8	27	65
CHP-5	Rørdal	45	3.0	28	72

[1] Initial water saturation.
[2] final water saturation after first waterflood

Table 18.1: Petrophysical data for outcrop chalk plugs.

18.2.3 Wettability alteration

The first attempt to restore reservoir wettability by re-aging of core plugs was carried out to overcome the concern regarding whether cleaning changed the wettability from that originally in the reservoir (Anderson 1986; Buckley, Bousseau et al. 1995). Cleaned cores were prepared with brine and drained to an initial water saturation of 18 to 30% PV using Ekofisk crude oil. Two re-aging techniques, proposed and used by others (Anderson 1986; Buckley, Bousseau et al. 1995), were employed: 1) aging for at least one year at room temperature, about 22°C, and 2) aging for 1000 hours at reservoir temperature. Re-aging was performed on Tor formation plugs (Graue and Baldwin 1995a), preserved Upper- and Lower- Ekofisk formation, Ekofisk core (Graue and Baldwin 1995b) and several outcrop chalks (Graue and Baldwin 1995c). The room temperature aging, although long, had no effect on the final production but affected the rate of imbibition. This decrease in imbibition rate was suspected to be the results of a thixatropic effect of the oil that occurred while the oil was static rather than a change of sample wettability (Graue and Baldwin 1995c). At elevated temperature, short-term aging made too large a change in apparent wettability, some of the aged plugs imbibed no water at all (Graue and Baldwin 1995b). These results indicated that these two proposed methods for reproducing the original wettability conditions were not adequate for controlled studies on our outcrop chalk. This led to development of a dynamic aging technique that produced controlled wettability alteration, in a reproducible manner, for outcrop chalk.

The aging technique was modified several times (Graue, Aspenes et al. 2002; Graue, Viksund et al. 1999a,c), and eventually consisted of continuously flowing crude oil while aging and reversing the direction of flow several times during the process (Aspenes, Graue et al. 2003). This method secured little or no spatial variation in wetting preference and was verified by in situ wettability characterization using MRI and NMR T_2 measurements, (Johannesen, Steinsbø et al. 2006; Johannesen 2008). Currently, it is possible to reproducibly alter outcrop Rørdal chalk to reflect uniform wettability distribution at any desired wettability with a water index (I_w) from 1.0 to < 0.1 (Fernø, Torsvik et al. 2010). A sample with an I_w=1.0 is highly water-wet, while one with $I_w = 0.8$ to 0.4 is moderately water-wet and $I_w < 0.3$ represents a nearly neutral-wet core. Repeated wettability tests of oil recovery by spontaneous imbibition of water in core samples aged at different initial water saturation and varying length of the aging period confirmed that the established wetting preference in the laboratory was stable within $I_w \pm 0.04$ during two cycles (Steinsbø, Graue et al. 2014).

18.2.4 Residual oil saturation: emphasis on capillary number and wettability

The ratio of the viscous to capillary forces, commonly denoted on the capillary number N_c, is crucial for the remaining oil saturation. The impact on residual oil saturation by a systematic increase in N_c, was determined in homogeneous chalk at wettabilities varying from nearly neutral-wet to strongly water-wet conditions. In fractured chalk reservoirs waterflood residual oil saturation is strongly dependent on the wettability. The current results provide assistance in determining the potential target for tertiary oil recovery by measuring the amount of mobile oil at various N_c values. A series of displacements of oil by water injection at increasing constant pressures has been carried out to determine the relation between remaining oil and applied differential pressure in waterfloods at different wettability conditions, (**Fig. 18.2**). Maximum oil recovery at constant differential pressures occurred at wettability conditions reflecting an Amott Index to water at 0.3. The residual oil saturation decreased with increasing capillary number and a significant amount of trapped oil after completed spontaneous water imbibition was mobilized at moderately water-wet to nearly neutral-wet conditions. Distinct dome shaped curves of oil recovery as function of wettability, which is consistent with increase in oil recovery with increasing capillary number, reflected similarities to earlier results on waterflooding oil recovery (Jadhunandan and Morrow 1995).

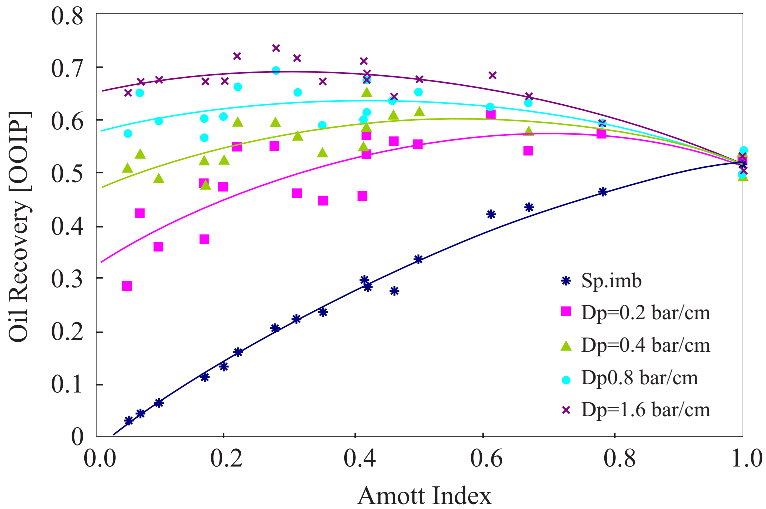

Figure 18.2: Waterflood oil recovery for different constant pressure injections and wettabilities, (Johannesen and Graue 2007).

18.3 Using visualization to study oil recovery mechanisms during waterfloods in chalk

18.3.5 Complementary imaging using MRI and NTI

The low permeability North Sea chalk reservoirs exhibit the characteristics of intense fracturing caused by tectonic activity. The tectonic history is very complex and consists of activities that induced an uplift of the graben margins that caused the chalk deposits to be buried deeper by gravity currents and associated slumping and sliding. As a result, the oil reserves in these reservoirs, found in the high porosity of the chalk matrix, are located in matrix blocks surrounded by interconnected fractures. At the University of Bergen, capillary continuity in such fractured chalk systems has been studied since the early 1990s. The core material used was mostly outcrop chalk obtained from the Portland quarry at Ålborg, Denmark. Portland chalk is of Maastrichtian age. It is characterized as fairly homogeneous and contains 99% calcite and 1% quartz and resembles the properties of the North Sea chalk on a microscopic level (Graue and Baldwin 1990). The porosity ranged from 40 to 50% and the permeability ranged from of 2-7 mD. Spontaneous imbibition of water from the fracture network into the matrix, and the subsequent movement of the expelled oil through the same fracture network is one of the production mechanisms. Imbibition studies and scaling helped to predict production rates. However, the effects of gravity and viscous displacement across fractures were not examined in these imbibition tests. Nuclear tracer imaging (NTI) and magnetic resonance (MRI) imaging were used in a complementary manner to study capillary continuity and block-to-block transfer at two different scales, (Aspenes, Ersland et al. 2008; Aspenes, Graue et al. 2002; Graue 1994, 1993; Graue, Aspenes et al. 2001a; Graue, Baldwin et al. 2003; Graue, Kolltveit et al. 1990; Graue, Viksund et al. 1999b). Blocks ($L \times H \times W = 20\,\text{cm} \times 10\,\text{cm} \times 5\,\text{cm}$) of fractured chalk served as models for fractured reservoir systems on the larger scale, (Haugen, Fernø et al. 2010). Complementary imaging has provided new and improved fundamental knowledge of fracture-matrix transfer and understanding of how oil recovery is affected by fractures. Magnetic Resonance Imaging (MRI) and Nuclear Tracer Imaging (NTI) enabled complementary investigations, (**Fig. 18.3**).

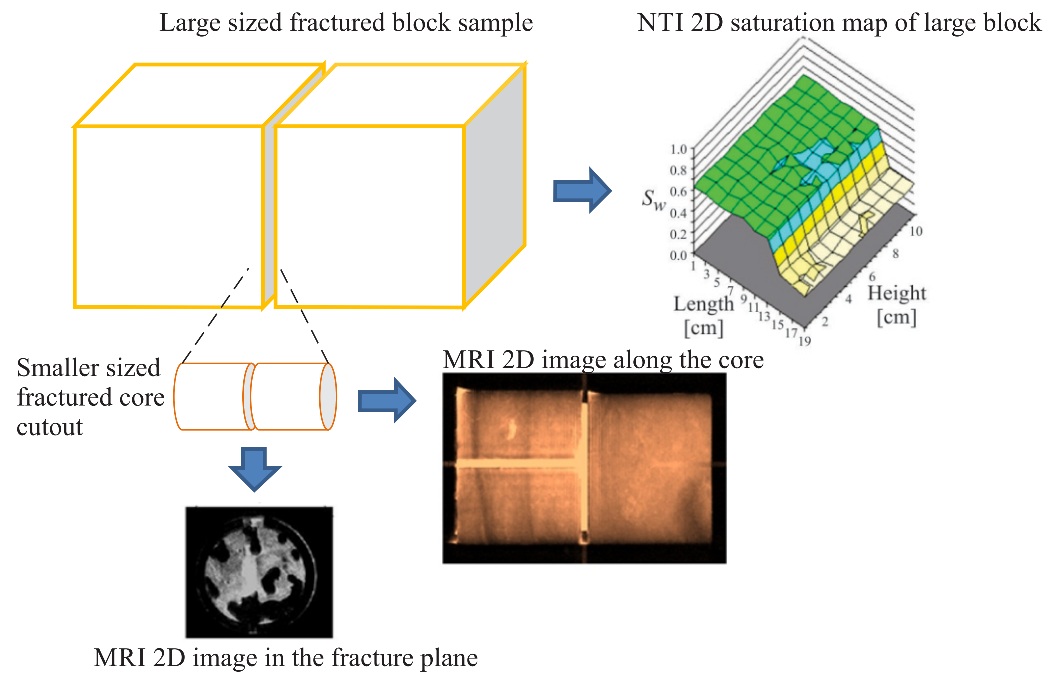

Figure 18.3: Complementary imaging of water flow in fractured chalk using NTI and MRI (Ersland, Fernø et al. 2010).

18.3.6 Large blocks of fractured chalk

The fractured blocks were formed by cutting the whole block and reassembling the parts to give open and 'closed' horizontal and vertical fractures. For the highly water-wet chalk, the fractures impeded and redirected water flow. In general, no fracture was crossed until the preceding matrix block was close to its final spontaneous imbibition endpoint, as shown in **Fig. 18.4** (left two columns) for the highly water-wet case. At strongly water-wet conditions, the dominating mechanism was spontaneous imbibition of water from fracture to matrix, displacing oil from each isolated matrix block until the endpoint for spontaneous imbibition was reached. At this point, the matrix capillary pressure was zero, and equal to the capillary pressure in the fracture. At moderately water-wet conditions, the presence of fractures was less prominent and water displaced oil with a uniform dispersed front. Water swept across fractures, through capillary contacts, increasing the total oil recovery by adding a viscous component to the displacement.

Fig. 18.4 shows the effect of wettability, and compares the dynamic in-situ imaging of water saturation development at various times, represented by various pore volumes (PV) of water injected, during waterfloods at strongly water-wet conditions (left) to moderately water-wet conditions (right) in fractured chalk blocks. The embedded fracture network was identical for both waterfloods and is indicated in first figure before start of waterflood. Moderately water-wet conditions reflect in this case an Amott-Harvey water index, I_w, of 0.6. As can be seen from Fig. 18.4, the waterfront propagation for the moderately water-wet block is much more uniform compared to the block by block displacement for the strongly water-wet case. This observation indicates that the recovery mechanisms change towards more viscous dominant flow regimes at less water-wet conditions.

Additional block experiments were performed to compare: 1) two methods of preparing 'closed' fractures in the blocks, 2) constant pressure versus constant rate waterfloods, 3) the role of chalk obtained from two different sources (Viksund, Graue et al. 1998) and 4) total recovery from whole and fractured blocks. There was no measurable difference between the saturation developments in blocks containing either coarse or smooth faces at the fracture. This suggested that the observed effect, i.e., lack of flow across a 'closed' fracture until the matrix nearly reached its imbibition endpoint for highly water-wet chalk, is a property of the matrix rather than the shape or roughness of its surface. No difference in saturation development was observed between waterflooding a block at a constant pressure differential versus constant flow rate, although the imbibition rate was slower for the constant pressure experiment (Aspenes, Ersland et al. 2008). No significant difference in oil recovery was observed between the fractured and un-fractured blocks at strongly water-wet conditions. At less water-wet conditions, the oil production was lower when the blocks were fractured implying that the fractures allowed the oil to be by-passed by the imbibing water. Experiments were made to specifically determine the impact of fracture-to-matrix permeability on total oil recovery and thereby determine whether viscous displace-

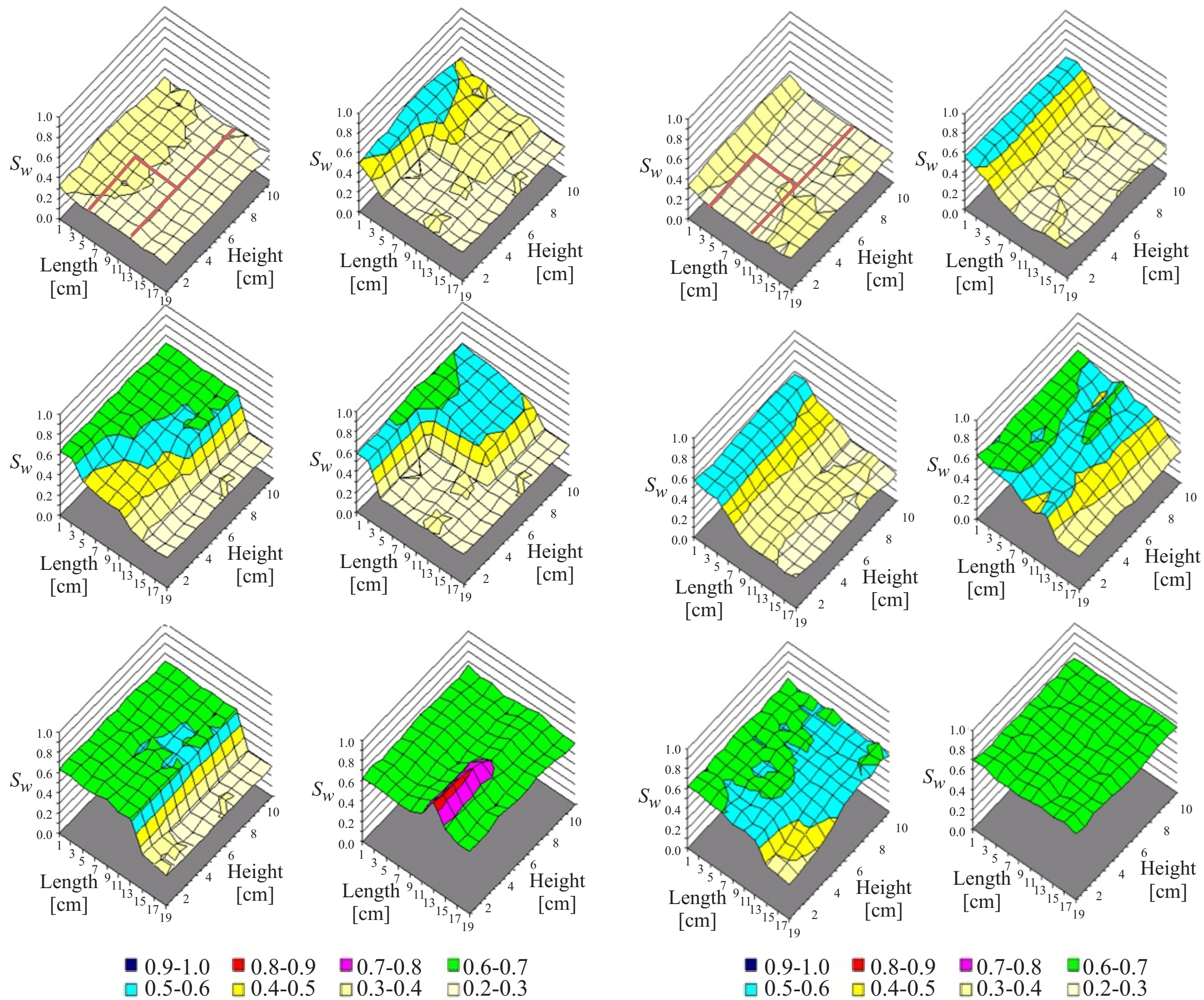

Figure 18.4: Nuclear Tracer Imaging of waterfloods in fractured chalk blocks. The waterfront propagation for the moderately water-wet block (right) is more uniform compared to the block by block displacement for the strongly water-wet case (left). The strongly water-wet case is shown in the two left columns, and the moderately water-wet case in the two right columns. Fracture configuration in water flood experiments are similar for the two experiments and indicated in first figure before the water flood started. Fracture marked with a double lined downstream was kept open using a spacer. The other fractures in the network were configured with matrix blocks face to face and confined with overburden pressure of approximately 10 bar (Ersland, Fernø et al. 2010).

ment contributed to the oil recovery in fractured chalk (Graue, Nesse et al. 2002a). The oil recovery depended on the fracture to matrix permeability ratio, were the increase in oil recovery with decreasing permeability ratio indicated that viscous displacement measurably added to the total oil production when the permeability ratio between the fracture system and the chalk matrix was less than 20 (Graue, Nesse et al. 2002b). Dania and Rørdal chalk were found to produce similar saturation development during constant rate waterfloods despite coming from different outcrop.

18.3.7 Numerical modeling of waterflooding fractured chalk blocks

The reason for determining field specific production mechanisms is to more accurately predict future reservoir performance and thus improve risk assessment. Numerical modeling (Graue, Moe et al. 2000; Haugen, Fernø et al. 2007, 2008) was performed using a compositional and black oil reservoir simulator with three input data sets: 1) both of the experimental P_c and k_r curves, 2) the experimental P_c curve and a k_r curve derived from history matching the production profile of the whole block and 3) the experimental k_r curve and a P_c curve derived from history matching the production profile of the whole block. This was done to determine whether it was possible to ascertain which of these input data could be most trusted. **Fig. 18.5** below show a comparison of experimental and simulated water saturation development in a fractured chalk block.

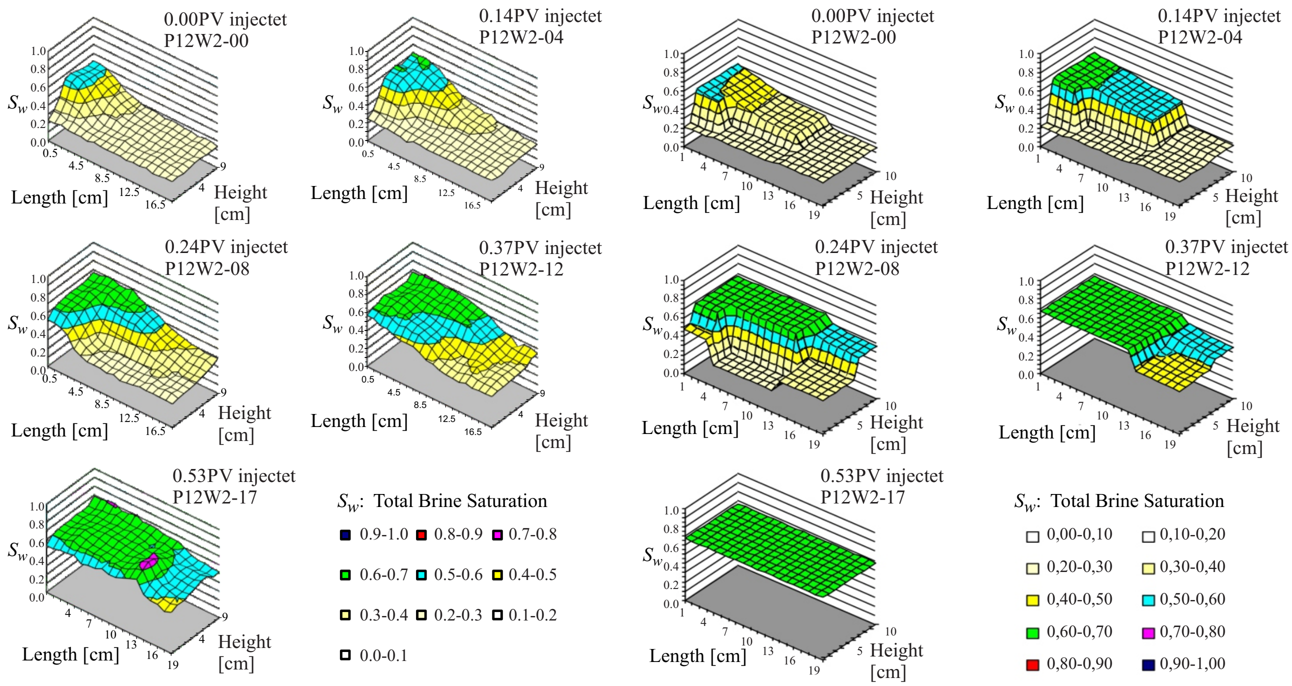

Figure 18.5: Comparison of experimental left two columns, and simulated, rightmost two columns saturation development for the second waterflood of a strongly water-wet block with fracture network indicated in first figure (Graue, Moe et al. 2000).

History matching both the production profile and the in-situ saturation distribution development gave higher confidence in the simulations. The numerical simulations indicated that the best matches were obtained using the experimental P_c data and the history matching k_r curve. When a good match of both the oil recovery profile and the in-situ fluid saturation development were obtained for the whole block, two fracture representations were used to model the fractured block. The first, a method based on history matching P_c in the fractures, had the most flexibility. The second method, representing the fractures by the fraction of effective matrix contact across them, was the easiest to use in the simulations and was based on a physical explanation that was consistent with the NTI and MRI experimental observations. An example of the fit to the 2-D saturation development is shown in Fig. 18.5 where the experimental observations are compared to the calculated saturation developments. Similar results were obtained for blocks with different wettabilities (Graue, Bognø et al. 2001; Graue, Moe et al. 2000; Moe, Graue et al. 2001). One major conclusion from these simulations was that currently available capillary pressure curve measurements, produced by commercial laboratories, could be used to give a good fit for chalk, but the relative permeability data, from the same source, did not provide as satisfactory match (Graue, Bognø et al. 2001; Moe, Graue et al. 2001).

18.3.8 Waterflood performance in fractured carbonate blocks: from strongly water-wet to oil-wet

Outcrop chalk may not be altered to oil-wet conditions using dynamic aging techniques. Chemical alteration of wettability to oil-wet conditions has been reported, but the relevance to reservoir conditions is not evident. To investigate how oil-wet conditions will affect waterflooding fractured rocks, outcrop limestone was used. This rock, Edward limestone from West Texas, has previously shown to be oil-wet after dynamic aging (Fernø, Ersland et al. 2007). **Fig. 18.6** illustrates how fractures impact waterflood oil recovery at oil-wet conditions, compared to strongly water-wet and less water-wet conditions.

Waterflood in fractured blocks

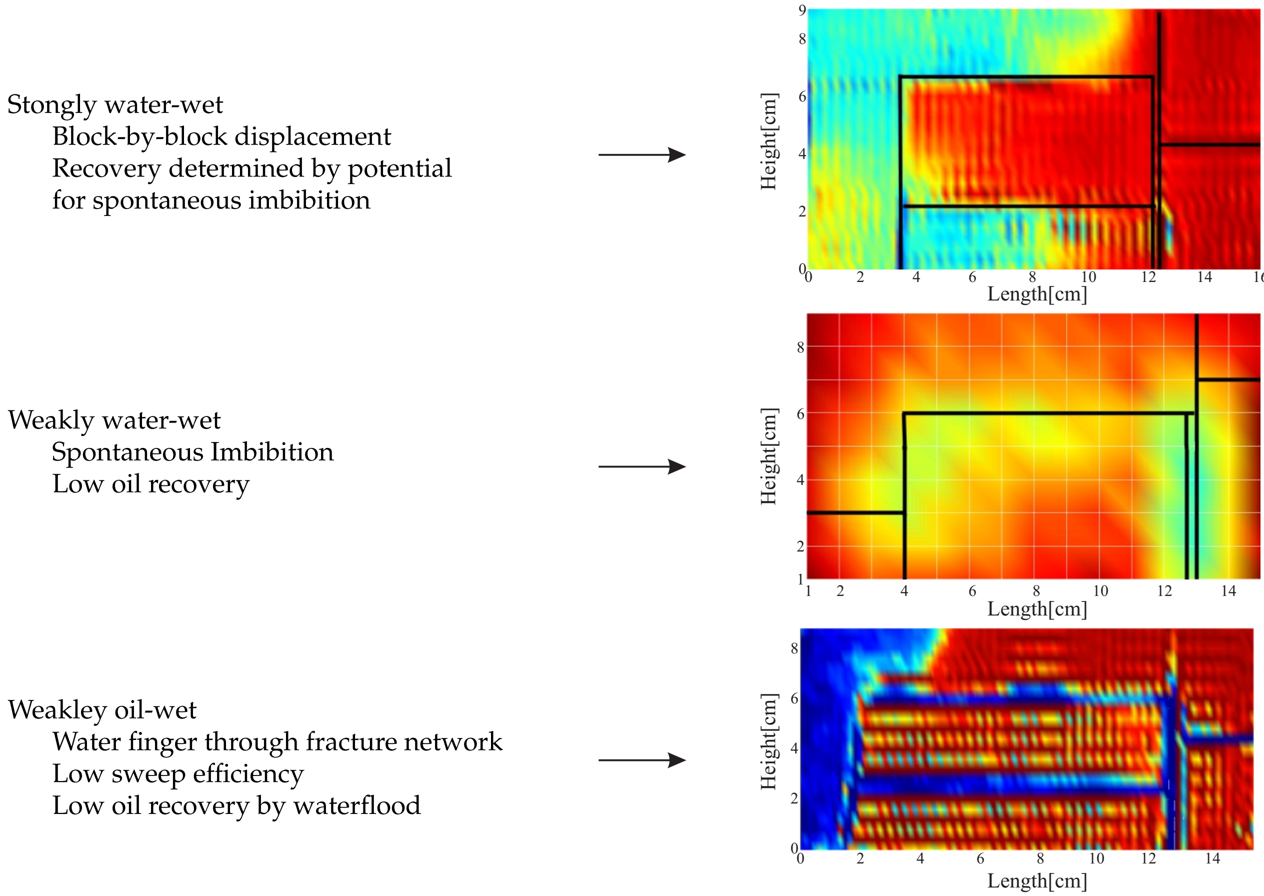

Figure 18.6: Impact from fractures on waterflood oil recovery at oil-wet conditions; compared to strongly water-wet and less water-wet conditions. Water saturation (blue) is measured with MRI for the three wetting states (Haugen, Fernø et al. 2010).

18.3.9 Capillary continuity - a view inside the fracture

NTI was used to study the impact of wettability on the saturation development in fractured systems, and the mechanisms for water transfer between fractures and the rock matrix. At strongly water-wet conditions, the first matrix block reached its imbibition potential ($P_c = 0$) before the water moved into the next matrix block. The oil was expelled on a block-by-block basis. At moderately water-wet conditions, however, the impact from fractures seemed to be less profound. Water moved across the fractures at lower water saturations, propagating through the system as in a continuous block, through capillary contacts (Graue, Bognø et al. 2001; Graue, Viksund et al. 1999b). The NTI method supplied quantitative information of saturations and flow behavior on a larger scale, but failed to monitor the saturation development inside the fractures. MRI was utilized to obtain a better spatial resolution for monitoring the detailed flow transfer mechanisms into and across the fractures. High spatial resolution MRI images were obtained of water saturation development inside an open fracture, that split a core plug in a vertical plane perpendicular to the direction of flow. Two distinct mechanisms for wetting phase transport were found (Aspenes, Ersland et al. 2008; Aspenes, Graue et al. 2002), corroborating the theory for obtaining capillary continuity by establishing wetting phase bridges, see **Fig. 18.7a**.

Two stacked core plugs, separated by an open fracture, were used to experimentally simulate the fractured system. **Fig. 18.7b** shows the orientation of the two plugs, the open fracture and the MRI slice used for these images.

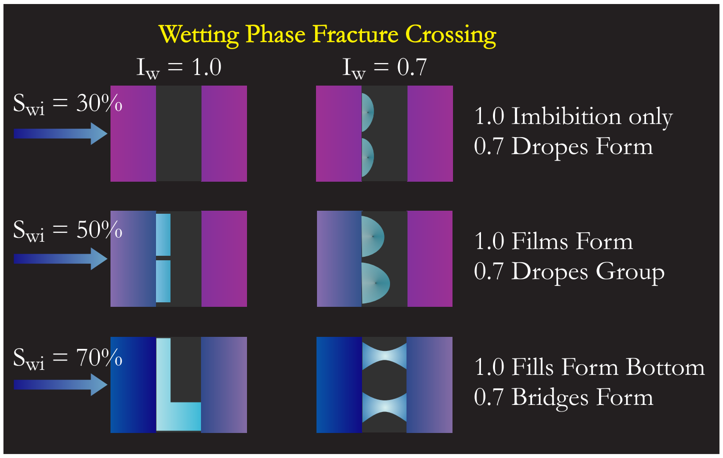

(a) Diagram illustrating the process of fracture crossing

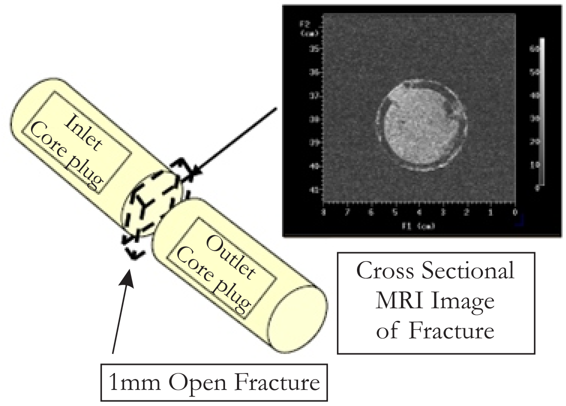

(b) Orientation of MRI slice (rectangular box) and sample MRI image showing oil filling the open fracture (Graue, Aspenes et al. 2001b).

Figure 18.7

Fractures were identified as these initially are filled with either oil or Deuterium (D_2O); heavy water is used to cancel MRI signals from the aqueous phase. Water was identified by only background signals, while oil appears as bright in the images. The MRI images of water saturation development in the fracture clearly revealed two distinct mechanisms for wetting phase transport in a stacked system with an open embedded fracture of 2–3 mm aperture. When strongly water-wet, the inlet plug reached its spontaneous imbibition endpoint (zero capillary pressure) before water entered the fracture. The water filled the fracture from the bottom and displaced the oil upwards at the rate of water injection. The water was detected as no signal (black) whereas the oil appeared bright on the MRI images, (**Fig. 18.8**).

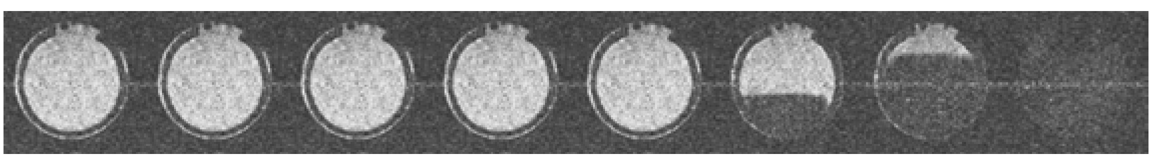

Figure 18.8: Facture filling in water-wet core (Aspenes, Graue et al. 2002).

For less water-wet conditions, (**Fig. 18.9**), water droplets formed on the exit face of the inlet plug and formed wetting phase bridges between the two plugs. This occurred before the inlet core reached its spontaneous imbibition endpoint. The fracture filled slowly, and the bridges increased in diameter and additional bridges formed. The capillary continuity of the wetting phase, transmitting differential pressure across the fracture, provided a viscous pressure component in the downstream plug that added to the total oil recovery beyond the spontaneous imbibition potential. These results corroborated the earlier larger scale NTI results and provided detailed dynamic information of the nature of flow across fractures for different wetting states.

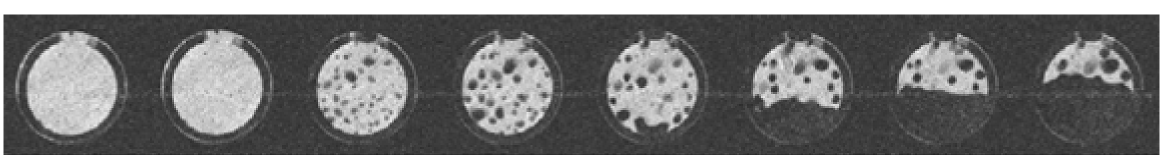

Figure 18.9: Fracture crossing in a moderately water-wet core (Aspenes, Graue et al. 2002).

18.3.10 Wetting phase bridges increase recovery

In the stacked core system above with one open fracture perpendicular to the flow direction, as shown in Fig. 18.8 and 18.9, water was ultimately forced to enter the downstream outlet core plug due to lack of alternative exits and a constant supply of water at the inlet end face. To create a model where individual matrix blocks were surrounded by fractures, a vertical fracture along the long axis of the outlet core piece established a system with isolated matrix blocks, (**Fig. 18.10**). This fracture provided an alternative path for the wetting phase to escape the system without going into the isolated matrices. The main objective was to see if stable wetting phase bridges still formed as observed in earlier stacked core experiments. In the previous MRI experiments, the core system was sleeved and the wetting phase was ultimately forced to cross the fracture into the next core. An open vertical slit from the transverse fracture to the outlet provides a path for the wetting phase to escape the system without going into the isolated matrices (Aspenes, Ersland et al. 2008). In that case, there would be no block-to block transfer and the contribution to oil recovery would be through imbibition only, (Fig. 18.10, right). However, if stable wetting phase bridges, observed in earlier stacked core experiments, formed across open fractures, a viscous force applied to the isolated matrices could increase recovery beyond the spontaneous imbibition potential, (Fig. 18.10, left).

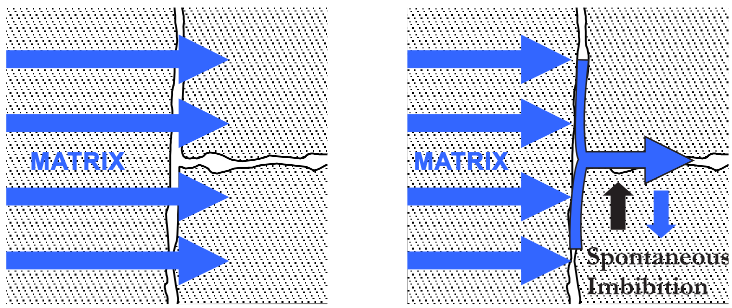

Figure 18.10: Schematic waterflood in fractured chalk with escape fracture. This experiment was designed to determine the role of wetting phase bridges on oil recovery.

Wetting phase bridges across open fractures formed despite having alternative outlets with higher flow properties (the escape fracture). The study also showed that the bridges added a viscous component to recovery of oil from the blocks surrounded by fractures. Water bridges were stable for days and resulted in oil recovery exceeding the spontaneous imbibition potential in excess of 10 percent. However, further increase in differential pressure did not increase the oil recovery from isolated blocks further. It seemed to be a threshold value for what the water bridges were able to exert on isolated matrix. When the differential pressure was increased by a factor of 10, from 0.2 psi to approximately 2 psi, no further oil was recovered from the isolated matrix blocks. The fluid saturation dynamics are shown by a series of images shown in **Fig. 18.11**. Each set of images corresponds to a time step; the large image showing the oil saturation distribution in the transverse open fracture and the associated smaller image shows the oil saturation in the inlet core and in the open vertical escape fracture separating the two core halves at the outlet of the stacked core system. In the transverse image, the flow direction is from the inlet plug, out of the image plane toward the reader to enter the outlet isolated plug halves. Because only bulk oil is imaged, dark spots represent water bridges while dark grey spots represent a water droplet that did not establish contact across the fracture. The black area surrounding the image is the spacer defining the open fracture. In the small image, showing the escape fracture, the injection of water is from the right through the un-fractured inlet block towards the open fracture on the left hand side of the image. Two experiments are presented in Aspenes, Ersland et al. (2008). The first were conducted with a low constant differential pressure and the second as a constant flow rate experiment at a much higher pressure. Fig. 18.11 shows the nature of wetting phase bridging in the constant rate experiment.

18.4 Mixing of injection and connate water during waterflooding

18.4.1 The influence of initial water saturation

The mixing of injection water and in-situ water and their saturation distributions during waterflooding were determined in chalk using NTI. One objective of this work was to determine when, or if, in-situ water, often considered immobile water, could be produced. Four different initial water saturations were used to determine the impact of initial water saturation on both water mixing and movement of the in-situ water at different wettabilities (Graue, Fernø et al. 2012a; Graue, Ramsdal et al. 2014). Injected and in situ water were labelled with separate radioactive tracers for the in-situ water and the injected water. The sample was prepared by saturating the sample with the in-situ water and bringing the sample to initial water saturation by flooding with decane.

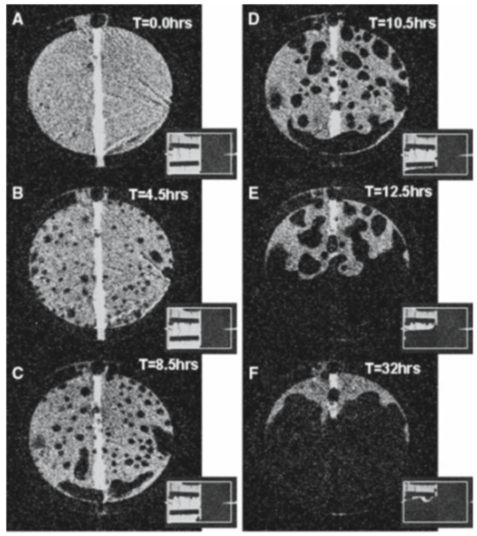

Figure 18.11: The in-situ saturation development inside a fracture during waterflood in chalk at near neutral, but slightly water-wet conditions ($I_w = 0.3$). Oil distribution in the transverse fracture (large image) and in the escape fracture (small image) during the water flood at constant rate. Water (D_2O) appears as the black phase (Aspenes, Ersland et al. 2008).

The sample was then water flooded with the injection water and both waters were monitored in the core and effluent using NTI. A bank of in-situ water formed ahead of the injection water, as can be seen in **Fig. 18.12** at strongly water-wet conditions. The maximum saturation of the bank increased with decreasing initial water saturation, while the length of the bank increased as S_{wi} increased. The produced water was initially pure in-situ water, followed by a mixed zone of both injection and in-situ water and finally pure injection water. All of the in-situ water, or at least, its dissolved salt was displaced in each of the waterfloods. The time lag between the production of the in-situ water and the injection water was dependent on the initial water saturation and wettability (Graue, Fernø et al. 2012b). These results imply that the so-called immobile or connate water, and/or its salts, can be displaced by the injection of water during a waterflood and may explain the observation of connate water salts in production wells after water break through. In addition, because of the formation of the in-situ water bank, the injection water may not contact the displaced oil. This observation has serious implications for the transport of chemicals to the water/oil interface by the injected water, as required for some proposed secondary and tertiary oil recovery processes.

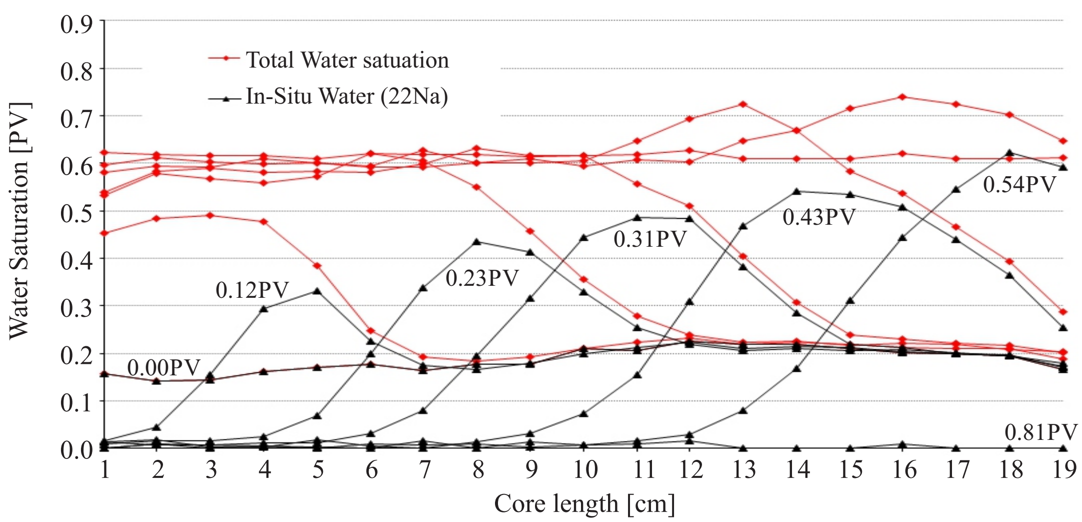

Figure 18.12: Mixing of injection water and in-situ water at strongly water-wet conditions.

18.4.2 The influence of wettability

Emphasizing the impacts by various wettability conditions on water mixing, experimental results of the mixing of injection water and in-situ water during oil production by waterflooding two outcrop chalk samples at three different wettabilities were performed (Graue, Fernø et al. 2012b). The displacement of in-situ, or "connate", water by the injected water was determined using nuclear tracer imaging (NTI). For all three wettabilities investigated, strongly water-wet ($I_w = 1.00$), moderately water-wet ($I_w = 0.44$) and less water-wet ($I_w = 0.28$) conditions, the connate water was fully removed from the core by the injected water. The connate water accumulated in front of the injected water, and constituted a large fraction of the water that immiscibly displaced the oil from the core plug. The connate water bank was less pronounced at reduced water-wet conditions, and the mixing between in-situ and injected water was increased at less water-wet conditions. Connate water breakthrough was observed at one mobile-oil-pore-volume of water injected at all three wettabilities. Breakthrough of the injected water was delayed at strongly water-wet conditions compared with less water-wet conditions, where both water phases were produced simultaneously.

18.4.3 Water mixing during spontaneous imbibition

The displacement of connate water by spontaneously imbibing water was determined at different wettability conditions (Graue and Fernø 2011). The development and distribution of both aqueous phases were determined by nuclear tracer imaging (NTI) to obtain 1D fluid saturation profiles. Two boundary geometries were applied to investigate the displacement and water mixing during strictly counter-current imbibition (One-End-Open: OEO) and during both co- and counter-current imbibition (Two-Ends-Open: TEO). The connate water was displaced from the open end face exposed to the invading water phase for both boundary geometries and all wettabilities, but the rate and displacement efficiency were highly influenced by the matrix wettability. The development of in-situ water saturation for a strongly water-wet case is shown in **Fig. 18.13**. The average connate water saturation did not change during spontaneous imbibition, but the distribution of the connate water changed as the invading water phase saturation increased in all tests. A connate water bank formed at strongly water-wet conditions for both boundary conditions. At the end of the test the connate water accumulated in the middle of the core at TEO imbibition and at the closed end face during OEO. In both cases the connate water accumulation constituted the entire fraction of water saturation, with little or no mixing between the connate and invading water phase during the displacement. At less water-wet conditions the connate water banking was reduced and the mixing of waters was increased. The invading water displacement of the in-situ water was also reduced, and the aqueous phases mixed by diffusion when redistribution of fluids stopped.

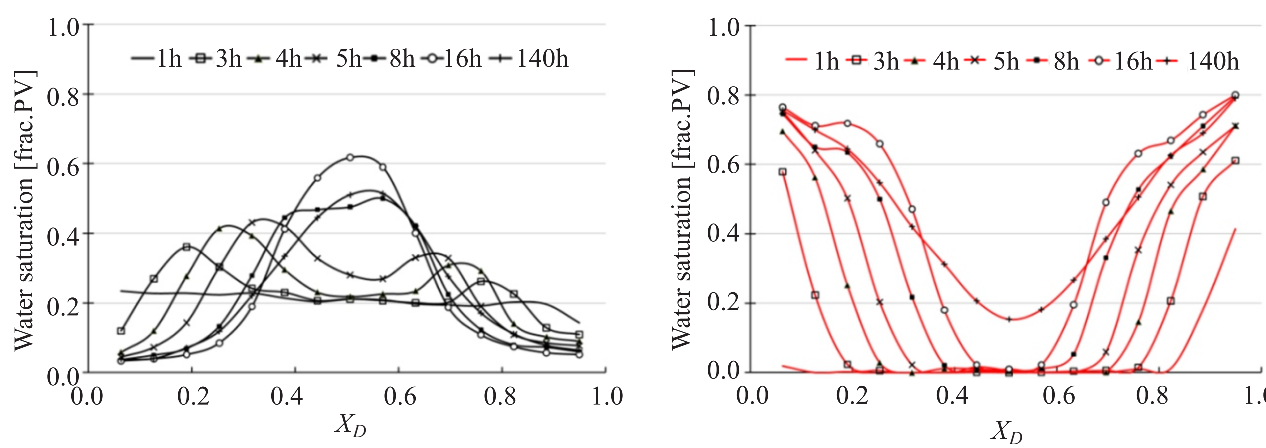

Figure 18.13: The development of in-situ water saturation (left) and invading water phase (right) as a function of dimensionless core length for strongly water-wet chalk sample C2 with the TEO boundary geometry during spontaneous imbibition (Graue and Fernø 2011).

18.5 Conclusions

- The imbibition differences between the different Ekofisk formations were not an artifact produced by sample storage or preservation.

- Production of oil by spontaneous imbibitions was observed in the laboratory for up to seven months, thus, short-term imbibition tests, couple of days, do not accurately reflect the spontaneous imbibition endpoint.
- Outcrop chalk was found that had pore characteristics and imbibition properties of highly water-wet Ekofisk reservoir chalk.
- The wettability of outcrop chalk could be altered to cover the range of wettabilities observed in North Sea reservoir chalk.
- Waterflooding of larger fractured, outcrop chalk blocks, as a function of wettability, showed that for highly water-wet chalk the fractured stopped water flow until the imbibition endpoint was reached, while for the same fracture orientation at less water-wet conditions the water crossed the fracture as if it were not there.
- Magnetic resonance imaging showed that water continuity could be achieved across fractures for less water-wet chalk by forming droplets on the outlet face of the initial matrix, which in turn formed bridges across the fracture and increased the recovery beyond the spontaneous imbibition potential.
- The water bridges formed across a fracture provide a mechanism for viscous displacement in fractured chalk and a lower residual oil endpoint.
- Preliminary attempts to use these water-crossing mechanisms in numerical modeling were successful at predicting both production and the in-situ saturation development inside the larger, fractured chalk block experiments.
- Independently monitoring both in-situ and injected water showed that an in-situ water bank formed ahead of the injected water, this explains the production of formation water during sea water injection and implies that the flowing oil may be isolated from the injected water.

Nomenclature

k_r = relative permeability, L^2
I_w = wettability index
N_c = capillary number
P_c = capillary pressure, m/Lt^2
S_w = water saturation

Subscripts

c = capillary
f = final
i = initial
r = relative
w = water, wettability

Abbreviation

MRI = magnetic resonamce imaging
NTI = nuclear tracer imaging
OEO = one-end-open
RDI = relative displacement index
TEO = two-end-open

References

Anderson, W.G., 1986. Wettability Literature Survey - Part 1: Rock/Oil/Brine Interaction and the Effects of Core Handling on Wettability. *Journal of Petroleum Technology*, **38** (10): 1125–1144. SPE-13932-PA. Octber. URL `http://dx.doi.org/10.2118/13932-pa`.

Aspenes, E., Ersland, G. et al., 2008. Wetting phase bridges establish capillary continuity across open fractures and increase oil recovery in mixed-wet fractured chalk. *Transport in Porous Media*, **74** (1): 35–47. URL http://dx.doi.org/10.1007/s11242-007-9179-3.

Aspenes, E., Graue, A., and Ramsdal, J., 2003. In situ wettability distribution and wetting stability in outcrop chalk aged in crude oil. *Journal of Petroleum Science and Engineering*, **39** (3): 337–350. URL http://dx.doi.org/10.1016/S0920-4105(03)00073-1.

Aspenes, E., Graue, A. et al., 2002. Fluid Flow in Fractures Visualized by MRI During Waterfloods at Various Wettability Conditions-Emphasis on Fracture Width and Flow Rate. In *SPE Annual Technical Conference and Exhibition*. Society of Petroleum Engineers. URL http://dx.doi.org/10.2118/77338-MS.

Buckley, J.S., Bousseau, C., and Liu, Y., 1995. Wetting Alteration by Brine and Crude Oil: From Contact Angles to Cores. Paper SPE 30765 presented at SPE Ann. Tech. Conf. and Exib., Dallas, TX, USA. 22 October. URL http://dx.doi.org/10.2118/30765-PA.

Ersland, G., Fernø, M.A. et al., 2010. Complementary imaging of oil recovery mechanisms in fractured reservoirs. *Chemical Engineering Journal*, **158** (1): 32–38. 15 March. URL http://dx.doi.org/10.1016/j.cej.2008.11.049.

Fernø, M.A., Ersland, G. et al., 2007. Impacts From Fractures On Oil Recovery Mechanisms In Carbonate Rocks At Oil-Wet And Water-Wet Conditions-Visualizing Fluid Flow Across Fractures With MRI. In *International Oil Conference and Exhibition in Mexico*. Society of Petroleum Engineers. URL http://dx.doi.org/10.2118/108699-MS.

Fernø, M.A., Torsvik, M. et al., 2010. Dynamic laboratory wettability alteration. *Energy & Fuels*, **24** (7): 3950–3958. URL http://dx.doi.org/10.1021/ef1001716.

Graue, A., 1993. Nuclear Tracer Saturation Imaging of Fluid Displacement in Low-Permeability Chalk. In *Low Permeability Reservoirs Symposium*. Society of Petroleum Engineers, Denver, Colorado. 26–28 April. URL http://dx.doi.org/10.2118/25899-MS.

Graue, A., 1994. Imaging the Effects of Capillary Heterogeneities on Local Saturation Development in Long Corefloods. *SPE Drilling & Completion*, **9** (01): 57–64. March. URL http://dx.doi.org/10.2118/21101-PA.

Graue, A., Aspenes, E. et al., 2001a. MRI tomography of saturation development in fractures during waterfloods at various wettability conditions. In *SPE Annual Technical Conference and Exhibition*. Society of Petroleum Engineers. URL http://dx.doi.org/10.2118/71506-MS.

Graue, A., Aspenes, E. et al., 2001b. MRI Tomography of Saturation Development in Fractures during Waterfloods at Various Wettability Conditions. Tech. rep., University of Bergen, Norway. Reservoir and Production Technology Report 17018, 13 August.

Graue, A., Aspenes, E. et al., 2002. Alteration of wettability and wettability heterogeneity. *Journal of Petroleum Science and Engineering*, **33** (1): 3–17. URL http://dx.doi.org/10.1016/S0920-4105(01)00171-1.

Graue, A. and Baldwin, B.A., 1990. Rock Properties and Fluid/Rock Characterization of Chalk Outcrop Materia. Tech. rep., University of Bergen, Norway. Production Technology Report 13222. 21 September.

Graue, A. and Baldwin, B.A., 1995a. The Significance of Aging on the Imbibition of Restored State, Tor Formation Ekofisk Core. Tech. rep., University of Bergen, Norway. Research and Services Report 15518, 2 February.

Graue, A. and Baldwin, B.A., 1995b. The Significance of Aging on the Imbibition of Restored State, Upper and Lower Ekofisk Formation, Ekofisk Core. Tech. rep., University of Bergen, Norway. Production Technology Report No. 15527, 12 April.

Graue, A. and Baldwin, B.A., 1995c. The Significance of Aging on the Imbibition of Various Outcrop Chalks Core. Tech. rep., University of Bergen, Norway. Production Technology Report No. 15543, 29 August.

Graue, A., Baldwin, B.A., and Weseloh, C.J., 1986. Imbibition and Relative Displacement Index of Restored State North Sea Chalk Core Samples from Well 2/4 A-6. Tech. rep., University of Bergen, Norway. Research and Services Report 2952. 28 August.

Graue, A., Baldwin, B.A. et al., 2003. Complementary imaging techniques applying NTI and MRI determined wettability effects on oil recovery mechanisms in fractured reservoirs. In *SCA annual conference, Pau, France*. Society of Core Analysts. 21–24 September.

Graue, A., Bognø, T. et al., 2001. Wettability effects on oil-recovery mechanisms in fractured reservoirs. *SPE Reservoir Evaluation & Engineering*, **4** (06): 455–466. URL http://dx.doi.org/10.2118/74335-PA.

Graue, A. and Fernø, M.A., 2011. Water mixing during spontaneous imbibition at different boundary and wettability conditions. *Journal of Petroleum Science and Engineering*, **78** (3): 586–595. URL http://dx.doi.org/10.1016/j.petrol.2011.07.013.

Graue, A., Fernø, M.A. et al., 2012a. Water Mixing During Waterflood Oil Recovery: The Effect of Initial Water Saturation. *SPE Journal*, **17** (01): 43–52. URL http://dx.doi.org/10.2118/149577-PA.

Graue, A., Fernø, M.A. et al., 2012b. Wettability effects on water mixing during waterflood oil recovery. *Journal of Petroleum Science and Engineering*, **94–95**: 89–99. September. URL http://dx.doi.org/10.1016/j.petrol.2012.06.020.

Graue, A., Kolltveit, K. et al., 1990. Imaging fluid saturation development in long-core flood displacements. *SPE Formation Evaluation*, **5** (04): 406–412. URL http://dx.doi.org/10.2118/17438-PA.

Graue, A., Moe, R. et al., 2000. Comparison of numerical simulations and laboratory waterfloods with in-situ saturation imaging of fractured blocks of reservoir rocks at different wettabilities. In *SPE International Petroleum Conference and Exhibition in Mexico*. Society of Petroleum Engineers. 1–3 Febryary. URL http://dx.doi.org/10.2118/59039-MS.

Graue, A., Nesse, K. et al., 2002a. Impact Of Fracture Permeability On Oil Recovery In Moderately-Water-Wet Fractured Chalk Reservoirs. Tech. rep., University of Bergen, Norway. Reservoir and Production Technology Report 17101, 13 May.

Graue, A., Nesse, K. et al., 2002b. Impact of fracture permeability on oil recovery in moderately water-wet fractured chalk reservoirs. In *SPE/DOE Improved Oil Recovery Symposium*. Society of Petroleum Engineers. URL http://dx.doi.org/10.2118/75165-MS.

Graue, A., Ramsdal, J., and Fernø, M.A., 2014. Mobilization of Immobile Water: Connate-Water Mobility During Waterfloods in Heterogeneous Reservoirs. *SPE Journal*, **20** (01): 88–98. URL http://dx.doi.org/10.2118/170249-PA.

Graue, A., Viksund, B.G., and Baldwin, B.A., 1999a. Reproducible wettability alteration of low-permeable outcrop chalk. *SPE Reservoir Evaluation & Engineering*, **2** (02): 134–140. URL http://dx.doi.org/10.2118/55904-PA.

Graue, A., Viksund, B.G. et al., 1999b. Large-Scale Two-Dimensional Imaging of Wettability Effects on Fluid Movement and Oil Recovery in Fractured Chalk. *SPE Journal*, **4** (01): 25–36. URL http://dx.doi.org/10.2118/54668-PA.

Graue, A., Viksund, B.G. et al., 1999c. Systematic wettability alteration by aging sandstone and carbonate rock in crude oil. *Journal of Petroleum Science and Engineering*, **24** (2): 85–97. URL http://dx.doi.org/10.1016/S0920-4105(99)00033-9.

Haugen, Å., Fernø, M.A., and Graue, A., 2007. Comparison of numerical simulations and laboratory waterfloods in fractured carbonates. In *SPE Annual Technical Conference and Exhibition*. Society of Petroleum Engineers, Anaheim, California, USA. 11–14 November. URL http://dx.doi.org/10.2118/110368-MS.

Haugen, Å., Fernø, M.A., and Graue, A., 2008. Numerical Simulation and Sensitivity Analysis of In Situ Fluid Flow in MRI Laboratory Waterfloods of Fractured Carbonate Rocks at Different Wettabilities. In *SPE Annual Technical Conference and Exhibition*. Society of Petroleum Engineers, Denver, Colorado, USA. 21–24 September. URL http://dx.doi.org/10.2118/116145-MS.

Haugen, Å., Fernø, M.A. et al., 2010. Wettability impacts on oil displacement in large fractured carbonate blocks. *Energy & Fuels*, **24** (5): 3020–3027. 20 April. URL http://dx.doi.org/10.1021/ef1000453.

Jadhunandan, P.P. and Morrow, N.R., 1995. Effect of wettability on waterflood recovery for crude-oil/brine/rock systems. *SPE reservoir engineering*, **10** (01): 40–46. SPE-22597-PA. February. URL `http://dx.doi.org/10.2118/22597-PA`.

Johannesen, E., Steinsbø, M. et al., 2006. Wettability characterization by NMR T2 measurements in chalk. In *International Symposium of the Society of Core Analysts, Trondheim, Norway*. Society of Core Analysts. SCA2006-39. 12–16 September. URL `http://www.researchgate.net/profile/James_Howard22/publication/267774101_WETTABILITY_CHARACTERIZATION_BY_NMR_T_2_MEASUREMENTS_IN_CHALK/links/551a99c70cf2f51a6fea78f6.pdf`.

Johannesen, E.B., 2008. *NMR characterization of wettability and how it impacts oil recovery in chalk*. Ph.D. thesis, Dept. of Physics and Technology. Bergen, University of Bergen.

Johannesen, E.B. and Graue, A., 2007. Systematic investigation of waterflood reducing residual oil saturations by increasing differential pressures at various wettabilities. In *Offshore Europe*. Society of Petroleum Engineers, Aberdeen, Scotland, U.K. 4–7 September. URL `http://dx.doi.org/10.2118/108593-MS`.

Lie, M.K., 1995. *Evaluation of outcrop chalk as analogues for north sea chalk reservoirs*. Master's thesis, Master Thesis in Reservoir Physics at University of Bergen (in Norwegian).

Moe, R., Graue, A. et al., 2001. Numerical Simulation of Waterfloods in Fractured Chalk at Moderately-Water-Wet Conditions. Tech. rep., University of Bergen. Reservoir and Production Technology Report 16429. 24 January.

Steinsbø, M., Graue, A., and Fernø, M.A., 2014. A systematic investigatin of wetting stability in aged chalk. In *International Symposium of the Society of Core Analysts*. Society of Core Analysts, Avignon, France. SCA2014-037. 8–12 September. URL `https://www.researchgate.net/profile/Martin_Ferno/publication/275153582_A_Systematic_Investigation_of_Wetting_Stability_in_Aged_Chalk/links/5534e51e0cf2df9ea6a3f22f.pdf`.

Viksund, B.G., Graue, A. et al., 1998. 2-D Imaging of Waterflooding Fractured Chalk Blocks, Part III: Fracture Roughness, Waterflood Method and Chalk Source. Tech. rep., . Reservoir and Production Technology Report 15709. 18 May.

Chapter 19

Surfactant Flooding

Ingebret Fjelde

19.1 Introduction

The wettability of the reservoir rocks controls the fluid distributions and the flow properties in the reservoir rocks (Willhite 1986; Jadhunandan and Morrow 1995). It affects most of the petrophysical properties including capillary pressure, relative permeability, electrical properties, waterflooding behavior and enhanced oil recovery (EOR) mechanisms (Zhou, Morrow et al. 2000; Morrow and Mason 2001; Tong, Morrow et al. 2003; Hirasaki and Zhang 2004). Many of the carbonate reservoirs are naturally fractured, and they typically have high permeability fractures and low permeability rock matrix (Akbar, Chakravorty et al. 2000; Roehl and Choquette 2012; Chilingar and Yen 1983). Many of these carbonate reservoirs have wettability in the range mixed-wet to oil-wet. The high matrix and fracture permeability contrast and the mixed-wet to oil-wet characteristics often lead to poor waterflooding efficiency in these reservoirs. The wettability of the chalk fields on the Norwegian Continental Shelf (NCS) is in general more water-wet than the other types of carbonate reservoirs. E.g., the Ekofisk field has been reported to have wettability in the range from strongly water-wet to neutral (mixed-wet) (Hamon 2004; Spinler, Zornes et al. 2000; Hallenbeck, Sylte et al. 1991), and the Valhall field has been characterized with wettability in the range from weakly water-wet to slightly oil-wet (Eltvik, Skoglunn et al. 1990; Springer, Olsen et al. 1996; Webb, Black et al. 2005).

When the Ekofisk field development was approved and commissioned by pressure depletion, the estimated oil recovery was 18 OOIP% (Jensen, Harpole et al. 2000). The fractured network in the Ekofisk field was identified early (Hamon 2004; Thomas, Dixon et al. 1987). The waterflooding potential in the Ekofisk field was evaluated, and waterflooding pilots were carried out. The potential for waterflooding was first shown in a pilot in the Tor formation (Hallenbeck, Sylte et al. 1991) and later in pilots in the Ekofisk formation (Sylte, Hallenbeck et al. 1988; Sulak 1991; Hermansen, Thomas et al. 1997). Due to the promising pilots, waterflooding has been implemented in the whole Ekofisk field. The extensive waterflooding of the field has increased the current oil recovery estimate to 50 %OOIP (NPD 2004). Early in the waterflood it was belived that the main recovery mechanisms in waterflooding the Ekofisk field was spontaneous imbibition (Hamon 2004; Thomas, Dixon et al. 1987). The focus for the EOR research was therefore first to alter the wettability to more water-wet and thereby improve the spontaneous imbibition of water (Jensen, Harpole et al. 2000). Wettability alteration by surfactants was therefore studied in many projects (Milter and Oxnevad 1996; Standnes and Austad 2000). Later viscous flooding of the rock matrix has been found to also be an important recovery mechanism in waterflooding of the Ekofisk field, especially in the less fractured parts of the field. Results from pore network simulations show the variation in spontaneous imbibition, residual oil saturation (S_{orw}) and relative permeability of water at S_{orw} ($k_{rw}(S_{orw})$) in the Ekofisk field, **Fig. 19.1** (Hamon 2004).

The fracture characteristics and wettability are today known to vary in the chalk fields on the NCS. In the more fractured zones/formations, spontaneous imbibition is the dominating recovery mechanism during waterflooding, but viscous flooding of the rock matrix dominates in the less fractured zones/formations. The largest potential for altering the wettability to more water-wet conditions by surfactants, have the less water-wet zones dominated by spontaneous imbibition. In the less fractured zones, the surfactant may reduce the interfacial tension (σ) and thereby reduce S_{or}. These two types of surfactant flooding are presented in the two next sections.

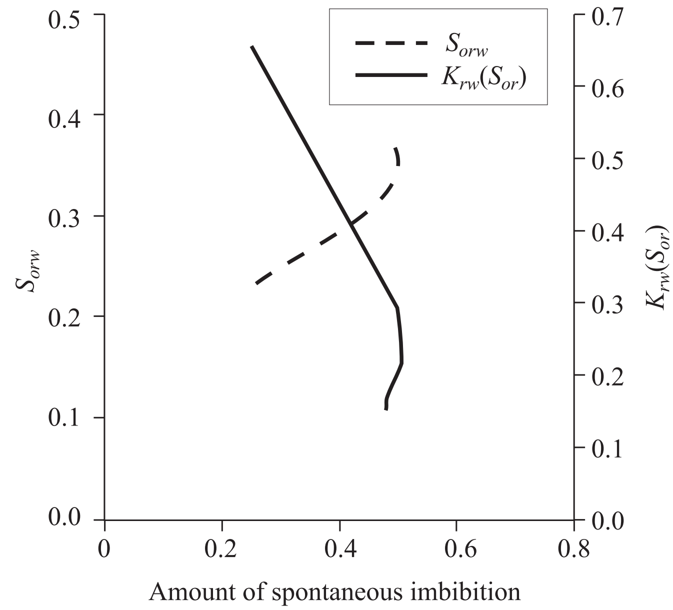

Figure 19.1: Pore network simulations show variation in spontaneous imbibition, S_{orw} and $k_{rw}(S_{orw})$ in the Ekofisk field Hamon (2004).

19.2 Surfactant flooding in chalk dominated by spontaneous imbibition

Since the chalk reservoirs on the NCS were first characterized to be fractured with spontaneous imbibition as the dominating recovery mechanism in waterflooding, the main EOR focus was to alter the wettability to more water-wet condition and thereby improve spontaneous imbibition. Surfactant structures were therefore screened for their potential to improve spontaneous imbibition (Austad, Milter et al. 1997; Standnes and Austad 2000). Dimensionless time (t_D) can be used to scale spontaneous imbibition results to correct for important parameters like dimensions, permeability, porosity, σ and viscosities (Zhou, Morrow et al. 2000):

$$t_D = t\sqrt{\frac{k}{\phi}}\frac{\sigma}{\sqrt{\mu_w\mu_o}}\frac{1}{L_c^2}, \tag{19.1}$$

where t is imbibition time, k is permeability, ϕ is porosity (fraction), σ is interfacial tension, μ_w is viscosity of water phase, μ_o is viscosity of oil phase, and L_c is core characteristic length. L_c is defined by:

$$L_c = \sqrt{\frac{V}{\sum_{i=1}^{n}\frac{A_j}{X_{ai}}}}, \tag{19.2}$$

where V is bulk volume of core samples, A_i is area perpendicular to the i'th imbibition direction and X_{Ai} is distance from A_i to the no-flow boundary.

Even though the surfactants mainly should alter the wettability, they will also reduce σ between the oil and water phases and reduce the spontaneous imbibition rate. This was not observed for the cationic surfactants of type alkyltrimethylammonium that were the first surfactant products evaluated in laboratory experiments (Austad, Milter et al. 1997; Standnes and Austad 2000, 2003). These surfactants gave moderat σ reduction between oil and water phases, from 20–30mN/m in the water/oil-system down to 1–5mN/m in the surfactant/oil-systems. They were found to alter the wettability of chalk to more water-wet and thereby to increase the spontaneous imbibition of water. Oil properties, brine composition, temperature, rock properties, rock composition and surfactant concentration are reported to be important for this type of wettability alteration. Examples of spontaneous imbibition experiments with the surfactant dodecyltrimethyl ammonium bromide are shown in **Fig. 19.2**. When this surfactant was added to the brine, the spontaneous imbibition was faster and higher than for the brine. Improvement in the spontaneous imbibition rate was also observed when the brine was replaced by the surfactant solution. Wettability alteration of chalk and other carbonate rocks by anionic and nonionic surfactants has also been reported in the literature (Spinler, Zornes et al. 2000; Seethepalli, Adibhatla et al. 2004; Xie, Weiss et al. 2004; Sharma, Mohanty et al. 2013; Chen and Mohanty 2013; Babadagli

2006). In some studies, reduction in spontaneous imbibition rate has been reported, e.g., Zhou, Morrow et al. (2000).

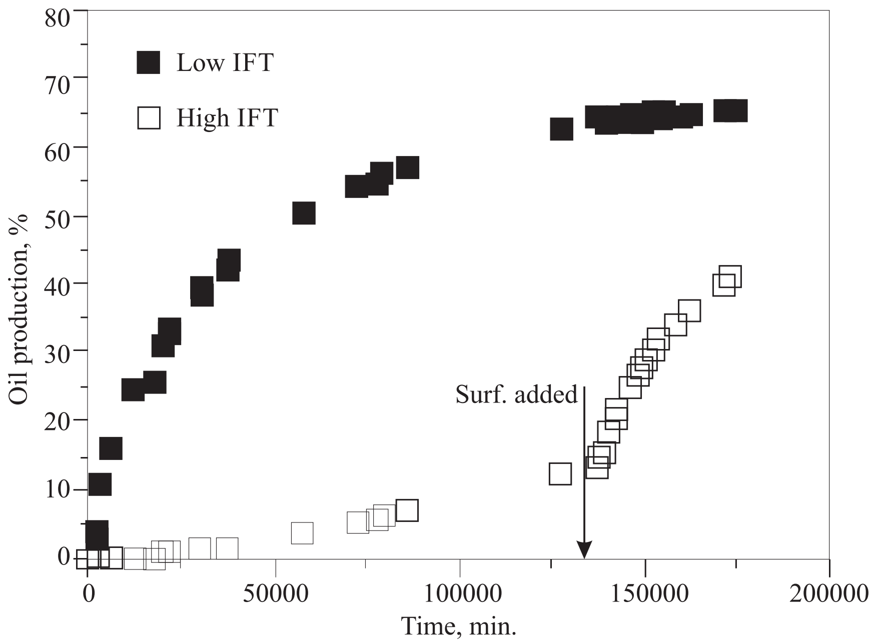

Figure 19.2: Comparison of spontaneous imbibition of brine (high IFT) and cationic surfactant solution (low IFT) Austad, Milter et al. (1997).

When the capillary forces are reduced, the gravity may become dominant (Masalmeh and Oedai 2009). The ratio between gravitational and capillary forces in a porous medium can be described by the dimensionless Bond number (B_o), defined by:

$$B_o = \frac{\Delta \rho g L^2}{\sigma}, \tag{19.3}$$

where $\Delta\rho$ is difference in density of the two phases, g is gravitational acceleration, L the characteristic length and σ the interfacial tension.

Reduction of the σ will increase the Bond number. The Bond number in spontaneous imbibition experiments with limestone was low ($B_0 = 10^{-7}$–10^{-6}) with brine (20–30mN/m), but was higher with moderate σ reduction (1–5mN/m) ($B_o = 10^{-5}$–10^{-4}) (Fjelde 2004). Gravity forces become important for Bond number above 10^{-5} (Chen, Lucas et al. 2000). The gravity forces can therefore be important in spontaneous imbibition experiments (Rostami Ravari, Strand et al. 2011). Spontaneous imbibition results have also been scaled by including the effect of gravity in the dimensionless time (Morrow and Xie 2001). Surfactant can also be used in surfactant-enhanced gravity drainage in carbonate rocks (Masalmeh and Oedai 2009).

19.3 Surfactant flooding in chalk dominated by viscous flooding of matrix

Surfactant flooding with low σ has the potential to reduce S_{or} of the rock matrix and thereby improve the oil recovery (Iglauer, Wu et al. 2010; Rao, Ayirala et al. 2006; Reppert, Bragg et al. 1990; Maerker, Gale et al. 1992; Alveskog, Holt et al. 1998). The theory for surfactant flooding was developed for water-wet sandstone reservoirs where the residual oil left after waterflooding is trapped as discontinuous droplets (Zolotukhin and Ursin 2000; Chatzis and Morrow 1984). These droplets can be mobilized by increasing the ratio between viscous and capillary forces, defined by the capillary number (N_c). Several definitions of N_c are in use (Iglauer, Wu et al. 2010; Rao, Ayirala et al. 2006; Lake 1989; Delshad, Bhuyan et al. 1986; Chatzis and Morrow 1984; Stegemeier 1974). The most common one is:

$$N_c = \frac{v\mu}{\sigma}, \tag{19.4}$$

where v is the Darcy velocity, μ is the flowing phase viscosity, and σ the interfacial tension between the two phases. N_c can also be defined as (Delshad, Bhuyan et al. 1986; Mohanty and Salter 1983):

$$N_c^{'} = \frac{k\Delta P}{L\sigma}, \tag{19.5}$$

where k is the permeability of the porous media, L its length, ΔP the differential pressure and σ the interfacial tension between the two phases.

The potential for surfactant flooding is often described by the capillary desaturation curve (CDC) which gives S_{or} as function of N_c, see **Fig. 19.3** (Lake 1989). The typical, and commonly accepted, shape of the CDC suggests that S_{or} is at a plateau at low N_c-values until a critical N_c value (N_{cc}) is reached. At N_c above N_{cc}, S_{or} decreases and tends to zero at large N_c values. In waterflooding of the main parts of the oil reservoir, N_c is low. By adding surfactants to the injected water, the σ between oil and water can significantly be reduced, and N_c is increased above N_{cc}. The σ between the reservoir oil and brine is typically in the range 20–30mN/m. To achieve very low S_{or}, σ often has to be reduced by a factor in the range 10^3–10^5.

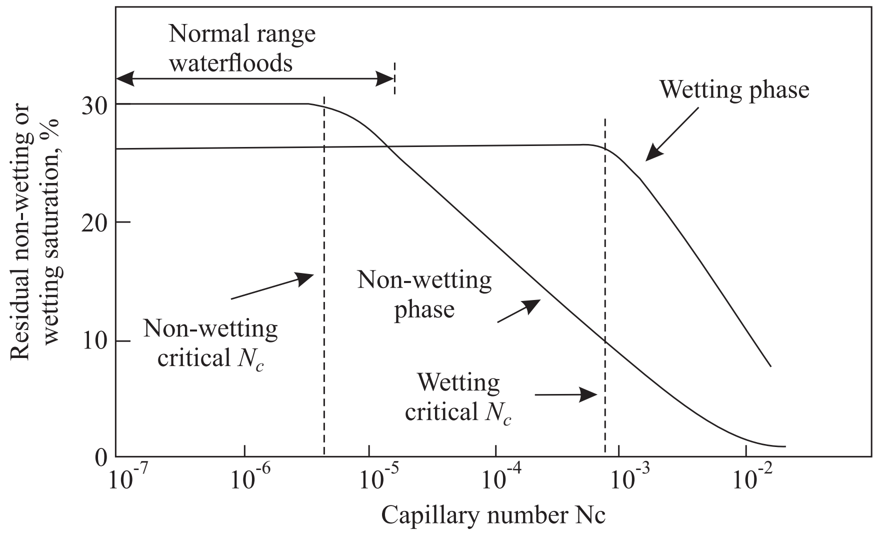

Figure 19.3: Capillary desaturation curves Lake (1989).

Many surfactant flooding studies have been carried out based on the assumption that the sandstone reservoirs are strongly water-wet. Today many of the sandstone oil reservoirs are characterized as mixed-wet. The mixed-wet conditions were first described by Salathiel et al. (1973). Still the commonly accepted practice is that the CDC concept, for strongly water-wet conditions, is adapted and used for other wettability conditions. Lake (1989) indicated that the CDC for a wetting phase should be at N_c 1–3 log-units higher than for the non-wetting phase (Fig. 19.3). Waterflooding and surfactant flooding experiments were performed in water-wet and mixed-wet Berea outcrop sandstone, and in mixed-wet reservoir sandstone rock (Fjelde, Lohne et al. 2015). At mixed-wet conditions, S_{or} was not reached with realistic injection volumes. For both waterflooding and surfactant flooding the remaining oil saturation (ROS) was found to strongly depend on the volumes injected. Typical CDC shapes were obtained for similar core plugs at water-wet conditions (See **Fig. 19.4a**). When ROS was plotted vs N_c, atypical CDC shapes were obtained at mixed-wet conditions (See **Fig. 19.4b**). The focus should therefore be on the alteration of k_r-curves by the surfactant rather than reduction of S_{or}. In the same paper it is shown that simulation of surfactant flooding in mixed-wet formations require a fair representation of the N_c-dependent k_r-curvature. It was also recommended by Fjelde, Lohne et al. (2015) to always evaluate capillary end effects to secure that additional oil production due to reduced end effects is not erroneously included in the surfactant flooding potential.

Even though the chalk reservoirs are not characterized as strongly water-wet, they are often preferential water-wet (on the water-wet side). Atypical CDC has been measured for chalk rocks. An example of CDC for a reservoir chalk (Fjelde 2008) is given in **Fig. 19.5**. Similar atypical CDC has been reported for limestones, see **Fig. 19.6** (Kamath, Meyer et al. 2001). When atypical CDC shape is measured for chalks or other carbonate rocks, similar procedure as recommended for mixed-wet sandstone should be used (Fjelde, Lohne et al. 2015).

Screening of surfactant systems with low σ to be used in surfactant flooding of the carbonate rock matrix, can be done as screening of surfactant systems for surfactant flooding of sandstone rocks. The relationship between the surfactant structure and the performance can be used to develop the surfactant formulation (Adkins, Arachchilage et al. 2012; Solairaj, Britton et al. 2012). The σ should be low in the surfactant flooding, and the surfactant retention should be low. Increase in pH to above pH=9 by adding an alkaline, can alter the charge of carbonate minerals from positive to negative and reduce the retention of anionic surfactants (Hirasaki and Zhang 2004). This can also alter the wettability to more water-wet. Increase in pH to this level is not possible in sea water, but is possible after softening of the sea water. The selected surfactant structures should be stable at

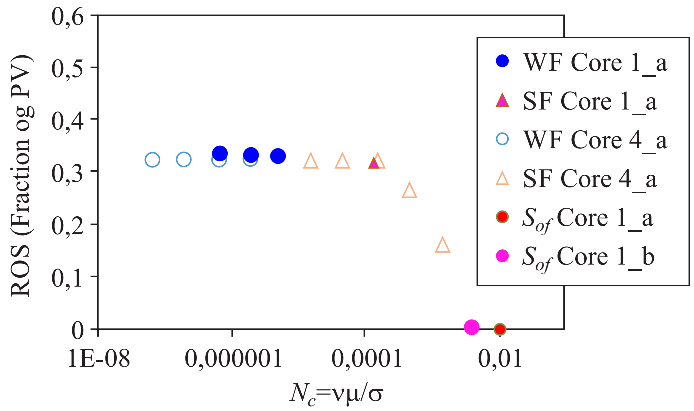

(a) Water-wet

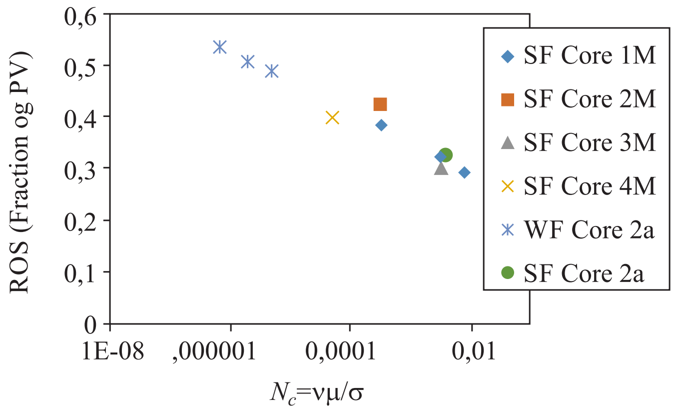

(b) Mixed-wet

Figure 19.4: Measured CDC (ROS vs N_c) during waterflooding (WF) and surfactant flooding (SF): a. Water-wet conditions and b. Mixed-wet conditions. ROS is plotted because the true S_{or} was not reached in the floods at mixed-wet conditions. Surfactant solution in equilibrium with STO, except core 2a (S_{of} is S_o determined by accessible water volume) Fjelde, Lohne et al. (2015).

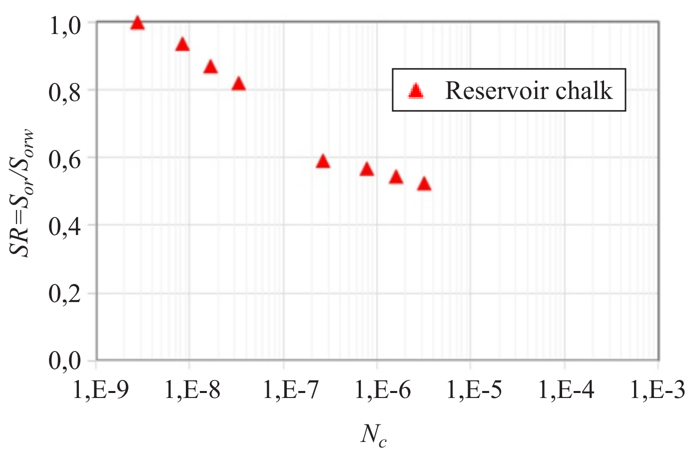

Figure 19.5: Measured CDC for reservoir chalk (Fjelde 2008). SR is S_{or} normalized with respect to measured S_{orw} for waterflooding at lowest N_c.

reservoir conditions. The surfactant system should not cause formation damage, and should give high recovery in core floods. The surfactant formulation should also be environmentally acceptable.

In surfactant flooding of sandstone reservoirs, it is crucial to have good mobility control to obtain high recovery (Lake 1989). A polymer is then injected behind the surfactant slug and also in the surfactant slug if necessary. The size of the polymer molecules/structures that is usually used for mobility control in sandstone rocks, can be larger than 1μm (Sorbie 1991). This is larger or in the same range as the pore throats of chalk rocks

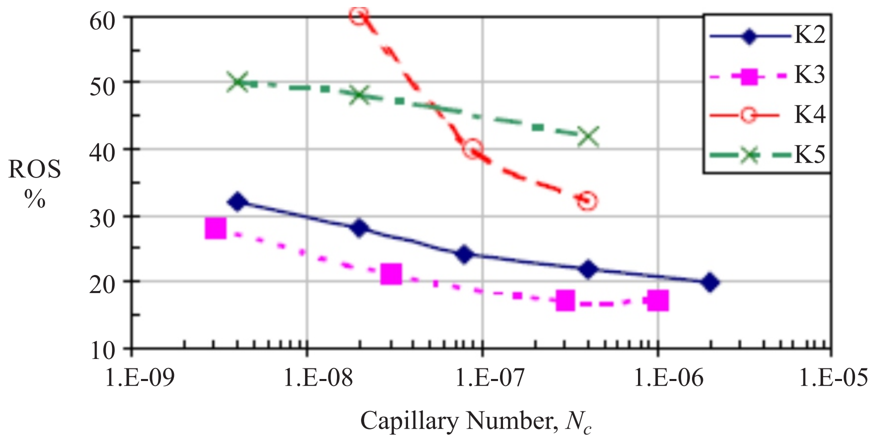

Figure 19.6: CDC for different types of limestones Kamath, Meyer et al. (2001).

(Milter and Oxnevad 1996). These EOR-polymers may therefore not enter the chalk matrix. It is also important that the transport of oil from the rock matrix to the fractures is not reduced by the polymer. To improve the displacement in the rock matrix, the polymer has to enter the matrix. Polymers with lower molecular weights than the standard EOR-polymers are therefore required for mobility control in surfactant flooding of chalk matrix. Very few polymer floods have been carried out in carbonate rocks and then with permeability higher than 10mD (Sheng, Leonhardt et al. 2015). This permeability is higher than the permeability of the chalk matrix. Examples of injection of polymer in carbonate rocks can be found in the literature, but with higher permeability than of the chalk matrix. The NVP ter-polymer Superpusher SAV301 was injected to the Estalliada carbonate rock with permeability of 150mD (Kulawardana, Koh et al. 2012), and sulfonated polyacrylamide was injected to reservoir carbonate with permeability of 135–633mD (Wang, Han et al. 2015).

19.4 Combination of wettability alteration and low interfacial tension

Change in brine composition has also been reported to alter the wettability of chalk to more water-wet and increase the spontaneous imbibition (Strand, Standnes et al. 2003; Puntervold and Austad 2007; Yu, Evje et al. 2008b; Yu, Kleppe et al. 2008; Yu, Evje et al. 2008a; Fjelde and Aasen 2009). As mention above, increase in pH can also alter the wettability of carbonate rocks (Hirasaki and Zhang 2004). Combination of wettability alteration by optimized water composition or wettability modifier chemicals, and surfactant flooding at reduced σ may be beneficial. Alteration of wettability to more water-wet condition can accelerate the production due to k_{ro} improvement and/or improve the spontaneous imbibition, while the σ reduction can reduce S_{or} in the chalk matrix.

Nomenclature

A_i = area perpendicular to the i'th imbibition direction, [L^2]
B_o = Bound number
g = acceleration of gravity, [L/t^2]
k = permeability, [L^2], mD
k_{ro} = relative permeability to oil, [L^2], mD
k_{rw} = relative permeability to water, [L^2], mD
L = length, characteristic length, [L]
L_c = core characteristic length, [L]
N_c = capillary number
N_{cc} = critical capillary number
S_{or} = residual oil saturation
S_{orw} = residual oil saturation after waterflooding
SR = normalized residual oil saturation
t = time, [t], min
t_D = time dimensionless
v = Darcy velocity, [L/t]

V = bulk volume, [L^3]
X_{A_i} = distance from A_i to the no-flow boundary
$\Delta\rho$ = difference in density of the two phases, [m/L^3]
ΔP = differential pressure, [m/L^2]
μ = viscosity, [m/Lt], cp
μ_o = viscosity of oil phase, [m/Lt], cp
μ_w = viscosity of water phase, [m/Lt], cp
ϕ = porosity
σ = interfacial tension, [m/t^2], mN/m

Abbreviations

CDC = desaturation curve
EOR = enhanced oil recovery
NCS = Norwegian continental shelf
ROS = remaining oil saturation
SF = surfactant flooding
STO = standard stocktank oil
WF = water flooding

References

Adkins, S., Arachchilage, P. et al., 2012. Development of thermally and chemically stable large-hydrophobe alkoxy carboxylate surfactants. In *SPE Improved Oil Recovery Symposium*. Society of Petroleum Engineers, Tulsa, Oklahoma, USA. SPE-154256-MS. 14–18 April. URL `http://dx.doi.org/10.2118/154256-MS`.

Akbar, M., Chakravorty, S. et al., 2000. Unconventional approach to resolving primary and secondary porosity in Gulf carbonates from conventional logs and borehole images. In *Abu Dhabi International Petroleum Exhibition and Conference*. Society of Petroleum Engineers, Abu Dhabi, United Arab Emirates. SPE-87297-MS. 13–15 October. URL `http://dx.doi.org/10.2118/87297-MS`.

Alveskog, P.L., Holt, T., and Torsæter, O., 1998. The effect of surfactant concentration on the Amott wettability index and residual oil saturation. *Journal of Petroleum Science and Engineering*, **20** (3): 247–252. 3–4 June. URL `http://dx.doi.org/10.1016/S0920-4105(98)00027-8`.

Austad, T., Milter, J. et al., 1997. Spontaneous imbibition of water into low permeable chalk at different wettabilities using surfactants. In *International Symposium on Oilfield Chemistry*. Society of Petroleum Engineers, Houston, Texas. SPE-37236-MS. 18–21 February. URL `http://dx.doi.org/10.2118/37236-MS`.

Babadagli, T., 2006. Evaluation of the critical parameters in oil recovery from fractured chalks by surfactant injection. *Journal of Petroleum Science and Engineering*, **54** (1): 43–54. 1–2 November. URL `http://dx.doi.org/10.1016/j.petrol.2006.07.006`.

Chatzis, I. and Morrow, N.R., 1984. Correlation of capillary number relationships for sandstone. *Society of Petroleum Engineers Journal*, **24** (05): 555–562. SPE-10114-PA. October. URL `http://dx.doi.org/10.2118/10114-PA`.

Chen, H., Lucas, L. et al., 2000. Laboratory monitoring of surfactant imbibition using computerized tomography. In *SPE International Petroleum Conference and Exhibition in Mexico*. Society of Petroleum Engineers, Villahermosa, Mexico. SPE-59006-MS. 1–3 Ferbruary. URL `http://dx.doi.org/10.2118/59006-MS`.

Chen, P. and Mohanty, K., 2013. Surfactant-mediated spontaneous imbibition in carbonate rocks at harsh reservoir conditions. *SPE Journal*, **18** (01): 124–133. SPE-153960-PA. January. URL `http://dx.doi.org/10.2118/153960-PA`.

Chilingar, G.V. and Yen, T.F., 1983. Some Notes on Wettability and Relative Permeabilities of Carbonate Reservoir Rocks, II. *Energy Sources*, **7** (1): 67–75. October. URL `http://dx.doi.org/10.1080/00908318308908076`.

Delshad, M., Bhuyan, D. et al., 1986. Effect of capillary number on the residual saturation of a three-phase micellar solution. In *SPE Enhanced Oil Recovery Symposium*. Society of Petroleum Engineers, Tulsa, Oklahoma. SPE-14911-MS. 20–23 April. URL `http://dx.doi.org/10.2118/14911-MS`.

Eltvik, P., Skoglunn, T., and Skinnarland, O., 1990. Valhall waterflood pilot - a study of water injection in a fractured reservoir. 11–12 June.

Fjelde, I., 2004. IRIS-report. Tech. rep., IRIS.

Fjelde, I., 2008. IRIS-report. Tech. rep., IRIS.

Fjelde, I., Lohne, A. et al., 2015. Critical Aspects in Surfactant Flooding Procedure at Mixed-wet Conditions. In *EUROPEC 2015*. Society of Petroleum Engineers, Madrid, Spain. SPE-174393-MS. 1–4 June. URL `http://dx.doi.org/10.2118/174393-MS`.

Fjelde, I.F. and Aasen, S.M.A., 2009. Improved Spontaneous Imbibition of Water in Reservoir Chalks. In *IOR 2009 - 15th European Symposium on Improved Oil Recovery*. EAGE. 27 April. URL `http://dx.doi.org/10.3997/2214-4609.201404826`.

Hallenbeck, L.D., Sylte, J.E. et al., 1991. Implementation of the Ekofisk field waterflood. *SPE Formation Evaluation*, **6** (03): 284–290. SPE-19838-PA. September. URL `http://dx.doi.org/10.2118/19838-PA`.

Hamon, G., 2004. Another Look at Ekofisk Wettability. SCA2004-01. 5–9 October.

Hermansen, H., Thomas, L.K. et al., 1997. Twenty five years of Ekofisk reservoir management. In *SPE Annual Technical Conference and Exhibition*. Society of Petroleum Engineers, Society of Petroleum Engineers (SPE), San Antonio, Texas. SPE-38927-MS. 5–8 October. URL `http://dx.doi.org/10.2118/38927-MS`.

Hirasaki, G.J. and Zhang, D.L., 2004. Surface Chemistry of OIl Recovery From Fractured, Oil-Wet, Carbonate Formations. *SPE Journal*, **9** (02): 151–162. SPE-88365-PA. URL `http://dx.doi.org/10.2118/88365-PA`.

Iglauer, S., Wu, Y. et al., 2010. New surfactant classes for enhanced oil recovery and their tertiary oil recovery potential. *Journal of Petroleum Science and Engineering*, **71** (1): 23–29. 1–2 March. URL `http://dx.doi.org/10.1016/j.petrol.2009.12.009`.

Jadhunandan, P.P. and Morrow, N.R., 1995. Effect of wettability on waterflood recovery for crude-oil/brine/rock systems. *SPE reservoir engineering*, **10** (01): 40–46. SPE-22597-PA. February. URL `http://dx.doi.org/10.2118/22597-PA`.

Jensen, T.B., Harpole, K.J., and Østhus, A., 2000. EOR Screening for Ekofisk. In *SPE European Petroleum Conference*. Society of Petroleum Engineers, Paris, France. SPE-65124-MS. 24–25 October. URL `http://dx.doi.org/http://dx.doi.org/10.2118/65124-MS`.

Kamath, J., Meyer, R.F., and Nakagawa, F.M., 2001. Understanding waterflood residual oil saturation of four carbonate rock types. In *SPE Annual Technical Conference and Exhibition*. Society of Petroleum Engineers, New Orleans, Louisiana. SPE-71505-MS. 30 September – 3 October. URL `http://dx.doi.org/10.2118/71505-MS`.

Kulawardana, E.U., Koh, H. et al., 2012. Rheology and transport of Improved EOR polymers under harsh reservoir conditions. In *SPE Improved Oil Recovery Symposium*. Society of Petroleum Engineers, Tulsa, Oklahoma, USA. SPE-154294-MS. 14–18 April. URL `http://dx.doi.org/10.2118/154294-MS`.

Lake, L.W., 1989. *Enhanced oil recovery*. Old Tappan, New Jersey, Prentice Hall Inc. URL `http://www.osti.gov/scitech/biblio/5112525`.

Maerker, J., Gale, W. et al., 1992. Surfactant flood process design for Loudon. *SPE reservoir engineering*, **7** (01): 36–44. SPE-20218-PA. February. URL `http://dx.doi.org/10.2118/20218-PA`.

Masalmeh, S.K. and Oedai, S., 2009. Surfactant Enhanced Gravity Drainage: Laboratory Experiments and Numerical Simulation Model. SCA2009-06. 27–30 September.

Milter, J. and Oxnevad, I.E.I., 1996. Spontaneous imbibition in two different chalk facies. *Petroleum Geoscience*, **2** (3): 231–240. August. URL `http://dx.doi.org/10.1144/petgeo.2.3.231`.

Mohanty, K.K. and Salter, S.J., 1983. Multiphase flow in porous media: III. Oil mobilization, transverse dispersion, and wettability. In *SPE Annual Technical Conference and Exhibition*. Society of Petroleum Engineers, San Francisco, California. SPE-12127-MS. 5–8 October. URL `http://dx.doi.org/10.2118/12127-MS`.

Morrow, N.R. and Mason, G., 2001. Recovery of oil by spontaneous imbibition. *Current Opinion in Colloid & Interface Science*, **6** (4): 321–337. August. URL `http://dx.doi.org/10.1016/S1359-0294(01)00100-5`.

Morrow, N.R. and Xie, X., 2001. Oil recovery by spontaneous imbibition from weakly water-wet rocks. *Petrophysics*, **42** (04): 313–322. SPWLA-2001-v42n4a1. July. URL https://www.onepetro.org/journal-paper/SPWLA-2001-v42n4a1.

NPD, 2004. *Petroleum resources on the Norwegian Continental Shelf. Fields and discoveries*. Norwegian Petroleum Directorate. URL http://www.npd.no/Global/Engelsk/3-Publications/Resource-report/Resource-report-2014/Resources-2014-nett.pdf.

Puntervold, T. and Austad, T., 2007. Injection of seawater and mixtures with produced water into North Sea chalk formation: Impact on wettability, scale formation and rock mechanics caused by fluid-rock interaction. In *SPE/EAGE Reservoir Characterization and Simulation Conference*. Society of Petroleum Engineers, Abu Dhabi, UAE. SPE-111237-MS. 28–31 October. URL http://dx.doi.org/10.2118/111237-MS.

Rao, D.N., Ayirala, S.C. et al., 2006. Impact of low-cost dilute surfactants on wettability and relative permeability. In *SPE/DOE Symposium on Improved Oil Recovery*. Society of Petroleum Engineers, Tulsa, Oklahoma, USA. SPE-99609-MS. 22-26 April. URL http://dx.doi.org/10.2118/99609-MS.

Reppert, T., Bragg, J. et al., 1990. Second Ripley surfactant flood pilot test. In *SPE/DOE Enhanced Oil Recovery Symposium*. Society of Petroleum Engineers, Tulsa, Oklahoma. SPE-20219-MS. 22-25 April. URL http://dx.doi.org/10.2118/20219-MS.

Roehl, P.O. and Choquette, P.W., 2012. *Carbonate petroleum reservoirs*. Springer Science & Business Media, New York.

Rostami Ravari, R., Strand, S., and Austad, T., 2011. Combined surfactant-enhanced gravity drainage (SEGD) of oil and the wettability alteration in carbonates: the effect of rock permeability and interfacial tension (IFT). *Energy & Fuels*, **25** (5): 2083–2088. URL http://dx.doi.org/10.1021/ef200085t.

Salathiel, R. et al., 1973. Oil recovery by surface film drainage in mixed-wettability rocks. *Journal of Petroleum Technology*, **25** (10): 1–216. SPE-4104-PA. October. URL http://dx.doi.org/10.2118/4104-PA.

Seethepalli, A., Adibhatla, B. et al., 2004. Physicochemical interactions during surfactant flooding of fractured carbonate reservoirs. *SPE journal*, **9** (04): 411–418. SPE-89423-PA. December. URL http://dx.doi.org/10.2118/89423-PA.

Sharma, G., Mohanty, K. et al., 2013. Wettability alteration in high-temperature and high-salinity carbonate reservoirs. *SPE Journal*, **18** (04): 646–655. SPE-147306-PA. April. URL http://dx.doi.org/10.2118/147306-PA.

Sheng, J.J., Leonhardt, B. et al., 2015. Status of polymer-flooding technology. *Journal of Canadian Petroleum Technology*, **54** (02): 116–126. SPE-174541-PA. March. URL http://dx.doi.org/10.2118/174541-PA.

Solairaj, S., Britton, C. et al., 2012. New correlation to predict the optimum surfactant structure for EOR. In *SPE Improved Oil Recovery Symposium*. Society of Petroleum Engineers, Tulsa, Oklahoma, USA. SPE-154262-MS. 14–18 April. URL http://dx.doi.org/10.2118/154262-MS.

Sorbie, K.S., 1991. *Polymer-Improved Oil Recovery*. Blackie and Sons Ltd., Glasgow, Scotland.

Spinler, E., Zornes, D. et al., 2000. Enhancement of oil recovery using a low concentration of surfactant to improve spontaneous and forced imbibition in chalk. In *SPE/DOE Improved Oil Recovery Symposium*. Society of Petroleum Engineers, Tulsa, Oklahoma. SPE-59290-MS. 3–5 April. URL http://dx.doi.org/10.2118/59290-MS.

Springer, N., Olsen, D. et al., 1996. Rock mechanics and water injection: Chalk characterization and description. 7–9 October.

Standnes, D.C. and Austad, T., 2000. Wettability alteration in chalk: 2. Mechanism for wettability alteration from oil-wet to water-wet using surfactants. *Journal of Petroleum Science and Engineering*, **28** (3): 123–143. November. URL http://dx.doi.org/10.1016/S0920-4105(00)00084-X.

Standnes, D.C. and Austad, T., 2003. Wettability alteration in carbonates: Interaction between cationic surfactant and carboxylates as a key factor in wettability alteration from oil-wet to water-wet conditions. *Colloids and Surfaces A: Physicochemical and Engineering Aspects*, **216** (1): 243–259. 15 April. URL http://dx.doi.org/10.1016/S0927-7757(02)00580-0.

Stegemeier, G.L., 1974. Relationship of trapped oil saturation to petrophysical properties of porous media. In *SPE Improved Oil Recovery Symposium*. Society of Petroleum Engineers, Tulsa, Oklahoma. SPE-4754-MS. 22-24 April. URL http://dx.doi.org/10.2118/4754-MS.

Strand, S., Standnes, D.C., and Austad, T., 2003. Spontaneous imbibition of aqueous surfactant solutions into neutral to oil-wet carbonate cores: Effects of brine salinity and composition. *Energy & fuels*, **17** (5): 1133–1144. July. URL http://dx.doi.org/10.1021/ef030051s.

Sulak, R.M., 1991. Ekofisk Field: the First 20 years. *JPT*, **43** (10): 1265–1271. SPE-20773-PA. October. URL http://dx.doi.org/10.2118/20773-PA.

Sylte, J., Hallenbeck, L. et al., 1988. Ekofisk formation pilot waterflood. In *SPE Annual Technical Conference and Exhibition*. Society of Petroleum Engineers, Houston, Texas. SPE-18276-MS. 2–5 October. URL http://dx.doi.org/10.2118/18276-MS.

Thomas, L.K., Dixon, T.N. et al., 1987. Ekofisk Waterflood Pilot. *Journal of Petroleum Technology*, **39** (02): 221–232. SPE-13120-PA. February. URL http://dx.doi.org/10.2118/13120-PA.

Tong, Z., Morrow, N., and Xie, X., 2003. Spontaneous imbibition for mixed-wettability states in sandstones induced by adsorption from crude oil. *Journal of Petroleum Science and Engineering*, **39** (3): 351–361. September. URL http://dx.doi.org/10.1016/S0920-4105(03)00074-3.

Wang, J., Han, M. et al., 2015. Surfactant Adsorption in Surfactant-Polymer Flooding for Carbonate Reservoirs. In *SPE Middle East Oil & Gas Show and Conference*. Society of Petroleum Engineers, Manama, Bahrain. SPE-172700-MS. 8–11 March. URL http://dx.doi.org/10.2118/172700-MS.

Webb, K.J., Black, C.J.J. et al., 2005. A laboratory study investigating methods for improving oil recovery in carbonates. In *International Petroleum Technology Conference*. International Petroleum Technology Conference, Doha, Qatar. IPTC-10506-MS. 21–23 November. URL http://dx.doi.org/10.2523/IPTC-10506-MS.

Willhite, G.P., 1986. *Waterflooding*, vol. 3. Society of Petroleum Engineers, Richardsion, Texas. URL http://store.spe.org/Waterflooding--P81.aspx.

Xie, X., Weiss, W.W. et al., 2004. Improved oil recovery from carbonate reservoirs by chemical stimulation. In *SPE/DOE Symposium on Improved Oil Recovery*. Society of Petroleum Engineers, Tulsa, Oklahoma. SPE-89424-MS. 17–21 April. URL http://dx.doi.org/10.2118/89424-MS.

Yu, L., Evje, S. et al., 2008a. Analysis of the Wettability alteration process during seawater imbibition into preferentially oil-wet chalk cores. In *SPE Symposium on Improved Oil Recovery*. Society of Petroleum Engineers, Tulsa, Oklahoma, USA. SPE-113304-MS. 20–23 April. URL http://dx.doi.org/10.2118/113304-MS.

Yu, L., Evje, S. et al., 2008b. Wettability Alteration by Spontaneous Imbibition of Sulphate Containing Water onto Chalk Core with Different Boundary Conditions. SCA2008-42. 29 October – 2 Novemberb. URL https://www.researchgate.net/profile/Svein_Skjaeveland/publication/264264117_Wettability_alteration_by_spontaneous_imbibition_of_sulphate_containing_water_onto_chalk_core_with_different_boundary_conditions._SCA2008-42/links/54770bf50cf245eb43729bb5.pdf.

Yu, L., Kleppe, H. et al., 2008. Modelling of wettability alteration processes in carbonate oil reservoirs. *Networks and Heterogeneous Media*, **3** (1): 149. URL http://jgmaas.com/SCA/2008/SCA2008-42.pdf.

Zhou, X., Morrow, N.R. et al., 2000. Interrelationship of wettability, initial water saturation, aging time, and oil recovery by spontaneous imbibition and waterflooding. *SPE Journal*, **5** (02): 199–207. SPE-62507-PA. June. URL http://dx.doi.org/10.2118/62507-PA.

Zolotukhin, A.B. and Ursin, J.R., 2000. *Introduction to Petroleum Reservoir Engineering*. Høyskoleforlaget AS — Norwegian Academic Press, Norway.

Chapter 20

Sweep Improvements: Mobility and Conformance Control

Dimitrios Georgios Hatzignatiou

20.1 Introduction

One of the big challenges engineers face with water and EOR-agent flooding is related to injectant's higher mobility compared to formation oil, causing it breakthrough at production wells before adequately sweeping to the reservoir, thus bypassing large volumes of formation oil. The presence of reservoir heterogeneities (such as natural fractures, faults, high permeability zones, etc.) and density difference between displacing and displaced fluid exacerbate the injectant's tendency to contact and mobilize oil only from parts of the formation (Sorbie 1991).

Waterflood of the Ekofisk field, for example, has been proven a success significantly improving oil recovery factors through a combination of waterflooding, well stimulation and monitoring, extensive infill drilling, and overall field optimization (Thomas, Dixon et al. 1987; Hermansen, Thomas et al. 1997; Hermansen 2008). This is in addition to arresting formation collapsing experienced during the pre-water injection period. However, the increase of water production is rapid during the last few years and means for addressing water production levels while maintaining/improving oil production need to be identified and field implemented. In the meantime large amounts of oil remain in the formation due to reservoir heterogeneities (e.g., natural fractures), injected water's mobility and fluids segregation in the formation. Injected water flows mainly through the fractured network and previously unswept formation areas, thus getting re-circulated. This decreases formation sweep, does not contribute effectively in the mobilization of formation oil, increases oil production cost (fluid lifting, separation and water re-injection) with consequences well documented in the literature.

Reduced sweep of an oil-bearing formation occurs both due to reservoir heterogeneities and injected fluid mobility compared to formation oil which results to viscous fingering phenomena even in homogeneous formations. In reality there is a combined effect of these factors which yields reduced sweep efficiencies and large volumes of remaining oil. For the case of reservoir heterogeneities, conformance control techniques can be employed to isolate highly conductive paths and divert the injected fluids to unswept formation regions. Such techniques include use of organic or inorganic gels which can be selectively placed in the formation, either near the wellbore or deep in the formation to address unwanted fluids (water and/or gas) production. With regards to mobility of the injected fluid, polymers or foams can be used for water- or gas- based injected fluid, respectively, to reduce its mobility, dampen viscous fingering phenomena, increase formation sweep and thus recovery of remaining oil.

This chapter aims at addressing means and technologies to divert injected fluids away from existing highly-conductive paths (faults, extended natural fractures and/or networks, highly conductive reservoir layers) into reservoir regions which remain unswept - conformance control - thus (a) reducing the amount of circulated, and at the same time inefficient, volume of injected fluids and (b) increasing the reservoir sweep efficiency, and thus oil production and oil recovery factors. In addition, means of controlling viscous fingering phenomena, by engaging fluids (polymers, foams) that delay and control the progress (speed) of the injected water or EOR fluids, will also be addressed as processes for improving oil recovery while reducing breakthrough times and produced volumes of injected fluids. Emphasis will be placed in naturally fractured, carbonate reservoirs.

20.2 Key technical issues

The key EOR issue is that the injected fluids should contact and mobilize waterflood residual or remaining oil in the fractured chalk reservoir. For example injected fluid should (a) not flow preferentially through the fracture system, (b) under multiphase flow conditions be able to imbibe into the matrix blocks (not prevented/restricted by capillary forces) in relatively high process (not like diffusion), and (c) contact and mobilize residual oil. Addressing these issues at laboratory scale is the first step. Upscaling the lab results to field scale with a subsequent validation with a pilot testing is very important for a successful application of this technology.

Critical operational and logistical issues for implementing a selected EOR process need to be examined carefully. Such issues include additional logistics and operating costs (e.g., EOR fluids supply and transportation, chemical costs, production facilities requirements, environmental impact, oil price, impact on wells/reservoir). The impact of the EOR fluids on the chalk mechanical properties (via chalk dissolution, alteration and/or compaction) and wells' mechanical integrity is also another issue that needs to be addressed prior to a successfully tested EOR technique is applied at a field-wide scale.

"Viscosifying" the injected water (Ghedan and Poettmann 1991) or "closing" the highly conductive natural fractures will help to direct the water into previously unswept areas that improving formation's macroscopic sweep efficiency and the opportunity to displace more oil from the surrounding matrix (Masalmeh, Blom et al. 2011). In the industry in addition to the traditional polymer injection field applications there is the extensive use of polymer gels, solid particulate systems and silicate gels that have been either field-applied/pilot-tested or proposed for field applications.

20.3 Formation sweep improvement solutions

This section addresses potential solutions for combating low formation sweep efficiency which, in addition to low oil recovery factors, it is often associated with water production problems since the very early stages of a producer's life. Formation sweep efficiency is exacerbated in the cases of gas-based EOR processes compared to water-based ones. Enick, Olsen et al. (2012) provided a review paper to address the chemical means for CO_2 flooding mobility control and conformance control problems originated by the low viscosity and low density of CO_2 at reservoir conditions. The various cases addressed by the authors for gas injection EOR schemes included WAG processes, application of direct CO_2 thickeners, use of small-molecule CO_2 thickeners, and CO_2 foams. Following an extensive review of ongoing research activities, Enick, Olsen et al. (2012) concluded that although small molecule CO_2 thickeners have been identified capable of increasing CO_2 viscosity by 50% to 500%, this can be achieved only at relative high concentrations of 2 wt% to 10 wt%. Therefore, due to the high costs associated with the synthesis of those CO_2 thickeners no field pilot attempt has been conducted.

Increasing formation sweep can be achieved by several technologies. In addition to chemical mobility and/or conformance control, technologies such as, infill well drilling that decreases well spacing, adjustment of the well flow patterns, use of smart well completions or sweeping individually reservoir layers through multiple completions, are some of the solutions which can be employed to avoid large disparities in sweep efficiency among the various formation regions. However, in reality a mixture of some of these solutions will be engaged depending on the causes of low sweep efficiency, type and degree of reservoir heterogeneities, operating environment (offshore/onshore), solutions' effectiveness and associated costs. In this chapter the main emphasis will be related to the use chemical mobility and conformance control for achieving improved sweep efficiencies.

20.3.1 Mobility/conformance control types diagnostics

In order to treat the low sweep efficiency properly, the root problem must be investigated, identified and possible solutions screened, categorized and ranked according to their success possibilities, well/field characteristics, field location, prior experience, as well as risks for success/failure. Although water production issues may arise for several reasons, in this chapter we will focus on water and EOR fluids production problems associated with oil displacement processes or water/gas production originated due to the presence of highly conductive paths in the reservoir such as faults, natural fractures, or super high permeability zones.

In the following, the most important cases for low sweep efficiency and related solutions are presented. It should be noted that these cases discussed here are pertaining the formation sweep and not to water production problems which may be associated with causes such as, for example, flow behind pipe, casing leaks, corrosion failures, etc. will not be addressed. In addition, the emphasis will be on naturally fractured chalk systems.

Injected fluids viscous fingering occurs even in homogenous reservoirs causing areal sweep efficiency problems. When the oil formation is associated with an underlying aquifer and/or a gas cap, viscous fingering, due to the adverse mobility ratio between the aquifer water (or gas-cap gas) and formation oil, can also occur in the vertical direction, thus exacerbating the total volumetric sweep of the reservoir. The presence of reservoir heterogeneities in formations containing viscous oil compounds the fluids-mobility driven viscous fingering, i.e., poor formation sweep. The more viscous the oil, the more pronounced the viscous fingering effects and the poorer the oil recovery.

Reservoirs with distinct, individual and separated layers which are not in communication except through the wellbores can be easily handled once the oil production from a given layer diminishes considerably making the injected fluid(s) process non-practical or even uneconomical. In this type of reservoirs, if EOR/IOR fluids are bullheaded into the well, they will have the tendency to move through the most conductive layer/zone, thus leaving the less conductive layers/zones poorly swept. This conformance issue gets aggravated once the injected fluid breaks through the production well; this causes injected fluids to be re-circulated through the formation, thus decreasing oil production and increasing oil production costs due to the lifting, separation, cleaning, and reinjection costs of injected fluids. Selective isolation of the swept, high permeability zone(s) will cause a rearrangement of the injected fluids thus giving the opportunity for the less prolific zones to be also swept.

Layered systems with communication in the reservoir are characterized by a layered structure with the individual layers being in communication in the reservoir. Thus, injected fluids will tend to move through the most conductive layers due to viscous forces. However, gravity and capillary forces may also be important, depending on the layer rock and fluid properties, reservoir structure, layer order, etc., in defining the distribution of fluids in the formation as a function of time. In general, layered reservoirs with crossflow in the formation are difficult to be dealt with by any means, and especially without the use of deep reservoir treatments.

In naturally fractured reservoirs, natural fractures are normally encountered in carbonate formations and may present severe difficulties for addressing formation sweep depending on the fractures density, aperture, and length, as well as fracture orientation, both with regards to the injection and production wells and their direction being either vertical or horizontal (see for example Hatzignatiou (1999); Hatzignatiou and McKoy (2000)). These are the most important parameters which dictate the sweep efficiency of the formation as well as our ability to effectively intervene to improve this situation. At this point, one needs to differentiate between the naturally occurring fractures in a formation and those that are created artificially, i.e., hydraulic fractures, either willingly to enhance the productivity/injectivity of a well which can be low for several reasons or unintentionally due to injection BHP exceeding the formation parting pressure and/or thermal effects encountered when injecting a cold injectant such as sea water. Although this chapter will not deal with hydraulically induced fractures, this type of fracture can in general be easier to deal with compared to naturally existing ones in order to address formation sweep efficiency issues.

Natural fractures can be encountered in the form of either distinct or isolated fracture, or alternatively occur as part of a fracture network. The former may actually not interfere with the formation sweep depending on its size and orientation. Intermediate fracture-spacing density displaying directional permeability trends may create significant issues with regards to the areal sweep efficiency of the formation (Sydansk 2007; Sydansk and Romero-Zerón 2011). Natural fracture networks with a high fracture density are generally not suitable for conformance control. As a matter of fact the presence of high density fractures will in general decrease the size of oil-bearing matrix blocks, thus providing a better access to and resulting in faster depletion rates compared to a low fracture density reservoir with large oil-bearing matrix blocks. However, in this latter case it often happens that large fractures may be developed from existing ones due to, for example, thermal cooling effects following cold water or EOR fluids injection. This case is sometimes referred to as fracture channeling (Sydansk and Romero-Zerón 2011).

The presence of natural fractures or faults can adversely impact economics of oil recovery due to water flow originated by either an underlying aquifer or injected water. In production wells, water flowing through natural fractures/faults connecting to the well can increase significantly the well's water cut affecting oil production rates. Apart of the increased production cost, high water-cuts inhibit oil production and may lead to an early well abandonment and associated loss of oil reserves. In waterflood or EOR recovery processes, water or EOR fluid injected into reservoir can contribute to cycling of drive fluid, high water or EOR fluid cut at neighboring production wells, poor volumetric sweep efficiency, high rate of reservoir pressure decline, and loss of oil production (and reserves) stored in the formation matrix. For either case, addressing water production will lead to increased oil production rates and oil reserves and will improve the field economics. For the waterflood or EOR recovery process, the objectives will be to (a) control the mobility of the injected drive fluid to increase its residence time into formation which will promote spontaneous imbibition, enhance oil recovery, and decrease drive-fluid cut, and/or eventually (b) divert the injected drive fluid into unswept reservoir regions, thus improving formation sweep and recovery of oil reserves.

The mobility of the injected fluids in a natural fractured reservoir can be addressed with the use of polymers and/or foams. The oil production mechanisms in such systems should be carefully considered and examined prior to undertaking any such steps in the field. Adverse interaction between the fracture network and matrix blocks interfaces will have serious consequences on the oil recovery. For the case of fractured-channels, these few and enlarged fractures will form a higher than average conductivity paths which may be potentially intervened in order to divert the injected fluids into other regions of the formation.

Oil and gas production problems associated with NFRs become more pronounced in the case of horizontal wells. These wells have, in general, higher degree of probability than the vertical ones of intercepting natural fractures (Hatzignatiou 1999; Hatzignatiou and McKoy 2000). In addition, due to economic reasons, many horizontal wells have open-hole completions with or without a slotted liner or pre-perforated uncemented liner (Lane and Seright 2000). These types of horizontal well completions render the isolation of an offending wellbore region for water control treatment as not feasible. However, even in cased-cemented horizontal wells, the primary cement bond quality is often poor due to cement loss into the natural fractures or faults (Lane and Seright 2000). Mechanical integrity problems associated with the formation surrounding a horizontal well in carbonate reservoirs, such as chalk, and/or significant reservoir rock dissolution aggravate the water production control and formation sweep efficiency issues.

Thief zones in the form of highly conductivity zones, solution channels and interconnected vuggy porosity may cause serious problems on the formation sweep. Interconnected vuggy channels or solution channels may be a large aperture flow conduits. Solutions channels are practically horizontal flow channels of a limited length and are also associated with carbonate formations. Conformance control gels can be engaged to address sweep efficiency issues developed due to the presence of thief zones in a reservoir unit.

20.3.2 Mobility control

The main issues related to fluid injection (water or EOR agent) into an oil-bearing formation are its mobility and density with reference to reservoir oil. Depending on their relative magnitudes compared to oil, a highly mobile injected fluid will have the tendency to flow faster than the displaced oil thus fingering through the formation. Fingering phenomena do occur in homogeneous formations, but they can be exaggerated in the presence of reservoir heterogeneities in the form of highly conductive paths such as high permeability thief zones, reservoir layering, natural fractures, etc. In addition, depending on the relative density of the injected fluid compared to formation oil, the injected fluid will have the tendency to override formation oil in case of gas injection, or underride it such as in cases of water injection. It has been observed in the lab, and also field tested, that the addition of fluid ”thickeners” in the form of polymers or foams could be greatly help to reduce the injected fluid mobility, thus increasing the formation sweep and the amount of recovered oil. Other means of controlling injected gas mobility is through the use of processes such as Water Alternating Gas (WAG), Simultaneous Water and Gas (SWAG), Foam Assisted Water Alternating Gas (FAWAG) (Permata and Hatzignatiou 2011).

Polymers

The addition of a water-soluble, high molecular weight polymer into injected water increases its viscosity and improves the sweep efficiency of formation oil by reducing the mobility ratio. For the case of hydrolyzed polyacrylamides (HPAM) the mobility ratio reduction is also caused by reduced effective water permeabilities caused by the polymer adsorption on to the surface of the rock. Adsorbed polymer onto the rock coats the rock surfaces with a hydrophilic film which swells when water passes over it; this causes the water effective permeability to be reduced. The phenomenon of polymer coat swelling does not occur in the presence of oil, which implies that polymers can reduce to a large extent water mobility in relatively low oil saturation regions, thus increasing oil recovery factors (Sparlin 1976). Hatzignatiou, Moradi et al. (2013, 2015) investigated the impact of formation wettability on the retention of injected polymer and reported that polymer retention and IPV are affected by the formation rock wettability.

From an engineering perspective, which seeks economic viability and efficiency, polymer flooding is a very effective method for improving oil recovery with regards to pressure maintenance and mobility control. Even though the cost of operating a polymer flood is relatively low compared to other forms of enhanced and improved oil recovery, polymer injection may still an expensive endeavor and has therefore warranted attention from researchers.

The behavior of HPAM macromolecules has been of special interest due to their somewhat complex behavior in a porous media. A recent study conducted by Stavland, Jonsbraaten et al. (2010), which focused on developing a model to describe the complex behavior of HPAM as a function of their injection rate through porous media, has resulted in a relationship that uses bulk rheological parameters to calculate the apparent viscosity of the polymer solution in the porous media. The newly created model is especially important in that it can handle the whole range of polymer flow regimes from lower Newtonian to degradation flow regime. The ability to model polymer degradation, which occurs at very high flow rates, is particularly of interest since previous models have only succeeded in modeling up to the shear thickening regime (Hatzignatiou, Norris et al. 2013).

The selection of the appropriate polymer for mobility control should be based on a screening of the most promising polymers using the following criteria: (a) injectivity - polymer should be able to be injected into formation without causing fractures and its injection rate be able to be sustained over time; (b) water viscosity enhancement and/or effective water permeability reduction - the identified polymer should increase the in situ water viscosity and/or reduce the effective water permeability; (c) low adsorption - polymer should have a low interaction with the formation rock and the adsorbed amount of polymer on to formation rock should be low; and (d) stability - polymer should be stable at reservoir conditions (resistant to thermal and biological degradation).

The reservoirs that have the highest potential for polymer flooding will be reservoirs (a) containing viscous oil, i.e., the possibility to reduce the mobility ratio, (b) with high permeability reservoirs, which will allow better polymer injectivity, (c) with moderate temperatures, which improves the thermal stability, and (d) containing low salinity and low divalent ion concentrations formation brine, which will promote better control of the viscosifying effects of synthetic polymers.

Foams

In a mobility control process, good foam stability to oil and low surfactant adsorption are essential, while for gas diverting applications intermediate- or low-oil stability might be sufficient, but strong and viscous foam is required (Kristiansen and Holt 1992). In either case, foam has to propagate away from the wellbore in order to create an efficient formation flooding process (Mannhardt and Svorstøl 1999).

Based on laboratory foam studies, Bernard and Holm (1964) have shown that rock-sample gas relative permeability was reduced significantly in the presence of foams. Another study of foam rheology in porous media showed that foam must be treated as two-phase flow and that the liquid relative permeability curve is the same as it would be in the presence of a continuous gas phase, (Bernard and Jacobs 1965).

The significant increase of gas viscosity in the foam as foam propagates through the reservoir, especially in cases that involves strong foam, is one of the most important properties that make foams highly applicable as mobility control agents. Gas flow, in the form of bubbles separated by lamellae, exhibits more resistance produced not only by viscous shear stresses in thin films between the pore walls and gas liquid interface, but also by the forces required to push lamellae through constricted pore throats (Nguyen, Alexandrov et al. 2000).

Zhang and Seright (2007) considered the use of foams and polymers as means for improving vertical sweep efficiency in reservoirs containing layers with and without crossflow during waterflooding and chemical flooding. Based on the fact that foams collapse in low permeability formations, provided that the capillary forces are sufficiently high to drain water from foam films (limiting-capillary-pressure effect) (Schramm 1994; Kim, Dong et al. 2005) it appears that in certain cases, this may allow a gas/water/surfactant formulation to penetrate into low permeability zones to a much greater extent than that of a polymer solution. Although it appears that vertical sweep efficiency could be higher in a foam flood than during a polymer one, viscous fingering associated with high mobility gas flow could impact negatively this possibility. According to the authors, foams generally will not be superior to polymers considering the challenges in formulating them as per requirements stated above, limitations on foam propagation due to surfactant retention, and limitations on their stability under reservoir conditions. However, under the following circumstances foams can provide improved sweep in layered systems compared to polymer solutions: (a) can form in high permeability zones but not in low permeability ones, (b) there is no crossflow occurring between the high and low permeability zones, and (c) the foam resistance factor in the high permeability zones is high enough to overcome the permeability contrast and the unfavorable mobility ratio between the gas bank and the oil/water bank in the less permeable zones (Zhang and Seright 2007).

For carbonate field cases, and especially in chalk reservoirs, the issues of in situ foam generation, foam strength and stability, and surfactant retention in the porous medium require special attention. In addition, the surface charge of the carbonate reservoir rock will also dictate the selection and use of appropriate surfactants to limit their retention in the formation while at the same time enabling the formation of sufficiently strong and stable foam for controlling the mobility of EOR injected fluids. Jensen, Harpole et al. (2000) screened several EOR methods for improving oil recovery at Ekofisk following waterflooding. Initial studies conducted for EOR low-concentration surfactant flooding were terminated due to the high surfactant adsorption especially at low temperature water injection regions.The influence of the fractured nature of carbonate formations on the behavior, stability and effectiveness of foam to recover formation oil have been partly addressed in the literature. Yan, Miller et al. (2006) used experiments to verify a theory developed for foam flow through a uniform fracture, and stated that the foam apparent viscosity is due to liquid between bubbles and the resistance to deformation of bubbles interfaces as they pass through the fracture. The foam apparent viscosity increases with the gas fractional flow and, for a given bubble size, is larger in wider fractures; this suggests that foam can divert injected fluid from wider to thinner fractures. The transport of the injected foaming agent solution is governed by convective flow, pore-scale diffusion, and retention. The latter will be affected by several factors such as type and concentration of used surfactant, formation temperature, brine salinity and presence of multivalent ions, minerals composing the fracture/matrix interface, surface area of fracture/matrix interface, reservoir fracture intensity, and transport rate in both fracture network and matrix. Bodin, Delay et al. (2003a,b) stated that the main solute-transport processes in low-permeability rocks, where advection in the matrix is negligible, are advective transport in fractures, hydrodynamic dispersion along fractures, molecular diffusion from fractures to matrix, sorption reactions on fracture/matrix and within matrix, and decay reactions.

The importance of surfactant adsorption on carbonate minerals for CO_2 flooding as compared to micellar flooding, the surfactant/mineral-rock interaction and distinct role of main carbonate minerals in the form of dissolution, interaction, and precipitation were highlighted by Ahmadall, Gonzalez et al. (1993). The authors concluded that the use of a cationic surfactant with an appropriate level of added multivalent electrolyte can reduce drastically surfactant adsorption in EOR application in carbonate reservoirs.

Static and dynamic experiments were conducted by Alkan, Goktekin et al. (1991) to investigate the use of in situ generated foam to improve mobility ratio and injection profile in an immiscible CO2 injection process at Bati Raman heterogeneous, fractured limestone field containing a 12–13 ° API oil. The effectiveness of three ethoxylated surfactants was tested in terms of foam generation, foam stability, and retention at reservoir salinity conditions, as well as the resulted mobility reduction in artificially fractured core samples. Spinler, Zornes et al. (2000) investigated the use of low surfactant concentrations, 100–500 ppm, to improve oil recovery in a fractured Kansas outcrop chalk and field reservoir formation. Several concentrations of commercial surfactants were screened for long term stability at high temperature in seawater based on cloud point, precipitation, and the stability of surface tension. Spontaneous imbibition tests conducted at ambient and reservoir temperatures in moderately water-wet reservoir chalk samples showed that a selected surfactant added at low concentrations to the imbibition water reduced the residual oil saturation over imbibition tests conducted without surfactant. Forced imbibition tests resulted in reduced residual oil saturations over cases without using surfactant, even though the use of low surfactant concentrations did not lower the oil-water interfacial tension below single digits. Lab data indicated that low adsorption at reservoir conditions could be obtained below CMC for some surfactants.

In an experimental approach, Haugen, Fernø et al. (2012) used C_{14+} alpha olefin sulfonate (AOS), linear C_{12-16} AOS, and the C_{15-18} internal olefin sulfonate (IOS) to study foam flow in fractured, oil-wet carbonate (limestone) rocks and determine its viability as an EOR agent for this type of reservoirs; the effect of rock wettability on oil recovery during foam flow was also addressed. Both in-situ generated (co-injection of surfactant solution and nitrogen gas, with a surfactant/gas ratio ranging from 0.9 to 0.92) and pre-generated foam options were used; the former foam turned out to be weak in smooth-walled fractures, thus yielding insufficient fluid diversion from the fractures and gas injection exhibited low (up to 10% of OOIP) additional oil recovery. On the other hand, injection of pre-generated foam resulted in reduced gas mobility, fluid diversion into oil saturated matrix and thus significant additional oil recovery, up to 78% of OOIP, for a high number of injected pore volumes. In general, injection of water, surfactant or gas resulted in an approximate 10% of OOIP incremental oil recovery.

The retention of two branched ethoxylated (EO) sulphonates in fractured outcrop Liege chalk samples was studied by Fjelde, Zuta et al. (2008). The authors reported that increasing the surfactant degree of ethoxylation decreased the surfactant retention on to the chalk formation saturated with formation water. The presence of residual oil saturation after waterflooding decreased the retention of 7-EO and increased the retention of the 12-EO branched ethoxylated sulphonate surfactant compared to the cases in the absence of residual oil. Formation temperature also influenced the amount of surfactant retention with the 12-EO branched ethoxylated sulphonate surfactant yielding the lowest retention at 55°C and the highest retention at 70°C. Zuta and Fjelde (2010) addressed the transport of CO_2-foaming agents in CO_2-foam processes in fractured chalk formations and stated that the process is rather slow and dependent on the matrix block size, CO_2 foaming agent concentration, and oil presence. Simulation results indicated that both molecular diffusion and adsorption are important transport mechanisms with the latter delaying the transport of CO_2 foaming agents in fractured chalk formations.

Recently, Chen, Elhag et al. (2014) proposed the use of switchable ethoxylated alkyl amine surfactants to improve sweep efficiency for CO_2 EOR flooding in formations with temperature up to 120°C and in the presence of high-salinity brine (182 g/L NaCl). In the presence of an aqueous phase with a pH < 6, these surfactants switch from the nonionic state in dry CO_2 to a cationic one. The high hydrophilicity in the protonated cationic state facilitated stabilization of lamellae between bubbles in CO2/water foams. The cationic head-group reduces the adsorption of ethoxylated alkyl amines on the positively charged calcite in the presence of CO_2 dissolved in brine. In addition, surfactant partition coefficients (0–0.04) favored the water phase over the oil phase, which results in reducing surfactant losses to the oil phase for efficient surfactant usage. In the nonionic form, the surfactant was soluble in CO_2 at 120°C, and 3,300 psia at a concentration of 0.2% (w/w); surfactant solubility CO_2 and favorable CO_2/water partition coefficient are beneficial for transport of surfactant through the CO_2-flow pathways. Finally, the surfactant was used to form CO_2/water foams, without forming stable/viscous oil/water emulsions. This results in low CO_2 mobility in regions of low oil saturation and high contact with oil at the displacement front.

20.3.3 Conformance control

Chemical solutions have a large range of application in terms of formation depth away from the wellbore and can address several water-type problems. Appropriate chemicals systems can be either injected to near-well areas to block the most water productive layers (with a higher efficiency compared with mechanical techniques) or used as in-depth treatments to block high water permeability fractures/faults/zones. These chemicals are injected as solutions and gels are formed within the reservoir. These gels are designed to be strong enough for long periods of time, at formation temperature, salinity, and pH; they are also able to withstand the applied pressure during hydrocarbon production. The resulting profile modification (conformance control) diverts injected water to unswept reservoir zones and improves the distribution of fluids in heterogeneous reservoirs (Simjoo, Vafaie Sefti et al. 2007). With significant advantages such as high control of setting time, flexibility for pumping without a work-over rig, deeper penetrations into formation, easy removal from wellbore by water recirculation, etc., chemical solutions have been used often and with a high success rate (Perez, Fragachan et al. 2001).

The chemicals mostly used for water shut-offs are crosslinked polymer and sodium silicate gels. The former are obtained by cross-linking high and/or low molecular weight polymers with crosslinkers (normally metal ions or metallic complexes). The chemical gelling solution (gelant) is prepared by adding the polymer to water, followed by a crosslinker. Under a specific temperature and time, a crosslinking (gelation) reaction starts between the two components to form a three-dimensional cross-linked polymer network, which is referred to as "gel". Silicate gels are created based on the principle of reducing its pH, normally done by adding acidic activators to the aqueous solution of sodium silicate. The use of silicate gels for petroleum application has been documented since 1922; however, their benefits and field potential were not appreciated for a long time (Lakatos and Lakatos-Szabó 2012; Vinot, Schechter et al. 1989), mainly due to the poor understanding of the silicate gelation mechanism especially under reservoir conditions. There are numerous field and experimental studies illustrating the beneficial use of polymer gels for conformance control. For example, recently Brattekås, Haugen et al. (2013) investigated the use of a combined mobility control (cross-linked Cr(III)-acetate HPAM polymer gel) followed by chase fluid injection (water, surfactant, or CO_2 foam) to enhance oil recovery in heavily fractured, oil-wet carbonate rock samples.

Polymer Gels

Polymer macromolecules are linked together by crosslinkers (normally metal ions or metallic complexes) forming a viscous gel in the formation. When reservoir temperatures are in excess of 250°F the use of organic crosslinking agents may be more appropriate. Polymer gels have mostly been used for water shut-off applications, and can be used for both sealing and disproportionate permeability reduction.

Polymers, both hydrolyzed polyacrylamides (HPAM) and biopolymers, are mainly used for water shut-off applications. HPAM polymers have a good ability of plugging of pores or fissures, because of their viscosity and the formed gel strength. Biopolymers have the ability to form physical network above critical concentration. Generally, as a result of the limited strength, they are not suitable for fracture treatment and are more suitable for plugging pores or fissures (note that the gel strength will be a function of the treated zone width, fracture aperture, etc.). There are also ungelled polymers/viscous systems, which have the ability to reduce the water permeability more than the oil permeability. The advantages with these systems are that they can be bullheaded into an un-fractured well without zonal isolation. On the other hand, they are not strong enough to seal vugs and big voids, and there is also a risk of reducing the oil permeability. General issues with polymers are gelation control, adsorption/retention and deep penetration because of their inherent viscosity.

Solid particulates

Movable "soft" microgels are effective means for deep reservoir injection profile control and/or disproportional permeability reduction (DPR) systems. Microgels are formed at polymer concentrations below the critical overlap concentration of polymer and are dominated by intramolecular crosslinking. Discontinuous microgels are low- concentration acrylamide-polymer gels formed at the surface with a very narrow particle-size distribution (Chauveteau, Denys et al. 2002). Colloidal Dispersion Gels (CDG) can be described as bulk gels that require low polymer and crosslinker concentrations, thus making the injection of large volumes economical while permitting in-depth placement (Mack and Smith 1994), but their field application is rather limited due to their rather restricted reservoir temperatures of less than 195°F and a salinity range of up to 5000 mg/l (Coste, Liu et al. 2000). According to Mack and Smith (1994) high molecular weight polymers with large degree of hydrolysis yield better gels, the polymer-to- aluminum ratio of 20:1 to 100:1 work the best, the CDG system they used worked well up to 30 000 ppm TDS, and the reaction rate should be slow enough to provide sufficient in-depth placement.

Nano-sized or micro-sized, crosslinked polymer particles, which are designed to swell approximately 10 times their original size when exposed to a high temperature, have found recent deep-reservoir applications. BrightWater is one of such gels introduced and field-applied by Frampton, Morgan et al. (2004) and Pritchett, Frampton et al. (2003); generally, it has found applications in reservoirs with temperatures up to 285°F and salinities of up to 120 000 ppm.

Micrometer- to millimeter-sized Preformed Particle Gels (PPG) have been developed and field-tested to overcome potential in situ gelation drawbacks related to polymer gel crosslinking (Coste, Liu et al. 2000; Bai, Liu et al. 2007). The main difference of PPGs with the microgel systems is due to swelling time and ratio as well as particle size. PPGs are mainly used to treat fractures or fracture-like channels and designed to withstand temperatures up to 250°F and salinities up to 300 000 mg/l (Bai, Liu et al. 2007).

Deep reservoir placement of pH sensitive polymers has been introduced by Al-Anazi and Sharma (2002). In general, a polyelectrolyte, which can create a molecular-network microgel in solution, is placed in a high conductivity path. The injected fluid reacts with formation minerals (e.g., carbonate) and experiences an increase in pH which causes the polymer to swell up to 1000 times of its own volume and drastically increase its apparent viscosity (Choi, Ermel et al. 2006); the viscosity characterization was reported by Huh, Choi et al. (2005). These polyelectrolytes (e.g., anionic derivatives of polyacrylic acid) may form rigid gels in the porous media which can resist applied pressure gradients, can be broken down with the use of a mild acid wash and flowback (if and when it is required), are sensitive to the presence of divalent cations resulting to precipitates (thus requiring the use of a formation preflush to reduce/eliminate such tendencies) and exhibit temperature tolerance (at least up to approximately 180°F).

Silicate Gels

Sodium silicate is manufactured by heating silica and sodium carbonate to temperatures above 1300°C to form a water-soluble glass referred as "water glass" (Iler 1979). Although the sodium silicate chemistry is complex and not fully understood, the author provides the basic fundamental equilibria involved. Generally, sodium silicates are identified by the SiO_2:Na_2O ratio, n. Alkalinity increases by decreasing n. The commercial sodium silicates are produced as glasses having n varying in the range of 1.6 to 3.9. At a given ratio, the density of a solution is dependent on total solids content. The higher the ratio is, the lower the density at a given concentration. The viscosity of a sodium silicate solution is a function of concentration, density, ratio n and temperature; viscosity increases when the ratio n increases. Since sodium silicates are alkaline fluids, they display tendencies for precipitation in the presence of divalent ions, dissolution of clay minerals, and lowering of oil/water interfacial tension (Mayer, Berg et al. 1983; Mohnot, Bae et al. 1987).

The gelation process of a sodium silicate solution can be initiated by decreasing the pH, e.g., by adding an acid to the solution. Such systems have been applied for many years and a significant amount work has been done on optimizing silicate/acid systems water for control purposes (Stavland, Jonsbråten et al. 2011b). Despite the fact that acids have been widely used, there are plenty of other chemicals (inorganic, organic and natural minerals) that can be used as gelling agents; see for example Krumrine and Boyce (1985) who presented an overview of such agents. Stavland, Jonsbråten et al. (2011a) presented a kinetics equation for estimating the bulk gelation time of a silicate gel system, formed by a sodium silicate solution with 2M HCl activator, by assuming the temperature dependency is given by the Arrhenius equation. Hatzignatiou, Helleren et al. (2014) used a commercial simulator to model sodium silicate reaction kinetics and history match dynamic experimental results for sand-pack plugging. Pham and Hatzignatiou (2016) studied a commercially available sodium silicate system and developed a unified sol-gel transition (gelation) time correlation, which included all relevant parameters such as (a) sodium silicate solution concentration; (b) activator concentration; (c) temperature;

and (d) divalent ion (Ca^{2+} and Mg^{2+}) concentration.

Among the various existing techniques for water control, silicate gel systems are known to be an effective and environmentally friendly method for managing water production. These gel systems usually content two main components, the liquid silica and activator. Silicate gel can be used in water control and near well applications due to their (a) deep penetration into the treated zone because of their low initial viscosity, (b) good thermal and chemical stability, (c) low cost, (d) environmental friendliness, and (e) easy removal in case of a failure (Lakatos, Lakatos-Szabó et al. 1999). Jurinak and Summers (1991) reported the use of silicate gels in several well interventions such as water- injection-profile modification, water-production control and remedial casing repair with a mixed success.

The main advantages of silicate gels are low viscosity of treating solutions; short to moderate pumping time before gelation onset; flexible chemical mechanism; good chemical stability; excellent thermal and mechanical resistivity; easy gel breaking in case of technical failure; simple and cost-effective surface technology; relative inexpensive; and environmentally “green” chemicals. Various silicate-based technologies have been used several times in field applications worldwide demonstrating good field experience as well as lessons to learn. Until 2012, more than 80 jobs were performed with 60 to 65% of the treatments deemed technically successful and 40% of the jobs as economic (Lakatos and Lakatos-Szabó 2012). For example, in June 2011, a single well pilot injection of sodium silicate in the Snorre NCS oil field was carried out successfully. Acid hydrochloric acid (HCl) was used as activator in this job. An in-depth permeability restriction of approximately 40 m away from the wellbore and permeability reduction of more than 100 were achieved and confirmed by post fluid infectivity measurements and transient falloff tests (Skrettingland, Giske et al. 2012).

The disadvantages of silicate gels are related to their blocking effect and gelation mechanisms. More specifically, the silicate gel tends to shrink (syneresis) over time, thus reducing the gel’s blocking effect; formed gel is rigid and prone to fracture; silicates are prone to form precipitates instead of gel; and since the gelation of silicate is a function of pH, temperature and concentrations of the reacting components, the gelation time might be difficult to control as its mechanisms have not been fully understood (Lakatos and Lakatos-Szabó 2012).

Various studies and tests have been performed to overcome the mentioned shortcomings, such as the use of different additives. For example, addition of acid phosphate into alkaline silicate reduced influence of salinity of formation water on the gelling time (Beecroft and Maier 1969); the gelation of a silicate system still happened even though the pH remained constant (> 11) when adding hydrolysable esters into the alkaline silicate solution as a dispersed phase (micro-emulsion) (Vinot, Schechter et al. 1989); Glyoxal and urea were also tested as gelling agent (activator) for sodium silicate gelling system (Nasr-El-Din and Taylor 2005). These works have also shown that as a result of a unique gelation mechanism, the properties of gel and the chance to have permanent and efficient barrier formation under harsh reservoir conditions were significantly improved (Lakatos, Lakatos-Szabó et al. 1999).

Alkaline fluids, such as sodium silicate, are not miscible with seawater or magnesium-rich formation water (hard brines). In particular, sodium silicate reacts with Mg^{2+} and Ca^{2+} and forms Mg-Ca-silicate complexes which may precipitate or activate gelation. According to Mayer, Berg et al. (1983) the injection of large preflush volumes of soft water may be required to displace formation water and avoid near-wellbore plugging. However, since mixing between the injected sodium silicate and formation water will always take place, the preflush soft-water volume can be viewed as one of the parameters which control the invasion depth of the sodium silicate (Skrettingland, Dale et al. 2014). Bulk fluid studies conducted by Pham and Hatzignatiou (2016) have also revealed precipitation tendencies of a commercial sodium silicate system in the presence of magnesium ions.

Skrettingland, Dale et al. (2014) investigated the effect of in-depth mixing of diluted sodium silicate, varied from 0.4 to 4.0 wt% SiO_2, and formation water (mixture of seawater diluted in distilled water with fractions ranging from 0.1 to 1). Mobility reduction, RF, declined slowly as more silicate was injected; permeability was partially regained after the injection of 5000 ppm KCl brine due to dissolution of precipitated species. The observed mobility reduction depended on water salinity (i.e., calcium and magnesium ion concentrations), silicate concentration, and formation porosity, but apparently not on permeability; the latter indicates that permeability reduction is related to surface area rather than pore size. The maximum mobility reduction observed was approximately 14 when displacing seawater with 4 wt% SiO_2 through a reservoir rock with porosity of 30%. Ion analysis of effluent revealed suppressed calcium and magnesium concentrations, which indicates precipitation of these ions in the core. A white precipitate was also observed in the first effluent samples after breakthrough which contains calcium, magnesium and silicate. The authors stated that the silicate retention is low and controlled primarily by the silicate precipitation. Core flood experiments at residual oil saturation using Snorre stock tank oil revealed no impact on reactions between oil and the alkaline sodium silicate; an observed small amount of incremental oil production was attributed to an IFT reduction.

20.3.4 Mobility/conformance control diagnostics

A multidisciplinary approach is required in evaluating the problem type, screening and addressing potential means of resolving it, and designing effective well/reservoir treatments for improving mobility and/or conformance control solutions. Depending on the problem type the depth of treatment within the reservoir will be of a primary importance. For example, watered out formation layers in a layered formation without crossflow can be easily isolated by a variety of solutions ranging from mechanical to chemical and near-wellbore to deep-placement. However, the no-crossflow requirement needs to be properly and effectively evaluated otherwise the applied solution will be either ineffective or short-lived.

Normally, one should start by gathering all existing data ranging from reservoir geology, well production and well completion schemes, well patterns, well logging data both open- and cased-hole ones, well testing and pressure transient analyses, tracer testing and evaluations, production well monitoring data, 4D seismic, and history-matched reservoir simulation models. Sydansk and Romero-Zerón (2011) provided a summary of required data/tests compiled from the works of Soliman, Creel et al. (2000); Seright, Lane et al. (2003); Jaripatke and Dalrymple (2010). Based on the review and analyses conducted from the available data, carefully selected additional data acquisition could be conducted to supplement existing information, clarify and conclude on the current problem identification.

Integration of all existing and newly acquired data and analyses will assist greatly in identifying the root of the poor sweep efficiency problem, screen and evaluate potential treatments, quantify well intervention costs and risks as well as likelihood of achieving the objective for improving formation sweep. Only having undergone such a process the proper solution should be designed and field applied. Statistics from the Permian Basin, related to the success ratio of a conformance treatment as a function of the type of diagnostic parameters used, indicate that the average success rate when all diagnostic parameters were used was 88.6%; this rate declined down to 51.6% when no diagnostic technique was used in the selection of the appropriate well treatment (Soliman, Creel et al. 2000).

20.4 Chemical screening characteristics

Chemicals for water of EOR fluids management are widely used worldwide in onshore and offshore environments and for both sandstone and carbonate formation treatments. The chemicals must be screened to ensure that the desired properties are met; however, depending on the field location environmental restrictions may apply which could result to selecting not the most effective chemicals, but rather the ones which are permitted to be pumped. Nevertheless, these chemicals must be thoroughly evaluated in the lab using representative core samples and selected based on criteria dictated by the field operator, environmental guidelines, costs, HSE, reservoir properties, and last but not least, the properties of the chemicals themselves. The main selection criteria for water or EOR fluids management chemicals (mobility or conformance control) are: HSE; reservoir properties (formation temperature, salinity, multivalent ions); gel (gelation/placement, gelant injectivity, gel strength, permeability reduction, dehydration/shrinkage,); polymer (mechanical degradation, bacterial degradation, chemical stability), rock/fluid interactions (retention/adsorption, fracture/matrix interface properties); as well as price and accessibility.

20.5 Field cases - mobility and conformance control applications

In this section field cases from China and USA for both mobility control and profile modification will be briefly presented and experience gained from such applications will be highlighted.

20.5.1 Polymer flooding - daqing oilfield, China

The world's largest polymer flood has been implemented in the Daqing field, China, a large river-delta/lacustrine-facies, multilayer, heterogeneous sandstone in an inland basin (Wang, Seright et al. 2008; Wang, Dong et al. 2009). The field was discovered in 1959 with water injection initiated in 1960; waterflood increased oil recovery by 10–12% of OOIP. Polymer flood (using high-molecular-weight HPAMs) was implemented in December 1995 and by 2007, 22.3% of total production from the Daqing oil field was attributed to polymer flooding. Polymer flooding is expected to increase ultimate oil recovery to more than 50% of OOIP (Wang, Seright et al. 2008; Wang, Dong et al. 2009). The reservoir depth is approximately 1000 m and the formation (Saertu) under polymer flood has a net average thickness of 6.1 m, average air permeability of 1.1 μm^2 , and a Dykstra-Parsons permeability coefficient ranging from 0.5–0.8. Its reservoir properties, 45°C temperature, around 9 mPa·s oil viscosity at reservoir conditions, and total salinity, 3000–7000 mg/L, make this field a very good candidate for polymer flooding.The gained benefits of zone management (profile modification) versus time were evaluated and guidelines for candidate wells and layers for such treatment were drawn (Wang, Seright et al. 2008; Wang, Dong et al. 2009). For some Daqing wells with significant permeability differential between layers and no crossflow, injecting polymer solutions separately into different layers improved flow profiles, reservoir sweep efficiency, and injection rates, and reduced the water cut in production wells. Simulation studies and pilot tests the favorable conditions for separate layer injection were established (Wu, Chen et al. 2005).

Polymers with 12–35 million Daltons molecular weights were designed and supplied to meet field requirements. The 12–16 million Dalton molecular weight HPAM polymer has a 40 cp viscosity, which is considered to overcome the unfavorable mobility ratio of 9.4 and the up to 4:1 encountered permeability differentials. Polymer viscosities measured prior to (35–40 cp) and after injection into formation displayed an over 50 % reduction in the polymer solution's viscosity due to mechanical degradation. Most of the viscosity loss took place between the high pressure injection pumps, mixing system and near wellbore (Wang, Dong et al. 2009). Injected polymer solution concentrations determine the required size of polymer slug. Higher polymer concentrations could shorten the time required for the polymer flood and also reduce the wells' water cut. Wang, Seright et al. (2008) stated that laboratory measurements on representative core samples showed retention levels of 126 μg/g for a 15 million Dalton HPAM polymer, and 155 μg/g for a 25 million Dalton HPAM polymer. These polymer retention numbers result to a 65% and 80% depletion of a 1 PV 1000 mg/l injected polymer solution, respectively.

The injection rates were evaluated to be less than 0.14–0.20 PV/year, depending on well spacing; for a 250 m well spacing the polymer injection rate was less than 0.16 PV/year (Wang, Seright et al. 2008; Wang 2013). Bactericide (formaldehyde) was used to prevent biological degradation and low applied shear rates to reduce mechanical degradation (Wang, Dong et al. 2009). The optimum polymer-injection volume varied around 0.7 PV, depending on the water cut. The average polymer concentration was designed to be about 1000 mg/L, but for an individual injection station, it could be as high as 2000 mg/L or even more (Wang, et al., 2008; Wang, 2013). Typical polymer bank sizes range from 640–700 mg/L·PV compared to the initial ones of 240–380 mg/L·PV used in the initial pilots. From experience, once the water cut reaches the level of 92% to 94% the polymer injection should be ceased.

On some Daqing wells, oil recovery could be enhanced by 2 to 4% of OOIP following a profile modification before polymer injection. These benefits were decreased if the conformance control was implemented after the half-life of a polymer flood. Wells that were considered as candidates for such treatment included (a) injection wells with downhole pressures lower than a typical injection well at the onset of polymer flood and (b) injection wells with offset producers producing at larger than the average water cuts. Layers that were considered as good candidates included layers (a) with good lateral connectivity between wells, (b) layers with high permeability differential compared to adjacent layers, (c) which have good permeability-thickness products, (d) which exhibit effective isolation with adjacent layers, (e) that produce at high water cut levels, and (f) which have high injectivity index per unit height compared to other layers (Wang, Seright et al. 2008; Wang, Dong et al. 2009).

Well spacing, permeability ratio between zones, and connectivity factor (pore volumes accessed by the injected polymer divided by the total pore volume) between injector/producer are key factors when designing the well pattern. The connectivity factor was determined to be greater than 70% when designing the well pattern. Also zones of similar properties should be combined to promote more uniform formation sweep. For polymer flooding, Wang, Dong et al. (2009) stated that the permeability ratio should be less than 5, while the combined thickness should be at least 5 m. The well pattern chosen for Daqing was the five-spot one with well spacing reduced from the original 500–600 m down to 175–250 m ones.

Polymer flood in Daqing can be distinguished into five stages shown in **Fig. 20.1** (Wang, Seright et al. 2008; Wang, Dong et al. 2009). Stage 1: polymer injected less than 0.05 PV - water cut is yet to decrease. Stage 2: polymer injected in the range of 0.05–0.2 PV - water cut declines and approximately 15% of the incremental oil from polymer flood is produced during this stage. Stage 3: polymer injected in the range of 0.2–0.4 PV - oil production reaches its peak value and associated water cut is relatively stable; approximately 40% of the incremental oil from polymer flood is produced during this stage. Stage 4 polymer injected in the range of 0.4–0.7 PV - areal sweep efficiency reaches its maximum value, oil production declines and associated water cut increases; approximately 30% of the incremental oil from polymer flood is produced during this stage. Stage 5: polymer injected is over 0.7 PV - the last stage that lasts until the well's ever increasing water cut reaches its maximum value of 98%; approximately 10% of the incremental oil from polymer flood is produced during this stage.

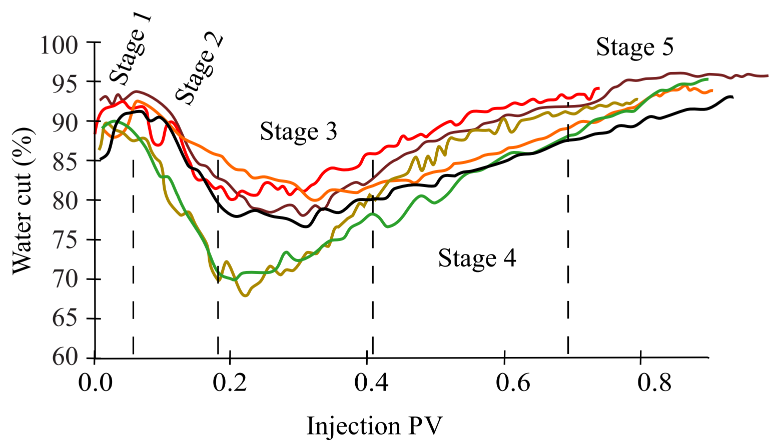

Figure 20.1: Five stages of water cut development during polymer flood in Daqing oil field.

20.5.2 Well crossing a fault in the Prudhoe bay field - North Slope of Alaska, USA

A production well drilled on the periphery of the Prudhoe Bay field encountered lost circulation problems during drilling beginning at 11,,327 md-ft; from this point on fluid returns were approximately 70%. Gamma ray and neutron revealed washed out shale at that depth, and cement bond logs showed a poor cement bond from this depth to the depth at which the well was terminated, 11,853 md-ft or 9,009 ft TVD. This waterflood producer was located approximately 50 ft above an underlying aquifer and in a region of the field with formation thickness of less than 50 ft, perm,eability ranging from 50 to 100 mD, temperature of 195°F and pressure around 3,200 psi. Initially the well produced 500 STB/D with a 24% water cut; however, after three months of production the oil rate declined down to 400 STB/D and the water cut increased up to 90%. Production logs showed that all production was originated between 11,327 ft and 11,345 ft, i.e., at and near the suspected fault location. Produced water analyses showed that the water had the same composition as the aquifer water (Lane and Sanders 1995; Lane and Seright 2000).

Squeeze cement was considered and rejected due to the potential presence of fault connecting the well with the aquifer, thus giving very low possibilities for success. The decision was made to plug the faulted interval and for some distance away from the wellbore with the use of a polymer gel. Since mechanical zone isolation during treatment was not an option, due to poor cement bond, a bullhead treatment of a gel system, previously tested successfully in isolating natural fractures, was selected. This gel system that uses a low concentration (0.3–1.2% w/w) of a polymer with molecular weight over 1 million Dalton can be pumped even after full gelation (Lane and Seright 2000). The well treatment called for a 12,000 bbls upper limit gel volume based on the existing information at a pumping rate of 2 BPM; the treatment job lasted approximately 100 hrs with much of the gelation taking place during pumping. The production history of the treated well shown in **Fig. 20.2**, both for prior and after well treatment, displays the beneficial effects of the treatment. Shutting off the water originated from the fault system reduced the well's water cut, improved the well hydraulics and increased oil production. **Table 20.1** provides historical production for the treated well; the well's oil productivity index (PI) remained stable after one month following treatment, whereas the well's initial water PI decreased by 25%. The observed post-job reduction in the oil PI was attributed to temporary perforation plugging by dehydrated gel during the lengthy job treatment; the well's oil PI was gradually restored during production and applied high pressure drawdowns (Lane and Seright 2000).

20.5.3 Foam-gel conformance treatment in the Rangely CO_2 flood - Colorado, USA

The Rangely Weber Sand Unit CO_2 flood began in 1986; in 1999 there were 372 active producers and 300 active injectors, 259 of which were WAG CO_2injectors. WAG CO_2 injection to recover a relatively light oil takes place into Pennsylvanian-Permian Weber Sand Unit which is a 200 m thick sequence of sandstones, siltstones and shales; the latter are normally effective vertical flow barriers stratifying the formation into six producing zones (Wackowski and Masoner 1995). The importance of conformance improvement due to preferential flow through the natural fracture network leading to premature CO_2 breakthrough times was recognized early by the field operator. An improved conformance of the injected CO_2 was expected to reduce operating costs and increase oil recovery.

A number of mechanical methods and chemical treatments were employed to achieve this goal. Dual injection strings and selective injection equipment were used to improve control of the injection profile. In addition,

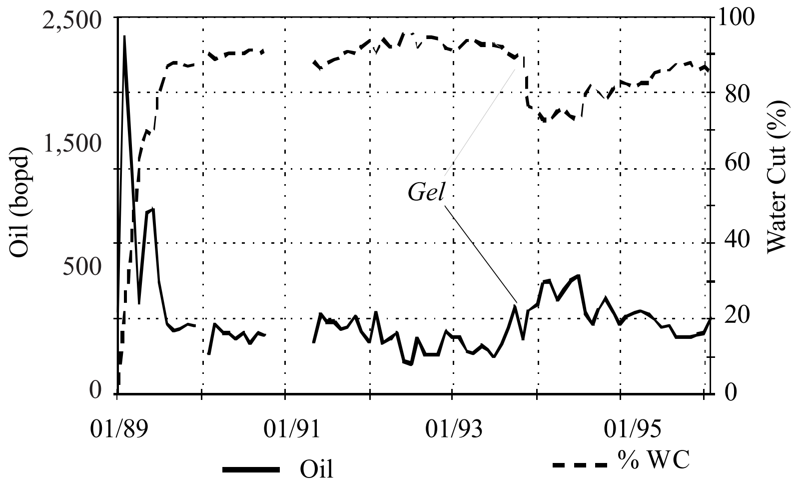

Figure 20.2: Intervened production well history prior and after water shutoff treatment.

Time	Oil Rate (STB/D)	Water Rate (STB/D)	WC (%)	Oil PI (STB/D/psi)	Water PI (STB/D/psi)
Nov. 1993	466	4290	90	0.32	2.95
Post-job	543	1700	76	0.24	0.74
1 month past	727	1895	72	0.30	0.78
1 year past	665	2175	77	-	-
1.5 years past	567	2410	81	-	-

Table 20.1: Treated well historical production data, (Lane and Seright 2000).

chemical treatments, polymer gels and CO_2 foam, were also applied to improve the volumetric sweep efficiency. While these treatments improved local sweep efficiency and oil recovery, economics limited the maximum treatment volume per injector well to 15 000–20 000 bbl. Certain regions of the Rangely reservoir required considerably larger treatment volumes to reduce the permeability of a larger volume of the fracture network and improve conformance in a larger volume of the well pattern (Hughes, Friedmann et al. 1999).

The design called for a large volume of CO_2 foam placed into the fracture network, and conversion of the injected fluid system into a robust gel capable of diverting subsequently injected fluids. The design injection fluids called for a 0.5 wt% surfactant (Alcohol Ether Sulphate - AES) and a 0.5–1 wt% HPAM with a low degree of hydrolysis (0.5–1%) along with a 100–2000 mg/l of added Cr(III) acetate. Sodium lactate was added to give molar ratios lactate/acetate up to 2, and a delayed released bicarbonate buffer (urea) aiming to control the pH at around 4.5. The pumped foam-gel formulation was 80 vol% CO_2, 6.3 g/l active polymer, 0.5 wt% active surfactant and 3 g/l urea with the pump time been around 12.8 days (Hughes, Friedmann et al. 1999).

Three large-volume foam-gel treatments were successfully placed. The first 36 400 bbl treatment (Treatment I) was implemented in November of 1996 and resulted in an increased of the pattern oil rate from 260 barrels of oil per day (BOPD) in March 1997 to ±330 BOPD in August 1998. The second 43,450 bbl and third 44 700 bbl treatments increased the corresponding patterns' oil rates by 9% and 13%, respectively (Hughes, Friedmann et al. 1999). In Treatment I the pattern oil rate was first stabilized accompanied by a decrease in the pattern gas rate. The first positive oil rate response was observed 6–8 months after treatment and was dominated by the response at producer wells lying to the west/southwest and/or east/southeast of the treated LNH A9X injection well. **Fig. 20.3a** illustrates the well layout in the treated well pattern for Treatment I. The injection well LNH A9X and producers LHA8, EM60X, and EM11 have shown signs of rapid communication (Fig. 20.3a). The treated injector was an open-hole completion well with the injected fluids accessing 600 ft open hole in the interval between 6,030 ft and 6,630 ft; the left panel of **Fig. 20.3b** displays the pre-treatment well injectivity profile with a CO_2 and water well injectivity in the range of 8–18 bbl/D/psi and 4–12 bbl/D/psi, respectively.

The main conformance issue was the excess access of inject fluids into zone 7, and the lack of injectivity into zones 3 and 5. The right panel of Fig. 20.3b illustrates the post-treatment LNH A9X injection profile indicating that the water was diverted from the upper region of zone 1 intervals (6030–6100 ft) and zone 7 ones (6440–6540 ft) into underperformed zones 3 and 5. Fig. 20.4a displays the pre- and post-treatment pattern oil production history. Prior to Treatment I, the rate of decrease of oil production rate was -128 BOPD/yr. After treatment, oil production rate stabilized at a rate of ±250 BOPD followed by a gradual increase to ±320 nine months later. Fig. 20.4b shows the individual well contribution to the pattern oil production rate (the main contribution to the increased oil rate was from wells EM90X, EM11 and EM60X).

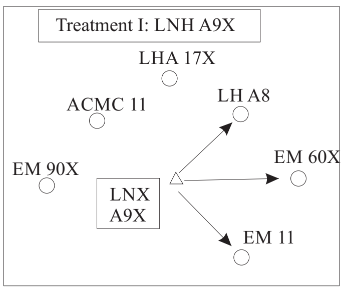

(a)

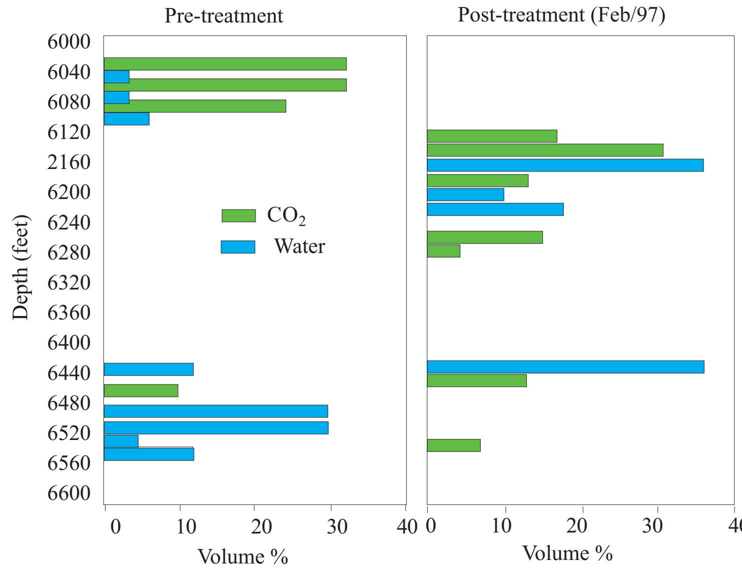

(b)

Figure 20.3: Treatment I: (a) Schematic diagram illustrating the relative location of the treated injection well (LNH A9X) with respect to the surrounding oil produces and rapid communication trends, and (b) pre- and post-treatment injection profile surveys.

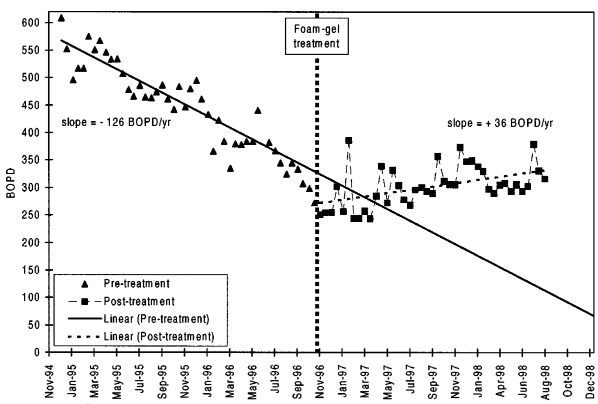

(a)

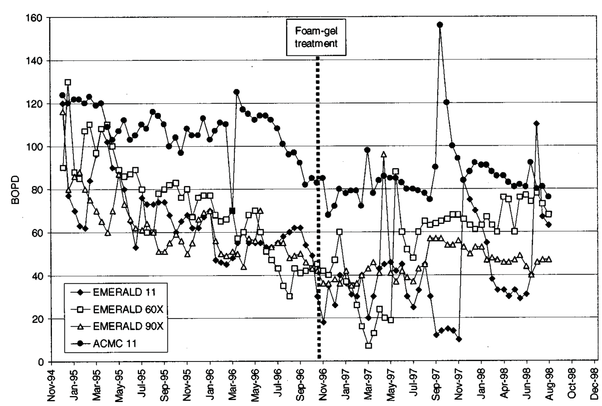

(b)

Figure 20.4: Treatment I: Pre- and post-treatment oil production history for (a) pattern and (b) producing wells EM11, EM60X, EM90X AND ACM11 (Hughes, Friedmann et al. 1999).

20.6 Concluding Remarks

Experience and knowledge gained from laboratory experiments, well and reservoir engineering evaluations, as well as field applications in many parts of the globe have shown that the existing chemicals have yielded positive results for managing unwanted fluids production and maximizing the oil recovery thought either mobility or conformance control well treatments.

This chapter introduced the issues behind low formation sweep efficiency, provided an integrated approach for evaluating the root of the problem, introduced key characteristics required for the injected chemicals and concluded by referring to successful field applications in various case problems and in various parts of the globe. However, it was also stated that depending on the existing well and reservoir characteristics as well as environmental restrictions, challenges may arise in specific case problems which may result in suboptimum well treatments and oil recoveries. There are, therefore, several existing challenges that require to be addressed and opportunities to be attained for further increasing oil recovery factors in an economical and environmental way, especially from mature oil fields in the North Sea.

Nomenclature

f_w = water fractional flow
F_r = resistance factor
f_{wp} = polymer fractional flow
k = permeability, L^2, mD
L_p = linear penetration distance, L, ft
M = mobility ratio
q_o = oil rate, L^3/t, STB/D
q_w = water rate, L^3/t, STB/D
r_p = radial penetration distance, L, ft
S_o = oil saturation
S_{oi} = initial oil saturation
S_{orw} = waterflood residual oil saturation
ϕ = porosity

Subscripts

1 = layer 1
2 = layer 2
o = oil
oi = initial oil
orw = residual oil waterflood
p = penetration, polymer
r = resistance, residual
w = water, waterflood

Abbreviations

AOS = alpha olefin sulfonate
BHP = bottom hole pressure
CDG = colloidal dispersion gels
CMC = critical micellar concentration
DPR = disproportional permeability reduction
EO = ethoxylated
FAWAG = foam assisted water alternating gas
HPAM = hydrolyzed polyacrylamides
HSE = health, safety, environment
IOS = internal olefin sulfonate
NFR = naturally fractured reservoir
OOIP = original oil in place
SWAG = simultaneous water and gas
WAG = water alternating gas

References

Ahmadall, T., Gonzalez, M.V. et al., 1993. Reducing surfactant adsorption in carbonate reservoirs. *SPE reservoir engineering*, **8** (02): 117–122. SPE-24105-PA. May. URL `http://dx.doi.org/10.2118/24105-PA`.

Al-Anazi, H.A. and Sharma, M.M., 2002. Use of a pH Sensitive Polymer for Conformance Control. Paper SPE 73782 presented at the SPE International Symposium on Formation Damage Control, Lafayette, Louisiana, USA. 20–21 February. URL `http://dx.doi.org/10.2118/73782-MS`.

Alkan, H., Goktekin, A., and Satman, A., 1991. A Laboratory Study of CO_2-Foam Process for Bati Raman Field, Turkey. In *Middle East Oil Show*. Society of Petroleum Engineers. SPE-21409-MS. URL `http://dx.doi.org/10.2118/21409-MS`.

Bai, B., Liu, Y. et al., 2007. Preformed Particle Gel for Conformance Control: Transport Mechanism Through Porous Media. *SPE Reservoir Evaluation & Engineering*, **10** (2). April. URL `http://dx.doi.org/10.2118/89468-PA`.

Beecroft, W. and Maier, L., 1969. US Patent No. 808312.

Bernard, G. and Jacobs, W.L., 1965. Effect of Foam on Trapped Gas Saturation and on Permeability of Porous Media to Water. *Society of Petroleum Engineers Journal*, **5** (4). December. URL `http://dx.doi.org/10.2118/1204-PA`.

Bernard, G.G. and Holm, L.W., 1964. Effect of Foam on Permeability of Porous Media to Gas. *Society of Petroleum Engineers Journal*, **4** (3). September. URL `http://dx.doi.org/10.2118/983-PA`.

Bodin, J., Delay, F., and de Marsily, G., 2003a. Solute transport in a single fracture with negligible matrix permeability: 1. fundamental mechanisms. *Hydrogeology Journal*, **11** (4): 418–433. a. URL `http://dx.doi.org/10.1007/s10040-003-0268-2`.

Bodin, J., Delay, F., and de Marsily, G., 2003b. Solute transport in a single fracture with negligible matrix permeability: 2. mathematical formalism. *Hydrogeology Journal*, **11** (4): 434–454. b. URL `http://dx.doi.org/10.1007/s10040-003-0269-1`.

Brattekås, B., Haugen, Å. et al., 2013. Fracture Mobility Control by Polymer Gel- Integrated EOR in Fractured, Oil-Wet Carbonate Rocks. In *EAGE Annual Conference & Exhibition incorporating SPE Europec*. Society of Petroleum Engineers. Paper SPE-164906 presented at EAGE Annual Conference & Exhibition incorporating SPE Europec, London, UK. 10–13 June. URL `http://dx.doi.org/10.2118/164906-MS`.

Chauveteau, G., Denys, K., and Zaitoun, A., 2002. New Insight on Polymer Adsorption Under High Flow Rates. Paper SPE 75183 presented at the SPE/DOE Improved Oil Recovery Symposium, Tulsa, Oklahoma, USA. 13–17 April. URL `http://dx.doi.org/10.2118/75183-MS`.

Chen, Y., Elhag, A.S. et al., 2014. Switchable Nonionic to Cationic Ethoxylated Amine Surfactants for CO2 Enhanced Oil Recovery in High-Temperature, High-Salinity Carbonate Reservoirs. *Society of Petroleum Engineers*, **19** (02): 249–259. SPE-154222-PA. April. URL `http://dx.doi.org/10.2118/154222-PA`.

Choi, S.K., Ermel, Y.M. et al., 2006. Transport of a pH-Sensitive Polymer in Porous Media for Novel Mobility-Control Applications. Paper SPE 99656 presented at the SPE/DOE Improved Oil Recovery Symposium, Tulsa, Oklahoma, USA. 22–26 April. URL `http://dx.doi.org/10.2118/99656-MS`.

Coste, J.P., Liu, Y. et al., 2000. In-Depth Fluid Diversion by Pre-Gelled Particles. Laboratory Study and Pilot Testing. Paper SPE 59362 presented at the SPE/DOE Improved Oil Recovery Symposium, Tulsa, Oklahoma, USA. 3–5 April. URL `http://dx.doi.org/10.2118/59362-MS`.

Enick, R.M., Olsen, D. et al., 2012. Mobility and Conformance Control for CO_2 EOR via Thickeners, Foams, and Gels - A Literature Review of 40 Years of Research and Pilot Tests. Paper SPE 154122 presented at the SPE Improved Oil Recovery Symposium, Tulsa, Oklahoma, USA. 14–18 April. URL `http://dx.doi.org/10.2118/154122-MS`.

Fjelde, I., Zuta, J.F., and Hauge, I., 2008. Retention of CO_2-Foaming Agents on Chalk: Effects of Surfactant Structure, Temperature, and Residual-Oil Saturation. Paper SPE-113259-MS presented at SPE Symposium on Improved Oil Recovery,, Tulsa, Oklahoma, USA. 20–23 April. URL `http://dx.doi.org/10.2118/113259-MS`.

Frampton, H., Morgan, J.C. et al., 2004. Development of a Novel Waterflood Conformance Control System. Paper SPE 89391 presented at the SPE/DOE Improved Oil Recovery Symposium, Tulsa, Oklahoma, USA. 17–21 April. URL `http://dx.doi.org/10.2118/89391-MS`.

Ghedan, S.K. and Poettmann, F.H., 1991. Effect of Polymers on the Imbibition Process: A Laboratory Study. *SPE Reservoir Engineering*, **6** (1): 84–90. February. URL `http://dx.doi.org/10.2118/20244-PA`.

Hatzignatiou, D.G., 1999. Reservoir Engineering Aspects of Horizontal Wells in Stochastic Naturally Fractured Gas Reservoirs. Paper SPE 54626 presented at SPE Western Regional Meeting, Anchorage, Alaska. 26–27 May. URL `http://dx.doi.org/10.2118/54626-MS`.

Hatzignatiou, D.G., Helleren, J. et al., 2014. Numerical Evaluation of Dynamic Core-Scale Experiments of Silicate Gels for Fluid Diversion and Flow-Zone Isolation. *SPE Production & Operations*, **29** (02): 122–138. SPE-170240-PA. May. URL `http://dx.doi.org/10.2118/170240-PA`.

Hatzignatiou, D.G. and McKoy, M., 2000. Probabilistic Evaluation of Horizontal Wells in Stochastic Naturally Fractured Gas Reservoirs. Paper SPE/CIM 65459 presented at SPE/CIM Horizontal Well Technology Conference, Calgary, Canada. 6–8 November. URL `http://dx.doi.org/10.2118/65459-MS`.

Hatzignatiou, D.G., Moradi, H., and Stavland, A., 2013. Experimental Investigation of Polymer Flow through Water- and Oil-Wet Berea Sandstone Core Samples. Paper SPE 164844 presented at the SPE EUROPEC and EAGE Annual Meeting, London UK. 10–13 June. URL `http://dx.doi.org/10.2118/164844-MS`.

Hatzignatiou, D.G., Moradi, H., and Stavland, A., 2015. Polymer flow through water-and oil-wet porous media. *Journal of Hydrodynamics, Ser. B*, **27** (5): 748–762. URL `http://dx.doi.org/10.1016/S1001-6058(15)60537-6`.

Hatzignatiou, D.G., Norris, U.L., and Stavland, A., 2013. Core-scale simulation of polymer flow through porous media. *Journal of Petroleum Science and Engineering*, **108**: 137–150. URL `http://dx.doi.org/10.1016/j.petrol.2013.01.001`.

Haugen, Å., Fernø, M.A. et al., 2012. Experimental Study of Foam Flow in Fractured Oil-Wet Limestone for Enhanced Oil Recovery. *SPE Reservoir Evaluation & Engineering*, **15** (02): 218–228. SPE-129763-PA. April. URL `http://dx.doi.org/10.2118/129763-PA`.

Hermansen, H., 2008. The Ekofisk field: achieving three times the original value. In *19th World Petroleum Congress*. World Petroleum Congress. WPC-19-3966. URL `https://www.onepetro.org/conference-paper/WPC-19-3966`.

Hermansen, H., Thomas, L.K. et al., 1997. Twenty five years of Ekofisk reservoir management. In *SPE Annual Technical Conference and Exhibition*. Society of Petroleum Engineers, Society of Petroleum Engineers (SPE), San Antonio, Texas. SPE-38927-MS. 5–8 October. URL `http://dx.doi.org/10.2118/38927-MS`.

Hughes, T.L., Friedmann, F. et al., 1999. Large-Volume Foam-Gel Treatments to Improve Conformance of the Rangely CO_2 Flood. *SPE Reservoir Evaluation & Engineering*, **2** (1): 14–24. SPE-54772-PA. February. URL `http://dx.doi.org/10.2118/54772-PA`.

Huh, C., Choi, S.K., and Sharma, M.M., 2005. A Rheological Model for pH-Sensitive Ionic Polymer Solutions for Optimal Mobility Control Applications. Paper SPE 96914 presented at the SPE Annual Technical Conference and Exhibition, Dallas, Texas. 9–12 October. URL `http://dx.doi.org/10.2118/96914-MS`.

Iler, R.K., 1979. *The Chemistry of Silica, Solubility, Polymerization, Colloid and Surface Properties, and Biochemistry*. Wiley-Interscience Publication, John Wiley & Sons Inc., New York.

Jaripatke, O.A. and Dalrymple, E.D., 2010. Water-Control Management Technologies: A Review of Successful Chemical Technologies in the Last Two Decades. Paper SPE 127806 presented at the SPE International Symposium and Exhibition on Formation Damage Control, Lafayette, Louisiana, USA. 10–12 February. URL `http://dx.doi.org/10.2118/127806-MS`.

Jensen, T.B., Harpole, K.J., and Østhus, A., 2000. EOR Screening for Ekofisk. In *SPE European Petroleum Conference*. Society of Petroleum Engineers, Paris, France. SPE-65124-MS. 24–25 October. URL `http://dx.doi.org/http://dx.doi.org/10.2118/65124-MS`.

Jurinak, J.J. and Summers, L.E., 1991. Oilfield Applications of Colloidal Silica Gels. *SPE Production Engineering*, **6** (04): 406–412. November. URL `http://dx.doi.org/10.2118/18505-PA`.

Kim, J.S., Dong, Y., and Rossen, W.R., 2005. Steady-State Flow Behavior of CO_2 Foam. *SPE Journal*, **10** (4): 405–415. December. URL `http://dx.doi.org/10.2118/89351-PA`.

Kristiansen, T.S. and Holt, T., 1992. Properties of Flowing Foam in Porous Medium Containing Oil. Paper SPE/DOE 24182 presented at the SPE/DOE Enhanced Oil Recovery Symposium, Tulsa, Oklahoma. 22–24 April. URL `http://dx.doi.org/10.2118/24182-MS`.

Krumrine, P.H. and Boyce, S.D., 1985. Profile Modification and Water Control With Silica Gel-Based Systems. Paper SPE 13578 presented at the SPE Oilfield and Geothermal Chemistry Symposium, Phoenix, Arizona. 9–11 March. URL `http://dx.doi.org/10.2118/13578-MS`.

Lakatos, I. and Lakatos-Szabó, J., 2012. Reservoir Conformance Control in Oilfield Using Silicates: State-of-the-Arts and Perspectives. Paper SPE-159640-MS presented at the SPE Annual Technical Conference and Exhibition, San Antonio, Texas. 8–10 October. URL `http://dx.doi.org/10.2118/159640-MS`.

Lakatos, I., Lakatos-Szabó, J. et al., 1999. Application of Silicate-Based Well Treatment Techniques at the Hungarian Oil Fields. Paper SPE 56739 presented at the 1999 SPE Annual Technical Conference and Exhibition, Houston, Texas, USA. 3–6 October. URL `http://dx.doi.org/10.2118/56739-MS`.

Lane, R.H. and Sanders, G.S., 1995. Water Shutoff Through Fullbore Placement of Polymer Gel in Faulted and in Hydraulically Fractured Producers of the Prudhoe Bay Field. Paper SPE 29475 presented at the SPE Production Operations Symposium, Oklahoma City, Oklahoma. 2–4 April. URL `http://dx.doi.org/10.2118/29475-MS`.

Lane, R.H. and Seright, R.S., 2000. Gel Water Shutoff in Fractured or Faulted Horizontal Wells. Paper SPE 65527 presented at the SPE/CIM International Conference on Horizontal Well Technology, Calgary, Alberta, Canada. 6–8 November. URL `http://dx.doi.org/10.2118/65527-MS`.

Mack, J.C. and Smith, J.E., 1994. In-Depth Colloidal Dispersion Gels Improve Oil Recovery Efficiency. Paper SPE 27780 presented at the SPE/DOE Improved Oil Recovery Symposium, Tulsa, Oklahoma, USA. 17–20 April. URL `http://dx.doi.org/10.2118/27780-MS`.

Mannhardt, K. and Svorstøl, I., 1999. Effect of Oil Saturation on Foam Propagation in Snorre Reservoir Core. *Journal of Petroleum Science and Engineering*, **23** (3-4): 189–200. October. URL `http://dx.doi.org/10.1016/S0920-4105(99)00016-9`.

Masalmeh, S.K., Blom, C.P.A. et al., 2011. Simultaneous Injection of Water and Polymer (SIWAP) to Improve Oil Recovery and Sweep Efficiency from Layered Carbonate Reservoirs. Paper SPE 144865 presented at the SPE Enhanced Oil Recovery Conference, Kuala Lumpur, Malaysia. 19–21 July. URL `http://dx.doi.org/10.2118/144865-MS`.

Mayer, E.H., Berg, R.L. et al., 1983. Alkaline Injection for Enhanced Oil Recovery - A Status Report. *Journal of Petroleum Technology*, **35** (01): 209–221. January. URL `http://dx.doi.org/10.2118/8848-PA`.

Mohnot, S.M., Bae, J.H., and Foley, W.L., 1987. A Study of Mineral/Alkali Reactions. *SPE Reservoir Engineering*, **2** (04): 653–663. November. URL `http://dx.doi.org//10.2118/13032-PA`.

Nasr-El-Din, H.A. and Taylor, K.C., 2005. Evaluation of Sodium Silicate/Urea Gels used for Water Shut-off Treatments. *Journal of Petroleum Science and Engineering*, **48** (3-4): 141–160. September. URL `http://dx.doi.org/10.1016/j.petrol.2005.06.010`.

Nguyen, Q.P., Alexandrov, A.V. et al., 2000. Experimental and Modeling Studies on Foam in Porous Media: A Review. Paper SPE-58799-MS presented at the SPE International Symposium Damage, Lafayette Louisiana. 23–24 February. URL `http://dx.doi.org/10.2118/58799-MS`.

Perez, D., Fragachan, F. et al., 2001. Application of Polymer Gel for Establishing Zonal Isolation and Water Shutoff in Carbonate Formation. *SPE Drilling & Completion*, **16** (3): 182–189. SPE-73196-PA. September. URL `http://dx.doi.org/10.2118/73196-PA`.

Permata, P. and Hatzignatiou, D.G., 2011. Feasibility Study of Gas-Based EOR Processes in a North Sea Oil Reservoir. *J. of Pet. Sci. & Eng.*, **76**: 3–4, 155–171. URL `http://dx.doi.org/10.1016/j.petrol.2011.01.007`.

Pham, L.T. and Hatzignatiou, D.G., 2016. Rheological evaluation of a sodium silicate gel system for water management in mature, naturally-fractured oilfields. *Journal of Petroleum Science and Engineering*, **138**: 218–233. URL http://dx.doi.org/10.1016/j.petrol.2015.11.039.

Pritchett, J., Frampton, H. et al., 2003. Field Application of a New In-Depth Waterflood Conformance Improvement Tool. Paper SPE 84897 presented at the International Improved Oil Recovery in Asia Pacific, Kuala Lumpur, Malaysia. 20–21 October. URL http://dx.doi.org/10.2118/84897-MS.

Schramm, L.L., 1994. *Foams: Fundamentals and Applications in the Petroleum Industry*. Advances in Chemistry Series 242, American Chemical Society, Washington, DC.

Seright, R.S., Lane, R.H., and Sydansk, R.D., 2003. A Strategy for Attacking Excess Water Production. *SPE Production & Facilities*, **18** (03): 158–169. SPE-84966-PA. August. URL http://dx.doi.org/10.2118/84966-PA.

Simjoo, M., Vafaie Sefti, M. et al., 2007. Polyacrylamide Gel Polymer as Water Shut-off System: Preparation and Investigation of Physical and Chemical Properties in One of the Iranian Oil Reservoirs Conditions. *Iran. J. Chem. Chem. Eng.*, **26** (4): 99–108. Autumn. URL http://www.ijcce.ac.ir/article_7611_1415.html.

Skrettingland, K., Dale, E.I. et al., 2014. Snorre In-depth Water Diversion Using Sodium Silicate - Large Scale Interwell Field Pilot. Paper SPE 169727-MS presented at SPE EOR Conference at Oil and Gas West Asia, Muscat, Oman. 31 March – 2 April. URL http://dx.doi.org/10.2118/169727-MS.

Skrettingland, K., Giske, N.H. et al., 2012. Snorre In-depth Water Diversion Using Sodium Silicate - Single Well Injection Pilot. Paper SPE 154004 presented at SPE Improved Oil Recovery Symposium, Tulsa, Oklahoma, USA. 14–18 April. URL http://dx.doi.org/10.2118/154004-MS.

Soliman, M.Y., Creel, P. et al., 2000. Integration of Technology Supports Preventive Conformance Reservoir Techniques. Paper SPE 62553 presented at the SPE/AAPG Western Regional Meeting, Long Beach, California, USA. 19–22 June. URL http://dx.doi.org/10.2118/62553-MS.

Sorbie, K.S., 1991. *Polymer-Improved Oil Recovery*. Blackie and Sons Ltd., Glasgow, Scotland.

Sparlin, D., 1976. An Evaluation of Polyacrylamides for Reducing Water Production. *Journal of Petroleum Technology*, **28** (8): 906–914. SPE-5610-PA. August. URL http://dx.doi.org/10.2118/5610-PA.

Spinler, E., Zornes, D. et al., 2000. Enhancement of oil recovery using a low concentration of surfactant to improve spontaneous and forced imbibition in chalk. In *SPE/DOE Improved Oil Recovery Symposium*. Society of Petroleum Engineers, Tulsa, Oklahoma. SPE-59290-MS. 3–5 April. URL http://dx.doi.org/10.2118/59290-MS.

Stavland, A., Jonsbraaten, H.C. et al., 2010. Polymer Flooding - Flow Properties in Porous Media versus Rheological Parameters. Paper SPE 131103 presented at the SPE EUROPEC/EAGE Annual Conference and Exhibition, Barcelona, Spain. 14–17 June. URL http://dx.doi.org/10.2118/131103-MS.

Stavland, A., Jonsbråten, H.C. et al., 2011a. In-Depth Water Diversion Using Sodium Silicate - Preparation for Single Well Field Pilot on Snorre. Paper presented at the 16th European Symposium on Improved Oil Recovery, Cambridge, UK. 12–14 April. URL http://dx.doi.org/10.3997/2214-4609.201404788.

Stavland, A., Jonsbråten, H.C. et al., 2011b. In-Depth Water Diversion Using Sodium Silicate on Snorre - Factors Controlling In-Depth Placement. Paper SPE 143836 presented at the SPE European Formation Damage Conference, Noordwjik, The Netherlands. 7–10 Juneb. URL http://dx.doi.org/10.2118/143836-MS.

Sydansk, R.D., 2007. Polymers, Gels, Foams, and Resins., In *Petroleum Engineering Handbook: Reservoir engineering and petrophysics*, eds., L. Lake, J. Fanchi, M. F, K. Arnold, J. Clegg, E. Holstein, and H. Warner, , Chap. 13, 1149–1260. Society of Petroleum Engineers. URL http://books.google.no/books?id=yjxSAQAAIAAJ.

Sydansk, R.D. and Romero-Zerón, L., 2011. Reservoir Conformance Improvement. *Society of Petroleum Engineers, Richardson, Texas, USA*.

Thomas, L.K., Dixon, T.N. et al., 1987. Ekofisk Waterflood Pilot. *Journal of Petroleum Technology*, **39** (02): 221–232. SPE-13120-PA. February. URL http://dx.doi.org/10.2118/13120-PA.

Vinot, B., Schechter, R.S., and Lake, L., 1989. Formation of Water-Soluble Silicate Gels by the Hydrolysis of a Diester of Dicarboxylic Acid Solubilized as Microemulsions. *SPE Reservoir Engineering*, **4** (3): 391–397. SPE-14236-PA. August. URL http://dx.doi.org/10.2118/14236-PA.

Wackowski, R.K. and Masoner, L.O., 1995. Rangely Weber Sand Unit CO_2 Project Update: Operating History. *SPE Reservoir Engineering*, **10** (03): 203–207. August. URL `http://dx.doi.org/10.2118/27755-PA`.

Wang, D., 2013. Chapter 4 - Polymer Flooding Practice in Daqing. In J. Sheng, ed., *Enhanced Oil Recovery Field Case Studies*, 83–116. Gulf Professional Publishing, Boston. ISBN 978-0-12-386545-8. URL `http://dx.doi.org/10.1016/B978-0-12-386545-8.00004-X`.

Wang, D., Dong, H. et al., 2009. Review of Practical Experience by Polymer Flooding at Daqing. *SPE Reservoir Evaluation & Engineering*, **12** (3): 470–476. SPE-114342-PA. June. URL `http://dx.doi.org/10.2118/114342-PA`.

Wang, D., Seright, R.S. et al., 2008. Key Aspects of Project Design for Polymer Flooding at the Daqing Oilfield. *SPE Reservoir Evaluation & Engineering*, **11** (6): 1117–1124. SPE-109682-PA. December. URL `http://dx.doi.org/10.2118/109682-PA`.

Wu, L., Chen, P., and Lu, J., 2005. Study of Injection Parameters for Separate Layers During the Period of Polymer Flooding. *Petroleum Geology & Oilfield Development in Daqing*, **24** (4): 75–77.

Yan, W., Miller, C.A., and Hirasaki, G.J., 2006. Foam sweep in fractures for enhanced oil recovery. *Colloids and Surfaces A: Physicochemical and Engineering Aspects*, **282–283**: 348–359. A Collection of Papers in Honor of Professor Ivan B. Ivanov (Laboratory of Chemical Physics and Engineering, University of Sofia) Celebrating his Contributions to Colloid and Surface Science on the Occasion of his 70th Birthday. 20 July. URL `http://dx.doi.org/http://dx.doi.org/10.1016/j.colsurfa.2006.02.067`.

Zhang, G. and Seright, R.S., 2007. Conformance and Mobility Control: Foams versus Polymers. Paper SPE 105907 presented at the SPE International Symposium on Oilfield Chemistry, Houston, Texas, USA. 28 February–2 March. URL `http://dx.doi.org/10.2118/105907-MS`.

Zuta, J. and Fjelde, I., 2010. Transport of CO_2-Foaming Agents During CO_2-Foam Processes in Fractured Chalk Rock. *SPE Reservoir Evaluation & Engineering*, **13** (04): 710–719. SPE-121253-PA. August. URL `http://dx.doi.org/10.2118/121253-PA`.

Chapter 21

CO_2 Injection for EOR

Martin Anders Fernø, Geir Ersland, and Arne Graue

21.1 Introduction

The rate of new discoveries compared to produced oil reserves has been declining in the last decades (Alvarado and Manrique 2010), and many of the existing oil fields are approaching the end of waterflooding and are near the tail end production. Enhanced oil recovery (EOR) processes are designed to maximize oil recovery, extend the field life and increase profitability of the fields by extracting the residual oil that is left behind after conventional recovery methods such as waterflooding. One attractive EOR method is the injection of a miscible gas into the oil reservoir that mixes with the oil and displaces it towards the producing well. Depending on reservoir pressure, temperature and oil composition, a range of available gases have the ability to develop miscibility with crude oil (Lambert, Marino et al. 1996; Skjæveland and Kleppe 1992). One such gas is carbon dioxide (CO_2). The apparent opposite interests with rising world energy demand and anthropogenic climate change may be combined through Carbon Capture, Utilization and Sequestration (CCUS) to reduce greenhouse gas emissions through safe CO_2 storage in mature oil fields and incremental oil recovery for energy consumption (Falcone and Harrison 2013). Meanwhile, current CO_2 EOR projects mainly use CO_2 piped from rapidly depleting natural CO_2 reservoirs, and readily available CO_2 sources are decreasing, increasing the need for anthropogenic CO_2.

Injection of CO_2 may be an attractive EOR method depending on the reservoir quality and crude oil, and may favorably change the physical properties of the oil phase to increase flow through 1) oil swelling, 2) reduction of oil viscosity, 3) increased oil density, 4) vaporization and extraction of hydrocarbon components up to C_{30}, 5) reduction of interfacial tension, and, 6) the ability to achieve miscibility with crude oil at relatively low pressure (Ahmed 1994; Holm 1976; Holm and Josendal 1974; Lambert, Marino et al. 1996; Skjæveland and Kleppe 1992). In the US, CCUS in the form of CO_2 injection for EOR has been implemented for 40 years, largely because of availability of CO_2 (from large natural sources and natural gas plants) and extensive CO_2 pipeline infrastructure (Enick, Olsen et al. 2012; Lambert, Marino et al. 1996; National Energy Technology Laboratory 2010). In the North Sea, however, CO_2 EOR is still not realized, although identified as particularly attractive area because of light crude and favorable reservoir geology compared with American fields (Blunt, Fayers et al. 1993). Two CCS (Carbon, Capture and Storage) projects have so far been implemented on the Norwegian Continental Shelf (NCS), where a total of 13 Mt CO_2 has been stored into two saline aquifers since 1996 (Eiken, Ringrose et al. 2011). These projects were mainly realized as a result of Norwegian taxation on CO_2 emissions on NCS.

Naturally fractured reservoirs are highly heterogeneous in terms of porosity and permeability (Chilingar and Yen 1983; Fernø 2012) and the conductive fracture system usually leads to rapidly declining production and low total recoveries (Allan and Sun 2003; Alvarado and Manrique 2010). High mobility of CO_2 compared to oil and water leads, in many cases, to poor volumetric sweep efficiency limited by gravity tonguing and/or viscous fingering (Hirasaki and Zhang 2004; Lescure and Claridge 1986). The high residual oil saturation after waterflooding makes carbonate reservoirs good candidates for CO_2 enhanced oil recovery (EOR). The injected CO_2 typically achieves miscibility with oil at lower pressures compared to the frequently used gases including (N_2) and methane (CH_4) and is less prone to gravity segregation (Brock and Bryan 1989; Bui 2013). Still, the poor sweep efficiency during CO_2 injections in heterogeneous reservoirs remains a severe problem, and typically 10–20% OOIP incremental recoveries are reported on the field scale during miscible CO_2 (Enick, Olsen et al. 2012). Hence, the need for mobility and conformance control during CO_2 flooding is critical and has led to an extensive study of numerous methods to mitigate the problem. Studies conducted indicate that the Ekofisk field could be a candidate for CO_2 for EOR and storage (Jensen, Harpole et al. 2000). However, the study points out that CO_2 is currently too expensive, and not available in a large enough quantity. The current focus on CCUS might, however, provide a less expensive source of CO_2. With the help of tax, or other economic incentives, governments can create a demand for CO_2, making it a commodity (Hustad and Austell 2004). In order for this to become a realistic option it is also necessary to make the CO_2-flooding process more efficient.

This chapter provides an introduction to challenges for the success of a CO_2 EOR projects, from the reservoir engineer prospective. Important parameters that control the efficiency of CO_2 injection for oil recovery will be reviewed, with emphasis on miscible CO_2 injection for EOR in naturally fractured chalk reservoirs. Laboratory results designed to investigate the CO_2 oil recovery will be discussed and show that diffusion of CO_2 from a fracture is an effective recovery mechanism in system with small fracture spacing. At increased size, the production rate from diffusion alone drops dramatically, and additional CO_2 mobility mechanisms should be implemented. Visualizations of the displacement will be discussed to shed light on the transport of CO_2 into the matrix and numerical simulations model has been developed and validated against laboratory tests to study different parameters that control oil recovery by diffusion.

21.2 CO_2 injection for EOR in fractured reservoirs

In a highly fractured reservoir, miscible CO_2 flooding as an EOR technique rely on diffusion as an important driving mechanism (Alavian and Whitson 2012; Darvish, Lindeberg et al. 2006; Hoteit and Firoozabadi 2006), and an efficient oil recovery therefore requires high fracture density to minimize diffusion lengths. Diffusion is often neglected as a production mechanism during modelling of CO_2 injection in oil reservoirs as it is computationally expensive and assumed to be of minor importance. Whereas this might be true for most conventional reservoirs, it is not true for heavily fractured reservoirs and in laboratory experiments, where the diffusion distances are much smaller. Underestimating the contribution from diffusion in laboratory experiments can create a mismatch if the experimental results are used to predict field behavior. That is because at laboratory scale a low volume of CO_2 is needed to get very high recovery, especially at miscible conditions, whereas at field scale a large volumes of CO_2 are usually recycled into the reservoir.

We here report on laboratory CO_2 injection in fractured carbonate rock samples to study recoverable oil by diffusive mixing (Fernø, Steinsbø et al. 2015). The injected CO_2 will follow the path of least resistance in the fracture, whereas the majority of oil is located in the oil saturated matrix block adjacent to the CO_2 filled fracture. Oil is produced by diffusion only because the viscous forces are limited due to the high transmissibility of the fracture and the low viscosity of the injected CO_2. A one component pure mineral oil (decane) was used as the oleic phase in the experiment to achieve first contact miscible conditions with CO_2 at pressures below 10 MPa, to eliminate the effect of oil composition and to promote repeatability between tests.

21.2.1 Experimental procedure

Fig. 21.1 shows the procedure to prepare fractured core plugs: (A) core plugs were cut at S_{wi} (or dry for baseline tests) along the core length; (B) a 1 mm thick polyoxymethylene (POM) spacer containing separate apartments connected by high conductive flow channels was placed in the fracture; (C–F) the fractured core plug was reassembled, wrapped in aluminum foil to reduce contact between CO_2 and the rubber sleeve; (E–H) aluminum foil was wrapped over inlet and outlet end pieces to further reduce and minimize CO_2 contact with rubber before the fractured core plug was placed in a core holder with overburden pressure. Effective oil permeability in the fractured core plug was measured during injection of oil to fill the fracture.

Fig. 21.2 shows the 7 step block preparation procedure: (1) a rectangular block was cut from a larger slab of chalk and gently washed in distilled water to remove access dust and loose particles. The dimensions were measured, (2) the fracture network was obtained by cutting the matrix with a band saw in an interconnected fracture system, with direct contact between injector and producer. Both horizontal and vertical fractures were cut to increase the tortuosity of the fracture system. POM spacers were placed in each fracture to keep a constant aperture, (3) an epoxy layer was applied using a two component epoxy resin, (4) aluminum foil was wrapped around the block to reduce CO_2 diffusion out of the block, (5) a second epoxy layer was applied, (6) aluminum end pieces were attached to each end face, (7) a final epoxy layer was applied to hold the end pieces in place.

Fig. 21.3 shows the experimental setup for the CO_2 injections. The pore pressure ranged between 86–107 bars, ensuring first-contact miscible conditions between CO_2 and n-decane (Ayirala, Xu et al. 2006). Oil production was measured downstream at ambient pressure in a graded cylinder; pore pressure and differential pressure were also recorded. The confinement pressure was maintained at approximately 15 bars above the

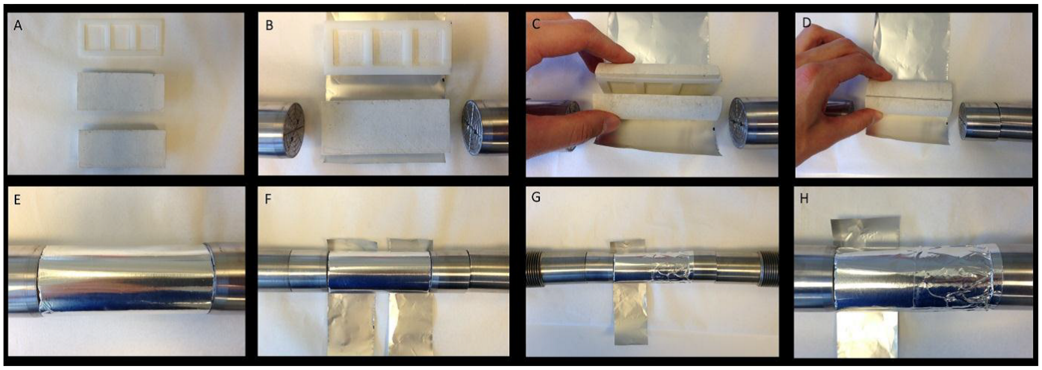

Figure 21.1: The preparatory procedure for fractured core plugs for CO_2 injection tests (Baird 2013).

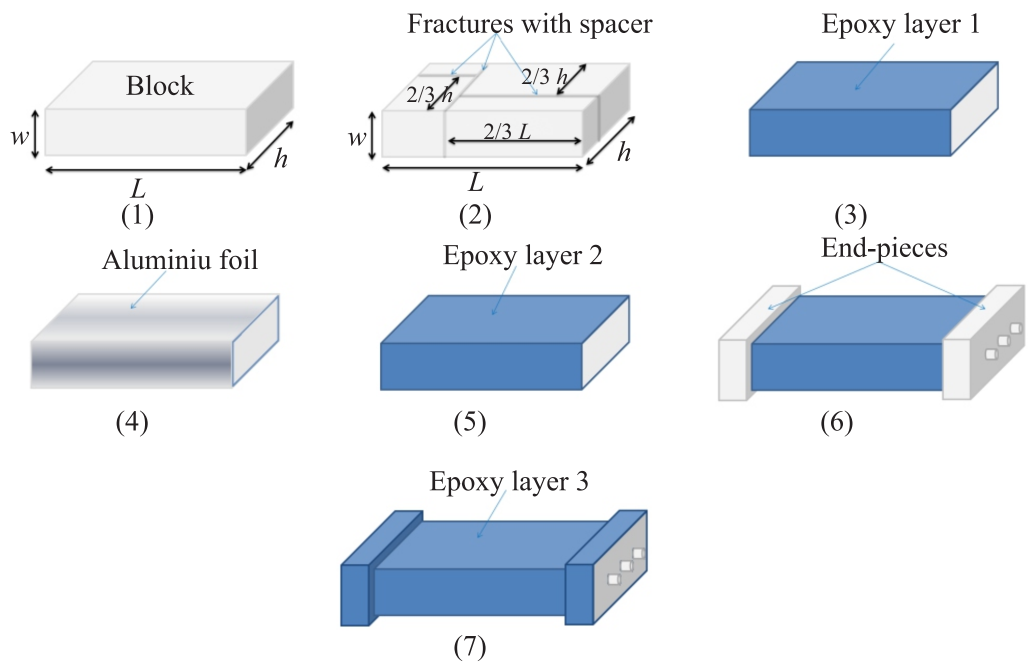

Figure 21.2: Laboratory procedure for fractured block preparation for CO_2 injection tests.

pore pressure. The injection rate was varied between 1 and 4 cm^3/hr. The rectangular blocks were all flooded with an injection rate of 12 cm^3/hr. The reported oil recovery values are from the matrix only in the fractured core plugs.

21.2.2 Secondary CO_2 injection in strongly water-wet core plugs

Seven secondary CO_2 injection tests were performed in whole (3 core plugs) and fractured with an open fracture (4 core plugs). All cores were strongly water-wet and the injection rate was 2 cm 3/hr for core plug PC1 and 4 cm 3/hr for all other tests. **Table 21.1** lists key core properties and final recoveries for the 5 injection tests.

Fig. 21.4 shows the development in average oil saturation during CO_2 injection in whole (core plugs PC1, PC13 and PC15) and fractured (core plugs PC2, PC7, PC9 and PC17) core plugs. The presence of water reduced the oil recovery efficiency during CO_2 injection when compared to baseline tests (PC15 and PC17), both with respect to final recovery and the number of pore volumes needed to reach final recovery. The higher total oil recovery for core plugs without initial water (PC15 and PC17) is attributed to CO_2 being less soluble in water than oil at experimental conditions, and the presence of water reduced the CO_2-oil diffusion in a water-wet porous medium by reducing the contact area between oil and CO_2 (Grogan and Pinczewski 1987; Shyeh-Yung 1991; Zekri, Shedid et al. 2007). The rate of diffusion depends on several parameters including tortuosity, temperature, pressure, concentration gradient and water shielding (Alavian and Whitson 2010; Ghedan 2009; Skjæveland and Kleppe 1992).

The oil production for both whole cores with irreducible water saturation (core plugs PC1 and PC13) was

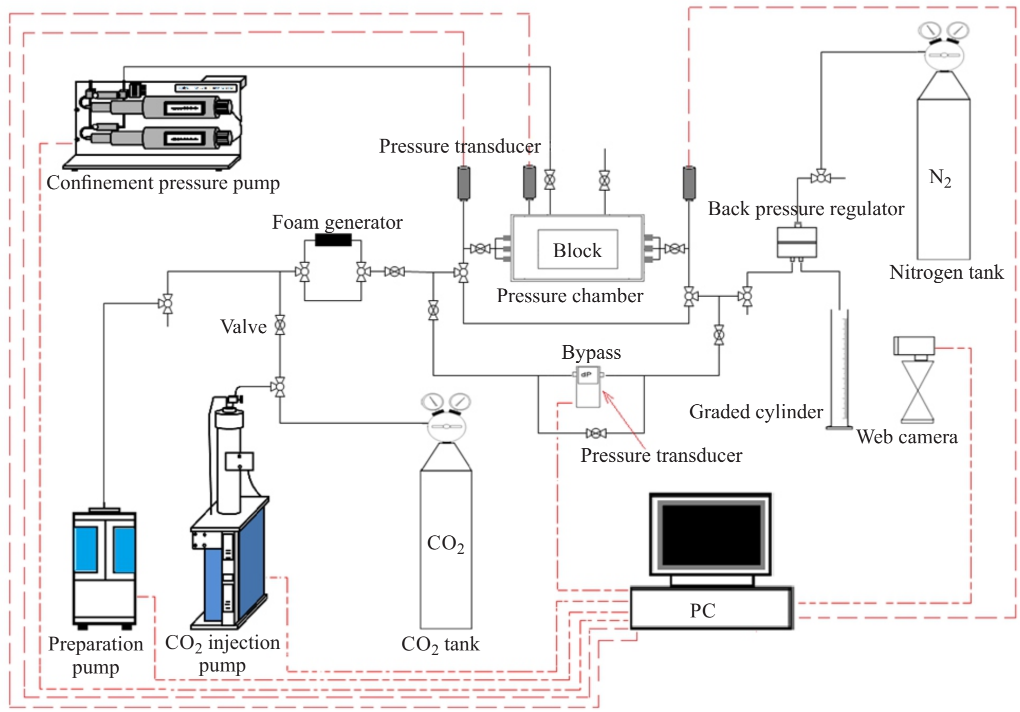

Figure 21.3: Experimental setup used for CO_2 injection tests in fractured and whole core plugs and rectangular blocks.

Core	State	S_{wi}	k_{mat} [mD]	k_{frac} [mD]	S_{or}	RF @ 1 PV	RF @ 2 PV	RF_{tot}	PV @ RF_{tot}
PC1	WHOLE	0.34	3.7	n.a.	0.00	0.93	1.00	1.00	1.6
PC13	WHOLE	0.34	3.8	n.a.	0.00	0.82	0.98	1.00	2.1
PC15	WHOLE	0.00	4.4	n.a.	0.00	0.87	0.99	1.00	2.08
PC2	OPEN	0.34	3.4	2247	0.10	0.28	0.40	0.84	11.2*
PC7	OPEN	0.30	3.2	1855	0.10	0.24	0.41	0.85	11.6
PC9	OPEN	0.35	3.5	2190	0.14	0.25	0.41	0.79	7.5*
PC17	OPEN	0.00	-	1879	0.09	0.28	0.44	0.91	6.75*

Table 21.1: Secondary CO_2 injection in strongly water-wet whole and fractured core plugs.

* final oil recovery not established

RF_{tot}=100% OOIP, identical to the baseline test. The time to reach final recovery varied between 40 hours (core plug PC13) and 60 hours (core plug PC1), reflecting the higher CO_2 injection rate for core plug PC13 (4cm 3/hr) compared with core plug PC1 (2cm 3/hr). The increased injection rate resulted, however, in less efficient displacement for core plug PC13, requiring 2.1 PV CO_2 compared to 1.6 PV injected for core plug PC1. For fractured core plugs, the presence of water reduced the rate of recovery compared to the baseline test: after 1 PV injected the average production was RF=25.6% OOIP (baseline: 28.8% OOIP); after 2 PV injected average RF=40.6% OOIP (baseline: 46.7% OOIP) with the difference increasing with the number of pore volumes injected.

21.2.3 Length of diffusion and oil recovery during CO_2 injection in fractured systems

Fig. 21.5 compares oil recovery during CO_2-injection in rock samples with different diffusion lengths (D_L). The diffusion lengths varied from 0.00 cm in the whole core PC15 to 11.9 cm in whole core PC19, where CO_2 was injected across the inlet end face only. Core plug PC19 was positioned vertically to ensure contact between the injected CO_2 and the oil saturated porous chalk at all times. Two blocks were used with a range of diffusion

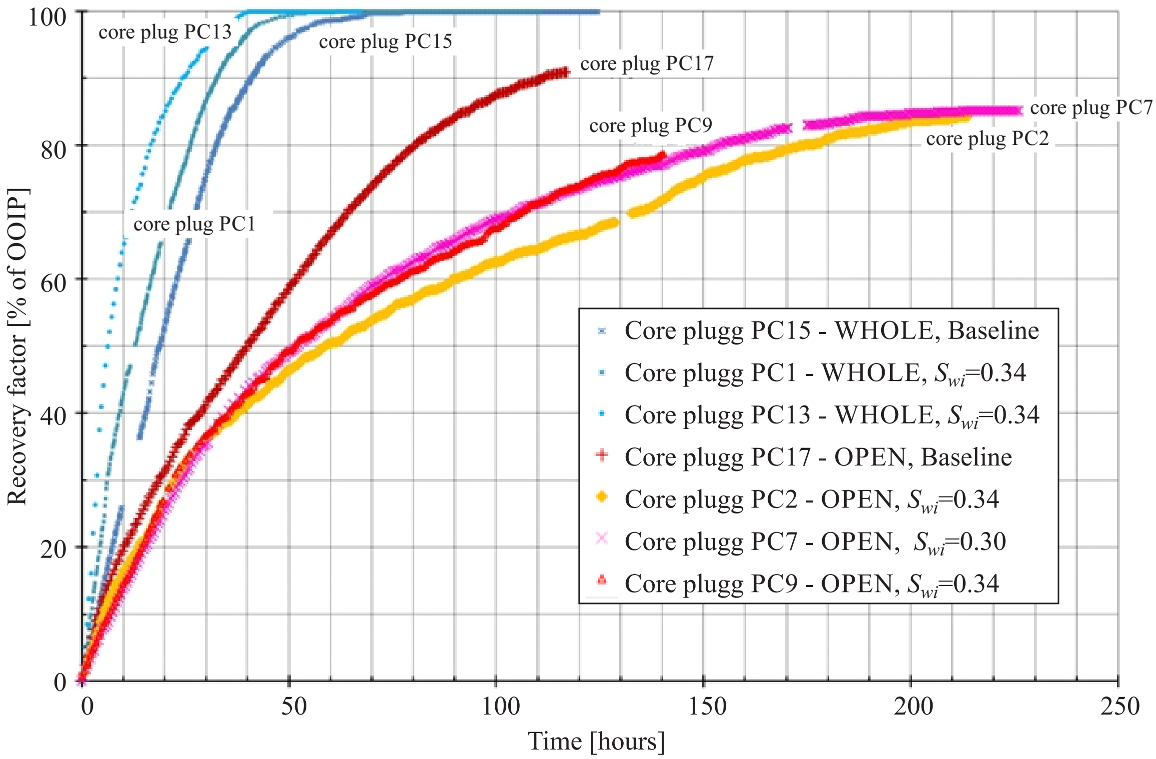

Figure 21.4: Average oil saturation as a function of time during CO_2 injection in whole core plugs (core plugs PC1 and PC13) and fractured core plugs (core plugs PC2, PC7 and PC9). A consistent shift to lower oil recovery with the presence of an irreducible water phase present in the pore space for both whole and fractured core plugs was observed when compared to baseline tests (core plugs PC15 and PC17).

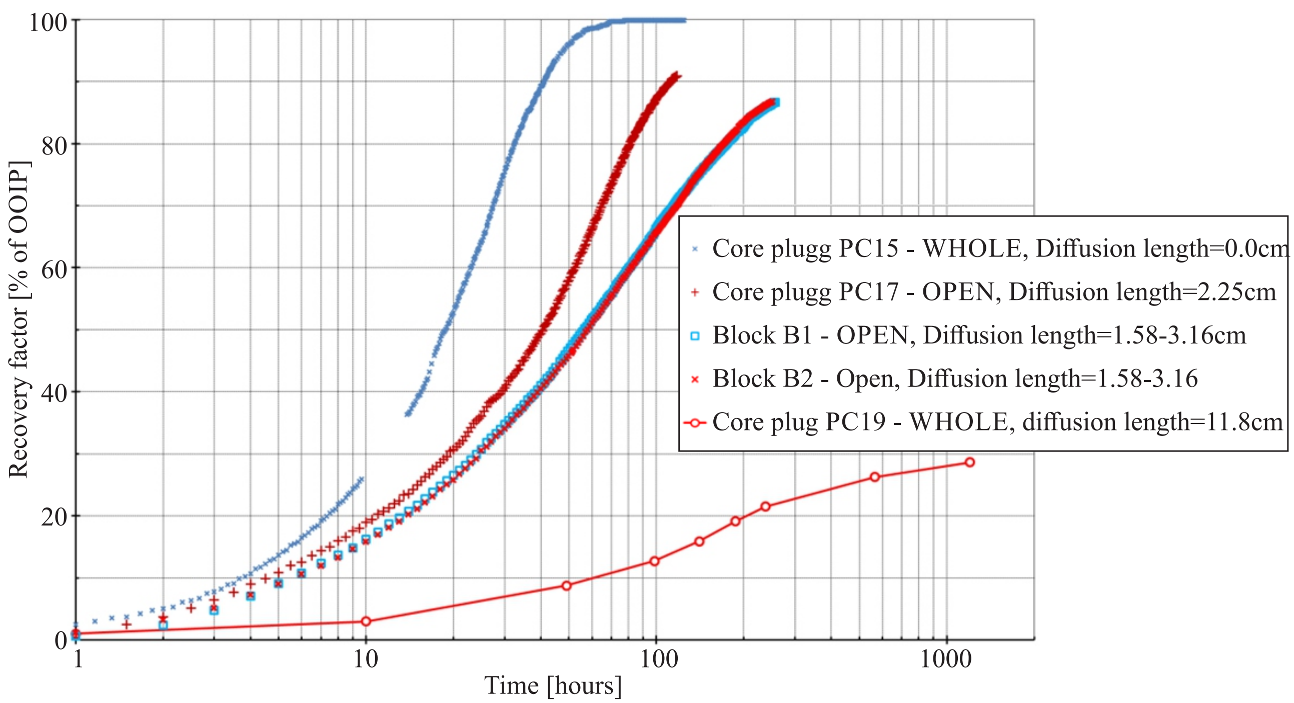

Figure 21.5: Oil recovery vs. time during CO_2 injection in rock samples with different diffusion lengths. The diffusion lengths vary from 0.00 cm in whole core PC15 to 11.9 cm in whole core PC19. Two identical blocks with a several diffusion lengths were used. Note logarithmic x-axis.

lengths within the block ranging between 1.58 – 3.16 cm. Key numbers are listed in **Table 21.2**. An equivalent diffusion length was calculated for core plug PC17 based on a rectangular shaped sample with the same surface area.

Sample	State	Diffusion length [cm]	S_{or}	RF @ 1 PV	RF @ 2 PV	RF_{tot}	PV @ RF_{tot}
PC15	WHOLE	0.00	0.00	0.87	0.99	1.00	2.08
B1	OPEN	1.58-3.16	0.13	0.40	0.66	0.87	4.0
B2	OPEN	1.58-3.16	0.13	0.85	0.94	0.87	2.2*
PC17	OPEN	2.25†	0.09	0.28	0.40	0.91	11.2*
PC19	WHOLE	11.86	0.71	0.05	0.10	0.29	38.2*

Table 21.2: Comparison between secondary CO_2 in fractured systems with variable diffusion length.

* final oil recovery not established
† calculated equivalent to rectangular shape

The oil recovery during pure CO_2 injection in fractured core/block samples at first contact miscible conditions is solely depending on dispersion (mechanical dispersion and molecular diffusion), driving CO_2 from the fracture to the matrix. Fig.21.5 clearly demonstrates that the controlling factor for the oil recovery efficiency during CO_2 injection is the distance the CO_2 must diffuse from the fracture to the oil saturated matrix. In a cylindrical core plug with a longitudinal fracture, the distance is the width of an equivalent rectangle with the same volume as a half cylinder. Blocks B1 and B2 have a range of diffusion lengths, and demonstrate the excellent reproducibility between repeated tests in similar systems. The system with the largest diffusion length (core plug PC19) produced the least amount of oil, and the production did not exceed RF=29% OOIP, even after 1200 hours of injection.

Fig. 21.6 shows the calculated oil production rates observed in systems with variable diffusion lengths. The oil production rate is the slope in each point on the oil recovery curve. The unit used for the production rate ($\Delta S_o/\Delta t$) describes the displacement efficiency during the CO_2 injection: an oil production rate of 1.0 means that one unit of CO_2 injected displace one unit of oil, and an oil production rate of 0.5 means that two units of CO_2 injected displace one unit of oil.

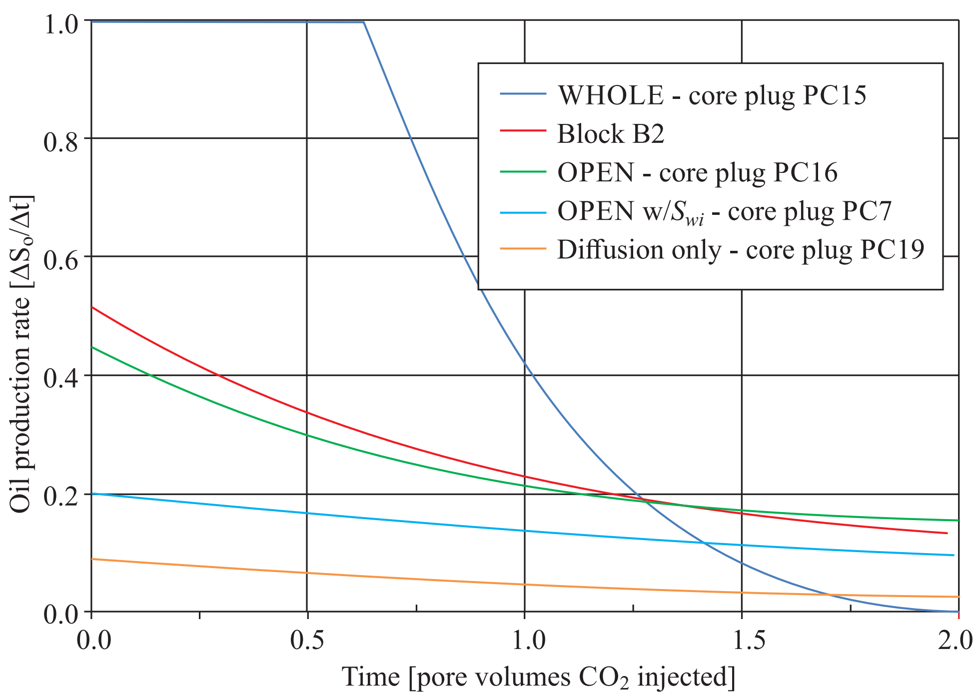

Figure 21.6: Oil production rates ($\Delta S_o/\Delta t$) versus pore volumes injected during secondary CO_2 injection for whole and fractured rock samples with different diffusion lengths.

The highest oil production rate was observed for the whole core plug PC15, where the oil production rate was 1.0 until 0.6 PVs injected when the breakthrough of CO_2 at the outlet was observed. The production rate after CO_2 breakthrough decreased rapidly to zero after 2 PVs injected. The initial oil production rate for block B2 was above 0.5, showing that the CO_2 injection was effective in the heavily fractured system. The oil production rate steadily decreased to 0.13 after 2 PV injected. In comparison, the initial oil production rate for the fractured core plug PC16 was initially lower (0.44) during the first 1.25 PVs injected, after which the production rate was higher than block B2. This behavior results from by the presence of smaller diffusion length ($D_L = 1.58$cm) in parts of the fractured block B2, compared to a constant $D_L = 2.25$cm in core plug PC16. Shorter diffusion lengths reduce the time oil is produced during CO_2 injection and therefore increase the rate of production at the start of the CO_2 injection. After 1.25 PVs CO_2 injected the oil production rate for core plug PC16 was larger than block B2, suggesting that the oil was produced from the parts on the block with longer diffusion lengths up to $D_L = 3.16$cm. The lowest production rate was observed in the system with the longest diffusion length $D_L = 11.86$cm, consistently below 0.1 and decreasing with time. The effect of water on the oil production rate during secondary CO_2 can be observed by comparing core plugs PC7 and PC19: similar rock properties and identical injections, with the only difference being the presence of 34% immobile water in the pore space at the start of the CO_2 injection for core plug PC7. The presence of water dramatically reduced the initial production rate (0.20) compared to the production rate without water (0.44). The production rate without water was more than twice the production rate with an irreducible water phase during the first 0.25PV injected.

21.2.4 Visualization of CO_2 diffusion in fractured chalk

EOR by CO_2 diffusion in fractured reservoirs during CO_2 injection was experimentally investigated using standard size fractured core samples (Eide, Ersland et al. 2015; Eide, Fernø et al. 2015). Local fluid saturations and dynamic oil displacement patterns were imaged using a medical computer tomography scanner. Experiments were performed at supercritical CO_2 conditions above MMP between the oil and the CO_2. **Fig. 21.7** shows development in spatial oil recovery during injection of supercritical CO_2 injection in a fractured, 100% oil saturated core plug.

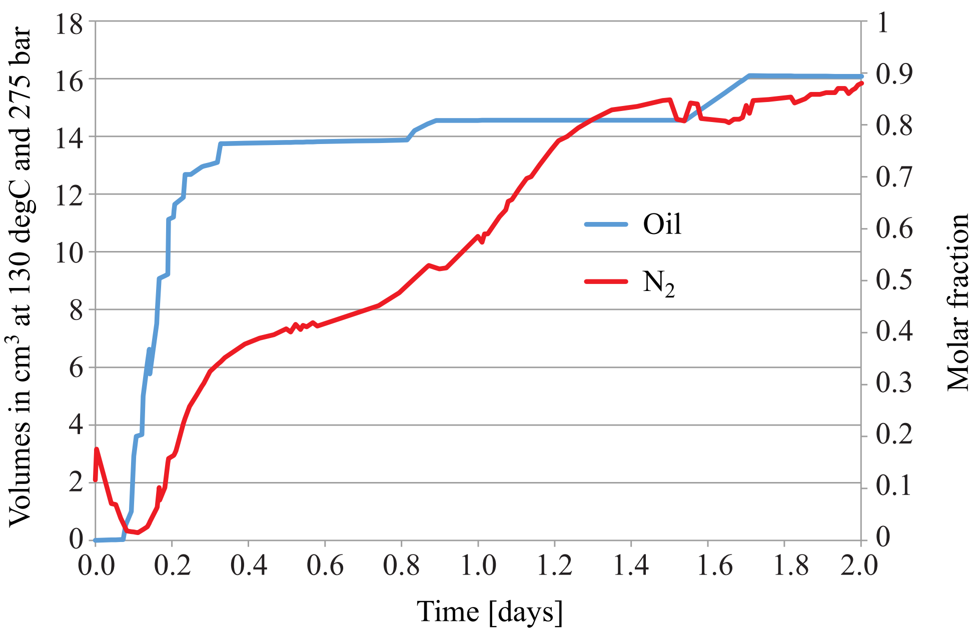

Figure 21.7: Development in oil saturation development during supercritical CO_2 injection in a fractured chalk core plug. Warm colors indicate high oil saturations and cold colors indicate low oil saturation. The core is horizontally digitally sliced perpendicular to the fracture to observe recovery mechanisms from a birds-eye view. Total recovery after 7 pore volumes was 96% OOIP.

The CT images, and the absence of a significant differential pressure, confirmed that molecular diffusion from the CO_2 filled fracture to the oil-filled matrix displaced the oil. Total recovery was 96% OOIP after approximately 7 pore volumes of CO_2 injected. After 1.1 hours CO_2 injection the oil saturation was decreasing in the bottom part of the fracture (at the inlet), and the fracture was fully saturated with CO_2 after 1.8 hours. Oil is produced by diffusion along the whole length of the fracture (L). The supporting columns in the POM spacer (see Fig. 21.1), located at $1/3L$ and $2/3L$, can be observed and continue to be visible up to 56 hours of injection due to a lower CO_2 concentration at those positions. At 3.1 hours the CO_2 has filled the void at the outlet which is evident from the reduction in oil saturation at the top of the image. After 3.0 hours the oil saturation drops uniformly with no difference between the inlet and the outlet. After 5.7 hours the scanning interval was lowered as the production was slower. This can be seen as the larger time difference in subsequent images, but the change in oil saturation is less significant. Oil production was stopped at 117.8 hours when the drop in oil saturation was very slow due to a small saturation gradient between the fracture and the matrix. At this point the oil saturation was almost uniform in the sample.

The injected CO_2 initially flowed only in the fracture and displaced oil here first. The observed symmetric reduction in oil saturation validated diffusion as the main recovery mechanism. Residual oil saturation versus the square root of time was linear, also indicating that diffusion was the only production mechanism in the fractured rock with declining production as time progressed due to the longer diffusion distance. This demonstrates that CO_2 injection and oil recovery by diffusion may be a viable recovery mechanism in fractured reservoirs, but the production rate depends on the fracture spacing. It is also shown that care should be taken when laboratory tests are used to predict field performance and highlights the importance of including diffusion as a production mechanism in some fractured reservoirs. The use of in-situ saturation data means that it is possible to identify heterogeneities in the core samples and get representative values. It also made it possible to identify where the oil is produced from and get local saturation values.

21.2.5 Tertiary CO_2 injection after a waterflood

Tertiary CO_2 injection for EOR is currently the most realistic CO_2 EOR method to be applied on a large scale, using mature oil fields that have been waterflooded for a long time. In this scenario, the injected CO_2 must contact the residual oil after waterflood, and the oil recovery efficiency is no longer only dependent on diffusion. The reservoir wettability determines the location of the residual oil saturation after a waterflood, and at water-wet conditions oil is trapped as discontinuous droplets in the center of the pore. For water-wet system, the injected CO_2 must therefore diffuse through the water to reach the residual oil at the pore-scale. **Fig. 21.8** shows the development in oil saturation during the CO_2 injection in a chalk core plug P2 visualized with MRI Brautaset, Ersland et al. (2008). The injected CO_2 after the waterflood mobilize oil at the inlet and push an oil

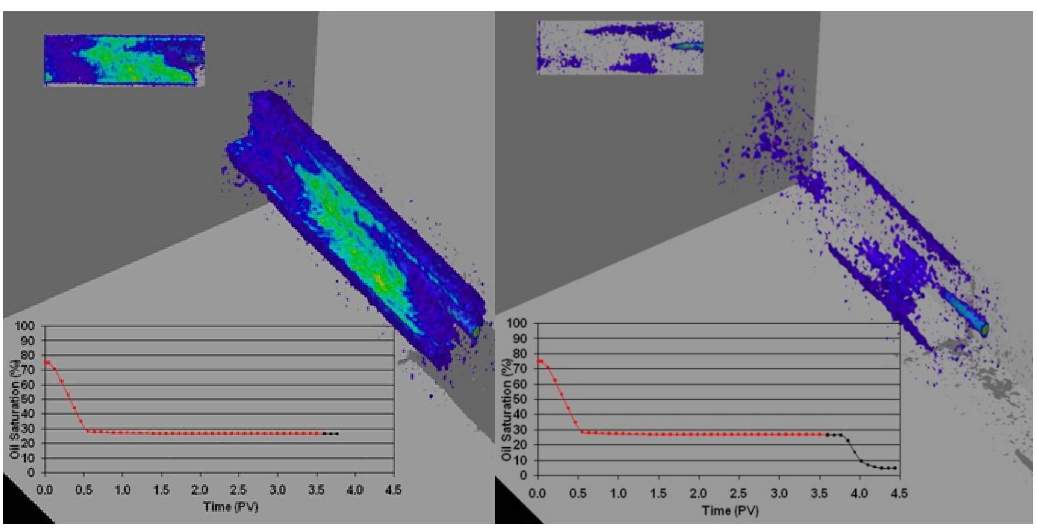

Figure 21.8: Development in oil saturation during tertiary CO_2 injection after a waterflood in a chalk core plug visualized with MRI. The development in average oil recovery vs time, a two dimensional cross-section through the core and the three dimensional spatial distribution of the oil saturation is shown. Left: An oil bank moves towards the outlet after 0.26 PV CO_2 injected. Right: Residual oil saturation after 0.94 PV CO_2 injected was $S_{OR} = 0.048$.

bank through the core towards the outlet. The residual oil after the CO_2 flood was Sor=0.048 resulting in a final recovery of 93.6 %OOIP, see **Table. 21.3**.

In a similar test, CO_2 was injected through a fractured chalk core subsequent to a waterflood.**Fig. 21.9** shows tertiary CO_2 injection into a waterflooded strongly water-wet fractured chalk plug. In contrast to the whole core

Sample	Length [cm]	Dia [cm]	k [mD]	ϕ [frac]	I_{A-H} [-1,1]	WF %OOIP	3^{nd} CO_2 %OOIP	CO_2 inj. [PV]	Final RF %OOIP
P2	10.02	3.81	3.96	0.48	0.25	64.1	29.5	0.94	93.6
COJ 2	10.90	5.07	2.95	0.45	1.00	52.2	9.4	0.52	61.6

Table 21.3: Comparison between tertiary CO_2 injection with and without fractures

system, the presence of fractures resulted in poor incremental oil recovery during the CO_2 injection. Fractures limit the sweep of the injected CO_2, without displacing oil from the adjacent matrix blocks.

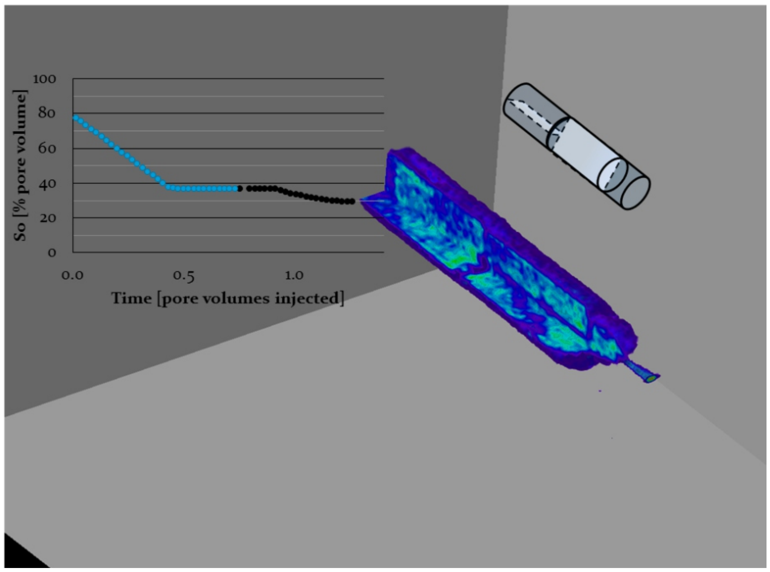

Figure 21.9: Development in oil saturation during tertiary CO_2 injection after a waterflood in a fractured chalk core plug visualized with MRI. The fracture network is schematically shown in upper, right corner. The injected CO_2 did not produce oil from the matrix blocks

Compared to secondary CO_2 injection, the increased water saturation in the matrix at the start of the CO_2 injection resulted in a significantly lower oil production, suggesting a water shielding effect. Residual oil after waterflooding in the strongly water-wet systems is trapped in the center of the pore as a result of capillarity, and the injected CO_2 phase must initially diffuse through the water layer to mix and thus mobilize oil. Increased water saturation after waterflooding resulted in thicker water layers and reduced production rate of oil. The 9.4% OOIP incremental oil recovery observed from core plug COJ 2 was produced from the inlet core only. The MRI images show no additional recovery from the matrix blocks adjacent to the fracture.

21.3 Mobility Control for CO_2 EOR in fractured reservoirs

As demonstrated above, CO_2 injection for EOR may be an attractive oil recovery mechanism in systems with small diffusion lengths. In fractured systems, however, the sweep efficiency is poor, and large amounts of CO_2 must be recycled as a result of the early breakthrough in the production well from CO_2 in the fracture network. This adds significant costs to the CO_2 EOR projects and should be avoided. A potential method to improve the poor macroscopic sweep efficiency is to reduce the mobility of the injected CO_2. Reduction in gas mobility by CO_2 foam injection provides improved mobility and conformance control and will reduce recycling costs and increase the unit oil produced/unit CO_2 injected ratio. One promising solution of CO_2 mobility control is the injection of a surfactant solution alongside CO_2 to create foam, see (e.g., Hirasaki, Miller et al. 2011; Li, Yan et al. 2010; Rossen 1995). CO_2 foam effectively increases the gas viscosity to produce a more favorable mobility ratio to increase sweep, and thereby improve oil recovery. So far only limited field implementation is observed due to inaccurate simulation tools for foam behavior in a reservoir. Nevertheless, the injection of foam in naturally fractured reservoirs is increasingly recognized as a potential EOR technique (Haugen, Fernø et al.

2012; Kovscek, Tretheway et al. 1995; Pancharoen, Fernø et al. 2012; Yan, Miller et al. 2006; Fernø, Gauteplass et al. 2014), specifically see Farajzadeh, Wassing et al. (2010) and references therin.

21.3.1 Tertiary CO_2-foam injections

Tertiary CO_2 foam injections were performed in two fractured block samples, both after waterflood (block B3) and after pure CO_2 injection (block B2 and core plug EDW35). Additional oil recovery was observed in both cases and the final recovery after CO_2 foam was identical for both blocks (RF= 68.4% OOIP). The oil recovery during tertiary CO_2 and CO_2 foam injections after waterflooding may be evaluated using blocks B2 and B3, see **Table 21.4**.

Sample	System description	WF % OOIP	3nd CO_2 % OOIP	3nd CO_2-foam % OOIP	Final RF % OOIP
P2	Whole	64.1	29.5	-	93.6
COJ 2	Frac Core	52.2	9.4	-	61.6
EDW35	Frac Core	41.1	11.0	12.3	64.6
B2	Frac Block	59.6	6.8	2.0	68.4
B3	Frac Block	60.7	-	7.7	68.4

Table 21.4: Oil production during waterfloods, CO_2 and CO_2 foam injections for five injection tests.

Fig. 21.10 compares tertiary oil production during CO_2 foam injection (block B3) and CO_2 injection (block B2) subsequent to the waterflood. Oil production is given in % produced of residual oil after waterflooding, SOR,WF. Both blocks had identical fracture and matrix networks and had equal dimensions and rock properties. Similar oil saturation endpoints after the waterflood (Block B2: RF= 59.6% OOIP, $S_o = 0.40$; Block B3: RF= 60.7% OOIP, $S_o = 0.39$) make it possible to directly compare the efficiency between CO_2 and CO_2 foam in identical systems. A significantly accelerated oil recovery was observed during CO_2 foam injected compared to pure CO_2 injection: oil recovery after 0.4 PVs CO_2 injected was 19.6% $S_{or,\text{wf}}$ for CO_2 foam, compared with only 11.6% $S_{or,\text{wf}}$ for CO_2.

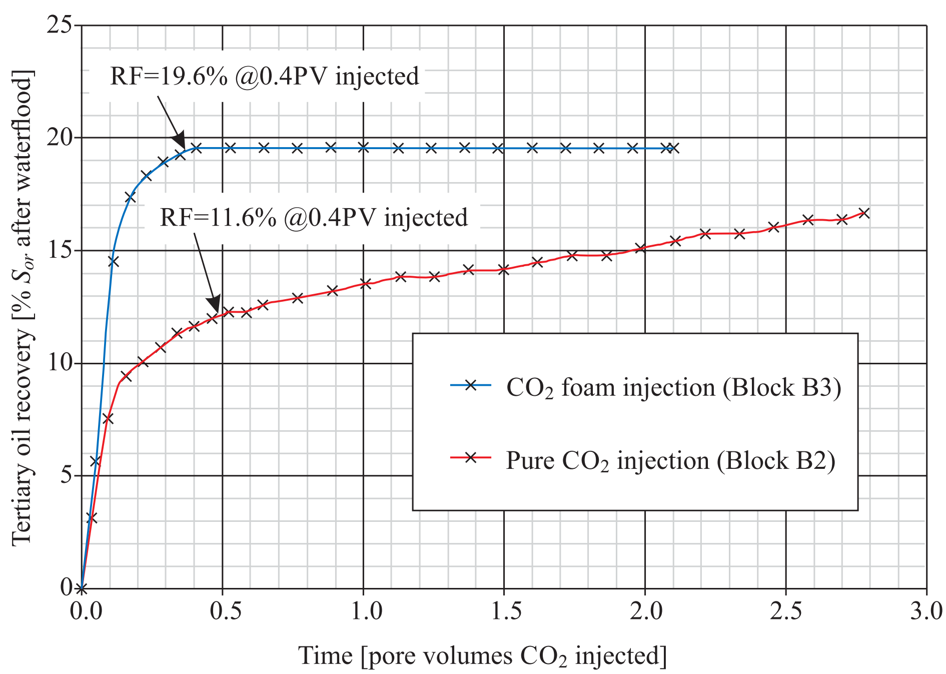

Figure 21.10: Comparison of tertiary oil production in fractured block samples during CO_2 foam injection (block B3) and CO_2 injection (block B2) subsequent to waterflooding. Oil production is % residual oil after waterflooding, $S_{or,\text{wf}}$. A significantly accelerated oil recovery was observed during CO_2 foam injected compared to pure CO_2 injection.

Reduction in CO_2 mobility by foam contributed to reduce the amount of CO_2 needed to by more than 1 magnitude (over 12 times) and made the CO_2 injection significantly more effective, consumption: 0.17PV CO_2 was injected to produce 17.0% $S_{or,f}$ during tertiary CO_2-foam injection, compared to 2.78PV to produce RF=17.0 % $S_{or,wf}$ during tertiary CO_2 injection. The initial oil production rate (change in oil saturation per time) during CO_2-foam was 0.68, compared to 0.47 for pure CO_2 injection. The CO_2-foam production rate remained larger than the CO_2 production rate during the first 0.3 PVs injected: 43% larger at start of injection; 79% larger after 0.10PV; 104% larger after 0.15PV; 124% larger after 0.20PV; 99% larger after 0.25PV. After 0.4 PV injected, the oil production stopped in block B3.

Fig. 21.11 shows the average oil saturation and differential pressure for the water-wet core plug EDW35 during waterflood, pure CO_2 injection and CO_2 foam injection. Waterflood oil recovery was 39.7% of OOIP after 0.4 PV injected, with a total of 2.8 PV water injected. The CO_2 injection recovered an additional 10.2% OOIP after 0.2PV (2.6 PV CO_2 injected in total), whereas the subsequent CO_2 foam injection gave 13% of OOIP (8.5PV injected). Oil production during CO_2 foam was observed after 5PV injected, after an increase in differential pressure.

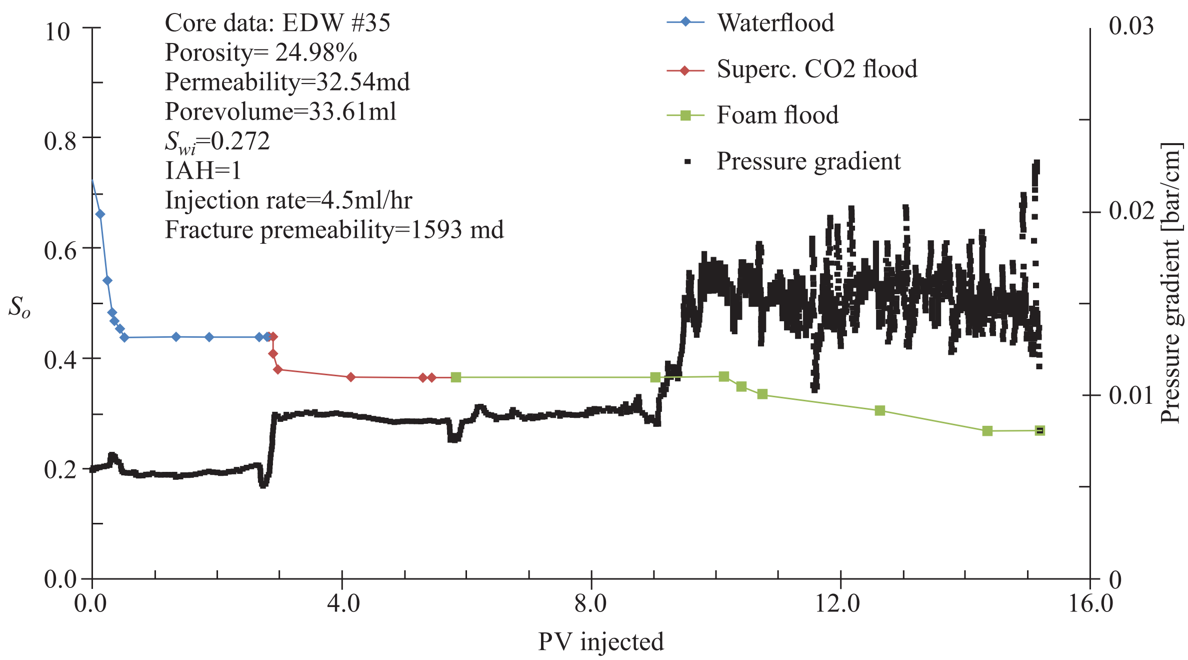

Figure 21.11: Differential pressure and saturation profile for EDW35 (fractured water-wet core) during waterflood, CO_2 and CO_2 foam flood. Injection rate was equal to 4.5 ml/hr. CO_2 injected at near miscible conditions (Haugen, Mani et al. 2014).

21.4 Conclusions

In the laboratory, using standard sized core plugs, CO_2 injection is a very effective recovery method at above MMP, with high ultimate oil recovery values (RF 90% OOIP). The efficient oil recovery is due to first-contact miscibility between CO_2 and oil. The impact from negative effects applying CO_2 injection, including the high CO_2 mobility, viscous fingering and channeling and gravity segregation only have a minor effect in core floods because of the rapid rate of diffusion at this scale; in particular in fractured core plugs due to the large surface exposure area between residual oil and CO_2.

The enhanced oil recovery (EOR) potential during secondary and tertiary CO_2 injection in fractured oil reservoirs was evaluated in systematic laboratory tests. The results demonstrate a significant oil recovery potential during secondary CO_2 injection, in both whole and fractured core plugs. The presence of fractures, however, dramatically reduced the oil production rate in cases where oil recovery was mainly driven by diffusion. The observed production rate correlated with the length of diffusion from the fracture to the matrix: a larger distance from the fracture to the center of the matrix block reduced the oil recovery rate.

Oil recovery by CO_2 oil diffusion was visualized with nuclear magnetic resonance (MRI) and x-ray computer tomography (CT). The development in local CO_2 and oil saturations was imaged during injection tests, both with and without residual water present. Visualization with MRI showed oil recoveries above 90% OOIP without fractures. The presence of fractures dramatically reduced oil recovery by diffusion during tertiary CO_2 injection because the residual oil is surrounded by water leading to a water-shielding effect. Water reduced the rate of production by reducing the pore space and changes the tortuosity and CO_2 flow paths.

Foam mobility control during tertiary CO_2 injection after waterfloods in fractured systems accelerated oil recovery and increased oil production by 70% within 0.4 PV CO_2 injected compared to pure CO_2 injection. CO_2-foam injection produced 20% of the residual oil after waterflood (7% OOIP). An increased oil production rate (more than double) was observed with CO_2-foam compared to pure CO_2 injection during the first 0.3 PV injected. Additionally, mobility control by foam reduced the amount of CO_2 needed by more than 1 order of magnitude (over 12 times) to produce the same amount of oil.

Nomenclature

D_L = diffusion length, L
$I_{\text{A-H}}$ = Amott-Harvey wettability index
k = absolutt permeability, L^2
k_{frac} = permeability in fracrured system, L^2
k_{mat} = permeability of rock matrix, L^2
L = fracture length, L
RF_{tot} = total oil recovery factor
S_{or} = residual oil saturation
$S_{or,\text{wf}}$ = residual oil saturation after waterflooding
S_{wi} = initial water saturation
ϕ = porosity
ΔS_o = change in oil saturation
Δt = change in time

Subscripts

A-H = Amott-Harvey
frac = fracture
mat = matrix
tot = total
L = length
o = oil
or = residual oil
or, wf = residual oil, after waterflooding
wi = initial water

Abbreviation

CCS = carbon, capture and storage
CCUS = carbon capture, utilization and sequestration
NCS = norwegian continental shelf
POM = polyoxymethylene
RF = recovery factor
WF = water flooding

References

Ahmed, T.H.M.T., 1994. Prediction of CO2 Minimum Miscibility Pressures. SPE Latin America/Caribbean Petroleum Engineering Conference, Buenos Aires, Argentina. 27–29 April. URL http://dx.doi.org/10.2118/27032-MS.

Alavian, S.A. and Whitson, C.H., 2010. CO2 EOR Potential in Naturally Fractured Haft Kel Field, Iran. *SPE Reservoir Evaluation & Engineering*, **13** (4): 720–729. URL http://dx.doi.org/10.2118/139528-PA.

Alavian, S.A. and Whitson, C.H., 2012. Modeling CO2 Injection Including Diffusion in a Fractured-Chalk Experiment with Initial Water Saturation. Carbon Management Technology Conference, Orlando, Florida, USA. 7–9 February. URL `http://dx.doi.org/10.7122/149976-MS`.

Allan, J. and Sun, S.Q., 2003. Controls on Recovery Factor in Fractured Reservoirs: Lessons Learned from 100 Fractured Fields,. SPE Annual Technical Conference and Exhibition,Denver, Colorado. 5–8 October. URL `http://dx.doi.org/10.2118/84590-MS`.

Alvarado, V. and Manrique, E., 2010. Enhanced Oil Recovery: An Update Review. *Energies*, **3** (9): 1529–1575. URL `http://dx.doi.org/10.3390/en3091529`.

Ayirala, S.C., Xu, W., and Rao, D.N., 2006. Interfacial Behaviour of Complex Hydrocarbon Fluids at Elevated Pressures and Temperatures. *The Canadian Journal of Chemical Engineering*, **84** (1): 22–32. URL `http://dx.doi.org/10.1002/cjce.5450840105`.

Baird, S., 2013. *CO2 EOR by Diffusion in Fractured Chalk*. Master's thesis, University of Bergen, Bergen.

Blunt, M., Fayers, F., and Jr., F.M.O., 1993. Carbon dioxide in enhanced oil recovery. *Energy Conversion and Management*, **34** (9–11): 1197–1204. Proceedings of the International Energy Agency Carbon Dioxide Disposal Symposium. URL `http://dx.doi.org/10.1016/0196-8904(93)90069-M`.

Brautaset, A., Ersland, G. et al., 2008. Using MRI to Study In situ Oil Recovery During CO2 Injection in Carbonates. SCA International Symposium Abu Dhabi, UAE. 29 October – 2 November.

Brock, W.R. and Bryan, L.A., 1989. Summary Results of CO2 EOR Field Tests, 1972 –1987. Low Permeability Reservoirs Symposium, 6–8 March, Denver, Colorado. URL `http://dx.doi.org/10.2118/18977-MS`.

Bui, L.H., 2013. *Near-Miscible CO2 Application to Improve Oil Recovery*. Master's thesis, University of Kansas. 108 pp.

Chilingar, G.V. and Yen, T.F., 1983. Some Notes on Wettability and Relative Permeabilities of Carbonate Reservoir Rocks, II. *Energy Sources*, **7** (1): 67–75. October. URL `http://dx.doi.org/10.1080/00908318308908076`.

Darvish, G.R., Lindeberg, E.G.B. et al., 2006. Reservoir Conditions Laboratory Experiments of CO2 Injection Into Fractured Cores. SPE Europec/EAGE Annual Conference and Exhibition, 12-15 June, Vienna, Austria. URL `http://dx.doi.org/10.2118/99650-MS`.

Eide, Ø., Ersland, G. et al., 2015. CO2 EOR by Diffusive Mixing in Fractured Reservoirs. *PETROPHYSICS*, **56** (1): 23–31. URL `http://www.researchgate.net/profile/Martin_Ferno/publication/275153483_CO2_EOR_by_Diffusive_Mixing_in_Fractured_Reservoirs/links/5534e4220cf2df9ea6a3f178.pdf`.

Eide, Ø., Fernø, M.A. et al., 2015. Visualization of Carbon Dioxide Enhanced Oil Recovery by Diffusion in Fractured Chalk. *SPE Journal*. URL `http://dx.doi.org/10.2118/170920-PA`.

Eiken, O., Ringrose, P. et al., 2011. Lessons learned from 14 years of {CCS} operations: Sleipner, In Salah and Snøhvit. *Energy Procedia*, **4** (0): 5541–5548. 10th International Conference on Greenhouse Gas Control Technologies. URL `http://dx.doi.org/http://dx.doi.org/10.1016/j.egypro.2011.02.541`.

Enick, R.M., Olsen, D. et al., 2012. Mobility and Conformance Control for CO_2 EOR via Thickeners, Foams, and Gels - A Literature Review of 40 Years of Research and Pilot Tests. Paper SPE 154122 presented at the SPE Improved Oil Recovery Symposium, Tulsa, Oklahoma, USA. 14–18 April. URL `http://dx.doi.org/10.2118/154122-MS`.

Falcone, G. and Harrison, R., 2013. Deciding Whether to Fund Either CCS or CCUS Offshore Projects: Are We Comparing Apples and Pears in the North Sea? SPE Annual Technical Conference and Exhibition, 30 September-2 October, New Orleans, Louisiana, USA. URL `http://dx.doi.org/10.2118/166388-MS`.

Farajzadeh, R., Wassing, L.B.M., and Boerrigter, P.M., 2010. Foam Assisted Gas Oil Gravity Drainage in Naturally-Fractured Reservoirs. SPE Annual Technical Conference and Exhibition, 19-22 September, Florence, Italy. URL `http://dx.doi.org/10.2118/134203-MS`.

Fernø, M.A., 2012. Introduction to Enhanced Oil Recovery (EOR) Processes and Bioremediation of Oil-Contaminated Sites. In L. Romero-Zerón, ed., *Introduction to Enhanced Oil Recovery (EOR) Processes and Bioremediation of Oil-Contaminated Sites*, Chap. Enhanced Oil Recovery in Fractured Reservoirs,. InTech. URL `http://dx.doi.org/10.5772/34732`. ISBN: 978-953-51-0629-6. May.

Fernø, M.A., Gauteplass, J. et al., 2014. Experimental Study of Foam Generation, Sweep Efficiency and Flow in a Fracture Network. In *SPE Annual Technical Conference and Exhibition*. Society of Petroleum Engineers. URL http://dx.doi.org/10.2118/170840-MS.

Fernø, M.A., Steinsbø, Ø. et al., 2015. Parametric Study of Oil Recovery during CO_2 iinjection in Fractured Chalk: Influence of fractured permaeability, diffusion length and water saturation. *Jorurnal of Natural Gas Science and Engineering*, In Press.

Ghedan, S.G., 2009. Global Laboratory Experience of CO2-EOR Flooding,. SPE/EAGE Reservoir Characterization and Simulation Conference, 19-21 October, Abu Dhabi, UAE. URL http://dx.doi.org/10.2118/125581-MS.

Grogan, A.T. and Pinczewski, W.V., 1987. The Role of Molecular Diffusion Processes in Tertiary CO2 Flooding. *Journal of Petroleum Technology*, **39** (5): 591–602. URL http://dx.doi.org/10.2118/12706-PA.

Haugen, Å., Fernø, M.A. et al., 2012. Experimental Study of Foam Flow in Fractured Oil-Wet Limestone for Enhanced Oil Recovery. *SPE Reservoir Evaluation & Engineering*, **15** (02): 218–228. SPE-129763-PA. April. URL http://dx.doi.org/10.2118/129763-PA.

Haugen, Å., Mani, N. et al., 2014. Miscible and immiscible foam injection for mobility control and EOR in fractured oil-wet carbonate rocks. *Transport in Porous Media*, **104** (1): 109–131. URL http://dx.doi.org/10.1007/s11242-014-0323-6.

Hirasaki, G., Miller, C.A., and Puerto, M., 2011. Recent Advances in Surfactant EOR. *SPE Journal*, **16** (4): 889–907. URL http://dx.doi.org/10.2118/115386-PA.

Hirasaki, G.J. and Zhang, D.L., 2004. Surface Chemistry of OIl Recovery From Fractured, Oil-Wet, Carbonate Formations. *SPE Journal*, **9** (02): 151–162. SPE-88365-PA. URL http://dx.doi.org/10.2118/88365-PA.

Holm, L.W., 1976. Status of CO2 and Hydrocarbon Miscible Oil Recovery Methods. *Journal of Petroleum Technology*, **28** (1): 76–84. SPE-5560-PA. URL http://dx.doi.org/10.2118/5560-PA.

Holm, L.W. and Josendal, V.A., 1974. Mechanisms of Oil Displacement By Carbon Dioxide. *Journal of Petroleum Technology*, **26** (12): 1427–1438. SPE-4736-PA. URL http://dx.doi.org/10.2118/4736-PA.

Hoteit, H. and Firoozabadi, A., 2006. Numerical modeling of diffusion in fractured media for gas injection and recycling schemes. SPE Annual Technical Conference and Exhibition, 24–27 September, San Antonio, Texas, USA. URL http://dx.doi.org/10.2118/103292-MS.

Hustad, C.W. and Austell, J.M., 2004. Mechanisms and incentives to promote the use and storage of CO 2 in the North Sea. In M.M. Roggenkamp and U. Hammer, eds., *In European Energy Law Report I*, 355–380. Intersentia.

Jensen, T.B., Harpole, K.J., and Østhus, A., 2000. EOR Screening for Ekofisk. In *SPE European Petroleum Conference*. Society of Petroleum Engineers, Paris, France. SPE-65124-MS. 24–25 October. URL http://dx.doi.org/http://dx.doi.org/10.2118/65124-MS.

Kovscek, A.R., Tretheway, D.C. et al., 1995. Foam flow through a transparent rough-walled rock fracture. *Journal of Petroleum Science and Engineering*, **13** (2): 75–86. URL http://dx.doi.org/http://dx.doi.org/10.1016/0920-4105(95)00005-3.

Lambert, M.R., Marino, S.D. et al., 1996. Implementing CO2 Floods: No More Delays! Permian Basin Oil and Gas Recovery Conference, 27-29 March, Midland, Texas. URL http://dx.doi.org/10.2118/35187-MS.

Lescure, B.M. and Claridge, E.L., 1986. CO2 Foam Flooding Performance vs. Rock Wettability. SPE Annual Technical Conference and Exhibition, 5-8 October, New Orleans, Louisiana. URL http://dx.doi.org/10.2118/15445-MS.

Li, R.F., Yan, W. et al., 2010. Foam Mobility Control for Surfactant Enhanced Oil Recovery. *SPE Journal*, **15** (4): 928–942. URL http://dx.doi.org/10.2118/113910-PA.

National Energy Technology Laboratory, N., 2010. Carbon Dioxide Enhanced Oil Recovery-Untapped Domestic Energy Supply and Long Term Carbon Storage Solution. *The Energy Lab*. URL http://www.netl.doe.gov/File%20Library/Research/Oil-Gas/enhanced%20oil%20recovery/co2%20eor/NETL_CO2-EOR-Primer.pdf.

Pancharoen, M., Fernø, M.A., and Kovscek, A.R., 2012. Modeling foam displacement in fractures. *Journal of Petroleum Science and Engineering*, **100**: 50–58. URL `http://dx.doi.org/http://dx.doi.org/10.1016/j.petrol.2012.11.018`.

Rossen, W.R., 1995. Foams in Enhanced Oil Recovery, In *Foams Theory, Measurements, and Applications.*, eds., R.K. Prud'homme and S.A. Khan, , Chap. 11. Foams in Enhanced Oil Recovery, 414–457. Taylor & Francis Inc, New York. ISBN 0-8247-9395-1. URL `https://www.ebook.de/de/product/3802723/robert_k_prud_homme_foams.html`.

Shyeh-Yung, J.G.J., 1991. Mechanisms of Miscible Oil Recovery: Effects of Pressure on Miscible and Near-Miscible Displacement of Oil by Carbon Dioxide. SPE Annual Technical Conference and Exhibition, 6-9 October, Dallas, Texas. URL `http://dx.doi.org/10.2118/22651-MS`.

Skjæveland, S.M. and Kleppe, J., eds., 1992. *SPOR Monograph. Recent Advances in Improved Oil Recovery Methods for North Sea Sandstone Reservoirs*. Norwegian Petroleum Directorate, Stavanger.

Yan, W., Miller, C.A., and Hirasaki, G.J., 2006. Foam sweep in fractures for enhanced oil recovery. *Colloids and Surfaces A: Physicochemical and Engineering Aspects*, **282–283**: 348–359. A Collection of Papers in Honor of Professor Ivan B. Ivanov (Laboratory of Chemical Physics and Engineering, University of Sofia) Celebrating his Contributions to Colloid and Surface Science on the Occasion of his 70th Birthday. 20 July. URL `http://dx.doi.org/http://dx.doi.org/10.1016/j.colsurfa.2006.02.067`.

Zekri, A.Y., Shedid, S.A., and Almehaideb, R.A., 2007. Possible alteration of tight limestone rocks properties and effect of water shielding on the performance of supercritical CO2 flooding for carbonate formation. SPE Middle East Oil and Gas Show and Conference, Kingdom of Bahrain. 11–14 March. URL `http://dx.doi.org/10.2118/104630-MS`.

Chapter 22

Air Injection

Roman Berenblyum, Arvid Østhus, Sigmund Stokka, and Leonid Surguchev

22.1 Introduction

In all secondary and tertiary processes, fluids are injected into the reservoir to displace, bank and produce resident hydrocarbons. Air injection and the resulting in-situ combustion recovery method is a proven technology, which has found a quite wide application as an Enhanced Oil Recovery (EOR) method for heavy oil recovery in many countries (Yannimaras and Tiffin 1995; Yannimaras and Mustoni 1996; Yannimaras 1996; Musin and Diyashev 1994; Surguchev 1987) over a period of more than 60 years.

The main agent of the process is air, which is inexpensive and easily available. A total consumption of 5 to 10% of oil in place can be expected to maintain a propagating in-situ combustion/oxidation process. Schematically the air injection process is illustrated in **Fig. 22.1**. The combustion front is moving behind the oil displacement front. Behind the combustion zone is a burned zone, while ahead of it is an evaporation zone containing steam, nitrogen, hydrocarbon gases and combustion gases. Ahead of the evaporation zone is the condensation zone and then follows the water bank, oil bank and the unswept zone. The flue gas and steam generated at the combustion front are stripping, swelling and heating the contacted oil. The oil with reduced viscosity is more easily moved towards production wells.

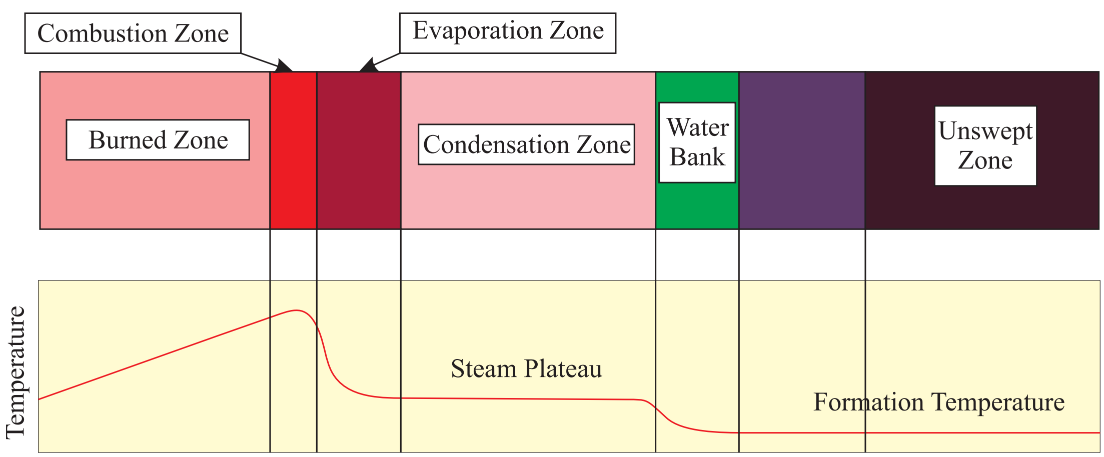

Figure 22.1: Schematic of the air injection process

The process can lead to a high recovery within a relatively short time period by achieving very high displacement efficiency. In-situ combustion accelerates oil production and can potentially result in that all remaining oil in place is being produced from the region swept by air. The propagation of the combustion and displacement fronts in the reservoir is uncertain. Monitoring and control of combustion front movement is important. Premature breakthrough of flue gas in production wells can cause exploitation problems (communication, corrosion, environmental aspects etc.) (Musin and Diyashev 1994; Surguchev 1987). Simulations with accurate handling of the combustion reactions at reservoir conditions allow evaluating and designing the efficient field application of the process (Oballa, Coombe et al. 1993; Rubin and Buchanan 1985). In the 1950-70 period, air injection into light oil reservoirs was narrowly tested in the form of tertiary fireflooding. Air injection/in-situ combustion was shown to be technically feasible in light oil reservoirs following water flooding, but economics was challenging. In the 1980s, air injection was shown to be technically and economically interesting in secondary applications in certain light oil reservoirs. Several field applications to light oil reservoirs showed oil recovery increase by 15-40% of OOIP. NGL extraction was a major contributor to economic success. Key air injection application to light oil reservoirs are: Medicine Pole Hills Unit (Fassihi, Yannimaras et al. 1996; Kumar and Fassihi 1995), Buffalo Red River (Fassihi, Yannimaras et al. 1997; Gutierrez, Miller et al. 2008), Horse Creek (Clara, Zelenko et al. 1998), West Heidelberg Unit (Huffman, Benton et al. 1983) and Gnedintsi (Busto, Sauacut et al. 1991). No air injection / in-situ combustion projects in chalk reservoirs have been identified in the literature. In a fractured reservoir, a diffusion process is required for the air to enter the rock matrix, and the process itself might also behave somewhat differently from the illustration in Figure 1. Air injection in carbonate reservoirs, however, have been tested with some success in USA. The best studied field case is Medicine Pole Hills Unit (MPHU) in North Dakota (Kumar and Fassihi 1995). A unit comprising 9600 acres with 13 producing wells was formed in July 1985 and air injection operations commenced in October 1987. The combination of light oil (39 API), carbonate formation, hot reservoir (230 ^{0}F) and low permeability (1-30 md) makes this a unique air injection project. The application of air injection in MPHU doubled oil recovery from approximately 15% OOIP to 30% OOIP. **Fig. 22.1** summarises oil production and air injection history from MPHU.

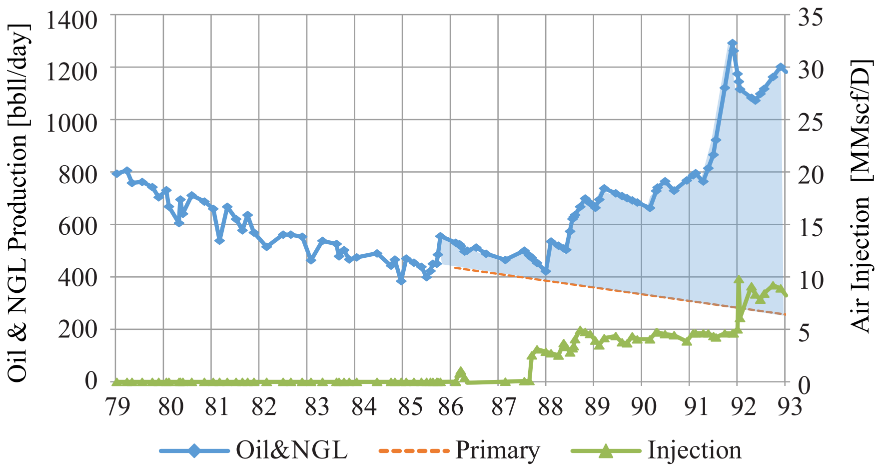

Figure 22.2: Oil and NGL production (blue line) in bbl/d, air injection (green line) in MMscf/d and estimated effect from air injection (blue shaded area) for Medicine Pole Hills Unit. Digitized from Kumar and Fassihi (1995)

W. Hackberry is a salt-dome field located in Southwestern Louisiana. Air injection commenced in 1994 and incremental oil was produced from 1996 (Gillham, Cerveny et al. 1998). The project tested air injection in a waterflooded reservoir at 3000 psig reservoir pressure and in a depleted reservoir (500 psig) with a gas cap and a thin oil rim. The plot below shows that the project generated incremental oil above the normal decline trend, see **Fig. 22.3**.

Turta and Singhai (1998) addressed the reservoir engineering aspects of air injection as an Enhanced Oil Recovery (EOR) method for low permeability light oil reservoirs. A classification of various air injection processes is presented and discussed in this paper. Air injection into an oil reservoir results in four main types of processes:

1. Immiscible air flooding with oxidation
2. Immiscible air flooding without oxidation
3. Miscible air flooding with oxidation
4. Miscible air flooding without oxidation

The last two processes are commonly known as high pressure air injection (HPAI) processes. According to the intensity of oxidation, either the low temperature oxidation (LTO) or the high temperature oxidation (HTO) reactions can dominate the development of the process. Actually, when HTO takes place in the immiscible air flooding, the classic in-situ combustion process is obtained, while if only LTO takes place, the process is called LTO-IAF (LTO combined with immiscible air flooding).

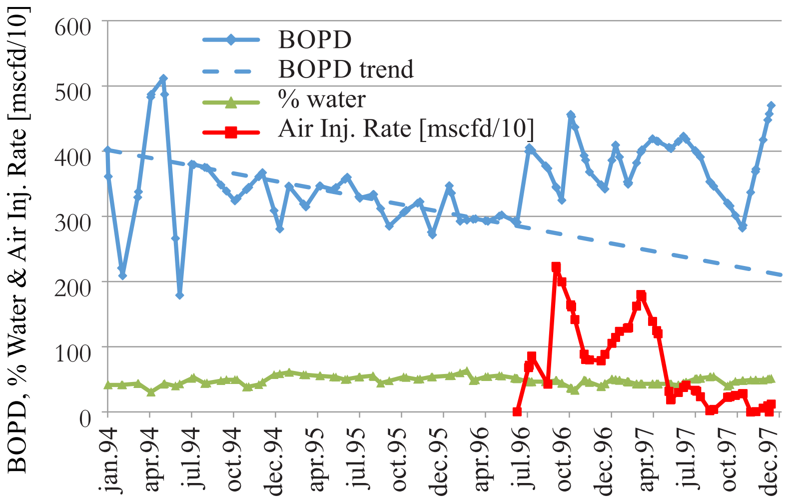

Figure 22.3: Barrels of oil produced (in blue line with blue diamonds) vs production trend (in dashed blue line), water cut in % (green line with triangles) and air injection rate in mcfd/10 (red line with squares) for W. Hackberry field. Digitised from Gillham, Cerveny et al. (1998)

As a part of Joint Chalk Research Phase V (JCR V) in period 1997-99, air injection was studied in project 5 titled "Air injection in North Sea Environment". D.V. Yannimaras, Amoco stated the following in his report of June 1998, titled "Technical Update on Air Injection for Crude Oil Recovery from Carbonate Reservoirs": "Air is a low cost injectant and, depending on circumstances, it can serve multiple functions. In the reservoir, air may be used as an agent of oxidation and heat release, of pressurization, of in-situ gas stripping and also of miscibility. In many deep, hot reservoirs, ignition will spontaneously occur following air injection and the agent of pressurization will be the combustion product gases ahead of the combustion front. Moreover, if the reservoir is at sufficient depth and the oil is of appropriate composition, miscibility may develop between the combustion product gases and oil in-place. Miscibility then will be another mechanism also influencing the ultimate oil recovery. Therefore, air injection may be broadly regarded as an improved recovery operation."

JVR V contained results from air injection combustion tube (CT) experiments, studies of mechanical properties before and after combustion, studies of mineralogy and texture changes due to combustion and screening reservoir simulation studies of potential incremental recovery due to air injection. Both combustion tube experiments and accelerating rate calorimetry (ARC) indicated potential for increased recovery due to air injection. Geomechanical studies indicated reduction in yield strength and Young's modulus due to combustion, and scanning electron microscope (SEM) studies indicated only minor changes in texture and mineralogy due to combustion. A more detailed description of above mentioned laboratory procedures is presented further in this chapter.

The screening simulation study was based on CT and ARC results and concluded that air injection could potentially result in incremental oil as high as 5–7% OOIP. The screening model results represent an optimistic estimate of oil recovery by air injection due to favourable modelling premises. For example, it is likely that incremental hydrocarbon recovery by air injection would be dramatically reduced if there were preferential flow of injected gas through a fracture network, allowing injected air to bypass waterflood residual oil in the chalk matrix. Also, related operational factors such as increased corrosion or the impact of the air injection process on mechanical properties of chalk (with consequent impact on seabed subsidence and/or wellbore integrity) have not been fully investigated.

As there were no experience reported in open literature for air injection offshore in low permeable chalk reservoirs it was considered necessary to perform in depth studies to evaluate the potential for application of this technology for such fields, building on the results obtained in JCR V. Supported by the European Commission through the fifth framework program, the Ekofisk Field owners (Production License 018) joined forces with leading European research institutes and a contractor to investigate the potential of air injection as a cost effective IOR method for a fractured chalk field, such as the Ekofisk field. Results of this study, named AirOil, was presented by Stokka, Østhus et al. (2005). The subject paper reports results obtained during 2001–2004 to evaluate the potential through screening studies, extensive laboratory experiments, reservoir simulations, design of processing facilities and project feasibility evaluations. An extensive knowledge base of the air injection process for light oil fractured reservoirs was established.

This chapter attempts to summarise air injection related results and experiences gained from JCR V and

AirOil studies. Both projects evaluated applicability of air injection to light oil carbonate fields of the North Sea. JCR V research activities focused on mechanical (Powell 1999), textural and/or mineralogical (Rett 1999) changes to Austin outcrop chalks and potential incremental hydrocarbon recovery (Harpole and Østhus 1999). The AirOil project combined laboratory studies of the combustion process, effect of different physical forces (diffusion, capillary and gravity) as well as air injection performance in core tests and computer simulations on different scales (lab and field) (Stokka, Østhus et al. 2005). The findings from both projects are used as illustrative examples in the corresponding sections of the chapter.

22.2 Air injection in light oil reservoirs

The main differences in the air injection mechanisms in light compared to heavy oil (oils are usually defined as heavy if their API gravity is below 20) reservoirs are:

- Flue gas drive (i.e. pressure maintenance, gasflood, oil stripping, oil swelling, etc.) is the main driving mechanism in light oils in the beginning of air injection process.
- While for heavy oils thermal effects are the main driving mechanisms, for light oils, thermal effects become important later in the project (i.e. after 1 PV of air injected). Thermal effects provide displacement of residual oil (to gas and steam) and mobility control effects.

Light oil reservoirs are usually deep enough and hot enough, that spontaneous ignition and combustion of the in-situ hydrocarbons occur following air injection. The ignition delay time for the reservoir with temperatures above 150–200°F(app. 60–100°C) could be in the range of several hours. The important processes contributing to the improved oil recovery by air injection in light oil reservoirs are Musin and Diyashev (1994):

- stripping and vaporizing of oil as well as possible miscibility effects by generated CO_2,
- swelling of the oil by combustion gases,
- oil banking and improved sweep,
- pressurization and voidage replacement,
- HPHT displacement conditions, water at supercritical conditions,
- reduction of oil viscosity due to increasing temperature,
- better mobility ratio.

In order to design the process for a particular reservoir it is vitally important to:

1. Study kinetics, activation energy, reactive oil properties. This is done by, for example, Differential Thermal Analyser (DTA) under low pressure (up to 100 bar), Accelerating Rate Calorimeter (ARC) with pressure of up to 450 bar or in a disc reactor, Ramped Temperature Oxidation (RTO) at reservoir conditions.
2. Evaluate oxidation process, quantify performance, calibrate simulation model using combustion tube test
3. Perform state-of-the-art simulation including physics and chemistry of the process.

Process kinetics may be schematically described with the following reactions:

- Bond Scission Reactions (Oxidation Reaction):

$$Hydrocarbon + O_2 \rightarrow Carbonoxides + Water + Energy \tag{22.1}$$

  This reaction is dominant for light oils at temperatures above 150^0C and for heavy oils above 350^0C.

- Oxygen Addition Reactions (Oxidation Reaction):

$$Hydrocarbon + O_2 \rightarrow Oxygenated\ \ compounds + Energy \tag{22.2}$$

  Oxygenated components are primarily aldehydes, alcohols, ketons, hydroperoxides, which are ineffective in mobilising oil and form stable emulsions with water. This reaction is dominant for heavy oil at temperatures below 300^0C or for light oil at temperatures below 150^0C

- Pyrolisis Reactions (Thermal Cracking):

$$Hydrocarbon_{(\text{liquid})} \xrightarrow{Energy} HC_{(\text{liquid or solid})} + HC_{(gas)}. \tag{22.3}$$

  Thermal Cracking, unlike combustion are endothermic reactions (require energy, rather than generate it) and are not important for light oils. For heavy oils, coke (solid HC) is source of fuel for bond scission reaction.

In simulation models, reaction kinetics is formulated as:

$$r_k = r_{fk} e^{\frac{-E_{act}}{TR}} C_1^{0k,1} ... C_{nc}^{0k,nc}, \tag{22.4}$$

where stoichiometric coefficients, concentration factors, reaction rate, reaction enthalpy are unknowns in the model and need to be calibrated over actual measurements. Simulation tools, therefore, should be capable of:

- Correctly resolving for energy conservation and thermal modeling
- Modeling chemical reactions
- Handling four phases: water, oil, gas, solid
- Representing a multi-component systems using compositional or K value pseudo-compositional approaches

22.3 Evaluation of air injection in light oil chalk reservoirs

As any other IOR/EOR technique an air injection process has to go through several phases prior to application to a particular reservoir. These phases typically are:

- Initial screening based on in-house or general experience in the industry
- Laboratory study
- Simulations and pilot preparations
- Pilot and analysis, evaluation of full field potential
- Field applications.

This chapter concentrates mostly on the second and third stages. Details on the methods of initial screening may be found elsewhere in the literature (Surguchev, Reich et al. 2011; Alvarado, Ranson et al. 2002) and are, at least in principal, similar to all methods. Pilot and field applications including infrastructure and economics are just briefly touched upon at the end of the chapter. Assuming that initial screening confirmed feasibility of the method for the particular field, a set of laboratory studies are to be carried out. For a complex recovery process such as air injection an elaborate study is needed to understand the essence of the process and design a field application. An experimental study should be planned in order to set the basis for reservoir simulations and process evaluation.

22.3.1 Experimental studies

A typical set of experimental studies to evaluate the air injection process includes Accelerated Rate Calorimetry (ARC) and Combustion Tube (CT) cell followed by simulation of experiments in order to tune the simulation model. ARC tests are aimed at evaluation of kinetics and mechanisms, while CT are aimed at mimicking the process at reservoir conditions. Additional experiments are often carried out and also described in this chapter.

Accelerated rate calorimetry

The key goal in ARC study is to qualify air injection candidates by confirming extent and continuity of the low-temperature-oxidation (LTO) isotherm and evaluating the autoignition potential (Yannimaras and Tiffin 1995). The isotherm resulting from ARC study is reported as a Self Heat Rate (or Temperature rate) in degrees $^0C/min$ as a function of temperature. Two examples in **Fig. 22.4** are showing results from: a successful test with good isotherm continuity (blue diamonds); and a failed air injection candidate showing bad isotherm continuity (red squares).

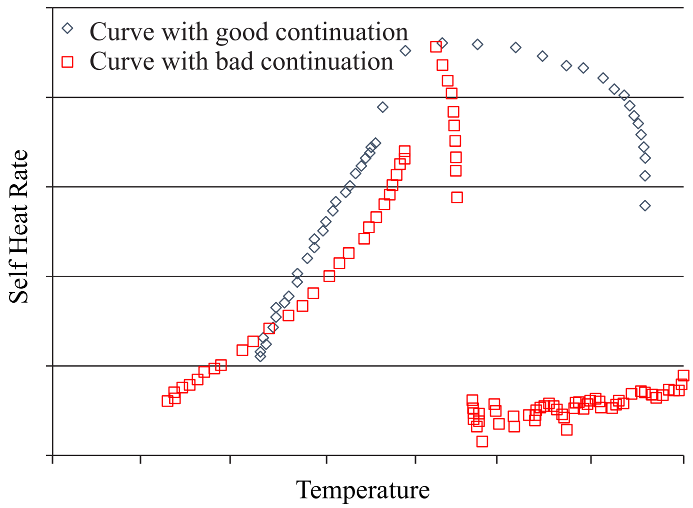

Figure 22.4: Self heat rate vs temperature plot showing a curve with good (blue diamonds) and bad (red squares) continuity, redrawn.

Such experiments conducted for Ekofisk crude oil, for example, showed that the rate of reaction was influenced significantly by the temperature, and initial saturations of oil and brine (Greaves, Bentaher et al. 2005). Ekofisk crude oil was found to be sufficiently reactive in the temperature range of 130–150°C and all the oxygen charged into the reactor was completely consumed over a number of days. Autoignition for Ekofisk oil started in the temperature range of 155–200°C.

Combustion tube cell

The combustion tube cell essentially represents an increment of the reservoir and is designed to answer the questions of how much air is needed and oil consumed in the reaction, and if the combustion front would propagate. The combustion tube is usually several meters long with a diameter of approximately 10cm. It should be equipped with an array of temperature sensors inside the tube, which would be used to measure the temperature of the progressing combustion front and serve as crucial parameters for tuning the reservoir model. The produced fluids are separated, and gas flow rate, CO and CO_2 production, and O_2 combustion are also monitored.

Adiabatic disc reactor

The adiabatic disc reactor allows to characterise the kinetics of the oxidation and combustion reactions using core plugs at reservoir conditions. Experiments are to be carried out with step wise increase of the temperature via heaters wired around the core while measuring the oxygen consumption and exothermic response of the system. The stepwise increase should continue until the core temperature would start increasing by itself. The core temperature is then allowed to evolve freely and the system should be controlled to be at adiabatic conditions. Different initial conditions (brine concentration, reservoir temperature and pressure) could be tested. A core experiment with Ekofisk oil, for example, showed that the autoignition temperature increases with increasing initial water saturation, and varies in the range 160–350°C.

Diffusion experiment

In the conditions of fractured chalk gas diffusion is the process controlling gas flows between high permeable flowing fractures and low permeable matrix storage. In the experiment carried out the rate of diffusion of nitrogen and oxygen into a matrix plug was measured under reservoir conditions of pressure, temperature and fluid saturations. The experimental setup is illustrated in **Fig. 22.5**.

A 20 cm^3 pore volume cylindrical chalk sample was mounted into a steel reactor and was sealed except at the top of the core. A narrow flow space, the diffusion chamber, allowed for flow of air past the top side of the plug. Synthetic air, composed of 20% O_2 and 80% N_2, was injected through the diffusion chamber. The effluent from the chamber was continuously analyzed, thus to determine the amount and type of hydrocarbons diffusing out of the core as well as the amount of O_2 and N_2 diffusing into the core. The molar fractions of produced O_2, N_2, C1, C2 and C3 are shown in **Fig. 22.6**. As expected the O_2 and N_2 concentrations increase with time while the

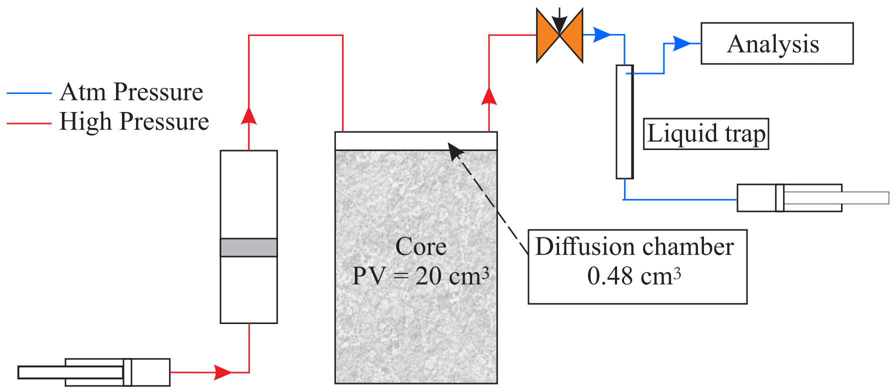

Figure 22.5: Experimental setup for diffusion experiments, redrawn.

hydrocarbon component fractions decrease.

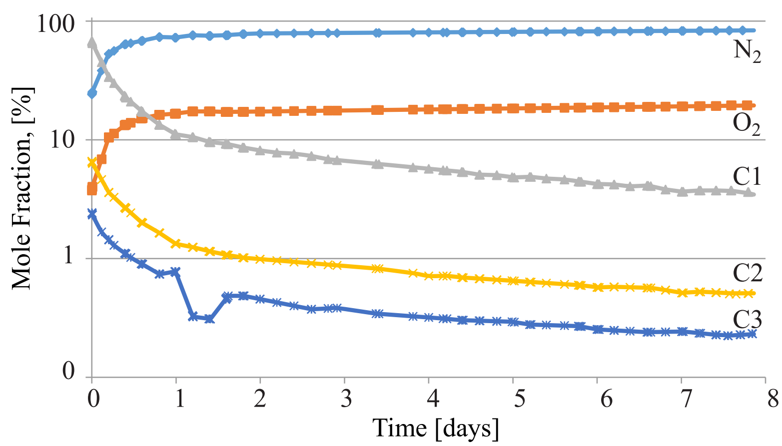

Figure 22.6: Produced gas composition vs. time for O_2, N_2, C1, C2 and C3, redrawn.

Flue gas flooding test

A flue gas flooding test was carried out on a composite Ekofisk core (six plugs) assuming waterflooded reservoir conditions (60°C, 320 bar and 70% water saturation). Nitrogen was injected from the top of a vertically mounted core and was allowed to pass outside the core but inside the sleeve, thus simulating nitrogen flow through a reservoir fracture. Hydrocarbons in the core could only be produced through diffusion. The experiment demonstrated that the lighter hydrocarbons were stripped from the reservoir oil originally present in the matrix. The experiment therefore confirming that gasses formed during combustion would diffuse into the matrix and efficiently produce oil. The cumulative oil production and nitrogen content in the produced gases of the two first gas sweeps are shown in **Fig. 22.7**. Flue gas sweep efficiency was estimated at 9% of the hydrocarbon pore volume after 2.15 pore volume flue gas injection.

Subsidence and compaction

One of the key questions in the chalk reservoirs is stability of a brittle rock. Compaction, while yielding a positive recovery effect by "squeezing" the oil out of the shrinking pores causes subsidence and weakening of the brittle rock structure. Together with water weakening of chalk (Madland, Zangiabadi et al. 2009) it may cause losses of productivity and well collapses. It is, therefore, crucial to understand the effect of the in-situ oxidation process on the rock structure. In the past SEM (scanning electronic microscope), EDS (Energy-dispersive X-ray spectroscopy) on Austin chalk (Powell 1999) and SEM + mercury porosimetry on Ekofisk cores (Stokka, Østhus et al. 2005) were used to determine mineralogical and structural changes. Both "unaltered" and "combusted" cores were analyzed. For the Ekofisk cores, for example, the samples came from the experiments performed

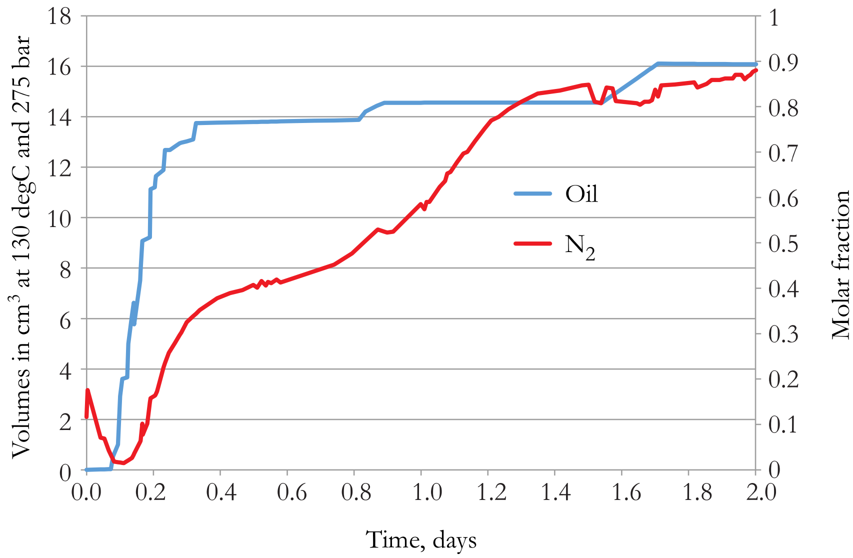

Figure 22.7: Long core experiment with flue gas flooding showing early N_2 breakthrough and oil production due to Flue gas sweep, redrawn.

in the diffusion chamber and the adiabatic disc reactor, and had been exposed to temperatures of 80°C and 490°C, respectively. Constrained pore volume compressibility measurements on these plugs, indicated that combustion has weakened the chalk. Austin chalk experiments also showed decrease in mechanical properties of the chalk. Based on the obtained results it was concluded that low temperature oxidation would not lead to any increased compaction and subsidence. The high temperature case should yield additional subsidence, however, high temperature combustion process did not alter pore geometry by melting or destroying grains other than depositing carbon rich coating on the grains. The estimated field subsidence is not considered to be prohibitive for an eventual air injection project at the Ekofisk field. However, near wellbore effects might increase well failure risks and could potentially be of a serious concern.

Computer simulations of laboratory experiments

Laboratory data do not only provide necessary understanding of the process specifics for the particular field, but also allows calibration of simulation models. First stage of such calibration is simulation of laboratory experiments on the lab scale to obtain reservoir simulation parameters. Simulations of the diffusion experiment and the adiabatic disc reactor experiment carried out for the Ekofisk oil resulted in a good match of the activation energies for those two experiments. The diffusion coefficients used were based on kinetic theory of gases and allowed to successfully represent the experiments. Parameters used in the simulations are listed in **Tables 22.1 and 22.2**.

Component	Mol. fraction	Mol. weight g/molar	$D_{gas-gas}$ $10^{-3} m^2/day$
N_2	0.0010	28	4.8
O_2	0.0000	32	4.9
CO_2	0.0083	44	4.0
CO	0.0000	28	3.4
C1	0.4406	16	5.5
LITE	0.1210	35	2.2
MEDIUM	0.0844	80	1.8
HEAVY	0.3445	254	1.0

Table 22.1: Diffusion coefficients used in simulations

Activation energy from diffusion experiment	36-40 kJ/mol
Activation energy from adiabatic disc reactor experiment	36-40 kJ/mol

Table 22.2: Activation energy estimates from simulation of experiments

These values were used in the field simulations. It was observed that the self-ignition temperature increased with increasing water saturation. Indeed, if no water is present in the system, the heat released is transferred to the rock and the oil. However, when water is present, for the same heat rate released by the reactions, the heat transferred to the oil is smaller since part of it is transferred to the water.

22.3.2 Reservoir scale simulations

Reservoir scale simulations need to be based on the results of the experimental study. Scaling up these results from core to the field level possesses a significant challenge for the reservoir simulation practice. This question is not discussed in this chapter, however, it could be mentioned that representing the details of chemical processes on reservoir scale grids currently seems impossible due to required grid detailisation and corresponding simulation time penalty. It is, nevertheless, possible through a careful step-by-step procedure to scale up the results from core to field level provided that numerical dispersion is carefully controlled during each scale up stage and the resulting simulation case is within a certain time step and grid size limits. The first step towards reservoir scale simulation is often a preliminary screening carried out on representative mechanistic models of the field.

Preliminary air injection potential evaluation

The work carried out as a part of JCR V (Harpole and Østhus 1999) was based on a small sector model of the Ekofisk field. The primary goal was to evaluate the potential of a tertiary air injection following the waterflood. Simulation results showed significant gravity overrides and resulted in up to 7% STOOIP recovery increase. In the AirOil project a similar mechanistic 5-spot element study was carried out. The study was used to evaluate air injection efficiency at different stages of field development. The air injection process-specific parameters (chemical reactions, stoichiometry coefficients and other) and fluid description were heavily based on a light oil data set that has been used successfully in the past by Amoco to simulate in-situ combustion of light oils. History match simulations of a combustion tube experiment have been used to calibrate the simulation model to current task. The simulation results presented in **Fig. 22.8** show efficiency of air injection applied at different stages of field development starting with air injection as primary recovery (blue line), after depletion (purple line) to several stages of waterflooding (two green lines). Application of air injection as a secondary method allows to recover additional 11% of STOOIP compared to waterflooding. Application of the method at later stages yields lower overall efficiency, yet extra 5-7% of STOOIP can be recovered with tertiary air injection. These results are in good agreement with the estimates carried out in the JCR V study. It is important to notice that no attempt to optimize the injection/production strategy was undertaken in this study. The injection and production wells were perforated in the whole section of the thick productive formation. Selective completion and recompletion of the wells can further improve the sweep efficiency of the air injection process.

Field pilot screening

Next phase after the potential of the method has been established both through the laboratory study and preliminary simulations is a field pilot. Selection of the pilot area for the field is a complex process involving not only IOR/EOR experts, but production engineers and operational staff. A selected area first needs to be representative of the field or the area to which the method would be expanded. It is also needed to be somewhat isolated and the fluid flow processes in the area should be well understood (Bargas 1987). After a pilot area is selected a segment model encapsulating the area in question is created. While creating a sector model is always challenged by properly handling mass and energy flow on the segment boundaries, working with the full field model, at a current moment, still seem to be unfeasible. The smaller sector model allows increasing grid resolution in the study area and improving understanding of fluid distribution prior to and during the air injection process. A sector model with its shorter runtimes should also allow to carry out a rather large number of simulation scenarios in order to fully investigate recovery strategy. For the air injection process it is essential

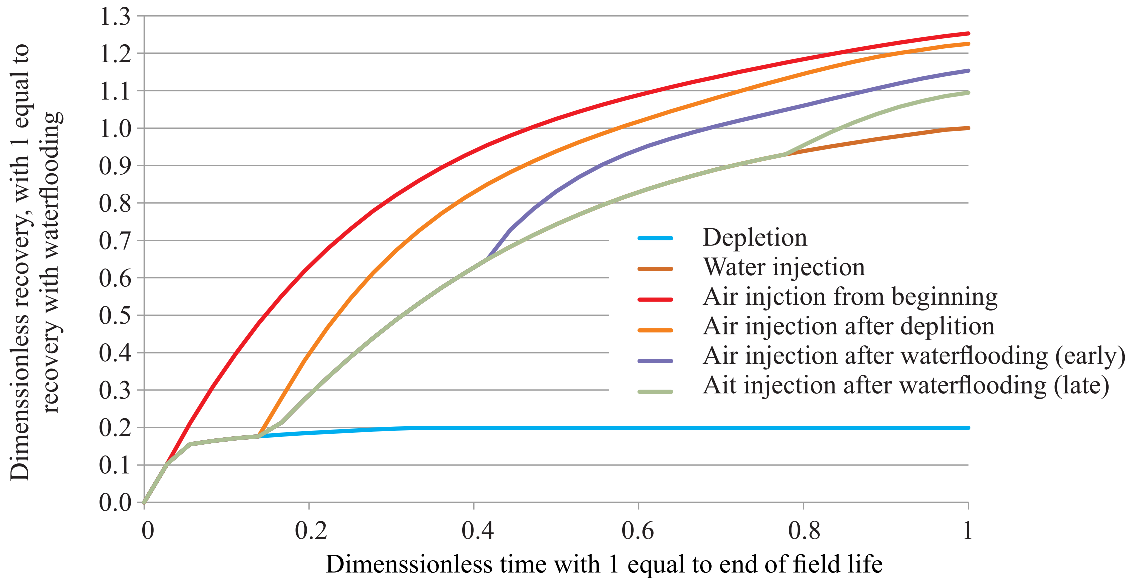

Figure 22.8: Air Injection potential evaluation. Dimensionless recovery (with waterflooding giving recovery of 1) vs dimensionless time (1 equal end of field life) for several scenarios: Depletion (blue); Waterflooding(brown); Air injection from beginning (red), after deplition (orange), after waterflooding at early (violet) and late (green) stages, redrawn.

not only to have a proper initial fluid distribution and pressures, but also a temperature profile. An example of the pilot simulations on the segment model for the Ekofisk field may be found in Stokka, Østhus et al. (2005).

Several of the best scenarios are then transferred to the full field model. Effects of larger grid and time step sizes should be carefully studied and controlled in this process. The full field simulation including the pilot air injection should allow looking on the effect of the process to the nearby areas and verifying validity of the segment runs.

A thorough monitoring program is an extremely important part of the field pilot. It helps to evaluate the performance of the pilot project, to provide information as to the state of the oxidation reaction and to protect the production wells /facilities from damage due to corrosion or heat breakthrough. Measurements of reservoir pressure and temperature (including distributed temperature sensing where possible), pressure fall-off and step rate tests, and injection/production profiles on involved wells prior to pilot initiation should help to establish baseline conditions for the pilot and will supply useful data for the simulation work. Wells included in the field pilot should also monitor temperature, pressure and fluid production and makeup. Analysis of production gas is crucial in air injection projects. Determination of hydrocarbons, oxygen, nitrogen, carbon dioxide and carbon monoxide in the produced gas stream provide important information on project performance and warns about potential safety and corrosion problems. The arrival of the combustion front is preceded by changes like: (1) a decrease in water salinity, (2) an increase in organic acid content of the water (lower pH), (3) an increase in CO_2 or O_2 in the produced gas, (4) a change in the appearance of the produced fluid, and (5) an increase in corrosion rate, leak frequency and amount of iron in the produced water.

The results from the pilot screening are used to improve and advance available simulation models. If pilot test results are considered successful a field wide implementation strategy including optimisation of further drilling campaigns, completion designs, injection and production schemes and regimes need to be developed, utilising both segment (for detailed, in-depth tests) and full field (for overall field performance optimisation) simulation models.

22.3.3 Surface facilities and wells

Wells and surface facilities have to be designed with respect to high temperature, varying gas composition and high reactive activity of oxygen. This task possesses additional complexities for mature offshore installations. From the injection site, key complexity are in air compressors (resulted gas is hot and extremely reactive), well completion to prevent tubing leaks and oxygen backflow if there is an interruption in air injection. On the production side key, complexity for in-situ combustion for the surface equipment compared to primary operations is due to the production of gas containing corrosive substances and a crude stream which may contain stable emulsions. An elaborate monitoring system is required to detect the approaching combustion front and avoid oxygen breakthrough. Utilisation of smart completions should be evaluated to improve sweep of the reservoir by injected air, control and balance an oil to air ratio. At the current stage of technological development neither surface facilities nor well construction are show stoppers, however top-side and well completion design need to be matured prior to field implementation.

22.3.4 Safety and risks

Several potential safety hazards and production risks could be associated with the air injection process. One of those is formation of premixed gas and oxidant zones in the reservoir due to possible interruptions in injection. Generally it can be imagined that such mixtures could detonate, however research carried out by Rogg, Hermann et al. (1985) could be interpreted to mean that borehole explosions will not propagate into the reservoir. Compressors are another potential safety hazard, however, much higher temperature than the operating ones is required for them to explode. Injection of high pressure gas generally is a safety hazard and necessary measures accounting for high chemical activity of the gas need to be included in facilities and wells design basis. Finally an elaborate monitoring program is needed to monitor propagation of the oxidation front. Combined with wells constructed to prevent potential leakages of combustion gasses or oxygen this should provide safe operations. Safety and risk issues must of course be evaluated and screened in the pilot preparation and field implementation phases.

22.3.5 Economic evaluation

One of the key elements in evaluating the economics of the project is to account for risk and uncertainty. Such evaluation is usually based on a number of simulation scenarios combined with uncertainty ranges in costs related to equipment, materials and electricity; oil and gas prices; as well as taxation. Uncertainties could be represented in a tornado diagram and a cumulative probability plot showing distribution of calculated net present value for the project.

22.4 Conclusions

Laboratory experiments, computer simulations and previous experience of air injection confirmed it as a feasible recovery process also for light oil chalk reservoirs. Air injection could be applied as a primary, secondary or tertiary method.

The investigation of the air injection process in fractured chalks showed that gravity, diffusion and stripping of lighter hydrocarbons would have a dominant effect on recovery, compared to oil banking, steam washing and oil viscosity reduction mechanism dominating more "conventional" reservoirs.

Additional subsidence and compaction caused by air injection and in-situ oxidation and combustion were estimated, and were not considered to be prohibitive for fractured chalk fields. However, possible well failures caused by compaction is a serious concern.

It was demonstrated that a stable combustion front can form and propagate under favourable reservoir conditions (low water saturation), and that additional hydrocarbons will be produced from carbonates. If a proper monitoring and detection program is implemented it is unlikely that uncontrolled oxygen breakthrough will occur in the producing wells.

Evaluations showed large variations in potential improved oil recovery from 5–7 (as a tertiary method) up to 20–25 (as a primary method) % STOOIP in favorable conditions and early phase application (Stokka, Østhus et al. 2005; Harpole and Østhus 1999). It is advisable to further continue evaluations of the air injection process for chalk fractured reservoir of the North Sea.

Nomenclature

$C_1^{0k,1}$ to $C_{nc}^{0k,nc}$ = concentrations of reactants in respective powers
E_{act} = activation energy
R = gas constant,$\mathrm{mL^2/t^2T}$
r_k = kinetic reaction rate
r_{fk} = frequency factor of kinetic reaction
T = temperature, T

Subscripts

1..cn= indexes identifying reactants
act= activation
fk= frequency of kinetic reaction
k= kinetic

Abbreviation

ARC = accelerated rate calorimetry
CT = combustion tube
DTA = diferential thermal analyser
LOT = low temperature oxidation
RTO = ramped temperature oxidation
SEM = scanning electron microscope

References

Alvarado, V., Ranson, A. et al., 2002. Selection of EOR/IOR opportunities based on machine learning. In *European Petroleum Conference*. Society of Petroleum Engineers. URL `http://dx.doi.org/10.2118/78332-MS`.

Bargas, C.L., 1987. Selection Criteria for the Salt Creek WC2 Immiscible $C0_2$ Demonstration Pilot. Tech. rep., Amoco Prod. Co. memorandum 87159ART0229. Tulsa, OK, 6/11/1987.

Busto, J.L., Sauacut, R., and Garcia Rivero, J.G., 1991. Prediction of Horizontal Wells Production, Economic Evaluation and Comparison with Other Investment Alternatives. In *13th World Petroleum Congress*. World Petroleum Congress, Buenos Aires Argentina.

Clara, C., Zelenko, V. et al., 1998. Appraisal of the Horse Creek Air injection project performance. In *Abu Dhabi International Petroleum Exhibition and Conference*. Society of Petroleum Engineers. URL `http://dx.doi.org/10.2118/49519-MS`.

Fassihi, M.R., Yannimaras, D.V., and Kumar, V.K., 1997. Estimation of Recovery Factor in Light-Oil Air-Injection Projects. *SPE Reservoir Engineering*, **12** (03): 173–178. Paper SPE 28733 presented at the 1994 International Petroleum Conference and Exhibition of Mexico, Veracruz. August. URL `http://dx.doi.org/10.2118/28733-pa`.

Fassihi, M.R., Yannimaras, D.V. et al., 1996. Economics of Light Oil Air Injection Projects. In *SPE/DOE Improved Oil Recovery Symposium*. Society of Petroleum Engineers. 21–24 April. URL `http://dx.doi.org/10.2118/35393-ms`.

Gillham, T.H., Cerveny, B.W. et al., 1998. Low Cost IOR: An Update on the W. Hackberry Air Injection Project. In *SPE/DOE Improved Oil Recovery Symposium*. Society of Petroleum Engineers (SPE). SPE 39642. URL `http://dx.doi.org/10.2118/39642-MS`.

Greaves, M., Bentaher, A.H., and Rathbone, R.R., 2005. Air Injection into Light Oil Reservoirs. Oxidation Kinetics and Simulation. In *European Symposium on Improved Oil Recovery, Budapest*. 25–27 April.

Gutierrez, D., Miller, R.J. et al., 2008. Buffalo Field High-Pressure Air Injection Projects 1977 to 2007: Technical Performance and Operational Challenges. In *SPE Symposium on Improved Oil Recovery*. Society of Petroleum Engineers (SPE). 20–23 April. URL `http://dx.doi.org/10.2118/113254-ms`.

Harpole, K. and Østhus, A., 1999. Joint Chalk Research V: Potential For Oil Recovery By Air Injection Following Waterflooding In a North Sea Chalk Reservoir. Tech. rep., Phillips Petroleum Company, Technology and Services Division.

Huffman, G.A., Benton, J.P. et al., 1983. Pressure Maintenance by In-Situ Combustion, West Heidelberg Unit, Jasper County, Mississippi. *Journal of Petroleum Technology*, **35** (10).

Kumar, V.K. and Fassihi, M.R., 1995. Case History and Appraisal of the Medicine Pole Hills Units Air Injection Project. *SPE Reservoir Engineering Journal*, **10**: 198–202. Paper SPE 27792.

Madland, M.V., Zangiabadi, B. et al., 2009. Rock Fluid Interactions in Chalk with $MgCl_2$ and Na_2SO_4 Brines with Equal Ionic Strength. In *Presented at the IOR 2009 symposium (EAGE) in Paris, France*.

Musin, M.M. and Diyashev, e.a., 1994. Analysis of Pilot Areas Development after In-situ Combustion. In *Proceedings of Int. Conf. on Development of Hard-Accessible Oils and Natural Bitumens*. Kazan, Russia. October.

Oballa, V., Coombe, D., and Buchanan, W.L., 1993. Factors Affecting the Thermal Response of Naturally Fractured Reservoirs. *Journal of Canadian Petroleum Technology*, **32** (08): 31. Can. J. Pet. Tech. October. URL `http://dx.doi.org/10.2118/93-08-04`.

Powell, B.N., 1999. Joint Chalk Research V: Mineralogical and Textural Changes Induced in Austin Chalk by Experimental Combustion. Tech. rep., Phillips Petroleum Company, Technology and Services Division.

Rett, D.W., 1999. Joint Chalk Research V: Austin Chalk Air Injection - Combustion Study, Mechanical Properties of Austin Chalk Before and After combustion. Tech. rep., Phillips Petroleum Company, Technology and Services Division.

Rogg, B., Hermann, D., and Adomeit, G., 1985. Shook Induced Flow in Regular Arrays of Cylinders and Packed Beds. *Int. J. Heat Mass Transfer*, **28**: 2285–2298.

Rubin, E. and Buchanan, W.L., 1985. A General Purpose Thermal Model. *Society of Petroleum Engineers Journal*, **25** (02): 202–214. Society of Petroleum Eng. J. April. URL `http://dx.doi.org/10.2118/11713-PA`.

Stokka, S., Østhus, A., and Frangeul, J., 2005. Evaluation of Air Injection as an IOR Method for Giant Ekofisk Chalk Field. In *SPE paper 97481, SPE International Improved Oil Recovery Conference in Asia Pacific held in Kuala Lumpur, Malaysia*. 5-6 December. URL `http://dx.doi.org/10.2118/97481-MS`.

Surguchev, L.M., 1987. Assessment of the Efficiency of Thermal EOR Methods by the Use of Primary Resources. In *Proceedings of the Academy of Sciences EOR Conference*. Baku. November.

Surguchev, L.M., Reich, E.M. et al., 2011. A Muliti-Stage Approach to IOR/EOR Screening and Potential Evaluation. In *Brasil Offshore*. Society of Petroleum Engineers, Macaé, Brazil. SPE-143789-MS. 14–17 June. URL `http://dx.doi.org/10.2118/143789-MS`.

Turta, A.T. and Singhai, A.K., 1998. Reservoir Engineering Aspects of Oil Recovery from Low Permeability Reservoirs by Air Injection. In *SPE 48841 presented at the SPE International Oil and Gas Conference and Exhibition in China, Beijing*. 2–6 November. URL `http://dx.doi.org/10.2118/48841-MS`.

Yannimaras, D.V., 1996. Air Injection Economics & the Effect of Project Size. Tech. rep., EPTG, AMOCO. December.

Yannimaras, D.V. and Mustoni, J.L., 1996. Implementation Concepts and Experience with Field Air Injection Projects. Tech. rep., EPTG, AMOCO. November.

Yannimaras, D.V. and Tiffin, D.L., 1995. Screening of Oils for In-Situ Combustion at Reservoir Conditions by Accelerating-Rate Calorimetry. *SPE Reservoir Engineering*, **10** (01): 36–39. SPE Reservoir Engineering, February. February. URL `http://dx.doi.org/10.2118/27791-pa`.

Chapter 23

Microbial Methods

Harald Berland and Ole Torsæter

23.1 Introduction

North Sea reservoirs are located 1.6–6 km below the seabed with pressures ranging from 15–80 MPa with temperatures between 40–200 °C. These are high temperature reservoirs that consist of sandstone and fractured chalk pores filled with reservoir fluids, formation water, oil and gas (Myhr, Lillebø et al. 2002). For many years it was believed that these reservoirs were sterile, but global findings of microorganisms with similar characteristics have revealed a microbial population well adapted to the in-situ reservoir conditions providing growth and survival of aerobe or anaerobe, (Adkins, Cornell et al. 1992; Telang, Ebert et al. 1997; Voordouw, Armstrong et al. 1996) mesophile to hyper thermophile microbes (Gerday and Glansdorff 2007; Grabowski, Nercessian et al. 2005; Takahata, Nishijima et al. 2000; Stetter, Huber et al. 1993; Dahle, Garshol et al. 2008; Nilsen, Beeder et al. 1996; Castorena-Cortés, Zapata-Peñasco et al. 2012). In chalk reservoirs population of sulphate- nitrate-, manganese- and iron reducing prokaryotes have been found in wellhead samples together with methanogens, acetogens and fermentative prokaryotes (Castorena-Cortés, Zapata-Peñasco et al. 2012; Nazina, Shestakova et al. 2013). In this section, a short overview are presented about the biotope, modes of life, phylogeny and methods to attribute beneficial microbial activities.

23.2 Chalk biotope

A distinct trait of about chalk reservoirs in the North Sea are the conjoining of high porosity, overpressure, high oil saturation and high fracture permeability. Aqueous phase movement governs transport of bacteria through this porous media, where bacteria are exposed to attenuation through adhesion onto surfaces, or are strained or trapped in interstitial pores slowing down the transport. The effect of straining or trapping are considered important when the particle diameter exceeds 5% of the initial pore size (Jenkins and Lion 1993; McDowell-Boyer, Hunt et al. 1986). Experiments with Bacillus and Pseudomonas species have though shown to penetrate low permeability chalk cores (2–4 mD), and Draugen PW enrichment culture have passed through a Liege chalk cores (0,28–0,6 md), while a 100 md Berea sandstone could limit the instantaneous penetration of a mixed bacteria culture (Halim, Shapiro et al. 2014; Kaster, Hiorth et al. 2012; Jenneman, McInerney et al. 1985). Pore throat and tortuosity may be crucial for bacteria penetration together with the tendency for bacteria to strongly adhere to surfaces (Jenneman, McInerney et al. 1985; Davis and Updegraf 1954). As a general observation a microbe needs about 10 pore volumes to penetrate a water saturated sand stone core, a transport time that are significantly reduced when the core becomes more mixed wet. Fractures in the rock matrix would in addition ease the transport of microbes through the rock formation into low permeable zones, where microbes disintegrates or causes a permeability reduction (Bulut, Waites et al. 1999; Zhang, She et al. 2010; Bryant and Britton 2004). The huge rock surface in porous media constitute a natural hinder for particle movement, but compared to particles, microbes actively uses surfaces exposed to a water flow to improve their growth abilities by settling and establishment of a biofilm. Biofilm contains cells, cell debris and metabolic by-products etc. that are imbedded in a protective slimy polysaccharide layer that prevents the microbes of being washed out from the area, securing a stable supply of oil and other rock-bound minerals for growth (Vasconcellos, Dellagnezze et al. 2011). In this position microbes can simultaneous harvest extra nutrient from the water flow and narrow the water dilution rate of extracellular chemicals as surfactants and enzymes that the microbes have produced to utilize the rock-associated chemicals. The biofilm will expand until the nutrients get depleted and the film starts to breaks off, releasing starved cells and biofilm debris into the water stream (Kim and Fogler 2000). During starvation many microbes enters a survival state that often includes a formation of small and tough survival units as spores, or causes the cell to shrink, induce microbial motion or leads to a cell surface change that decreases the attachment to the rock surface (Takahata, Hoaki et al. 2001; Cusack, Lappin-Scott et al. 1992; Kim and Fogler 1999; Cunningham, Sharp et al. 2007). A shift in surface charge from a hydrophobic to a hydrophilic state may reduce the microbial attachment to rocks or dissolves aggregates, since a hydrophilic cell surface cannot aggregate strongly due to the external water flow. This may change if the ionic strength of the cell suspension is above 40 mol/m^3 that promotes cell adhesion, in contrast to biofilm aggregations that are propagated by the formation of extracellular polymeric substances (Nomura, Narahara et al. 2009). The microbial responds to starvation have actively been employed to increase the injection and transportation rate of exogenous microbes that are injected in the reservoir to induce a physiochemical change as employed in MEOR stimulations (Cunningham, Sharp et al. 2007; Brown 2010; Gao 2011).

A hydrostatic pressure up to 380 bars is generally assumed to be nonlethal to piezophiles, but exert adverse growth effects of organisms adapted to atmospheric pressure (Abe 2007; Bartlett 2002). Those effects depend on the duration of pressure in combination with temperature, pH and the culture media. All strains of piezophiles belongs to γ-proteobacteria or Crenarchaea except for Desulfovibrio and Marinitoga which is a member of the δ-proteobacteria and Thermotogales respectively (Gerday and Glansdorff 2007). In analysis of Ekofisk PW samples, 10% of the well population have been reported to be associated with piezophile Thermotogales, while 40% of the Archaea population was dominated by Thermococcus 33% and Methanococcus 9%. By introducing a high pressure to procaryotes a long list of cellular processes and structures would be impaired, such as cell mobility, cell division and nutrient uptake etc. (Abe 2007). In addition, an increase in pressure will change the chemical equilibrium for many nutrients and change the uptake and growth conditions that affects the microbial distribution in the area (Abe 2007). An increase in load pressure will increase the solvability of gasses as CO_2 in the water, causing calcite to solve while an increase in temperature will shift the equation towards a calcite precipitation. This indicate that the true reservoir pH measured in depressurized Ekofisk PW samples of 7,4 probably are closer to a pH of 5,4 favouring the growth of moderate acidophiles embracing the majority of the reservoir population. The microbial population living in reservoirs generally cope with additional environmental extremes such as high salinity and temperatures. Temperature appear to be the major limiting factor for microbial growth in a reservoir (Wilhelms, Larter et al. 2001), while a change in salt concentration could be adapted by multiple ways of regulating the osmotic equilibrium in the cell, both narrowing the population diversity (Gerday and Glansdorff 2007; Kaster, Bonaunet et al. 2009). One of the most extremophile bacteria, able to deal with both high temperature and salinities is the anaerobe fermentative bacteria Halothermothrix orenii that is found in salt lakes area and thrives at salt concentration of 20% with a temperature up to 68°C (Cayol, Ollivier et al. 1994). In Ekofisk the anaerobe genus Thermoanaerobacter and Thermococcus have been found to dominate the microbial population from high temperature and saline wells, both capable of growing at low pH (4.0, 6.0) at high temperature ~70°C, and salinities varying between 3 to 4% (Balows, Truper et al. 1992).

Microbes with a growth optimum above 80 °C are rare even though the thermo stability of cellular constituents as adenosine triphosphate (ATP), amino acids and peptides in the cell should sustain temperatures up to 150 °C (Gerday and Glansdorff 2007). Lethal temperatures may then not occur until as much as 10,000 m below the surface (Pedersen 2000) but as temperature accelerates chemical reactions it affects the availability of nutrients attending to the proposed oligotrophic conditions. Microorganisms isolated from Ekofisk produced water samples comprise of meso- to hyper thermophilic species that may have their origin from the reservoir or have been added to the reservoir during drilling or water injection (Pedersen 2000; L'Haridon, Reysenbacht et al. 1995). In the colder injector site psychrophilic aerobe seawater microbes usually dominates the population and hold an uncertain activity towards the chemicals near the injector site (Berland, Kaster et al. 2008). Since oil fields are generally isolated from the surface water their redox potential are very low and electron acceptors such as oxygen, nitrate and ferric ion are generally absent (Magot, Ollivier et al. 2000). This will affect the concentration and distribution of injected substances as oxygen, that in additions suffer from a low solvability in saline and high temperature waters. Transportation of oxygen into the reservoir will then be limited and the conditions will favor anaerobic respiration and microbes that are able to degrade oil and fatty acids using other electron acceptors than oxygen. If the redox reactions occurred in order to their thermodynamic possibilities, a microbial mediated sequence of redox reactions will occur applying the oxidant with the highest redox potential first, before the less energy developing reactions are utilized. The majority of the microbial driven reactions reflects the redox potential in an ecological succession of microorganisms that often starts with aerobic heterotrophs, denitifiers, fermenters, sulphate reducers and then species belonging to the methanogenic group. Anaerobic processes utilize most commonly nitrate, sulphate and carbonate as an electron acceptors or organic compounds as an electron donor and acceptor in a fermentative reactions, producing nitrite, sulphide, CO_2 among a waste of organic products. The activity in the subsurface environments varies then with the availability of an energy source, nutrients, water chemistry and the geochemical conditions of the surrounding matrix affecting competition and the microbial diversity.

23.3 Microbial community in chalk

It has taken over a century of scientific progress to realize Darwin's prophecy of making true genealogical trees of each great kingdom in nature (Woese 1994). The progress in exploring the enormous phylogenetic record laid buried in the sequences of macromolecules, made it possible to evolutionary organized the prokaryotes, regardless of habitat and metabolic activity. Prokaryotes are now divided into Bacteria and Archaea, representing fundamentally distinct domain of life, though with similar overall cellular architecture and metabolic diversity (exception of methanogenesis) (Cavicchioli 2007).

The microbial composition in carbonate petroleum reservoir fluids indicate a low diversity assemblage of Bacteria and Archaea that hold a divers metabolic activity (Adkins, Cornell et al. 1992; Kaster, Bonaunet et al. 2009). From the 16S rRNA gene studies, these communities are dominated by thermophile fermenters capable of reducing sulphur compounds, that are similar to observations found in high temperature sandstone reservoirs (Kaster, Bonaunet et al. 2009). The Archaea and Bacteria domain communities are dominated by Crenarchaeota, Euryarchaeota and Proteobacteria, Bacteroidetes respectively. Within these, aerobe and anaerobe organotrophs from the genera Pseudomonas, Actinobacter, Brachymonas and Thauera, Bacteroides, Thermoanaerobacter, Thermococcus have been retrieved together with sulphate reducers as Desulfoglaeba, Desulfomicrobium, Desulfovibrio, Thermotoga, Caminicella, Archaeoglobus, etc. (Nazina, Shestakova et al. 2013; Kaster, Bonaunet et al. 2009; Castorena-Cortés, Zapata-Peñasco et al. 2012). Methanogenesis is seen as a minor process in carbonates with species belonging to the genera Methanolobus, Methanobulbus and Methanococcus (Nazina, Shestakova et al. 2013). Among these genera, metabolites such as CO2, CH4, ethanol, acetone, acetate and other organic acids are common. In addition the microbial activity have been responsible for mobilizing heavy crude oil from carbonates by reducing the oil viscosity as a plausible mixed response of metabolite production and the increased conversion of crude oil into lighter alkanes as C8–C30 (Castorena-Cortés, Zapata-Peñasco et al. 2012; Gaytán, Mejía et al. 2015).

16S rRNA have shown to be a powerful tool in order to investigate the population diversity, microbial interactions and metabolic pathways that can be applied to reduce detrimental microbial activity or to attribute beneficial mechanisms. Awareness of interpreting the results should though be made, since sampling methodology and differences between adjacent wells and sampling time have been reported, probably reflecting the geochemical and time production differences between the wells (Kaster, Bonaunet et al. 2009).

23.4 MEOR in chalk

A main difference between MEOR and other EOR methods is that MEOR is not limited to a single mechanism. There are many different mechanisms by which bacteria can increase oil recovery from a reservoir, and it is not rare that more than one of these mechanisms will be active for a given bacteria assuming it has access to nutrients, a carbon source and oxygen (for aerobic bacteria), and that the environmental conditions are favorable for the bacteria's development. Understanding these mechanisms is the key for developing efficient MEOR technology. In the following, the MEOR mechanisms will be addressed in the context of typical chalk reservoir and production properties.

23.4.1 Reduction in interfacial tension

Based on experimental data from the literature (Gray, Yeung et al. 2008) the interfacial tensions (IFT) obtained during MEOR processes is varying from almost no decrease to as low as 6×10^{-3} mN/m. The general discussion indicates that the IFT in the range of the lowest value will reduce the residual oil. However, that requires that the microbes are flowing in the fractures and deliver surfactants far into the reservoir where the surfactants can enter into the matrix blocks. The nice thing about this process compared to conventional surfactant flooding is that potential adsorption losses of surfactants are avoided. Laboratory experiments (Kaster, Hiorth et al. 2012; Halim, Shapiro et al. 2014) show that bacteria are moving through chalk pore space with permeability less than 5 md . This happens even though the bacteria size is comparable with the pore size. A main reason might be that the bacteria are not rigid and they can change shapes due to the forces acting during flow. A possible recovery mechanism in a water-wet chalk will be that a bacteria solution imbibes from the fractures into the matrix blocks and due to lower interfacial tension obtained in the matrix blocks higher oil recovery will be obtained.

23.4.2 Wettability

The initial wettability condition has a great impact on the effectiveness of bacteria, because it affects the distribution of the remaining oil in the porous space. If the oil forms a continuous connected film it is much easier to move than if it is left in scattered drops **Fig. 23.1**. However, in fractured chalk reservoirs an important oil recovery mechanism is water imbibition which requires that the chalk is water-wet and the remaining oil is immobile oil droplets. In this case the bacteria may be spread quickly deep into the reservoir through the fractured network and are imbibed into the matrix blocks. There the microbes may produce surfactants and reduce the oil/water interfacial tension and interact with the droplets and create instability which may finally result in mobilization.

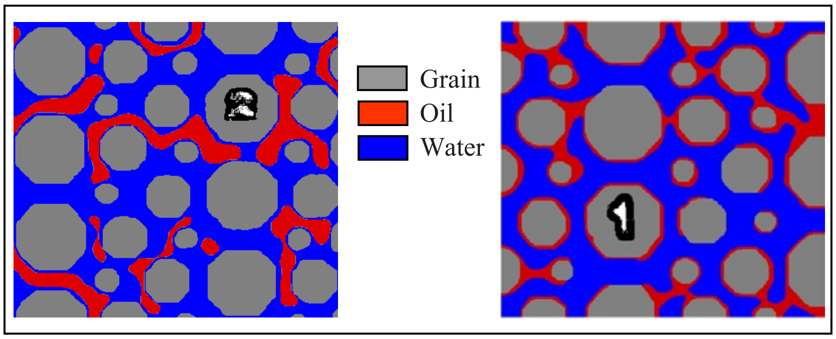

Figure 23.1: Water-wet (left) and oil-wet (right) glass micromodel (Afrapoli, Crescente et al. 2009).

In cases where chalk is weakly water-wet, neutral- or oil-wet a wettability change to more water-wet would be preferable. This is seen in **Fig. 23.2** where the water relative permeability curves change to the right (giving higher oil recovery) during the progress of a MEOR flooding (Afrapoli, Crescente et al. 2012). A MEOR process in a fractured chalk reservoir might bring bacteria to matrix blocks in large volumes of the reservoir and establishing a biofilm in the outer matrix block walls. A few experiments (Gandler, Gbosi et al. 2006; Kaster, Hiorth et al. 2007; Afrapoli, Alipour et al. 2010; Crescente 2012) indicate that these biofilms may change a hydrophobic surface to more hydrophilic. If this is the case in a fractured chalk reservoir the water imbibition due to capillary drive will give increased oil recovery.

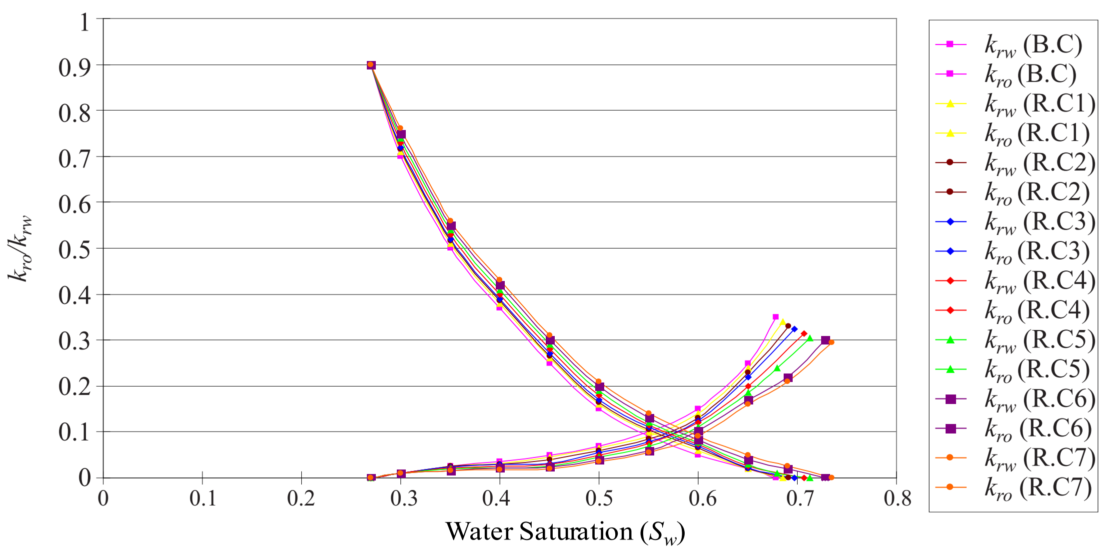

Figure 23.2: The relative permeability curves for different time steps during a MEOR process. The initial water relative permeability curve is the upper one and when the MEOR process is finished the water relative permeability curve is the lower one, redrawn from Afrapoli, Crescente et al. (2012).

23.4.3 Changes in flow pattern

The most successful MEOR field trials have been related to flow diversion from high permeability channels (Awan, Teigland et al. 2008). On the meter scale the main permeability contrast in fractured chalk reservoirs is between fracture permeability and matrix block permeability. In a MEOR process the fractures will be the main transport pathway far into the reservoir and the bacteria will most likely not block the fractures since the ratio between fracture opening to bacteria size is 100 or more. However, change in flow pattern in the matrix pore bacteria may happen and result in improved oil recovery. Laboratory studies on MEOR in chalk have shown decrease in permeability after injection of bacteria (Halim, Shapiro et al. 2014; Kaster, Hiorth et al. 2012). This permeability reduction is due to microbes attaching the surface of the chalk and can be approximated by using simple surface area considerations (Kaster, Hiorth et al. 2012). The specific surface area (S_{rock} =(wetted surface/flow volume)) of the chalk is according to Carman-Kozeny equation:,

$$S_{\text{rock}} = \sqrt{\frac{\phi}{2\tau k}}, \tag{23.1}$$

where ϕ is porosity and τ is tortuosity. If we assume the bacteria to be spherical the surface area per m^3 of fluid is

$$S_b = N_b \cdot \pi \cdot D_b^2, \tag{23.2}$$

where D_b is the diameter of bacteria and N_b is the number of bacteria that has attached to the rock surface per m^3 fluid. Assuming that the permeability is inverse proportional with the square of specific surface area the following relation is obtained;

$$\frac{k_{\text{MEOR}}}{k} = \left(\frac{S_{\text{rock}}}{S_{\text{rock}} + S_b}\right)^2 = \left(1 + \sqrt{\frac{2\tau k}{\phi}} N_b \cdot \pi \cdot D_b^2\right)^{-2}, \tag{23.3}$$

where k_{MEOR} is the permeability of the rock after a MEOR process. By using bacteria data and chalk parameters as shown in **Tab. 23.1** the permeability after microbial flooding is 98% of initial permeability. This is a rough estimate and bigger reduction after MEOR flooding of chalk is observed by Halim, Shapiro et al. (2014). The low values may be due to establishment of a filtercake at the inlet, precipitation of bacterial metabolites, bacterial aggregation and other causes.

Parameter	k (10^{-15} m^2)	ϕ	τ	N_b (10^{16} m^{-1})	D_b (10^{-6} m)	$\frac{k_{\text{MEOR}}}{k}$
Value	4	0.3	3	1	1	0.98

Table 23.1: Input parameters to permeability reduction calculation.

This shows that bacteria adsorption will have minor effect on permeability in low permeability rock like chalk. As seen from **Eq. 23.3** it will be a bigger reduction in permeability for highly permeable rocks. However, even though the effect on permeability is minor the attachment of bacteria on the chalk surface may affect the microscopic flow pattern and together with wettability effects this may have a positive effect on the imbibition oil recovery in chalk matrix blocks.

23.4.4 Additional mechanisms

During MEOR flooding in fractured chalk, carbon dioxide (CO_2) is produced during metabolism or by the reaction between metabolic acids and the carbonate rock. Laboratory experiments indicate that carbonate dissolution may occur (Jimoh, Rudyk et al. 2011) but most researchers rule out dissolution as a process that increases the chalk permeability. However, due to CO_2 production the rock can become weaker which may require models that couple geochemical and flow processes. CO_2 production during a MEOR process may repressurize the reservoir and decrease the viscosity. The effects on recovery in a chalk reservoir will require thorough analysis since they are function of parameters like saturated versus unsaturated oil (determines the type of drive mechanism) and relative permeability.

23.4.5 Modelling

Oil companies are reluctant to apply a production method that cannot give reliable forecasts for future field performance. Chalk reservoirs with dual porosity properties are challenging to simulate by itself and a MEOR process simulator for such reservoirs is not available at the present time. However, simulation of the MEOR processes in conventional reservoirs has progressed considerably lately, but still the models are inadequate as prediction tools. As long as the mechanisms are poorly understood the simulation modelling will only be of conceptual character. The chemical flooding simulator UTCHEM (Delshad, Asakawa et al. 2002) has a dual porosity formulation and a MEOR formulation that includes permeability reduction due to bacterial retention and formation of surfactant and polymer bio-products. To merge these formulations is for sure a challenge.

An interesting approach to MEOR simulation is the application of a compositional streamline simulator (Nielsen, Jessen et al. 2010) which is based on standard IMPEC (implicit pressure, explicit composition) framework and thereby are flow and reactive transport decoupled. For chalk reservoirs the simulator will not handle the mechanisms adequately, but the simulator has the potential to be a nice tool for studying both microscopic and macroscopic displacement efficiency of MEOR.

The mechanistic approach to model the reservoir souring process in the Ekofisk Field is an interesting starting point for a comprehensive fractured chalk MEOR simulation model (Burger, Jenneman et al. 2005). The model evaluates and forecasts the souring of a fractured reservoir. Included in the formulation is development of a biofilm on fracture faces and transport of nutrients in injection water and formation water in the chalk matrix. The model is based on microbiology principles, capillary imbibition waterflood processes, flow of water through the fractured chalk reservoir, and the thermodynamics of H_2S equilibrium. The approach used in the process of converting a special purpose simulation model for a conventional reservoir to be applicable for a fractured chalk reservoir is interesting and a similar approach could maybe be used as the first step towards a dual porosity MEOR model.

23.4.6 Practical aspects

Fig. 23.3 illustrates schematically the flooding procedure and necessary equipment for injection of microorganisms and nutrients. The microbes and nutrients are inexpensive, easy to handle, and eco-friendly. For a reservoir with on-going water injection the equipment requirements and logistics, even for offshore operations, are modest. Minor modifications of existing facilities are needed, marginal increase in difficulty, operating costs are low, and there will be minimal impact on other operations on the platform. According to Jensen, Harpole et al. (2000), the potential incremental costs will be (1) a tank for generation of microbial culture, (2) chemical injection pumps and (3) laboratory facilities. The cost aspect of the MEOR operations will not be affected by the reservoir type (sandstone or chalk) but the uncertainty regarding MEOR process performance in the reservoir rock is maybe greater for chalk reservoirs.

The main challenge for MEOR application in chalk reservoirs is to reduce the uncertainty in the improved oil recovery estimates. However, a nice aspect regarding chalk reservoirs is that these reservoirs are produced slower than sandstone reservoirs and thereby will they be less time critical for EOR. More time is therefore available for attacking the problem of recovery uncertainty. The challenge can only be solved by further investigations on the following subject areas:

- Microbial strains for chalk reservoir environment (pressure, temperature, water salinity, oil composition, prevailing indigenous microbial communities) have to be identified.

- Rates of biochemical processes have to be developed to ensure that enough microbial biomass and metabolites are produced.

- Laboratory studies on chalk core plugs to evaluate recoveries. This is a multidisciplinary task between microbiologists and reservoir engineers.

- A MEOR simulation model for dual porosity chalk reservoirs should be developed

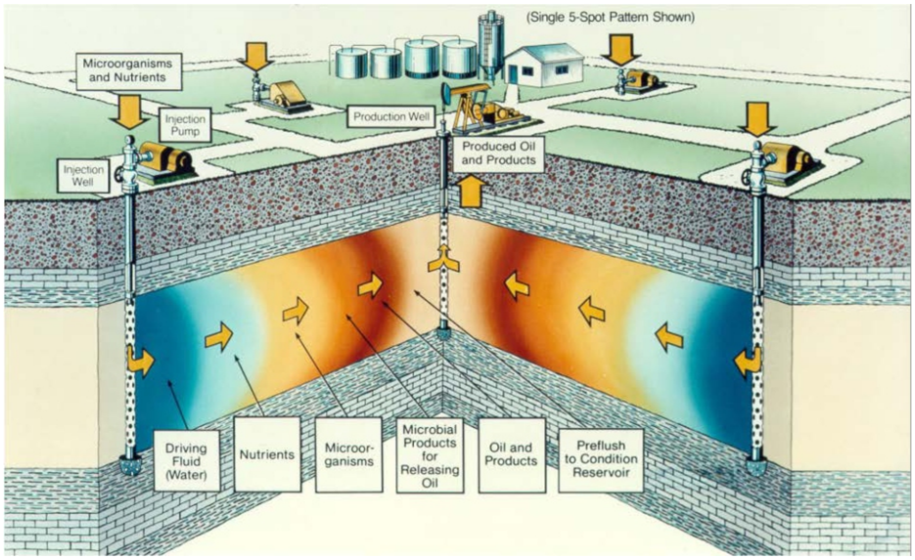

Figure 23.3: Example of injection pattern in a microbial enhanced oil recovery process (www.netl.doe.gov)

Nomenclature

ϕ = porosity
σ = interfacial tension
θ = contact angle
τ = tortuosity (square of the ratio between actual flow length and the straight line)
a = length of block sides
b = fracture opening
D_b = diameter of bacteria
k = absolute permeability
k_f = fracture network permeability
k_{MEOR} = permeability after MEOR flooding
k_{ro} = relative permeability for oil
k_{rw} = relative permeability for water
N_b = number of bacteria per m^3
Nc = capillary number
S_{rock} = specific surface area (wetted surface / flow volume)
S_b = surface area of a bacteria
u = flow velocity

Subscripts

b = bacteria
f = fracture
MEOR = Microbial EOR
rock = rock
ro = relativ oil
rw = relative water

Abbreviation

16S rRNA = is a universal phylogenetic marker for bacteria and archaea. Short conserved ribosomal RNA sequences.
IFT = interacial tension
IMPEC = implicit pressure, explicit composition
MEOR = microbial enhanced oil recovery
UTCHEM = chemical fooding simulator

References

Abe, F., 2007. Exploration of the effects of high hydrostatic pressure on microbial growth, physiology and survival: perspectives from piezophysiology. *Biosci. Biotechnol. Biochem.*, **71** (10): 2347–2357. October. URL http://www.ncbi.nlm.nih.gov/pubmed/17928722.

Adkins, J.P., Cornell, L.A., and Tanner, R.S., 1992. Microbial composition of carbonate petroleum reservoir fluids. *Geomicrobiology Journal*, **10** (2): 87–97. URL http://dx.doi.org/10.1080/01490459209377909.

Afrapoli, M.S., Alipour, S., and Torsæter, O., 2010. Effect of Wettability and Interfacial Tension on Microbial Improved Oil Recovery with Rhodococcus sp 094. Paper SPE-129707 presented at SPE Improved Oil Recovery Symposium, Tulsa, Oklahoma, USA. 24–28 April. URL http://dx.doi.org/http://dx.doi.org/10.2118/129707-MS.

Afrapoli, M.S., Crescente, C. et al., 2009. The effect of bacterial solution on the wettability index and residual oil saturation in sandstone. *Journal of Petroleum Science and Engineering*, **69** (3–4): 255–260. URL http://dx.doi.org/http://dx.doi.org/10.1016/j.petrol.2009.09.002.

Afrapoli, M.S., Crescente, C.M. et al., 2012. Simulation Study of Displacement Mechanisms in Microbial Improved Oil Recovery Experiments. Paper SPE 153323 presened at SPE EOR Conference at Oil and Gas West Asia, Muscat, Oman. 16–18 April. URL http://dx.doi.org/dx.doi.org/10.2118/153323-MS.

Awan, A.R., Teigland, R., and Kleppe, J., 2008. A Survey of North Sea Enhanced-Oil-Recovery Projects Initiated During the Years 1975 to 2005. *SPE Reservoir Eval. & Eng*, **11**: 497–512. URL http://dx.doi.org/http://dx.doi.org/10.2118/99546-PA.

Balows, A., Truper, H.G. et al., 1992. *The Procaryotes*. New York, NY: Springer-Verlag.

Bartlett, D.H., 2002. Pressure effects on in vivo microbial processes. *Biochimica et Biophysica Acta (BBA) - Protein Structure and Molecular Enzymology*, **1595** (1–2): 367–381. URL http://dx.doi.org/http://dx.doi.org/10.1016/S0167-4838(01)00357-0.

Berland, H., Kaster, K. et al., 2008. MEOR, A study of microbes and mechanisms at Ekofisk chalk reservoir. Tech. rep., IRIS report 2008-212.

Brown, L.R., 2010. Microbial enhanced oil recovery (MEOR). *Current Opinion in Microbiology*, **13** (3): 316–320. Ecology and industrial microbiology * Special section: Systems biology. URL http://dx.doi.org/10.1016/j.mib.2010.01.011.

Bryant, S. and Britton, L., 2004. Mechanistic understanding of microbial plugging for improved sweep efficiency. Tech. rep., The University of Texas at Austin. In Final Scientific/Technical Report.

Bulut, S., Waites, W.M., and Mitchell, J.R., 1999. Effects of Combined Shear and Thermal Forces on Destruction of Microbacterium lacticum. *Applied and Environmental Microbiology*, **65** (10): 4464–4469. URL http://aem.asm.org/content/65/10/4464.abstract.

Burger, E.D., Jenneman, G.E. et al., 2005. A Mechanistic Model To Evaluate Reservoir Souring in the Ekofisk Field. Paper SPE-93297 presented at SPE International Symposium on Oilfield Chemistry, The Woodlands, Texas. 2–4 February. URL http://dx.doi.org/http://dx.doi.org/10.2118/93297-MS.

Castorena-Cortés, G., Zapata-Peñasco, I. et al., 2012. Evaluation of indigenous anaerobic microorganisms from Mexican carbonate reservoirs with potential {MEOR} application. *Journal of Petroleum Science and Engineering*, **81**: 86–93. URL http://dx.doi.org/http://dx.doi.org/10.1016/j.petrol.2011.12.010.

Cavicchioli, R., 2007. *Archaea: molecular and cellular biology.* ASM Press. URL http://www.cabdirect.org/abstracts/20073220049.html;jsessionid=0D18929059A8C1A8FA81BC178423159C#.

Cayol, J.L., Ollivier, B. et al., 1994. Isolation and Characterization of Halothermothrix orenii gen. nov., sp. nov., a Halophilic, Thermophilic, Fermentative, Strictly Anaerobic Bacterium. *International Journal of Systematic Bacteriology*, **44** (3): 534–540. URL http://dx.doi.org/10.1099/00207713-44-3-534.

Crescente, C.M., 2012. *Experimental Studies of Microbial Enhanced Oil Recovery*. Ph.D. thesis, Norwegian University of Science and Technology, Department of Petroleum Engineering and Applied Geophysics.

Cunningham, A.B., Sharp, R.R. et al., 2007. Effects of starvation on bacterial transport through porous media. *Advances in Water Resources*, **30** (6–7): 1583–1592. Biological processes in porous media: From the pore scale to the field. URL `http://dx.doi.org/http://dx.doi.org/10.1016/j.advwatres.2006.05.018`.

Cusack, F., Lappin-Scott, H. et al., 1992. Enhanced Oil-Recovery - 3-Dimensional Sandpack Simulation of Ultramicrobacteria Resuscitation in Reservoir Formation. *Journal of General Microbiology*, **138**: 647–655. URL `http://mic.sgmjournals.org/content/138/3/647.full.pdf`.

Dahle, H., Garshol, F. et al., 2008. Microbial community structure analysis of produced water from a high-temperature North Sea oil-field. *Antonie van Leeuwenhoek*, **93** (1-2): 37–49. URL `http://dx.doi.org/10.1007/s10482-007-9177-z`.

Davis, J.B. and Updegraf, D.M., 1954. Microbiology in the petroleum industry. *Bacteriol Rev*, **18** (4): 215–238. December.

Delshad, M., Asakawa, K. et al., 2002. Simulations of Chemical and Microbial Enhanced Oil Recovery Methods. Paper SPE-75237 preseted at SPE/DOE Improved Oil Recovery Symposium, Tulsa, Oklahoma. 13–17 April,. URL `http://dx.doi.org/dx.doi.org/10.2118/75237-MS`.

Gandler, G., Gbosi, A. et al., 2006. Mechanistic Understanding of Microbial Plugging for Improved Sweep Efficiency. *SPE*. Paper SPE-100048 presented at SPE/DOE Symposium on Improved Oil Recovery, Tulsa, Oklahoma,. 22–26 April. URL `http://dx.doi.org/http://dx.doi.org/10.2118/100048-MS`.

Gao, C., 2011. Microbial enhanced oil recovery in carbonate reservoir: an experimental study. Paper SPE-143161-MS presented at SPE Enhanced Oil Recovery Conference, Kuala Lumpur, Malaysia. 19–21 July. URL `http://dx.doi.org/10.2118/143161-MS`.

Gaytán, I., Mejía, M. et al., 2015. Effects of indigenous microbial consortia for enhanced oil recovery in a fragmented calcite rocks system. *Journal of Petroleum Science and Engineering*, **128**: 65–72. URL `http://dx.doi.org/http://dx.doi.org/10.1016/j.petrol.2015.02.028`.

Gerday, C. and Glansdorff, N., eds., 2007. *Physiology and Biochemistry of Extremophiles*. American Society of Microbiology. URL `http://www.asmscience.org/content/book/10.1128/9781555815813`.

Grabowski, A., Nercessian, O. et al., 2005. Microbial diversity in production waters of a low-temperature biodegraded oil reservoir. *FEMS Microbiology Ecology*, **54** (3): 427–443. URL `http://dx.doi.org/10.1016/j.resmic.2005.03.009`.

Gray, M., Yeung, A. et al., 2008. Potential microbial enhanced oil recovery processes: A critical analysis. Paper SPE-114676-MS presented at SPE Annual Technical Conference and Exhibition, Denver, Colorado, USA. 21–24 September. URL `http://dx.doi.org/10.2118/114676-MS`.

Halim, A., Shapiro, A. et al., 2014. Experimental Study of Bacterial Penetration into Chalk Rock: Mechanisms and Effect on Permeability. *Transport in Porous Media*, **101** (1): 1–15. URL `http://dx.doi.org/10.1007/s11242-013-0227-x`.

Jenkins, M.B. and Lion, L.W., 1993. Mobile bacteria and transport of polynuclear aromatic hydrocarbons in porous media. *Applied and Environmental Microbiology*, **59** (10): 3306–3313. URL `http://aem.asm.org/content/59/10/3306.abstract`.

Jenneman, G.E., McInerney, M.J., and Knapp, R.M., 1985. Microbial Penetration through Nutrient-Saturated Berea Sandstone. *Applied and Environmental Microbiology*, **50** (2): 383–391. URL `http://aem.asm.org/content/50/2/383.abstract`.

Jensen, T.B., Harpole, K.J., and Østhus, A., 2000. EOR Screening for Ekofisk. In *SPE European Petroleum Conference*. Society of Petroleum Engineers, Paris, France. SPE-65124-MS. 24–25 October. URL `http://dx.doi.org/http://dx.doi.org/10.2118/65124-MS`.

Jimoh, I.A., Rudyk, S.N., and Søgaard, E.G., 2011. Microbial Fluid-rock Interactions in Chalk Samples and Salinity Factor in Divalent Ca2+ Ions Release for Microbial Enhanced Oil Recovery Purposes. *Chemical Engineering Transactions*, **24**: 889–894. URL `http://dx.doi.org/DOI:10.3303/CET1124149`.

Kaster, K., Bonaunet, K. et al., 2009. Characterisation of culture-independent and -dependent microbial communities in a high-temperature offshore chalk petroleum reservoir. *Antonie van Leeuwenhoek*, **96** (4): 423–439. URL `http://dx.doi.org/10.1007/s10482-009-9356-1`.

Kaster, K.M., Hiorth, A. et al., 2007. Biofilms a possible mechanism of enhanced oil recovery. In . IRIS. Poster presented at Thermophiles Conference Bergen, Norway. 24–27 September. URL http://www.iris.no/publications/414551636/2007-320.

Kaster, K.M., Hiorth, A. et al., 2012. Mechanisms Involved in Microbially Enhanced Oil Recovery. *Transport in Porous Media*, **91** (1): 59–79. URL http://dx.doi.org/10.1007/s11242-011-9833-7.

Kim, D.S. and Fogler, H.S., 1999. The effects of exopolymers on cell morphology and culturability of Leuconostoc mesenteroides during starvation. *Applied Microbiology and Biotechnology*, **52** (6): 839–844. URL http://dx.doi.org/10.1007/s002530051601.

Kim, D.S. and Fogler, H.S., 2000. Biomass evolution in porous media and its effects on permeability under starvation conditions. *Biotechnology and Bioengineering*, **69** (1): 47–56. URL http://dx.doi.org/10.1002/(SICI)1097-0290(20000705)69:1<47::AID-BIT6>3.0.CO;2-N.

L'Haridon, S., Reysenbacht, A.L. et al., 1995. Hot subterranean biosphere in a continental oil reservoir. *Nature*, **377** (6546): 223–224. URL http://dx.doi.org/10.1038/377223a0.

Magot, M., Ollivier, B., and Patel, B., 2000. Microbiology of petroleum reservoirs. *Antonie van Leeuwenhoek*, **77** (2): 103–116. URL http://dx.doi.org/10.1023/A:1002434330514.

McDowell-Boyer, L.M., Hunt, J.R., and Sitar, N., 1986. Particle transport through porous media. *Water Resources Research*, **22** (13): 1901–1921. URL http://dx.doi.org/10.1029/WR022i013p01901.

Myhr, S., Lillebø, B.L. et al., 2002. Inhibition of microbial H2S production in an oil reservoir model column by nitrate injection. *Applied Microbiology and Biotechnology*, **58** (3): 400–408. URL http://dx.doi.org/10.1007/s00253-001-0881-8.

Nazina, T.N., Shestakova, N.M. et al., 2013. Functional and phylogenetic microbial diversity in formation waters of a low-temperature carbonate petroleum reservoir. *International Biodeterioration & Biodegradation*, **81**: 71–81. Special Issue: 3rd International Symposium on Applied Microbiology and Molecular Biology in Oil Systems. URL http://dx.doi.org/http://dx.doi.org/10.1016/j.ibiod.2012.07.008.

Nielsen, S.M., Jessen, K. et al., 2010. Microbial Enhanced Oil Recovery: 3D Streamline Simulation with Gravity Effects. Paper SPE-131048 presented at SPE EUROPEC/EAGE Annual Conference and Exhibition, Barcelona, Spain. 14–17 June. URL http://dx.doi.org/dx.doi.org/10.2118/131048-MS.

Nilsen, R.K., Beeder, J. et al., 1996. Distribution of thermophilic marine sulfate reducers in north sea oil field waters and oil reservoirs. *Applied and Environmental Microbiology*, **62** (5): 1793–1798. URL http://aem.asm.org/content/62/5/1793.abstract.

Nomura, T., Narahara, H. et al., 2009. The role of microbial surface properties and extracellular polymer in Lactococcus Lactis aggregation. *Advanced Powder Technology*, **20** (6): 537–541. URL http://dx.doi.org/http://dx.doi.org/10.1016/j.apt.2009.07.003.

Pedersen, K., 2000. Exploration of deep intraterrestrial microbial life: current perspectives. *FEMS microbiology letters*, **185** (1): 9–16. URL http://dx.doi.org/10.1111/j.1574-6968.2000.tb09033.x.

Stetter, K.O., Huber, R. et al., 1993. Hyperthermophilic archaea are thriving in deep North Sea and Alaskan oil reservoirs. *Nature*, **365** (6448): 743–745. URL http://dx.doi.org/10.1038/365743a0.

Takahata, Y., Hoaki, T., and Maruyama, T., 2001. Starvation survivability of Thermococcus strains isolated from Japanese oil reservoirs. *Archives of Microbiology*, **176** (4): 264–270. URL http://dx.doi.org/10.1007/s002030100318.

Takahata, Y., Nishijima, M. et al., 2000. Distribution and Physiological Characteristics of Hyperthermophiles in the Kubiki Oil Reservoir in Niigata, Japan. *Applied and Environmental Microbiology*, **66** (1): 73–79. URL http://dx.doi.org/10.1128/AEM.66.1.73-79.2000.

Telang, A.J., Ebert, S. et al., 1997. Effect of nitrate injection on the microbial community in an oil field as monitored by reverse sample genome probing. *Applied and Environmental Microbiology*, **63** (5): 1785–1793. URL http://aem.asm.org/content/63/5/1785.abstract.

Vasconcellos, S.P., Dellagnezze, B.M. et al., 2011. The potential for hydrocarbon biodegradation and production of extracellular polymeric substances by aerobic bacteria isolated from a Brazilian petroleum reservoir. *World Journal of Microbiology and Biotechnology*, **27** (6): 1513–1518. URL `http://dx.doi.org/10.1007/s11274-010-0581-6`.

Voordouw, G., Armstrong, S.M. et al., 1996. Characterization of 16S rRNA genes from oil field microbial communities indicates the presence of a variety of sulfate-reducing, fermentative, and sulfide-oxidizing bacteria. *Applied and Environmental Microbiology*, **62** (5): 1623–1629. URL `http://aem.asm.org/content/62/5/1623.abstract`.

Wilhelms, A., Larter, S.R. et al., 2001. Biodegradation of oil in uplifted basins prevented by deep-burial sterilization. *Nature*, **411** (6841): 1034–1037. June. URL `http://dx.doi.org/10.1038/35082535`.

Woese, C.R., 1994. There must be a prokaryote somewhere: microbiology's search for itself. *Microbiological Reviews*, **58** (1): 1–9. 1 March. URL `http://mmbr.asm.org/content/58/1/1.short`.

Zhang, F., She, Y. et al., 2010. Response of microbial community structure to microbial plugging in a mesothermic petroleum reservoir in China. *Applied Microbiology and Biotechnology*, **88** (6): 1413–1422. URL `http://dx.doi.org/10.1007/s00253-010-2841-7`.

Chapter 24

Geomechanics Applications

Tron Golder Kristiansen

24.1 Field application of the geomechanics models

Rock mechanics, or geomechanics, has been one of the focus areas of chalk research since the chalk reservoirs were discovered, especially after the discovery of seafloor subsidence over fields like Ekofisk, Valhall and Eldfisk in the eighties. The need to understand the constitutive behavior of the chalk was important to accurately predict future seafloor subsidence. The constitutive behavior of chalk reservoirs has been a bit more complicated compared with many other types of reservoirs in the industry, so the chalk models have always been some of the more advanced models in the industry. The following are a couple of short sections illustrating some of the current-day applications of geomechanical modeling of the chalk fields. For more details around the historical developments see (Andersen 1995). For more details on chalk geomechanics please read the earlier chapters in this textbook on rock mechanics/geomechanics, Chapter 6 Rock Mechanics and Chapter 14 Geomechanical Modeling.

24.1.1 Compaction and subsidence

The compaction and subsidence modeling has been the main driver for rock mechanics testing and research in JCR over the years. Currently these models are built on a routine basis and used to evaluate how various development scenarios could impact the seafloor subsidence. The importance of this work is linked to the air gap of the platforms used. If the air-gap is too small the platforms may not be safe for people to work on during storms and may have to be evacuated in bad weather. The Ekofisk platforms were first jacked up 6 meters (Nagel 2001) in 1987. Then the Ekofisk barrier wall was installed (Nagel 2001) in 1989. Valhall was installed with larger air gap allowance and is still in operation after experiencing close to 6.5m of subsidence. A new combined processing and hotel platform was installed in 2010 and the old 3 platform central complex will be abandoned within the next few years. The Tyra field was also reported to be closed during 2018 in 2017. This was also reported to be due to loss of air gap due to subsidence. There has also been presented plans to redevelop the field. **Fig. 24.1** shows a typical numerical model used for managing chalk fields.

Fig. 24.2 shows how faults are included in the model. **Fig. 24.3** shows some more details of the faults implemented in the model while **Fig. 24.4** and **24.5** shows typical output products for the geomechanics models in terms of maps or 3D shapes of the rock deformations at certain points in time during the field life. Typical subsidence uncertainty for a chalk field is shown in Fig. 24.1 (Kristiansen and Plischke 2010).

The lower 3 cases in Fig. 24.6 are based on prediction of strong repressurization resulting from the waterflooding at Valhall, but with varying water weakening assumptions based on laboratory experiments. The difference between the two families of cases is that in the highest two cases one investigates a worst case scenario from a subsidence point of view, a weak repressurization. The differences within the two groups are the magnitude of the water weakening used. The strongest is the one reported from the Ekofisk field (Gauer, Sylte et al. 2002) instead of the one from Valhall laboratory data. One can see that the uncertainty in repressurization in this case has the largest impact on predicted subsidence.

Measured subsidence data and most recent predictions are shown in (Fig. 24.6b). Predictions are done in 2008. Measured subsidence data up to 2009 are included. Results are within uncertainty envelope from 2003 and along most likely scenarios (Kristiansen and Plischke 2010) . Major uncertainties were related to

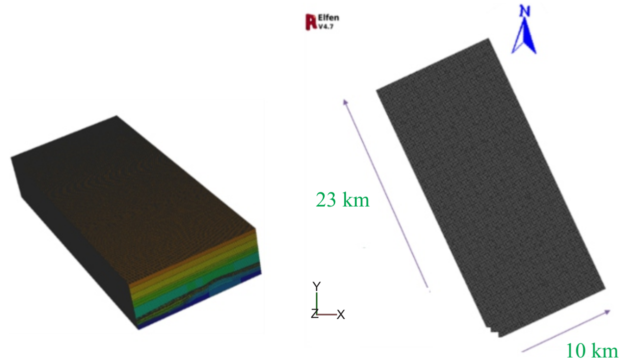

Figure 24.1: Overview of a geomechanics model mesh in 3D (left) and in plan view with dimensions (right) for the Valhall-Hod fields. The total number of finite elements are around 3 million in this case, but much larger models are feasible. The model has around 30 geologic layers. Courtesy of Aker BP.

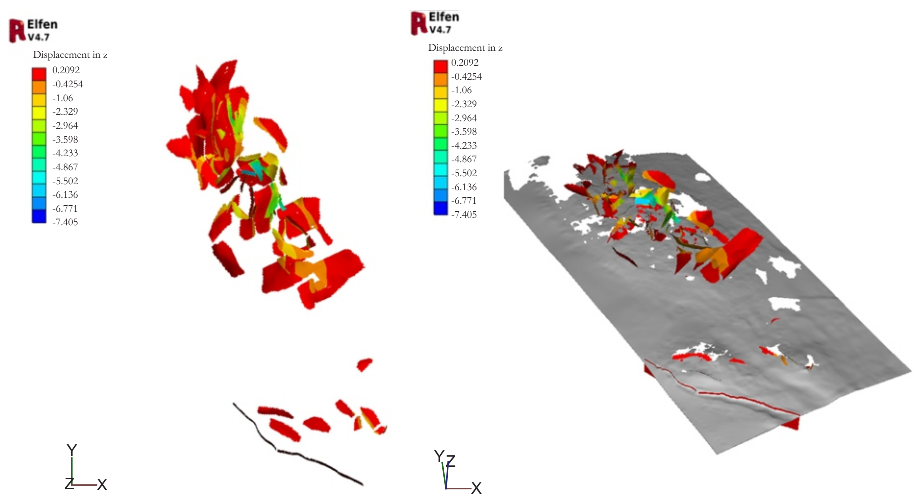

Figure 24.2: The faults in a geomechanics model shown (left). 69 of the largest faults were selected in this case. Many of the faults extend up into the overburden above the top of the reservoir (right). Courtesy of Aker BP.

reservoir management decisions. The case producing most subsidence is an early blowdown after a potential unsuccessful waterflood.

The use of these full field models has ben extended to more than compaction and subsidence prediction as we will see in some of the following sections on casing deformations, well planning, 4D seismic, microseismicity and coupled modeling.

24.2 Chalk production

Chalk production has been a topic of interest since the early days of JCR. The background was experiences with chalk influx failures in both Valhall and Eldfisk and Tyra (Risnes 1990). The initial work was based on the classical work on sandstones (Bratli and Risnes 1981), but extended to chalk (Risnes and Horsrud 1985). Numerical modeling was performed by Plischke and Pisarsky (1992) as part of JCR III. This work gave insight into other potential mechanisms around perforations.

A majority of the influx failures, 80%, could completely be removed by carefully controlling the opening of the well chokes, Kristiansen and Meling (1996). The other 20% of the failures may be related to a combination of multiphase flow effects and rapid triggering of instability in undrained conditions in the near wellbore area. Selection of completion methods and completion geometry details had a significant impact on chalk production, Kristiansen (1996).

More advances in modeling chalk production was presented by Crook, Yu et al. (2008). They were developing a model to reproduce the chalk liquefaction laboratory experiments performed by Flatebø (2005). Crook, Yu et al. (2008) were using a further extension of the commercially available SR3 (soft rock model 3) constitu-

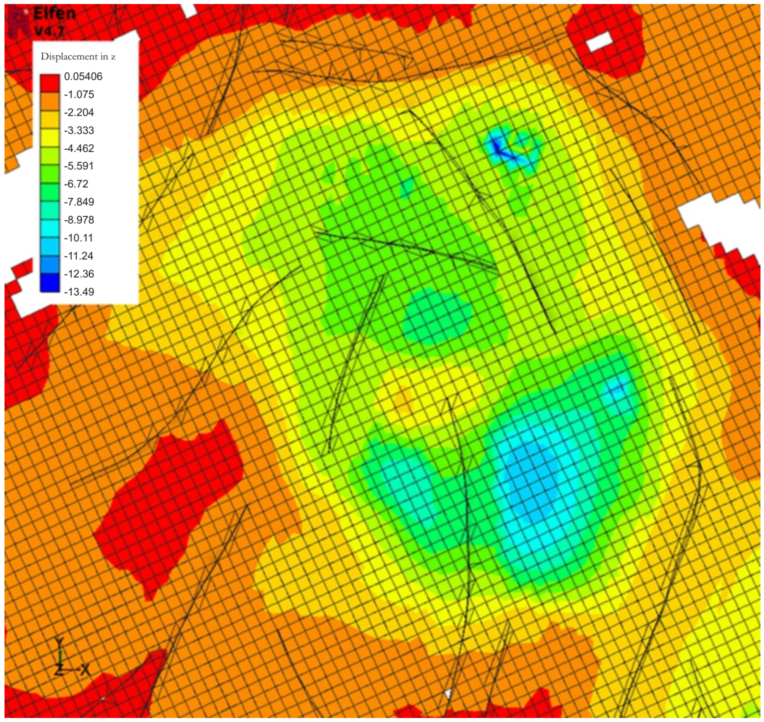

Figure 24.3: A plan view close up of faults in the crestal basin at the top Tor M0 layer Valhall at some point in the depletion history. Courtesy of Aker BP.

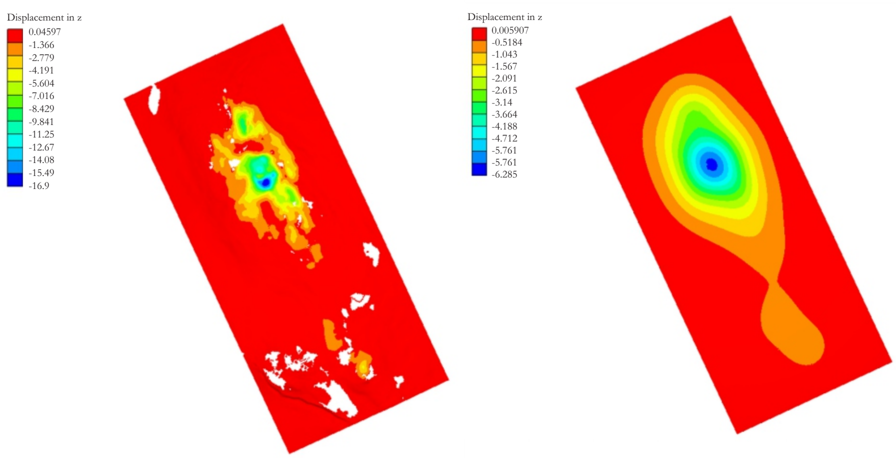

Figure 24.4: Predicted vertical displacement on top reservoir (compaction) layer (left) and at the seafloor (subsidence) (right) in a scenario for 2048 in the Valhall-Hod area. Courtesy of Aker BP.

tive model in the finite element software Elfen. **Fig. 24.7** is showing the numerical simulation of the laboratory experiments in more detail.

More recent work is ongoing to better understand all the potential mechanisms associated with chalk production to come up with a robust and hopefully rather simple prediction model, Papamichos, Berntsen et al. (2012).

24.3 Casing deformations

Casing deformations in chalk fields have been experienced due to the compaction and subsidence (Schwall and Denney 1994; Kristiansen, Barkved et al. 2000) but also due to chalk production (Pattillo and Kristiansen 2002) and stimulation (Furui, Fuh et al. 2009).

A joint project between the Ekofisk and Valhall licenses were initiated in the mid 1990s with Center for

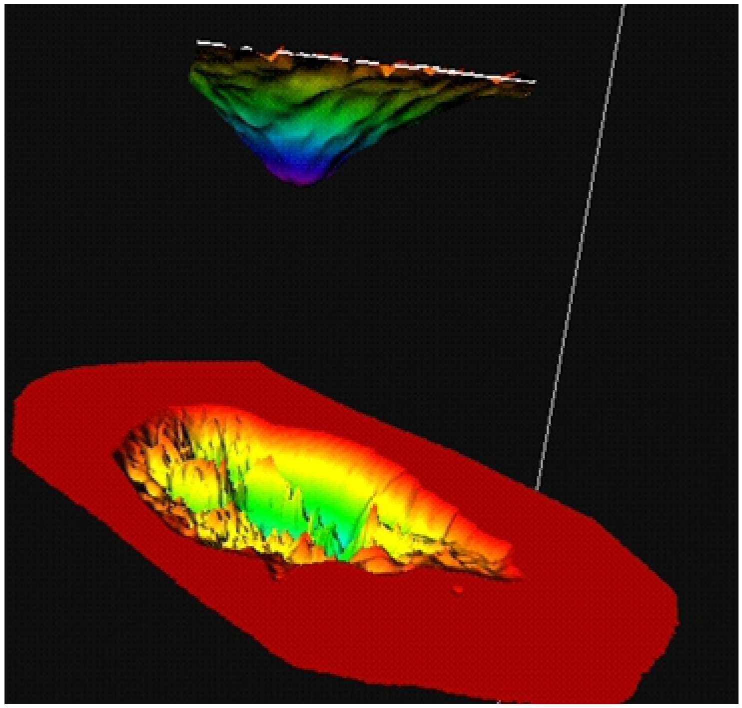

Figure 24.5: Example of a 3D representation of vertical displacement at top reservoir and at seafloor. Note that the reservoir compaction is smoothed through the overburden and the result is a smoother subsidence bowl on the seafloor. Courtesy of Aker BP.

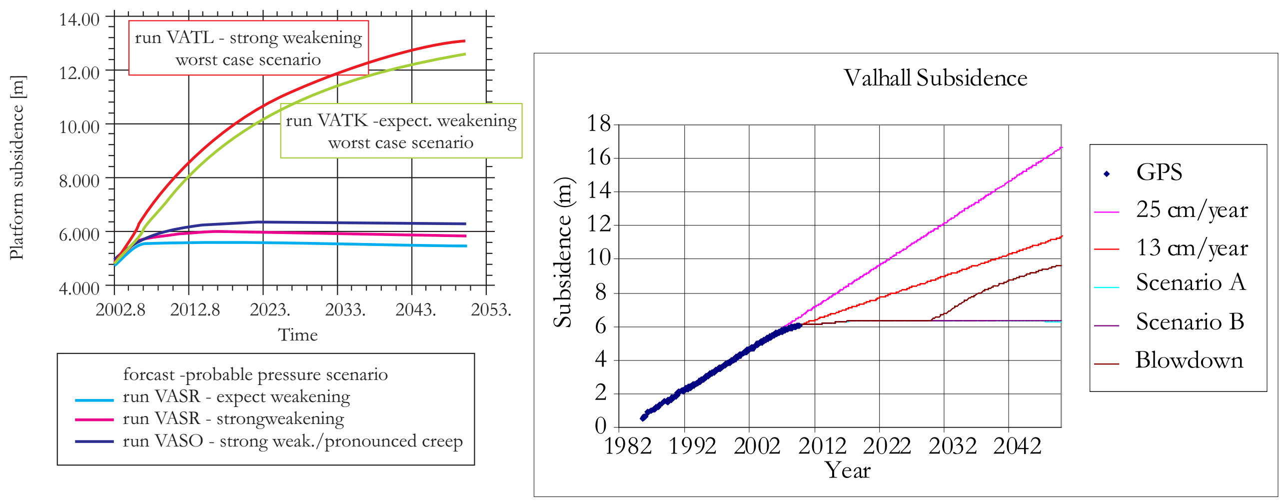

(a) (b)

Figure 24.6: : Uncertainty envelope for subsidence developed in 2003 for Valhall (a). Measured subsidence data and most recent predictions (b) (Kristiansen and Plischke 2010).

Frontier Engineering Research (CFER), Kaiser, Roggensack et al. (1996). The main findings of this study as implemented at Valhall is presented by Kristiansen, Barkved et al. (2000). The main solution implemented was to extend heavy wall (high thickness/diameter ratio) liner laps up across the areas of highest risk for fault re-activation, that could be determined from microseismic monitoring.

More details on the reservoir section can be found in the work by Pattillo, Moschovidis et al. (1995) and Pattillo and Kristiansen (2002).

Again, the solution was high thickness/diameter ratio pipe to combat non-uniform loading. The work by Furui, Fuh et al. (2009) conclude that the loading condition for acid fractured Ekofisk wells is a buckling failure mode also in horizontal wells, but the solution is in this case also a higher thickness/diameter ratio pipe or use of screens instead of perforated completions. **Fig. 24.8** shows a comparison of standard oil field tubulars and the ones used to prevent collapse in some of the chalk fields. **Fig. 24.9** shows an example of modelling shear of a well structure across a fault as experienced in the overburden in many chalk fields.

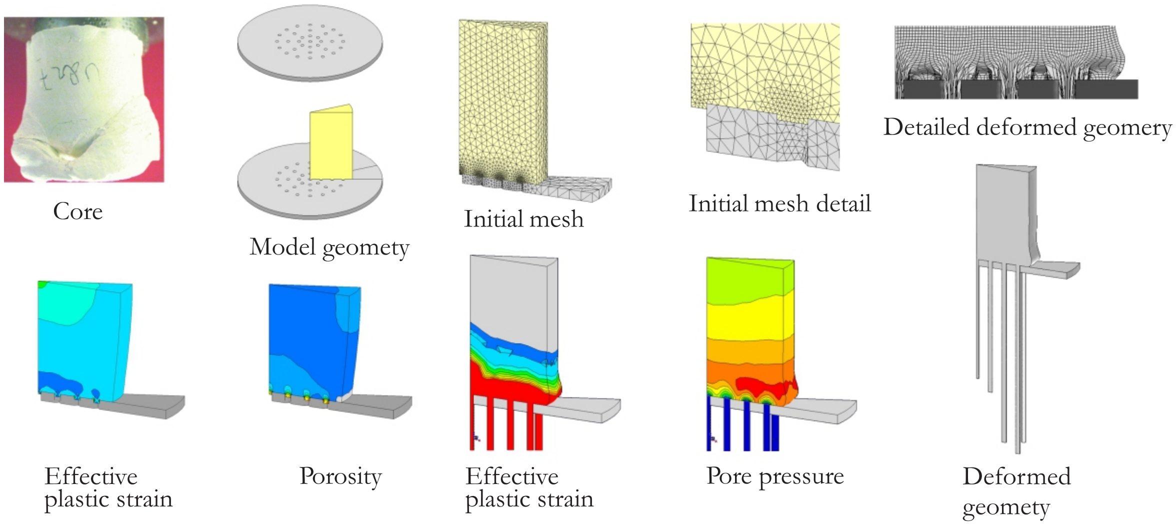

Figure 24.7: An illustration of the modeling of chalk liquefaction using the constitutive model developed by Crook, Yu et al. (2008). Courtesy of Aker BP and Rockfield.

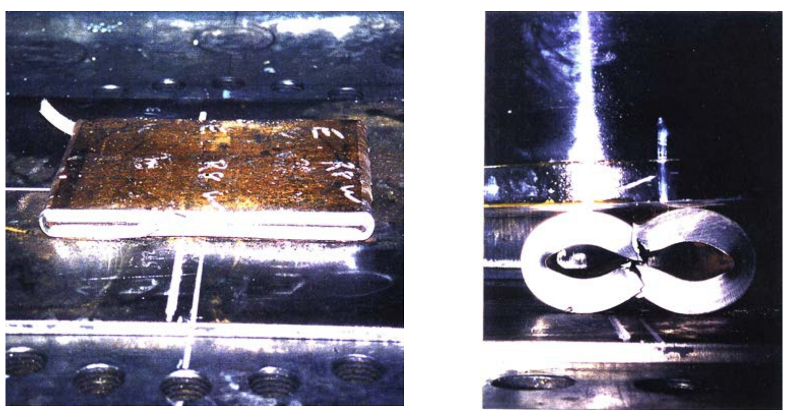

Figure 24.8: Standard oilfield liner tubulars (low thickness/diameter ratio) exposed to a line load (left). Thick walled liner tubulars (high thickness/diameter ratio) used in weak chalk reservoirs exposed to a very high line load (right). From Kaiser, Roggensack et al. (1996).

24.4 Water injection modeling

A creative use of geomechanics modeling as part of waterflooding chalks was presented by Jørgensen (2002) and implemented on Halfdan, to reduce risk of transversely growing fractures between 3000-meter-long producers and injectors with only a well spacing of 183 meters. By injecting water at matrix rates initially the pore pressure will increase and the bulk volume of the rock mass around the well is increasing (if the thermal volume shrinkage is much less, which is the case in high porosity chalk). This will alter the stress distribution around the well and at some point in time an induced fracture, following a rapid increase in injection pressure, will start to propagate along the wellbore axis, even if the initial in-situ stress state may have favored a transverse fracture.

The initial work by Jørgensen (2002) was based on linear elasticity, but the concept has also been tested on a case using a thermo-elasto-plastic material model with water weakening for a mature chalk field that had

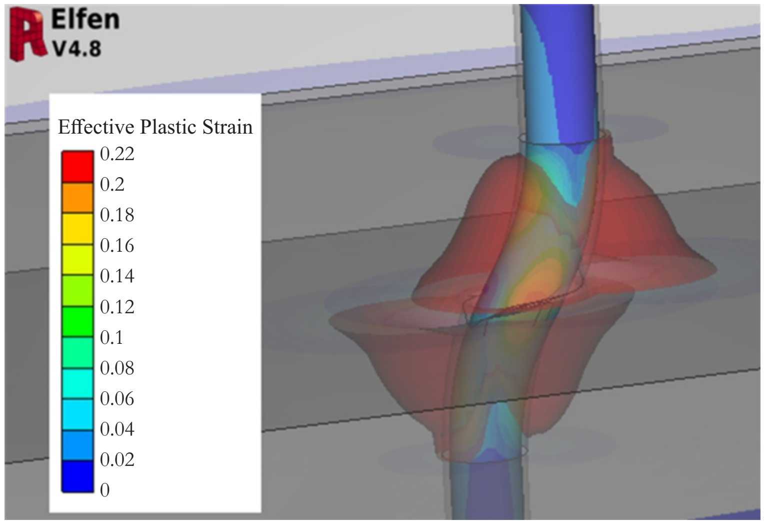

Figure 24.9: : Iso-surface of shear zone plastic strains showing damage in the formation above and below the fault plane as well as plastic strains in the outer casing. Courtesy of Aker BP.

experienced severe depletion. The concept did also work in this more complex case based on the numerical modeling, if the total horizontal stress anisotropy did not exceed 2%. The thermal strains did also result in a larger resistance to the re-orientation of the horizontal stresses. **Fig. 24.10** shows results from the modeling.

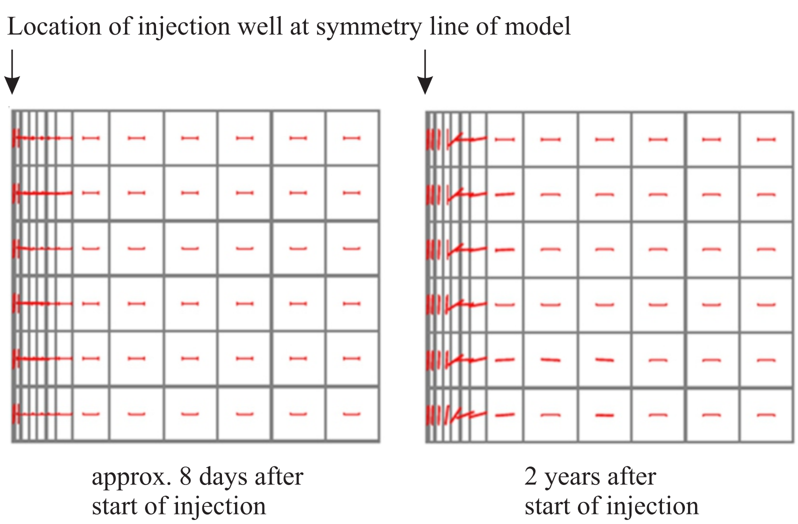

Figure 24.10: Map of maximum horizontal stress direction around a horizontal injector showing stress re-orientation after 8 days and 2 years of injection below the fracturing pressure using a thermo-elasto-plastic model with water weakening. Courtesy of Aker BP and ISAMGEO.

The main challenge with implementing this technique on water injectors is the lack of short term verification of the exact direction of fracture growth in the field. 4D seismic can be used over a longer time period.

24.5 4D seismic

The first linkage between subsidence and 4D seismic in the chalk reservoirs was made by Guilbot and Smith (2002) based on the first 4D seismic survey at Ekofisk. They reported large seismic timeshifts. Similar and additional observations were reported from the first 4D on Valhall, Barkved, Buer et al. (2003). A detailed review of deformations outside the reservoir as predicted by geomechanical modeling and observed in seismic is given by Kristiansen, Barkved et al. (2005). Most of the published material around this time was based on 4D in the chalk fields. One of the reasons being that these fields typically had geomechanics models available that could be used to compare to the observed seismic attributes. Herwanger and Koutsabeloulis (2011) includes a table of publications up until 2011. **Fig. 24.11** shows a comparison between volumetric strain and timeshifts. **Fig. 24.12** also show the linkage between stress and shear wave splitting as observed in the shallow layers at Valhall on seismic compared to the direction and magnitude of the second largest principal stress vector on the seafloor from the geomechanics model.

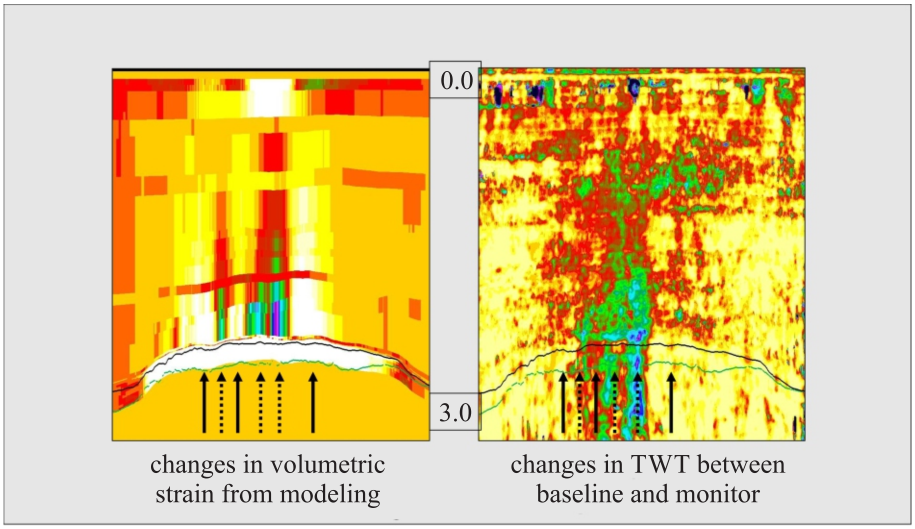

Figure 24.11: Comparison of volumetric strain from geomechanics model (left) to timeshifts between baseline and monitor survey (right). From Kristiansen, Barkved et al. (2005).

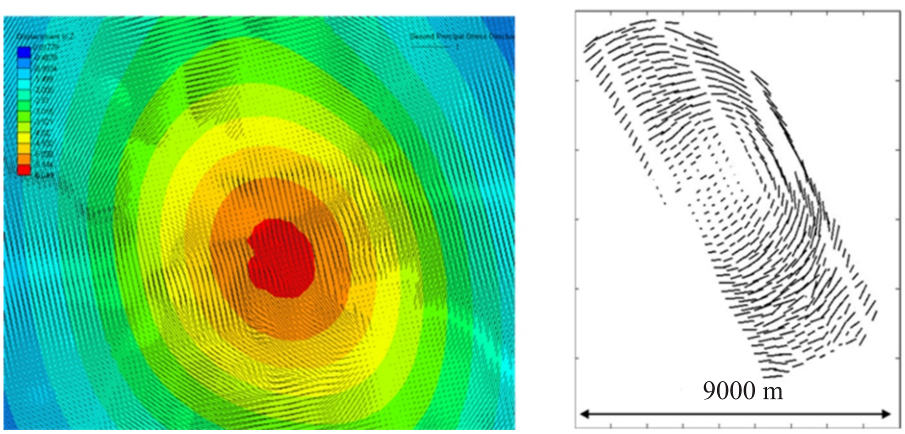

Figure 24.12: Comparison of the direction and magnitude of the second largest principal stress vector on the seafloor from the geomechanics model (left) and the shear wave splitting magnitude and direction (right). Courtesy of Aker BP.

Fig. 24.13 shows a typical application of 4D to verify the geomechanics model, where geomechanics model attributes are cross-correlated with related seismic attributes.

24.6 Wellbore stability

The impact of subsidence on drilling in the overburden was first time pointed out and quantified by Kristiansen, Barkved et al. (2005) for Valhall. The rather small total stress changes resulted in mud losses across faults and wellbore stability problems in high angle wells that had been drilled with higher angles and same mud weight earlier in field life. Kristiansen and Flatebo (2009) present how one can use the output from the full field geomechanics model in well planning to reduce the risk and cost of drilling wells into the heavily compacted and subsiding Valhall field. **Fig. 24.14** is shown an example of the use of the geomechanics model output in well planning. **Fig. 24.15** is shown how synthetic seismic timeshifts generated from the geomechanics model output can be compared to the observed seismic timeshifts to check if the "map is in line with the terrain".

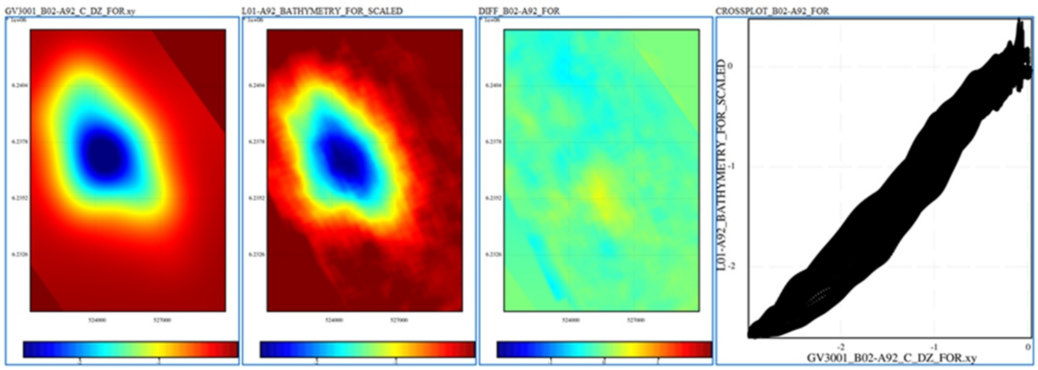

Figure 24.13: Predicted vertical displacement at seafloor from geomechanics model (left), measured vertical displacement from 4D seismic data (second from left), difference map between the two previous maps (third from left) and a crossplot of the data (right). Courtesy of Aker BP.

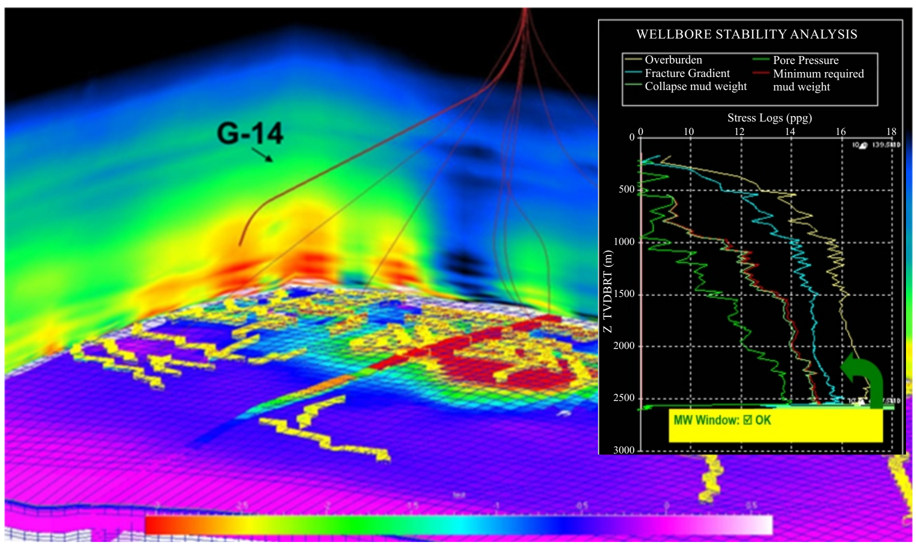

Figure 24.14: A cut of a shear stress cube in the overburden of Valhall from the geomechanics model. The bottom surface is the top of the reservoir model. The pore pressure, stress and wellbore stability plot insert shows the modified trajectory with lower inclination through the red high shear stress that creates a drilling window between the borehole collapse and the minimum stress curves. Courtesy of Aker BP.

24.7 Coupled modeling

The flow models used in the oil and gas industry is approximating pore volume deformation due to injection and production using a constant rock compressibility number or a pore volume multiplier look-up table. Permeability changes are linked to pore volume changes as discussed in earlier sections of this book and can be used in the pore volume multiplier look-up tables.

The weakness in the current reservoir simulation approach in the industry is that the pore volume modifiers and permeability modifiers can only be linked to the pore pressure in the reservoir flow model. This has been pointed out since the early 1990s, (Heffer, Last et al. 1992; Koutsabeloulis, Heffer et al. 1994). The alternative has been to either couple the flow models to the geomechanics models in different ways or work on a model where all the equations are solved simultaneously. Both approaches are quite computer intensive so the majority of work in this area has been more of a research type than day to day use by the reservoir engineers in the oil companies.

Chalk reservoirs should be a type of reservoir where this technology should have the largest impact because of the high compressibility of the matrix rock combined with the relative low matrix permeability.

Important work on the chalk reservoirs is the work by Gutierrez and Lewis (1998), which used an approach where all the equations were solved simultaneously. They studied a simplistic geometry of the Ekofisk field with a few wells in the center of the field. One observation is a feature that cannot be observed in standard

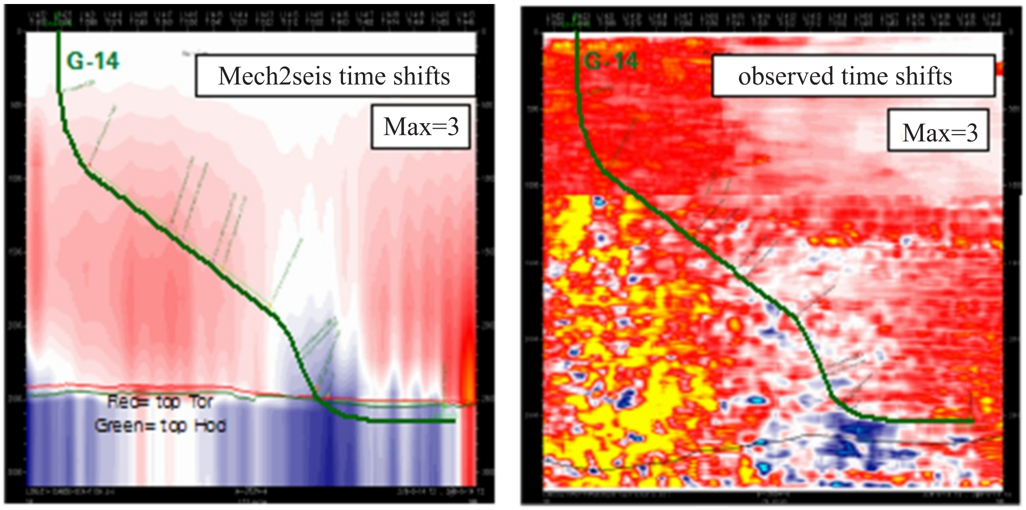

Synthetic timeshifts from Geomechanics model Observed imeshift from seismic

Figure 24.15: Comparion of well trajectory in fig. 24.14 above in synthetic generated seismic timeshifts (left) from the geomechanics model and compared to observed seismic timeshifts (right), used to compare the "map with the terrain". Courtesy of Aker BP.

reservoir fluid flow modeling, – an increase in the pore pressure in the flank of the field as the field is produced from the crest. This is due to poroelastic behavior, a so- called Mandl-Cryer effect (Cryer 1963) or sometimes also referred to as a Noordbergum effect (Verruijt 1969), both from the geotechnical literature.

Similar observations were also made in an unpublished study using the same simulation software a bit earlier on a more detailed model of a chalk field so that the results that can be directly compared to the reservoir flow model for the Valhall field, see **Fig. 24.16** from work by Ghafouri and Lewis (1997). In this work one can also see significant impact on the pore pressure distribution in the field when solving the full set of equations for multiphase flow and deformation in porous media. The stress arching is more pronounced over the short axis of the field.

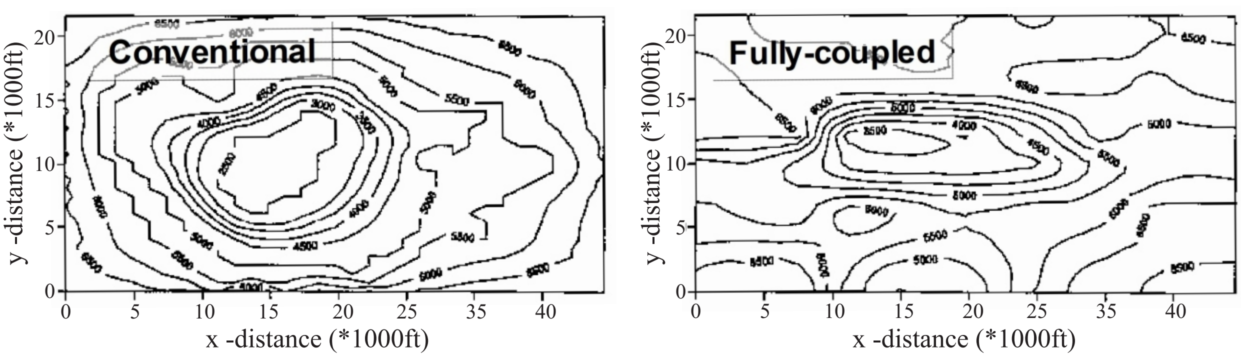

Figure 24.16: Pore pressure distribution in a Tor layer at Valhall comparing a uncoupled traditional reservoir simulator (left) with a fully coupled fluid flow and deformation solution (right) from an unpublished study by Ghafouri and Lewis (1997).

These observations resulted in numerous studies on coupled modeling for chalk fields where one looked at various coupling strategies and simplifications to provide these more physical correct models for reservoir engineers (Chin and Thomas 1999; Chin, Thomas et al. 2002; Thomas, Chin et al. 2003; Samier, Onaisi et al. 2008; Pettersen and Kristiansen 2009). However, the models are still not used as a default model for the chalk fields, most likely due to the added complexity and the increased computational cost.

24.8 Microseismic

Microseismic monitoring was reported from the Ekofisk and Valhall fields in the late 1990s by Maxwell, Young et al. (1998) and Maxwell (2000). Several hundreds of microseismic events where recorded around the monitoring wells in both the reservoir and the overburden. The induced microseismic events are typically in the range -3 to 2 on the Richter scale. The microseismic events are a result of changing the stresses in the subsurface in response to production or injection in the chalk reservoirs. The stress changes are exceeding the shear failure strength of the faults and fractures and the movement of them is generating energy that can be detected by the geophones. The process is the same as for large natural earthquakes.

Kristiansen, Barkved et al. (2000) link the microseismicity to casing deformation as discussed in an earlier section above. The data from the Valhall overburden indicate slip of typically 2–3 mm over a fault surface of 10 m^2 in a typical induced event like this. This is typical numbers for a -2 event on the Richter scale. To fail a standard casing accumulated slip on a single fault must be in the order of 100 to 200 mm.

Modeling of microseismicity has been presented by Kristiansen, Barkved et al. (2005); Zhang, Koutsabeloulis et al. (2011); Angus, Dutko et al. (2015). The geomechanics models can be used to estimate the energy released from the re-activation event simulated by the model, see example from Angus, Dutko et al. (2015) in **Fig. 24.17**. There is more potential to use microseismic data combined with geomechanics modeling. It is believed that some of this technology will be developed for the oil and gas shales in the US, since there is currently a high interest in integrating these data sources in that part of the industry to optimize well stimulation.

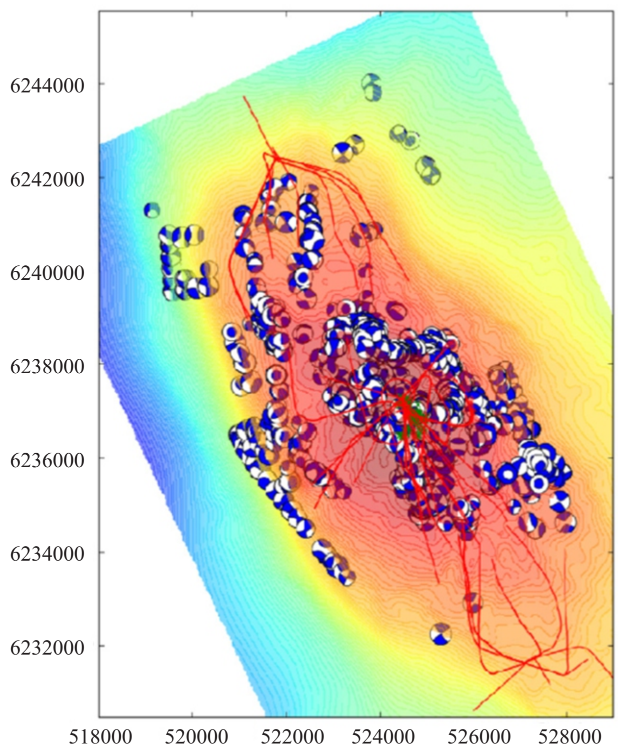

Figure 24.17: Predicted shear-type microseismic events (focal solutions) for 25 years of production at Valhall. The size of the focal sphere indicates the relative magnitude of the predicted event. The contour map is depicting the anticline structure. The green symbols are the location of the observed microseismic events in a monitored area and the red lines represent the locations of the wellbore trajectories (Angus, Dutko et al. 2015).

24.9 Summary

This chapter illustrates some numerical geomechanical-modeling applied to chalk fields. The applications are based on the understanding of chalk deformation as developed in the laboratory and discussed in detail in Chapter 6 Rock Mechanics in this book. This laboratory understanding is then used to develop a constitutive model for numerical implementation as discussed in Chapter 14 Geomechanical Modeling. Based on the work described in these two chapters one can address problems and answer questions for the management of the chalk fields as described in this chapter.

References

Andersen, M.A., 1995. *Petroleum Research in North Sea Chalk.* RF-Rogaland Research. Joint Chalk Research Program Phase IV.

Angus, D., Dutko, M. et al., 2015. Integrated hydro-mechanical and seismic modelling of the Valhall reservoir: A case study of predicting subsidence, AVOA and microseismicity. *Geomechanics for Energy and the Environment*, **2**: 32–44. URL `http://dx.doi.org/https://doi.org/10.1016/j.gete.2015.05.002`.

Barkved, O., Buer, K. et al., 2003. 4D Seismic Response of Primary Production and Waste Injection at the Valhall Field. 02 June. URL `http://www.earthdoc.org/publication/publicationdetails/?publication=3102`.

Bratli, R.K. and Risnes, R., 1981. Stability and Failure of Sand Arches. *Society of Petroleum Engineers Journal*, **21** (02): 236–248. 1. April. URL `http://dx.doi.org/10.2118/8427-pa`.

Chin, L. and Thomas, L., 1999. Fully Coupled Analysis of Improved Oil Recovery by Reservoir Compaction. *Society of Petroleum Engineers*. SPE-56753-MS. 3–6 October. URL `http://dx.doi.org/10.2118/56753-MS`.

Chin, L.Y., Thomas, L.K. et al., 2002. Iterative Coupled Analysis of Geomechanics and Fluid Flow for Rock Compaction in Reservoir Simulation. *Oil & Gas Science and Technology - Rev. IFP*, **57** (5): 485–497. URL `http://dx.doi.org/10.2516/ogst:2002032`.

Crook, A.L., Yu, J.G. et al., 2008. Computational Modelling of the Rate Dependent Deformation and Liquefaction of Chalk. *American Rock Mechanics Association*. Paper presented at The 42nd U.S. Rock Mechanics Symposium (USRMS), San Francisco, California. 29 June – 2 July. URL `https://www.onepetro.org/conference-paper/ARMA-08-176`.

Cryer, C.W., 1963. A COMPARISON OF THE THREE-DIMENSIONAL CONSOLIDATION THEORIES OF BIOT AND TERZAGHI. *The Quarterly Journal of Mechanics and Applied Mathematics*, **16** (4): 401–412. URL `http://dx.doi.org/10.1093/qjmam/16.4.401`.

Flatebø, R., 2005. *Stability and Flow of Chalk Near Production Wells*. Ph.D. thesis, Department of Petroleum Engineering, University of Stavanger, Norway.

Furui, K., Fuh, G.F. et al., 2009. A Comprehensive Modeling Analysis of Borehole Stability and Casing Deformation for Inclined/Horizontal Wells Completed in a Highly Compacting Chalk Formation. January. URL `http://dx.doi.org/10.2118/123651-ms`.

Gauer, P.R., Sylte, J.E., and Nagel, N.B., 2002. Ekofisk Field Well Log Decompaction. In *SPE/ISRM Rock Mechanics Conference*, 11. Society of Petroleum Engineers, Irving, Texas. URL `http://dx.doi.org/https://doi.org/10.2118/78177-MS`.

Ghafouri, H.R. and Lewis, R.W., 1997. Fully-Coupled Analysis of Production and Subsidence Valhall Oil Field, Norway, Phase III. techreport, report to Amoco Norway.

Guilbot, J. and Smith, B., 2002. Subsidence and compaction observations from 4-D seismic data. *The Leading Edge*.

Gutierrez, M. and Lewis, R.W., 1998. The Role of Geomechanics in Reservoir Simulation. Paper SPE-47392-MS presened at SPE/ISRM Rock Mechanics in Petroleum Engineering, Trondheim, Norway. 8–10 July. URL `http://dx.doi.org/10.2118/47392-MS`.

Heffer, K.J., Last, N.C. et al., 1992. The influence of natural fractures, faults and earth stresses on reservoir performance - geomechanical analysis by numerical modelling., In *North Sea oil and gas reservoirs-III*, eds., J.O. Aasen, E. Berg, A.T. Buller, O. Hjelmeland, R.M. Holt, J. Kleppa, and O. Torsæter, , Chap. 11, 201–211. Springer. ISBN 9789401043878.

Herwanger, J. and Koutsabeloulis, N., 2011. *Seismic geomechanics: How to build and calibrate geomechanical models using 3D and 4D seismic data. (EET 5)*. European Association of Geoscientists and Engineers. Seismic geomechanics: How to build and calibrate geomechanical models using 3D and 4D seismic data.

Jørgensen, O., 2002. Using flow induced stresses for steering of injection fracturesUsing flow induced stresses for steering of injection fractures. In *SPE/ISRM Rock Mechanics Conference*. Society of Petroleum Engineers. Paper SPE 78220 presented at SPE/ISRM Rock Mechanics Conference, Irving, Texas. 20–23 October. URL `http://dx.doi.org/10.2118/78220-MS`.

Kaiser, T., Roggensack, W.D., and Slack, M., 1996. Casing Damage & Well Optimization, Ekofisk & Valhall Overburden, Phase 1 & 2. resreport, Center for Frontier Engineering Research, Edmonton (CFER):. Report to Amoco Norway and Phillips Petroleum Company Norway.

Koutsabeloulis, N., Heffer, K. et al., 1994. Numerical geomechanics in reservoir engineering. *Computer Methods and Advances in Geomechanics*, **3**: 2097–2104. May.

Kristiansen, T., 1996. A Review of Completion Techniques and the Impact of Geomechanical Processes on their Performance in the Valhall Field. In *Fifth North Sea Chalk Symposium*.

Kristiansen, T.G., Barkved, O.I., and Pattillo, P., 2000. Use of passive seismic monitoring in well and casing design in the compacting and subsiding Valhall field, North Sea. In *SPE European Petroleum Conference*. Society of Petroleum Engineers.

Kristiansen, T.G., Barkved, O.I. et al., 2005. Production-induced deformations outside the reservoir and their impact on 4D seisimic. In *International Petroleum Technology Conference*. International Petroleum Technology Conference, International Petroleum Technology Conference. URL `http://dx.doi.org/10.2523/IPTC-10818-MS`.

Kristiansen, T.G. and Flatebo, R.E., 2009. 60 Days Ahead of Schedule–Reducing Drilling Risk at Valhall Using Computational Geomechanics. In *SPE/IADC Drilling Conference and Exhibition*. Society of Petroleum Engineers, Amsterdam, The Netherlands. SPE-119509-MS. 17–19 March. URL `http://dx.doi.org/10.2118/119509-MS`.

Kristiansen, T.G. and Meling, S., 1996. A production parameter analysis of chalk influxes in the Valhall field. In *Fifth North Sea Chalk Symposium*.

Kristiansen, T.G. and Plischke, B., 2010. History Matched Full Field Geomechanics Model of the Valhall Field Including Water Weakening and Re-pressurisation. Paper SPE-131505-MS presented at SPE EUROPEC/EAGE Annual Conference and Exhibition, Barcelona, Spain. 14–17 June. URL `http://dx.doi.org/10.2118/131505-MS`.

Maxwell, S., Young, R. et al., 1998. Microseismic logging of the Ekofisk reservoir. In *SPE/ISRM Rock Mechanics in Petroleum Engineering*. Society of Petroleum Engineers, Society of Petroleum Engineers. URL `http://dx.doi.org/10.2118/47276-ms`.

Maxwell, S.C., 2000. Comparison of Production Induced Microseismicity from Valhall and Ekofisk. *EAGE expanded abstracts*, **62**.

Nagel, N.B., 2001. Compaction and subsidence issues within the petroleum industry: From wilmington to ekofisk and beyond. *Physics and Chemistry of the Earth, Part A: Solid Earth and Geodesy*, **26** (1–2): 3–14. URL `http://dx.doi.org/10.1016/S1464-1895(01)00015-1`.

Papamichos, E., Berntsen, A.N. et al., 2012. Solids Production In Chalk. Janyary. URL `https://www.onepetro.org/conference-paper/ARMA-2012-479`.

Pattillo, P.D. and Kristiansen, T.G., 2002. Analysis of horizontal casing integrity in the Valhall field. In *SPE/ISRM Rock Mechanics Conference*. Society of Petroleum Engineers, Society of Petroleum Engineers. URL `http://dx.doi.org/10.2118/78204-MS`.

Pattillo, P.D., Moschovidis, Z.A., and Lal, M., 1995. An evaluation of concentric casing for nonuniform load applications. *SPE Drilling & Completion*, **10** (03): 186–192. September. URL `http://dx.doi.org/10.2118/29232-PA`.

Pettersen, Ø. and Kristiansen, T.G., 2009. Improved Compaction Modeling in Reservoir Simulation and Coupled Rock Mechanics/Flow Simulation, With Examples From the Valhall Field. *SPE Reservoir Evaluation & Engineering*, **12** (02): 329–340. URL `http://dx.doi.org/10.2118/113003-PA`.

Plischke, B. and Pisarsky, L., 1992. Chalk Fines Production, Final Report, Chalk Research Programme, Phase III, Project &A. resreport.

Risnes, R., 1990. Solids Production in Different Fields, Chalk Research Program - Phase II, Project 2 - Chalk Instability,. Tech. rep., .

Risnes, R. and Horsrud, P., 1985. Well Stability in Chalk Reservoir, Chalk Research Program, Project III. resreport, . April.

Samier, P., Onaisi, A. et al., 2008. A Practical Iterative Scheme for Coupling Geomechanics With Reservoir Simulation. *SPE Reservoir Evaluation & Engineering*, **11** (05): 892–901. URL `http://dx.doi.org/10.2118/107077-MS`.

Schwall, G.H. and Denney, C.A., 1994. Subsidence induced casing deformation mechanisms in the Ekofisk field. In *Rock Mechanics in Petroleum Engineering*, 9. Society of Petroleum Engineers, Delft, Netherlands. URL `http://dx.doi.org/10.2118/28091-MS`.

Thomas, L.K., Chin, L.Y. et al., 2003. Integrating geomechanics in full-field 3-D reservoir simulation–modeling techniques and field applications. In *Paper SPE 77724, presented at the SPE Applied Technology Workshop*, vol. 31.

Verruijt, A., 1969. Elastic storage of aquifers, In *Flow Through Porous Media*, ed., R.D. Wiest, , 331–376. Academic Press, New York.

Zhang, X., Koutsabeloulis, N. et al., 2011. Modelling of depletion-induced microseismic events by coupled reservoir simulation: application to Valhall field. Paper SPE-143378-MS presented at SPE EUROPEC/EAGE Annual Conference and Exhibition, Vienna, Austria. 23–26 May. URL `http://dx.doi.org/10.2118/143378-MS`.

Part IV

Field Histories

Chapter 25

Field data

25.1 Ekofisk

Field Name	**Ekofisk**
License holders %	Total (39.896%) ConocoPhillips (35.112%) Eni (12.388%) Statoil (7.604%) Petoro (5.0%)
Location Map (Enclosure)	See below
# Platform installations	5 wellhead platforms, 1 SS template, process platform, quarter
Oil Export route	Pipeline to Teesside, UK
Gas export route	Pipeline to Emden Plant, Germany
Reservoir Pressure at Datum - initial and current (psia)	Initial: 7100 psia (@10400 tvdss, current: 5840 psia
Initial Reservoir Temperature (°C)	130 C
Reservoir Depth Range (m ss)	2896 mss Top Ekofisk Fm - 3307 mss FWL in Tor Fm.
Stratigraphic units in production	Ekofisk Fm (Danian) & Tor Fm (Maastrichtian)
Stratigraphic units under water injection	Ekofisk Fm (Danian) & Tor Fm (Maastrichtian)
Initial Porosity range (%)	25–45%
S_{wi} range (%)	5–25%
Initial Matrix permeability range (md)	1–10 md
Initial Effective permeability range (md)	1–220 md
Oil API grade	39 Deg
Initial Solution GOR range (Scf/Stb)	1520
Initial Bubble point pressure range (psia)	5600–5800
CO2, H2S contents (mole%)	CO_2 0.93–1.83%, H_2S 0%
Production start-up	1971
Waterflood start-up	1987
Current drive mechanisms	Water Injection and reservoir compaction
# of active production wells by 2011 (Of which horizontal, vertical)	101 (57, 44)
Reservoir completion types used in active production wells	Comingled
Stimulation techniques used in active production wells	Acid Fracturing
# of active water injection wells by 2011 (Of which horizontal, vertical)	37 (9, 28)
Reservoir completion types used in active injection wells	Comingled
Stimulation techniques used in active injection wells	Acid Fracturing

Near term completion types for new producers	Comingled or Intelligent well system
Near term stimulation techniques for new producers	Acid Fracturing
Near term completion types for new injectors	Comingled or Intelligent well system
Near term stimulation techniques for new injectors	Acid Fracturing
Current field Oil Production rate (2011) (Stb/d)	120,000
Current field Water Production rate (2011 (bbl/d)	215,000–220,000
Current field Gross Liquid Production rate (bbl/d)	340,000
Current field Water Injection rate & max WH pressure (bbl/d & psia)	400,000 bbl/day, 4200 psi WHP
Produced Water Re-injection & max WH pressure (bbl/d & psia)	N/A
Current Gas production rate (MMscf/d)	162
Artifical lift methods, # of active installations per method (2011)	Gas lift, about 50% of wells
Key constraints on production	Water handling
Key constraints on water injection	Reservoir backpressure
Waterflood Surveillance	
No. of 4D seismic surveys for waterflood monitoring. Possible to separate Sw changes from other effects?	5 streamline surveys, 3 LOFS surveys
Is cased hole logging routinely used to monitor waterflood development? Typical logging frequency per well.	1 well logged every second year.
Type of open hole logs run to estimate water saturation in flooded intervals. Do they give reliable results?	Resistivity. Room for improvement.
No. of wells successfully cored behind water front	5
Tracer in injection water used in all injectors? Normal frequency of tracer pulses per well.	Tracer in 12 injectors. 1 puls per well.
Analysis of produced water samples for ions, tracers, etc.	Yes
Is interference testing used on regular basis?	No
Typical particle content in injection water. Is injectivity observed to decrease with time?	Low. Decreasing injectivity with increased reservoir pressure.
Monitoring techniques for fracture growth in injectors	None
No. of dedicated observation/monitoring wells for waterflood. Logging types and frequency?	1 well. Pulsed Neutron every second year.
No. of wells used for compaction monitoring. Logging frequency?	1 well logged every second year. 5 wells logged irregularly due to restrictions or P&A.
Use of advanced logging for waterflood monitoring (DTS, EMS, passive seismic,..)	DTS planned.
Issues with current waterflood surveillance tools/technologies	Estimate S_w in flooded sections, 4D interpretation, WBM for NMR
Background papers for further reading (max. 3)	Avail. on: `http://www.onepetro.org/mslib/app/newSearch.do`

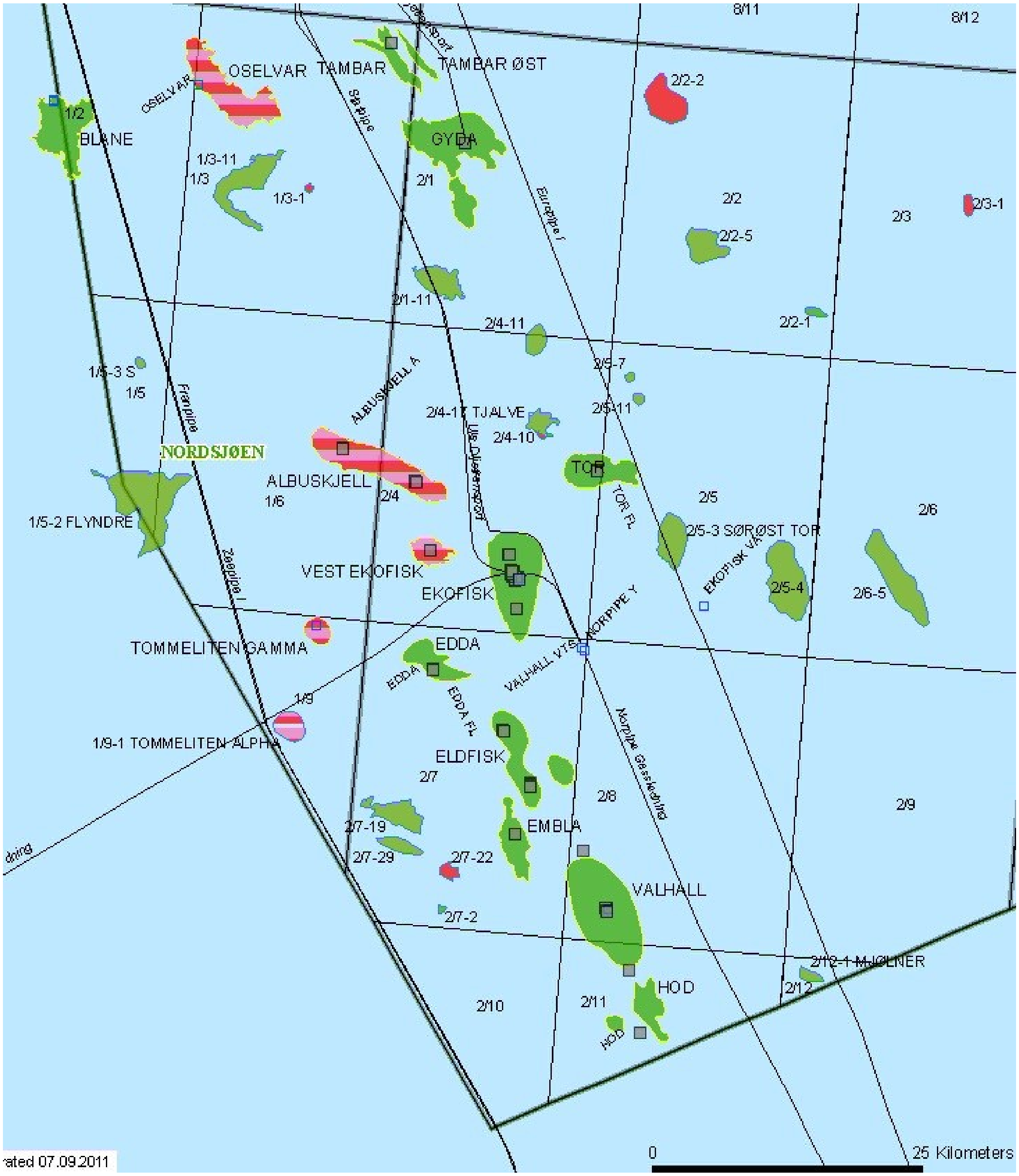

Figure 25.1: Ekofisk Field Location Map

25.2 Valhall

Field Name	**Valhall**
License holders %	BP (35.95); Hess (64.05)
Location Map (Enclosure)	Enclosed
# Platform installations	5 wellhead platforms; process platform, quarter
Oil Export route	Pipeline via Ekofisk facility to Teesside, UK
Gas export route	Pipeline to Emden Plant, Germany
Reservoir Pressure at Datum – initial and current (psia)	Initial: 6500 psia (@2500m TVDss); current: 2500–6000 psia
Initial Reservoir Temperature (°C)	93
Reservoir Depth Range (m ss)	2400–2700
Stratigraphic units in production	Tor & Hod formations
Stratigraphic units under water injection	Tor formation
Initial Porosity range (%)	Tor fm.: 30->50% (Crest) & 25–45% (flank); Hod fm: 25–43%
S_{wi} range (%)	Tor: 0-5% (crest) & 10–40 (flank); Hod: 20–60%
Initial Matrix permeability range (md)	Tor fm.: 1–20 mD; Hod fm: 0.1–7 mD
Initial Effective permeability range (md)	1–2000 mD (Tor fm)
Oil API grade	36
Initial Solution GOR range (Scf/Stb)	550–1700
Initial Bubble point pressure range (psia)	2500–4500
CO_2, H_2S contents (mole%)	0.3; 0
Production start-up	Oct. 1982
Waterflood start-up	Feb. 2006
Current drive mechanisms	Reservoir compaction, fluid expansion & in some areas waterflooding
# of active production wells by 2011 (Of which horizontal, vertical)	42 (40, 2)
Reservoir completion types used in active production wells	Cased, cemented and perforated, cased w/ sliding sleeves and external casing packers, semi-openhole (uncemented and preperforated)
Stimulation techniques used in active production wells	Proppant fracturing, acid fracturing (selective and limited entry bullhead), unstimulated
# of active water injection wells by 2011 (Of which horizontal, vertical)	5 (5, 0)
Reservoir completion types used in active injection wells	Cased, cemented and perforated, cased w/ sliding sleeves and external casing packers
Stimulation techniques used in active injection wells	Unstimulated, Acid fracturing (selective and limited entry bullhead).
Near term completion types for new producers	Cased, cemented and perforated, cased w/ sliding sleeves and external casing packers, semi-openhole (uncemented and preperforated), Fishbone completion
Near term stimulation techniques for new producers	Proppant fracturing, acid fracturing (selective and limited entry bullhead), unstimulated, Fishbones
Near term completion types for new injectors	Cased w/ sliding sleeves and external casing packers
Near term stimulation techniques for new injectors	Acid fracturing - selective treatment
Current field Oil Production rate (2011) (Stb/d)	45000
Current field Water Production rate (2011 (bbl/d)	10000

Current field Gross Liquid Production rate (bbl/d)	55000
Current field Water Injection rate & max WH pressure (bbl/d & psia)	40000; Injection rate limited by downhole pressure limits, injection header pressure is 4200 psi
Produced Water Re-injection & max WH pressure (bbl/d & psia)	No PWRI
Current Gas production rate (MMscf/d)	40
Artifical lift methods, # of active installations per method (2011)	Gaslift, 4
Key constraints on production	Well productivity, stability and integrity. Artificial Lifting problems. Scale management (future constraint).
Key constraints on water injection	Well injectivity, ability to inject above fracture pressure, max BHP constraints for integrity, WI plant performance
Waterflood Surveillance	
No. of 4D seismic surveys for waterflood monitoring. Possible to separate Sw changes from other effects?	9 LoFS surveys under waterflood (LoFS6 - LoFS14). Currently not possible to separate for Valhall
Is cased hole logging routinely used to monitor waterflood development? Typical logging frequency per well.	Yes. Saturation logging across Tor fm in 4 Hod formation producers. Saturation & compaction monitoring logging in an observation well. Frequency depends on access and expected water movements.
Type of open hole logs run to estimate water saturation in flooded intervals. Do they give reliable results?	Resistivity combined with density logs. Not much experience on Valhall.
No. of wells successfully cored behind water front	Currently none, but one failed attempt.
Tracer in injection water used in all injectors? Normal frequency of tracer pulses per well.	Yes. 1st tracer pulse injected shortly after injection start-up. Have plans for doing a 2nd tracer campaign in several injectors
Analysis of produced water samples for ions, tracers, etc.	Offshore analysis for Sr, Ba, SO_4, Mg, Cl once/week for selected wells. 11-ion analysis once a year. Sampling for tracer analysis is typically 1/month.
Is interference testing used on regular basis?	Standard interference testing is not used due to slow response times
Typical particle content in injection water. Is injectivity observed to decrease with time?	Filtering of the injected water down to 50 micron. Injectivity decrease observed in injectors.
Monitoring techniques for fracture growth in injectors	Falloff PTA
No. of dedicated observation/monitoring wells for waterflood. Logging types and frequency?	3 wells are used for BH pressure monitoring. One of these is used for compaction and saturation monitoring. Frequency depend on access.
No. of wells used for compaction monitoring. Logging frequency?	Currently one. Logging frequency depends on access.
Use of advanced logging for waterflood monitoring (DTS, EMS, passive seismic,..)	Permanent geophones installed in 1 injection well.
Issues with current waterflood surveillance tools/technologies	4D seismic: Techniques to separate changes in water saturation from other fluid and rock effects. Imaging through overburden gas.
Background papers for further reading (max. 3)	SPE83957, SPE108687, IPTC11276; Avail. on: `http://www.onepetro.org/mslib/app/newSearch.do`

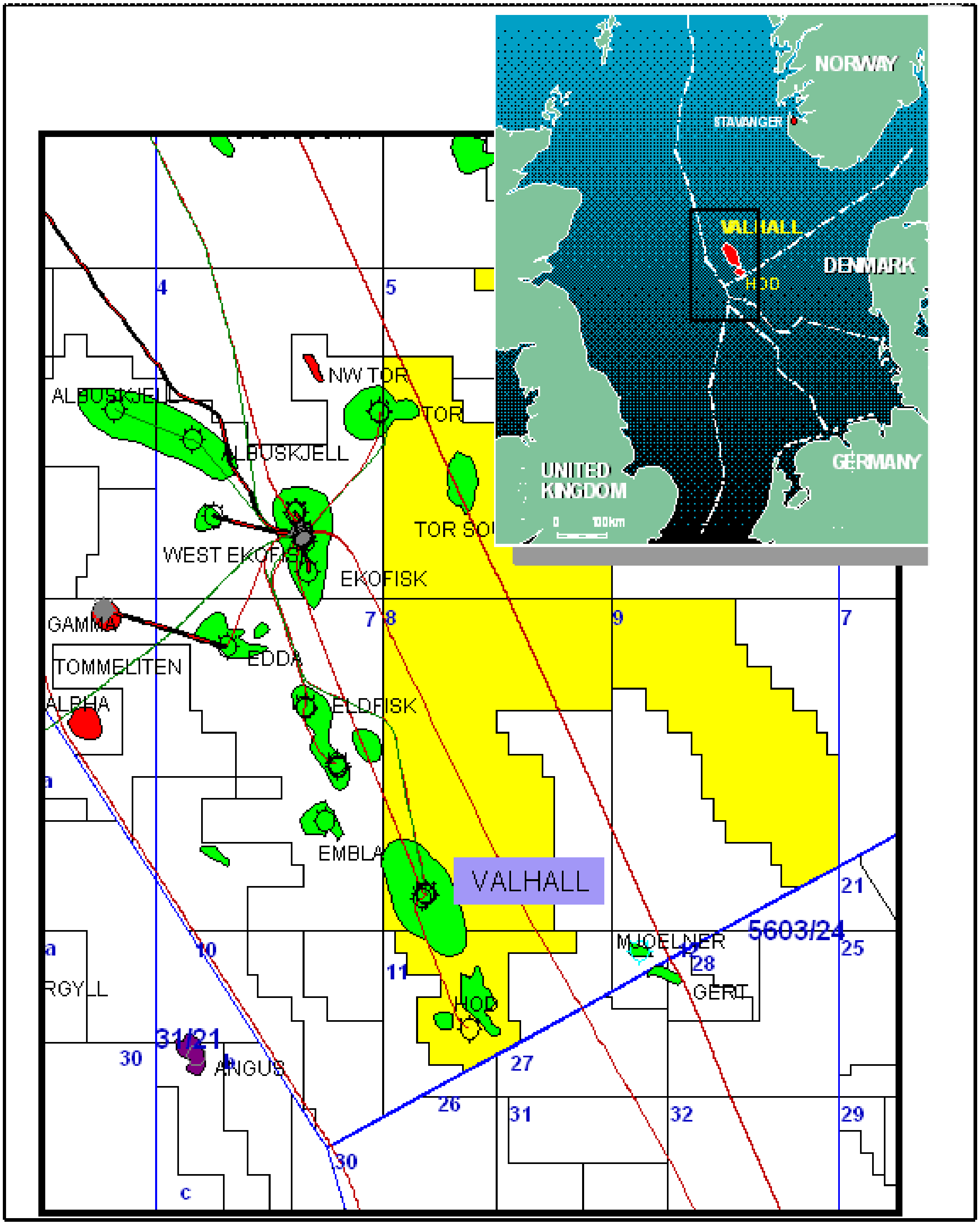

Figure 25.2: Valhall Field Location Map

25.3 Eldfisk

Field Name	**Eldfisk**
License holders %	Total (39.896%) ConocoPhillips (35.112%) Eni (12.388%) Statoil (7.604%) Petoro (5.0%)
Location Map (Enclosure)	See below
# Platform installations	2 WHP, 1 separation, 1 gas treatment
Oil Export route	Pipeline via Ekofisk facility to Teesside, UK
Gas export route	Pipeline to Emden Plant, Germany
Reservoir Pressure at Datum - initial and current (psia)	"Initial: 6840 psia @9400ft TVDss, current: 4600 psia"
Initial Reservoir Temperature (°C)	118°C (245°F)
Reservoir Depth Range (m ss)	2650–2950m tvdss
Stratigraphic units in production	Ekofisk Fm (Danian), Tor Fm (Maastrichtian) & Hod Fm (Cenomanian-Campanian)
Stratigraphic units under water injection	Ekofisk Fm (Danian), Tor Fm (Maastrichtian),
Initial Porosity range (%)	15–45%
S_{wi} range (%)	5–20%
Initial Matrix permeability range (md)	0.1–10 mD
Initial Effective permeability range (md)	up to 30 mD
Oil API grade	36–39° API
Initial Solution GOR range (Scf/Stb)	1490 (1450–2390)
Initial Bubble point pressure range (psia)	Alpha 4800 psia, Bravo 5600 psia
CO_2, H_2S contents (mole%)	
Production start-up	1979
Waterflood start-up	2000
Current drive mechanisms	Water Injection and reservoir compaction
# of active production wells by 2011 (Of which horizontal, vertical)	34 (25, 9)
Reservoir completion types used in active production wells	Commingled
Stimulation techniques used in active production wells	Acid fracturing
# of active water injection wells by 2011 (Of which horizontal, vertical)	9 (9, 0)
Reservoir completion types used in active injection wells	Commingled
Stimulation techniques used in active injection wells	Acid fracturing
Near term completion types for new producers	Commingled or intelligent well system
Near term stimulation techniques for new producers	Acid fracturing
Near term completion types for new injectors	Commingled or intelligent well system
Near term stimulation techniques for new injectors	Acid fracturing
Current field Oil Production rate (2011) (Stb/d)	50,000
Current field Water Production rate (2011 (bbl/d)	Bravo: 6500—7000 bwpd, Alpha: 25,000 bwpd
Current field Gross Liquid Production rate (bbl/d)	82,000 bwpd
Current field Water Injection rate & max WH pressure (bbl/d & psia)	105,000 bbl/day, 3800 psi WHP
Produced Water Re-injection & max WH pressure (bbl/d & psia)	N/A
Current Gas production rate (MMscf/d)	74

Artifical lift methods, # of active installations per method (2011)	Gas lift, about 50% of wells
Key constraints on production	Water handling
Key constraints on water injection	Reservoir backpressure
Waterflood Surveillance	
No. of 4D seismic surveys for waterflood monitoring. Possible to separate Sw changes from other effects?	2 streamline surveys
Is cased hole logging routinely used to monitor waterflood development? Typical logging frequency per well.	No
Type of open hole logs run to estimate water saturation in flooded intervals. Do they give reliable results?	Resistivity. Room for improvement.
No. of wells successfully cored behind water front	3
Tracer in injection water used in all injectors? Normal frequency of tracer pulses per well.	Tracer in 10 injectors. 1 puls per well.
Analysis of produced water samples for ions, tracers, etc.	Yes
Is interference testing used on regular basis?	No
Typical particle content in injection water. Is injectivity observed to decrease with time?	Low. Decreasing injectivity with increased reservoir pressure.
Monitoring techniques for fracture growth in injectors	None
No. of dedicated observation/monitoring wells for waterflood. Logging types and frequency?	0
No. of wells used for compaction monitoring. Logging frequency?	No compaction monitoring
Use of advanced logging for waterflood monitoring (DTS, EMS, passive seismic,..)	DTS planned for several injectors and producers.
Issues with current waterflood surveillance tools/technologies	Estimate S_w in flooded sections, 4D interpretation, WBA for NMR
Background papers for further reading (max. 3)	Avail. on: `http://www.onepetro.org/mslib/app/newSearch.do`

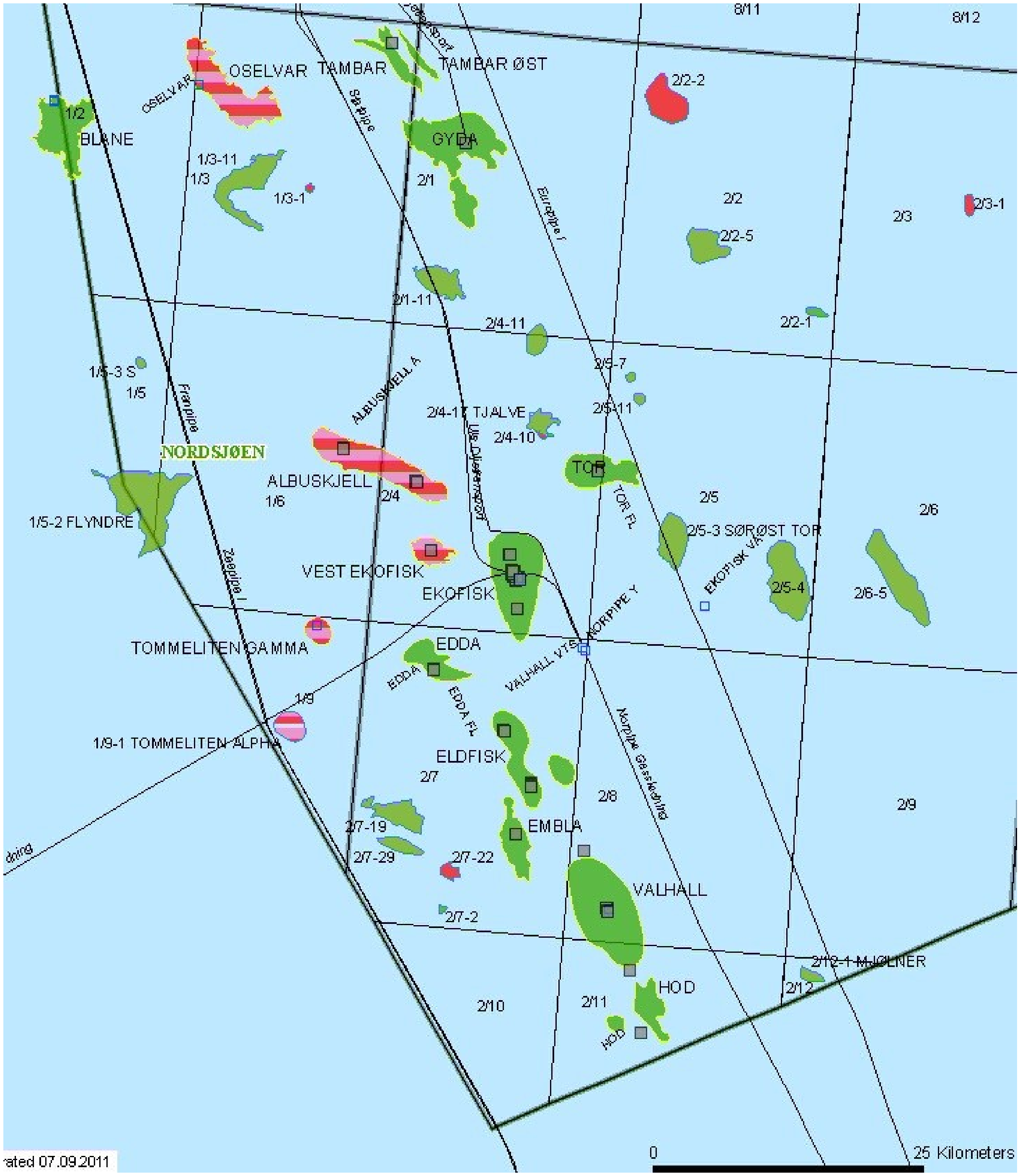

Figure 25.3: Eldfisk Field Location Map

25.4 Tor

Field Name	**Tor**
License holders %	COP 30.7%, Total 48.2%, ENI 10.8%, Statoil 6%, Petoro 3.7%
Location Map (Enclosure)	See below
# Platform installations	1 wellhead platform
Oil Export route	Pipeline via Ekofisk facility to Teesside, UK
Gas export route	Pipeline to Emden Plant, Germany
Reservoir Pressure at Datum – initial and current (psia)	Initial 7100 psi (10400ft) , current 3000-4500 psi
Initial Reservoir Temperature (°C)	138°C
Reservoir Depth Range (m ss)	2900–3300
Stratigraphic units in production	Ekofisk Fm (Danian) & Tor Fm (Maastrichtian)
Stratigraphic units under water injection	Ekofisk Fm (Danian) & Tor Fm (Maastrichtian)
Initial Porosity range (%)	Ekofisk fm 15–35%, Tor fm 25–45%
S_{wi} range (%)	Ekofisk: 25–55 (crest) & 50–70 (flank) & Tor: 10-30 (crest) & 20–60 (flank)
Initial Matrix permeability range (md)	0.1–1 md
Initial Effective permeability range (md)	Up to 200 md
Oil API grade	42
Initial Solution GOR range (Scf/Stb)	1000–1500
Initial Bubble point pressure range (psia)	3000–5000
CO_2, H_2S contents (mole%)	
Production start-up	1978
Waterflood start-up	1992
Current drive mechanisms	Aquifer influx. Water injection.
# of active production wells by 2011 (Of which horizontal, vertical)	1 horizontal, 4 vertical
Reservoir completion types used in active production wells	Cased, cemented and perforated.
Stimulation techniques used in active production wells	Acid fracturing
# of active water injection wells by 2011 (Of which horizontal, vertical)	One vertical injector
Reservoir completion types used in active injection wells	Cased, cemented and perforated.
Stimulation techniques used in active injection wells	-
Near term completion types for new producers	-
Near term stimulation techniques for new producers	-
Near term completion types for new injectors	-
Near term stimulation techniques for new injectors	-
Current field Oil Production rate (2011) (Stb/d)	4000
Current field Water Production rate (2011 (bbl/d)	6500
Current field Gross Liquid Production rate (bbl/d)	10 500
Current field Water Injection rate & max WH pressure (bbl/d & psia)	3000 & 250
Produced Water Re-injection & max WH pressure (bbl/d & psia)	-
Current Gas production rate (MMscf/d)	1.6

Artifical lift methods, # of active installations per method (2011)	Gaslift (5 wells)
Key constraints on production	Well productivity, stability and integrity. Artificial Lifting (gaslift) depends on amount of gas production.
Key constraints on water injection	Max 250 psi on injection pump pressure
Waterflood Surveillance	
No. of 4D seismic surveys for waterflood monitoring. Possible to separate Sw changes from other effects?	None.
Is cased hole logging routinely used to monitor waterflood development? Typical logging frequency per well.	No.
Type of open hole logs run to estimate water saturation in flooded intervals. Do they give reliable results?	Resistivity in new well (E18) pilot hole. However, it may be water swept by formation water or injection water.
No. of wells successfully cored behind water front	1 — E18 pilot hole. Dynamic model suggests behind water flood front but salinity of water suggests the zone may have been swept by aquifer influx.
Tracer in injection water used in all injectors? Normal frequency of tracer pulses per well.	No.
Analysis of produced water samples for ions, tracers, etc.	Yes, chlorides for salinity ppm.
Is interference testing used on regular basis?	No.
Typical particle content in injection water. Is injectivity observed to decrease with time?	No real injection taking place. It is more of a water dump with very little surface pressure applied. Change in injectivity is therefore difficult to measure.
Monitoring techniques for fracture growth in injectors	None.
No. of dedicated observation/monitoring wells for waterflood. Logging types and frequency?	None.
No. of wells used for compaction monitoring. Logging frequency?	None.
Use of advanced logging for waterflood monitoring (DTS, EMS, passive seismic,..)	None.
Issues with current waterflood surveillance tools/technologies	No injected water has been seen at any production well - difficult to interpret results or overall water flood performance.
Background papers for further reading (max. 3)	Avail. on: `http://www.onepetro.org/mslib/app/newSearch.do`

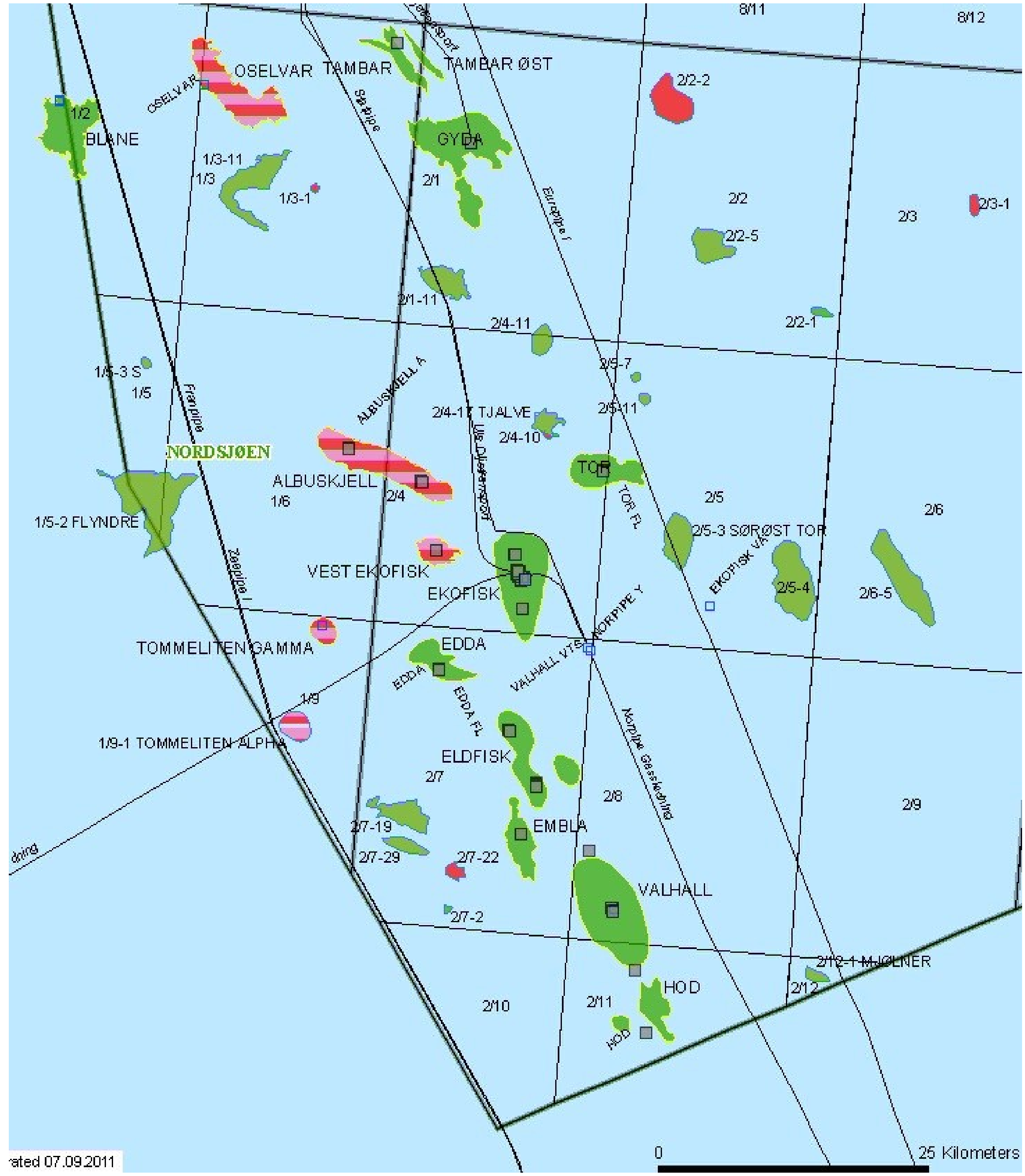

Figure 25.4: Tor Field Location Map

25.5 Dan

Field Name	Dan
License holders %	Current: Maersk (39% and operator), Shell (46%), Chevron (15%)
Location Map (Enclosure)	Enclosed
# Platform installations	7 wellhead platforms, 3 processing
Oil Export route	Pipeline to Gorm E, to shore
Gas export route	Pipeline to Tyra East, to shore
Reservoir Pressure at Datum – initial and current (psia)	Initial: 3815 psi @ datum 1840 m, Current: varying 2000–5000 psi
Initial Reservoir Temperature (°C)	80°C
Reservoir Depth Range (m ss)	1750–2300 m
Stratigraphic units in production	Ekofisk, Tor
Stratigraphic units under water injection	Ekofisk, Tor
Initial Porosity range (%)	Ekofisk: 28–40%, Tor: 25–35%
S_{wi} range (%)	10–100%
Initial Matrix permeability range (md)	Tor: 1–5 mD Ekofisk: 0.5–2.5 mD
Initial Effective permeability range (md)	Tor: 1–5 mD Ekofisk: 0.5–2.5 mD
Oil API grade	30
Initial Solution GOR range (Scf/Stb)	350–635
Initial Bubble point pressure range (psia)	2000–3815
CO_2, H_2S contents (mole%)	CO_2: 0.1, H_2S: 50–500 ppm
Production start-up	1972
Waterflood start-up	1988
Current drive mechanisms	Water injection
# of active production wells by 2011 (Of which horizontal, vertical)	57, all horizontal
Reservoir completion types used in active production wells	Cased, cemented, perforated, isolated with packers and sliding sleeves. Or (slotted) lined (CAJ). Or a mix.
Stimulation techniques used in active production wells	Sand/Acid/water frac, matrix acid, CAJ
# of active water injection wells by 2011 (Of which horizontal, vertical)	50, 18 vertical, 32 horizontal
Reservoir completion types used in active injection wells	Cased, cemented, perforated, isolated with packers and sliding sleeves. Or (slotted) lined (CAJ). Or a mix. 1 "smart" (SCRAMS).
Stimulation techniques used in active injection wells	Sand/Acid/water frac, matrix acid, CAJ
Near term completion types for new producers	Cased, cemented, perforated, isolated with packers and sliding sleeves. Or (slotted) lined (CAJ). Or a mix. Dual lateral. Smart.
Near term stimulation techniques for new producers	Acid frac, matrix acid, CAJ
Near term completion types for new injectors	Cased, cemented, perforated, isolated with packers and sliding sleeves. Or (slotted) lined (CAJ). Or a mix. Dual lateral. Smart.
Near term stimulation techniques for new injectors	Acid frac, matrix acid, CAJ
Current field Oil Production rate (2011) (Stb/d)	50 000
Current field Water Production rate (2011 (bbl/d)	250 000
Current field Gross Liquid Production rate (bbl/d)	300 000

Current field Water Injection rate & max WH pressure (bbl/d & psia)	300 Mbbl/d, 2900 psi (controlled by max THP or max Q)
Produced Water Re-injection & max WH pressure (bbl/d & psia)	2 well trial, max 11 Mbbl/d
Current Gas production rate (MMscf/d)	45
Artifical lift methods, # of active installations per method (2011)	Gas lift, 57
Key constraints on production	Well integrity
Key constraints on water injection	Frac pressure, conformance
Background papers for further reading (max. 3)	Available at SPE

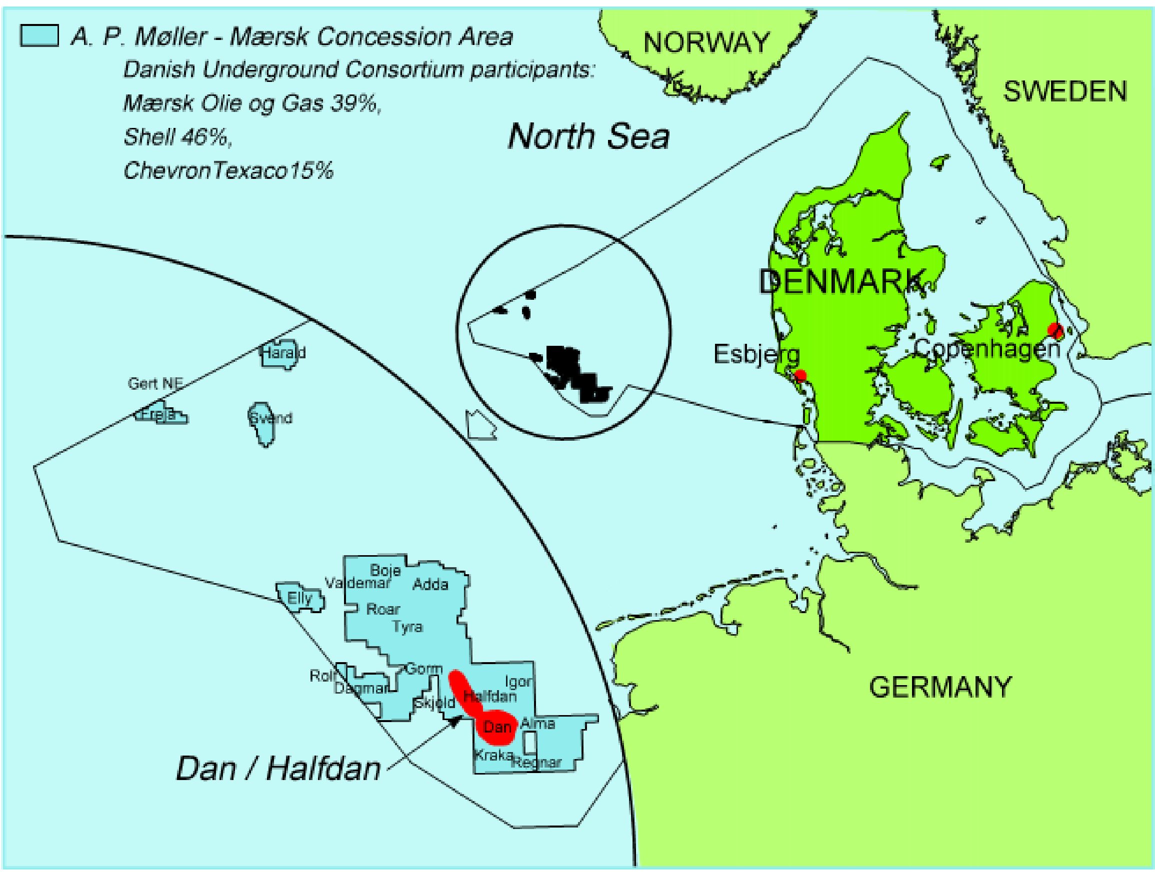

Figure 25.5: Dan Field Location Map

25.6 Halfdan

Field Name	**Halfdan**
License holders %	MOG (39); Shell (46); Chevron (15)
Location Map (Enclosure)	Enclosed
# Platform installations	4 Wellhead platforms; HBA, HBB, HCA, HDA 2 Accomodation platforms; HBC, HDB 1 Processing platform; HBD (+HDA)
Oil Export route	Pipeline via Gorm E facility to Fredericia, DK
Gas export route	Pipeline via Tyra facility then either to Denmark or via F3 facilities to the Netherlands
Reservoir Pressure at Datum - initial and current (psia)	Initial: 4188 Current: 1800-3100 (depending on location and Water injection)
Initial Reservoir Temperature (°C)	71@2012 ft TVDSS (1.5°F/100 ft)
Reservoir Depth Range (m ss)	2000–2200 m TVDSS
Stratigraphic units in production	Ekofisk, Tor
Stratigraphic units under water injection	Tor
Initial Porosity range (%)	2–45
S_{wi} range (%)	10–100
Initial Matrix permeability range (md)	0.4–8
Initial Effective permeability range (md)	0.4–8
Oil API grade	30
Initial Solution GOR range (Scf/Stb)	310–750
Initial Bubble point pressure range (psia)	4
CO_2, H_2S contents (mole%)	0.1–0.2 CO_2 & 0 H_2S
Production start-up	February 1999
Waterflood start-up	October 1999
Current drive mechanisms	Water injection
# of active production wells by 2011 (Of which horizontal, vertical)	34 (34,0)
Reservoir completion types used in active production wells	Cased, cemented, perforated, isolated with packers and sliding sleeves. Or (slotted) lined (CAJ). Or a mix.
Stimulation techniques used in active production wells	water frac, matrix acid, CAJ
# of active water injection wells by 2011 (Of which horizontal, vertical)	28 (28,0)
Reservoir completion types used in active injection wells	Cased, cemented, perforated, isolated with packers and sliding sleeves. Or (slotted) lined (Controlled Acid Jetted CAJ). Or a mix. 1 ”smart” (SCRAMS).
Stimulation techniques used in active injection wells	water frac, matrix acid, CAJ
Near term completion types for new producers	Cased, cemented, perforated, isolated with packers and sliding sleeves. Or (slotted) lined (CAJ). Or a mix. Dual lateral. Smart.
Near term stimulation techniques for new producers	Optimised hydrojetting, matrix acid, CAJ
Near term completion types for new injectors	Cased, cemented, perforated, isolated with packers and sliding sleeves. Or (slotted) lined (CAJ). Or a mix. Dual lateral. Smart.
Near term stimulation techniques for new injectors	matrix acid, CAJ
Current field Oil Production rate (2011) (Stb/d)	Ytd = 84,571 stb/d
Current field Water Production rate (2011 (bbl/d)	Ytd = 101,812 bbl/d

Current field Gross Liquid Production rate (bbl/d)	Ytd = 186,383 bbl/d
Current field Water Injection rate & max WH pressure (bbl/d & psia)	Ytd = 217,351 bbl/d Injection rate limited by downhole pressure limits, max WHP 2750 psi
Produced Water Re-injection & max WH pressure (bbl/d & psia)	No PWRI
Current Gas production rate (MMscf/d)	Ytd = 89.45 MMscf/d
Artifical lift methods, # of active installations per method (2011)	Gaslift, (31/34)
Key constraints on production	Well productivity, production stability and tubing integrity, allocation problems, scale management (future constraint)
Key constraints on water injection	Well injectivity, Frac pressure, WI plant performance, conformance
Background papers for further reading (max. 3)	Available at SPE

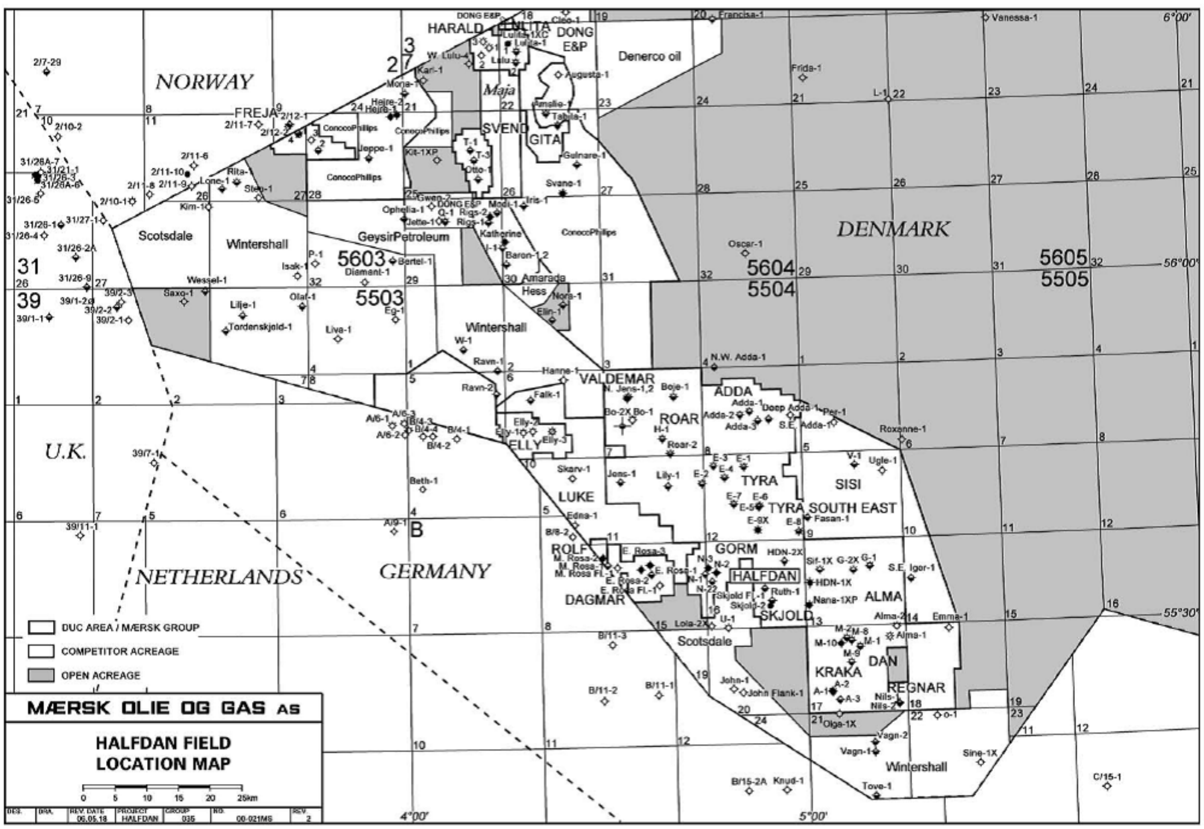

Figure 25.6: Halfdan Field Location Map

25.7 Gorm

Field Name	**Gorm**
License holders %	MOG 39%, Shell 46%, Chevron 15%
Location Map (Enclosure)	
# Platform installations	3 wellhead platforms, 3 other platforms
Oil Export route	Pipeline to Fridericia (DK)
Gas export route	Pipeline to Tyra facilities to Nybro (DK) and Den Helder (NL)
Reservoir Pressure at Datum – initial and current (psia)	4280 and 4500
Initial Reservoir Temperature (°C)	89
Reservoir Depth Range (m ss)	B block 1941 ft m TVDSS - 2140 m TVDSS Graben 2084 m TVDSS A block 1990 m TVDSS - 2057 m TVDSS
Stratigraphic units in production	Ekofisk and Tor
Stratigraphic units under water injection	Tor
Initial Porosity range (%)	15-45
S_{wi} range (%)	20–100
Initial Matrix permeability range (md)	1–10
Initial Effective permeability range (md)	0–10 mD - matrix around 1–2 mD
Oil API grade	33–35
Initial Solution GOR range (Scf/Stb)	600–850
Initial Bubble point pressure range (psia)	A-Block 3600
	B-Block 3300
CO_2, H_2S contents (mole%)	Initial $CO_2 < 1$ mol% H_2S initial none. Now it has been measured up to 8000 ppm in the gas stream when starting up wells after shut down
Production start-up	1981
Waterflood start-up	1989
Current drive mechanisms	Waterflood
# of active production wells by 2011 (Of which horizontal, vertical)	36 total (18, 18)
Reservoir completion types used in active production wells	Cased, cemented and perforated, cased w/ sliding sleeves and external casing packers, semi-openhole (uncemented and preperforated)
Stimulation techniques used in active production wells	Hydraulic sand fracs, WISPER, Matrix acid, High rate acid, Acid fracs.
# of active water injection wells by 2011 (Of which horizontal, vertical)	14 total (8, 6)
Reservoir completion types used in active injection wells	Cased, cemented and perforated, cased w/ sliding sleeves and external casing packers
Stimulation techniques used in active injection wells	Hydraulic sand fracs, Matrix acid, High rate acid
Near term completion types for new producers	Cased, cemented and perforated, cased w/ sliding sleeves and external casing packers, semi-openhole (uncemented and preperforated)
Near term stimulation techniques for new producers	Hydraulic sand fracs, Matrix acid, High rate acid
Near term completion types for new injectors	Cased, cemented and perforated, cased w/ sliding sleeves and external casing packers
Near term stimulation techniques for new injectors	Hydraulic sand fracs, Matrix acid, High rate acid

Current field Oil Production rate (2011) (Stb/d)	13
Current field Water Production rate (2011 (bbl/d)	78
Current field Gross Liquid Production rate (bbl/d)	81
Current field Water Injection rate & max WH pressure (bbl/d & psia)	100 000 at 3300 psia
Produced Water Re-injection & max WH pressure (bbl/d & psia)	100 000 at 3300 psia
Current Gas production rate (MMscf/d)	12
Artifical lift methods, # of active installations per method (2011)	Gas lift
Key constraints on production	Bedspaces hindering well intervention work
Key constraints on water injection	Number of wells, Schmoo
Background papers for further reading (max. 3)	Avail. on: `http://www.onepetro.org/mslib/app/newSearch.do`

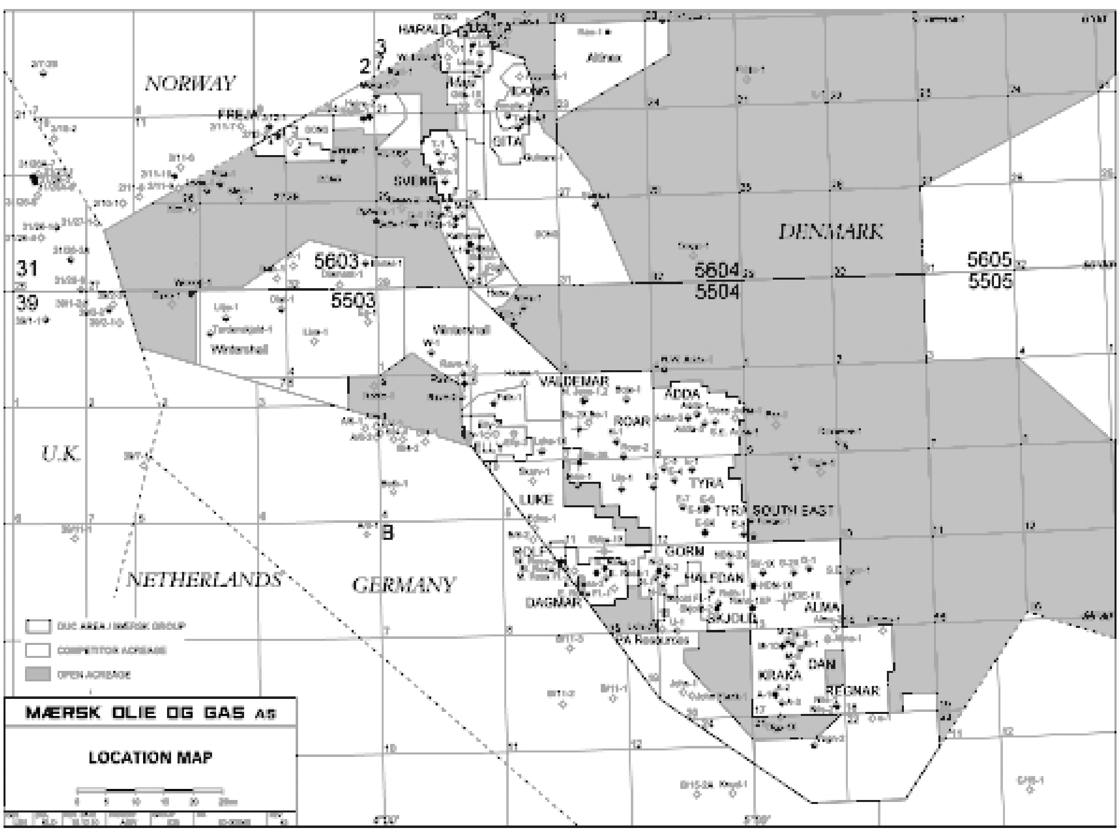

Figure 25.7: Gorm Field Location Map

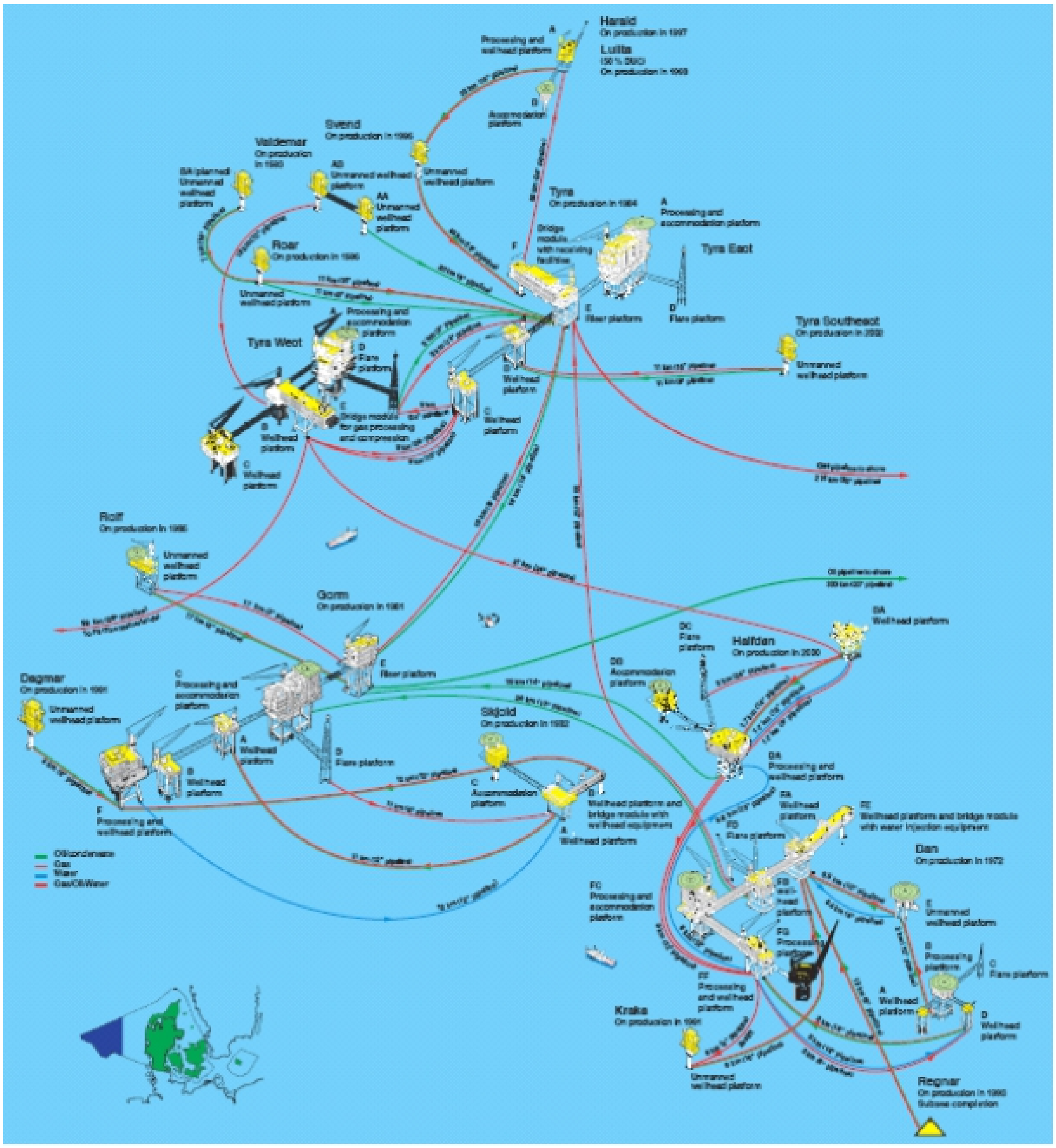

Figure 25.8: Gorm Field Location Map

25.8 Skjold

Field Name	**Skjold**
License holders %	Maersk Oil (39%); Shell (46%), Chevron (15%)
Location Map (Enclosure)	Enclosed
# Platform installations	2 bridge-linked wellhead platforms (1 manned)
Oil Export route	Pipeline via Gorm facility to Fridericia (DK)
Gas export route	Pipeline via Gorm & Tyra facilities to Nybro (DK) and Den Helder (NL)
Reservoir Pressure at Datum - initial and current (psia)	Initial: 3559 psia (@ 1600 m TVDss); current: 2700–3100 psia
Initial Reservoir Temperature (°C)	83
Reservoir Depth Range (m ss)	1400–2000
Stratigraphic units in production	Ekofisk & Tor formations
Stratigraphic units under water injection	Tor formation
Initial Porosity range (%)	Ekofisk fm.: 15–40%; Tor fm: 10–40%
S_{wi} range (%)	Ekofisk: 10–80%; Tor: 7–90%
Initial Matrix permeability range (md)	Ekofisk fm.: 0.1–7 mD; Tor fm: 0.1–5 mD
Initial Effective permeability range (md)	1–2000 mD (depending on fracture density)
Oil API grade	30
Initial Solution GOR range (Scf/Stb)	524
Initial Bubble point pressure range (psia)	3183
CO_2, H_2S contents (mole%)	0.33; 0 (initial); current H_2S levels in wells up to 0.2 mole% as a result of water injection (bacteria)
Production start-up	Nov. 1982
Waterflood start-up	Apr. 1986
Current drive mechanisms	Waterflooding
# of active production wells by 2011 (Of which horizontal, vertical)	17 (15, 2)
Reservoir completion types used in active production wells	Cased, cemented, perforated, isolated with packers and sliding sleeves. Or un-cemented slotted liner (CAJ).
Stimulation techniques used in active production wells	Matrix acidized, propped fracturing, acid fracturing
# of active water injection wells by 2011 (Of which horizontal, vertical)	9 (1, 8)
Reservoir completion types used in active injection wells	Cased, cemented, perforated, isolated with packers and sliding sleeves. Or un-cemented slotted liner (CAJ).
Stimulation techniques used in active injection wells	Matrix acidized, CAJ
Near term completion types for new producers	n.a.
Near term stimulation techniques for new producers	n.a.
Near term completion types for new injectors	n.a.
Near term stimulation techniques for new injectors	n.a.
Current field Oil Production rate (2011) (Stb/d)	15 000
Current field Water Production rate (2011 (bbl/d)	67 000
Current field Gross Liquid Production rate (bbl/d)	82 000
Current field Water Injection rate & max WH pressure (bbl/d & psia)	80 000, Injection rate reduced due to flooding of some producers
Produced Water Re-injection & max WH pressure (bbl/d & psia)	Injection water consists of a mix of seawater and produced water (approx. 50%–50%)
Current Gas production rate (MMscf/d)	12

Artifical lift methods, # of active installations per method (2011)	Gaslift, 14
Key constraints on production	Pipeline capacity
Key constraints on water injection	Well injectivity, WI plant performance, producer performance (impact on BSW)
Background papers for further reading (max. 3)	

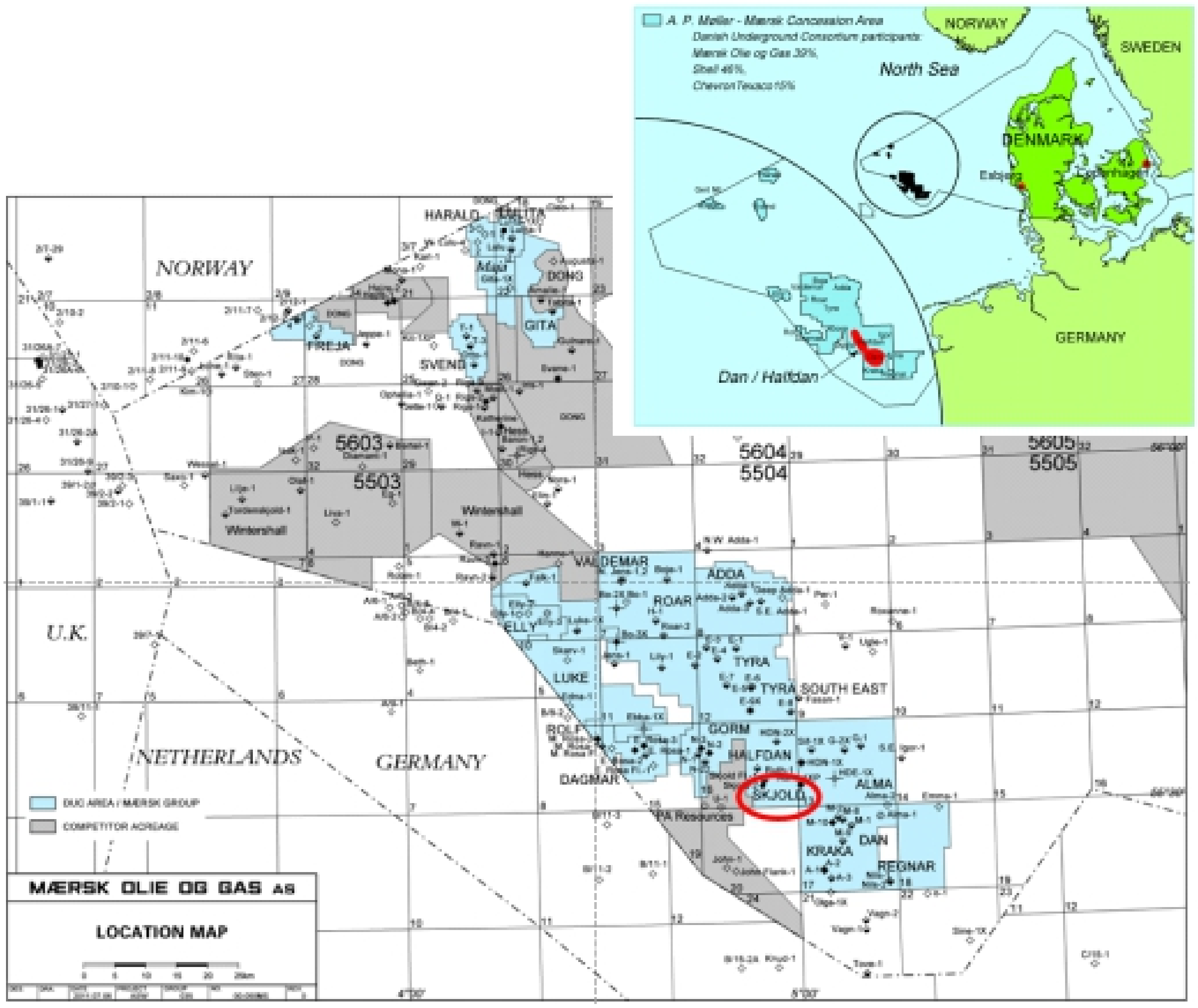

Figure 25.9: Skjold Field Location Map

25.9 Syd-Arne

Field Name	**South Arne**
License holders %	Hess 61.5% Dong 36.8% Danoil 1.7%
Location Map (Enclosure)	
# Platform installations	3
Oil Export route	Gravity base storage (500 MBO), tanker offload
Gas export route	Gas pipeline → Harald → Nybro
Reservoir Pressure at Datum - initial and current (psia)	6300 psi (initial) @ 2804 mSS; 2500–7500 psi (current)
Initial Reservoir Temperature (°C)	115°C
Reservoir Depth Range (m ss)	2650–3050 mTVDSS
Stratigraphic units in production	Tor, Ekofisk
Stratigraphic units under water injection	Tor, Ekofisk
Initial Porosity range (%)	15–45%
S_{wi} range (%)	2–60%
Initial Matrix permeability range (md)	0.05–2 mD
Initial Effective permeability range (md)	0.1–30 mD
Oil API grade	36.7 ° API
Initial Solution GOR range (Scf/Stb)	1200 scf/STB
Initial Bubble point pressure range (psia)	4800 psi
CO_2, H_2S contents (mole%)	CO_2 1.4%, H_2S < 10 ppm
Production start-up	July 1999
Waterflood start-up	December 2000
Current drive mechanisms	Water injection, depletion, compaction
# of active production wells by 2014 (Of which horizontal, vertical)	18 Horizontal of which 1 will be converted to injector end 2014
Reservoir completion types used in active production wells	Multizone Baker PSI (10), Multizone openhole production tubing with swell packers (2), limited entry openhole production tubing (1)
Stimulation techniques used in active production wells	Proppant fractures (7 wells), Acid fractures (11 wells)
# of active water injection wells by 2014 (Of which horizontal, vertical)	7 Horizontal
Reservoir completion types used in active injection wells	Multizone Baker PSI (5), Multizone openhole liner with swell packers (2)
Stimulation techniques used in active injection wells	Acid fracturing, acid limited entry, water fracturing
Near term completion types for new producers	Multizone openhole liner with swell packers
Near term stimulation techniques for new producers	Acid fracturing, ball activated SSDs
Near term completion types for new injectors	Multizone openhole liner with swell packers, ball activated SSDs
Near term stimulation techniques for new injectors	Acid fracturing, acid limited entry, water fracturing
Current field Oil Production rate (2014) (Stb/d)	25 000 BOPD
Current field Water Production rate (2014 (bbl/d)	45 000 BWPD
Current field Gross Liquid Production rate (bbl/d)	70 000 BLPD
Current field Water Injection rate & max WH pressure (bbl/d & psia)	Up to 80 000 BWPD (PWRI+SRP), 4900 psi SRP: Sulphate Removal Plant

Produced Water Re-injection & max WH pressure (bbl/d & psia)	Up to 50 000 BWPD, 4900 psi
Current Gas production rate (MMscf/d)	25 MMSCFD export, 38 MMSCFD gaslift
Artifical lift methods, # of active installations per method (2014)	Gas lift, 10 wells, 0–3 unloading valves, orifice and venturi operating valves
Key constraints on production	Water injection availability, proppant production, $CaCO_3$ scale in vertical sections, $BaSO_4$ scale in horizontal sections
Key constraints on water injection	Injection pressure limited by overburden fracture pressure, managing water short circuits, seal failures on PWRI pumps, SRP uptime
Waterflood Surveillance	
No. of 4D seismic surveys for waterflood monitoring. Possible to separate S_w changes from other effects?	3D seismic surveys were shot in 1995, 2005 and 2011.
	4D AVO inversion allows fluid type distinction and indications of compaction effects.
Is cased hole logging routinely used to monitor waterflood development? Typical logging frequency per well.	PLTs are performed regularly in both producers and injectors. Typically we have 2-3 PLTs per well. Logging frequency per well is about 4 years.
Type of open hole logs run to estimate water saturation in flooded intervals. Do they give reliable results?	Not been performed at South Arne.
No. of wells successfully cored behind water front	No wells cored behind water front at South Arne.
Tracer in injection water used in all injectors? Normal frequency of tracer pulses per well.	Tracers have been injected approximately twice in all injectors. Frequency is about every 4 years.
Analysis of produced water samples for ions, tracers, etc.	Produced water is analysed monthly for 12 different ions. Most importantly chloride and sulphate.
Is interference testing used on regular basis?	Interference testing is performed on an ad-hoc basis.
Typical particle content in injection water. Is injectivity observed to decrease with time?	The sea water injected is very clean < 1 my. The produced water injected is not regularly monitored, but is known to contain some solids occasionally.
Monitoring techniques for fracture growth in injectors	Pressure transient analysis and injectivity monitoring.
No. of dedicated observation/monitoring wells for waterflood. Logging types and frequency?	No dedicated observation wells at South Arne.
No. of wells used for compaction monitoring. Logging frequency?	No dedicated observation wells at South Arne.
Use of advanced logging for waterflood monitoring (DTS, EMS, passive seismic,...)	4D seismic shows water flooding.
Issues with current waterflood surveillance tools/technologies	We estimate sea-water break-through in producers based on chloride, but results are only an average of the horizontal reservoir section.
Background papers for further reading (max. 3)	Avail. on: `http://www.onepetro.org/mslib/app/newSearch.do` 130412-MS 130410-MS 86485-MS

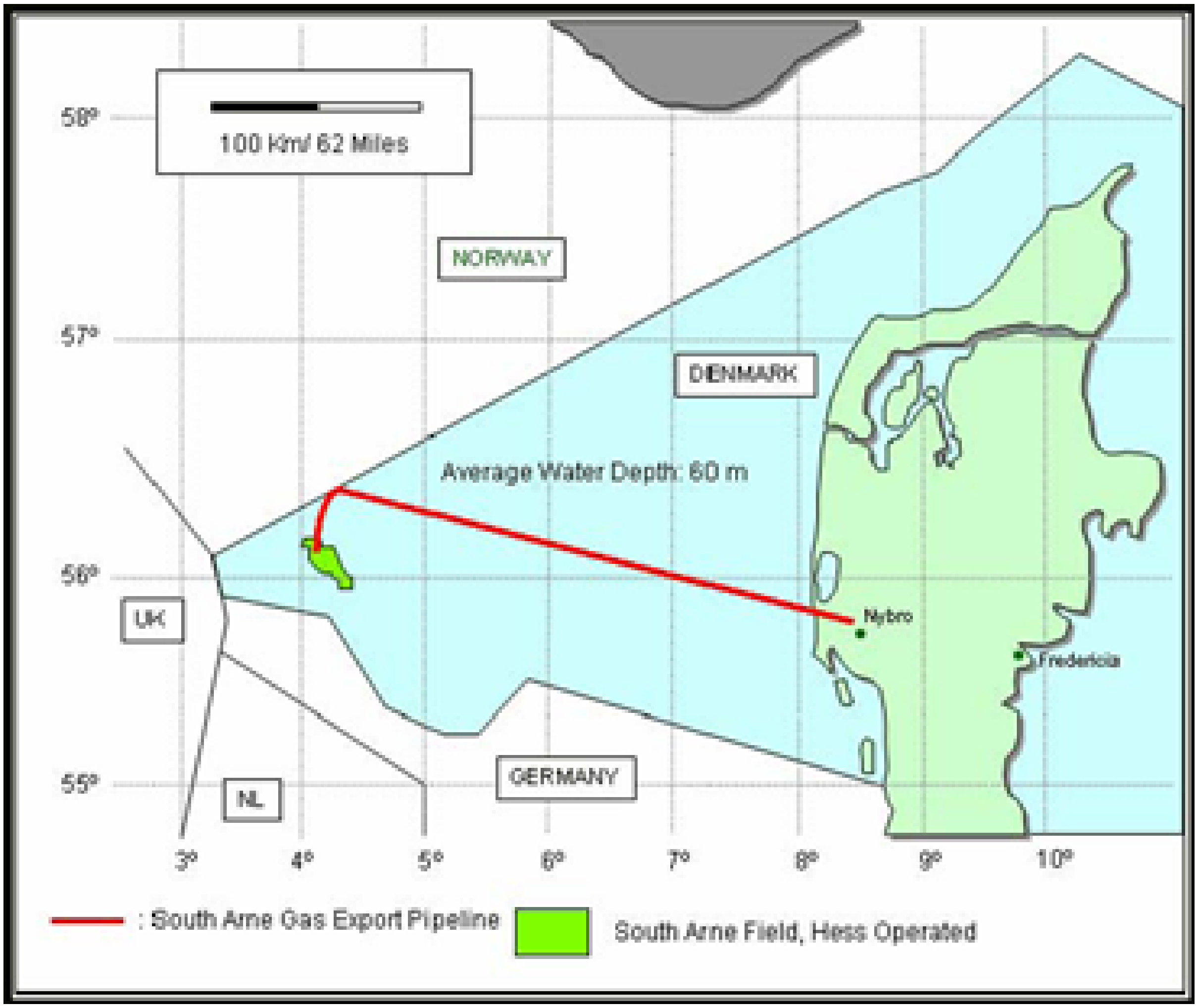

Figure 25.10: South Arne Field Location Map

25.10 UK fields

Field Name	**Machar**
License holders %	BP (100.00)
Location Map (Enclosure)	Enclosed
# Platform installations	2 subsea manifold tied-back to ETAP processing platform 35 km away
Oil Export route	Pipeline via FPS to Kinneil, Grangemeouth, UK
Gas export route	Pipeline via CATS to Teeside, UK
Reservoir Pressure at Datum - initial and current (psia)	Initial: 3800 psia (@2000m TVDss); current: 2300–3800 psia
Initial Reservoir Temperature (°C)	108
Reservoir Depth Range (m ss)	1300–2500
Stratigraphic units in production	Maureen (clastic), Ekofisk (clastic & chalk), Tor & Hod formations
Stratigraphic units under water injection	All the above but Maureen & Hod indirectly
Initial Porosity range (%)	Maureen 12–24%; Ekofisk: 12–28%; Tor fm: 12–28%; Hod fm: 8–20%
S_{wi} range (%)	Maureen: 10–25%; Tor: 5–35%; Hod: 5–35%
Initial Matrix permeability range (md)	Maureen 10–1000; Ekofisk sand 10–100; Ekofisk chalk 0.1–1 mD; Tor 0.1–10 mD; Hod 0.01–1 mD
Initial Effective permeability range (md)	0.1–1000 mD (Ekofisk & Tor fm)
Oil API grade	41
Initial Solution GOR range (Scf/Stb)	805
Initial Bubble point pressure range (psia)	3114
CO_2, H_2S contents (mole%)	1.6; 0
Production start-up	EWT 1994–1996. Platform: Aug 1998
Waterflood start-up	Oct. 1998
Current drive mechanisms	Waterflooding + Fluid Expansion & Gravity Drainage in secondary gas cap
# of active production wells by 2011 (Of which horizontal, vertical)	7. All are deviated but due to dip this makes them stratigraphically horizontal
Reservoir completion types in active production wells	Cased, cemented and perforated, cased with external casing packers,
Stimulation techniques in active production wells	Acid fracturing with diversion
# of active water injection wells by 2011 (Of which horizontal, vertical)	3. All are deviated but due to dip this makes them stratigraphically horizontal
Reservoir completion types in active injection wells	Cased, cemented and perforated.
Stimulation techniques used in active injection wells	Acid fracturing with diversion
Near term completion types for new producers	Cased, cemented and perforated
Near term stimulation techniques for new producers	Acid fracturing with diversion
Near term completion types for new injectors	Cased
Near term stimulation techniques for new injectors	Acid fracturing with diversion
Current field Oil Production rate (2014) (Stb/d)	15 000
Current field Water Production rate (2014 (bbl/d)	25 000
Current field Gross Liquid Production rate (bbl/d)	40 000
Current field Water Injection rate & max WH pressure (bbl/d & psia)	45 000. VRR = 1.0

Produced Water Re-injection & max WH pressure (bbl/d & psia)	PWRI in Palaeocene near CPF (35 km away)
Current Gas production rate (MMscf/d)	12
Artifical lift methods, # of active installations per method (2011)	Gaslift, 7
Key constraints on production	Facility constrained - slug-catcher and CPF PWRI.
Key constraints on water injection	No constraints
Background papers for further reading (max. 3)	SPE56974, SPE121483
Waterflood Surveillance	
No. of 4D seismic surveys for waterflood monitoring. Possible to separate S_w changes from other effects?	No 4D due to the difficulty of imaging steeply dipping structure
Is cased hole logging routinely used to monitor waterflood development? Typical logging frequency per well.	Yes but only in producers and injectors - there are no observation wells
Type of open hole logs run to estimate water saturation in flooded intervals. Do they give reliable results?	Full OH suite including resistivity / density / neutron / sonic. Analysis is complicated by varying water properties as injected seawater dissolves salts to make it saline.
No. of wells successfully cored behind water front	None
Tracer in injection water used in all injectors? Normal frequency of tracer pulses per well.	Yes. Tracers injected in early injectors provided valuable information on water movement
Analysis of produced water samples for ions, tracers, etc.	Field water samples 2-weekly. 11-ion analysis. No tracer analysis nowadays.
Is interference testing used on regular basis?	Not regularly but interference testing has been used successfully.
Typical particle content in injection water. Is injectivity observed to decrease with time?	Heavily fractured reservoir with injectors choked back so injectivity is not an issue.
Monitoring techniques for fracture growth in injectors	Falloff PTA performed but fracture length depends on injection rate & pressure
No. of dedicated observation/monitoring wells for waterflood. Logging types and frequency?	None
No. of wells used for compaction monitoring. Logging frequency?	None
Use of advanced logging for waterflood monitoring (DTS, EMS, passive seismic,...)	None
Issues with current waterflood surveillance tools/technologies	Ability to determine oil saturations with varying water properties.

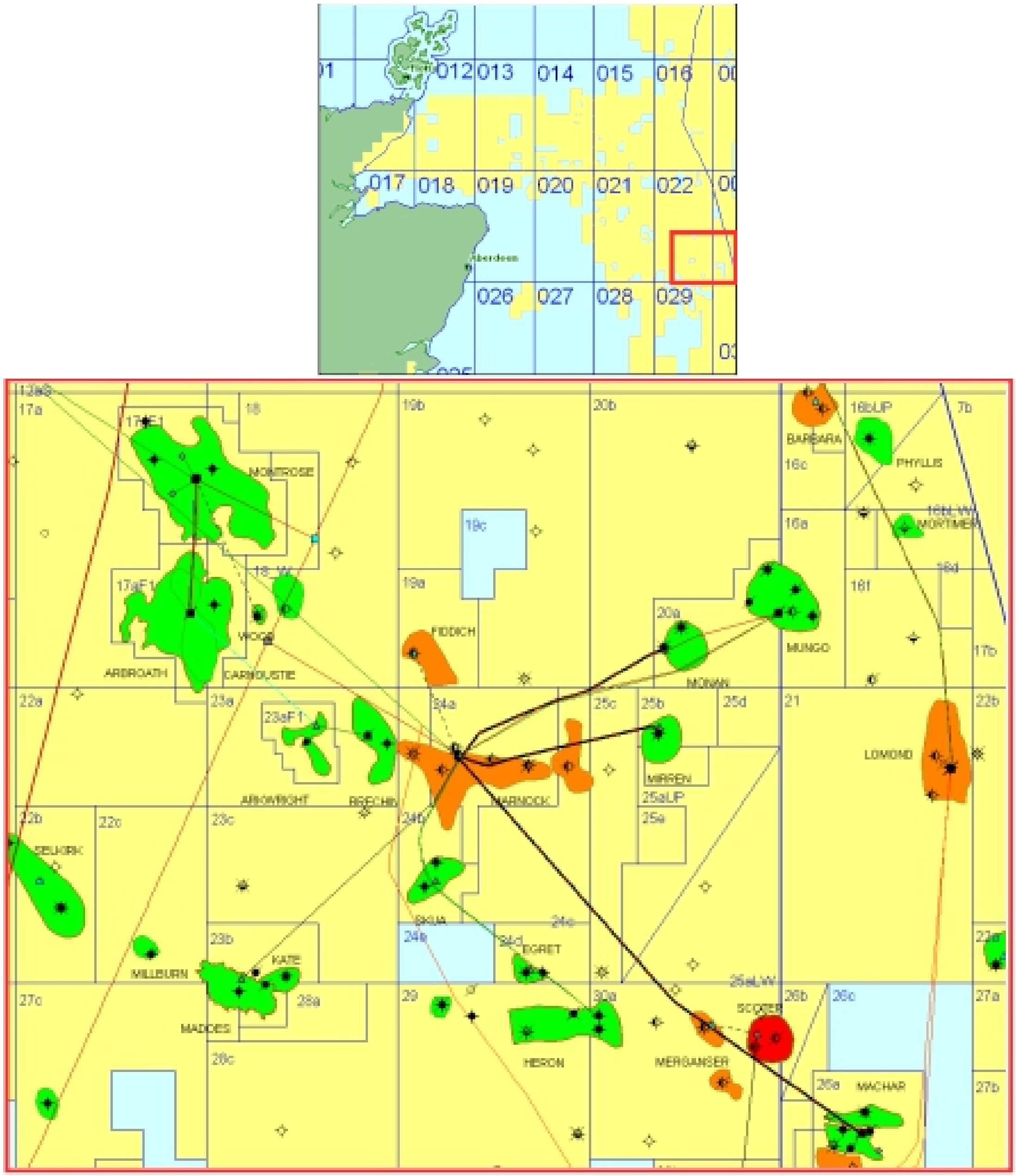

Figure 25.11: Machar Field Location Map (UKCS Block 23/26a)

Nomenclature/Abbreviation

AVO = amplified versus offset
BLPD = barrels of liquid per day
BOPD = barrels of oil per day
BWPD = barrels of water per day
BWS = basic sediment and water phase
CAJ = controlled acid jet
CATS = central area transmission system
CPF = central processing facility
DTS = digital transmission system
EMS = electronic massage system
ETAP = processing platform
EWT = extended well test

FSP = forties pipeline system
HBA = Halfdan B wellhead platform
HBB = Halfdan B riser platform
HBC = Halfdan B accommodation platform
HBD = Halfdan B processing platform
HCA = Halfdan unmanned wellhead platform
HDA = Halfdan A combined processing and wellhead platform
HDB = Halfdan A accommodation platform
LoFS = life of field seismic
NMR = nuclear magnetic resonance
PLT = production logging tool
PTA = pressure transient analysis
PWRI = produced water re-injected
Q = rate
SCRAMS = surface controlled reservoir analysis and management system
SRP = sulfate removal plant
SSD = sliding side door
TVDSS = total vertical depth subsea
THP = top hole pressure
Ytd year-to-date
VRR = voidage replacement ratio
WBM = water based mud
WH = wellhead
WHP = wellhead platform, wellhead pressure
WI = well injectivity
WISPER = widely spaced etched ridges